Nonmetal coordination chemistry: P-adducts of electrophilic, terminal phosphinidene complexes

Dissertation

zur

Erlangung des Doktorgrades (Dr. rer. nat.)

der

Mathematisch-Naturwissenschaftlichen Fakultät

der

Rheinischen Friedrich-Wilhelms-Universität Bonn

vorgelegt von

David Biskup

aus Adenau

Bonn, 2023

Angefertigt mit Genehmigung der Mathematisch-Naturwissenschaftlichen Fakultät
der Rheinischen Friedrich-Wilhelms-Universität Bonn

1. Gutachter: Prof. Dr. Rainer K. Streubel
2. Gutachter: Prof. Dr. Andreas Gansäuer

Tag der Promotion: 10.10.2023
Erscheinungsjahr: 2023

Hiermit versichere ich, dass die vorgelegte Arbeit persönlich, selbstständig und ohne Benutzung anderer als der angegebenen Hilfsmittel angefertigt wurde und alle Quellen kenntlich gemacht wurden.

To my grandparents

“Imagine all the people living life in peace. You may say that I’m a dreamer, but I’m not the only one. I hope someday you’ll join us and the world will be as one.”

– JOHN LENNON

PUBLIKATIONEN UND KONFERENZBEITRÄGE

Teilergebnisse aus dieser Dissertation wurden mit Genehmigung der Mathematisch-Naturwissenschaftlichen Fakultät der Universität Bonn vorab veröffentlicht.

VERÖFFENTLICHUNGEN

1. „*Challenging an old paradigm by demonstrating transition metal-like chemistry at a neutral nonmetal center*“; D. Biskup, G. Schnakenburg, R. T. Boeré, A. Espinosa Ferao, R. K. Streubel, *Nat. Commun.* **2023**, *14*, 6456. DOI: 10.1038/s41467-023-42127-3
2. „*A novel access to phosphanylidene-phosphorane complexes via P-donor substitution and a detailed bonding analysis*“; D. Biskup, G. Schnakenburg, R. T. Boeré, A. Espinosa Ferao, R. Streubel, *Dalton Trans.* **2023**, *52*, 13781–13786. DOI: 10.1039/D3DT02304D
3. „*Synthesis of a 1-aza-2-phospha-acenaphthene complex profiting from coordination enabled chloromethane elimination*“; D. Biskup, T. Bergmann, G. Schnakenburg, R. M. Gomila, A. Frontera, R. Streubel, *RSC Adv.* **2023**, *13*, 21313–21317. DOI: 10.1039/D3RA04352E
4. „*Synthesis of free and ligated 1,2-thiaphosphetanes – expanding the pool of strained P-ligands*“; A. W. Kyri, F. Gleim, D. Biskup, G. Schnakenburg, A. Espinosa Ferao, R. Streubel, *Chem. Commun.* **2019**, *55*, 1615–1618. DOI: 10.1039/C8CC09892A

KONFERENZBEITRÄGE

1. „19th European Workshop on Phosphorus Chemistry“ (EWPC-19) und „3rd Spanish Workshop on Phosphorus Chemistry“ (SWPC-3) in Donostia-San Sebastián (Spanien) vom 28.–30.03.2023; **Vortrag** „*Chemistry of P-adducts of electrophilic terminal phosphinidene complexes*“.
2. „Spring Meeting GDCh Working Group Phosphorus Chemistry“ in Dresden (Deutschland) vom 12.–13.03.2023; **Vortrag** „*Nonmetal coordination chemistry: Synthesis, properties and reactions of P-adducts of electrophilic terminal phosphinidene complexes*“.
3. „ACS Fall 2022 – Sustainability in a Changing World“ in Chicago, IL (USA) vom 21.–25.08.2022; **Posterbeitrag** „*Transition metal-like reactivity of ligand-to-phosphinidene complex adducts*“.

4. „16th International Symposium on Inorganic Ring Systems“ (IRIS16) in Graz (Österreich) vom 24.–29.07.2022; **Posterbeitrag** „*Chemistry of ligand-to-phosphinidene complex adducts, and the surprising formation of P_4*“.
5. „11. Deutsch-Österreichischer Mitarbeiterworkshop für Hauptgruppenelement-Chemie“ (MHC-11) in Bonn (Deutschland) vom 03.–05.09.2021; **Vortrag** „*Synthesis and Reactivity of Donor-to-Phosphinidene Complex Adducts*“.
6. „23rd International Conference on Phosphorus Chemistry“ (ICPC23) virtuell vom 05.–09.07.2021; **Posterbeitrag** „*Phosphorus, a metal copy? 1,2-Addition of primary amines to isonitrile-to-phosphinidene complex adducts*“.
7. „Online Workshop on Phosphorus Chemistry“ (OWPC 2021) virtuell vom 29.–31.03.2021; **Posterbeitrag** „*Formation and Reactions of Isonitrile-to-Phosphinidene Complex Adducts*“.
8. „17th European Workshop in Phosphorus Chemistry“ (EWPC-17) in Rennes (Frankreich) vom 26.–28.02.2020; **Posterbeitrag** „*Nucleophilic reactions at the P-center of Isonitrile-to-phosphinidene complex adducts*“.
9. „13th International Conference on Heteroatom Chemistry“ (ICHAC 2019) in Prag (Tschechische Republik) vom 30.06.–05.07.2019; **Posterbeitrag** „Reactivity of an Isonitrile-to-Phosphinidene Complex Adduct and its thermal stability“.
10. „16th European Workshop in Phosphorus Chemistry“ (EWPC-16) in Bristol (Vereinigtes Königreich) vom 24.–26.04.2019; **Posterbeitrag** „Reactions of Isonitrile-to-Phosphinidene Complex Adducts“.
11. „10. Deutsch-Österreichischer Mitarbeiterworkshop für Hauptgruppenelement-Chemie“ (MHC-10) in Tübingen (Deutschland) vom 15.–17.03.2019; **Vortrag** „*Reactions of Isonitrile-to-Phosphinidene Complex Adducts*“.

ACKNOWLEDGMENTS

First and foremost, I would like to express my gratitude to Prof. Dr. Rainer K. Streubel for the opportunity to perform my doctoral studies in his research group. I am very thankful for his invaluable guidance, support, constructive feedback and trust. Without the provided well-equipped inert-gas chemistry laboratory with its special unique instruments, the pursuit of the challenging research topic and the preparation of this dissertation would not have been possible. Furthermore, I am grateful for enabling the participation in many international conferences and workshops, the research stay in Japan and the invitation to many dinners with fruitful discussions not only on scientific topics.

I also would like to thank Prof. Dr. Andreas Gansäuer, Prof. Dr. Arne Lützen and Prof. Dr. Diana Imhof for their interest in my research project and their willingness to invest their valuable time to examine this thesis and be part of the doctoral committee.

I owe special thanks to Prof. Dr. Arturo Espinosa Ferao (University of Murcia, Spain) for all the performed high-level DFT calculations on my research topic as well as the long meetings with the productive discussions and explanations. Especially, I would like to acknowledge the fulfillment of several requests during the final stage of my doctoral studies.

I am very thankful to Prof. Dr. René T. Boeré (University of Lethbridge, Canada) for the workshop and tutorial on cyclic voltammetry as well as the extraordinary support in analyzing and interpreting the obtained data.

Furthermore, I would like to thank Prof. Dr. Norihiro Tokitoh (Kyoto University, Japan) for the hosting and the possibility to work in his laboratories during the short-term exchange program in Uji. I especially would like to express my gratitude to Prof. Dr. Yoshiyuki Mizuhata for the organization and supervision of the research stay as well as Dr. Yamato Omatsu for several scientific discussions and his recommendations for places of interest. I also want to thank the whole research group in Japan, especially Dr. Yamato Omatsu and Dr. Tatsuya Yanagisawa for several dinners and activities outside of the lab.

Without the careful and patient service of the analytical department, the research would not have proceeded such smoothly and properly. Therefore, I thank Dr. Gregor Schnakenburg and Charlotte Rödde for single crystal X-ray diffraction analyses, Dr. Senada

Nozinovic, Dipl.-Ing. Karin Prochnicki, Hannelore Spitz and Ulrike Weynand for recording the solution NMR spectra including several variable temperature and extended measurements, Dr. Marianne Engeser, Christine Sondag and Karin Peters-Pflaumbaum for recording the mass spectra and enabling conditions to perform the elaborate measurements of sensitive compounds, Dr. Sabine Rings, Charlotte Rödde and Hannelore Spitz for performing the elemental analyses, Mridhul Ram Kottayil Madam Ramachandran, Shahriar Kermanshahian and Kerstin Kühnel-Lysek for the time-consuming conscientious preparation of the elemental analysis samples. Special thanks also belong to the whole highly professional staff of the workshops of the chemical institutes: Tobias Schönberg and Thorsten Ullrich (glass blowing workshop), Bernhard Klöckner and his colleagues (electronics workshop), Ralf Batta and his colleagues (mechanical workshop), Wolfgang Klein †, Thomas Gerhards and Torsten Bartsch (janitorial services) and Kirsten Müller and her colleagues (chemical storage, ZVE).

For the generous financial support of this work and the participation at conferences, workshops and an exchange program, I am grateful to the Deutsche Forschungsgemeinschaft (STR 411/45-1), the University of Bonn, the Gesellschaft Deutscher Chemiker (GDCh), the Bonn International Graduate School of Chemistry (BIGS Chemistry) and the International Joint Usage/Research Center of the Institute for Chemical Research, Kyoto University (ICR-iJURC).

I also want to thank all former and present members of the research group of Prof. Dr. Rainer K. Streubel for all the scientific and non-scientific discussions, especially Dr. Andreas W. Kyri, Dr. Philip Junker and Dr. Alexander Schmer who introduced me to the chemistry of the research group, Philipp, Tim and Tatjana for advices on DFT calculations and Florian, Shahriar, Mridhul and all aforementioned members of the group for the moral support and the coffee breaks with the mostly scientific lively discussions.

Finally, I thank my family and friends for all their understanding and support during my doctoral studies: especially my wife Pauline who had to spend many nights and weekends alone or waiting *only* fifteen minutes in the car while I was working in the lab as well as the many relaxing strolls with Simba and Penny, my parents who supported me during all difficult stages, my grandmother for all the long brunches which always were a great compensation for the lab work and my parents-in-law as well as my “grandparents-in-law” who always were interested in my research and supported me a lot. I would like to especially thank Dr. Lothar Biskup and Andreas Schaefer for the revision of this thesis.

TABLE OF CONTENTS

1 INTRODUCTION

1.1 THE ELEMENT PHOSPHORUS AND ITS CHEMISTRY

Phosphorus is the 15th element in the periodic system and only one isotope, namely ^{31}P, is naturally existent.[1] It cannot be found uncombined as free element in nature. Due to its strong affinity to oxygen phosphorus usually is found as phosphate. The most important and common phosphorus containing minerals are the apatite $Ca_5(PO_4)_3(Cl,F,OH)$ and the phosphorite $Ca_3(PO_4)_2$.[2] Additionally phosphorus can be found rarely as iron-, aluminum- and rare-earth metal phosphates, *e.g.* vivianite $Fe_3(PO_4)_2 \cdot 8\ H_2O$, wavellite $Al_3(PO_4)_2(OH,F)_3 \cdot 5\ H_2O$ or monazite $(Ce,Th)(PO_4,SiO_4)$.[3] Thus, the synthesis and isolation of elemental phosphorus are energetically and economically costly. The discovery of the first elemental phosphorus is ascribed to the alchemist Henning Brand in 1669 who was searching for the philosopher's stone. For that, he glowed the white residue of evaporated urine observing radiation of light due to the chemiluminescence that is based on the oxidation of traces of evaporated white phosphorus P_4 by atmospheric oxygen to phosphorus trioxide P_2O_3 and further oxidation to phosphorus pentoxide P_2O_5 while releasing light. The white phosphorus was generated via reduction of ammonium sodium hydrogen phosphate $Na(NH_4)HPO_4$ by organic material.[4]

Elemental phosphorus exists in different allotropic modifications. White phosphorus consists of tetrahedral P_4 molecules as cubic modification. It is the starting material for the preparation of all other modifications and is synthesized by reducing fluorapatite (2.3–4.8 weight-% F) with coke in the presence of quartz in an electric arc furnace at 1400–1500 °C (Scheme 1). Upon cooling, P_2 dimerizes to P_4. Commercially available white phosphorus is purified by distillation and casted into bars.[3]

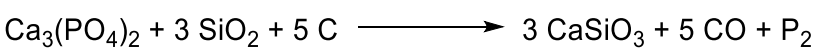

Scheme 1: Simplified equation of the carbothermal reaction of calcium phosphate to elemental phosphorus.[3]

Due to its high ring strain of 25 kJ/mol white phosphorus is highly reactive and ignites itself in air. Red phosphorus is the amorphous, polymeric modification and is synthesized by heating white phosphorus at 200–450 °C. Violet phosphorus also referred to as Hittorf's phosphorus is obtained by heating red phosphorus or white phosphorus at 550 °C for one to two weeks as monoclinic modification. It is the thermodynamically most stable modification between

550 and 620 °C. Above 620 °C it starts subliming under formation of white phosphorus. Black phosphorus has a higher density (ρ = 2.69 g/cm^3) than white phosphorus (ρ = 1.82 g/cm^3) or violet phosphorus (ρ = 2.36 g/cm^3). Therefore, its generation is favored by applying high pressures, meaning that white phosphorus is converted to the orthorhombic black modification at 200 °C under high pressure (12 kbar). If very large pressures (100 kbar) are applied the conversion is already completed after a short pressure surge. Black phosphorus conducts electricity as semi-conductor and thus has a metallic character. Black phosphorus can also be converted into high pressure modifications: at pressures above 83 kbar a rhombohedral modification (isotype to grey arsenic) and above 111 kbar a cubic modification is reversibly formed. Black phosphorus is the thermodynamically most stable modification up to 550 °C. Above this temperature, it converts to violet phosphorus. Fibrous red phosphorus, the latest discovered allotrope, is obtained by subliming red phosphorus using iodine as catalyst at 500–600 °C. The structure is related to violet phosphorus.[3,5]

Phosphorus can occupy all oxidation states between −III and +V (Table 1).[3]

Table 1: Examples of phosphorus containing compounds occupying oxidation states between −III and +V.[3]

oxidation state	Example
−III	PH_3
−II	P_2H_4
−I	$(PH)_n$
0	P_4
+I	H_3PO_2
+II	$H_4P_2O_4$
+III	H_3PO_3
+IV	$H_4P_2O_6$
+V	H_3PO_4

In the biosphere phosphorus also plays an important role as phosphates and phosphate esters, *e.g.* hydroxyapatite $Ca_5(PO_4)_3(OH)$ in bones and teeth, the phosphate-deoxyribose backbone in deoxyribonucleic acid (DNA), phospholipids (*e.g.* the bilayer in cell membranes), in the energy metabolism (*e.g.* adenosine triphosphate (ATP) or guanosine tri-phosphate (GTP)) or in intracellular cell signaling.[6,7] Blood has a phosphate concentration of 1 mM and it is a crucial buffer to keep the pH value of the blood constant at 7.4 due to the

presence of a mixture of $H_2PO_4^-$ and HPO_4^{2-}.[7] Additionally, organophosphates are cholinesterase inhibitors. They phosphorylate the hydroxy group of the serine molecule and thus, the organism cannot break the acetylcholine into choline and acetic acid anymore and poison itself.[8] This effect is used in agriculture in phosphorus-based insecticides, *e.g.* diisopropylfluorophosphate (DFP), parathion (*O,O*-diethyl-*O*-(4-nitrophenyl)phosphorothioate, E605), dimethoate (*O,O*-dimethyl-*S*-[2-(methylamino)-2-oxoethyl]phosphorodithioate), fenthion (*O,O*-dimethyl-*O*-[3-methyl-4-(methylsulfanyl)phenyl]phosphorothiorate) or chlorpyrifos (*O,O*-diethyl-*O*-(3,5,6-trichloropyridin-2-yl)phosphorothioate, CPS).[8,9] Furthermore, phosphoric acid and phosphates are also industrially relevant in the production of fertilizers, feedstuff, detergents, dairy products, textiles, disinfectant cleanser, precipitation agents in water softening, photography, baking aids, leather, paint, concrete retarders, ceramics and much more.[10] Another important usage are flame retardants in plastics that form a protective layer of phosphoric acid when they are burned.[11]

In organic and organometallic chemistry phosphorus is predominantly used in an oxidation state of +III since they show a higher and more interesting reactivity due to the free electron lone pair at the phosphorus atom. Since the non-bonding p-orbital of a phosphane (PR_3) is filled with electrons while its σ^*-orbital is empty, a phosphane generally behaves as good σ-donor and good π-acceptor.[12] Therefore, P^{III} compounds can operate as ligands in organic catalysis (*e.g.* DIPAMP (bis[(2-methoxyphenyl)phenylphosphanyl]ethane) in the catalysis of asymmetric hydrogenation[13] or BINAP (bis(diphenylphosphanyl)-1,1'-binaphtyl) and Xantphos ((9,9-dimethyl-9*H*-xanthene-4,5-diyl)bis(diphenylphosphane)) in the catalysis of cross coupling reactions, cyanide additions, CH functionalizations, polymerization reactions, carboxylation reactions, decarboxylative reactions, reductive aminations, decarbonylative reactions and reductive deoxygenations[14]) or as starting compounds in the Wittig reaction.[15] Although phosphorus plays a minor role in medicinal chemistry several examples of metal phosphorus complexes were developed as antitumor agents during the last decades.[16]

To describe the bonding situation of phosphorus more precisely the $\sigma^n\lambda^m$-notation is used where the σ^n-descriptor reflects the number *n* of σ-bonds and the λ^m-descriptor the number *m* of all bonds.[17,18] The most important bonding motifs of phosphorus (**I–VII**) are shown in Figure 1.

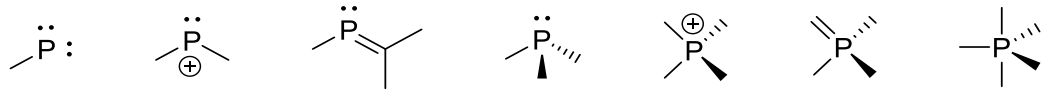

I **II** **III** **IV** **V** **VI** **VII**

Figure 1: Bonding motifs of phosphorus in different chemical environments.[17]

To clarify the ligating atom of a ligand molecule in a coordination complex the κ-convention is applied where the ligating atoms are indicated by the italicized element symbol preceded by the Greek letter κ.[19] An example is shown in Figure 2 displaying a dichloro(organyl)phosphane complex **VIII**.

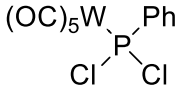

VIII

Figure 2: Pentacarbonyl{dichloro(phenyl)phosphane-κ*P*}tungsten(0) (**VIII**).

1.2 Low-valent phosphorus chemistry: going from carbenes to phosphinidenes

1.2.1 Phosphinidenes and related compounds

The most famous and very important class of low-valent compounds are singlet carbenes defined as divalent species with only six valence electrons not fulfilling the octet rule of main group elements and, hence, resulting in a high reactivity. Carbene complexes were known already since the beginning of the 20th century.[20] Complexes with late transition metals in low oxidation states bearing strong π-accepting coligands show an electrophilic character and are known as Fischer carbenes, named after complexes of the pioneering work of Fischer in 1964.[21] Nucleophilic complexes with early transition metals in high oxidation states without π-accepting coligands show a nucleophilic character, named as Schrock carbenes and usually are not heteroatom substituted.[22] However, it took more than 70 years until the first isolable carbene was reported by Bertrand in 1988[23] but some doubt about the bonding as to be a carbene was raised in the beginning. Thenceforth, the development of carbenes and their chemistry was rocketing, *e.g.* the synthesis of the first "bottleable" carbene as *N*-heterocyclic carbene (NHC) by Arduengo in 1991[24] or the more σ-donating and π-accepting cyclic alkyl(amino)carbenes (cAAC) by Bertrand in 2005.[25]

Related to singlet carbenes are the isoelectronic phosphenium ions (R_2P^+) **II** in phosphorus chemistry but since nitrenes (R-N) and phosphinidenes (to be named as phosphanediyl

according to IUPAC) (R-P) **I** are also isoelectronic and just differ by their local symmetry ($C_{\infty v}$ instead of C_{2v}), they generally can also be regarded as carbene analogs. This diagonal relationship was extensively described and expanded to the whole chemistry of carbon and phosphorus by Dillon, Mathey and Nixon in 1998.[26] Although singlet species such as carbenes,[27] silylenes[28] and nitrenes[29] are now well-established classes of compounds no isolable phosphinidene was known for a long time. The aforementioned symmetry difference has an enormous influence on the electronic ground state since the p_x- and p_y-orbitals are energetically degenerate resulting inevitably in a triplet (**I-t**) instead of a singlet ground state (**I-s**) (Figure 3).

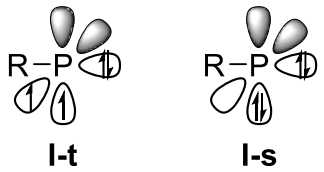

Figure 3: Triplet (**I-t)** and singlet (**I-s**) electronic configuration of phosphinidenes.

In the 1990s, first theoretical investigations on the electronic configuration of phosphinidenes have shown that changing the substituents from hydrogen, alkyl, aryl or halogen to π-donors like phosphanyl (PR_2) or amino (NR_2) groups can narrow the singlet-triplet gap and thus stabilize the singlet state.[30] Further theoretical studies confirmed this effect when very strong π-donor substituents or P-C bonds with higher orders are present.[31,32] Phosphinidenes have been known for decades only as short-lived, highly reactive species and were investigated spectroscopically and spectrometrically just in the gas phase or a cryogenic matrix,[33] or indirectly by trapping reactions.[34] Recently, the synthesis of the first and so far only stable singlet phosphinidene **X** was reported by Bertrand as sterically encumbered phosphanylphosphinidene via UV irradiation of the phosphaketene **IX** which had been accessed by a multistep synthetic protocol (Scheme 2).[35] An additional strong stabilization is described by the zwitterionic resonance structure **X'** that possesses a significant contribution to the real structure. Shortly afterward, examples of the electrophilic reactivity of this phosphinidene were reported.[36]

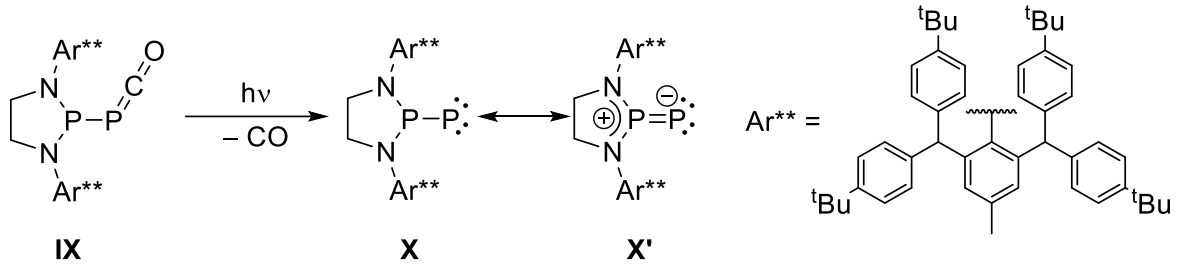

Scheme 2: Synthesis of the first stable singlet phosphanylphosphinidene **X**.[35]

Due to the overall extremely high reactivity associated with a transitory nature of phosphinidenes the concept of phosphinidenoid chemistry was introduced somehow in analogy to carbenoid chemistry. The latter possess a carbon center which is bound to an electropositive metal M and a good leaving group X, and both can be formally eliminated as MX to form the carbene.[37] However, these formal MX salt adducts of phosphinidenes have never been isolated or detected to date. Yoshifuji was the first who introduced the term "phosphinidenoid" in the literature which was proposed for the possible intermediate Mes*P(Cl)MgCl (**XII**) (Mes* = supermesityl = 2,4,6-$^{t}Bu_3C_6H_2$) occurring in the reduction of Mes*PCl_2 (**XI**) with magnesium, finally yielding the *E*-diphosphene Mes*P=PMes* (**XIII**) (Scheme 3).[38,39]

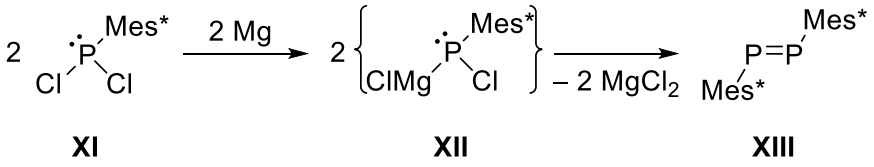

Scheme 3: Synthesis of the first *E*-diphosphene **XIII** via the proposed phosphinidenoid **XII** (Mes* = 2,4,6-$^{t}Bu_3C_6H_2$).

Similarly, respective Zn/Cl phosphinidenoids can be envisaged as intermediate in the synthesis of phosphanylidene phosphoranes.[40,41]

An aminophosphinidene transfer reagent was reported by Niecke and Streubel in 1990 using the 1,1'-chloro(silyl)diisopropylaminophosphane/HMPT system (HMPT = hexamethyl-phosphoric triamide) and later performed reactions with polar π-bond systems,[42,43,44] but no transfer reactions could be observed to alkenes or alkynes.[44]

Several donor-to-phosphinidene adducts have been reported in the last decades including carbene,[36,45,46] carbon monoxide,[35,46] isocyanide,[35,46,47] phosphane,[36,40,41,46,48,49] silylene[50] and nitrene adducts[43] that can undergo donor exchange reactions in various cases. Recently, an annelated 3a,6a-diaza-1,4-diphosphapentalene was described as intramolecularly stabilized singlet phosphinidene but no reactions with π-bond systems were reported.[51] In

2006, Mathey proposed a more reactive imidazole-stabilized arylphosphinidene as transient intermediate that decomposed to cyclopolyphosphanes when no trapping reagent was present and was trapped in presence of tetrachloromethane under formation of aryl(chloro)trichloromethylphosphane.[52] Unfortunately, reactions of the imidazole adduct with π-bonds were not reported.

1.2.2 Phosphinidene and phosphinidenoid transition metal complexes

Phosphinidenes (**I**) can be stabilized by transition metal complexation. The interaction of the filled p-orbital of the phosphinidene center (R-P) with an empty frontier orbital of the transition metal (M) is stabilizing the singlet state (Figure 4). The stabilization can be even more increased by π-backdonation of a filled d-orbital of the transition metal or π-donation of the substituent R into the remaining empty p-orbital of the P-center.[53]

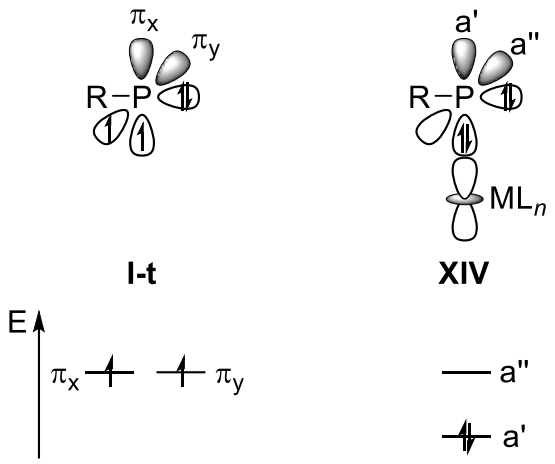

Figure 4: Stabilization of the singlet state by transition metal complexation forming complex **XIV**.

As for carbene complexes, the complexes can be divided into electrophilic (Fischer-type) and nucleophilic (Schrock-type) phosphinidene complexes. The coligands L of the transition metal fragment (ML_n) have the major influence on the nature of the electrophilicity and nucleophilicity of the phosphinidene complex.[54] While stable nucleophilic phosphinidene complexes are known since the 1980s (*e.g.* the first reported complex $Cp_2M{=}PMes^*$ (M = Mo, W; Cp = cyclopentadienyl) by Lappert in 1987[55] or the aminophosphinidene complex $Cp_2M{=}PN(H)Mes^*$ (M = Mo, W) by Niecke in 1989[56]), to date no neutral electrophilic, terminal phosphinidene complexes bearing only π-accepting coligands have been reported displaying the significantly larger stability of the nucleophilic phosphinidene complexes compared to the electrophilic ones. Neutral electrophilic phosphinidene complexes[48,57] were intensely studied

via thermal chelotropic elimination or extrusion-type chemistry using 7-phosphanorbornadiene,[58] phosphirane,[59] 2*H*-azaphosphirene[60,61,62] or phosphepine complexes.[63] But up to now, no spectroscopic data of neutral, terminal electrophilic phosphinidene complexes in condensed phase are known. Important studies on electrophilic phosphinidene complexes were reported by Mathey,[58,64,65] Lammertsma[66] and Streubel.[60,62] Especially the phenylphosphinidene tungsten(0) complex [$W(CO)_5$(PPh)] (**XVI**) that was obtained via the 7-phosphanorbornadiene complex **XV** was intensively explored. The transient phosphinidene complex **XVI** was proven by mass spectrometry and trapping reactions at 110 °C with alkenes, alkynes and butadiene to obtain phosphirane (**XVII**), 1*H*-phosphirene (**XVIII**) or 2,5-dihydro-1*H*-phosphole (**XIX**) complexes, respectively (Scheme 4).[58,64,65]

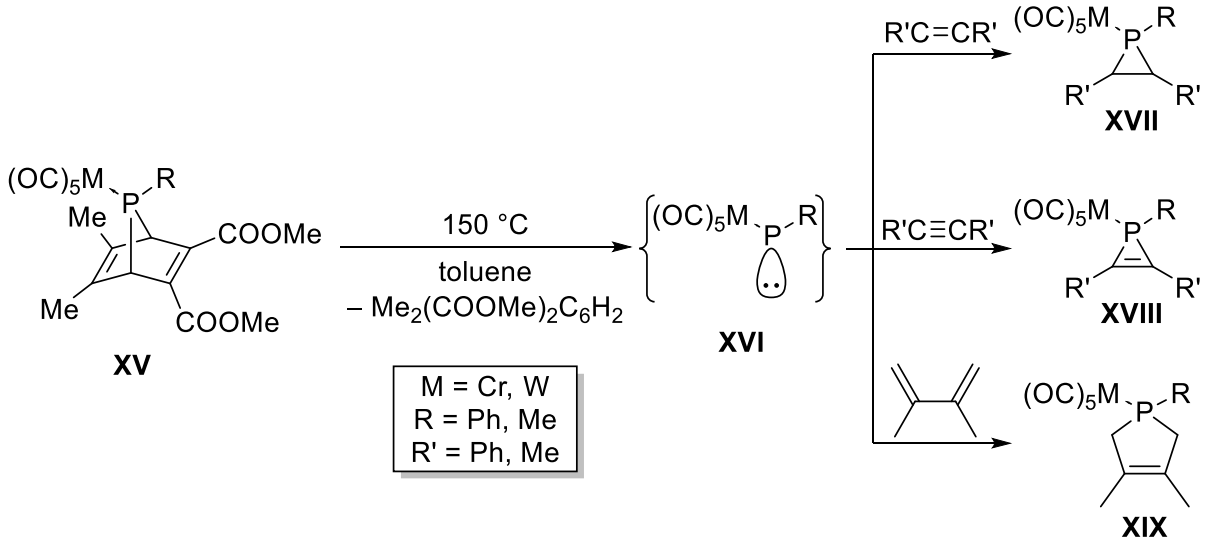

Scheme 4: Generation of the transient electrophilic phosphinidene complex **XVI** and trapping reactions.[58,64]

By addition of Ag^{I}, Pd^{II} and Cu^{I} salts the needed temperature could be reduced and thus, the reactions could be performed at 55 °C when catalytic amounts of CuCl were added.[64] Theoretical studies have shown that a chloride shift from copper to phosphorus within the formed heterodinuclear complex [$W(CO)_5\{\mu_2$-PhP}CuCl(solvent)] is occurring if a π-substrate is present (π-donor reagent or solvent) and thus, forming a Cu/Cl phosphinidenoid complex.[67] In 2006, Mathey also reported on the Cs/F phosphinidenoid complex by addition of CsF to the 7-phosphanorbornadiene complex **XV** in the presence of 18-crown-6 assuming that the Cs cation was fully separated and the fluorophosphanido complex was formed.[68] However, the chemistry of M/X phosphinidenoid complexes had started by Huttner in 1975, somehow, when lithium/chlorine exchange reactions starting from a dilithiophosphane complex were performed, but only a cyclotriphosphane complex and the phosphinidene

complex were observed by mass spectrometry.[69] Further attempts via metal/halogen exchange starting from a dichloro(organyl)phosphane complex by Huttner were also unsuccessful.[70] In 2005, Streubel reported on the first constitutional isomer of a phosphinidenoid complex using the bis(trimethylsilyl)methyl (bisyl) substituent at phosphorus namely [W(CO)$_5${P(bisyl)(CNLi{12-crown-4})}] with a remarkable stability.[71] It was not until 2007, that Streubel reported on the first kinetically stabilized *P*-bisyl substituted Li/Cl phosphinidenoid complex **XXII** with the lithium cation separated via ligation to 12-crown-4 and a donor solvent molecule.[72] The phosphinidenoid complex was either obtained by deprotonation of the bisyl(chloro)phosphane complex **XX** with lithium diisopropylamide (LDA) in the presence of 12-crown-4 at −80 °C, or by chlorine/lithium exchange of the bisyl(dichloro)phosphane complex (**XXI**) with *tert*-butyl lithium in the presence of 12-crown-4 at −80 °C (Scheme 5).[72] Due to the more time-consuming synthesis, and the occurrence of side reactions with the formed diisopropylamine,[72–74] the route using the lithium/chlorine exchange was used preferrentially.

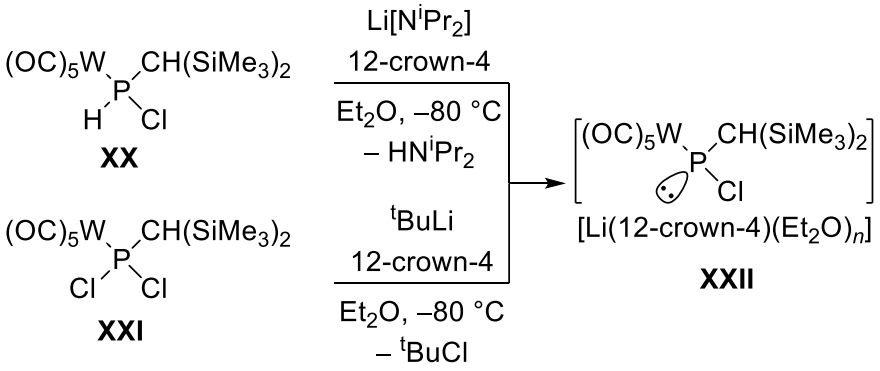

Scheme 5: Synthetic routes for the preparation of Li/Cl phosphinidenoid complex **XXII**.[72]

Above a temperature of −40 °C the phosphinidenoid complex started to decompose by formal dimerization via self-condensation/elimination processes to the mononuclear diphosphene complex **XXVI**.[72] When the halogen was changed from chlorine to fluorine the stability could be increased up to about 10 °C before furnishing complex **XXVI** (Scheme 6).[75] Thus, a trend of decreasing thermal stability when going for larger homologs of fluorine (F > Cl > Br > I) was established.[76]

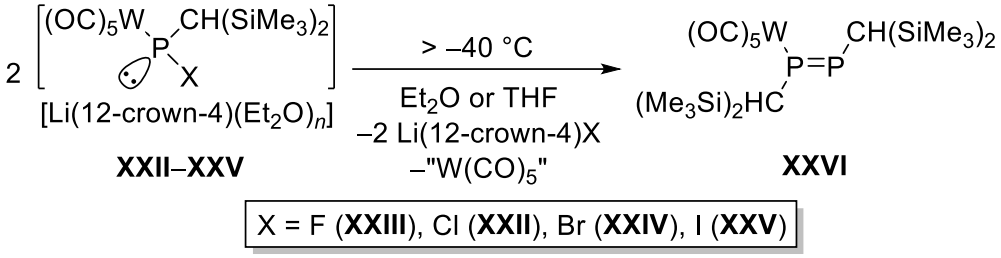

Scheme 6: Thermal decomposition of Li/X phosphinidenoid complexes **XXII–XXV**.

P-pentamethylcylopentadienyl (*P*-Cp*) substituted Li/Cl phosphinidenoid complexes **XXVII** are also only stable at low temperatures and decompose above −25 °C via intramolecular cycloaddition reactions with the Cp* group.[77] The introduction of the triphenylmethyl (CPh_3) *P*-substituent increased the stability of the Li/Cl phosphinidenoid complex **XXVIII** which was stable at ambient temperature for more than one day and isolable as solid.[78] Additionally the metal fragment of the various Li/Cl phosphinidenoid complexes could be changed to pentacarbonylchromium(0),[79,80] pentacarbonylmolybdenum(0)[79,80] and tetracarbonyliron(0).[81] Although no reactivity towards water was observed for the *P*-CPh_3 substituted group 6 metal complexes the respective iron(0) complex **XXIX** showed an increased reactivity towards water above −10 °C under formation of the formal OH-insertion product $[Fe(CO)_4\{P(CPh_3)(H)OH\}]$ (**XXX**) that could not be isolated and, thus, only the follow-up product **XXXI** was isolated after reaction of **XXX** with chlorotrimethylsilane in the presence of triethylamine (Scheme 7).[81]

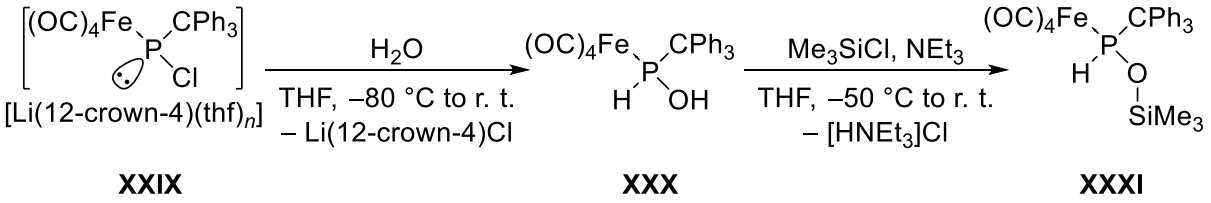

Scheme 7: Hydrolysis of the Li/Cl phosphinidenoid complex **XXIX**.[81]

The latest *P*-organyl substituted Li/Cl phosphinidenoid tungsten(0) and iron(0) complexes were reported recently by Streubel introducing the comparatively small(er) *tert*-butyl substituent showing a surprisingly high thermal stability up to 0 °C but decomposing unselectively above this temperature for M = W and to the dinuclear diphosphene complex $[Fe_2(CO)_8\{^tBuP{=}P^tBu\}]$ for M = Fe.[81,82]

Within the last 15 years, the manifold reactivity of Li/Cl phosphinidenoid complexes has been extensively studied by Streubel.[83] They can undergo nucleophilic and electrophilic reactions,[72,84–87] formal insertion reactions into OH- or NH-bonds,[78,81,88,89], ring expansion reactions,[90] 1,2-addition to polar π-systems[72,91–95] and oxidative single electron transfer

(SET) reactions.[96] Li/Cl aminophosphinidenoid complexes represent an exceptional case with their extremely low stability where only the *P*-NCy_2 substituted complex could be observed below −80 °C.[97]

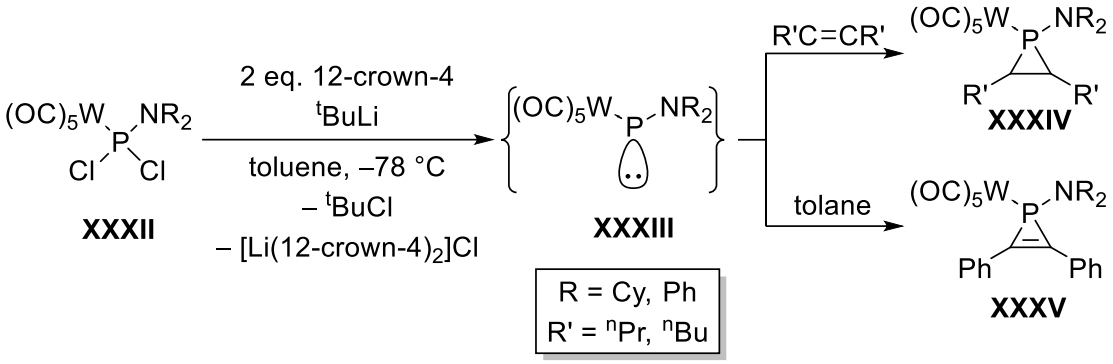

Scheme 8: Umpolung of a phosphinidenoid complex in apolar solvents and trapping reactions with alkenes and tolane under formation of complexes **XXXIV** and **XXXV**.[97]

When the chlorine/lithium exchange reaction of the amino(dichloro)phosphane complexes **XXXII** with *tert*-butyllithium in presence of two equivalents of 12-crown-4 was performed in toluene, a potential umpolung was observed increasing the electrophilic character and enabling even reactions with alkenes and alkynes at low temperatures forming the phosphirane **XXXIV** and 1*H*-phosphirene complexes **XXXV** and, hence, the phosphinidene complex **XXXIII** was proposed as intermediate (Scheme 8).[97]

In 2015, the synthesis and isolation of the first highly strained 3-imino-azaphosphiridine complexes **XXXVI** by reacting the Li/Cl phosphinidenoid complex **XXVII** with *N*,*N'*-diisopropyl- or *N*,*N'*-dicyclohexylcarbodiimide was reported (Scheme 9).[94]

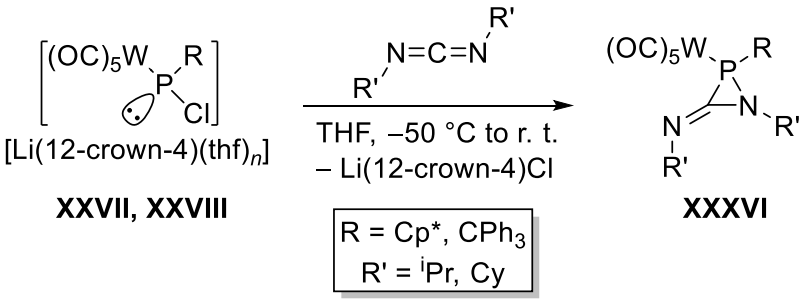

Scheme 9: Synthesis of the highly strained 3-imino-azaphosphiridine complexes **XXXVI**.[94,98]

Similar to the known oxaphosphirane,[78,82,92,95,99] 2*H*-azaphosphirene[62] and azaphosphiridine complexes[91,93,100,101] the 3-imino-azaphosphiridine complexes **XXXVI** reveal a high reactivity due to the high ring strain and the polar bonds in the ring. Hence, ring opening reactions with water,[94] insertion reactions of sulfur and selenium,[102] frustrated Lewis pair (FLP) type reactivity via ring expansion reactions with isocyanates, carbon dioxide[98] and carbon

monoxide,[103] and formal substitution reactions with isocyanides under formation of isocyanide-to-phosphinidene complex adduct **XXXVII** (Scheme 10) were discovered.[103]

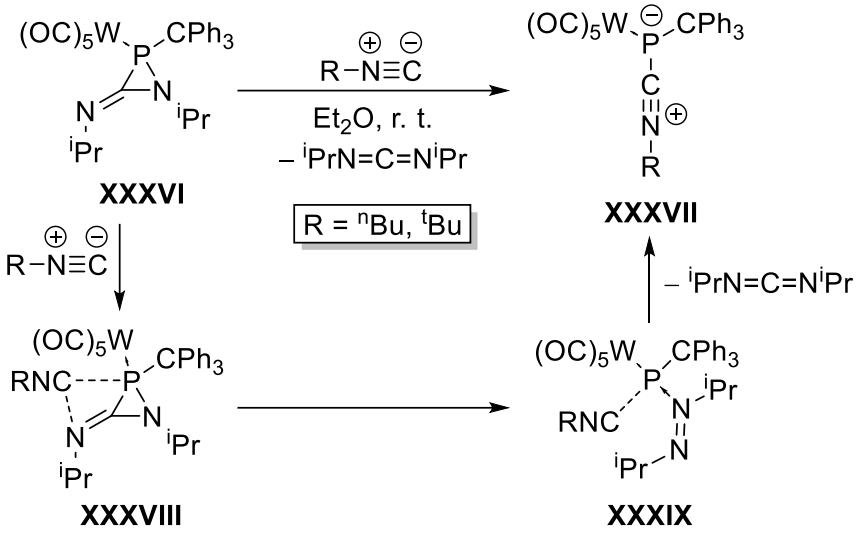

Scheme 10: Synthesis of the isocyanide-to-phosphinidene complex adduct **XXXVII** and a theoretically proposed reaction pathway.[98]

1.3 DONOR-TO-PHOSPHINIDENE COMPLEX ADDUCTS

1.3.1 C-donor adducts

Apart of the aforementioned isocyanide adduct **XXXVII** further isocyanide-to-phosphinidene complex adducts **XLI** were obtained when 2*H*-azaphosphirene complex **XL** reacted with cyclohexyl and *tert*-butyl isocyanide (Scheme 11).[104]

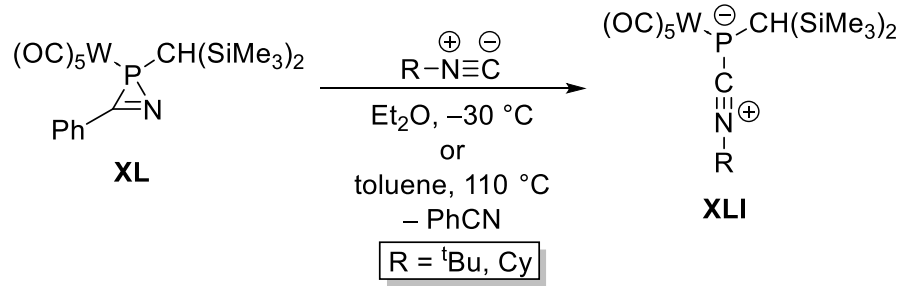

Scheme 11: Synthesis of isocyanide-to-phosphinidene complex adducts **XLI** via 2*H*-azaphosphirene complex **XL**.[104]

Adducts **XLI** revealed a low stability and, thus, already started decomposing during the reaction with *tert*-butyl isocyanide to yield a cyanophosphane complex under elimination of *iso*-butene and to a mononuclear diphosphene complex in case of cyclohexyl isocyanide. In contrast to the former, the cyclohexyl isocyanide adduct could be isolated via column chromatography whereas the *tert*-butyl isocyanide adduct was not isolated in pure form.[104]

In 2013, Scheer proposed the transient formation of the *tert*-butyl isocyanide stabilized dinuclear phosphinidene pentacarbonyltungsten(0) complex bearing pentamethyl-cyclopentadienyl (Cp*) as *P*-substituent but a bicyclic product by an intramolecular attack of the Cp* moiety was obtained as final product.[105]

C-donor carbenes have been used for the synthesis of phosphinidene complex adducts. In 2001, Weber reported on the first bis(amino)carbene-to-phosphinidene metal(0) complex adducts **XLII** by reacting Fischer arylcarbene complexes with an inversely polarized phosphaalkene.[106] NHC-to-phosphinidene copper(I), silver(I) and gold(I) complexes (**XLIII**) were prepared via direct syntheses or ligand exchange reactions by Tamm in 2015.[107] The first NHC-to-phosphinidene metal(0) complexes (**XLIV**) were investigated around the same time by reacting IMe_4 (1,3,4,5-tetramethylimidazol-2-ylidene) with phosphinidenoid-, chlorophosphane-, dichlorophosphane- and oxaphosphirane complexes using bisyl and triphenylmethyl as *P*-substituents.[85,108] For the triphenylmethyl case the adduct **XLIV** could be just obtained as minor product in the reaction mixture and, hence, was only investigated NMR-spectroscopically.[85] Further NHC-to-phosphinidene metal(0) complex adducts **XLV** were reported later using IDipp (1,3-bis(2,6-diisopropylphenyl)imidazol-2-ylidene) with R = H, Ph, Mes (2,4,6-trimethylphenyl) as *P*-substituents by Tamm.[109] Abnormal NHC-to-μ_2-aminophosphinidene complex adducts **XLVI** were reported by Carty in 2006.[110]

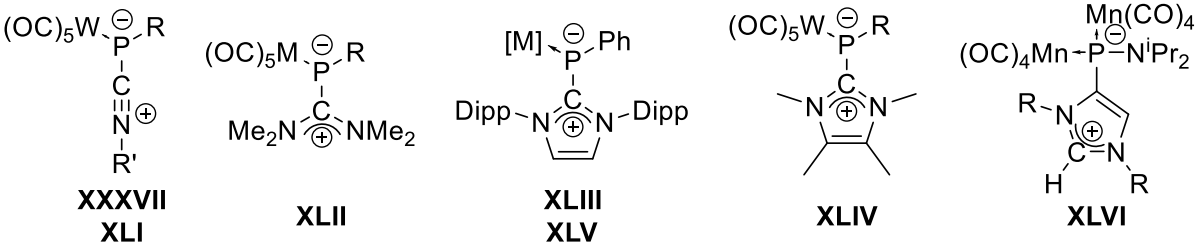

XXXVII: R = CPh_3, R' = ^{n}Bu, ^{t}Bu
XLI: R = $CH(SiMe_3)_2$; R' = ^{t}Bu, Cy
XLII: M = Cr, W; R = ^{t}Bu, $SiMe_3$
XLIII: [M] = CuCl, CuOTf AgCl, AuCl; R = Ph
XLIV: R = $CH(SiMe_3)_2$, CPh_3
XLV: [M] = $Mo(CO)_5$, $W(CO)_5$, $Rh(CO)_3$; R = H, Ph, Mes
XLVI: R = ^{t}Bu, Ad

Figure 5: C-donor-to-phosphinidene complex adducts **XXXVII** and **XLI–XLVI** (Dipp: 2,6-diisopropylphenyl, Cy: cyclohexyl, Mes: 2,4,6-trimethylphenyl, Ad: adamantyl).[85,103,104,106–110]

1.3.2 N-donor adducts

To date no stable N-donor-to-phosphinidene complexes are reported. Only a few examples are known describing such species as transient intermediates. In 1997, Streubel *et al.* proposed nitrile-to-phosphinidene complex adducts **XLVII** as transient species within the reaction of 2*H*-azaphosphirene complexes with dimethylacetylene dicarboxylate (DMAD) to form a [3+2] cycloaddition product.[111] A dimethyl cyanamide-to-phosphinidene complex adduct **XLVIII** was reported for a similar reaction of **XL** with DMAD under presence of dimethyl cyanamide.[112] In 2000, Streubel and Mathey proposed a 1-piperidinocarbonitrile-to-phosphinidene complex adduct **XLIX** as transient species upon reaction with the electrophilic phosphinidene complex **XVI** that was generated via thermal treatment of the 7-phosphanorbornadiene complex **XV**.[113] Thenceforth, similar transient species were reported but could not be isolated or spectroscopically observed[62,114] and remains subject of theoretical calculations.[32] A first attempt to synthesize an imidazole stabilized phosphinidene complex **L** were undertaken by Mathey in 2006 reacting complex **XV** with *N*-methylimidazole at elevated temperatures, but only cyclic polyphosphanes were obtained together with *N*-methylimidazole molybdenum complexes when no trapping reagent was provided; therefore, the adduct **L** was proposed only as intermediate.[52] Recently, promising theoretical results were obtained by Espinosa Ferao and Streubel illustrating the stability and accessibility of such P-adducts.[86]

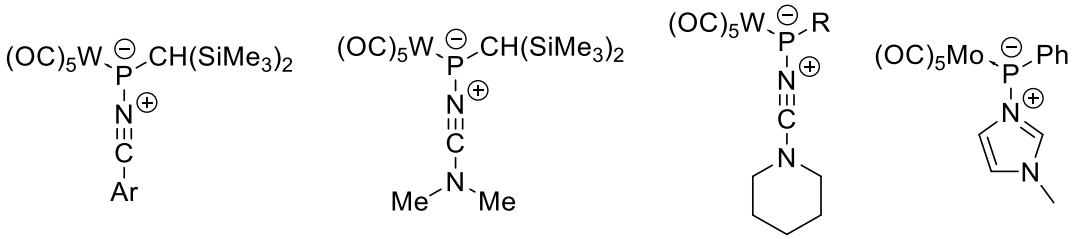

XLVII **XLVIII** **XLIX** **L**

XLVII: Ar = *p*-$MeOC_6H_4$, Ph, *p*-$F_3CC_6H_4$
XLIX: R = Me, Ph

Figure 6: N-donor-to-phosphinidene complex adducts **XLVII–L**.[52,111–113]

1.3.3 Phosphanylidene-phosphoranes and their complexes

In contrast to phosphonium-ylides and iminophosphoranes,[115] phosphanylidene-phosphoranes were less intensely studied due to their lower thermal stability and higher sensitivity. In 1961, Burg and Mahler prepared the first phosphanylidene-phosphorane **LII** by

reaction of tetrakis(trifluoromethyl)cyclotetraphosphane (**LI**) with trimethylphosphane at low temperatures (Scheme 12) and was only investigated ^{19}F NMR-spectroscopically in the first study.[116] Later the ^{31}P NMR chemical shifts of **LII** could be determined to 12.7 ppm and −81.0 ppm showing a large $^{1}J_{P,P}$ coupling constant of 436.5 Hz.[49,117]

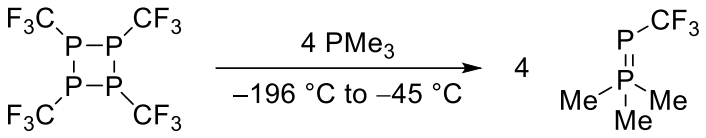

LI **LII**

Scheme 12: Synthesis of the first phosphanylidene-phosphorane **LII**.[116]

Further phosphanylidene-phosphoranes were prepared by Weber and Fluck[118], Fritz[119] and Regitz.[120] Later, Regitz and Bertrand described a 1,2-diphosphete derivative as cyclic phosphanylidene-phosphorane **LV** by irradiating a solution containing **LIII** and *tert*-butyl-phosphaalkyne under formation of the 2*H*-phosphirene **LIV** that rearranged to **LV** at ambient conditions (Scheme 13).[121,122] The 1λ^5,2λ^3-1,2-diphosphete **LV** can undergo oxidation reactions, addition reactions and complexation to transition metals.[122–124] A similar cyclic system was reported by Kilian in 2012.[125]

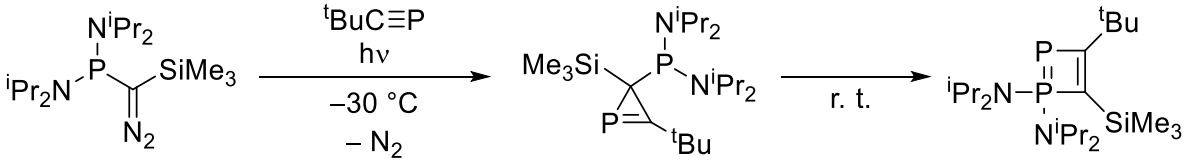

LIII **LIV** **LV**

Scheme 13: Synthesis of the 1λ^5,2λ^3-1,2-diphosphete **LV** via rearrangement of 2*H*-phosphirene **LIV**.[122]

Stable acyclic phosphanylidene-phosphoranes (**LVII**) were first synthesized by Protasiewicz analogous to a synthetic approach for phosphanylidene-phosphorane metal complexes of Mathey[126] by reducing Mes*PCl$_2$ (**LVI**) (Mes* = 2,4,6-tri-*tert*-butylphenyl) with zinc under presence of an excess of trimethylphosphane (Scheme 14).[41]

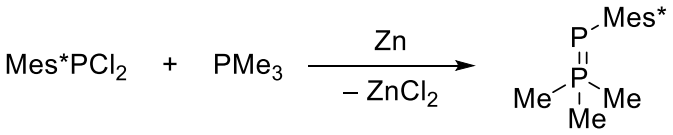

LVI **LVII**

Scheme 14: Synthesis of the stable acyclic phosphanylidene-phosphorane **LVII**.[41]

While the synthesis can be expanded using DmpPCl$_2$ (Dmp = 2,6-dimesitylphenyl) and triethylphosphane, the usage of sterically more demanding trialkylphosphanes reduced the

reaction progress extremely and using sterically less demanding substituents at the dichlorophosphane lead to the formation of thermally unstable products due to insufficient kinetic stabilization.[127] These phosphanylidene-phosphoranes behave as phospha-Wittig reagents[128,129] and react with aldehydes under formation of phosphaalkenes.[41] Remarkable is the generation of transient phosphinidenes upon irradiation of the mixed-valent phosphanylidene-phosphoranes forming diphosphenes or C-H insertion products and hence, proving indirectly the adduct-type structure **LVII''** of a phosphane to a phosphinidene (Figure 7).[130] Recently Ott reported on phospha-Wittig-Horner-type reactivity of a P-O functionalized phosphanylidene-phosphorane to synthesize phosphaalkenes.[131]

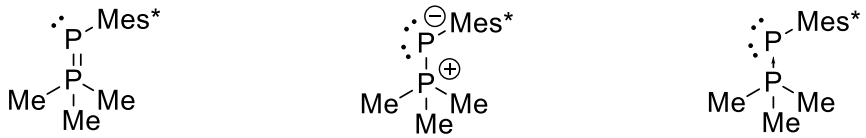

LVII **LVII'** **LVII''**

Figure 7: Valence isomeric structures of phosphanylidene-phosphorane **LVII**.

Theoretical calculations on the model system $H_3P{=}PH$ revealed that the highest occupied molecular orbital (HOMO) and the HOMO−1 is located mainly on the free electron pair of the phosphinidene fragment.[40] Reactions of the free electron pair with electrophiles confirmed the hypothesis.[132] In 1971, Burg prepared mononuclear and dinuclear phosphanylidene-phosphorane borane complexes observing a strong stabilization of **LII**.[117] Chromium(0)-, tungsten(0)- and iron(0) complexes were first prepared as thermally unstable species, *e.g.* via reduction of the dichlorophosphane complex **LVIII** with zinc under presence of tri-*n*-butylphosphane under formation of **LVIX** by Mathey several years later (Scheme 15) and were only proved indirectly via trapping reactions.[126,133,134] **LVIX** is further stabilized by the simultaneously formed zinc dichloride yielding complex **LX** being in an equilibrium.[126] The reactions also proceeded without addition of Zn but giving no stable product due to the missing stabilizing effect of the zinc dichloride.[126]

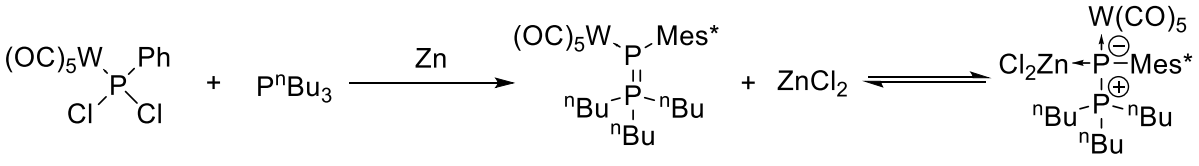

LVIII **LIX** **LX**

Scheme 15: Synthesis of phosphanylidene-phosphorane tungsten(0) complex **LIX** via reduction of **LVIII**.[126]

Complexes of the aforementioned cyclic phosphanylidene-phosphoranes of Kilian, Regitz and Bertrand were also prepared with a large variety of transition metals.[121,124,125,135] Gold and silver complexes of Protasiewicz's phosphanylidene-phosphoranes were reported in 2008.[136] A different route to phosphanylidene-phosphorane complexes was described by Scheer reacting a dinuclear *P*-Cp* substituted phosphinidene complex **LXI** with triethylphosphane under formation of complexes **LXII** and **LXIII** (Scheme 16).[137] Reactions with primary and secondary phosphanes proceeded similarly.[137,138]

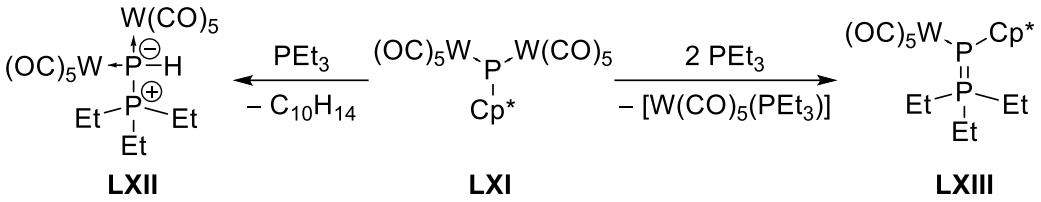

Scheme 16: Synthesis of mononuclear and dinuclear phosphanylidene-phosphorane complexes **LXII** and **LXIII**.[137]

Cationic phosphanylidene-phosphorane complexes were prepared and investigated by Carty but yielding thermally very stable compounds that did not show any further reactivity.[139]

1.4 CATIONIC LOW-COORDINATE PHOSPHORUS SPECIES

The first cationic dicoordinate phosphorus compounds **LXVI**, namely phosphamethine-cyanines, were described by Dimroth and Hoffmann in 1964 that were obtained via reaction of the 2-chlorobenzothiazolium salts **LXIV** with tris(hydroxymethyl)phosphane (**LXV**) in the presence of triethylamine (Scheme 17).[140,141]

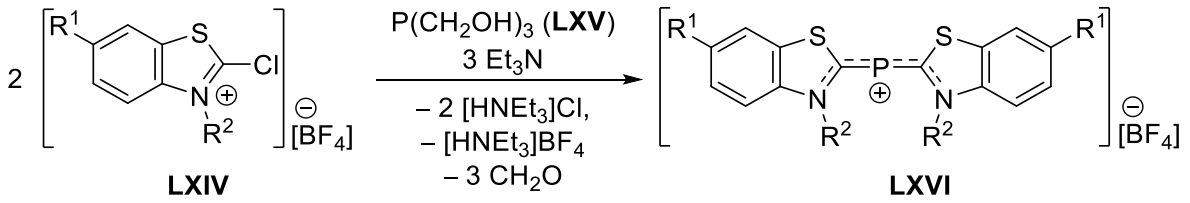

Scheme 17: Synthesis of the first stable phosphenium salt **LXVI**.[140,141]

The structures of **LXVI** were resolved by ^{31}P NMR spectroscopy, UV studies and X-ray crystallography.[142] The phosphenium center of **LXVI** is strongly stabilized by π donation of the electron-rich neighbour atoms and thus, delocalizing the charge by conjugation. Since this breakthrough, a broad range of π-donor stabilized phosphenium compounds were described, *e.g.* the amino(aryl)phosphenium salts **LXVII** or diaminophosphenium salts like the bis(diisopropylamino)phosphenium salt **LXVIII**,[143] 1,3,2-diazaphospholidinium salt **LXIX**[144] or

the 1,3,2-diazaphosphinanium salt **LXX** (Figure 8).[145] X-ray studies of **LXX** revealed that the positive charge is mainly localized on phosphorus.[146] However, the positive charge in the cyclic aminophosphenium salt **LXXI** is delocalized via conjugation.[147,148] A zwitterionic metallaphosphenium salt **LXXII** was reported by Niecke and Kröher in 1976,[149] and X-ray diffraction studies revealed a P-Al distance which was beyond the sum of van der Waals radii.[150]

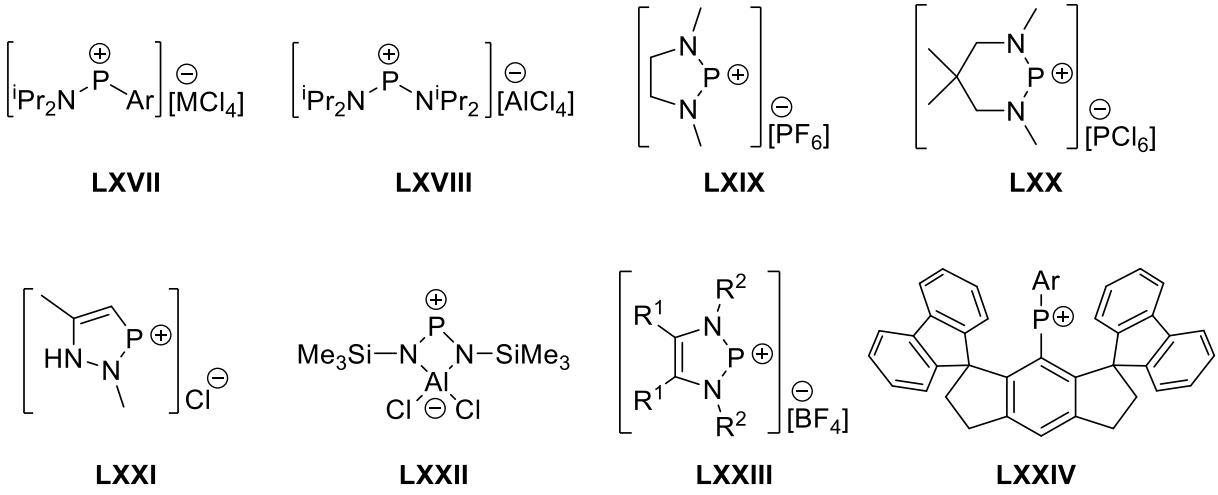

LXVII **LXVIII** **LXIX** **LXX**

LXXI **LXXII** **LXXIII** **LXXIV**

Figure 8: Examples of stable phosphenium salts **LXVII–LXXII**.[143–149]

1,3,2-Diazaphospholenium salts **LXXIII**, the analogs of *N*-heterocyclic carbenes, were prepared for the first time by Pudovik[151] and Denk,[152] and further deeply investigated by Gudat.[153] Recently, the synthesis of a kinetically stabilized donor-free phosphenium salt **LXXIV** was reported by Olaru, Mebs and Beckmann.[154]

Phosphenium salts are mostly prepared via halogen abstraction of halophosphanes.[155] Another interesting access was described by Grützmacher in 1999 by alkylation of Yoshifuji's bis(2,4,6-tri-*tert*-butylphenyl)diphosphene **LXXV**[39] using methyl trifluoromethanesulfonic acid under formation of the diphosphenium salt **LXXVI** (Scheme 18).[156]

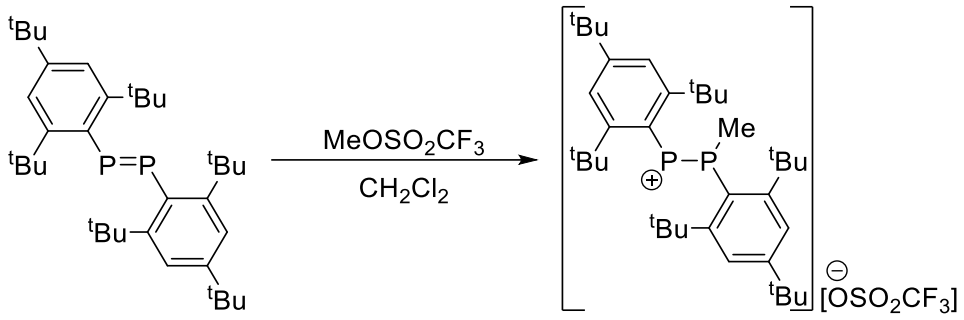

LXXV **LXXVI**

Scheme 18: Synthesis of the phosphanylphosphenium salt **LXXVI**.[156]

The case of nonmetal adducts started with a report of Burford on cationic, mono-coordinate phosphorus species such as the phosphadiazonium P-center **LXXVII** which was then expanded by the same author with studies on phosphenium adduct formation, *e.g.* the phosphenium adducts **LXXVIII–LXXX** (Figure 9), including donor substitution reactions.[157–168]

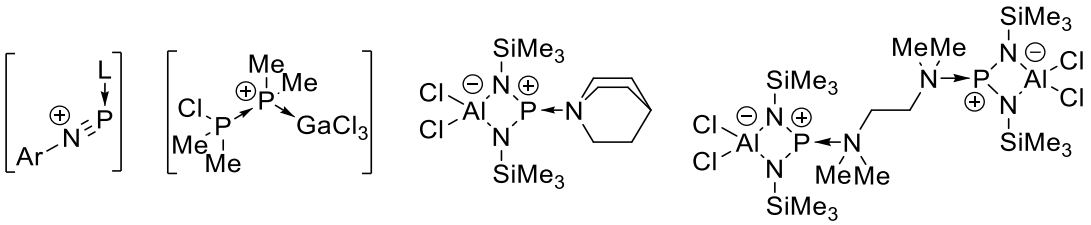

LXXVII **LXXVIII** **LXXIX** **LXXX**

Figure 9: Phosphadiazonium and phosphenium adducts **LXXVII–LXXX**.[157–168]

In 2001, Burford showed the substitution of a chlorodiphenylphosphane in the phosphenium adduct salt **LXXXI** by the stronger donating triphenylphosphane under formation of the salt **LXXXII** (Scheme 19).[164]

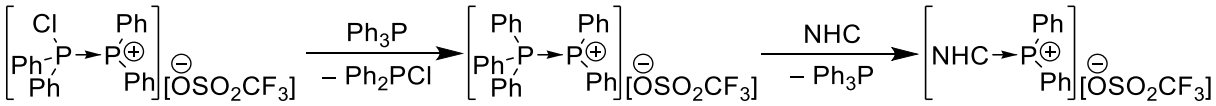

LXXXI **LXXXII** **LXXXIII**

Scheme 19: Ligand substitution reactions at a phosphenium center (NHC: 1,3-diisopropyl-4,5-dimethylimidazol-2-ylidene).[164]

A further substitution of the triphenylphosphane in **LXXXII** by an *N*-heterocyclic carbene also could be performed which was inspected by ^{31}P NMR spectroscopy.[164] Similar to carbene metal complexes, phosphenium metal complexes also can show an electrophilic or a nucleophilic character dependent on the nature of the metal, its coligands and the phosphenium fragment itself.[169] Hence, the P-center either behaves as a phosphenium or as a phosphanide. Several pathways to phosphenium metal complexes were described including

ligand substitution, salt metathesis, alkoxy abstraction, halogen abstraction and elimination reactions (Scheme 20).[169,170]

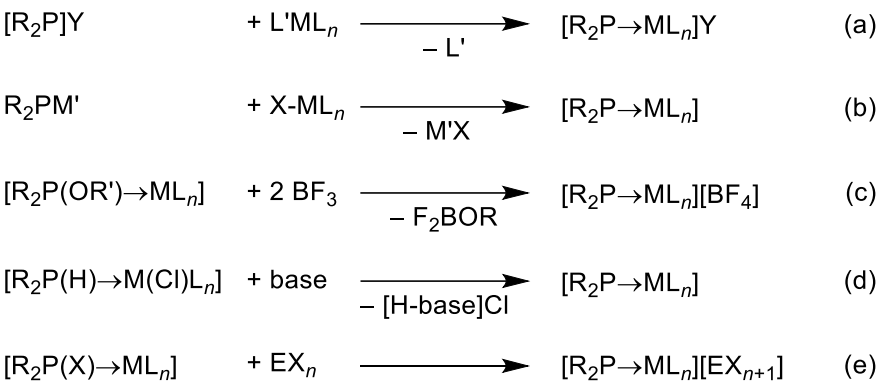

Scheme 20: Synthetic pathways to phosphenium metal complexes.[169,170]

Reactions of phosphenium complexes with neutral nucleophiles were only investigated sparsely, predominantly by Nakazawa and Gudat, in many cases observing reactions at the metal center instead of the P center and, thus, to date the class of donor-to-phosphenium complex adducts are only rarely reported and studied.[170–178] Very recently, the first *N*-donor-to-phosphenium complex adducts **LXXXV** were described by Ragogna and Gilroy where the *N*-donor center was directly linked as *P*-substituent.[178]

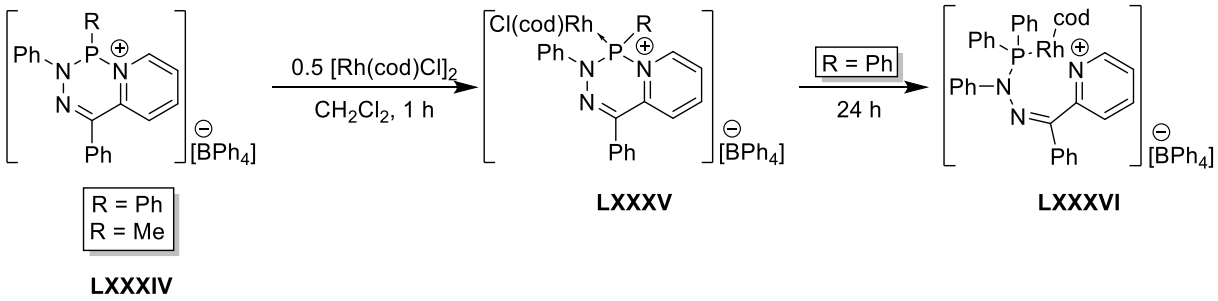

Scheme 21: Formation of the first *N*-donor-to-phosphenium complex adducts **LXXXV**.[178]

1.5 N-Donor-to-low valent metalloid element adducts

Neutral, low-coordinate metalloid-bound nitrile adducts were only rarely reported for silylenes, with Tokitoh being first.[179] The *end*-on (η^1) bound nitrile-to-silylene adduct **LXXXVIII** formed only transiently via the reaction of the disilene **LXXXVI** at elevated temperatures with *tert*-butylnitrile and rearranged to the formal *side*-on (η^2) bound nitrile-to-silylene adduct, the 2*H*-azasilirene **LXXXIX** (Scheme 22).

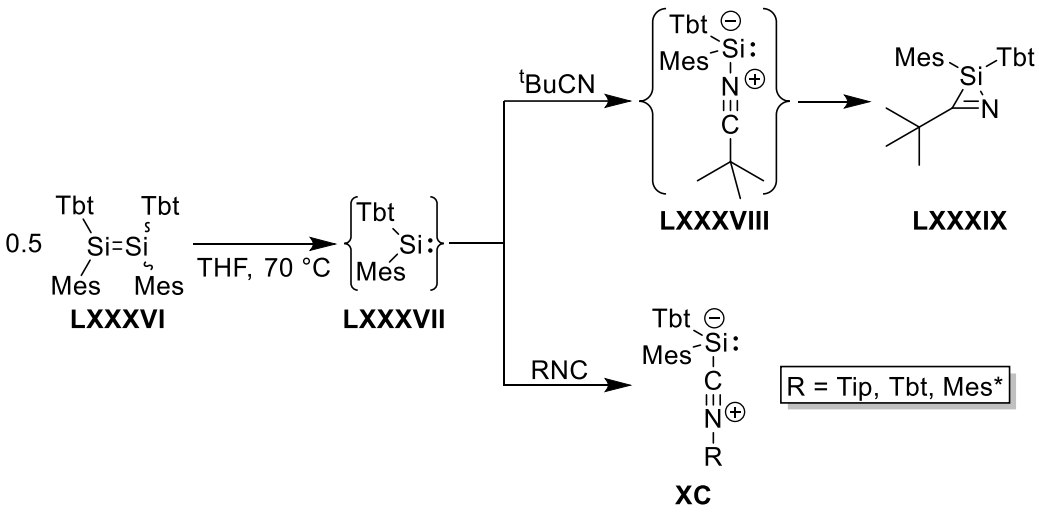

Scheme 22: Synthesis of the 2*H*-azasilirene **LXXXIX** via the nitrile-to-silylene adduct **LXXXVIII**, and of the isocyanide-to-silylene adduct **XC** (Tbt = 2,4,6-tris{bis(trimethylsilyl)methyl}phenyl; Tip = 2,4,6-triisopropylphenyl; Mes = 2,4,6-trimethylphenyl; Mes* = 2,4,6-tri-*tert*-butylphenyl).[179,180]

In contrast, the *end*-on (organic) isocyanide-to-silylene adduct **XC** could be isolated as stable compound using sterically demanding N-bound substituents,[180,181] following on an early hypothesis by Weidenbruch who had proposed such transient adducts as intermediates years before.[182] The *tert*-butyl isocyanide adduct **XCI** formed only transiently and decomposed rapidly to the cyanosilane **XCII** and *iso*-butene (**XCIII**) (Scheme 23).[183]

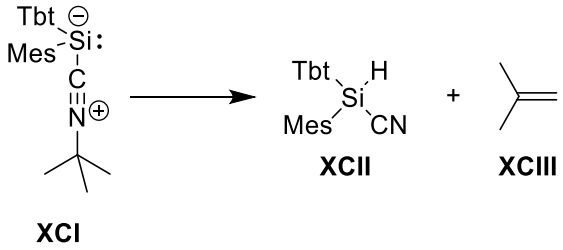

Scheme 23: Decomposition of the *tert*-butylisocyanide adduct **XCI** (Tbt = 2,4,6-tris{bis(trimethylsilyl)methyl}-phenyl; Mes = 2,4,6-trimethylphenyl).[183]

Furthermore, the isocyanide ligand could be substituted by another isocyanide derivative, thus indicating an equilibrium between R_2Si-CNR, the free silylene and the isocyanides.[183]

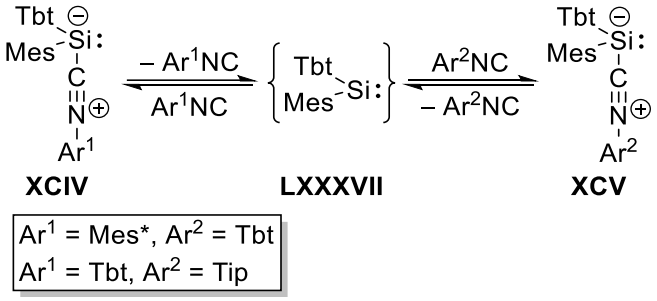

Scheme 24: Isocyanide substitution reactions of isocyanide-to-silylene adducts (Tbt = 2,4,6-tris{bis(trimethylsilyl)-methyl}phenyl; Tip = 2,4,6-triisopropylphenyl; Mes = 2,4,6-trimethylphenyl; Mes* = 2,4,6-tri-*tert*-butyl-phenyl).[183]

Iwamoto and Kira also synthesized the dialkylsilaketenimines **XCVII** via the Kira-type silylene **XCVI** without aromatic substituents at the silicon showing a slightly bent allenic structure in the solid state with a weak Si-C bond, *i.e.*, dissociation occurred above −30 °C (Scheme 25).[184]

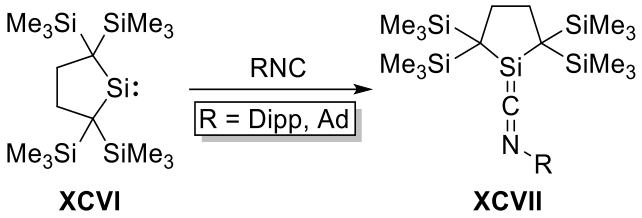

XCVI **XCVII**

Scheme 25: Reaction of the Kira-type silylene **XCVI** with isocyanides under formation of the dialkylsilaketenimines **XCVII** (Dipp: 2,6-diisopropylphenyl, Ad: adamantly).[184]

Recently, this field was expanded by Filippou demonstrating that an (organic) isocyanide can be also replaced in an oxidative fashion by reaction of the two-coordinate Si isocyanide compound **XCVIII** with Ge(Ar^{Mes})Cl (**XCIX**) under formation of the zwitterionic NHC-stabilized germasilyne **C** (Scheme 26).[185]

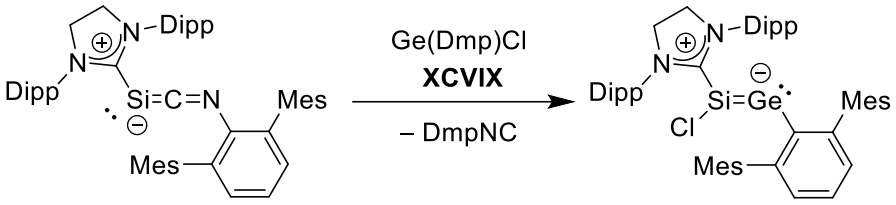

XCVIII **C**

Scheme 26: Synthesis of the NHC-stabilized germasilyne **C** via the Si(0) isocyanide compound **XCVIII** (Dipp = 2,6-diisopropylphenyl, Mes = 2,4,6-trimethylphenyl, Dmp = 2,6-dimesitylphenyl).[185]

In 2015, Scheschkewitz reported on the reactivity of an NHC-stabilized cyclic germylidene, the NHC-to-disilagermirane-3-ylidene adduct **CII** with xylyl isocyanide resulting in a ring expansion at the Si-Si bond forming the NHC-to-4-imino-1,3,2-disilagermetane-2-ylidene adduct **CIII**.[186]

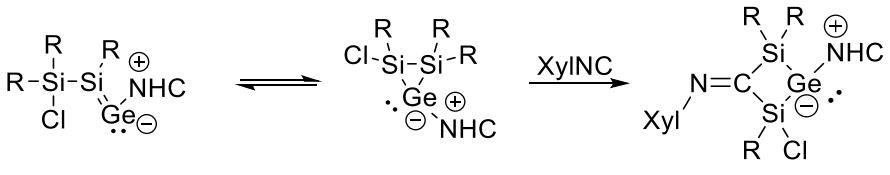

CI **CII** **CIII**

Scheme 27: Reactivity of the NHC-stabilized germylidene **CII** with xylyl isocyanide (Xyl = xylyl).[186]

To the best of my knowledge, isosteric carbon monoxide silylene adducts R_2Si-CO (**CIV**) were only investigated by computational studies and/or detected in cryogenic matrices.[187] In 2002, Tokitoh reported on the formation of azasilepines when reacting silylene **LXXXVII** with

pyridine (Scheme 28) or 4-dimethylaminopyridine (DMAP) (Scheme 29) supposing adduct structures as intermediates.[188]

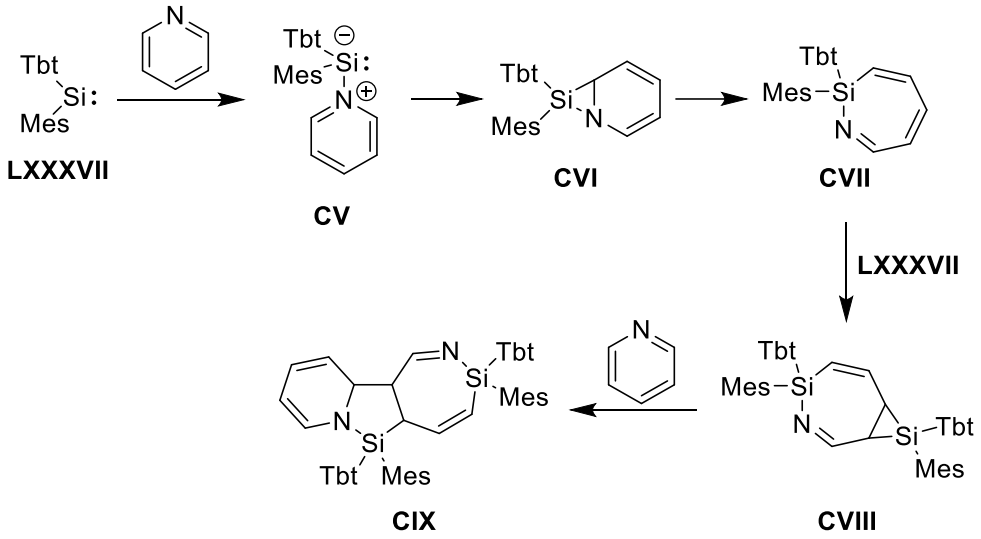

Scheme 28: Reaction of silylene **LXXXVII** with pyridine under formation of the transient pyridine-to-silylene adduct **CV** and its decomposition to compound **CIX** (Tbt = 2,4,6-tris{bis(trimethylsilyl)methyl}phenyl; Mes = 2,4,6-trimethylphenyl).[188]

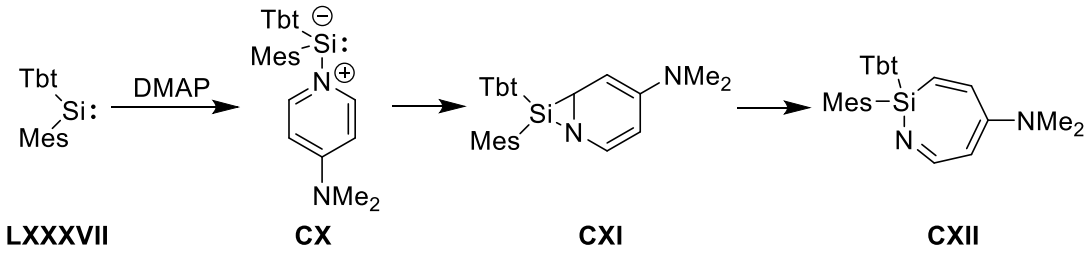

Scheme 29: Reaction of silylene **LXXXVII** with DMAP under formation of the transient DMAP-to-silylene adduct **CX** under formation of the 1,2-azasilepine **CXII** (Tbt = 2,4,6-tris{bis(trimethylsilyl)methyl}phenyl; Mes = 2,4,6-trimethylphenyl).[188]

Recently Inoue reported on the synthesis and isolation of stable DMAP-to-silylene adducts. Under elevated temperatures these adducts undergo 1,1 additions of dihydrogen and 1,2 additions of ethylene. In the absence of trapping reagents the DMAP adducts decompose to the disiletane, azasilepine or cyclotrisilane depending on the substituents at the silicon center (Scheme 30).[189]

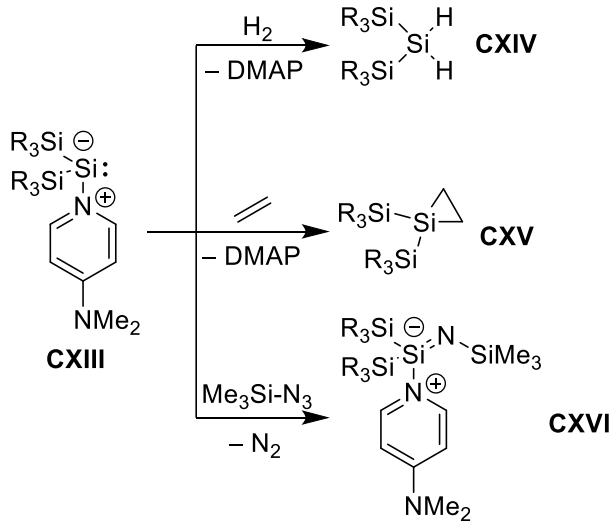

Scheme 30: Reactivity of the DMAP-to-silylene adduct **CXIII** towards dihydrogen, ethylene and trimethylsilyl azide.[189]

1.6 COORDINATION CHEMISTRY OF TRANSITION METALS

In the 19th century Werner reported his coordination theory,[190] one of the most important conceptional contributions to modern chemistry. Initially, a large range of complexes possessing neutral and anionic ligands L such as water, ammonia and halides were explored, and organic N- and P-ligands were added later on.[191] On the other hand, the important emergence of organometallic chemistry required ligands L such as carbon monoxide, isocyanide, carbenes and more sophisticated entities such as arenes, all of which have enriched numerous chemical opportunities including homogeneous catalysis or other applications.[191] Transition metal complexes with open coordination sites are prone to ligand additions which is an important feature of catalysis.[192] Transition metal complexes,[193–195] in general, display a great variety of different reactions which is illustrated hereafter for isocyanide complexes. Isocyanides are important ligands in organometallic chemistry which are isostructural with carbon monoxide. Nevertheless, isocyanides are poorer π-acids but stronger σ-donors than carbon monoxide.[196] Thus, isocyanide ligands have a strong affinity for transition metals forming neutral and cationic homoleptic metal isocyanide complexes as $M(CNR)_6$ or $M(CNR)_7^{2+}$ (M = Cr, Mo, W).[194,197,198] Metal isocyanide complexes are usually prepared by direct ligand exchange.[194] Isocyanides can coordinate in terminal and bridging fashions to the metal resulting in various structure motifs (Figure 10).[196]

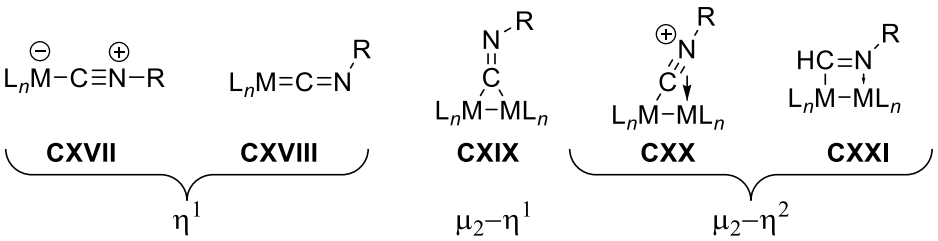

Figure 10: η^1, μ_2-η^1 and μ_2-η^2 isocyanide complexes **CXVII–CXXI**.[196]

Besides linear η^1 isocyanide ligands, also bent forms are known as $M(CNR)_2(L_2)_2$ (M = Mo, W; L_2 = dppe).[199] Bridging isocyanide ligands exist in monohapto[200] and dihapto fashions.[201]

The complexes show a broad reactivity, *e.g.* substitution,[202] redox[198,203], oxidative addition[204], insertion[205] and nucleophilic addition reactions.[206]

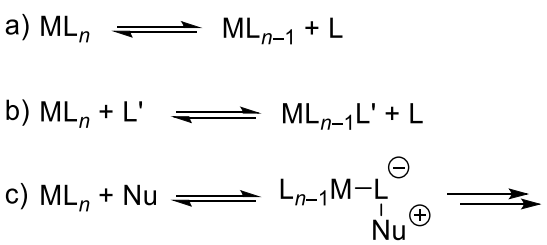

Scheme 31: Reactivity of transition metal complexes: a) dissociation, b) ligand substitution reactions and c) reactions at the metal-bound ligand to transition metal complexes.

Due to small energy gaps between the $1a_{2u}$ and $2a_{1g}$ molecular orbitals, isocyanide complexes additionally have a versatile photochemistry.[194] For example, amines and alcohols add to metal-bound isocyanides to form carbene complexes, thus representing an important example of ligand transformation unknown for metalloid and nonmetal complexes, so far.[207–209] First, the amine or the alcohol attacks the isocyanide carbon. Afterwards, a proton transfer occurs from the corresponding heterocarbene complex (Scheme 32). This either proceed intramolecularly via a four-center transition state or intermolecularly via a six-center transition state with a second amine or alcohol.[207,208] An intramolecular nucleophilic attack was reported by Hahn in 1993 of the 2-hydroxyphenyl isocyanide complex observing an equilibrium between the isocyanide and the carbene complex.[209] The resulting hetero-carbene ligands generally are better σ-donors but worse π-acceptors than the isocyanide ligands.[210]

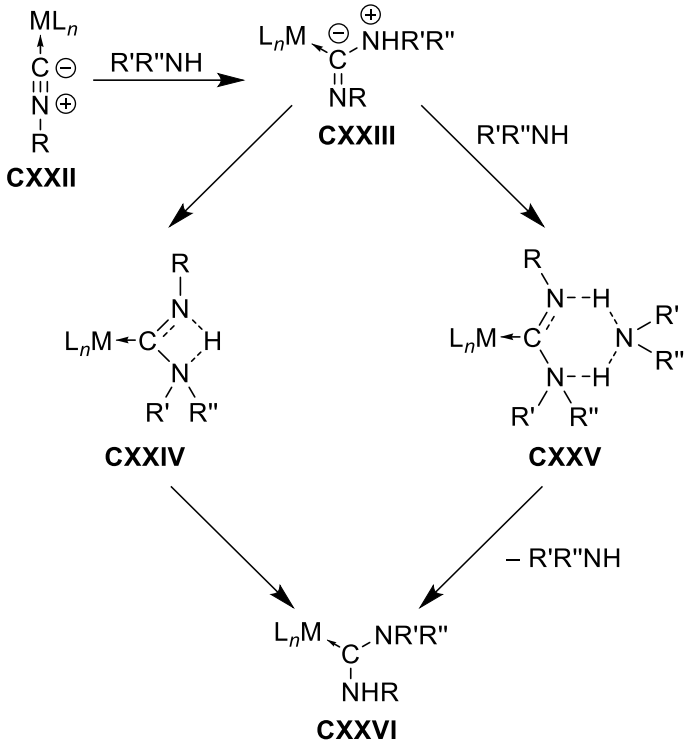

Scheme 32: Pathways of the proton transfer after a nucleophilic attack of an amine at the isocyanide ligand of a metal complex **CXXII**.

2 OBJECTIVE OF THIS WORK

The main focus of this work was on the development of facile syntheses of kinetically labile, donor-stabilized electrophilic, terminal phosphinidene complexes. This has to be seen against the background that most established methods require rather harsh thermal conditions to generate such reactive intermediates and/or very elaborate time-consuming methods. Therefore, the PhD project had several research lines:

1) Donor substitution reactions starting from very strained P-heterocycle complexes, *e.g.* 3-imino-azaphosphiridine complexes, or from labile, acyclic donor-to-phosphinidene complex adducts, and the latter required a new access.
2) Synthesis of various families of donor-to-phosphinidene complex adducts possessing various neutral monodentate donors with group 14 to 16 elements.
3) Study of the thermal dissociation of donors.
4) Testing the transformation of the donor molecule (= the ligand) at the phosphorus center via reactions with nucleophiles.
5) Protonation of donor-stabilized electrophilic, terminal phosphinidene complexes combining with attempts to abstract the donor from such complexes in order to access protonated electrophilic, terminal phosphinidene complexes. The latter would represent a new class of super-electrophiles.

3 RESULTS AND DISCUSSION

3.1 PREPARATION AND PROPERTIES OF DONOR-TO-PHOSPHINIDENE COMPLEX ADDUCTS

3.1.1 Isocyanide-to-phosphinidene complex adducts

3.1.1.1 Substitution reactions of 3-imino-azaphosphiridine complexes

The first concept to follow was based on the lead of Villalba Franco provided in 2015. According to his work, the synthesis of the highly strained 3-imino-azaphosphiridine complexes **4a,b** was performed analogously to the preparation of the known tungsten complex **4c**.[94,98] The Li/Cl phosphinidenoid complexes **2** were generated *in situ* by chlorine/lithium exchange reaction starting from the dichlorophosphane complexes **1**[78,80] and then reacted with diisopropylcarbodiimide (**3**) (Scheme 33). After extraction with *n*-pentane to separate the formed lithium salt and side products, the products were obtained in moderate to good yields (**4a**: 50.3 %, **4b**: 83.6 %).

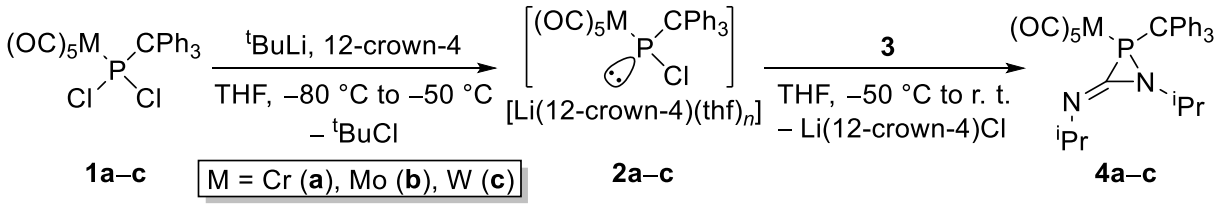

Scheme 33: Synthesis of azaphosphiridine complexes **4a–c** via the Li/Cl phosphinidenoid complexes **2a–c**.

The typical highfield shift of the ^{31}P NMR resonances by changing the metal to heavier homologs, known as heavy metal effect,[211] was also observed in case of **4a–c**. However, the resonance signals of the ^{31}P NMR spectra are downfield-shifted to the ones of known azaphosphiridine complex derivatives bearing no exocyclic π-bonds.[91,93,100,101] For the accurate assignment of all ^{1}H and ^{13}C{^{1}H} NMR data the measurement of ge-2D ^{1}H,^{15}N HMBC NMR spectra combined with phase-sensitive ge-2D ^{1}H,^{13}C HMBC and multiplicity-edited ^{1}H,^{13}C HSQC NMR experiments was necessary. The obtained ^{15}N{^{1}H} NMR data (Table 2) were compared to those of known free iminoaziridines[212] and, hence, assigning the isopropyl groups via the aforementioned 2D NMR experiments was straightforward.

Table 2: ^{31}P and $^{15}N\{^1H\}$ NMR data of 3-imino-azaphosphirdine complexes **3a,b** and **3c**.[98]

Compound	$\delta(^{31}P)$ / ppm	$^1J_{W,P}$ / Hz	$\delta(^{15}N)$ / ppm	solvent
4a	53.1	—	−169.5 (C=*N*-^{i}Pr), −285.2 (P-*N*-^{i}Pr)	$CDCl_3$
4b	23.6	—	−168.3 (C=*N*-^{i}Pr), −287.4 (P-*N*-^{i}Pr)	$CDCl_3$
4c[98]	2.1	257.4	—	$CDCl_3$

As already reported for the azaphosphiridine complex **4c**,[103] the complexes **4a,b** also can undergo substitution reactions. When *tert*-butyl isocyanide (**5**) is added to a solution of complexes **4** in diethyl ether at ambient temperature the conversion to the isocyanide-to-phosphinidene complex adducts **6** were observed (Scheme 34). The molybdenum complex **6b** showed a remarkable low stability and thus only a reaction mixture with a content of 13 % (by ^{31}P NMR integration) of the desired product and an unidentifiable mixture of unselective decomposition products was obtained.

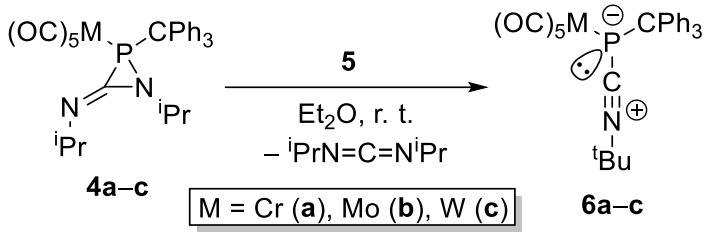

Scheme 34: Synthesis of the *tert*-butyl isocyanide-to-phosphinidene complex adducts **6c**[103] and **6a,b** via substitution reactions of azaphosphiridine complexes **4a–c**.

Due to the restricted thermal stability of complexes **4** in solution it was not possible to obtain a clean conversion to complexes **6** but also observing the decomposition into the 4-imino-1,3,2-diazaphosphetidine complexes **7** and isopropyl isocyanide-to-phosphinidene complex adducts **8** (Scheme 35, Table 3) as already described in previous studies.[102,213] As for **6b** the molybdenum complex **8b** showed a similar low stability under formation of an unselective decomposition product mixture revealing resonance signals at 122.1 ppm, 118.9 ppm, 109.3 ppm and 69.2 ppm (Figure 11).

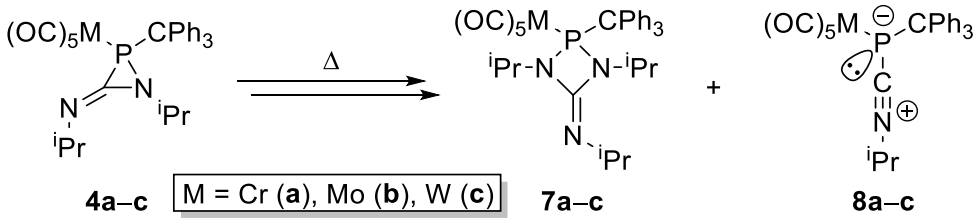

Scheme 35: Thermal decomposition of the azaphosphiridine complexes **4a–c** in solution.

Table 3: ^{31}P NMR data of the thermal decomposition products of **4a–c**.

Compound	δ(^{31}P) / ppm	$^{1}J_{W,P}$ / Hz	Solvent
7a	196.2	—	toluene
7b	173.2	—	toluene
7c[102]	150.8	288.3	Et_2O
8a	−12.5	—	toluene
8c[102]	−50.7	119.6	Et_2O

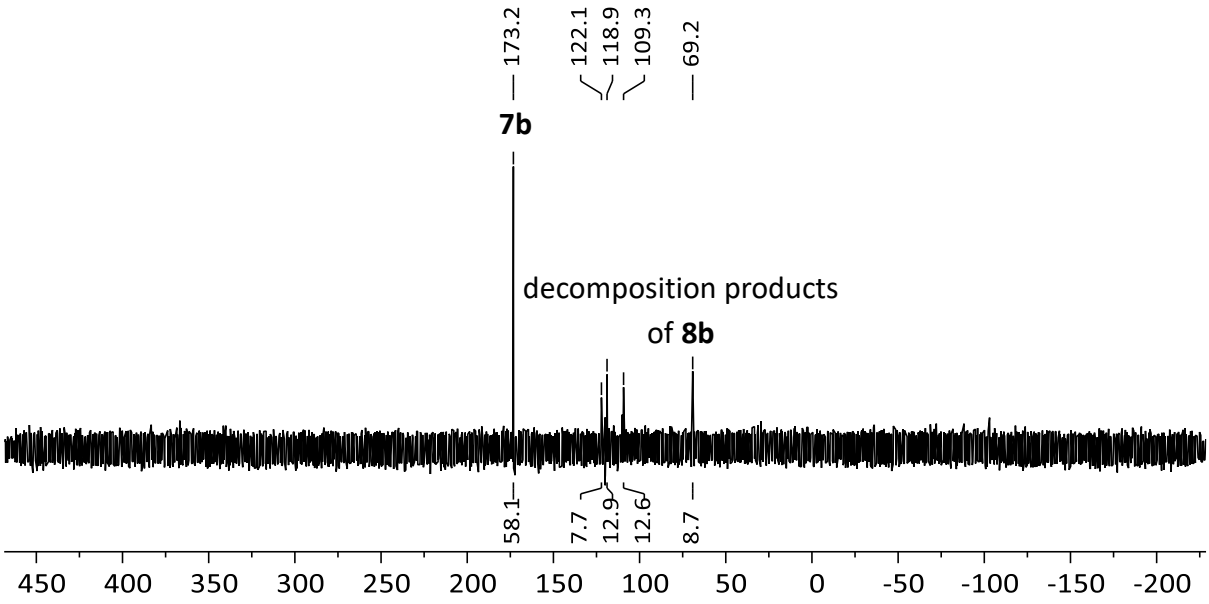

Figure 11: ^{31}P{^{1}H} NMR spectrum (121.51 MHz, 299 K, toluene) of the product mixture after heating complex **4b** at 60 °C in toluene for 3 days.

Thus, further purification of the obtained raw product of complexes **6** was required. Due to their instability column chromatographic purification was not eligible. Because of the similar solubility of the side products **7** and **8** washing procedures either led to low yields or unsatisfactory purity. Only a recrystallization of **6** in diethyl ether at low temperature was resulting in a clean product but generally also with low to medium yield. Additionally, complexes **4** are highly reactive towards water under formation of a formal carbene-to-phosphinidene oxide complex **9** as hydrolysis product (Scheme 36) and, hence, all chemicals and used glassware had to be dried carefully and a very strict exclusion of air was inevitable.[98,213] Otherwise, the reaction mixture contained up to 8 % of complexes **9**. Furthermore, it was possible to isolate the molybdenum complex **9b** by washing with an *n*-pentane/diethyl ether (50:1) mixture. The ^{31}P NMR data are shown in Table 4.

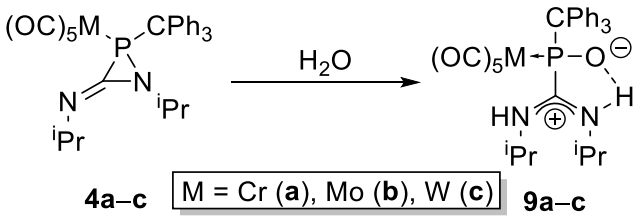

Scheme 36: Hydrolysis of the azaphosphiridine complexes **4**.

Table 4: $^{31}P\{^{1}H\}$ NMR chemical shifts and $^{1}J_{W,P}$ coupling constants of the hydrolysis products **9**.

Compound	$\delta(^{31}P)$ / ppm	$^{1}J_{W,P}$ / Hz	Solvent
9a	124.6	—	THF
9b	110.6	—	$CDCl_3$
9c[94]	92.4	285.6	$CDCl_3$

3.1.1.2 Synthesis of isocyanide adducts via Li/Cl phosphinidenoid complexes

To avoid the highly reactive 3-imino-azaphosphiridine complexes **4** and the consequential formation of side products **7–9** the direct reaction of the Li/Cl phosphinidenoid complexes **2** with *tert*-butyl isocyanide was tested. For that purpose, a slight excess of the isocyanide **5** was added to the freshly prepared complexes **2** at −50 °C and the reaction mixtures were allowed to slowly warm to ambient temperature yielding in a selective and full conversion to the isocyanide-to-phosphinidene complex adducts **6a,c** (Scheme 37). However, for M = Mo the complex **6b** already partially decomposed as described before and, hence, only could be obtained with a content of 76 % (by ^{31}P NMR integration) in the reaction mixture.

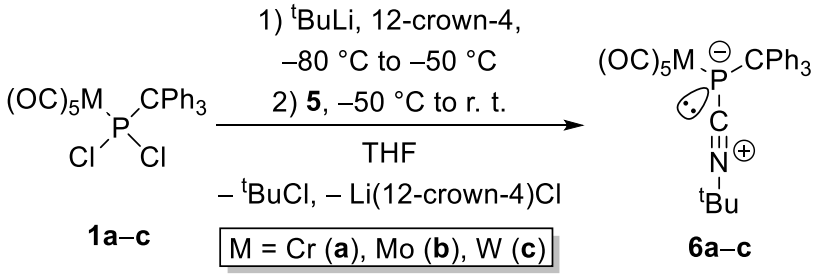

Scheme 37: Synthesis of the isocyanide-to-phosphinidene complex adducts **6** via intermediate Li/Cl phosphinidenoid complexes **2**.

After extraction with *n*-pentane and filtration at ambient temperature, complexes **6a,c** were obtained in good to excellent yields (**6a**: 94 % (before: 21 %) , **6c**: 82 % (before: 52 %[98,103])). The highfield-shifted ^{31}P NMR resonances of complexes **6** (**6a**: $\delta(^{31}P)$ = −11.4 ppm, **6b**: $\delta(^{31}P)$ = −29.0 ppm, **6c**: $\delta(^{31}P)$ = −50.5 ppm) compared to the starting material indicate an increased

electron density at phosphorus resulting in an increased shielding of the P nucleus as expected by its mesomeric structures (Figure 12). Furthermore, it was possible to assign all $^{13}C\{^{1}H\}$ NMR resonance signals including the *ipso*-carbon of the phenyl groups and the isocyanide carbon which was not reported before in literature.[98]

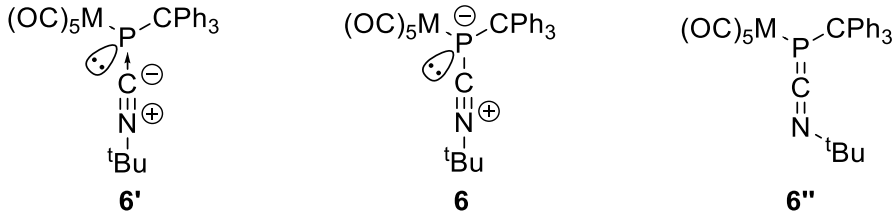

Figure 12: Valence isomeric structures of the isocyanide-to-phosphinidene complex adduct **6**.

The unique set of bond angles at phosphorus and the P-C1 and C1-N bond distances (Figure 13, Table 5) that are close to a typical P-C single and C≡N triple bond[214] give strong evidence that structure **6** represents the main contribution.

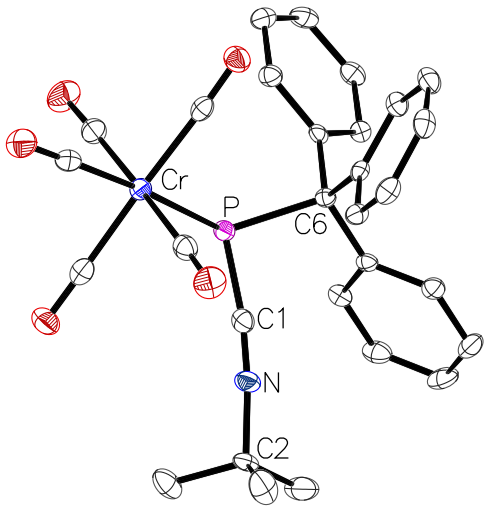

Figure 13: Molecular structure of **6a** in the single crystal lattice at 100(2) K. Thermal ellipsoids are set at 50 % probability level. Hydrogen atoms were omitted for clarity.

Table 5: Selected indicative bond lengths and bond angles of isocyanide-to-phosphinidene complex adducts **6**.

Bond lengths / Å and angles / °	6a	6c[103]
P-C1	1.750(2)	1.747(3)
C1-N	1.156(3)	1.156(3)
C1-P-M	101.57(8)	101.06(8)
C1-P-C6	98.18(10)	98.57(11)
C6-P-M	125.45(7)	124.25(7)
Σ∢P	325.20(25)	323.88(26)

Natural resonance theory (NRT) analyses[215] for the model *N*-methyl substituted complex **6c^{Me}**, that were conducted by Espinosa Ferao, validated the strong contribution of **6c$^{Me'}$** having a single P-C bond structure (34.2 %) (Scheme 38).[216]

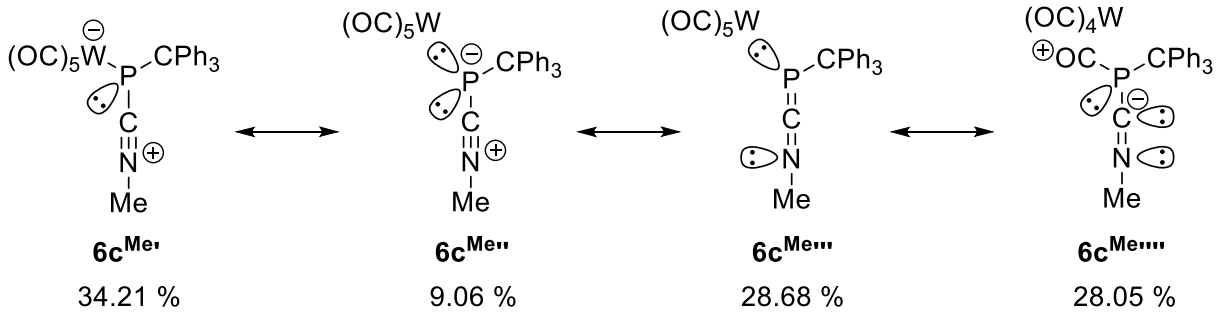

Scheme 38: NRT analysis of the model methylisocyanide-to-phosphinidene complex adduct **6c^{Me}**.

However, the isocyanide ligand is linked by a formal P=C double bond with a contribution of 28.7 % considering the twelve resonance structures contributing more than 2.1 %. The model compound **6c^{Me}** keeps a highly pyramidalized geometry at phosphorus ($\Sigma\sphericalangle P$ = 320.3°) and its valence isomer with a planar P center corresponds to the *vertex*-type transition state for the inversion at phosphorus with a remarkably low barrier ($\Delta\Delta G^{\ddagger}$ = 2.8 kcal/mol) compared to other three-coordinated P(III) species.[217]

3.1.2 Synthesis and properties of *N*-donor-to-phosphinidene complexes

Various families of *end*-on P-ligands of electrophilic, terminal phosphinidene complexes have been theoretically investigated recently.[86] According to a typical textbook on transition metal coordination chemistry, *N*-donors such as *N*-methylimidazole (*N*-MeIm) (**10**), 4-dimethylaminopyridine (DMAP) (**11**) and pyridine (Py) (**12**) should form mainly dative bonds in electrophilic phosphinidene complex adducts. To probe this concept and examine the option of a facile access to proposed hypothetical transient species, the aforementioned donors were reacted with *in situ* formed Li/Cl phosphinidenoid complexes **2** in THF at low temperatures. All reactions proceeded smoothly to yield almost selectively the donor-to-phosphinidene complex adducts **13** and **14**, except for the case of pyridine (**15**) which did not go to completion (contents at ambient temperature via $^{31}P\{^{1}H\}$ NMR integration: **15a** 74 %, **15b** 68 %) (for all following complexes "**a**" denotes M = Cr and "**b**" M = W) (Scheme 39).

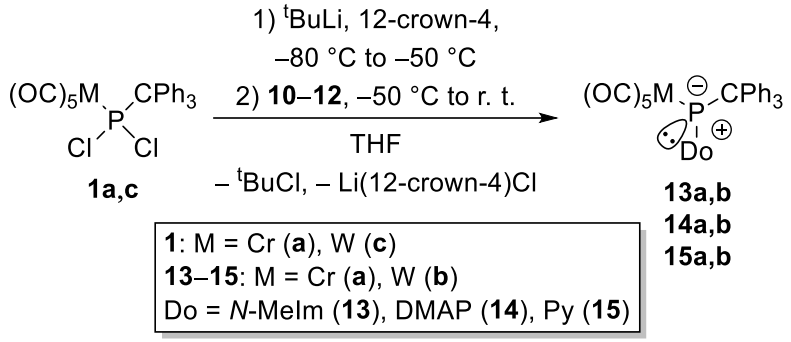

Scheme 39: Synthesis of *N*-donor-to-phosphinidene complexes **13–15**.

The phosphinidene complex adducts **13** and **14** were stable at ambient temperature and could be isolated via extraction of the residues using diethyl ether, subsequent filtration over silica gel and precipitation by slow addition of *n*-pentane. These complexes could be fully characterized. The resonance signal of the C^2H proton appear at 6.45 ppm for **13a** and 6.41 ppm for **13b** in the ^1H NMR spectra (Figure 14). Hence, the protons are highfield-shifted compared to **10**[218] due to coordination to the phosphinidene complex. The same effect is also observed for the $^{15}N\{^1H\}$ NMR resonances of the adducts that were found at −177.7 ppm (**13a**), −183.9 ppm (**13b**), −192.1 ppm (**14a**) and −193.9 ppm (**14b**) for the *P*-bound nitrogen nuclei while they were found at −111.4 ppm for **10**[219] and −112 ppm for **11**.[220] This highfield shift is similar to the one induced by coordination to transition metals with a coordination shift $\Delta\delta(^{15}N)$ of typically −50 ppm to −100 ppm, *e.g.* of −65.3 ppm for pyridine upon complexation in $[Pd(phen)(py)(C_2H_5)]CF_3SO_3$ (phen = 1,10-phenantroline) in CD_2Cl_2).[220,221]

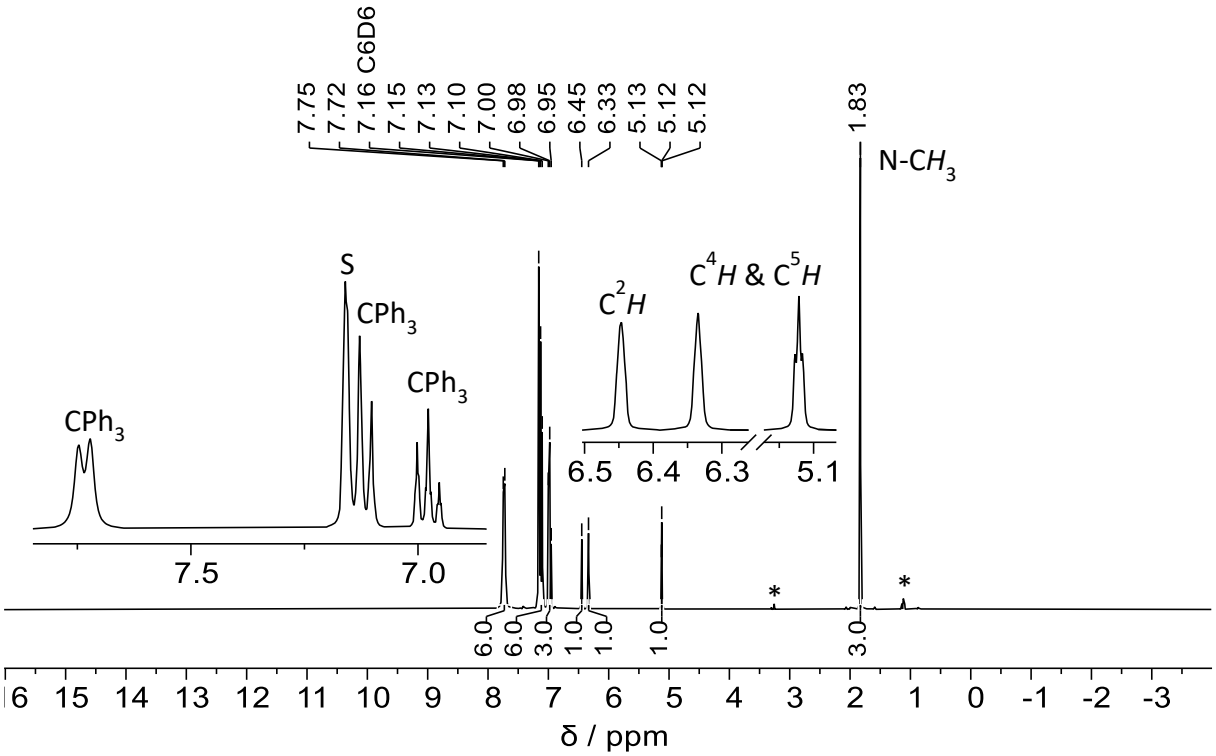

Figure 14: ^{1}H NMR spectrum (300.13 MHz, 300 K, C_6D_6) of complex **13a**. The resonances of traces of diethyl ether are marked with asterisks. The residual resonance signal of the deuterated solvent is marked with an "S".

Table 6: ^{31}P NMR data of Li/Cl phosphinidenoid complexes **2** and donor-to-phosphinidene complex adducts **13–15**.

Compound	δ(^{31}P) / ppm	$^{1}J_{W,P}$ / Hz	Solvent
13a	248.0	—	C_6D_6
13b	199.2	107.2	C_6D_6
14a	281.1	—	THF-d_8
14b	234.8	102.5	THF-d_8
15a[a]	335.5	—	THF
15b[a]	284.6	<100[b]	THF
2a[80]	310.4	—	THF-d_8
2b[80]	280.4	—	THF-d_8
2c[78]	252.1	77.6	$CDCl_3$

[a] Data obtained from the reaction mixture. [b] ^{183}W satellites lie inside the broadened signal.

The characteristic ^{31}P NMR data of complexes **13–15** (Table 6) are related to those of Li/X phosphinidenoid complexes present as ion pairs in solution. The remarkable downfield shift arises also from the less electron donating donor molecules attached to the low-valent phosphorus species compared to complex adducts **6** and, hence, accompanied by a lower

electron density at phosphorus and reduced electronic shielding of the ^{31}P nucleus. DFT calculations on the dative character by Espinosa Ferao strengthened this hypothesis (see also chapter 3.4.1 for more details).[216]

The molecular structures of **13** and **14** were confirmed by single crystal X-ray diffractions studies (Figure 15).

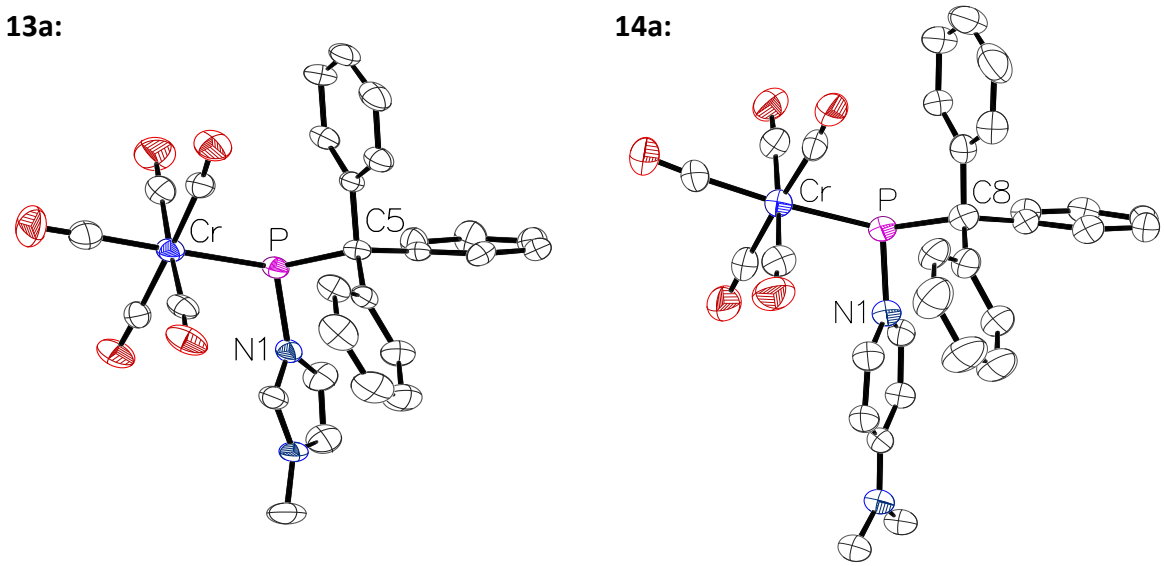

Figure 15: Molecular structures of **13a** and **14a** in the single crystal lattice at 180(2) K (**13a**) and 123(2) K (**14a**). Thermal ellipsoids are set at 50 % probability. Hydrogen atoms and solvent molecules were omitted for clarity.

Selected indicative bond lengths and angles are displayed in Table 8 and Table 9. The bond lengths within the imidazole and DMAP fragments of the adducts are very similar to those of the free donors[222,223] confirming the theoretically proposed dative character of the donor-P bond.

Table 7: Selected indicative bond lengths and bond angles of donor-to-phosphinidene complex adducts **13** and imidazole.[222]

Bond lengths / Å and angles / °	13a	13b	imidazole[222]
P-N1	1.817(2)	1.813(8)	—
N1-C1	1.330(3)	1.304(12)	1.3219(4)
N2-C1	1.338(3)	1.318(13)	1.3424(3)
N-P-M	109.27(7)	108.2(2)	—
N-P-C5	96.87(9)	97.0(4)	—
C5-P-M	117.84(8)	116.7(3)	—
Σ∢P	323.98(24)	321.9(9)	—

The unique set of bond angles at phosphorus and the P-donor bond lengths that are significantly elongated compared to typical P-N single bonds (*e.g.* 1.6742(16) Å in $[W(CO)_5\{P(CPh)_3(H)(pyrrolidin\text{-}1\text{-}yl)\}]$[224]) are supporting this hypothesis.

Table 8: Selected indicative bond lengths and bond angles of donor-to-phosphinidene complex adducts **14** and DMAP (**11**).[223]

Bond lengths / Å and angles / °	14a	14b	11[223]
P-N1	1.834(4)	1.826(8)	—
N1-C1	1.335(7)	1.372(11)	1.335(4)
N1-C5	1.368(7)	1.370(11)	1.337(3)
C1-C2	1.388(7)	1.354(12)	1.375(4)
C4-C5	1.384(7)	1.359(12)	1.381(3)
C2-C3	1.407(7)	1.421(12)	1.404(3)
C3-C4	1.394(8)	1.414(12)	1.403(3)
C3-N2	1.361(6)	1.333(10)	1.367(3)
N-P-M	108.87(14)	108.3(2)	—
N-P-C8	99.1(2)	100.2(3)	—
C8-P-M	117.19(18)	116.4(3)	—
Σ∢P	325.2(5)	324.9(8)	—

3.1.3 Synthesis and properties of phosphane-to-phosphinidene complex adducts

Introducing phosphanes as donor molecules would lead to the formation of phosphanylidene-phosphorane complexes that were shown previously to behave as phospha-Wittig reagent which can be used as source for a P_1 building block in the synthesis of phosphaalkenes.[41,128,129,134,225]

Phosphane-to-phosphinidene complex adducts **19–21** were obtained via reaction of the Li/Cl phosphinidenoid complexes **2** with trimethylphosphane (**16**), triethylphosphane (**17**) and tri-*n*-butylphosphane (**18**).

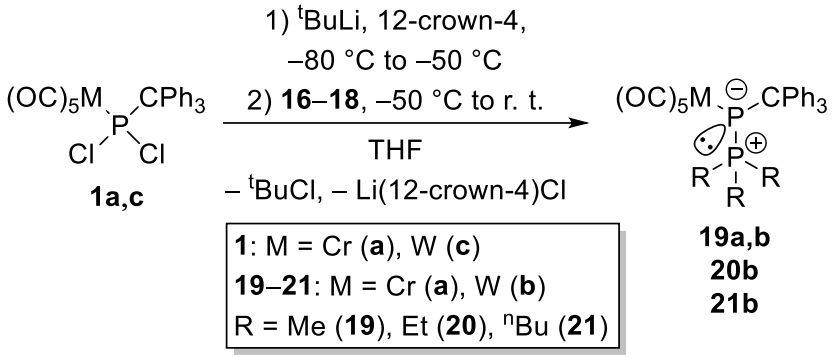

Scheme 40: Synthesis of phosphanylidene-phosphorane complexes **19–21**.

Complexes **19–21** were fully characterized. Compared to similar phosphanyl-phosphorane complexes of Mathey[126,133] and Scheer[137] the ^{31}P NMR chemical shifts of the phosphinidene fragments (Table 9) are significantly downfield shifted indicating a lower electron density at phosphorus which can be explained by a decreased donation of electrons from the trialkylphosphanes due to the steric repulsion induced by the triphenylmethyl substituent. This coincides with an increased polarization and, hence, an ionic-enhanced bonding with an increased s-character of the P-P bond causing an increase of the $^{1}J_{P,P}$ coupling constant as observed similarly for the P-C bond in alkylidene-phosphoranes.[226] Likewise, the $^{1}J_{W,P}$ coupling constant is also increasing with the larger s-character of the free electron pair involved in the complexation.

Table 9: ^{31}P NMR data of complexes **19–21** and similar complexes by Mathey and Scheer.[126,133,137]

Compound	δ(^{31}P) / ppm	$^{1}J_{P,P}$ / Hz	$^{1}J_{W,P}$ / Hz	solvent	lit.
19a	17.3 / 12.5	484.1	—	CD_2Cl_2	
19b	16.9 / −20.9	456.3	120.6	THF-d_8	
20b	33.3 / −28.6	476.9	123.9	C_6D_6	
21b	28.8 / −25.0	471.6	122.1	THF-d_8	
$[Cr(CO)_5\{P(Ph)P^nBu_3\}]$	34.1 / −60.8	440	—	THF	[126]
$[W(CO)_5\{P(Ph)P^nBu_3\}]$	30.9 / −100	444.3	102.5	THF	[133]
$[W(CO)_5\{P(Me)P^nBu_3\}]$	34.5 / −145.1	429.7	102.5	THF	[133]
$[W(CO)_5\{P(allyl)P^nBu_3\}]$	35.0 / −124.6	439.5	102.5	THF	[133]
$[W(CO)_5\{P(COOEt)P^nBu_3\}]$	31.9 / −87.2	368.7	109.9	THF	[133]
$[W(CO)_5\{P(COOEt)PEt_3\}]$	38.2 / −97.4	361.3	107.4	THF	[133]
$[W(CO)_5\{P(Cp^*)PEt_3\}]$	35.2 / −104.5	476	—	C_6D_6	[137]
$[W(CO)_5\{P(Cp^*)P(^iPr)_2Me\}]$	40.8 / −99.8	490	—	CD_2Cl_2	[137]

Single crystal X-ray diffraction studies confirmed the molecular structures (Figure 16). The weaker P-P interaction is reflected by the elongated P-P bonds approaching a typical P-P single bond length.[214] These observations are in agreement with DFT calculations of Espinosa Ferao (see chapter 3.4.1).[216] An additional steric pressure is applied for the case of chromium (**19a**) due to the shorter metal-phosphorus distance compared to the tungsten case resulting in an increased $^{1}J_{P,P}$ coupling constant and P-P bond length.

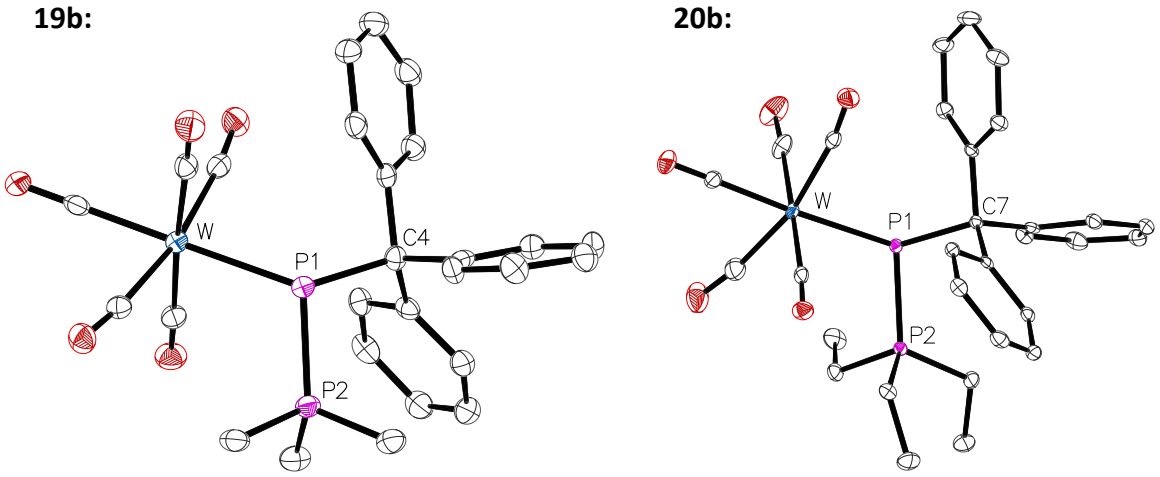

Figure 16: Molecular structures of **19b** and **20b** in the single crystal lattice at 123(2) K (for **19b**) and 100(2) K (for **20b**). Thermal ellipsoids are set at 50 % probability level. Hydrogen atoms were omitted for clarity. Selected bond lengths / Å and bond angles / °: **19b**: W-P1 2.6151(11), P1-C4 1.958(4), P1-P2 2.1584(14), P1-P2-W 109.87(5), P1-P2-C4 102.93(13), C4-P1-W 119.36(13); **20b**: W-P1 2.6373(6), P1-C7 1.945(2), P1-P2 2.1747(8), P1-P2-W 109.25(3), P1-P2-C7 103.45(8), C7-P1-W 116.69(7).

3.2 Cyclic voltammetry studies on P adduct complexes

The free electron pair at phosphorus, not involved into metal complexation, should provide for the donor-to-phosphinidene complex adducts a manifold of reactivity opportunities. The available free electron pair at phosphorus, largely representing the HOMO (see page 49), can be oxidized to obtain in a first step the corresponding radical cation which could form the respective dication under loss of a second electron (Scheme 41). The two-electron reduction is expected to occur at the metal center where the LUMO is largely located and, presumably, lead to a loss of the corresponding metallate and formation of the phosphinidene adduct.

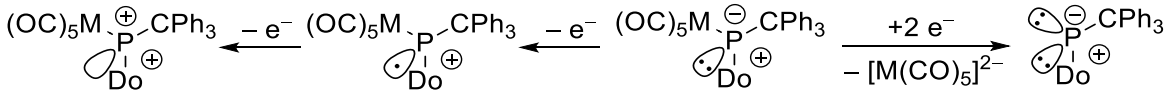

Scheme 41: Proposed redox reactions at the P-center of phosphinidene complex adducts.

To get first insights into the electrochemical properties of complexes **6**, **13**, **14** and **19–21** cyclic voltammograms were recorded in tetrahydrofuran using tetra-*n*-butylammonium hexafluoro-phosphate as electrolyte (**6c** and **13b**: Figure 17).

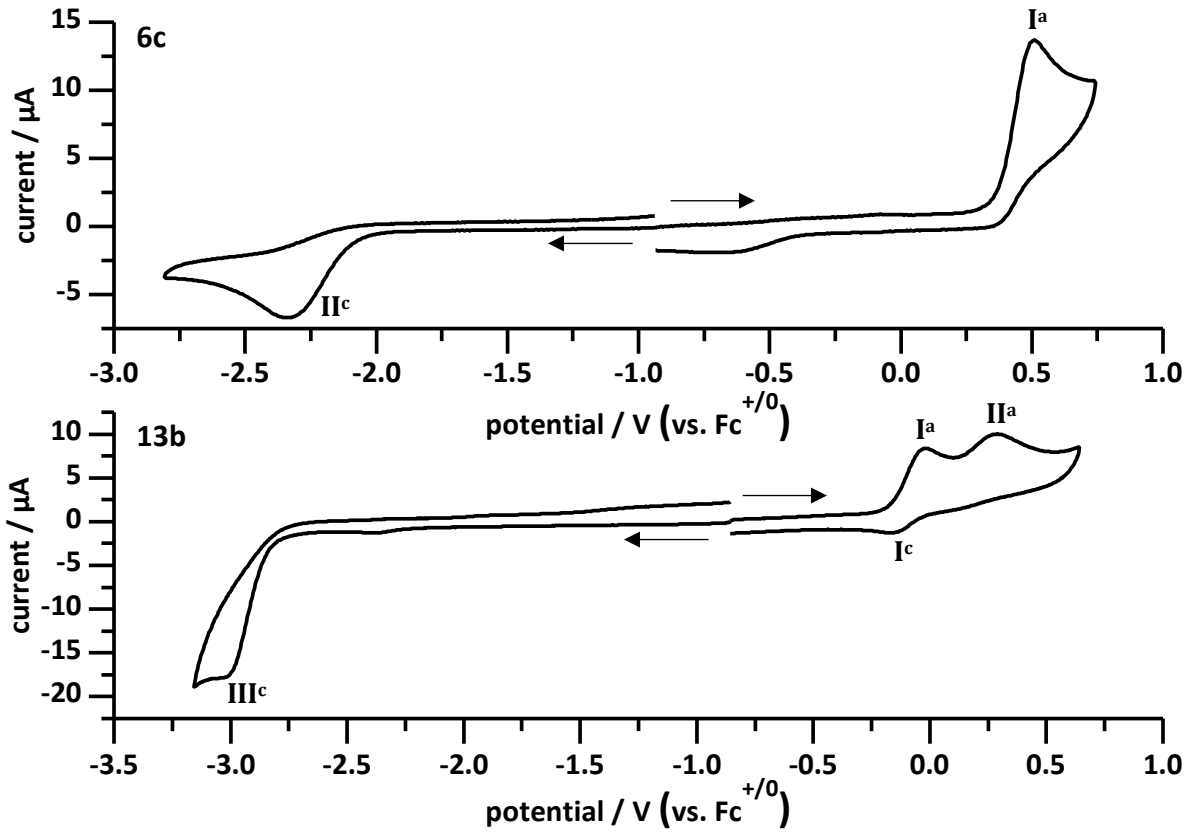

Figure 17: Overlay of cyclic voltammograms of **6c** and **13b** (1 mM) at a Pt electrode in a 0.2 M $^{n}Bu_4PF_6$/THF solution; oxidation parts with anodic initial scan direction and reduction parts with cathodic initial scan direction as denoted with arrows; scan rate: 200 mV/s; potentials are referenced against $Fc^{+/0}$.

All complexes except of **6** show a similar pattern in the cyclic voltammograms showing three redox processes. Therefore, first complexes **13**, **14** and **19–21** were studied, and for the first oxidation process a return wave can be observed that is getting suppressed by the second oxidation process. However, the second oxidation process as well as the reduction process do not show any return waves. The oxidation waves correspond to one-electron step processes while in the reduction process at least two electrons are involved. To assess the electrochemical reversibility of the first redox process I the difference of the anodic (E_p^{Ia}) and cathodic peak potentials (E_p^{Ic}), the so-called peak-to-peak separation ΔE_p and the ratio of the currents $|i_p^c/i_p^a|$ of the isolated process (by setting the upper potential limit in the minimum between the first (I^a) and second oxidation process (II^a); for **13b**: Figure 18) were determined (Table 10).

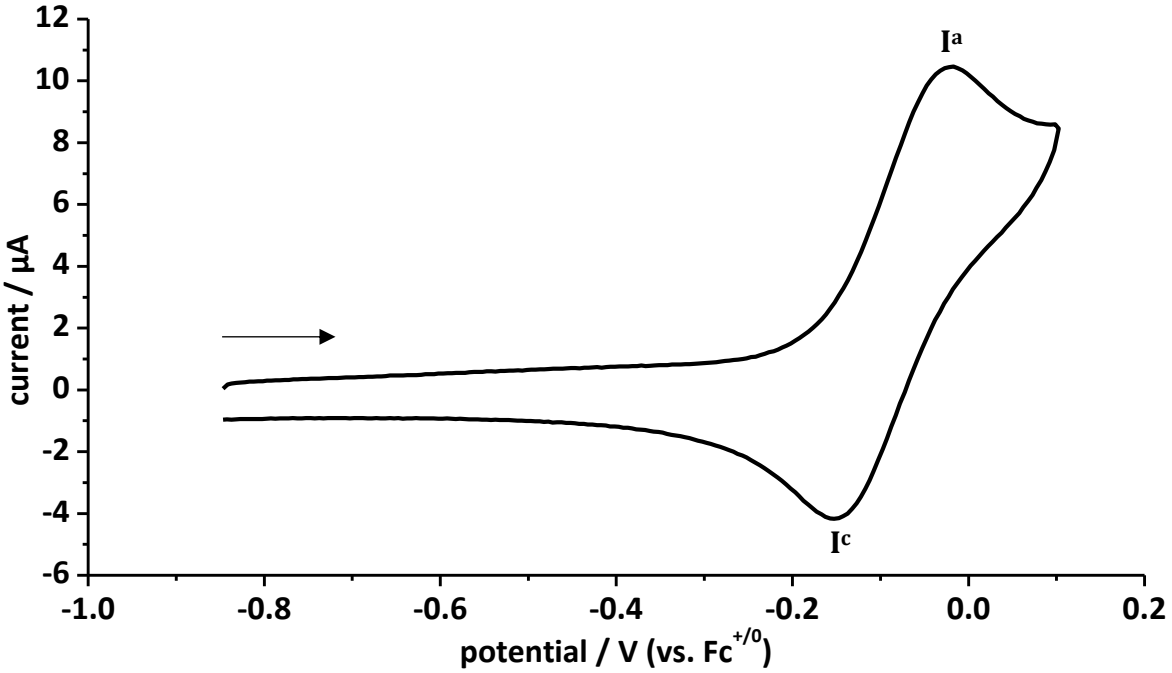

Figure 18: Cyclic voltammogram of the isolated first oxidation process (I) of **13b** (1 mM) at a Pt electrode in a 0.2 M $^{n}Bu_4PF_6$/THF solution; measurement with anodic initial scan direction (denoted with an arrow); scan rate: 200 mV/s; potentials are referenced against $Fc^{+/0}$.

According to the Nernst equation (eq. (*1*))[227] a theoretical value of 2.22 *RT*/*nF* and therefore of 57 mV/*n* is expected for the peak-to-peak separation ΔE_p at 25 °C if the process is reversible, where Φ_0 is the equilibrium potential, Φ_{00} the standard equilibrium potential, *R* the universal gas constant, *T* the temperature, *n* the number of transferred electrons, *F* the Faraday constant and $c_{ox/red}$ the concentration of the oxidized/reduced species.

$$\Phi_0 = \Phi_{00} + \frac{RT}{nF} ln \frac{c_{ox}}{c_{red}} \quad (1)$$

In practice non-linear diffusion phenomena and an uncompensated solution resistance are emerging and thus usually larger values for ΔE_p are observed.[228] Additionally, a theoretical width at half max on the forward scan of the peak of 59 mV is expected.[229,230] According to the obtained experimental values (Table 10) the first oxidation process can be considered as quasi-reversible and is proceeding via an $E_{rev}C_{irrev}$ mechanism.

Table 10: Anodic and cathodic peak potentials and currents, half-wave potentials $E^I_{1/2}$, ΔE_p and $|i^c_p/i^a_p|$ of the isolated first redox process I of compounds **13a,b**, **14b**, **19a,b**, **20b** and **21b**.

Compound	E^{Ia}_p / V	i^{Ia}_p / µA	E^{Ic}_p / V	i^{Ic}_p / µA	$E^I_{1/2}$ / V	ΔE^I_p / mV	$\lvert i^c_p/i^a_p \rvert$
13a	−0.08	6.10	−0.18	−6.28	−0.13	95	1.03
13b	−0.02	6.56	−0.16	−6.33	−0.09	146	0.96
14b	−0.04	2.06	−0.14	−1.78	−0.09	96	0.86
19a	0.12	6.54	−0.02	−6.02	0.05	136	0.92
19b	0.19	11.8	0.04	−11.7	0.12	145	0.99
20b	0.16	5.58	0.05	−5.63	0.10	110	1.01
21b	0.18	5.28	0.06	−5.20	0.12	125	0.99

To probe if the electrochemical processes are freely diffusion-controlled without involvement of electrode-absorption events the cyclic voltammograms were recorded at different scan rates (**13b**: Figure 19). In this case the peak current i_p should increase linearly with the square root of the scan rate ν according to the Randles-Ševčik equation (eq. (*2*)) where *A* is the electrode surface area, C^0 the bulk concentration of the analyte and D_{ox} is the diffusion coefficient of the oxidized species.[231,232]

$$i_p = 0.446nFAC^0 \left(\frac{nF\nu D_{ox}}{RT}\right)^{1/2} \quad (2)$$

The currents are increasing for higher scan rates due to a decrease of the size of the diffusion layer.[230,231] When the peak currents i_p of the cyclic voltammograms of the phosphinidene complex adducts are plotted against the square root of the scan rate $\nu^{1/2}$ for all cases a linear correlation was observed and linear fits can be applied with very good coefficients of determination $R^2 \geq 0.99$ proving a freely diffusion-controlled electrochemical process without participation of an electrode-absorption process (**13b**: Figure 20).

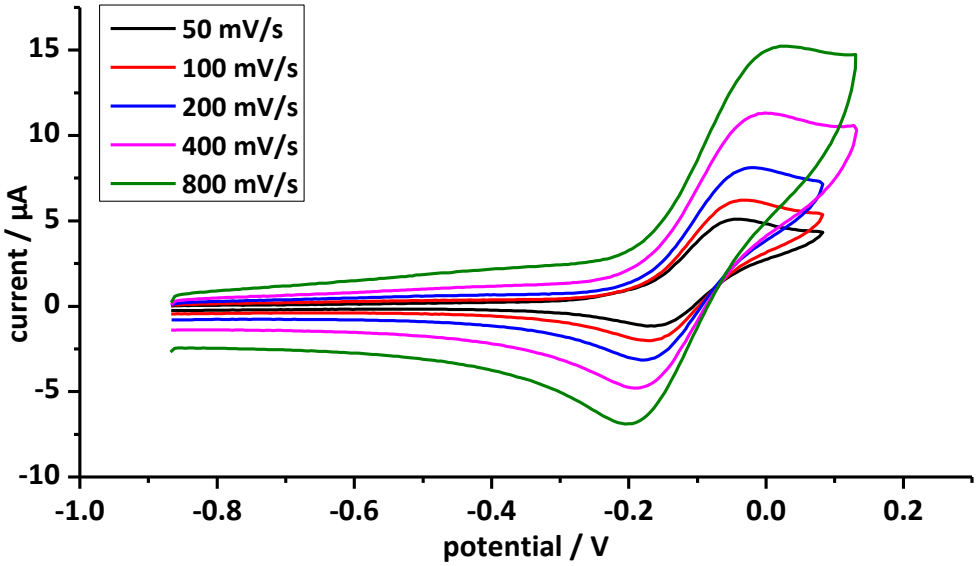

Figure 19: Cyclic voltammograms of the first redox event I of donor-to-phosphinidene complex adduct **13b** at scan rates of 50–800 mV/s; potentials are referenced against $Fc^{+/0}$.

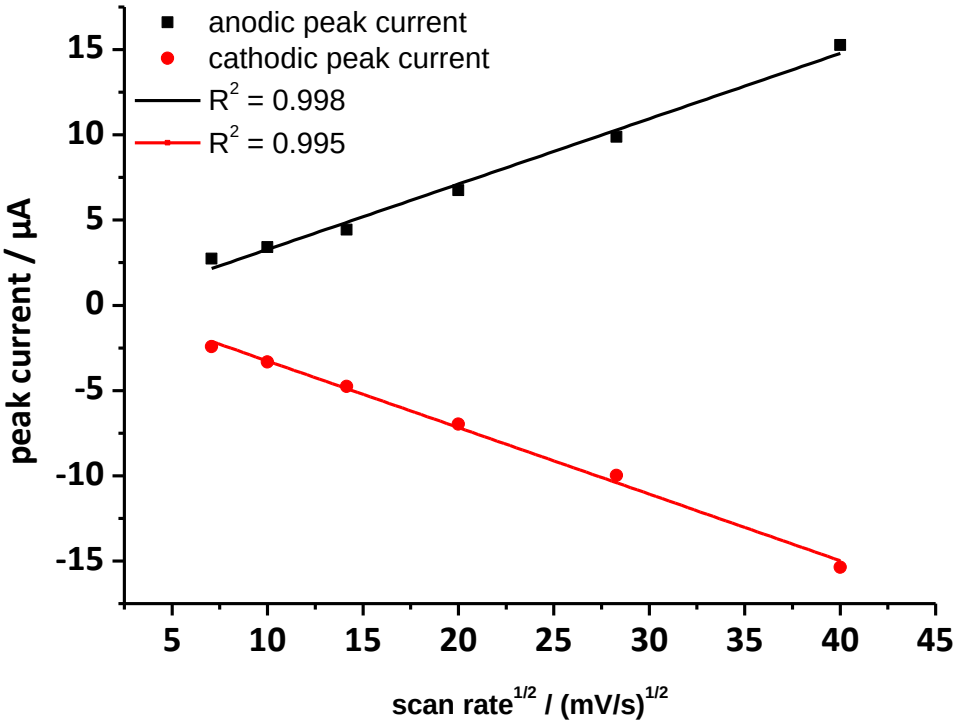

Figure 20: Dependency of the peak currents i_p of the first redox process I on the square root of the scan rate $\nu^{1/2}$ of **13b** at varying scan rates.

The second and third redox processes were also diffusion-controlled which was tested by variation of the scan rate (Figure 21) and checking the linear behavior of the peak potentials with the square root of the scan rate. The small waves that appeared in the cyclic voltammograms of the isolated third redox process by increasing the scan rate resulting from

decomposition of the electrolyte solution due to the low applied potentials lying outside of the solvent limits for stable measurement conditions. Furthermore, also no return waves were observed at higher scan rates for the second and third redox process and, hence, they proceed both via an $E_{irrev}C_{irrev}$ mechanism.

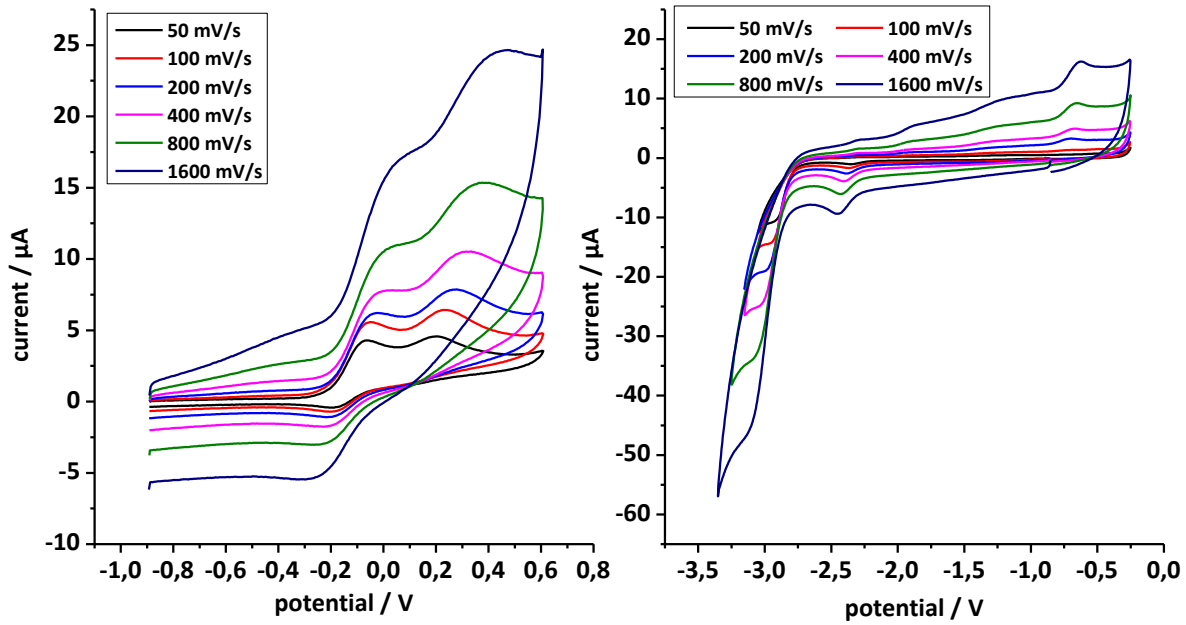

Figure 21: Cyclic voltammograms of the first and second (left) and third redox (right) redox process of complex **13b** at scan rates of 50–1600 mV/s; potentials are referenced against $Fc^{+/0}$.

However, complex **6** is behaving differently undergoing only two redox processes at a scan rate of 200 mV/s using an $^{n}Bu_4NPF_6$/THF electrolyte solution with anodic initial scan direction. The first redox process I^a is observed as oxidation wave at 0.51 V with initial scan into anodic direction. The second redox process II^c is observed as reduction wave at −2.34 V with initial scan into cathodic direction. While for redox process I^a no return wave can be observed, a low-current return wave (III^a) for redox process II^c could be observed with a peak potential of −0.10 V when a cathodic initial scan direction was used (Figure 22). The wave with a peak potential of −0.46 V is arising due to decomposition of the analyte as minor impurity. All observed waves were freely diffusion-controlled which was checked via a scan rate dependence of the current.

Unfortunately, the redox processes were not accessible chemically due to the potential of the first oxidation process lying too close to the one of the subsequent irreversible second oxidation, and the highly negative reduction potentials of the adducts.

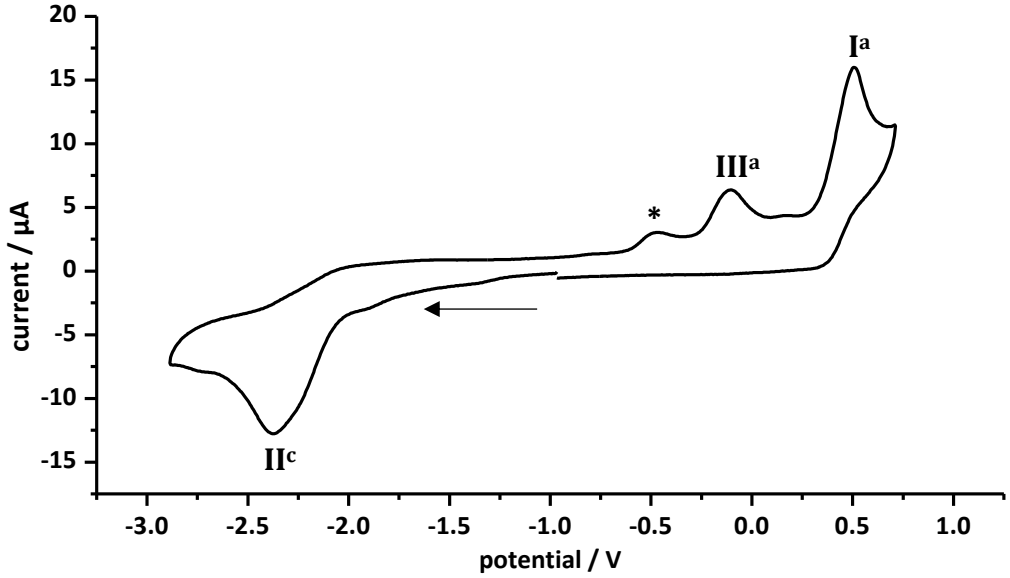

Figure 22: Cyclic voltammogram of complex **6c** (1 mM) at a Pt electrode in a 0.2 M $^{n}Bu_4PF_6$/THF solution; measurement with cathodic initial scan direction (denoted with an arrow); scan rate: 200 mV/s; potentials are referenced against $Fc^{+/0}$. A minor impuritiy due to decomposition of the analytes was denoted by an asterisk.

The energies of the highest occupied molecular orbitals (HOMO) and lowest unoccupied molecular orbitals (LUMO) of the donor-to-phosphinidene complex adducts were calculated at $CPCM_{tol}$/B3LYP-D3/def2-TZVP(ecp), $CPCM_{tol}$/PW6B95-D3/def2-QZVP(ecp)// $CPCM_{tol}$/B3LYP-D3/def2-TZVP(ecp) and $CPCM_{tol}$/PWPB95-D3/def2-QZVPP(ecp)//$CPCM_{tol}$/ B3LYP-D3/def2-TZVP(ecp) levels of theory by Espinosa Ferao (Table 11).[216] Since the first oxidation peak potentials E_p^{Ia} should reflect the HOMO energies and the first reduction peak potentials E_p^{IIIc} should reflect the LUMO energies, a linear correlation should be observed for the experimental peak potentials and the calculated redox orbital energies ε as shown in Figure 23 and Figure 24.

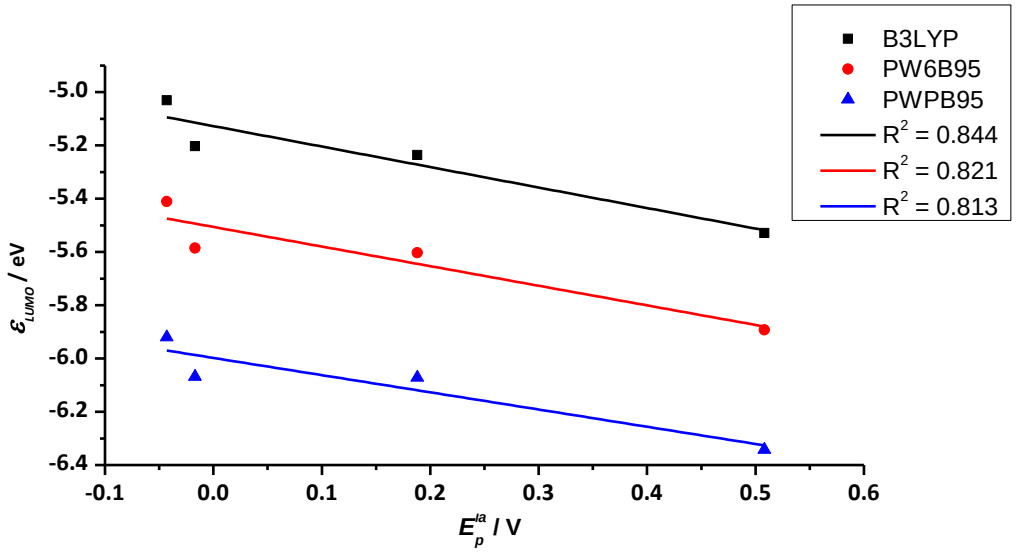

Figure 23: Plot of the LUMO energy ε_{LUMO} with the cathodic peak potentials of the first redox process E_p^{Ia} of donor-to-phosphinidene complex adducts **6c**, **13b**, **14b** and **19b** with linear fits; potentials are referenced against $Fc^{+/0}$.

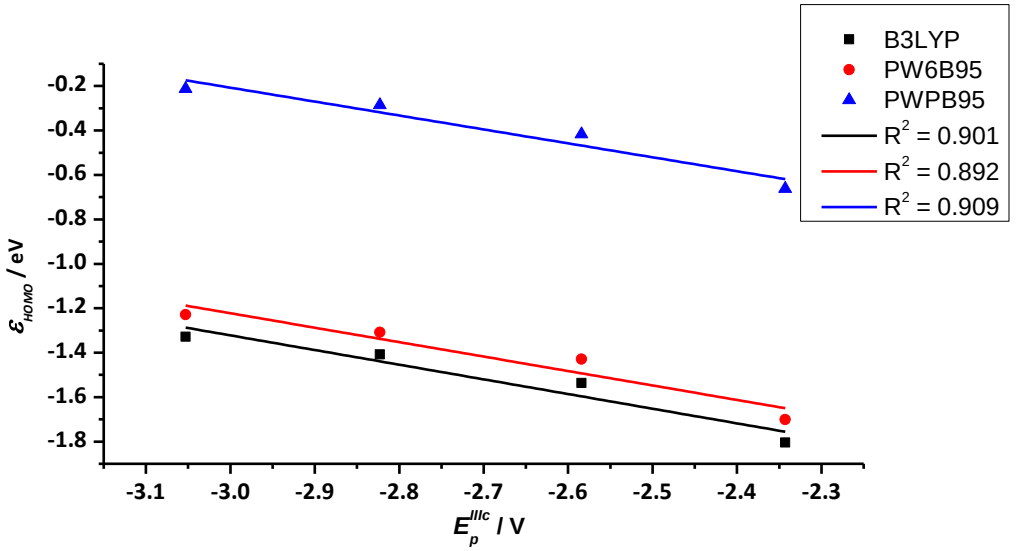

Figure 24: Plot of the HOMO energy ε_{HOMO} with the anodic peak potentials of the third redox process E_p^{IIIc} donor-to-phosphinidene complex adducts **6c**, **13b**, **14b** and **19b** with linear fits; potentials are referenced against $Fc^{+/0}$.

The experimental values of the peak potentials E_p^{Ia} and E_p^{IIIc} correlate well with the calculated HOMO and LUMO energies showing coefficients of determination of R^2 = 0.81–0.84 for the LUMO (Figure 23) and R^2 = 0.89–0.91 for the HOMO (Figure 24). The values correlated significantly better for the HOMO that is mainly presented by the free electron pair at phosphorus than for the LUMO which is mainly located on the metal fragment. The latter is in stark contrast to the situation ofhe model methylisocyanide adduct **6c^{Me}** where the LUMO is only marginally located on the metal fragment, but mainly on the donor molecule (Figure 25).

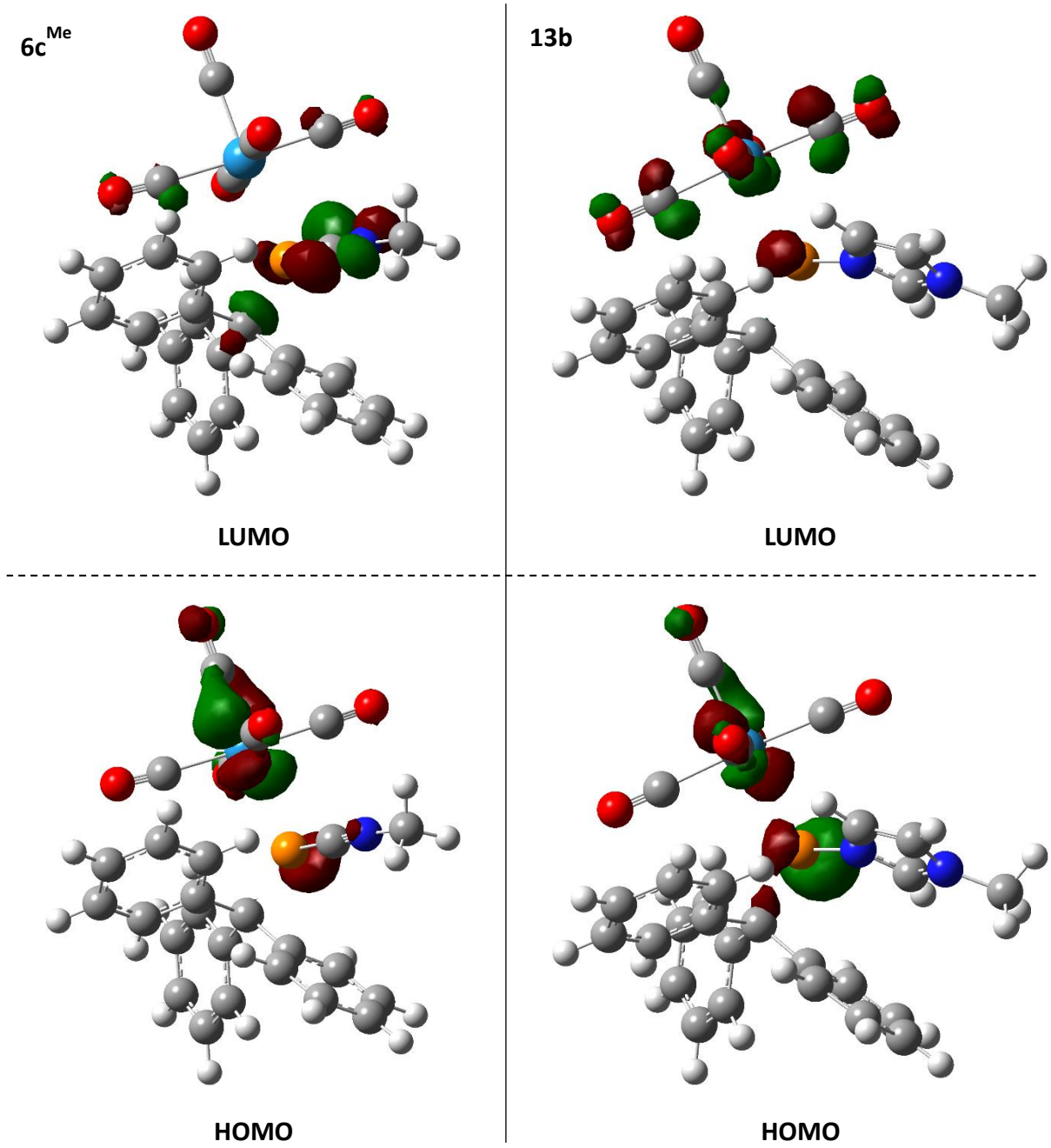

Figure 25: [CPCM$_{tol}$/B3LYP-D3/def2-TZVP(ecp)] lots of the LUMO (top) and HOMO (bottom) of donor-to-phosphinidene complex adducts **6c^{Me}** (left) and **13b** (right).[216]

The three different levels of theory do not show a significant difference in the quality of the correlation. Especially using the double hybrid functional PWPB95 does not give better results than the conventional hybrid functionals PW6B95 or B3LYP.

Table 11: Experimental anodic peak potential E_p^{Ia} of redox process I, cathodic peak potential E_p^{IIIc} of redox process III and the orbital energies of the HOMO and LUMO of donor-to-phosphinidene complex adducts **6c**, **13a,b**, **14b**, **19a,b**, **20b** and **21b**.

compound	E_p^{Ia} / V	E_p^{IIIc} / V	ε_{HOMO} / eV B3LYP / PW6B95 / PWPB95	ε_{LUMO} / eV B3LYP / PW6B95 / PWPB95
6c	−0.51	−2.34	−5.53 / −5.89 / −6.34	−1.81 / −1.70 / −0.66
13a	−0.08	−2.97	—	—
13b	−0.02	−3.05	−5.20 / −5.59 / −6.07	−1.33 / −1.23 / −0.21
14b	−0.04	−2.58	−5.03 / −5.41 / −5.92	−1.54 / −1.43 / −0.42
19a	0.12	−2.91	—	—
19b	0.19	−2.82	−5.24 / −5.60 / −6.07	−1.41 / −1.31 / −0.29
20b	0.16	−2.94	— / — / −6.00	— / — / −0.31
21b	0.18	−3.01	— / — / −6.04	— / — / −0.24

In 1987, Huttner described a correlation between the UV-vis absorption and the ^{31}P NMR chemical shift for phosphinidene-bridged dinuclear pentacarbonylmetal complexes and showed a correlation of the chemical shift with the inverse of the HOMO-LUMO gap.[233] Few years later, Niecke and Schoeller detected also a linear correlation of the ^{31}P NMR chemical shifts of iminophosphanes with their UV n-π* transitions also correlating with 1/Δ*E*(HOMO-LUMO) indicating a dominant paramagnetic contribution to the NMR chemical shift,[234] which was also observed for 7-phosphanorbornadienes.[235] For metallophosphaalkenes no direct correlation was described but trends were observed, *i.e.* small HOMO-LUMO gaps gave rise to significant low-field ^{31}P NMR chemical shifts.[236] Furthermore, nor for π-bridged bis(phospha-alkenes)[237] neither for diphosphenes[238,239] such a correlation was observed. If the diphosphene is η^1-complexed an increase of the HOMO-LUMO energy gap compared to the free ligand was observed together with the typical metal coordination shift of −30 to −130 ppm upon metal complexation and, hence, describing a trend but no direct correlation.[239,240]

To examine the situation for the donor-to-phosphinidene complex adducts the ^{31}P NMR chemical shifts were plotted inversely against the peak potential differences $\Delta E_p^{Ia,IIIc}$ of the first oxidation and first reduction process of the adducts expecting an inverse correlation since $\Delta E_p^{Ia,IIIc}$ should/could represent the HOMO-LUMO gap (Figure 26).

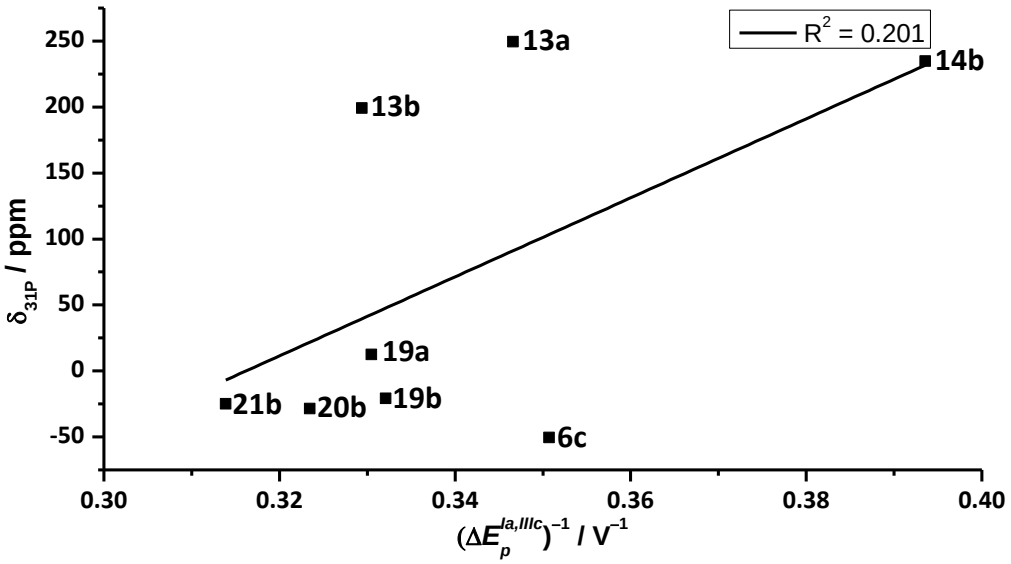

Figure 26: Correlation of the inverse values of the peak potential difference $\Delta E_p^{Ia,IIIc}$ and the ^{31}P NMR chemical shift of phosphinidene complex adducts **6c**, **13a,b**, **14b**, **19a,b**, **20b** and **21b**; potentials are referenced against $Fc^{+/0}$.

However, no inverse or positive correlation between the ^{31}P NMR chemical shift and the peak potential difference $\Delta E_p^{Ia,IIIc}$ was observed. Apparently, no significant contributions on the phosphorus nucleus chemical shielding in such adducts can be stated, especially if the HOMO and LUMO are both not located on phosphorus.[241] DFT calculations of Espinosa Ferao[216] show that the HOMOs of complexes **13**, **14** and **19–21** are predominantly located on phosphorus as free electron pair slightly mixed with the π orbital of W-CO bonds, but the LUMO is mainly contributing to the π* orbitals of the *trans*-C≡O coligands of the metal fragment and is only involved marginally in the σ* orbital of the P-M bond. In contrast, for the model isocyanide-to-phosphinidene complex adduct **6c^{Me}** the LUMO is only marginally contributing to the π* orbitals of the *trans*-C≡O coligands, but instead is significantly displaying the π* orbital of the C≡N bond in the donor molecule. Thus, only a good correlation of the chemical shifts is expected with the LUMO but not the HOMO energies. When the ^{31}P NMR chemical shifts are plotted against the respective peak potentials this behavior is reflected showing a very good linear correlation in the case of the anodic peak potential E_p^{Ia} with a coefficient of determination of $R^2 = 0.974$ but not for the case of the cathodic peak potential E_p^{IIIc} ($R^2 = -0.145$). The data for the isocyanide adducts **6** were excluded in these plots due to their significantly different nature in their electrochemistry (Figure 27). For lower anodic peak potentials E_p^{Ia} which reflect the HOMO energies, higher chemical shifts are observed. Weaker donor molecules coordinating to phosphorus decrease the electron density at the P center resulting in a downfield-shift in the ^{31}P NMR spectrum and, additionally, lead to an increase

of s-character of the free electron pair at phosphorus causing a lower molecular orbital energy. Therefore, the lower anodic peak potentials E_p^{Ia} correlate well with the ^{31}P NMR chemical shift.

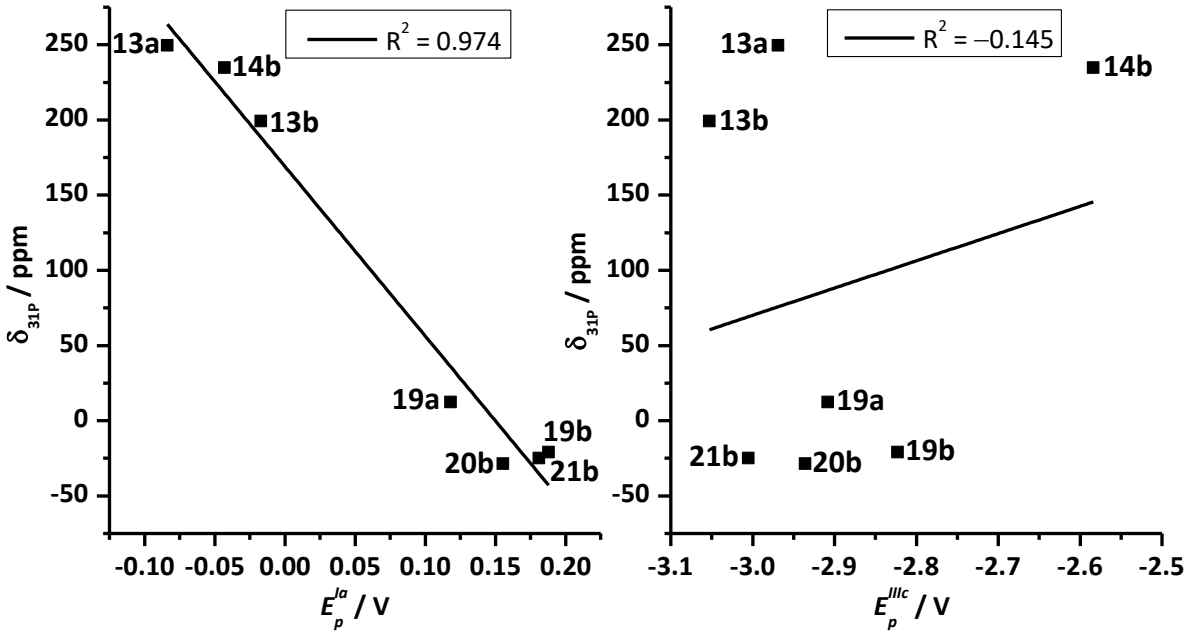

Figure 27: Correlation of the ^{31}P NMR chemical shifts of complexes **13a,b**, **14b**, **19a,b**, **20b** and **21b** with the anodic peak potentials E_p^{Ia} (left) and cathodic peak potentials E_p^{IIIc} (right) ; potentials are referenced against $Fc^{+/0}$.

In consequence of the increasing s-character of the free electron pairs at phosphorus for weaker donors, the $^1J_{W,P}$ coupling constants also correlate linearly with the anodic peak potentials E_p^{Ia} with a good coefficient of determination of $R^2 = 0.922$ (Figure 28).

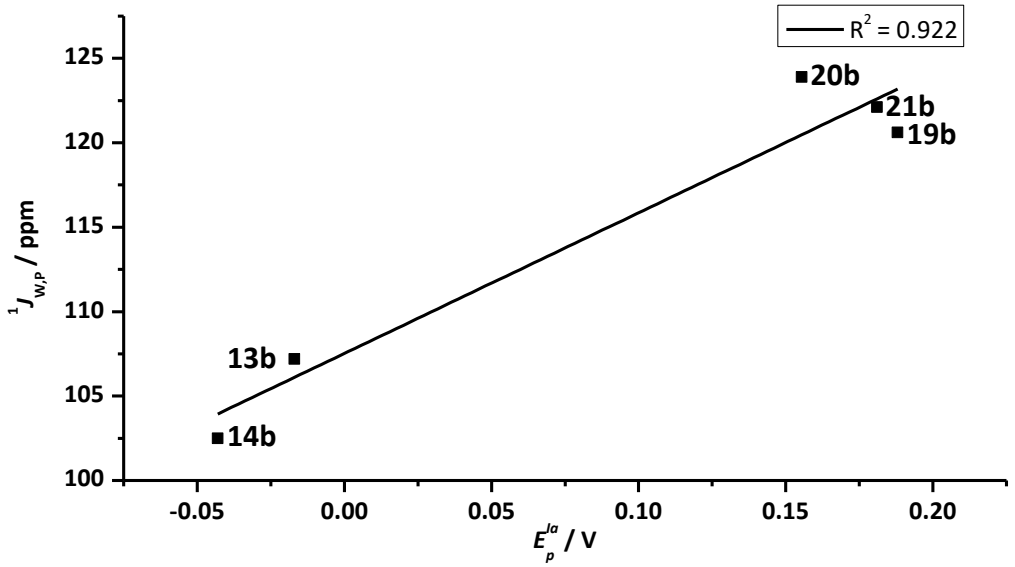

Figure 28: Correlation of the $^1J_{W,P}$ coupling constant with the anodic peak potential E_p^{Ia} of complexes **13b**, **14b**, **19b**, **20b** and **21b**; potentials are referenced against $Fc^{+/0}$.

Accordingly, again no correlation was found with the cathodic peak potential E_p^{IIIc} (R^2 = −0.038), the peak potential difference $\Delta E_p^{Ia,IIIc}$ (R^2 = 0.496) or its inverse $\left(\Delta E_p^{Ia,IIIc}\right)^{-1}$ (R^2 = 0.485).

As expected, the ^{31}P NMR chemical shifts neither correlated with the calculated LUMO energies nor with the HOMO-LUMO gap or its inverse as obtained by Espinosa Ferao.[216] Interestingly, the calculated HOMO energies did not correlate either (Figure 29).

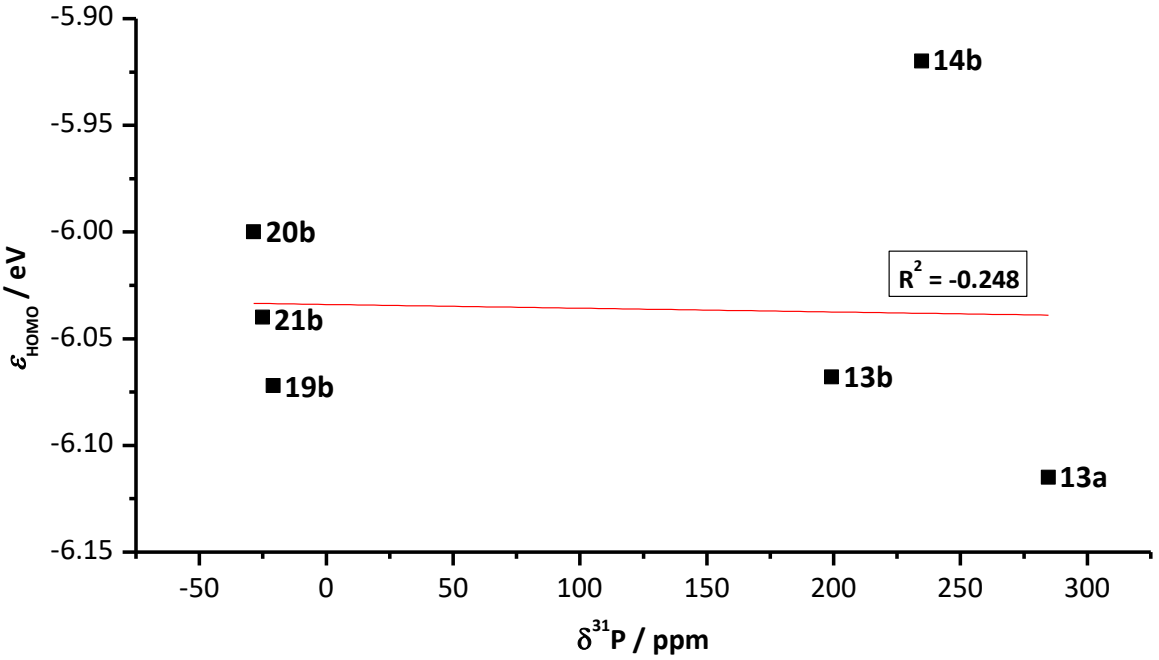

Figure 29: Correlation of the ^{31}P NMR chemical shifts of complexes **13b**, **14b**, **15b**, **19b**, **20b** and **21b** with the [CPCM$_{tol}$/PWPB95-D3/def2-QZVPP(ecp)//CPCM$_{tol}$/B3LYP-D3/def2-TZVP(ecp)] HOMO energies.[216]

3.3 Reactivity of donor-to-phosphinidene complex adducts

3.3.1 Thermal dissociation studies

3.3.1.1 Variable temperature NMR studies

The stability of the phosphinidene complex adducts **6**, **13** and **14** were probed via VT $^{31}P\{^1H\}$ NMR studies (above r.t.) to examine the thermal P-ligand dissociation and the formation of the free electrophilic, terminal phosphinidene complex **16**. When a solution of complex **6a** in chlorobenzene (as “almost inert” solvent) was heated to 95 °C (Scheme 42) a $^{31}P\{^1H\}$ NMR spectrum of the reaction mixture is showing only a singlet resonance signal at −520.8 ppm (Figure 30).

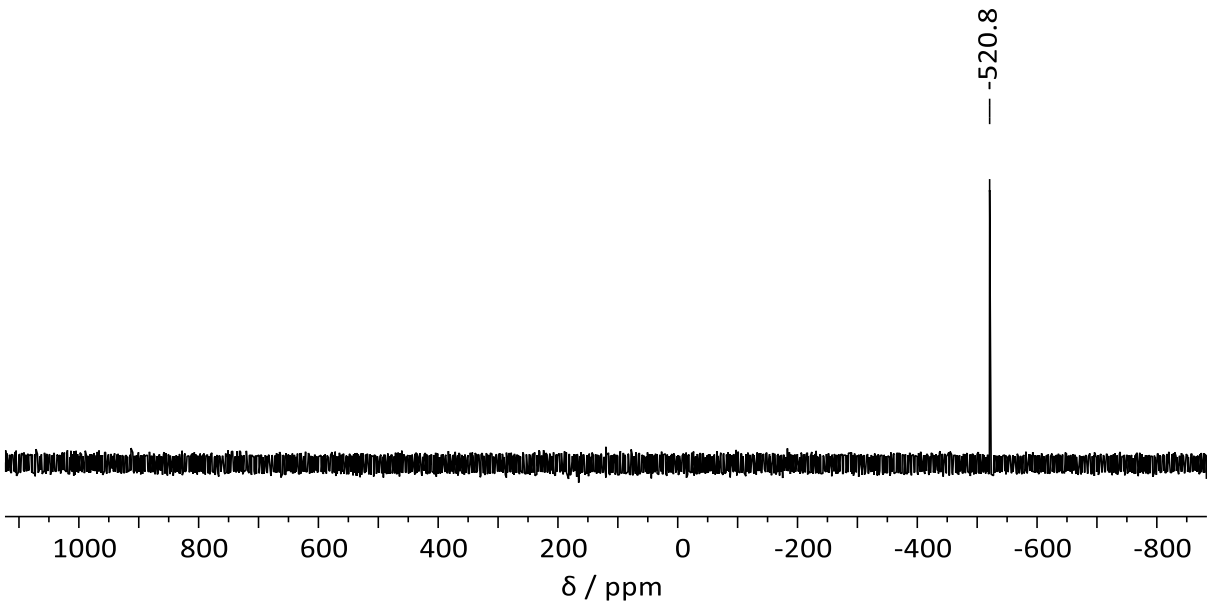

Figure 30: $^{31}P\{^{1}H\}$ NMR spectrum (121.51 MHz, 298 K, C_6H_5Cl) of a solution of **6a** after heating at 95 °C.

Such a strongly upfield shifted signal is specific for white phosphorus (**22**).[242] An authentic sample of **22** was added to the reaction solution confirming unequivocally the formation of white phosphorus as the only P-containing thermal decomposition product.

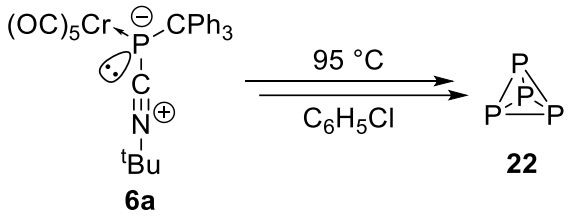

6a **22**

Scheme 42: Thermal decomposition of **6a** into white phosphorus (**22**) at 95 °C in chlorobenzene.

In contrast, the thermal treatment of tungsten complex **6c** gave only 1 % (by $^{31}P\{^{1}H\}$ NMR integration) of **22** which was observed next to several other smaller side products that could not be identified. The main decomposition product (86 % by ^{31}P NMR integration) showed a doublet resonance signal at −21.1 ppm ($^{1}J_{P,H}$ = 367.0 Hz, $^{1}J_{W,P}$ = 244.5 Hz) in the ^{31}P NMR spectrum.

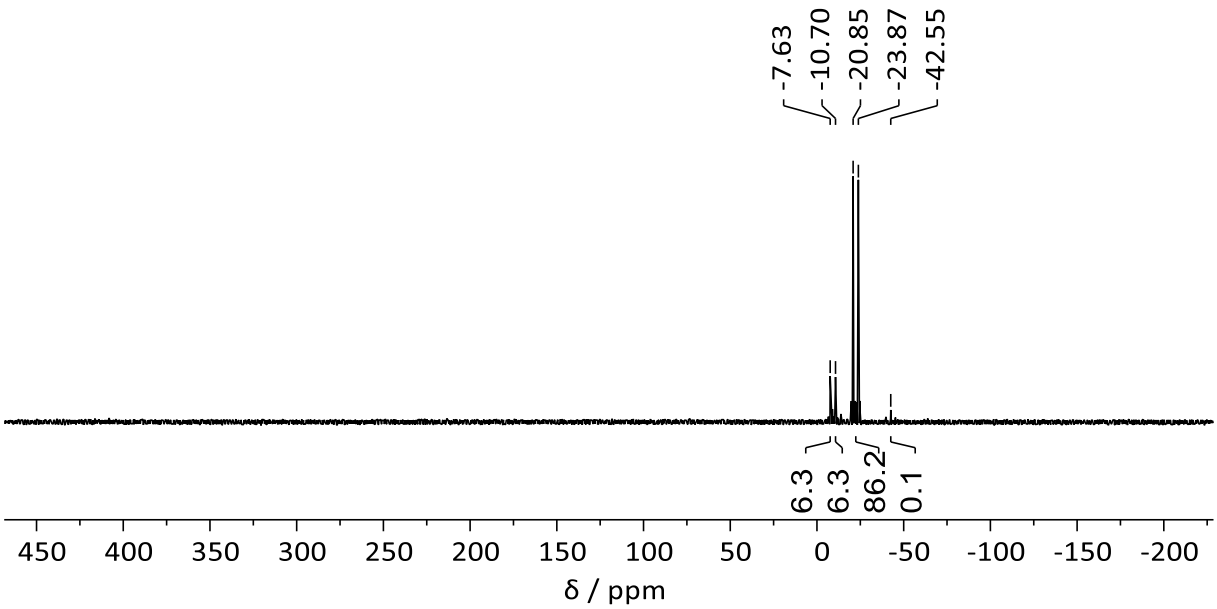

Figure 31: ^{31}P NMR spectrum (121.51 MHz, 298 K, C_6D_6) of a solution of **6c** after heating at 100 °C.

The main thermal decomposition product was identified as cyanophosphane complex **23b** that formed via 1,2-elimination of *iso*-butene (Scheme 43). The isolation of the product is described in chapter 3.3.3.1. In 2005, Ionescu *et al.* described a similar thermal decomposition of the less thermally stable *P*-bisyl substituted *tert*-butylisocyanide-to-phosphinidene complex adduct which already emerged under ambient conditions.[104]

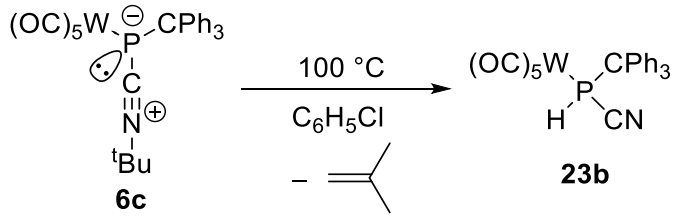

Scheme 43: Thermal decomposition of **6c** into cyanophosphane complex **23b** at 100 °C in chlorobenzene.

This difference in thermal stability of the chromium and tungsten complexes again corroborate the decreased P-donor bond strength caused by the shortening of the P-metal distance from tungsten to chromium as already indicated by the spectroscopic data of the adducts. In addition, the increased steric encumbrance at phosphorus is reducing the ability to accomplish a sufficient bending of the *tert*-butyl group to the P-center affording a 1,2-elimination of the *iso*-butene yielding complex **23b**.

The *N*-methylimidazole-to-phosphinidene complex adducts **13** behave similarly to complex **6a** under formation of white phosphorus but already at lower temperatures of around 80 °C. However, in case of **13a** an additional signal at 566.8 ppm (**27**) was observed in the VT ^{31}P{^{1}H} NMR spectra starting at 70 °C and reaching its maximum intensity at 80 °C, but fully vanished

again at 100 °C while the resonance signal of **22** reached its maximum intensity at 100 °C (Figure 32).

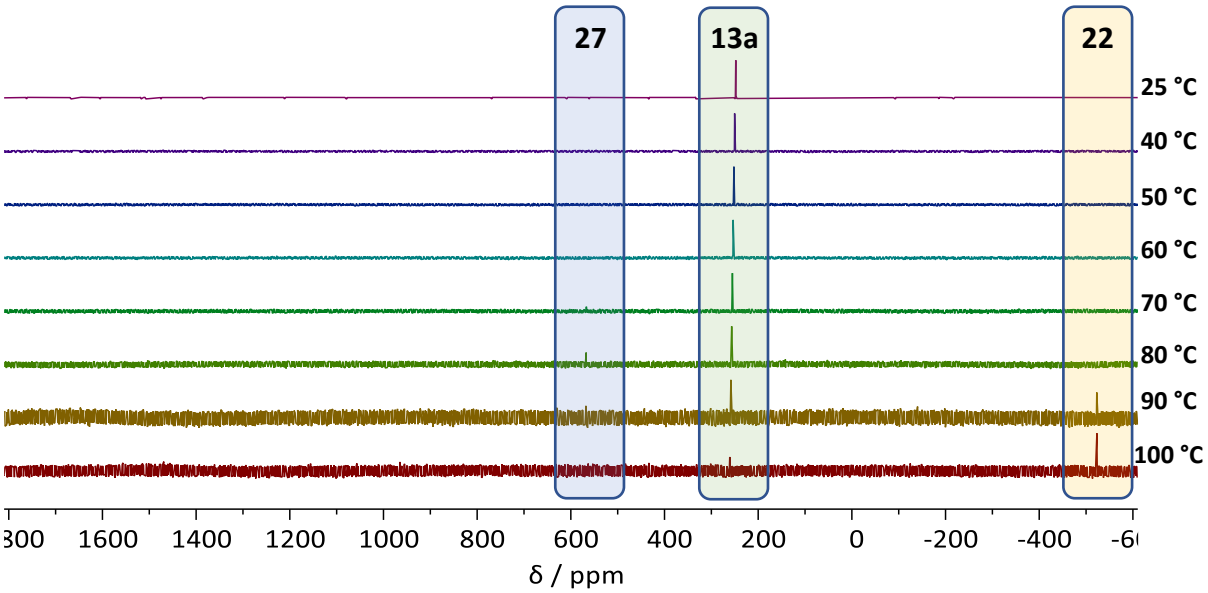

Figure 32: VT $^{31}P\{^{1}H\}$ NMR spectra (121.57 MHz, chlorobenzene) of a solution of **13a** at 25–100 °C.

The additional occurring resonance signal is characteristic for the *E*-triphenylmethyl-diphosphene (**27**) reported in 1999 by Schmutzler.[243] Hence, as first step of the thermal decomposition process of **13** the migration of the *N*-methylimidazole to the metal fragment under generation of the highly reactive transient phosphinidene **26** may occur which is then followed by immediate dimerization to obtain **27**.

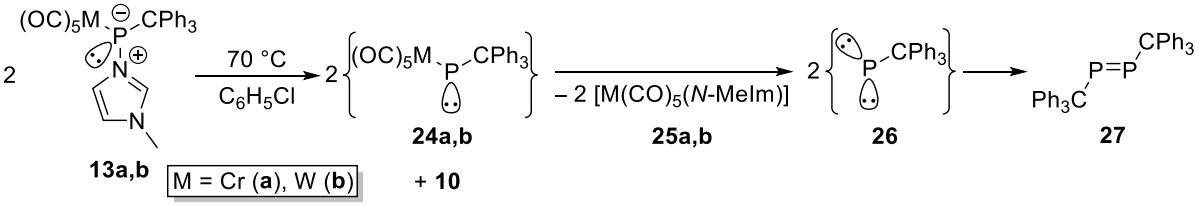

Scheme 44: Thermal decomposition of complex **13** to the diphosphene **27** via phosphinidene **26**.

Afterwards, a dimerization of the diphosphene **27** could happen followed by consecutive homolytic P-C bond cleavages to form triphenylmethyl radicals under formation of P-P bonds resulting, eventually, in the formation of white phosphorus (**22**) (Scheme 45). A similar formation of **22** was reported for the *E*-bis(pentamethylcyclopentadienyl)diphosphene via radical mechanism, but which was induced by UV irradiation.[244] Cowley described later the thermal decomposition of an unstable bis(silyl)diphosphene into the respective butterfly compound but did not observe the formation of white phosphorus.[245] A thermally induced radical cleavage of triphenylmethyl radicals from a diazadiphosphapentalene derivative under

formation of a P-P bond is described by Kornev in 2016 as a slow reaction in tetrahydrofuran at ambient conditions within two weeks that could be accelerated in refluxing toluene to two hours.[246]

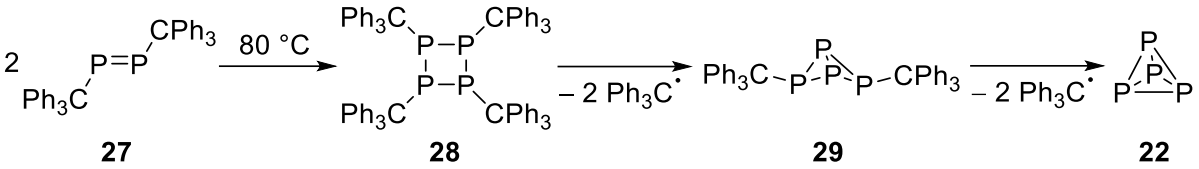

Scheme 45: Decomposition of the diphosphene **27** to white phosphorus (**22**) via the cyclotetraphosphane **28** and the P_4 butterfly compound **29**.

When a solution of complex **13a** in chlorobenzene was kept at 70 °C initially only the very slow formation of the diphosphene **27** was observed. After 48 hours, the $^{31}P\{^1H\}$ NMR spectrum showed the formation of **22** next to two triplet resonance signals which can be safely assigned to the butterfly complex **29** (−92.2 ppm (terminal), −335.5 ppm (bridgehead), $^1J_{P,P}$ = 189 Hz) (Figure 33).

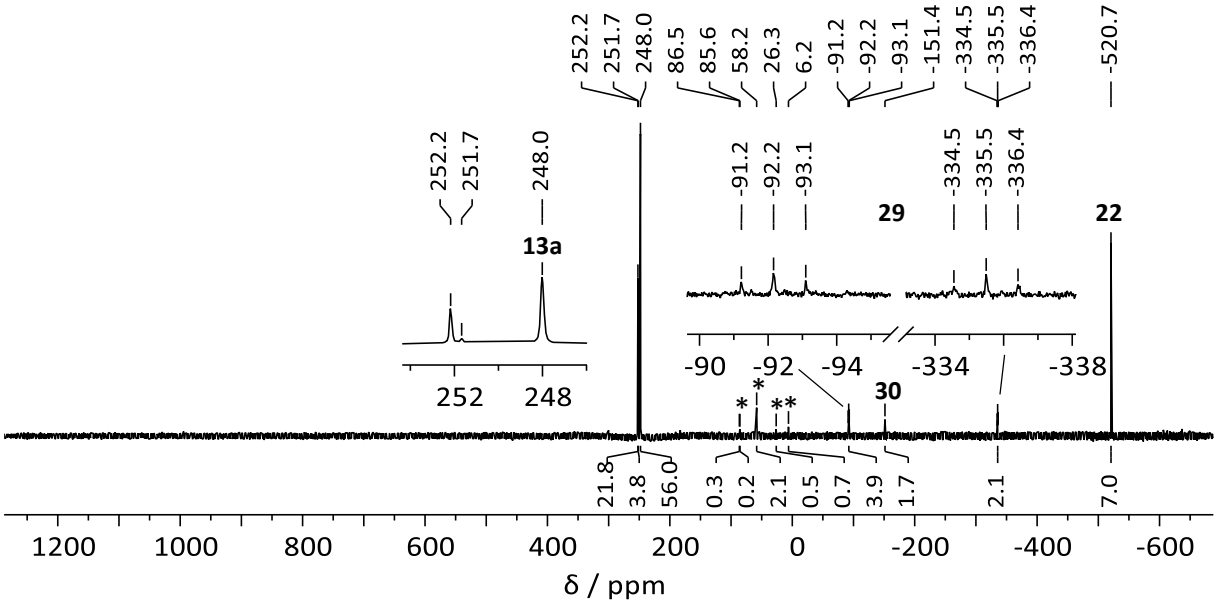

Figure 33: $^{31}P\{^1H\}$ NMR spectrum (202.48 MHz, 298 K, C_6H_5Cl) of a solution of **13a** after heating at 70 °C for 48 hours. Unidentified side products are marked with asterisks.

The resonance signals are very similar to analogous butterfly complexes (Table 12).

Table 12: ^{31}P NMR data of R_2P_4 butterfly compounds (Ar^{Dipp} = 2,6-(2,6-$^{i}Pr_2C_6H_3$)$_2C_6H_3$, Mes* = 2,4,6-$^{t}Bu_3C_6H_2$, Cp* = C_5Me_5, Cp^{BIG} = C_5(4-$^{n}BuC_6H_4$)$_5$, Cp''' = $C_5H_2{}^{t}Bu_3$, Cp^{4iPr} = $C_5H^{i}Pr_4$).

R	δ(^{31}P) / ppm *bridgehead*	δ(^{31}P) / ppm *terminal*	$^{1}J_{P,P}$ / Hz	reference
CPh_3	−335.5	−92.2	189	this work
$SiMe_3$	−333.9	−111.2	203.2	[245]
Ar^{Dipp}	−331.8	−163.0	189.2	[247]
Mes*	−272	−130	175.7	[248]
R_1 = CPh_3, R_2 = Mes*	−308.8	−105.5 (CPh_3), −127.5 (Mes*)	193.9 (CPh_3), 173.0 (Mes*)	[249]
Cp*	−369.8	−147.5	192	[244]
Cp^{BIG}	−308.2	−181.0	192	[250]
Cp'''	−307.3 – −366.0	−154.6 – −162.4	181–191	[250]
Cp^{4iPr}	−311.5 – −365.1	−134.2 – 140.8	176–180	[250]

Additionally, the formation of two broad resonances slightly downfield shifted to **13a** are observed presumably arising from ligand substitution at chromium by *N*-methylimidazole under loss of carbon monoxide. The other unidentified resonance signals (5 % by $^{31}P\{^{1}H\}$ NMR integration) likely arise from polyphosphanes as observed for similar compounds, reported by Mathey. Especially the signal at −151 ppm is characteristic for cyclotriphosphanes[251] that could occur via reaction of the diphosphene **27** with the transient phosphinidene **26** under formation of tris(triphenylmethyl)cyclotriphosphane (**30**) analogous to a similar reaction reported in 2011 by Streubel.[252] In the liquid injection field desorption (LIFDI) mass spectrum of **13a** the formation of the *N*-methylimidazole tungsten complex **25b** could be confirmed but nor **26** or its complexes **24** were observed in the mass spectra of **13**.

The thermal treatment of the DMAP adduct **14a** proceeded similarly under formation of **22** as observed in a VT NMR experiment (Figure 34). At 70 °C the formation of the diphosphene **27** and at 80 °C of the butterfly compound **29** and white phosphorus (**22**) was observed. At 90 °C the starting material **14a** was fully consumed and at 100 °C all intermediates were fully converted to **22**. However, during the study broad multiplets were observed at 170 ppm, 111 ppm and 97 ppm which were not observed before. These broad signals could belong to a branched oligophosphane due to its very similar pattern in the NMR spectra of comparable

derivatives,[253] showing a very similar signal shape of P_8R_6 phosphanes. Therefore, a tentative assignment to octaphosphane **31**, containing two cyclotetraphosphane units, is suggested.

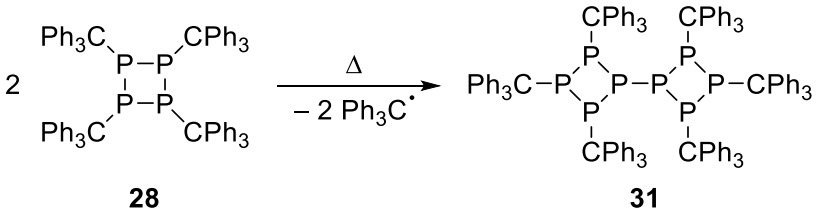

28 **31**

Scheme 46: Proposed formation of the branched octaphosphane **31**.

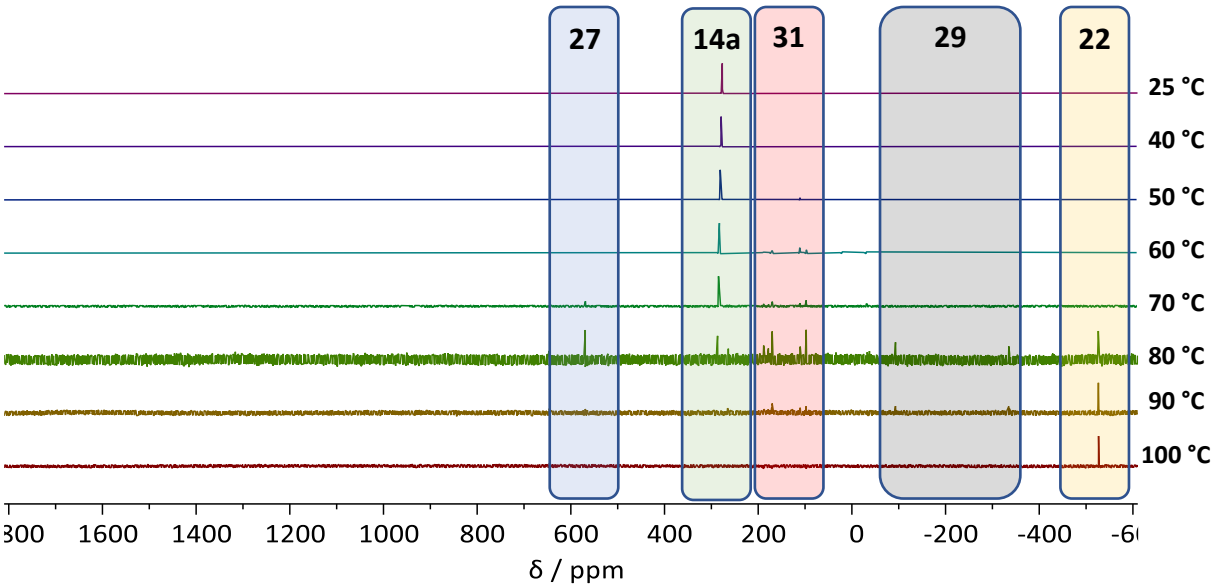

Figure 34: VT $^{31}P\{^1H\}$ NMR spectra (121.57 MHz, chlorobenzene) of a solution of **14a** at 25–100 °C.

The mass spectra of **14** again confirmed the formation of DMAP metal complexes [M(CO)$_5$(dmap)] (**32**) (M = Cr: m/z 314.0; W: m/z 446.0). Additionally, the formation of the free phosphinidene **26** (m/z 274.0) as well as the electrophilic, terminal phosphinidene tungsten complex **24b** (m/z 598.0) were identified in the electron impact ionization (EI) mass spectrum of **14b**.

3.3.1.2 Trapping reactions of transient electrophilic species

Phosphinidene **26** and its complexes **24a,b** were identified spectroscopically only in the gas phase via EI mass spectrometric experiments due to their high reactivity in condensed phase. Thus, additional clear-cut trapping experiments with apolar π-systems *videlicet* alkenes and butadiene were performed. It should be noted that such trapping reactions are of signature quality for electrophilic phosphinidene complexes and have been reported in

several cases, *e.g.* with alkenes[64] including ethylene,[254] alkynes,[58] methylene-cycloalkanes,[254] norbornadiene,[255] acrylic esters[64] and conjugated dienes.[64,256,257] As the first step of reactions with dienes the formation of 2-vinylphosphirane complexes via [1+2] cycloaddition is reported, which can rearrange thermally via a concerted [1,3] sigmatropic shift to give the phosphole complexes as formal [1+4] cycloaddition products.[256]

In the present study, first reactions with alkenes were investigated. Solutions of *N*-methylimidazole-to-phosphinidene complex adducts **13** in benzene were heated to 70 °C in the presence of ethylene (1 atm) (**33**), 1-pentene (10 eq.) (**34**) and 1-hexene (10 eq.) (**35**) which led to the clean formation of the respective phosphirane complexes **36–38** (Scheme 47).

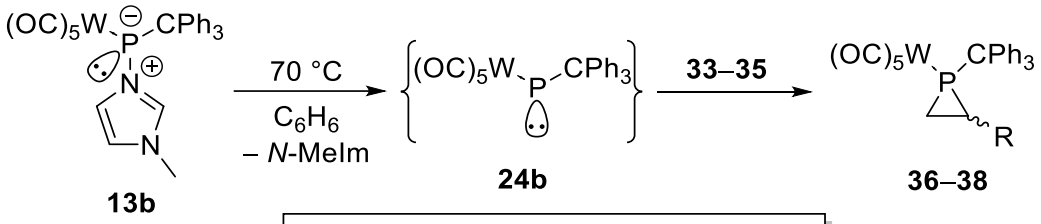

Scheme 47: Synthesis of phosphirane complexes **36–38** via trapping reactions of the electrophilic, terminal phosphinidene complex **24b** with ethylene (**33**), 1-pentene (**34**) and 1-hexene (**35**).

Compared to analogous *P*-phenyl and *P*-methyl substituted derivatives, the the ^{31}P NMR resonance signals of the phosphirane complexes **34–36** are downfield-shifted, a trend which was already observed for the terminal phosphorus of the butterfly compound **27**.

Table 13: ^{31}P NMR data of phosphirane complexes **36–38** and selected derivatives.

R	*P*-substituent	δ(^{31}P) / ppm	$^{1}J_{W,P}$ / Hz	Reference
H	CPh_3	−167.4	257.2	this work
H	Me	−199.3	254.1	[258]
H	Ph	−187.6	257.5	[254]
H	NEt_2	−111	278	[59]
^{n}Pr	CPh_3	−137.7 [−145.4]	259.8 [259.8]	this work
^{n}Pr	NCy_2	−133.1 [−140.0]	287.0 [281.8]	[97]
^{n}Bu	CPh_3	−137.4 [−145.5]	258.9 [260.2]	this work
^{n}Bu	Ph	−166.2 [−166.7]	257	[64]
^{n}Bu	NEt_2	−90.8 [−92.4]	278 [273]	[59]
^{n}Bu	NCy_2	−134.7 [−135.6]	287.6 [281.8]	[97]

Phosphirane complexes **37** and **38** were obtained as oils after column chromatography containing two isomers in a ratio of 31:69 and 36:46, respectively. Unfortunately, complex **36** could not be separated from minor side products via column chromatography. For **38** the ^{1}H NMR spectrum displayed a complicated set of resonance signals for the *n*-butyl group and the ring-protons due to the existence of two diastereomers (Figure 35). Nevertheless, all signals could be assigned correctly via 2D NMR experiments.

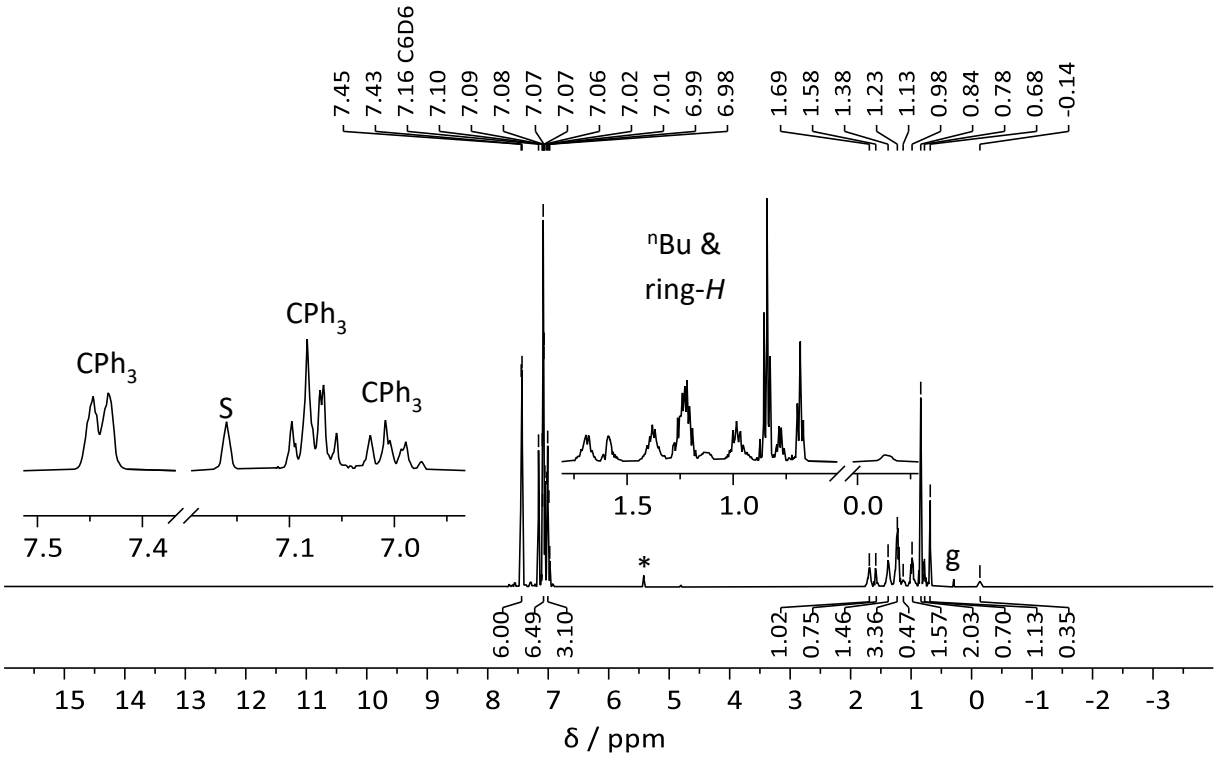

Figure 35: ^{1}H NMR spectrum (500.04 MHz, 298 K, C_6D_6) of phosphirane complex **38**. The resonance of traces of triphenylmethane is marked with an asterisk and of grease with a "g". The residual resonance signal of the deuterated solvent is marked with an "S".

Additionally, the diastereomers could be assigned via a ^{1}H,^{1}H 2D nuclear Overhauser effect spectroscopy (NOESY) experiment. The main isomer was identified as *trans*-phosphirane complex and the minor isomer as *cis*-phosphirane complex which can be explained by the steric repulsion of the triphenylmethyl and *n*-butyl substituents.

The mechanism was also studied computationally by Espinosa Ferao using the *P*-^{t}Bu substituted model complex **13b^{tBu}**.[216] In case of the formation of phosphirane complex **36^{tBu}** no transition state was found for the direct replacement of *N*-methylimidazole by ethylene (**33**) at phosphorus. Therefore, a two-step process consisting of an initial, moderately endergonic barrierless dissociation (ΔG_{comp} = 13.26 kcal/mol) of the ligand, followed by a barrierless rather exergonic chelotropic cycloaddition ($\Delta\Delta G$ = −35.8 kcal/mol) of the resulting

terminal phosphinidene complex with the C=C double bond was assumed. Interestingly, a low barrier was found for the case of *P*-amino substituted phosphinidene complexes.[97]

The terminal phosphinidene complex **24b** could also be trapped by 2,3-dimethyl-butadiene starting from the imidazole adduct **13b** in benzene and heating at 70 °C under formation of the 2,5-dihydro-1*H*-phosphole complex **39** (Scheme 48). Surprisingly, complex **39** could not be isolated using column chromatography and the product could only be obtained via crystallization from the reaction mixture.

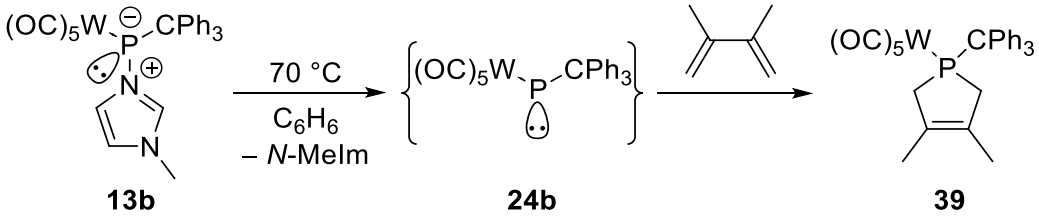

13b **24b** **39**

Scheme 48: Synthesis of 2,5-dihydro-1*H*-phosphole complex **39** via trapping reactions of the electrophilic, terminal phosphinidene complex **24b** with 2,3-dimethylbutadiene.

The ^{31}P NMR resonance signal (δ = 30.1 ppm) is slightly downfield shifted compared to similar derivatives (Table 14) being analogous to complexes **36–38**.

Table 14: ^{31}P NMR data of 2,5-dihydro-1*H*-phosphole complex **39** and selected derivatives.

***P*-substituent**	**δ(^{31}P) / ppm**	**$^{1}J_{W,P}$ / Hz**	**Reference**
CPh_3	30.1	241.8	this work
Ph	−3.2	—	[58]
$CH(CH)_2CH_2$	−12.1	—	[259]
Fc	−15.7	232	[260]
NEt_2	67.6	254	[59]
COOMe	4.2	222.6	[261]
CH_2Cl	1.5	239	[262]
Cl	103.6	264	[263]

The molecular structure of **39** was confirmed by single crystal X-ray diffraction analysis. The molecular structur reveals an angular sum at phosphorus of 308.96(38)° for the ligand only. The first value is close to the ideal angular sum of a tetrahedral geometry (Figure 36).

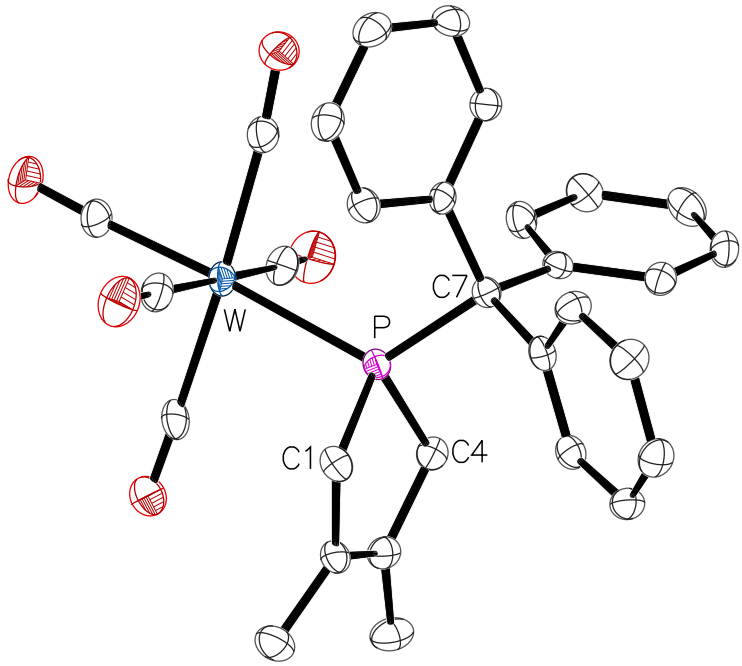

Figure 36: Molecular structures of **39** in the single crystal lattice at 123(2) K. Thermal ellipsoids are set at 50 % probability level. Hydrogen atoms were omitted for clarity. Selected bond lengths / Å and bond angles / °: W-P 2.5576(10), P-C1 1.856(3), P-C4 1.852(3), P-C7 1.929(3), C1-P-W 109.01(10), C1-P-C7 108.72(12), C4-P-W 111.48(9), C4-P-C1 93.68(13), C4-P-C7 106.56(13), C7-P-W 123.33(8).

3.3.2 Donor substitution reactions

Considering the ligand dissociation as typical feature of transition metal complexes, a potentially similar reactivity of donor-to-phosphinidene complex adducts was examined. At ambient conditions no dissociation of the donor-phosphorus bond in the *N*-methylimidazole-to-phosphinidene complex adducts **13** were observed generating the transient highly reactive phosphinidene complex **24**. Hence, no reaction with apolar π-systems such as alkenes, mentioned beforehand, was observed at ambient temperature. However, when stronger donors were added to a solution of **13** substitution reactions were already observed at ambient temperature (Scheme 49).

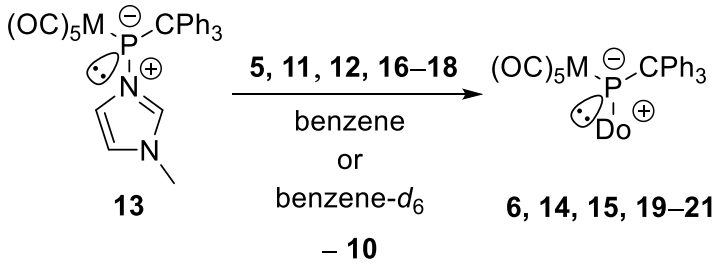

Scheme 49: *P*-donor substitution reactions at the *N*-methylimidazole-to-phosphinidene complexes **13**.

Ligand substitution reactions were computationally studied by Espinosa Ferao using the *P*-^{t}Bu substituted model complex **13b^{tBu}**.[216] The exchange reaction with methyl isocyanide exergonically furnishes the new model adduct complex **6c^{tBu}** ($\Delta\Delta G^{\ddagger}$ = 20.6 kcal/mol; $\Delta\Delta G$ = −6.9 kcal/mol).

Interestingly, the reaction of the *N*-methylimidazole-to-phosphinidene complex adduct **13b** with *N*-heterocyclic carbenes (NHCs) showed no clean conversion but somehow a higher selectivity than for the reaction with the Li/Cl phosphinidenoid complex. For the latter, no distinct main products were assignable. After stirring complex **13b** with 1.3 equivalents of 1,3,4,5-tetramethylimidazol-2-ylidene (IMe_4) in benzene-d_6 for 1.5 hours under ambient conditions adduct complex **40** was observed, but still 64 % of the starting material were left unreacted (Scheme 50). The ^{31}P NMR spectrum revealed a resonance signal at −38.3 ppm ($^{1}J_{W,P}$ = 116.9 ppm) for the main product (**40**) (Figure 37). The small $^{1}J_{W,P}$ coupling constant is very indicative for an increased electron density at phosphorus as before commonly observed for the adduct structures.

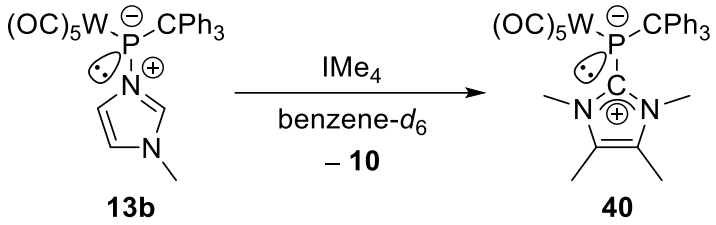

Scheme 50: Substitution reaction at the *N*-methylimidazole-to-phosphinidene complex **13b** with IMe_4.

Although complex **40** was already proposed before as minor product (6 % content in a reaction mixture) when dichlorophosphane complex **1c** had reacted with two equivalents of IMe_4, but in a former report[85] the assigned ^{31}P NMR resonance at −121.9 ppm ($^{1}J_{W,P}$ = 132.5 Hz) was not further confirmed. However, the ^{31}P NMR spectrum of the isolated and fully characterized respective *P*-bisyl substituted complex revealed a signal at −128.5 ppm ($^{1}J_{W,P}$ = 100.1 Hz).[85]

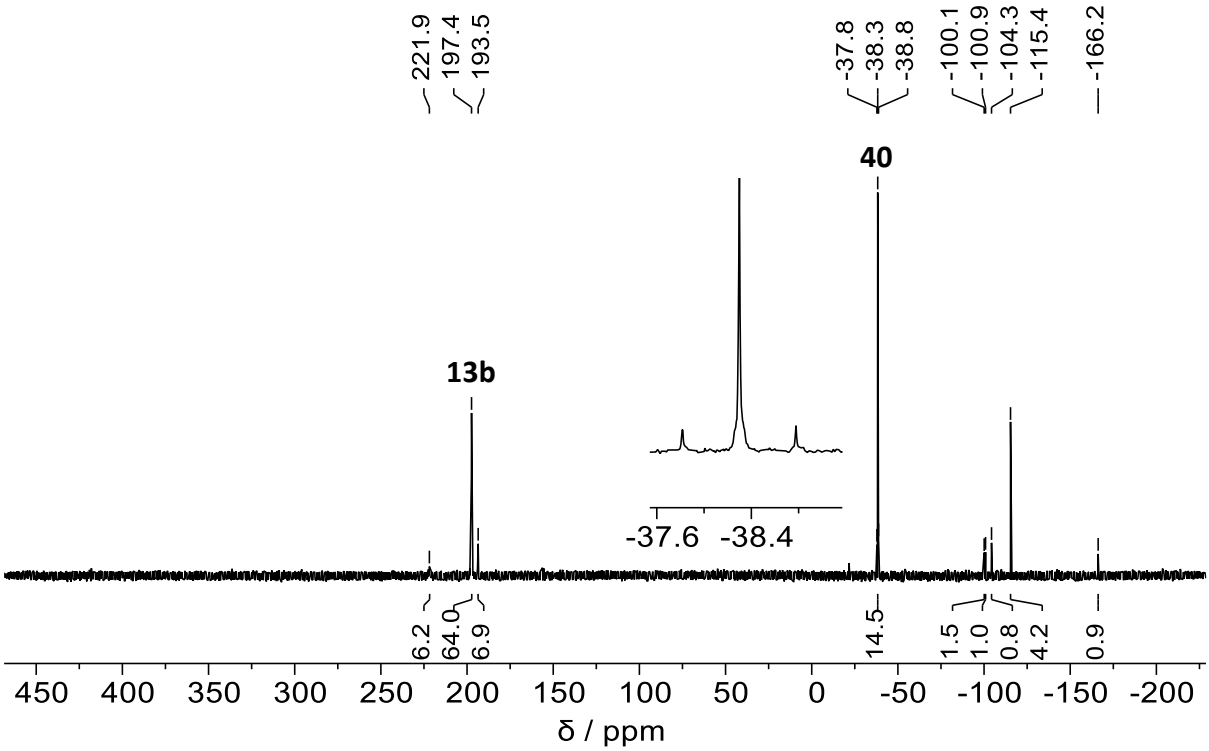

Figure 37: $^{31}P\{^{1}H\}$ NMR spectrum (121.51 MHz, 298 K, C_6D_6) of the reaction mixture of **13b** with IMe_4.

Having the background of the new results such a minor shift upon changing the *P*-substituent is suspicious, somehow, especially in case of a C-donor-to-phosphinidene complex, *e.g.* the *P*-bisyl substituted *tert*-butylisocyanide-to-phosphinidene complex adduct resonates at −136.6 ppm ($^{1}J_{W,P}$ = 194.5 Hz)[104] while the *P*-CPh_3 substituted adduct **6c** is found at −50.0 ppm ($^{1}J_{W,P}$ = 117.7 ppm)[103] and, hence, a downfield shift of 86.6 ppm was confirmed. Therefore, the here observed ^{31}P NMR chemical shift of −38.3 ppm for **40** seems to be much more reasonable and, hence, to be the correct value. Unfortunately, further stirring at ambient conditions led to an unselective progress and a decomposition of complex **40** within one day.

In contrast, reactions of **13b** with 2,3-bis(2,4,6-trimethylphenyl)imidazol-2-ylidene (IMes) or 1-(2,6-diisopropylphenyl)-3,3,5,5-tetramethylpyrrolidin-2-ylidene (Me_2cAAC) led to unselective reactions showing only non-complexed P-containing compounds in the ^{31}P NMR spectra.

3.3.3 Studies on the nucleophilic character of P-adduct complexes

Various transition metal complexes show a distinct nucleophilic character of the metal center,[264] *e.g.* the Brønsted-Lowry basicity with the pioneering work of Dessy, Pohl and King in 1966[265] as starting point of extensive investigations on such reactivities which is still an active research topic *inter alia* on transition metal hydrides.[266]

3.3.3.1 Reactions with Lewis acids

The nucleophilic character of the donor-to-phosphinidene complex adducts are determined by the availability/reactivity of the free electron pair at phosphorus. To probe this complex **13** was treated firstly with two labile tungsten complexes: $[W(CO)_5(NCMe)]$ (**41**) and $[W(CO)_5(thf)]$ (**42**) (Scheme 51).

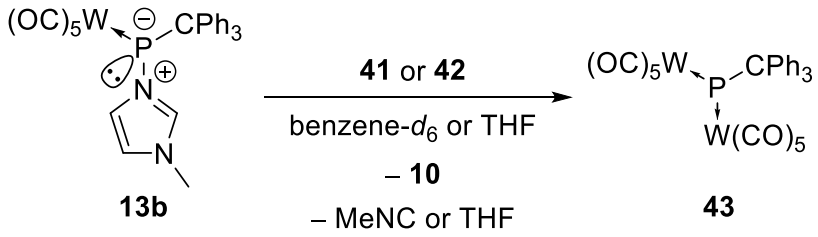

Scheme 51: Second complexation of **13** to a pentacarbonyltungsten(0) fragment under loss of the imidazole **10**.

Upon addition of **42** to **13** in benzene-d_6 a deep violet solution formed within a few minutes. The $^{31}P\{^1H\}$ NMR spectra revealed only a marginal conversion to **43** at ambient conditions with a maximum content of 3.6 % (via $^{31}P\{^1H\}$ NMR integration) after six hours showing a signature resonance signal at 811.2 ppm before it diminished and then vanished completely after three days under ambient conditions. Performing the reaction with freshly prepared **42** in tetrahydrofuran after one hour under ambient conditions still 46 % of complex **13** had not reacted (Figure 38). The main product **43** (content in the reaction mixture: 22 % via $^{31}P\{^1H\}$ NMR integration) was tentatively identified as dinuclear complex **43** at 791.5 ppm ($^1J_{W,P}$ = 185.0 Hz). However, also four further resonance signals were observed in the $^{31}P\{^1H\}$ NMR spectrum at 247.0 ppm (4 %), 182.2 ppm (9 %, $^1J_{W,P}$ = 193.9 Hz), 150.4 ppm (11 %, $^1J_{W,P}$ = 192.3 Hz) and 69.9 ppm (9 %, $^1J_{P,H}$ = 371.9 Hz, $^1J_{W,P}$ = 274.7 Hz). An *in situ* UV/vis spectrum (appendix, Figure 154) of the reaction mixture of complex **13b** with **41** in THF containing **43** showed a characteristic absorption at 540 nm which was assigned to a transition in the W-P-W π system.

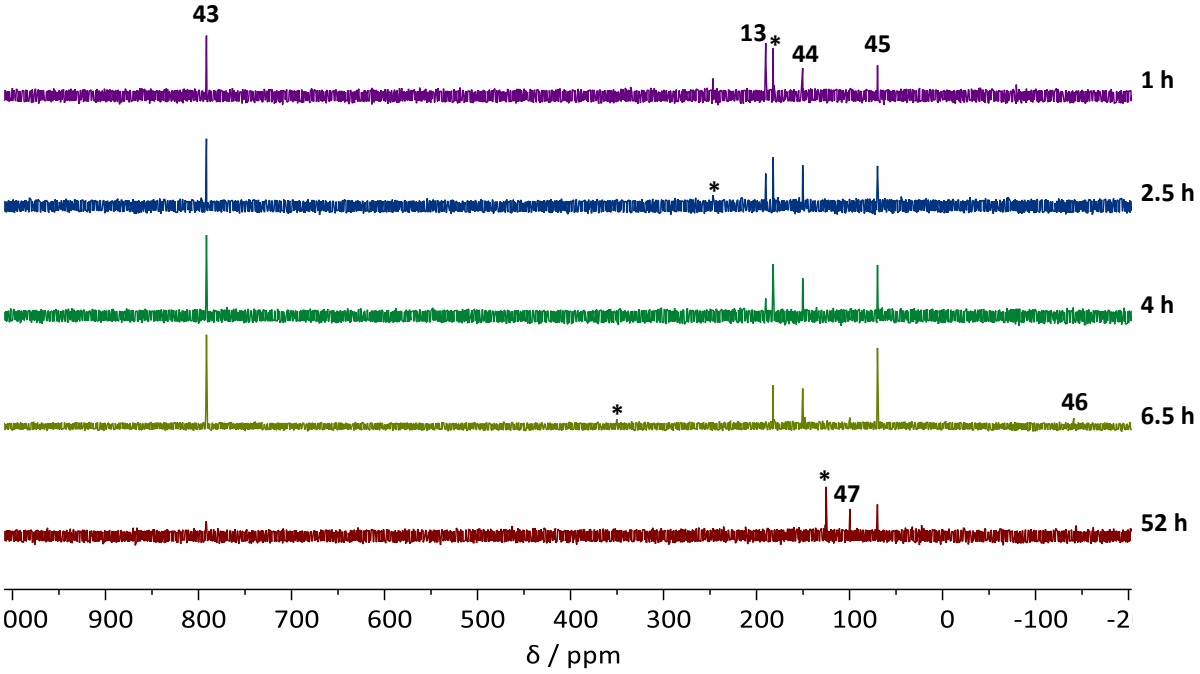

Figure 38: $^{31}P\{^{1}H\}$ NMR spectra (121.51 MHz, 298 K, THF) of the reaction mixture of complex **13** with **42** at various time steps of the reaction progress. Unidentifiable side products were marked with asterisks.

The dinuclear complex **43** is similar to dinuclear phosphinidene complexes described earlier by Huttner and Jutzi; the NMR parameters are of those are compiled on Table 15.[267–269]

Table 15: ^{31}P NMR and UV data of dinuclear phosphinidene complexes $[M_2(CO)_{10}(PR)]$.[267–269]

M	R	$\delta(^{31}P)$ / ppm	$^{1}J_{W,P}$ / Hz	color	λ_1 / nm (UV)	reference
W	CPh_3	791.5	185.0	deep violet	540	this work
Cr	Mes	1216	—	deep blue	584	[267]
W	Mes	961	176.4	deep blue	557	[267]
W	Bis	—	—	deep red	—	[267]
Cr	Cp*	1331	—	deep blue	605	[268]
W	Cp*	1074	177	deep blue	575	[268]
Cr	^{t}Bu	1362	—	deep blue	617	[269]

Dinuclear phosphinidene complexes either have a trigonal pyramidal geometry at phosphorus which can be viewed as doubly metallated phosphane (*e.g.* $[Pt_2(dippe)_2(\mu\text{-}PPh)]$ (dippe = 1,2-bis(diisopropylphosphino)ethane)) or a trigonal planar geometry which can be viewed as classical μ_2-bridged phosphinidene (*e.g.* $[W_2(\mu\text{-}PCp^*)(CO)_{10}]$).[270] DFT caluclations on complex **43** by Espinosa Ferao ($CPCM_{tol}$/B3LYP-D3/def-TZVP(ecp)) revealed a structure with a trigonal planar geometry with a sum of angles at phosphorus of 359.6°.

As first step the formation of the dinuclear *N*-methylimidazole-to-phosphinidene complex **44** is assumed which upon dissociation of the P-N bond formed **43**. The resonance signal at 150.4 ppm was assigned to **44** due to its broadened shape very similar to the one of **13** due to the hindered P-N rotation (Scheme 52). N-donor to dinuclear organyl phosphinidene complex adducts were already reported by Huttner in the 1980s, but unfortunately no ^{31}P NMR data were given and only the color change from blue to yellow was mentioned.[269,271]

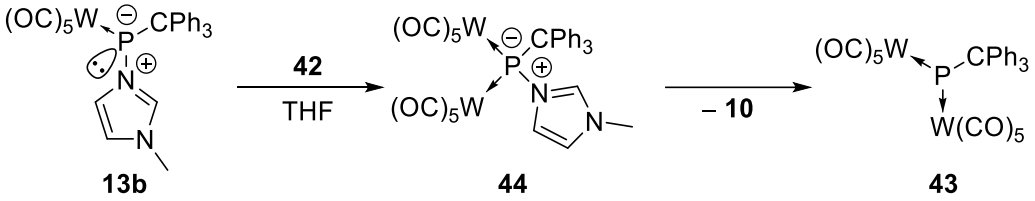

Scheme 52: Second metal complexation of **13b** via the proposed intermediate **44**.

The ^{31}P NMR spectrum of the reaction mixture has shown also a resonance at 69.9 ppm appearing as doublet which displayed the formation of a P-H bond. The formal C^2-H insertion product **45** (Scheme 53), resulting from the C^2-H activation of the dissociated *N*-methylimidazole (**10**) by complex **42,** could fit well to this resonance signal. Additionally, an analogous non-complexed benzimidazolyl(*tert*-butyl)phosphane has been reported by Kostyuk in 2012.

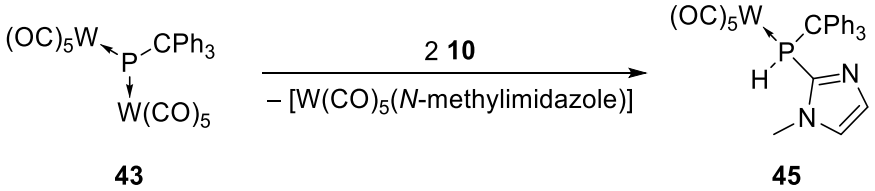

Scheme 53: Proposed formation of the imidazolyl(triphenylmethyl)phosphane complex **45**.

After 6.5 h complex **13** was fully consumed and **43** reached its maximum content in the reaction mixture. Additionally, two further signals with very low intensities appeared at 350.2 ppm (2 %) and −141.1 ppm (1 %). The latter is characteristic for phosphirane complexes (cf. chapter 3.3.1.2). Hence, the reaction of the transiently formed phosphinidene complex **24b** may have reacted with the backbone of the *N*-methylimidazole under formation of phosphirane complex **46** (Scheme 54).

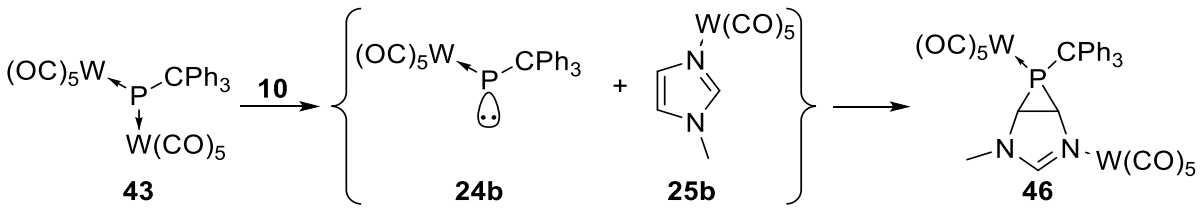

Scheme 54: Possible formation of the bicyclic phosphirane complex **46**.

After 52 hours new resonance signals emerged at 125.2 ppm (63 %, $^{1}J_{W,P}$ = 190.7 Hz) and 99.6 ppm (9 %, $^{1}J_{P,H}$ = 347.9 Hz, $^{1}J_{W,P}$ = 268.8 Hz) while the signal of **44** as well as the one at 182.2 ppm had vanished and the integrals of the signals of **43** and **45** decreased to 8 % and 20 %, respectively. The new signal at 99.6 ppm arose from the hydroxy(triphenylmethyl)phosphane complex **47** resulting from hydrolysis which was confirmed by the synthesis and isolation of complex **47b** (see chapter 3.3.3.2).

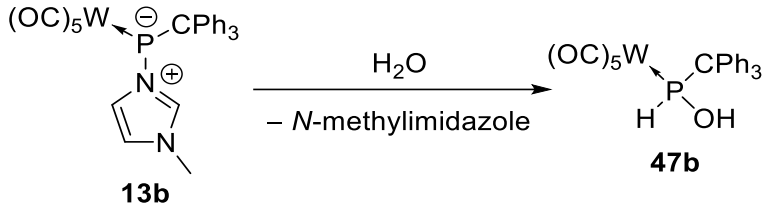

Scheme 55: Hydrolysis of complex **13b**.

Going from a transition metal Lewis acid to a metalloid Lewis acid, namely tris(pentafluorophenyl)borane (**48**) a similar reactivity is expected (Scheme 56).

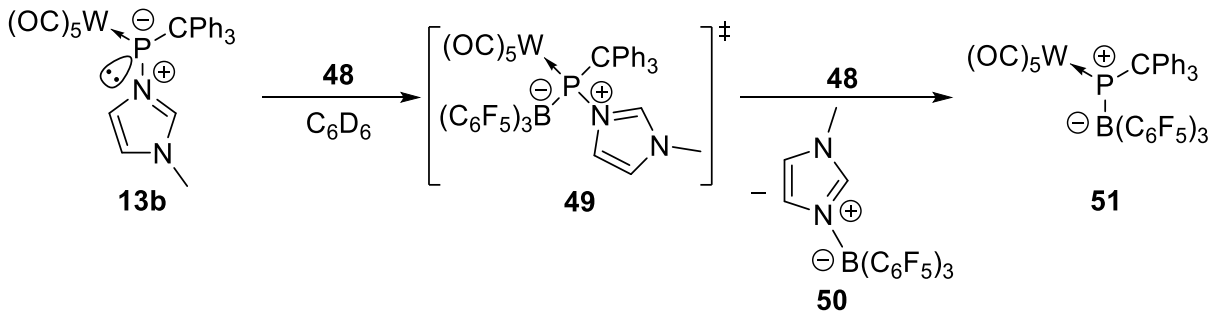

Scheme 56: Proposed formation of the phosphinidene complex borane adduct **51**.

When a slight excess (1.1 equivalents) of tris(pentafluorophenyl)borane (**48**) is added to **13** in benzene-d_6 under ambient conditions the reaction solution turned deep turkey-blue within 20 minutes. An *in situ* UV/vis spectrum of the reaction mixture (appendix, Figure 155) revealed an absorption at 578 nm which is in accordance to the observed color and differs significantly from the tris(pentafluorophenyl)borane radical anion (λ_{max} = 603 nm). Hence, the formation of the radical anion via a single electron transfer (SET) from complex **13b** to **48** is unlikely.[272] The $^{31}P\{^{1}H\}$ NMR spectrum of the reaction mixture that was measured immediately after the addition of **48** showed solely the formation of a compound with a resonance at −132.8 ppm ($^{1}J_{W,P}$ = 260.3 Hz) next to the unreacted starting material **13** (2 % conversion according to $^{31}P\{^{1}H\}$ NMR integration) (Figure 39). This signal is very similar to the one of **46** and thus expecting the analogous phosphirane complex **52** as formed product (Scheme 57). The strongly deshielded ^{31}P NMR resonance at 1040.3 ppm ($^{1}J_{W,P}$ = 180.1 Hz) is

assigned to the phosphinidene complex borane adduct **51** analogous to the dinuclear complex **43** which was found. Complex **51** would represent the first example ever of a μ_2-phosphinidene ligand bridging a transition metal and a metalloid center.

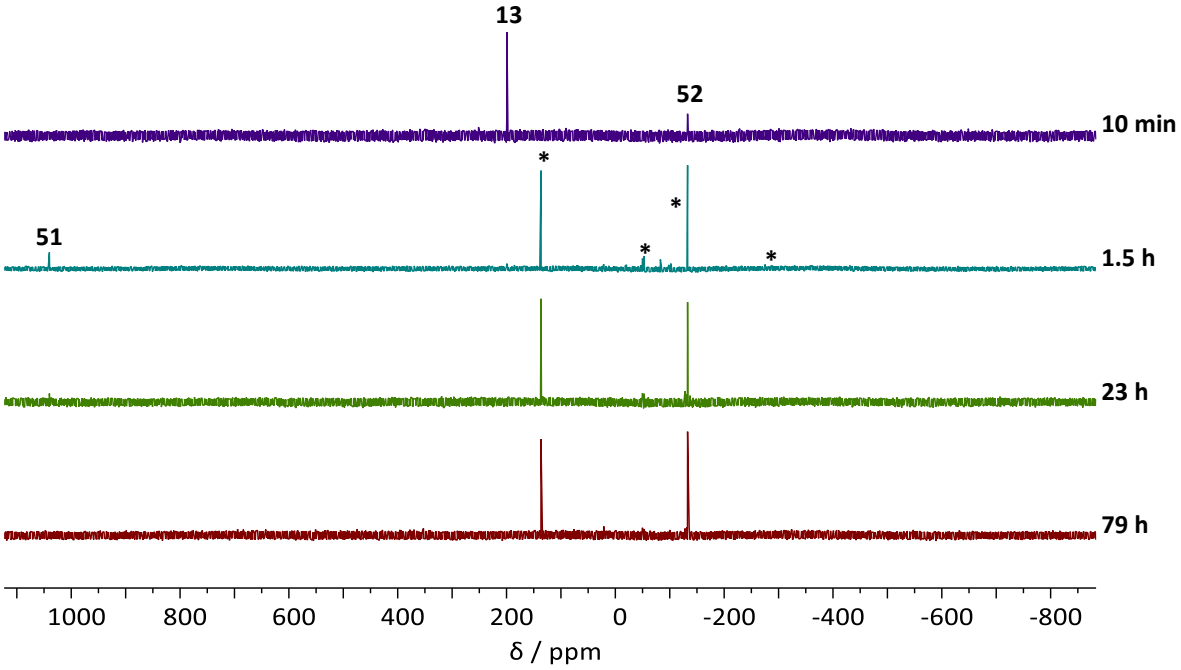

Figure 39: $^{31}P\{^1H\}$ NMR spectra (121.51 MHz, 298 K, C_6D_6) of the reaction mixture of complex **13** with **48** at various time steps of the reaction progress.

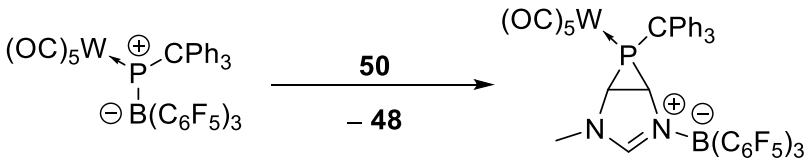

51 **52**

Scheme 57: Proposed formation of the phosphirane complex borane adduct **52**.

To enhance the formation of complex **51** a larger excess (3.4 equivalents) of the borane **48** was added to **13** to accelerate the reaction progress to the desired product **51**. The best outcome was obtained when the starting material **13** was fully consumed and stirring for 6.5 h at ambient temperature (Figure 40). Unfortunately, the high reactivity of the phosphinidene complex borane adduct **51** towards the side product **50** hindered its selective formation and isolation. Despite that the phosphirane complex **52** was formed as main product it could, unfortunately, not be isolated.

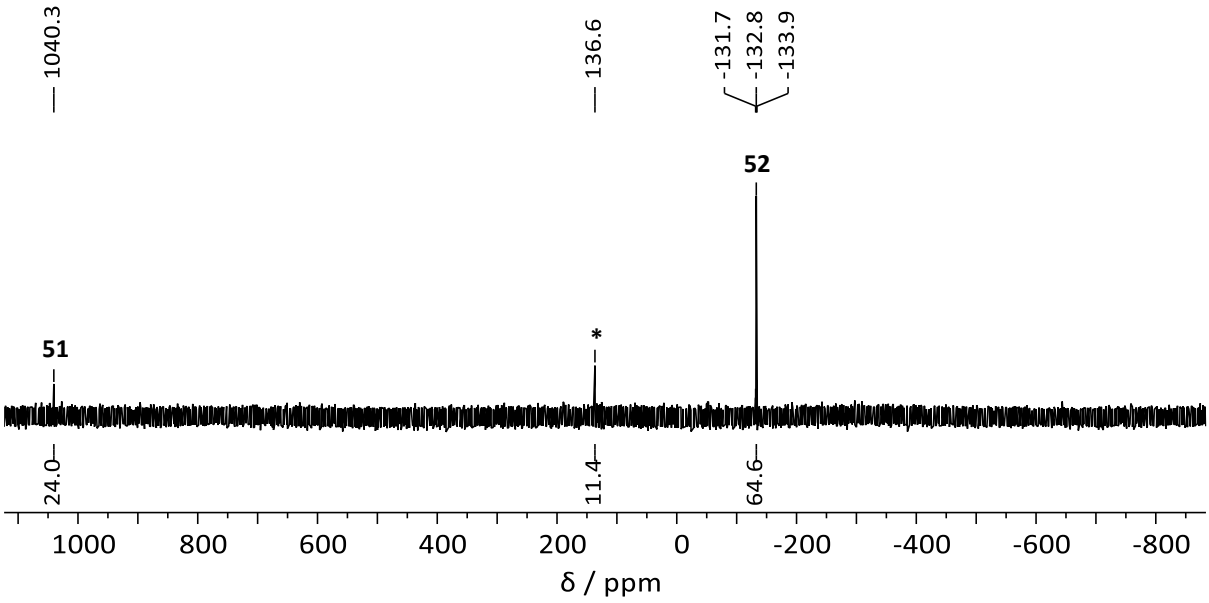

Figure 40: $^{31}P\{^{1}H\}$ NMR spectrum (121.51 MHz, 298 K, C_6D_6) of the reaction mixture of complex **13** with an excess of borane **48** after 6.5 h.

To achieve the formation of a borane adduct, possessing a higher stability, the idea came up to reduce significantly the steric bulk while still having a strong Lewis acidity. Therefore, the reaction of the *N*-methylimidazole-to-phosphinidene complex **13b** with the borane dimethylsulfide adduct (**53**) was tackled in the next experiment. The reaction proceeded smoothly under selective formation of the *N*-methylimidazole-to-*P*-stabilized phosphinidene complex borane adduct **54** (Scheme 58) and although the product was thermally unstable, it could be isolated via precipitation by slowly adding *n*-pentane to the reaction mixture and washing with *n*-pentane at −20 °C (or below). Additionally, the timespan of drying *in vacuo* (<0.02 mbar) at ambient temperature had to be reduced to a minimum.

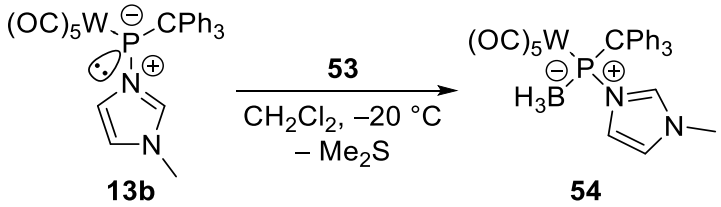

Scheme 58: Synthesis of the *N*-methylimidazole-to-*P*-stabilized phosphinidene complex borane adduct **54**.

Complex **54** showed a remarkably low solubility in all common organic solvents. Nevertheless, it was possible to obtain NMR spectra with a relatively low signal-to-noise ratio when dichloromethane-d_2 was used as solvent. The ^{31}P resonance signal of **54** was found at 163.5 ppm, highfield shifted compared to **13b** (no $^{1}J_{P,B}$ coupling constant could be determined because of the broadness of the resonance signals). Due to the borane adduct formation, the

rotation about the P-C bond was hindered and the *ortho*-CH groups differed significantly for each phenyl group (Figure 41).

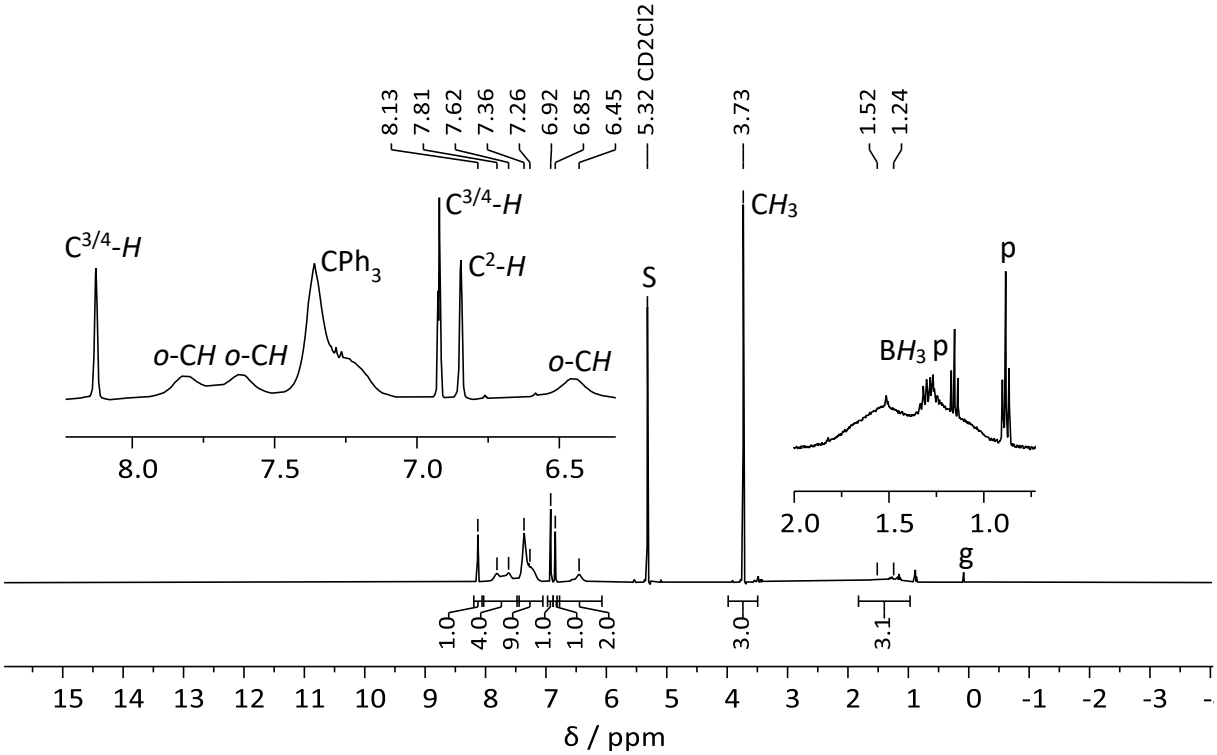

Figure 41: ^{1}H NMR spectrum (400.13 MHz, 298 K, CD_2Cl_2) of complex **54**. The resonance of traces of *n*-pentane is marked with a "p" and of grease with a "g". The residual resonance signal of the deuterated solvent is marked with an "S".

The BH_3 protons were found as very broad doublet between 1.24 ppm to 1.52 ppm. Complex **54** showed a resonance at −24.9 ppm as singlet signal in the ^{11}B NMR spectrum. Unfortunately, again the $^{1}J_{P,B}$ coupling constant could not be determined due to the broadness of the resonances signals.

In the ATR FTIR spectrum of complex **54** a band in the expected range, *i.e.*, at 2402 cm^{-1}, was found for the valence vibration of the B-H bond. Due to the low thermal stability of **54** no elemental analysis of the solid was possible but the molecular mass of the product was confirmed via high resolution mass spectrometry (HRMS) using the atmospheric pressure chemical ionization (APCI) method. Furthermore, single crystals were obtained from a concentrated solution in dichloromethane-d_2 at −40 °C that were suitable for an X-ray diffraction analysis; the molecular structure is shown in Figure 42.

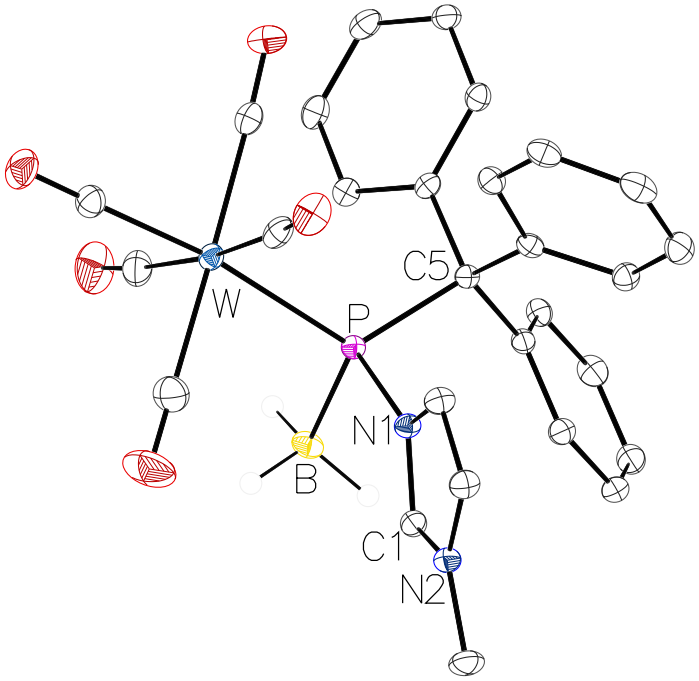

Figure 42: Molecular structure of **54** in the single crystal lattice at 100(2) K. Thermal ellipsoids are set at 50 % probability level. Hydrogen atoms and solvent molecules were omitted for clarity, except those bound to the boron atom. Selected bond lengths / Å and bond angles / °: W-P 2.5688(5), P-C5 1.9540(19), P-N1 1.8138(16), P-B 1.959(2), N1-P-W 107.17(5), N1-P-C5 101.73(8), N1-P-B 100.26(9), C5-P-W 121.14(16), C5-P-B 111.77(9), B-P-W 111.89(7).

The obtained molecular structure disclosed a slightly elongated P-CPh_3 bond of 1.9540(19) Å as expected due to the increased steric demand. The angular sum at phosphorus is 313.76(26)° being slightly smaller than the angular sum expected for a tetrahedral geometry. However, the repulsion of the sterically demanding triphenylmethyl substituent and the pentacarbonyl-tungsten fragment leads to an increased C5-P-W angle of 121.14(16)° and an decreased N1-P-B angle of 100.26(9)°.

Complex **54** reacted under ambient conditions in the solid state to yield a P-H containing compound, and if a reduced pressure was applied at ambient temperature the process was accelerated significantly. Nonetheless, after 12 hours under the aforementioned conditions still no full conversion was observed, but when dissolved in THF and heated to 60 °C the rearrangement reaction was completed within one day (Scheme 59).

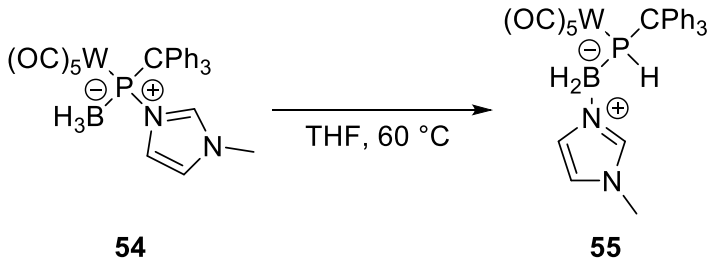

54 **55**

Scheme 59: Thermal rearrangement of adduct **54** in tetrahydrofuran to form complex **55**.

A strong highfield shift was observed in the ^{31}P NMR spectrum going from **54** to **55** revealing a resonance at −42.6 ppm ($^{1}J_{P,H}$ = 249.6 Hz, $^{1}J_{P,B}$ = 49.2 Hz). In the ^{1}H NMR spectrum the borane protons showed broad resonance with an integral of 2 protons, thus, indicating the formation of a B-H insertion product (Figure 43).

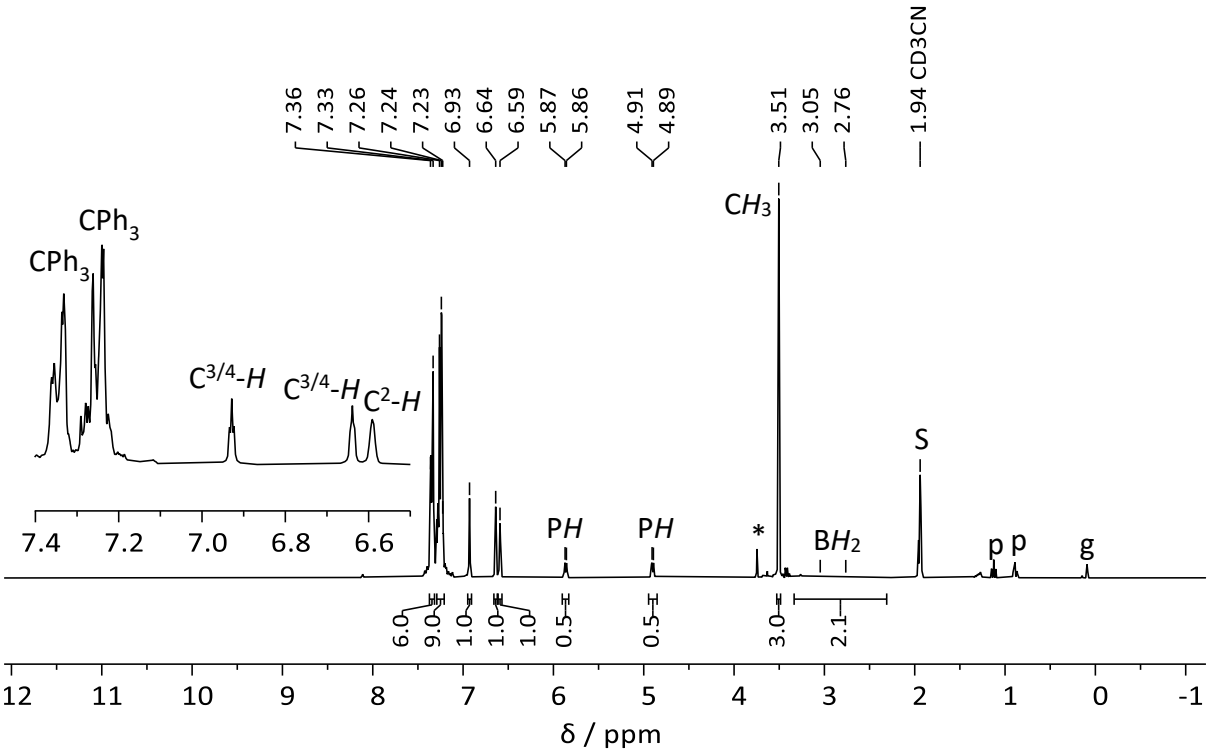

Figure 43: ^{1}H NMR spectrum (300.13 MHz, 298 K, CD_3CN) of complex **55**. The resonance of traces of an unkown side product is marked with an asterisk, of *n*-pentane with a "p" and of grease with a "g". The residual resonance signal of the deuterated solvent is marked with an "S".

At 5.38 ppm ($^{1}J_{P,H}$ = 289.04 Hz, $^{2}J_{B,H}$ = 4.40 Hz) the P*H* proton was observed showing a small coupling constant to the ^{11}B nucleus. Additionally, still the protons of the *N*-methylimidazole were present which portend the presence of an *N*-methylimidazole adduct. The loss of steric pressure due to migration of the *N*-methylimidazole to the borane the rotation about the P-C bond was again freely possible at ambient conditions and, thus, the *ortho*-CH protons of the phenyl groups were equivalent. The decomposition product was further confirmed by an APCI-HRMS and a single crystal X-ray diffraction analysis (Figure 44).

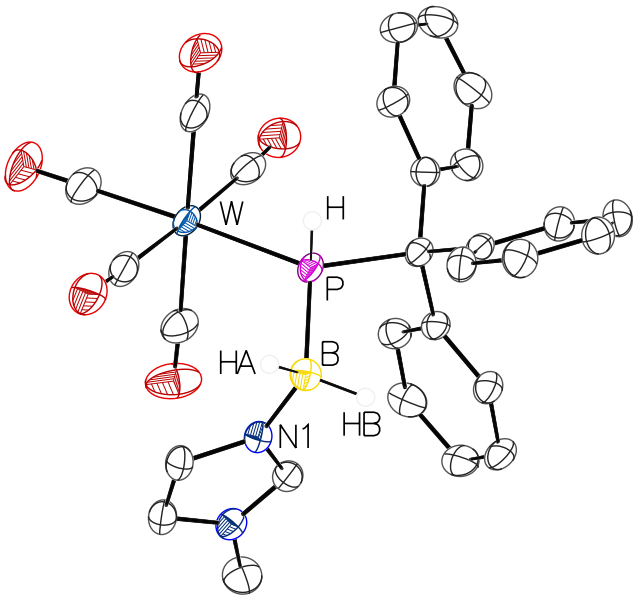

Figure 44: Molecular structure of **55** in the single crystal lattice at 100(2) K. Thermal ellipsoids are set at 50 % probability level. Hydrogen atoms and solvent molecules were omitted for clarity except for those bound to phosphorus and boron atoms. Selected bond lengths / Å and bond angles / °: W-P 2.5650(4), P-C5 1.9179(14), P-B 1.9904(16), N1-B 1.5586(19), C5-P-W 123.10(4), C5-P-B 107.48(6), B-P-W 118.20(5), N1-B-P 111.31(9).

3.3.3.2 Reactions with Brønsted-Lowry acids

3.3.3.2.1 Reactions with water and alcohols

To achieve a higher stability of the products with electrophiles, stronger acids have to be employed. For that, the reactivity of the *N*-methylimidazole-to-phosphinidene complex adducts **13** towards Brønsted-Lowry acids with increasing acidity was investigated. As products either the protonated adduct without dissociation of the *N*-methylimidazole or a formal insertion product under loss of the *N*-methylimidazole was expected. First, the reactions with water and alcohols were performed. While for *P*-CPh_3 substituted Li/Cl phosphinidenoid group 6 metal complexes no high reactivity towards water was observed (surprisingly), the adducts **13** showed a high reactivity towards water under formation of hydroxy(triphenylmethyl)phosphane complexes **56** strongly bound to *N*-methylimidazole via O-H···N hydrogen bonding (Scheme 60).

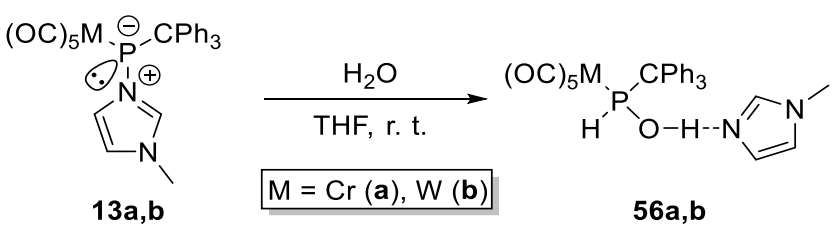

Scheme 60: Hydrolysis of the *N*-methylimidazole-to-phosphinidene complex adducts **13**.

The ^{31}P NMR spectrum of **56b** in THF-d_8 displayed a single resonance signal at 94.7 ppm ($^1J_{P,H}$ = 337.2 Hz, $^1J_{W,P}$ = 267.0 Hz). In the ^{1}H NMR spectrum the existence of one equivalent of *N*-methylimidazole is observed (Figure 45). Additionally, the O*H* proton is strongly deshielded showing a slightly broadened ^{1}H resonance signal at 12.94 ppm indicating the involvement in the rather strong hydrogen binding to the *N*-methylimidazole. The *N*-methylimidazole was neither separable from the hydroxy(triphenylmethyl)phosphane complex **47b** via evaporation *in vacuo* (<0.02 mbar) nor via recrystallization. However, it was possible to achieve a clean separation of complex **47b** and **10** via column chromatography at ambient temperature using silica gel as stationary phase and a diethyl ether/petroleum ether (40/65) mixture as mobile phase (eluent) under an Argon atmosphere (Scheme 61).

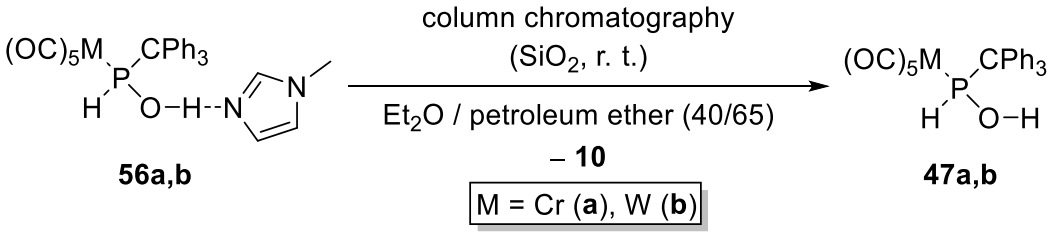

Scheme 61: Purification of the hydroxy(triphenylmethyl)phosphane complexes **47** via column chromatography.

The ^{31}P NMR resonance signal of **47b** was found slightly downfield-shifted compared to **56b** at 99.2 ppm ($^1J_{P,H}$ = 340.5 Hz, $^1J_{W,P}$ = 269.5 Hz). In the ^{1}H NMR spectrum of **47b** the resonance of the O*H* nucleus shifted by 4.55 ppm to highfield compared to the one of **56b** at 8.39 ppm being in accordance with the loss of the hydrogen bonding to the *N*-methylimidazole (Figure 45).

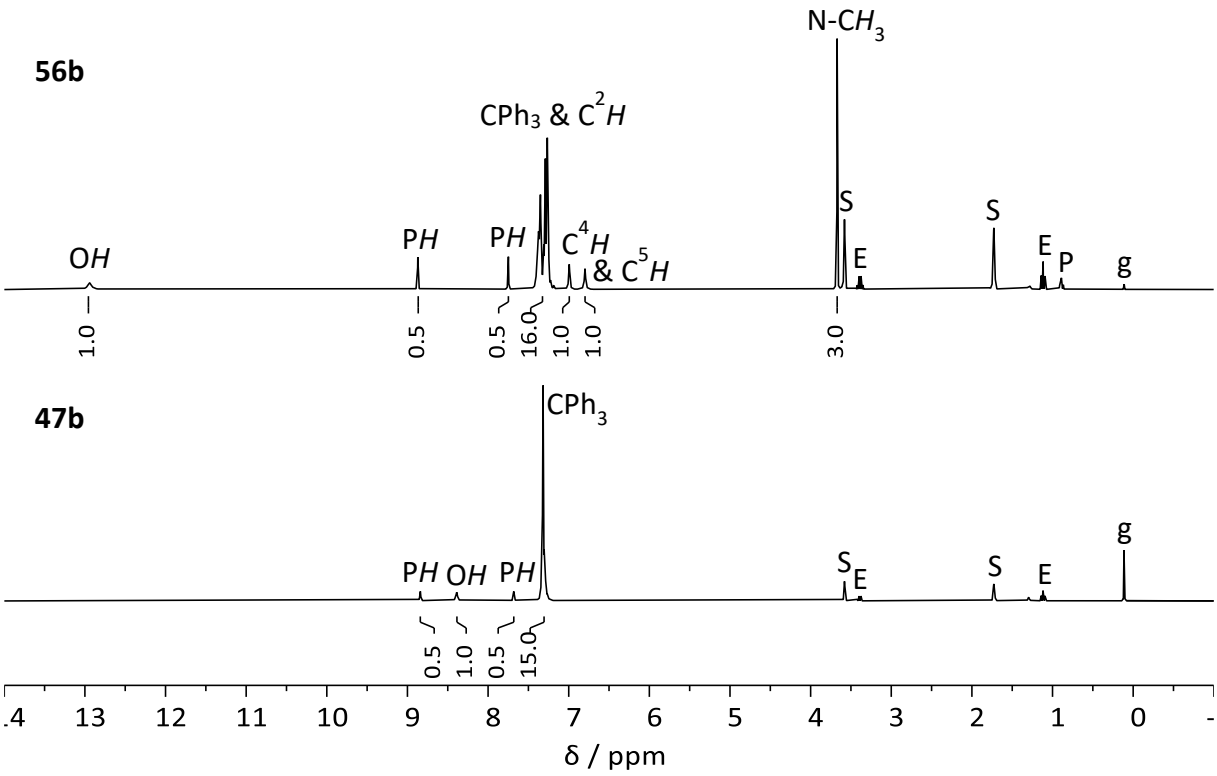

Figure 45: ^{1}H NMR spectra (300.13 MHz, 298 K, THF-d_8) of complexes **56b** (top) and **47b** (bottom). The resonances of traces of grease are marked with a "g", of diethyl ether with an "E" and of *n*-pentane with a "P". The residual resonance signal of the deuterated solvent is marked with an "S".

The highfield shift of the O*H* nucleus was significantly stronger if the weaker coordinating dichloromethane-d_2 was used instead as solvent for measurement of the ^{1}H NMR spectrum where the resonance signal appeared at 3.79 ppm ($^{2}J_{P,H}$ = 5.30 Hz) (Figure 46). The other proton resonances changed only marginally going from **56b** to the *N*-methylimidazole free complex **47b** or by changing the solvent confirming their non-involvement in hydrogen-bonding to **10** or solvents. The solvent change induced an additional slight downfield shift from 99.2 ppm to 100.7 ppm in the ^{31}P NMR spectrum.

The reaction with the chromium complex **13a** proceeded very similarly obtaining first the *N*-methylimidazole-to-hydroxy(triphenylmethyl)phosphane complex adduct **56a** ($\delta(^{31}P)$ = 142.2 ppm ($^{1}J_{P,H}$ = 330.3 Hz)) that was purified via column chromatography to obtain the final product **47a** ($\delta(^{31}P)$ = 147.5 ppm ($^{1}J_{P,H}$ = 330.0 Hz)).

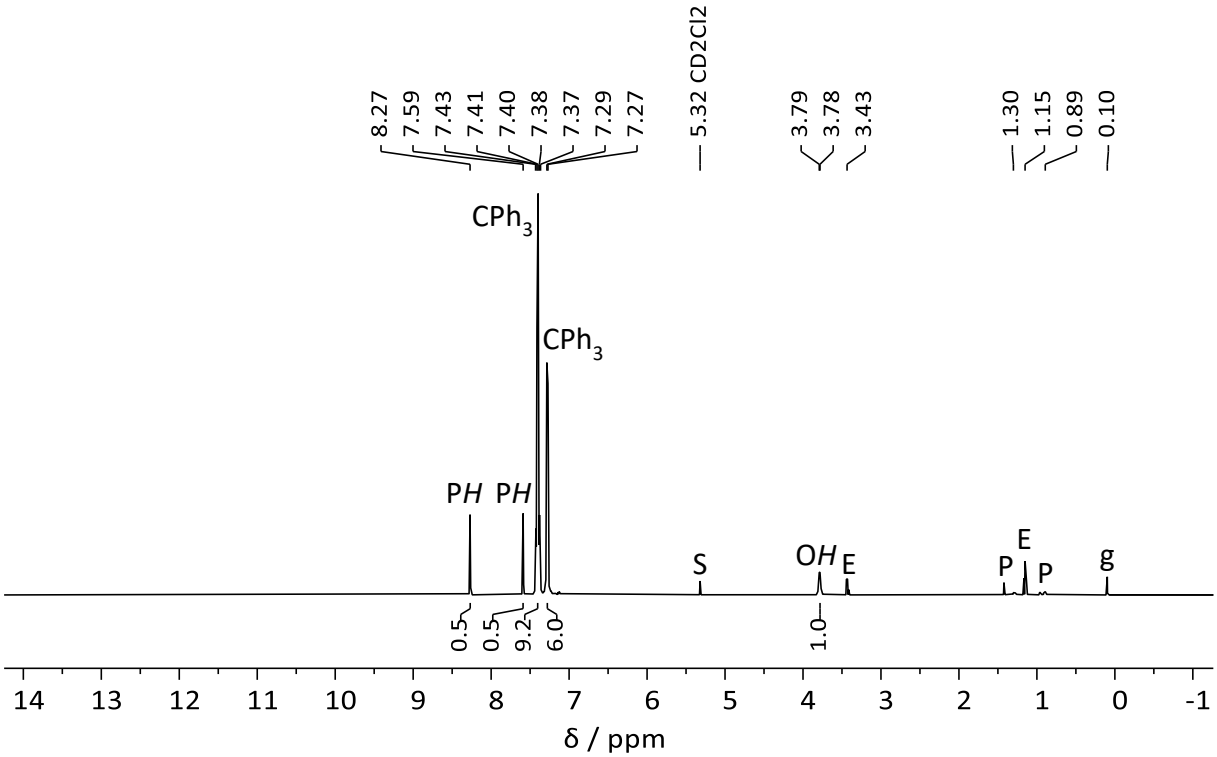

Figure 46: ^{1}H NMR spectrum (500.04 MHz, 298 K, CD_2Cl_2) of complex **47b**. The resonances of traces of grease are marked with a "g", of diethyl ether with an "E" and of *n*-pentane with a "P". The residual resonance signal of the deuterated solvent is marked with an "S".

The molecular structures of the hydroxy(triphenylmethyl)phosphane complexes **47** were confirmed by single crystal X-ray diffraction analysis (**47a**: Figure 47).

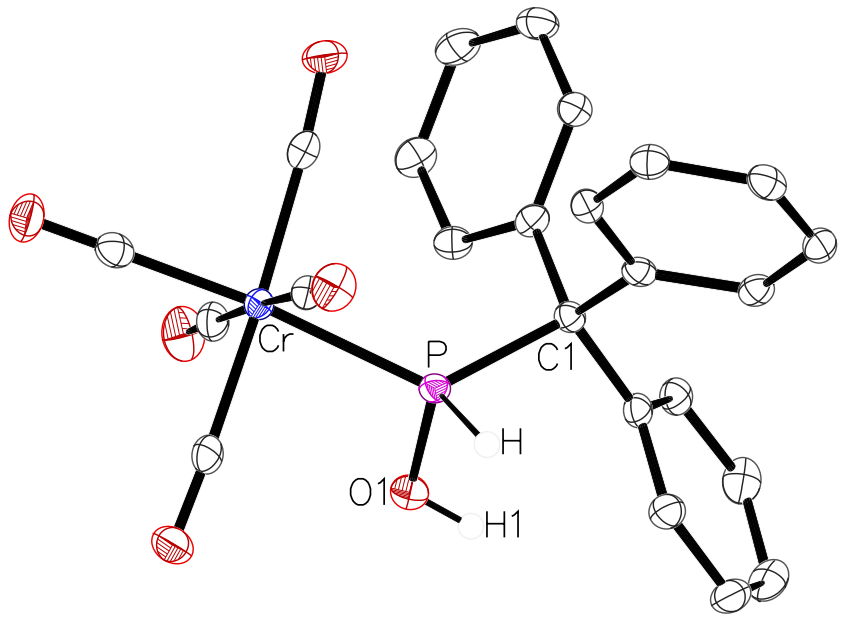

Figure 47: Molecular structures of **47a** in the single crystal lattice at 100(2) K. Thermal ellipsoids are set at 50 % probability level. Hydrogen atoms were omitted for clarity except for those bound to phosphorus and oxygen atoms. Selected bond lengths / Å and bond angles / °: Cr-P 2.3360(5), P-C1 1.9145(18), P-O1 1.6319(14), C1-P-Cr 128.33(6), O1-P-Cr 107.02(5), O1-P-C1 104.28(8).

The reaction of the *N*-methylimidazole-to-phosphinidene tungsten complex **13b** with methanol and *tert*-butanol gave analogous formal OH insertion products **57** ($\delta(^{31}P)$ = 127.2 ppm, $^{1}J_{P,H}$ = 342.7 Hz, $^{3}J_{P,H}$ = 12.5 Hz, $^{1}J_{W,P}$ = 274.1 Hz) and **58** ($\delta(^{31}P)$ = 97.4 ppm, $^{1}J_{P,H}$ = 322.3 Hz, $^{1}J_{W,P}$ = 282.6 Hz) which were identified via comparison of the ^{1}H and ^{31}P NMR spectra with the reported values of **57** that were obtained via the Li/Cl phosphinidenoid complex **2c** by Streubel and co-workers in 2014.[88]

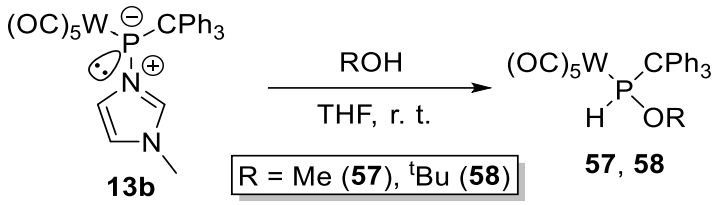

Scheme 62: Synthesis of alkoxy(triphenylmethyl)phosphane complexes **57** and **58**.

The reaction progress decreases strongly with increasing steric demand of the organic substituent of the alcohol. Thus, the reaction with methanol already was completed within less than one day but an almost full conversion (98 %) in the case of *tert*-butanol was only observed after 14 days.

3.3.3.2.2 Reactions with amines

Next, the reactions of **13b** with primary amines, *i.e.*, methylamine, isopropylamine and *tert*-butylamine, were performed using benzene-d_6 as solvent (Scheme 63).

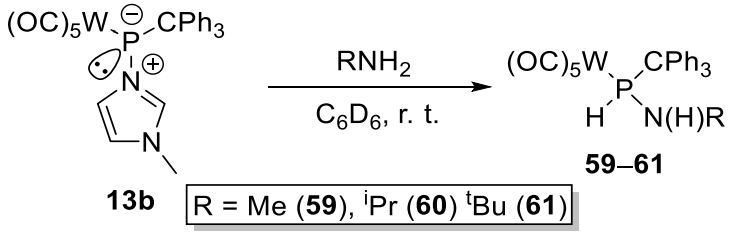

Scheme 63: Synthesis of the amino(triphenylmethyl)phosphane complexes **59–61**.

In all cases, the respective amino(triphenylmethyl)phosphane complexes **59–61** formed selectively that were already obtained previously via reactions with the Li/Cl phosphinidenoid complex **2c** by Majhi *et al.* in 2016.[89] The ^{1}H and ^{31}P NMR spectra of the reaction mixtures were in accordance with the reported data from literature (Figure 48, Table 16).

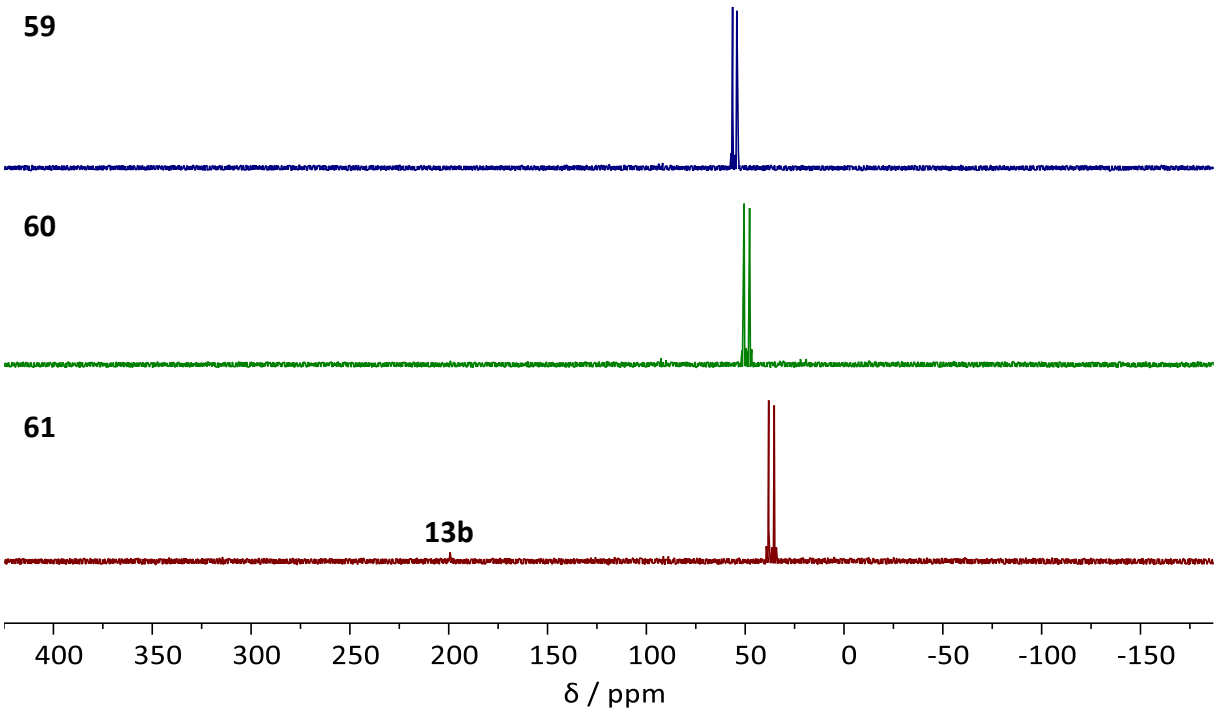

Figure 48: ^{31}P NMR spectra (**59**: 162.00 MHz, **60**, **61**: 121.51 MHz, 298 K, C_6D_6) of the reaction mixtures of **13b** with primary amines under formation of amino(triphenylmethyl)phosphane complexes **59–61**.

Table 16: Selected ^{31}P NMR data of amino(triphenylmethane)phosphane complexes **59–61**. Literature data are given in parentheses.[89]

Compound	R	δ(^{31}P) / ppm	$^1J_{P,H}$ / Hz	$^1J_{W,P}$ / Hz
59	Me	55.3 (57.4)	348.7 (346.1)	257.9 (258.4)
60	^{i}Pr	49.2 (49.3)	336.6 (332.6)	260.5 (260.5)
61	^{t}Bu	36.8 (37.2)	342.8 (342.3)	263.8 (263.8)

All reactions were completed within one day without any significant difference in the reaction progress with respect to the increasing steric demand.

3.3.3.2.3 Reactions with strong acids

When strong(er) Brønsted-Lowry acids were offered to the *N*-methylimidazole-to-phosphinidene complex adducts **13** an additional reaction with the *N*-methylimidazole (**10**) was observed under formation of the *N*-methylimidazolium salts. Hence, in this case the addition of two equivalents of the acids was essential. The reaction of the adducts **13** in dichloromethane with trifluoroacetic acid resulted in the formation of the trifluoroacetyl(triphenylmethyl)phosphane complexes **62** (Scheme 64).

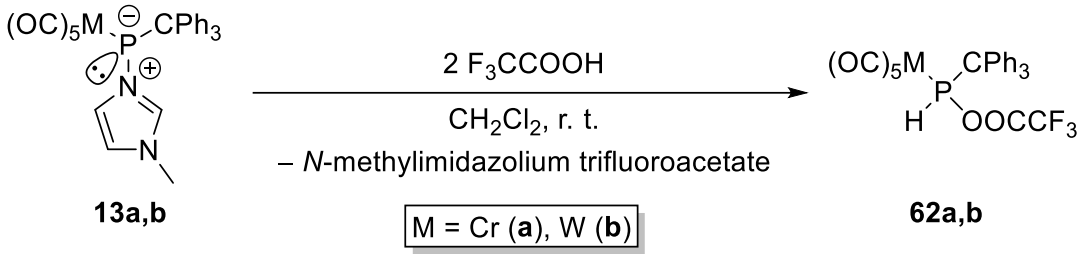

Scheme 64: Synthesis of trifluoroacetyl(triphenylmethyl)phosphane complexes **62**.

The products were extracted with *n*-pentane to separate from the formed *N*-methylimidazolium trifluoroacetate attaining very good yields of 96 % for **62a** and 78 % for **62b**, respectively. The ^{31}P NMR spectra of **62a** and **62b** showed slightly downfield-shifted resonance signals compared to the ones of the alkoxyphosphane and hydroxyphosphane complexes due to the larger negative inductive effect of the perfluorinated acetyl group (Figure 49, Table 17). In the same vein, the $^{1}J_{P,H}$ coupling constants of **62a,b** were relatively large compared to the ones of the beforehand obtained phosphane complexes.

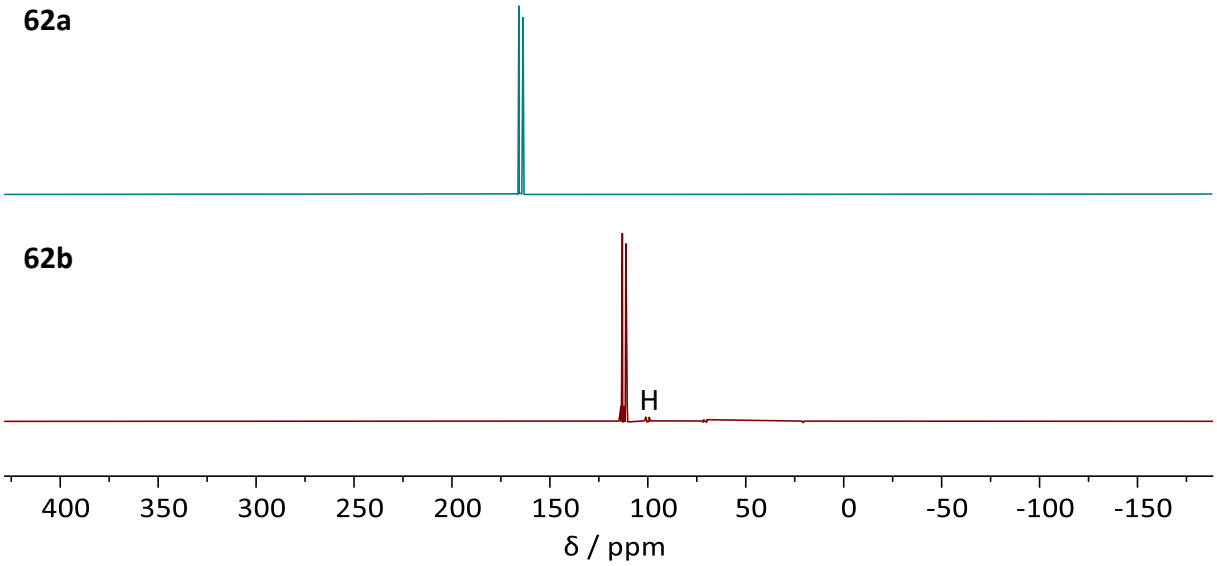

Figure 49: ^{31}P NMR spectra (**62a**: 162.00 MHz, **62b**: 202.44 MHz, 298 K, C_6D_6) of the trifluoroacaetyl-(triphenylmethyl)phosphane complexes **62**. The resonance of traces of the hydrolysis product **52a** was marked with an "H".

Table 17: ^{31}P NMR data of trifluoroacetylphosphane complexes **59**.

Compound	δ(^{31}P) / ppm	$^{1}J_{P,H}$ / Hz	$^{1}J_{W,P}$ / Hz
62a	164.8	350.1	—
62b	112.1	362.4	285.3

The P*H* proton nuclei of complexes **62** also were significantly deshielded and their ^{1}H resonance signals appeared at 8.19 ppm (**62a**) and 8.42 ppm ($^{2}J_{W,H}$ = 6.9 Hz) (**62b**) (**62a**: Figure 50).

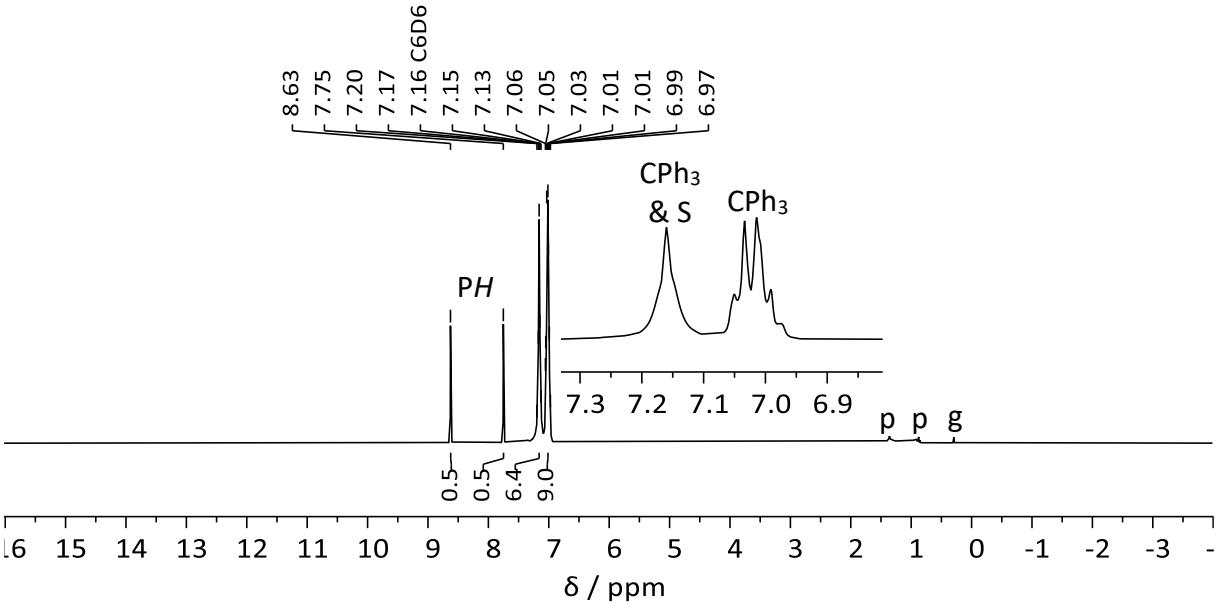

Figure 50: ^{1}H NMR spectrum (400.13 MHz, 298 K, C_6D_6) of complex **62a**. The resonances of traces of grease are marked with a "g" and of *n*-pentane with a "p". The residual resonance signal of the deuterated solvent is marked with an "S".

Single crystals of **62a,b** were analyzed by X-ray diffraction analysis and the results verified the proposed molecular structures (**62a**: Figure 51).

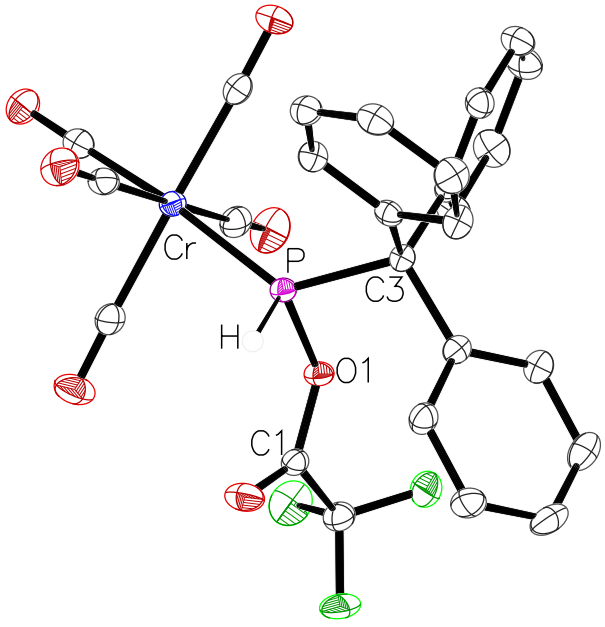

Figure 51: Molecular structures of **62a** in the single crystal lattice at 123(2) K. Thermal ellipsoids are set at 50 % probability level. Hydrogen atoms were omitted for clarity except for those bound to phosphorus atoms. Selected bond lengths / Å and bond angles / °: Cr-P 2.3224(5), P-C3 1.9148(16), P-O1 1.7017(10), C3-P-Cr 131.96(5), O1-P-Cr 106.46(4), O1-P-C3 97.56(6).

Furthermore, the *N*-methylimidazole-to-phosphinidene complex adduct **13b** was reacted with two equivalents of hydrogen chloride under formation of the chloro-(triphenylmethyl)phosphane complex **63** next to *N*-methylimidazolium chloride (Figure 52).

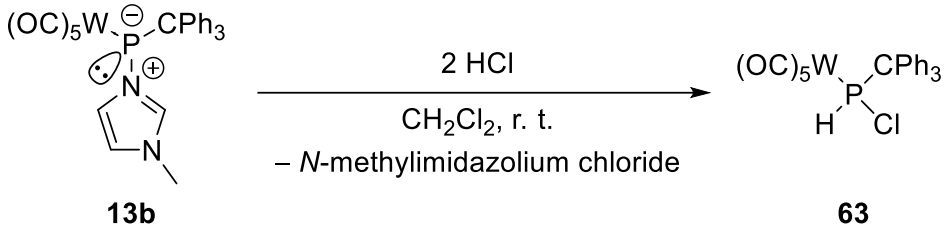

13b **63**

Figure 52: Synthesis of the chloro(triphenylmethyl)phosphane complex **63**.

Complex **63** was extracted from the reaction mixture using diethyl ether to yield the clean product. The ^{1}H and ^{31}P NMR data were in accordance to the ones obtained from the reaction of hydrogen chloride with the *tert*-butylamino(triphenylmethyl)phosphane complex **61** as reported by Streubel *et al.* in 2017.[224]

Table 18: ^{31}P NMR data of chloro(triphenylmethyl)phosphane complex **63** from this work and literature.[224]

Compound	**Solvent**	**δ(^{1}H) / ppm** P*H*	**δ(^{31}P) / ppm**	**$^{1}J_{P,H}$ / Hz**	**$^{1}J_{W,P}$ / Hz**
63 (this work)	CD_2Cl_2	8.00	71.2	345.3	270.9
63 (lit.[224])	$CDCl_3$	7.94	71.2	342.3	263.7

The previously reported yield of 53 % was increased to a quantitative yield by applying the route developed here and, hence, provides a much improved, alternative access to **63**.

3.3.3.2.4 Reactions with acids of weakly coordinating anions

To avoid the substitution of the P-bound *N*-methylimidazole of complexes **13** their reactivity towards acids with weakly coordinating anions[273] were tested. The reaction of the adducts **13** with one equivalent of trifluoromethanesulfonic acid led to the selective formation of the desired phosphanylimidazolium trifluoromethanesulfonate complexes **64** (Scheme 65).

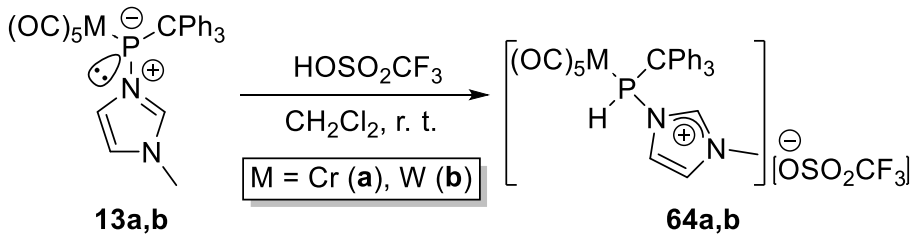

13a,b **64a,b**

Scheme 65: Synthesis of the phosphanylimidazolium trifluoromethanesulfonate complexes **64**.

The $^{31}P\{^{1}H\}$ NMR spectra displayed resonances at 116.4 ppm ($^{1}J_{P,H}$ = 362.2 Hz) for **64a** and 65.5 ppm ($^{1}J_{P,H}$ = 373.3 Hz, $^{1}J_{W,P}$ = 277.8 Hz) for **64b** (Figure 53).

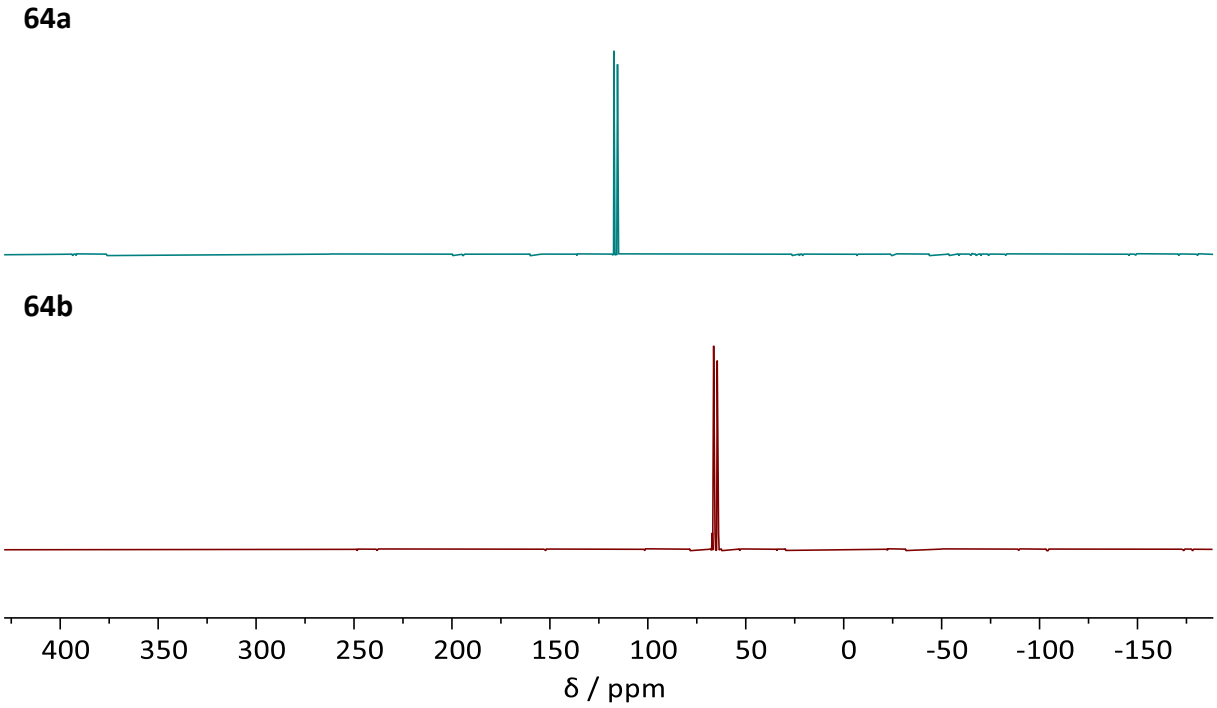

Figure 53: ^{31}P NMR spectra (202.44 MHz, 298 K, CD_2Cl_2) of phosphanylimidazolium trifluoromethansulfonate complexes **64**.

The highfield shift of **64** compared to the trifluoroacetylphosphane complexes **62** and the chlorophosphane complexes **63** is associated with the less electron-withdrawing character of the imidazolium moiety than of trifluoroacetyl or chloride resulting in a more shielded phosphorus nucleus. The P*H* and C^{2}*H* protons exhibited similar deshielded resonances in the ^{1}H NMR spectra (Table 19 , **64b**: Figure 54).

Table 19: Selected NMR data of complexes **64–66**.

Compound	$\delta(^{31}P)$ / ppm	$\delta(^{1}H)$ / ppm P*H*	$\delta(^{1}H)$ / ppm C^2H	$^{1}J_{P,H}$ / Hz
64a	116.4	8.94	9.11	362.2
64b	65.5	9.41	9.12	373.3
65a	131.8	—	—	342.0
65b	77.7	8.84	7.08	353.3
66a	132.0	8.34	7.03	341.9
66b	77.8	8.84	7.08	353.6

For the chromium complex **64a** the C^2H proton featured the largest chemical shift within the molecule while for the tungsten case (**64b**) the P*H* proton hold this feature. The observed deshielding of the C^2H proton presumably arose from a coordination of the trifluoromethanesulfonate as confirmed in the single crystal by X-ray diffraction analysis with a long O6-H1 distance of 2.405 Å (Figure 55). However, in both cases a partial positive charge is also expected on the phosphorus nucleus provoking both the PH and the C^2H protons to have a crucial acidic character.

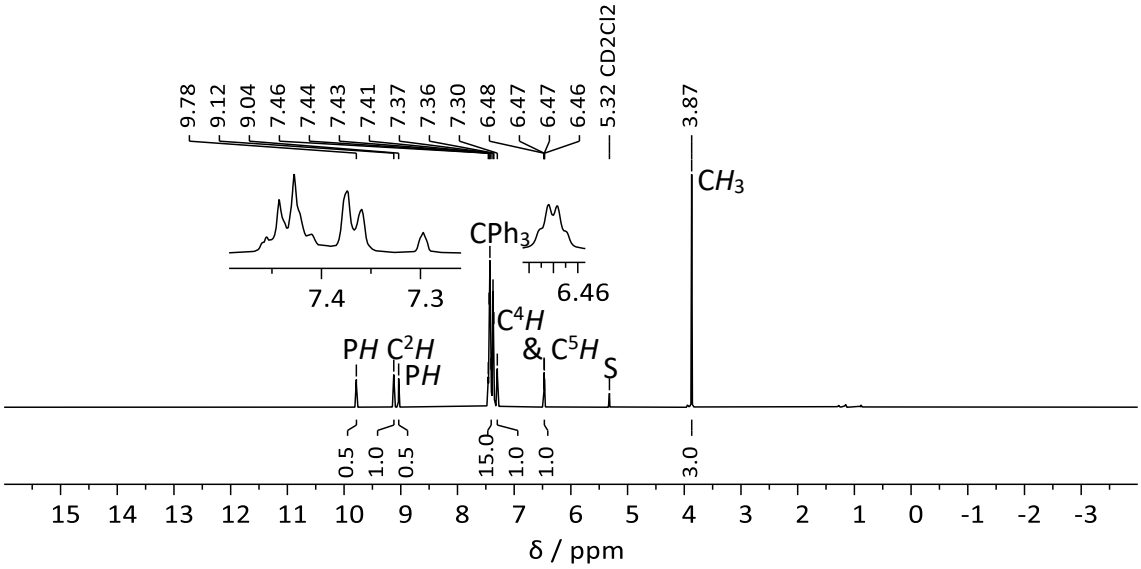

Figure 54: ^{1}H NMR spectrum (500.04 MHz, 298 K, CD_2Cl_2) of phosphanylimidazolium trifluoromethansulfonate complex **64b**. The residual resonance signal of the deuterated solvent is marked with an "S".

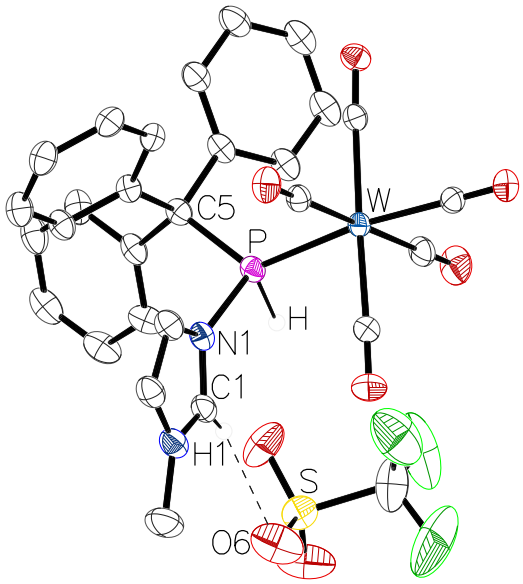

Figure 55: Molecular structure of **64b** in the single crystal lattice at 100(2) K. Thermal ellipsoids are set at 50 % probability level. Solvent molecules and hydrogen atoms were omitted for clarity except for those bound to phosphorus atoms or that are involved in hydrogen bonding. Selected bond lengths / Å and bond angles / °: W-P 2.4815(12), P-C5 1.894(5), P-N1 1.776(4), O6-H1 2.40499(10), N1-P-W 110.94(14), N1-P-C5 103.78(19), C5-P-W 127.57(15).

The phosphanylimidazolium complex cation is even more separated by introducing an even less coordinating anion namely the tetrakis[3,5-bis(trifluoromethyl)phenyl]borate ($[BAr^F_4]^-$). This was achieved via the reaction of the *N*-methylimidazole-to-phosphinidene complex adducts **13** with the established Brookhart's acid $[H(OEt_2)_2][B\{3,5\text{-}(F_3C)_2C_6H_3\}_4]$.

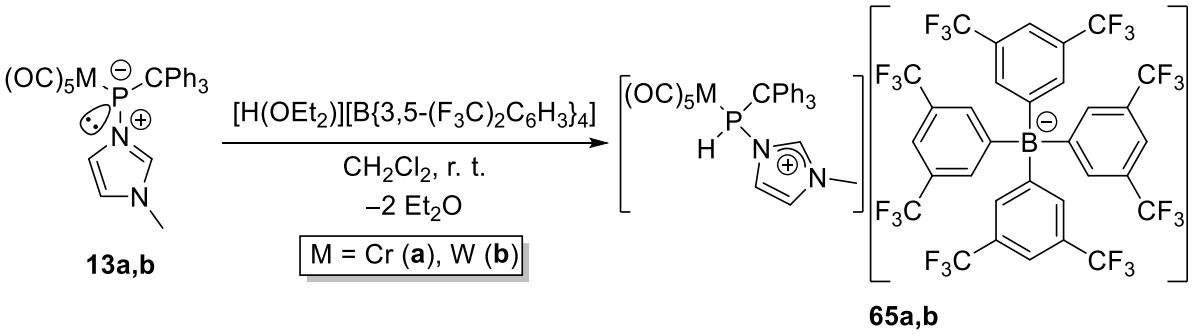

Scheme 66: Synthesis of phosphanylimidazolium complexes **65** with $[BAr^F_4]^-$ as counter anion.

The phosphorus nuclei of **65a** ($\delta(^{31}P)$ = 131.8 ppm, $^1J_{P,H}$ = 342.0 Hz) and **65b** ($\delta(^{31}P)$ = 77.7 ppm, $^1J_{P,H}$ = 353.3 Hz, $^1J_{W,P}$ = 283.9 Hz) are further downfield-shifted compared to the ones of **64a,b** (Table 19, Figure 56).

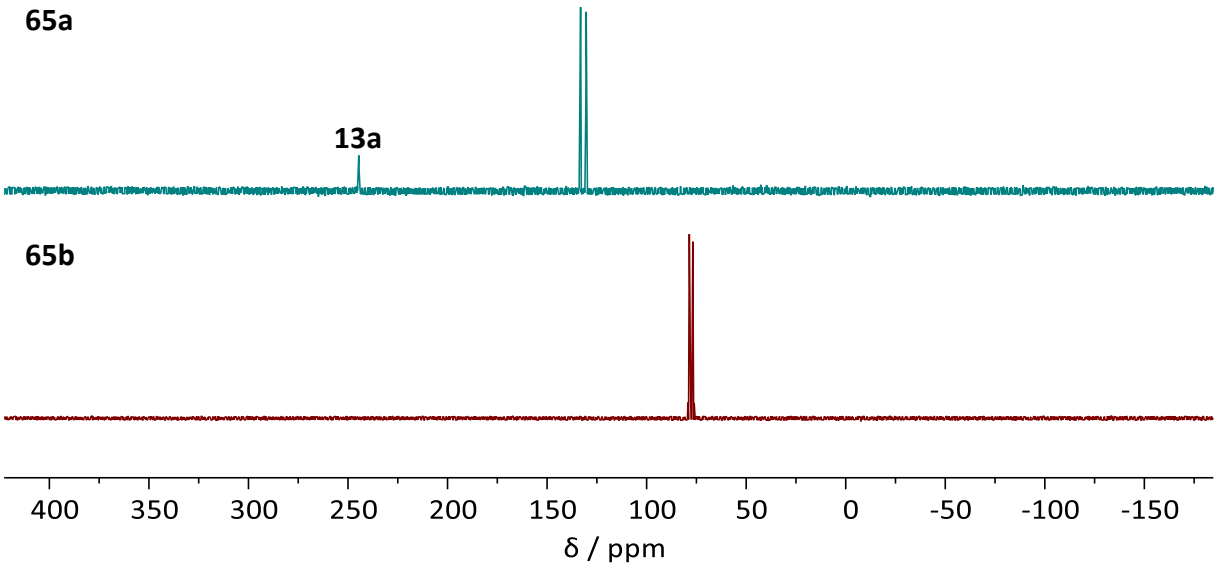

Figure 56: ^{31}P NMR spectra (**65a**: 121.51 MHz, 298 K, CH_2Cl_2; **65b**: 202.44 MHz, 298 K, CD_2Cl_2) of phosphanyl-imidazolium complexes **65**. The resonance of the starting material **13a** as side product was labeled accordingly.

Simultaneously, the ^{1}H NMR spectrum revealed a strong highfield-shift of the C^2*H* resonance compared to the ones of complexes **64** (**65b**: Figure 57).

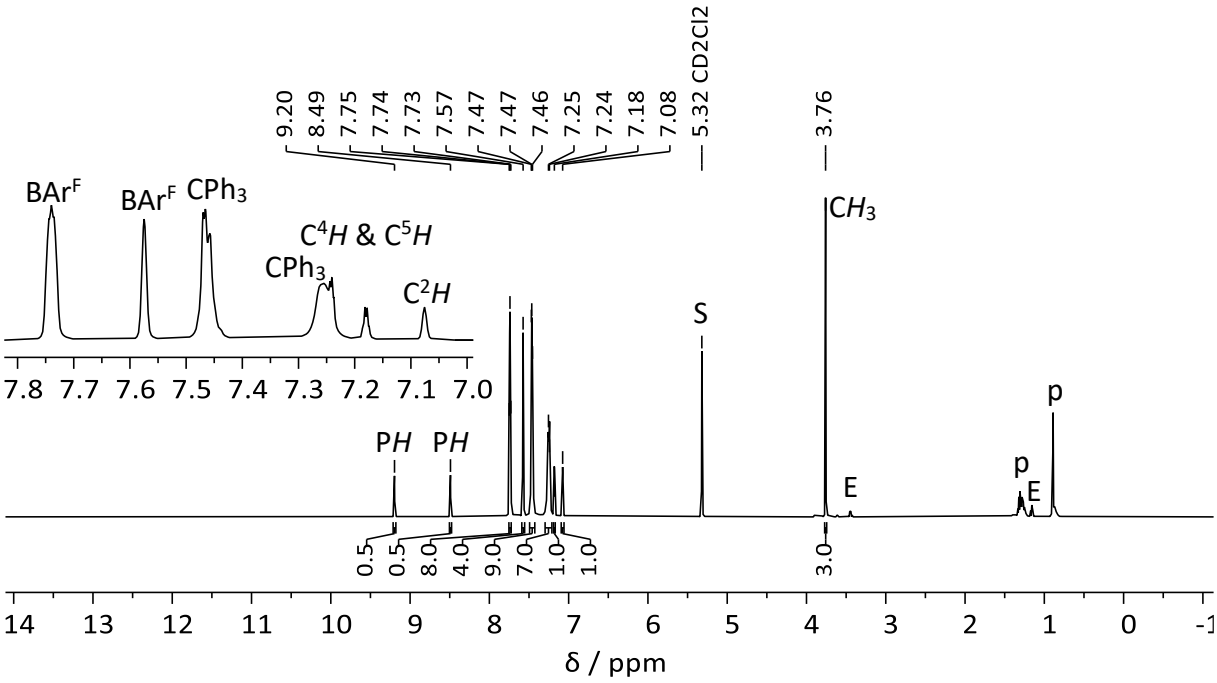

Figure 57: ^{1}H NMR spectrum (500.04 MHz, 298 K, CD_2Cl_2) of the phosphanylimidazolium complex **65b**. The resonances of traces of diethylether are marked with a "E" and of *n*-pentane with a "p". The residual resonance signal of the deuterated solvent is marked with an "S".

The further deshielding of the ^{31}P nuclei together with the stronger shielding of the C^2*H* nuclei of complexes **65** emerge from the complete loss of a coordination of the anion while the

trifluoromethanesulfonate still coordinated to the C^2*H* proton explaining its strong deshielded ^{1}H NMR resonance.

To verify the hypothesis of the influence of the anion on the shieldings Krossing's acid [H(OEt$_2$)$_2$][Al{OC(CF$_3$)$_3$}$_4$] was reacted with the *N*-methylimidazole-to-phosphinidene complex adducts **13**.

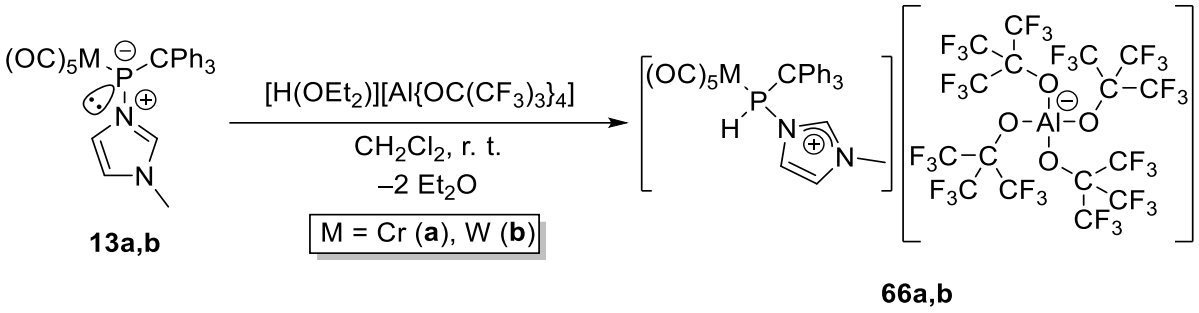

Scheme 67: Synthesis of phosphanylimidazolium complexes **66** with [Al{OC(CF$_3$)$_3$}$_4$]$^-$ as counter anion.

As expected the introduction of the tetrakis(nonafluoro-*tert*-butoxy)aluminate as weakly coordinating anion instead of [BAr$^F{}_4$]$^-$ led to no significant change in the ^{31}P NMR chemical shifts. In the ^{31}P NMR spectra the resonance signal of **66a** appeared at 132.0 ppm ($^1J_{P,H}$ = 341.9 Hz) and of **66b** at 77.8 ppm ($^1J_{P,H}$ = 353.6 Hz, $^1J_{W,P}$ = 283.8 Hz) (Table 19, Figure 58).

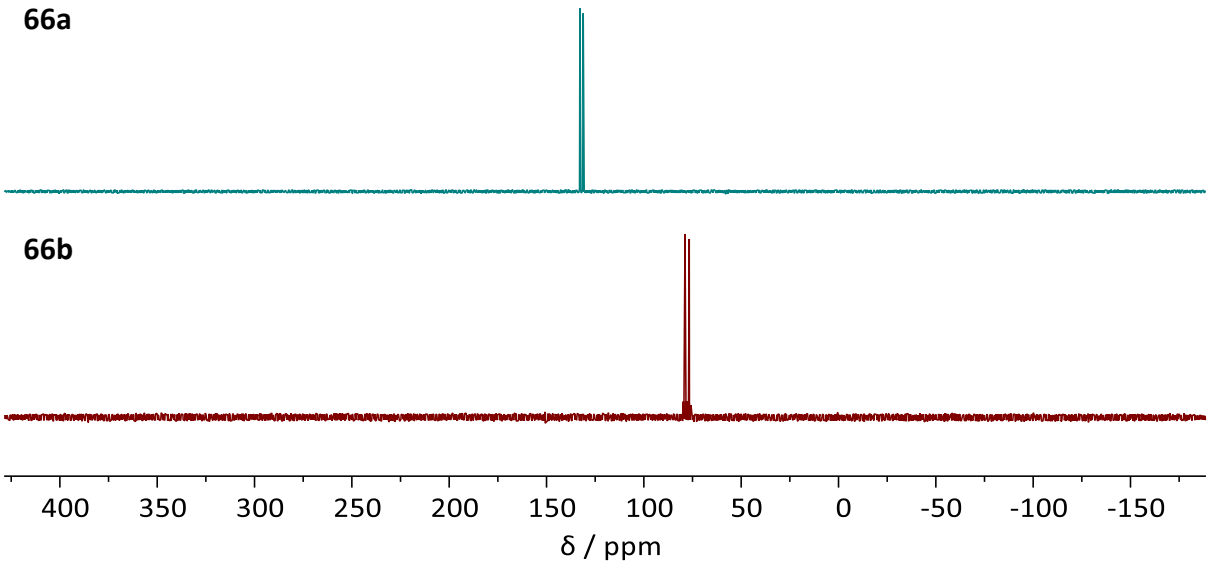

Figure 58: ^{31}P NMR spectra (**66a**: 202.44 MHz, **66b**: 162.00 MHz, 298 K, CD_2Cl_2) of phosphanylimidazolium complexes **66**.

Likewise, the ^{1}H NMR chemical shifts of the imidazolium protons as well as the proton directly bound to phosphorus did not change significantly (Table 19, Figure 59).

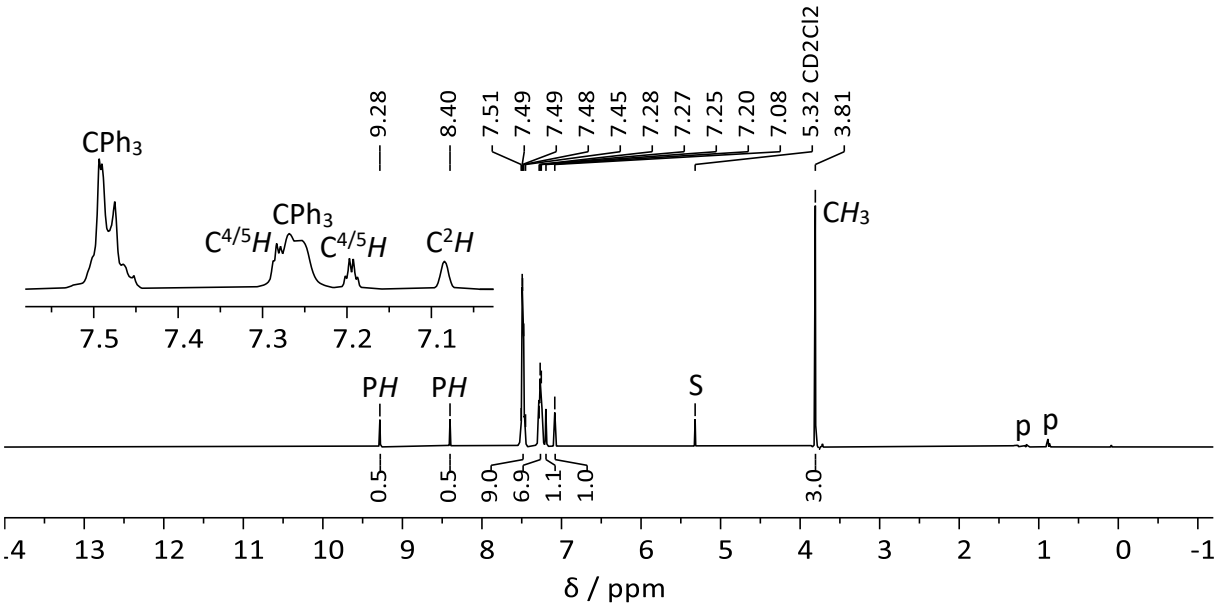

Figure 59: ^{1}H NMR spectrum (400.13 MHz, 298 K, CD_2Cl_2) of the phosphanylimidazolium complex **66b**. The resonances of traces of *n*-pentane are marked with a "p". The residual resonance signal of the deuterated solvent is marked with an "S".

2D NMR ^{1}H,^{15}N HMBC experiments revealed that the difference of the ^{15}N NMR chemical shifts of the two nitrogen nuclei within the imidazole moiety of phosphanylimidazolium complexes **64–66** approached to each other compared to the neutral *N*-methylimidazole-to-phosphinidene complexes **13** having a shift difference $\Delta\delta(^{15}N)$ of only 4.7 to 5.5 ppm for complexes **64** and of 8.5 ppm for complexes **65b** and **66** (Table 20).

Table 20: ^{15}N NMR data of complexes **13** and **64–66** obtained via ge-2D NMR ^{1}H,^{15}N NMR experiments.

Compound	**$\delta(^{15}N)$ / ppm** *N*-CH_3	**$\delta(^{15}N)$ / ppm** *N*-P	**$\lvert\Delta\delta(^{15}N)\rvert$ / ppm**
13a	−215.2	−177.7	37.5
13b	−215.2	−183.9	31.3
64a	−205.8	−200.3	5.5
64b	−205.0	−200.3	4.7
65b	−203.1	−194.6	8.5
66a	−204.2	−195.7	8.5
66b	−204.2	−195.7	8.5

This indicates a significant delocalization of the positive charge within the imidazolium ring of complexes **64–66** as expected. Interestingly, the ^{15}N NMR chemical shifts of the nitrogen nuclei in complexes **64** are most similar and, hence, exposing the stabilization of the positive charge in the imidazolium ring by coordination of the trifluoromethanesulfonate to the C^{2}*H*

proton. The molecular structure of complex **66b** was confirmed by single crystal X-ray diffraction analysis (Figure 60).

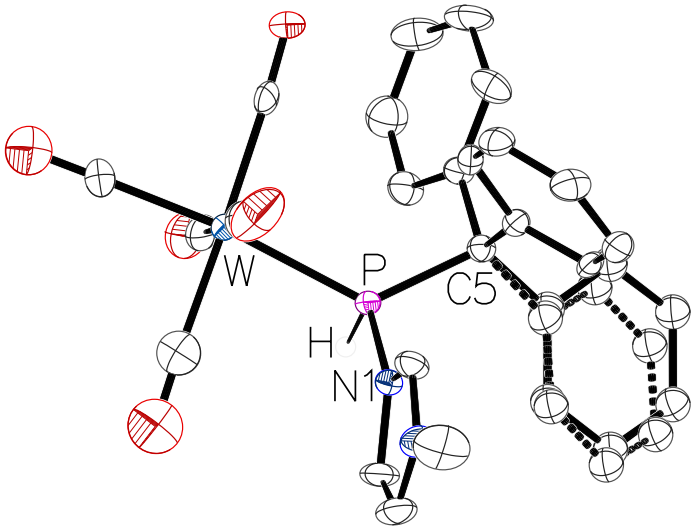

Figure 60: Molecular structure of **66b** in the single crystal lattice at 100(2) K. Thermal ellipsoids are set at 50 % probability level. A split layer site (50.6 %) is given with dashed lines. Hydrogen atoms were omitted for clarity except for those bound to phosphorus atoms. Selected bond lengths / Å and bond angles / °: W-P 2.4643(17), P-C5 1.923(7), P-N1 1.784(6), N1-P-W 111.5(2), N1-P-C5 105.2(3), C5-P-W 127.4(2).

The obtained phosphanylimidazolium complexes **64–66** can be described formally as *N*-methylimidazole-to-phosphenium complex adducts **64'–66'** (Figure 61).

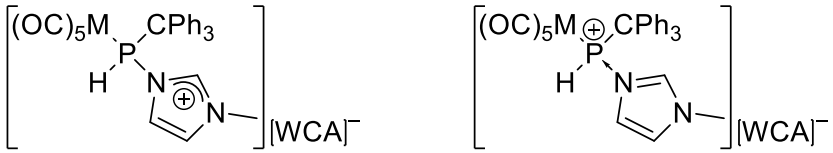

64–66 **64'–66'**

Figure 61: Phosphanylimidazolium complexes **64–66** and the formal representation as *N*-methylimidazole-to-phosphenium complex adducts **64'–66'**.

Reactions of phosphenium complexes with neutral nucleophiles were only investigated sparsely, predominantly by Nakazawa and Gudat, in many cases observing reactions at the metal center instead of the P center and thus to date the class of donor-to-phosphenium complex adducts are only rarely reported and studied.[170–178] Very recently, the first *N*-donor-to-phosphenium complex adduct was described by Ragogna and Gilroy where the *N*-donor center was directly linked as *P*-substituent.[178] Complexes **64–66** display the first example of a donor-stabilized phosphenium complex bearing a P-H bond and, in general, the first example of a donor-stabilized phosphenium group 6 metal complex. However, the first non-complexed NHC-stabilized phosphenium salt bearing hydrogen was reported in 2015 by Bertrand,

achieved via an inversely polarized *P*-H substituted phosphaalkene.[274] However, the structure may be better described as phosphanyl imidazolium salt.

The hydrogen atoms bound directly to phosphorus in complexes **64–66** are expected to have a high acidic character due to the proposed significant contribution of a phosphenium character. Especially this effect should be observed for complexes **65** and **66** since the anions are more innocent and no interaction with the C^2 bound hydrogen occurs.

Interestingly, when **66b** was dissolved in tetrahydrofuran or tetrahydrofuran-d_8 an immediate color change from colorless to yellow was observed. The ^{1}H and ^{31}P NMR spectra showed the formation of the *N*-methylimidazole-to-phosphinidene complex adduct **13b** showing that a deprotonation at the *P*-center occurred. Since no polymerization of the solvent was observed and a slightly broadened signal at 7.62 ppm with an integral of 1 proton appeared in the ^{1}H NMR spectrum when dissolved in THF-d_8 (Figure 62) presumably the compound [H(thf-d_8)$_4$][Al{OC(CF$_3$)$_3$}$_4$] has formed being in good accordance to the ^{1}H NMR data that were reported for the respective non-deuterated acid by Krossing when using dichloromethane-d_2 as solvent (Scheme 68).[275]

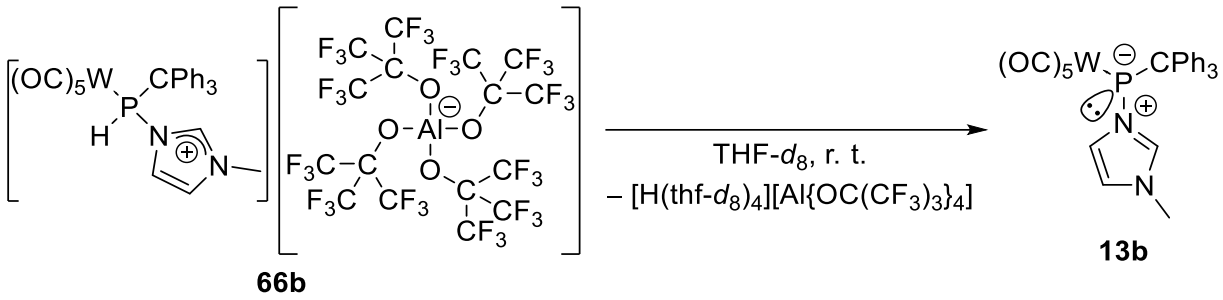

66b **13b**

Scheme 68: Decomposition of the phosphanylimidazolium complex **66b** in THF-d_8 to complex **13b** under the proposed formation of [H(thf-d_8)$_4$][Al{OC(CF$_3$)$_3$}$_4$].

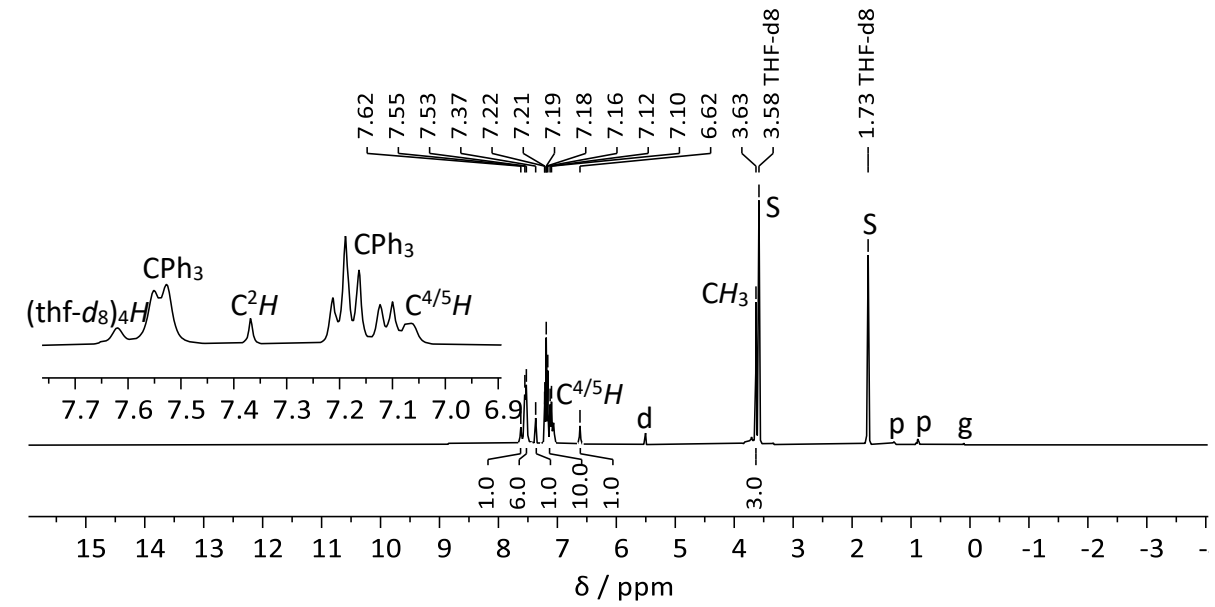

Figure 62: ^{1}H NMR spectrum (300.13 MHz, 298 K, THF-d_8) of the decomposition mixture of complex **66b** in THF-d_8. The resonances of traces of dichloromethane are marked with a "d", of *n*-pentane with a "p" and of grease with a "g". The residual resonance signals of the deuterated solvent are marked with an "S".

Furthermore, a solution of one equivalent of methyl lithium (as lithium bromide 1:1 adduct) in diethylether was added to a solution of the phosphanylimidazolium complex **66b** in dichloromethane immediately forming a yellow suspension under slight gas evolution (Scheme 69).

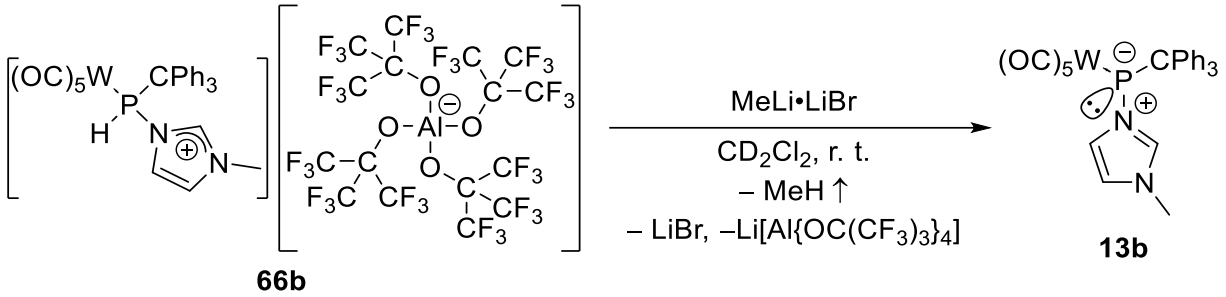

Scheme 69: Deprotonation of **66b** by methyl lithium under formation of **13b**.

The formation of methane was confirmed via its resonance signal at 0.21 ppm in the ^{1}H NMR spectrum. Unfortunately, a further unselective decomposition of complex **13b** was observed. Conceivably, the presence of lithium bromide is decreasing the dissociation temperature of the P-N bond under formation of the phosphinidene complex **24b** that is further decomposing into a mixture of unidentifiable products (Scheme 70).

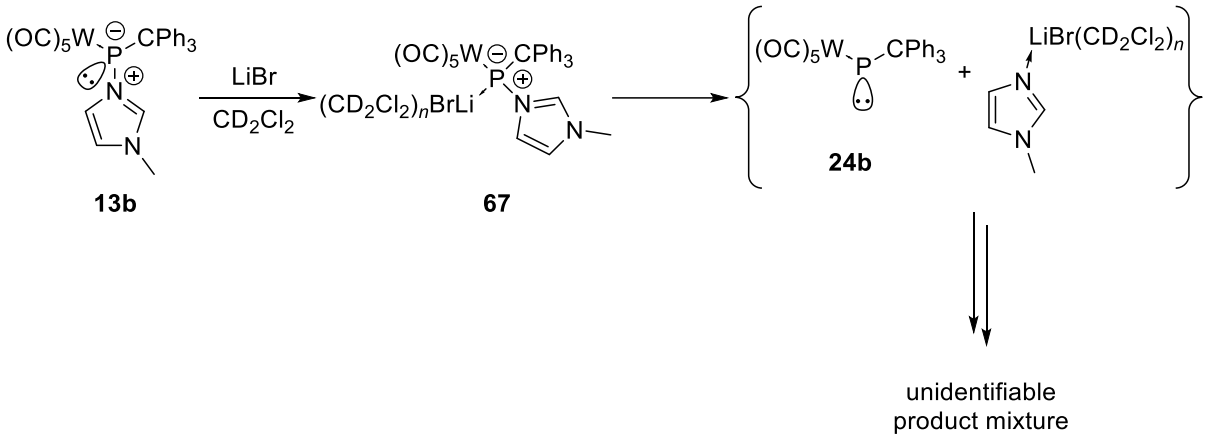

Scheme 70: Proposed decomposition of the *N*-methylimidazole-to-phosphinidene complex adduct **13b** in presence of lithium bromide.

To achieve a higher stability of the formal *N*-methylimidazole-to-phosphenium complex adducts a substitution of the *P*-bound hydrogen by an alkyl group is expedient and undesired simple side reactions as the deprotonation reaction can be prevented. For that, the *N*-methylimidazole-to-phosphinidene complex adduct **13b** was reacted with methyl trifluoromethanesulfonate (Scheme 71).

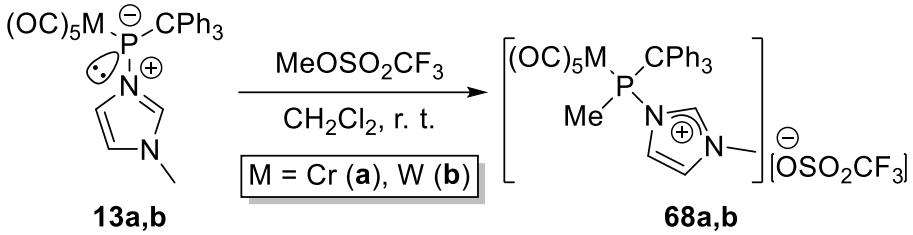

Scheme 71: Synthesis of methylphosphanylimidazolium complex **68**.

The ^{31}P NMR resonance signals of the selectively formed methyl(triphenylmethyl)phosphanyl-imidazolium complexes **68** were downfield-shifted compared to the respective *P*-H substituted complexes **64** and appeared at 165.1 ppm (**68a**) and 116.4 ppm ($^{1}J_{W,P}$ = 273.7 Hz) (**68b**) (Figure 63).

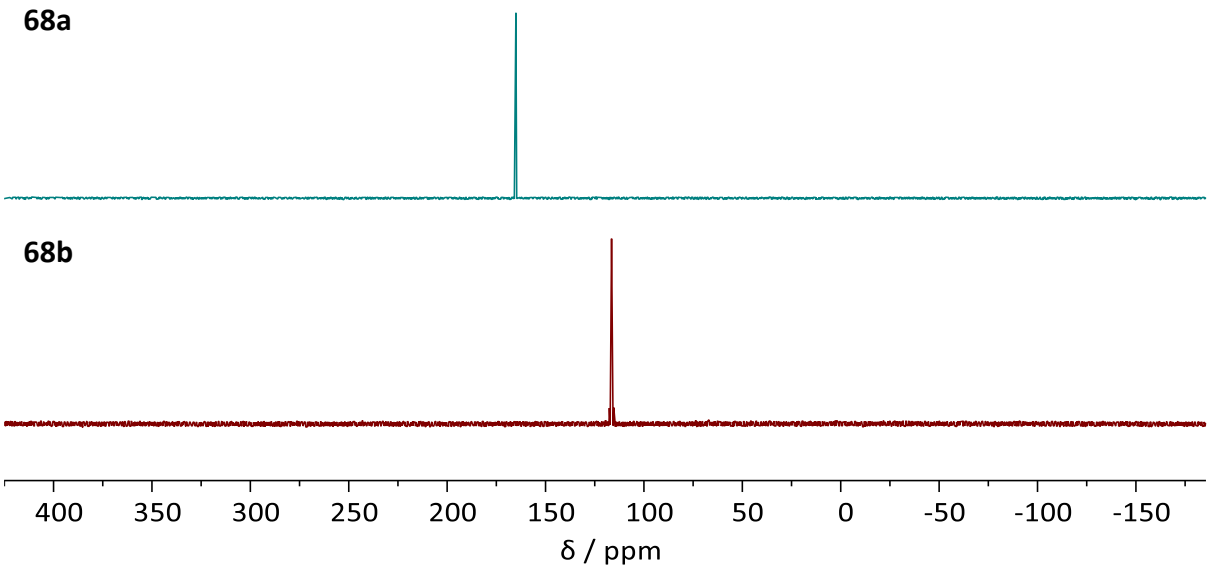

Figure 63: ^{31}P NMR spectra (**68a**: 202.44 MHz, 298 K, CD_2Cl_2, **68b**: 121.51 MHz, 299 K, CD_2Cl_2) of methylphosphanylimidazolium complexes **68**.

This is also reflected by the ^{15}N{^{1}H} NMR data obtained via ge-2D NMR ^{1}H,^{15}N HMBC experiments. The differences in the ^{15}N NMR chemical shifts $\Delta\delta(^{15}N)$ of the two nitrogen nuclei in complexes **68** are more than doubled (**68a**: $\Delta\delta(^{15}N)$ = 11.7 ppm, **68b**: $\Delta\delta(^{15}N)$ = 11.0 ppm) compared to the ones of complexes **64** again indicating weaker P-N interactions resulting in an increased phosphenium character. Nevertheless, the $\Delta\delta(^{15}N)$ values are still relatively small compared to the ones of the *N*-methylimidazole-to-phosphinidene complex adduct **13** showing that the positive charge still is significantly located within the *N*-methylimidazole moiety. Unexpectedly, in the ^{1}H and ^{13}C{^{1}H} NMR spectra the triphenylmethyl group produced complicated resonance signals where every phenyl group was different and thus displaying a hindered rotation of the P-C bond. Particularly the *ortho*-C*H* protons differ significantly for each phenyl group with broad resonance signals at 7.64 ppm, 7.30 ppm and 6.61 ppm. This indicates again the increased steric hindrance at phosphorus due to the alkyl substitution.

The greater stability of the *P*-Me derivative with respect to the *P*-H derivative enabled a less complicated growing of single crystals that were suitable for X-ray diffraction analyses (**68a**: Figure 65). As expected, the obtained molecular structure revealed an interaction of the trifluoromethanesulfonate anion with the C^2-bound hydrogen via hydrogen bonding with an H2-O7 distance of 2.17156(17) Å. The P1-N1 bond length of 1.778(4) Å is significantly shorter than the one in the *N*-methylimidazole-to-phosphinidene complex adduct **13b** indicating a stronger P-N bond having less dative character. However, also the N1-C2 and N2-C2 bond

lengths are very similar indicating a considerable covalency of the P-N bond together with a pronounced contribution of a delocalized positive charge within the imidazole ring.

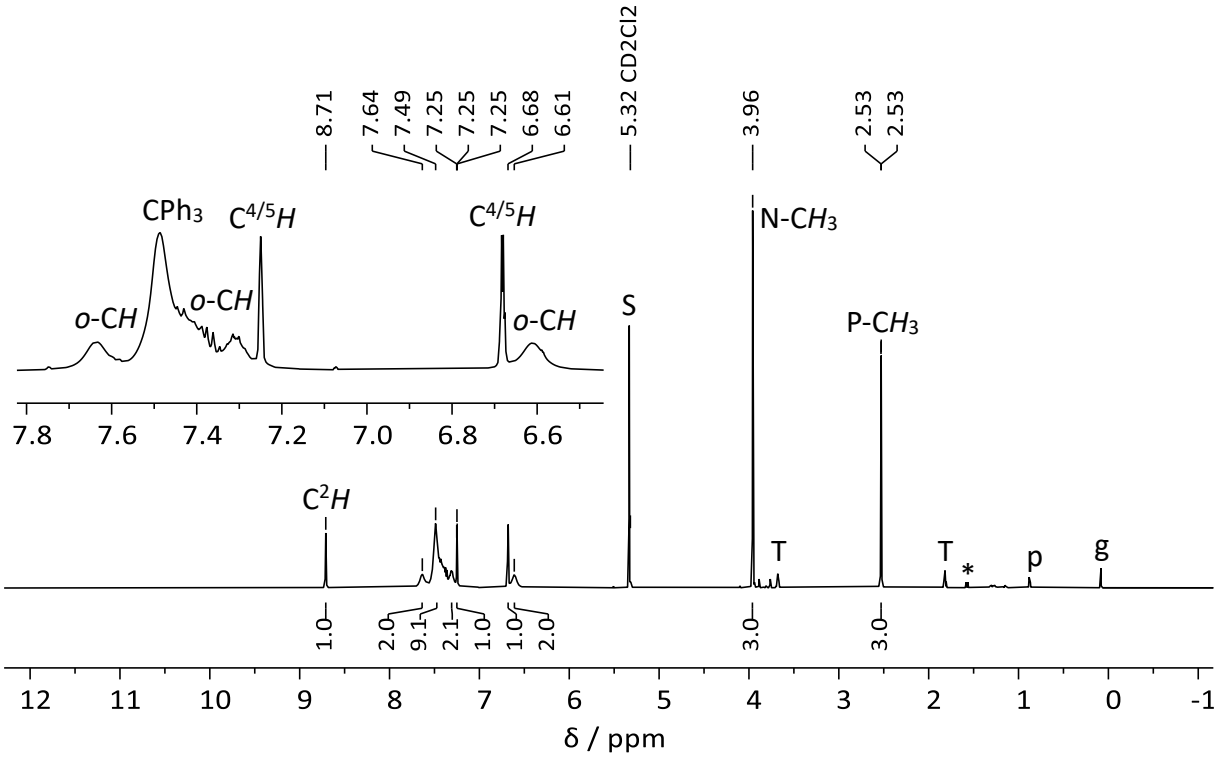

Figure 64: ^{1}H NMR spectrum (500.04 MHz, 298 K, CD_2Cl_2) of the methylphosphanylimidazolium complex **68b**. The resonances of traces of tetrahydrofuran are marked with a "T", of *n*-pentane with a "p" and of grease with a "g". The resonance of traces of an unidentified side product is marked with an asterisk. The residual resonance signal of the deuterated solvent is marked with an "S".

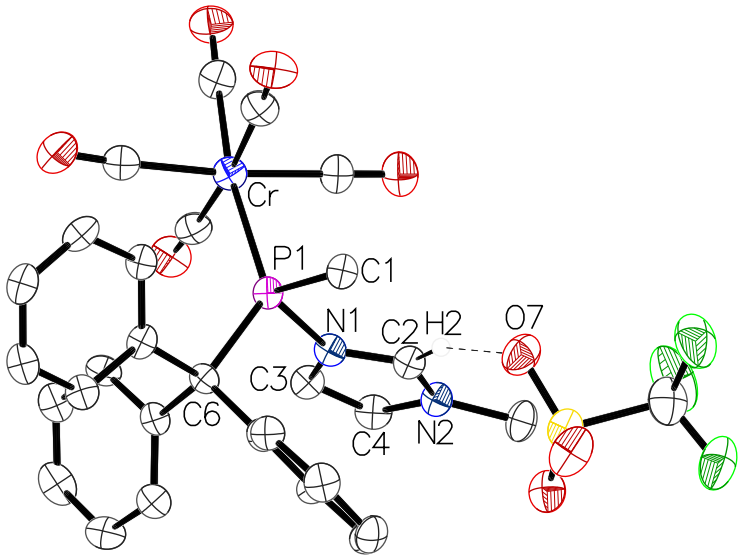

Figure 65: Molecular structures of **68a** in the single crystal lattice at 100(2) K. Thermal ellipsoids are set at 50 % probability level. Solvent molecules and hydrogen atoms were omitted for clarity except for those bound to phosphorus atoms. Selected bond lengths / Å and bond angles / °: Cr-P1 2.4024(15), P1-C1 1.828(5), P1-C6 1.935(5), P1-N1 1.778(4), N1-C2 1.338(7), N2-C2 1.328(7), H2-O7 2.17156(17), C1-P-Cr 111.61(18), C1-P1-C6 103.2(2), C6-P1-Cr 131.59(16), N1-P1-Cr 106.91(14), N1-P1-C1 98.3(2), N1-P1-C6 99.9(2).

Surprisingly, reactions of the isocyanide-to-phosphinidene complexes **6a,c** with trifluoromethanesulfonic acid as well as with methyl trifluoromethanesulfonate resulted in the selective formation of the thermal decomposition products under ambient conditions and thus facilitating a simple access to cyano(triphenylmethyl)phosphane complexes **23** (Scheme 72).

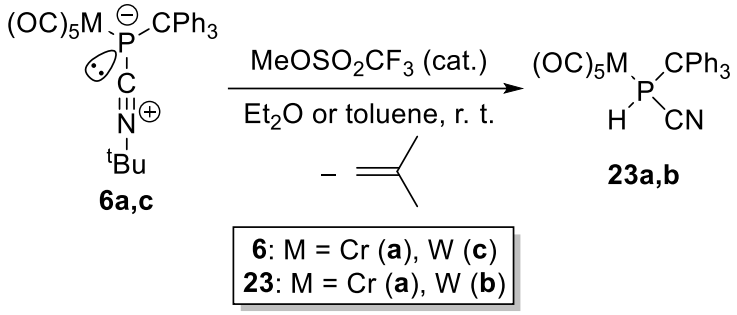

Scheme 72: Synthesis of cyano(triphenylmethyl)phosphane complexes **23**.

Complexes **23** are the formal insertion products of the phosphinidene complexes into hydrogen cyanide and, hence, can be indirectly integrated in the sequence of the Brønsted-Lowry acid reactions as product of a reaction with a very weak acid. In the ^{31}P NMR spectra the resonance signals of **23** were found most highfield shifted compared to all aforementioned acid reaction products at 27.0 ppm ($^{1}J_{P,H}$ = 354.4 Hz) (**23a**) and −22.4 ppm ($^{1}J_{P,H}$ = 367.3 Hz, $^{1}J_{W,P}$ = 244.6 Hz) (**23b**). This can be explained by the less electron-withdrawing effect of the cyano group which results in a stronger electronic shielding of the phosphorus nucleus.

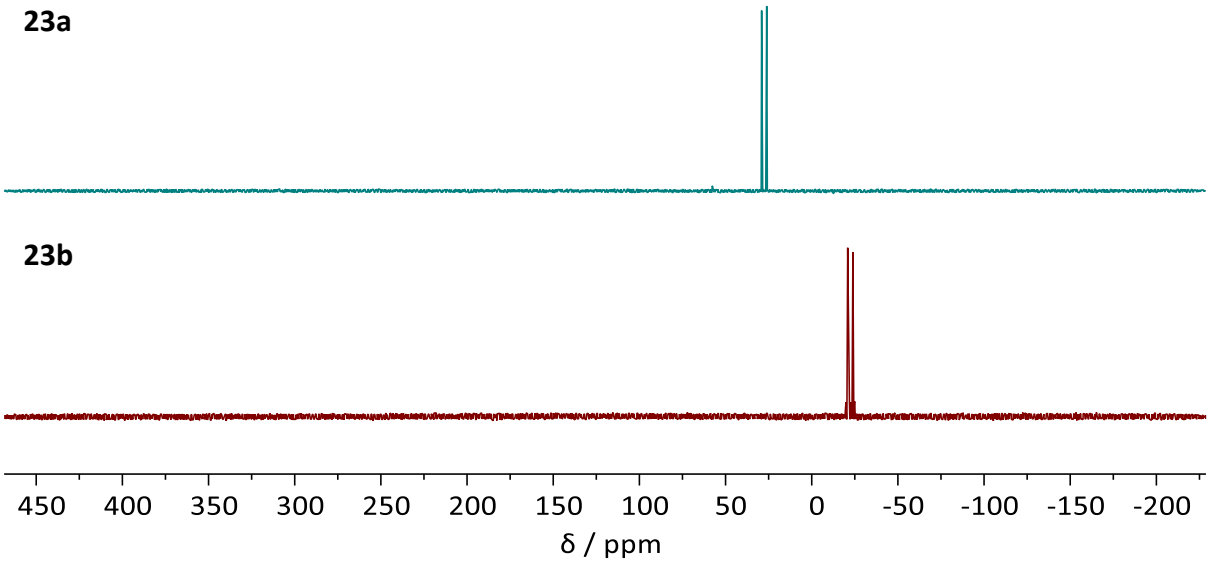

Figure 66: ^{31}P NMR spectra (121.51 MHz, **23a**: 299 K, C_6D_6, **23b**: 298 K, Et_2O) of cyano(triphenylmethyl)-phosphane complexes **23**.

This increased shielding is also reflected by the *P*-bound protons that are found at 5.69 ppm (**23a**) and 5.90 ppm (**23b**).

3.3.4 Donor-centered reactions of isocyanide-to-phosphinidene complex adducts

The shown dissociation and donor substitution reactions of the donor-to-phosphinidene complex adducts are very reminiscent to the reactivity of transition metal complexes and, hence, the adduct itself can also be described as ligand-to-nonmetal complex. As one litmus test of an *end*-on bound ligand nonmetal complex, the conversion of the P-donor unit was addressed focusing on the isocyanide ligand case.

The conversion of organic isocyanide ligands into heteroatom-substituted carbenes in transition metal complexes using primary amines is one of the earliest examples in organometallic chemistry.[193–195] Therefore, the isocyanide-to-phosphinidene complex adducts **6a,c** were treated with primary amines of different steric demand. The reaction of **6a,c** with methyl amine in THF at ambient temperature gave selectively the η^1-phosphaguanidine-κ*P* complexes **70a,b** (Scheme 73), but the products not only show the preference for a 1,2-addition of the N-H bond to the P-C bond of the donor but also a somewhat surprising protropic rearrangement as reveiled by the X-ray structure (below).

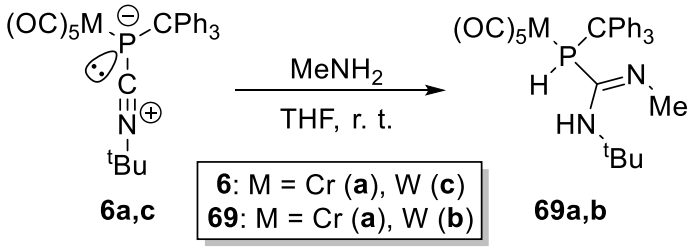

Scheme 73: Synthesis of η^1-phosphaguanidine-κ*P* complexes **69**.

The ^{31}P NMR spectra of the η^1-phosphaguanidine complexes **69a,b** displayed resonances at 14.4 ppm ($^1J_{P,H}$ = 339.5 Hz) (**69a**) and −27.2 ppm ($^1J_{P,H}$ = 349.2 Hz, $^1J_{W,P}$ = 220.5 Hz) (**69b**). The NMR data are in very good agreement with the one of the very few known η^1-phosphaguanidine complexes, namely [W(CO)$_2$(Cp){P(Ph)$_2$C(N-*p*-tol)N(H)*p*-tol}Cl] (*p*-tol = *para*-tolyl) (δ(^{31}P) = −25.6 ppm).[276] To test the outcome with a sterically more demanding amine, the reaction with isopropylamine in THF was examined which proceeded similarly with respect to the selective formation of the η^1-phosphaguanidine complexes **70a,b** (Scheme 74). But the reaction progress decreased strongly and a full conversion was observed only after one week. When the solvent was changed, *i.e.*, the reaction performed in neat

isopropylamine, the selective formation of complexes **70** was observed within one day Somewhat counterintuitively, the ^{31}P NMR resonances of complexes **70** were slightly downfield-shifted compared to complexes **69** despite the larger positive inductive effect of the isopropyl substituent. Apparently, the hybridization changes to have a higher p-orbital contribution in the P-C bond to sterically accommodate the larger group.

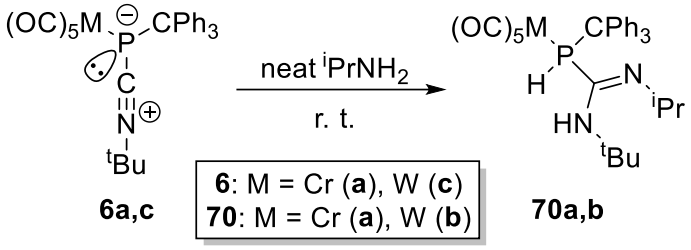

Scheme 74: Synthesis of η^1-phosphaguanidine-κ*P* complexes **70**.

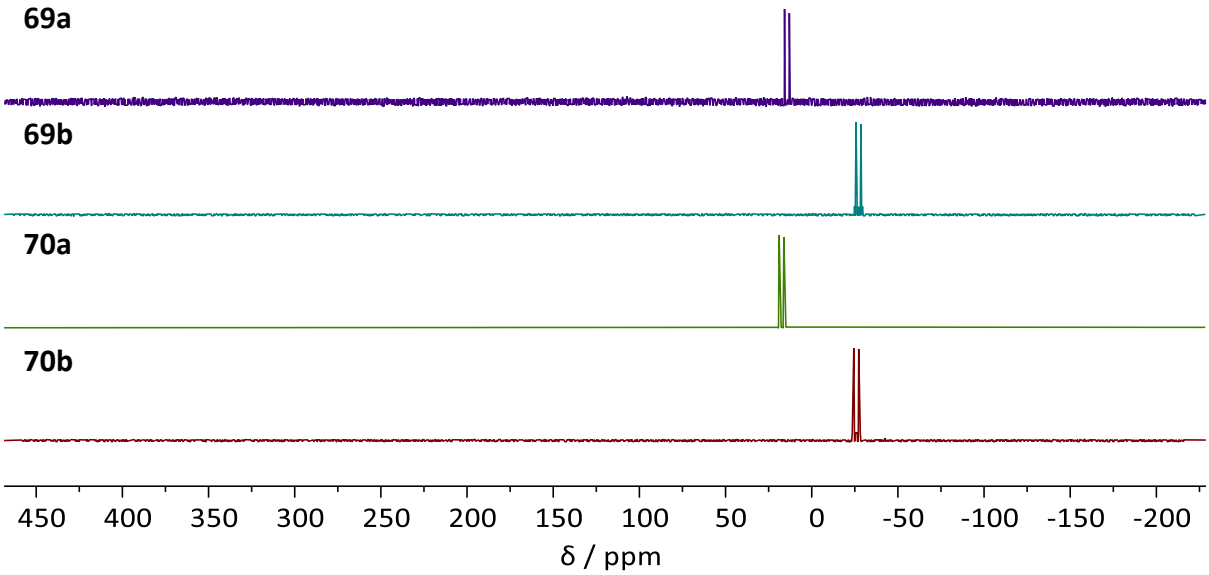

Figure 67: ^{31}P NMR spectra (121.51 MHz, **69a**: 299 K, C_6D_6, **69b**: 298 K, $CDCl_3$, **70a,b**: 298 K, C_6D_6) of the η^1-phosphaguanidine-κ*P* complexes **69** and **70**.

The molecular structures of complexes **69** and **70** were confirmed by singly crystal X-ray crystallography (Figure 68).

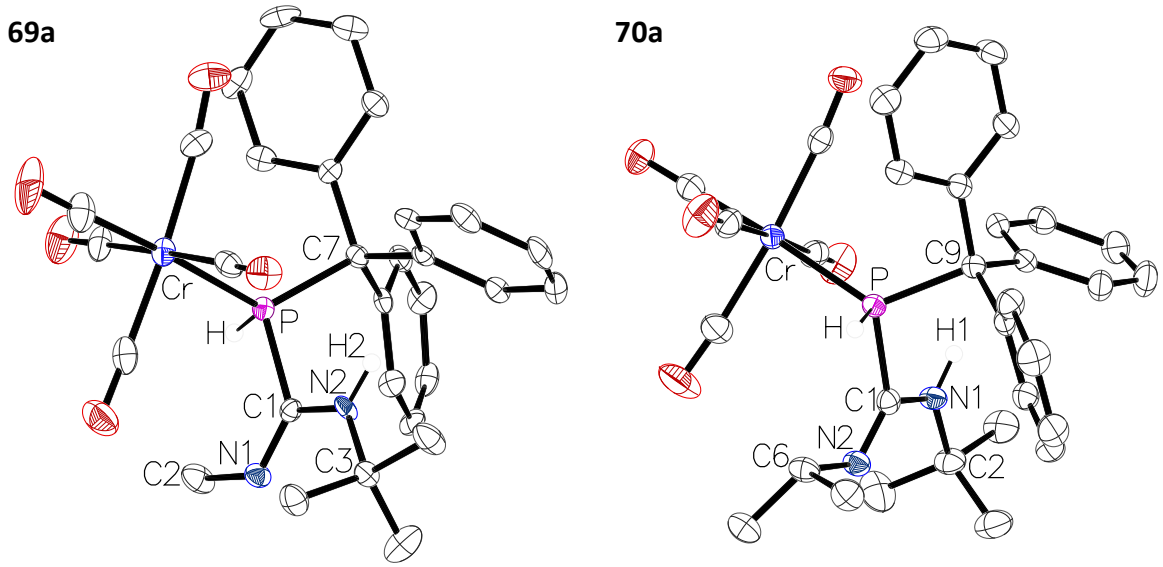

Figure 68: Molecular structures of **69a** and **70a** in the single crystal lattice at 123(2) K. Thermal ellipsoids are set at 50 % probability level. Hydrogen atoms were omitted for clarity except for those bound to phosphorus and nitrogen atoms. Selected bond lengths / Å and bond angles / ° (bond lengths and bond angles in square brackets are of the second independent molecule of **69a**): **69a**: Cr-P 2.3804(13) [2.3946(13)], P-C1 1.873(3) [1.873(3)], P-C7 1.938(3) [1.938(3)], N1-C1 1.270(4) [1.269(4)], N2-C1 1.368(4) [1.370(4)], C1-P-Cr 109.60(11) [108.87(11)], C1-P-C7 109.46(15) [109.16(15)], C7-P-Cr 127.27(11) [129.24(12)], N1-C1-N2 121.2(3) [121.4(3)]; **70a**: Cr-P 2.3952(6), P-C1 1.880(2), P-C9 1.948(2), N1-C1 1.369(3), N2-C1 1.278(3), C1-P-Cr 112.03(7), C1-P-C9 107.60(9), C9-P-Cr 126.93(6), N2-C1-N1 121.23(19).

A further increase of the steric demand of the amine by using *tert*-butylamine not only slowed down drastically the reaction with complexes **6a,c** – full conversion was not observed in THF under ambient conditions – but altered the entire reaction course (Scheme 75). In the case of the reaction with **6c**, the major product showed a resonance signal at −33.9 ppm ($^1J_{W,P}$ = 103.8 Hz) without any P,H coupling which is shlightly highfield-shifted compared to those of **69** and **70**. In order to achieve completion, the temperature was enhanced to 40 °C but no full conversion was achieved; beyond 40 °C the reaction became very unselective (Figure 69).

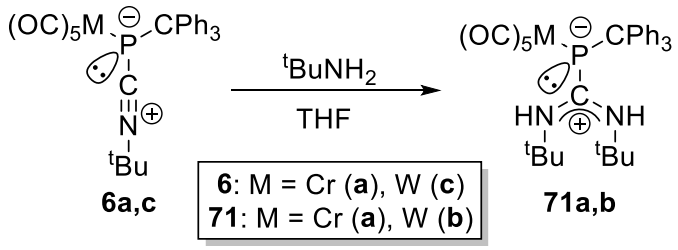

Scheme 75: Generation of diaminocarbene-to-phosphinidene complex adducts **71**.

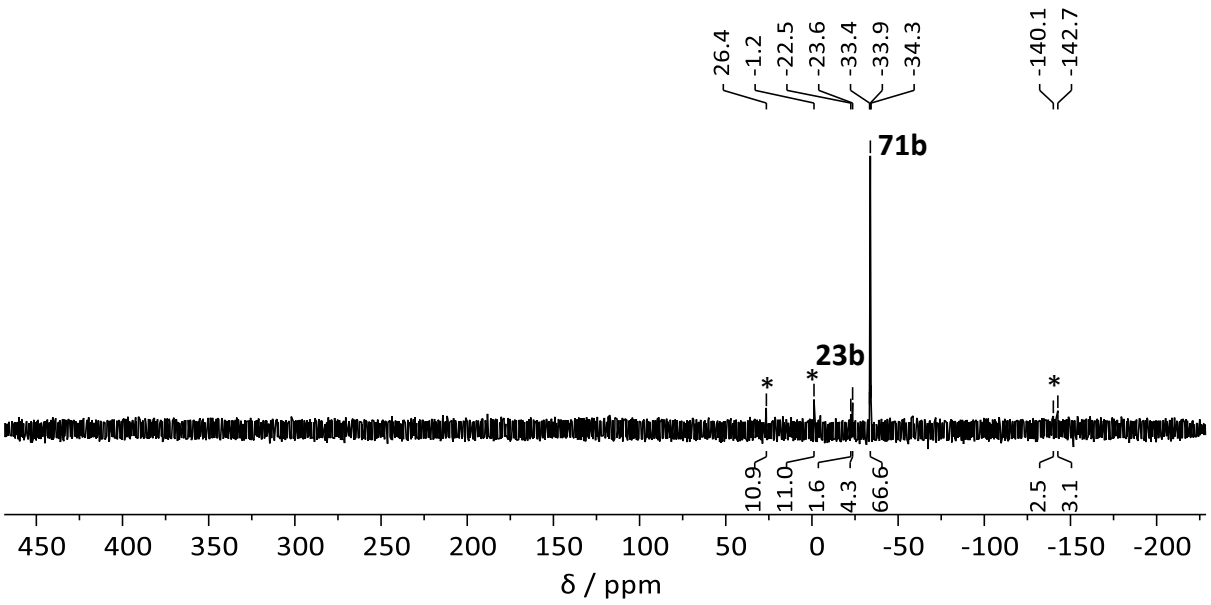

Figure 69: ^{31}P NMR spectrum (121.51 MHz, 298 K, THF) of the reaction mixture of **6b** with *tert*-butylamine after 27 days at 40 °C.

Furthermore, the small $^{1}J_{W,P}$ coupling constant in **71b** indicated an increased negative charge density at phosphorus similar to the isocyanide-to-phosphinidene complex adduct **6c**. These data imply the formation of the zwitterionic diaminocarbene-to-phosphinidene complex adducts **71**. As discussed beforehand for the case of the isocyanide-to-phosphinidene complex adducts **6** on the basis of an NRT analysis (see page 33), the alternative canonical form would represent a valence isomer, *i.e.*, the phosphaalkene complex **72** with a different geometry and hybridization at the P center (Figure 70), but it should have a smaller contribution to the ground state description and/or even could be just a transition state.

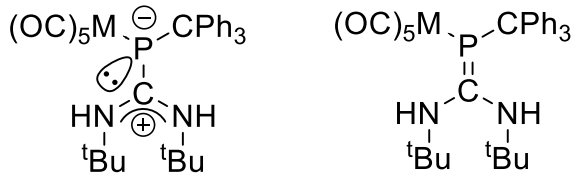

71 **72**

Figure 70: The diaminocarbene-to-phosphinidene complex adduct **71** and its hypothetical valence isomer **72**.

Early examples from the literature of then called inversely polarized phosphaalkene complexes, having two amino substituents at the carbon atom, have comparable ^{31}P NMR data, are $[W(CO)_5\{^tBuP{=}C(NMe_2)_2\}]$ ($\delta(^{31}P)$ = −25.1 ppm, $^{1}J_{W,P}$ = 153.5 Hz)[106] and $[W(CO)_5\{PhP(IDipp)\}]$ (IDipp = 1,3-bis(2,6-diisopropylphenyl)imidazole-2-ylidene) ($\delta(^{31}P)$ = −57.7 ppm, $^{1}J_{W,P}$ = 120 Hz).[109] In addition, the similarity of the chemical shift of **71b** and of IMe_4-to phosphorus complex adduct **40**, obtained within this work, is striking.

The reaction pathway of isocyanide-to-phosphinidene complex adduct **6c** towards alkyl amines was closely inspected by means of quantum chemical calculations at the $COSMO_{THF}$/CCSD(T)/def2-TZVPP(ecp) level by Espinosa Ferao (Figure 72).[216] For the sake of computational efficiency the simplified *P-tert*-butyl substituted pentacarbonyltungsten(0) model complex **6c^{tBu}** was used.

In case of methylamine, the nitrogen lone pair attacks the highly electrophilic isocyanide ligand C atom of the model complex **6c^{tBu}** in a nucleophilic manner under formation of the intermediate **73a^{E}** ("a" denotes R = Me and the superscript "*E*" or "*Z*" the configuration of the imine group) (Figure 71). After a [1,3]H shift via a moderate energetic barrier the very stable (model) phosphaguanidine complex **74a** is formed. After rotation about the P-C bond the rotamer **74a^{c}** (the superscript "c" denotes a conformational isomer) it could undergo a kinetically hampered [1,3]H shift from the phosphorus to the nitrogen atom originally belonging to the isocyanide donor (**74a^{c}**→**75a^{c}**) under formation of the more stable (model) diaminocarbene-to-phosphinidene complex adduct **75a^{c}**. The alternative mechanism via the *Z*-configured isomer **73a^{Z}** is unfavored compared to the aforementioned protropy in complex **73a^{E}**.

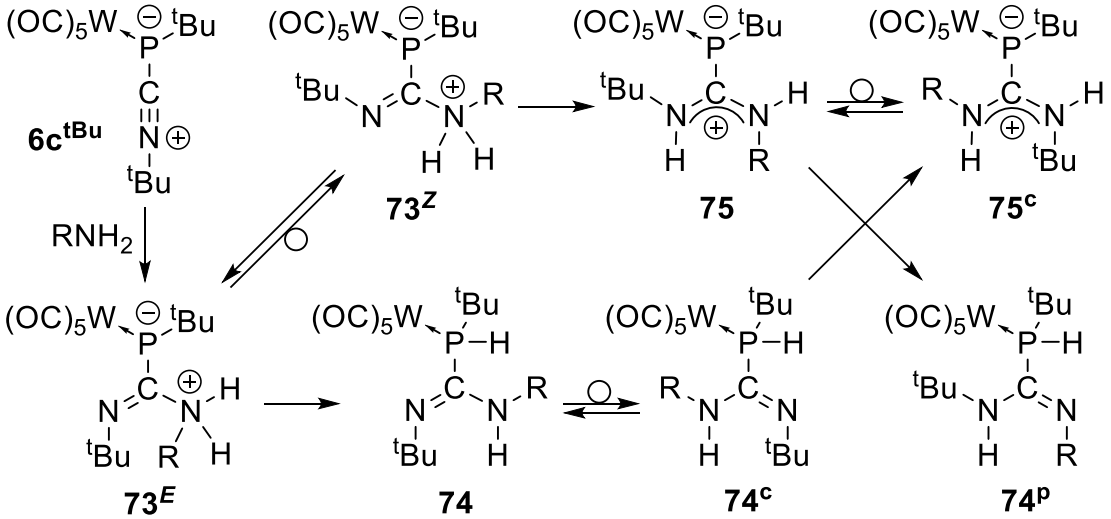

Figure 71: Proposed mechanism for the reaction of model isocyanide-to-phosphinidene complex adduct **6c^{tBu}** with alkyl amines.

The experimentally observed product with methylamine **69a** has a slightly different structure as the model complex **74a** or **74a^{c}** but a protomer **74a^{p}** (superscript "p" denotes the protomer). The proton transfer arises either intermolecularly (not studied) or intramolecularly from **75a**. In case of the reaction with phosphaguanidine, the phosphaguanidine complex

protomer **74b^{p}** ("b" denotes R = ^{i}Pr) ($\Delta G^{‡}$ = −12.6 kcal/mol) is more stable than its isomer **74b** ($\Delta G^{‡}$ = −10.9 kcal/mol).

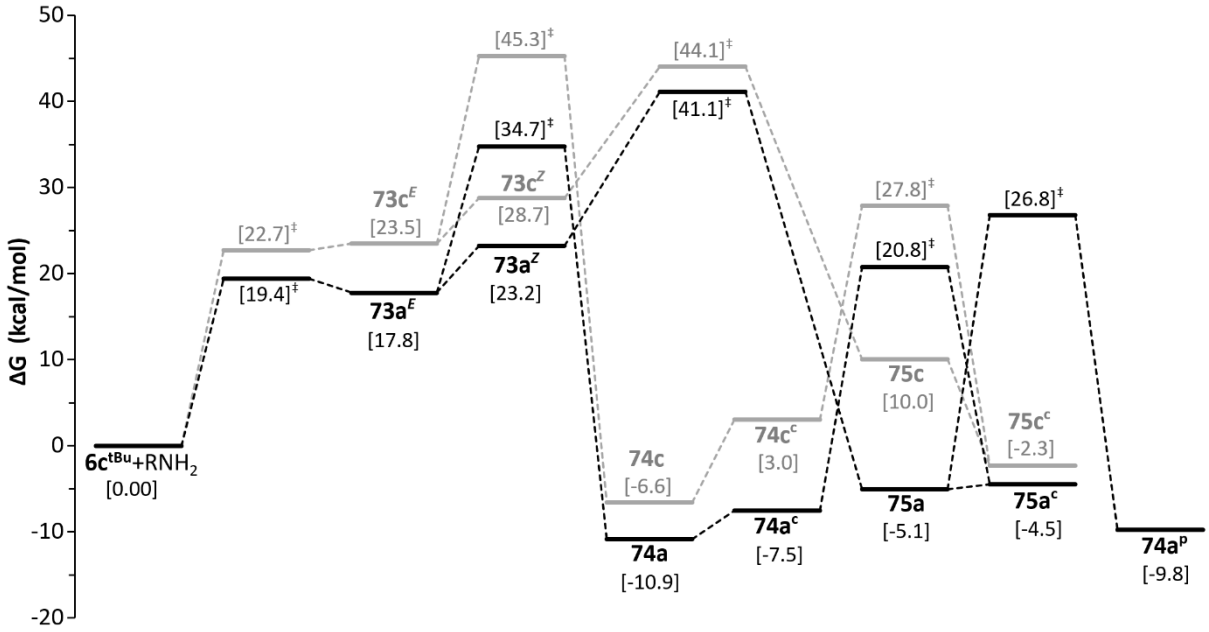

Figure 72: Computed [COSMO$_{THF}$/CCSD(T)/def2-TZVPPecp//COSMO$_{THF}$/B3LYP-D3/def2-TZVPecp] relative Gibbs free energy profile for the reaction of model isocyanide complex **6c^{tBu}** with methyl ("**a**" in black) and *tert*-butylamine ("**c**" in grey).

The sterically more demanding isopropylamine gives rise to similar or slightly higher energy model intermediates **73b^{E}** (ΔG = 20.5 kcal/mol), **74b** (ΔG = −10.9 kcal/mol) and the most stable final product **74b^{p}** (ΔG = −12.6 kcal/mol). This seems to indicate that the increase of steric bulk favors **74^{p}** over the initially formed intermediate **74** and, hence, points to a thermodynamic preference for the protomer also in case of reaction with methylamine when sterically crowded real triphenylmethyl group is used as P-substituent (**6c**^{tBu}).

As expected, the reaction with the sterically more demanding *tert*-butylamine gives rise to an even higher steps in the energy profile compared to methylamine (Figure 72). However, the lower barrier for the N-to-N proton transfer **73c^{Z}→75c** ($\Delta\Delta G^{‡}$ = 15.4 kcal/mol) compared to the N-to-P transfer **73c^{E}→74c** ($\Delta\Delta G^{‡}$ = 22.4 kcal/mol) is very remarkable. Thus, after rotation, the diaminocarbene adduct conformer **75c^{c}** is the kinetically preferred product. This is in good agreement with the experimental ^{31}P NMR spectroscopic observations in this case.

The C-P bond strength parameters in **75c^{c}** compared to reported model NHC-to-phosphinidene complex adducts[86] (d = 1.831/1.819 Å; WBI = 1.059/1.020; MBO = 1.036/1.071; ρ(r) = 0.1487/0.1473 au; ¼$\nabla^2\rho$(r) = −0.0473/−0.0180 e/Å^5) support the proposed

zwitterionic structure for the experimental (**71a**) or the model (**75**/**75^{c}**) diaminocarbene-to-phosphinidene complex adduct. Indeed, the above mentioned linkage should be better considered as a dative C→P bonding description according to the rather small electron transfer from the ligand to the phosphinidene complex fragment (Δq^{nat} = 0.412 e).

Computed ^{31}P NMR chemical shifts for the model phosphaguanidine complexes **74a^{p}** (−25.3 ppm) and **74b^{p}** (−22.3 ppm) are in very good agreement with the downfield-shift trend observed experimentally for the product with methylamine **69b** and isopropylamine **70b**, respectively.

3.4 DFT CALCULATIONS ON DONOR-TO-PHOSPHINIDENE COMPLEXES

3.4.1 Dativity of the P-donor interactions

The dative character of the described ligand-to-phosphinidene complexes (**6c^{Me}**, **13b**, **14b**, **15b**, **19b**, **20b**, **21b** the 1,3-dimethylimidazol-2-ylidene-to-phosphinidene complex adduct **40^{IMe2}** and **71**) was further investigated using Bader's quantum theory of atoms in molecules (QTAIM) by Espinosa Ferao.[216] The Holthausen-Cowley criteria for dative bonding are fulfilled by the L→P bond of complexes **13–15**, **19–21**, **40^{IMe2}** and **71** (Figure 73): existence of a bond critical point (BCP) closer to the electron acceptor center (P in these cases) with vanishing $\nabla^2\rho$ value, and displaying two valence-shell charge concentration (VSCC) regions located at the basin of the donor atom along the central part of the bond path.[277] Very recently, the relative charge concentration bands position parameter τ_{VSCC}, defined as the product of the two signed VSCC positions divided by the square of the bond path distance (to provide an adimensional quantity),[87] here τ_{VSCC} = 0.0013 together with the small positive value of $\nabla^2\rho$ at the BCP allows unequivocally assignment to a dative bonding. The positions of the minima for $VSCC_{N/C}$ and $VSCC_{P}$ (*e.g.* −0.624 Å and −0.007 Å, respectively, for **71**) were obtained by deconvolution of the central part of the $\nabla^2\rho$ plot along the L-P bond path into asymmetric Gaussian functions, as previously reported.[87] The plot of the Laplacian variation along the bond path of the phosphane adducts **19–21** showed a similar bonding feature as the halide (Cl^-, Br^- and I^-) adducts (Figure 74).[87] Therefore, the name of ionic-enhanced dative bonding is proposed for the phosphane-to-phosphinidene complex adducts **19–21**.

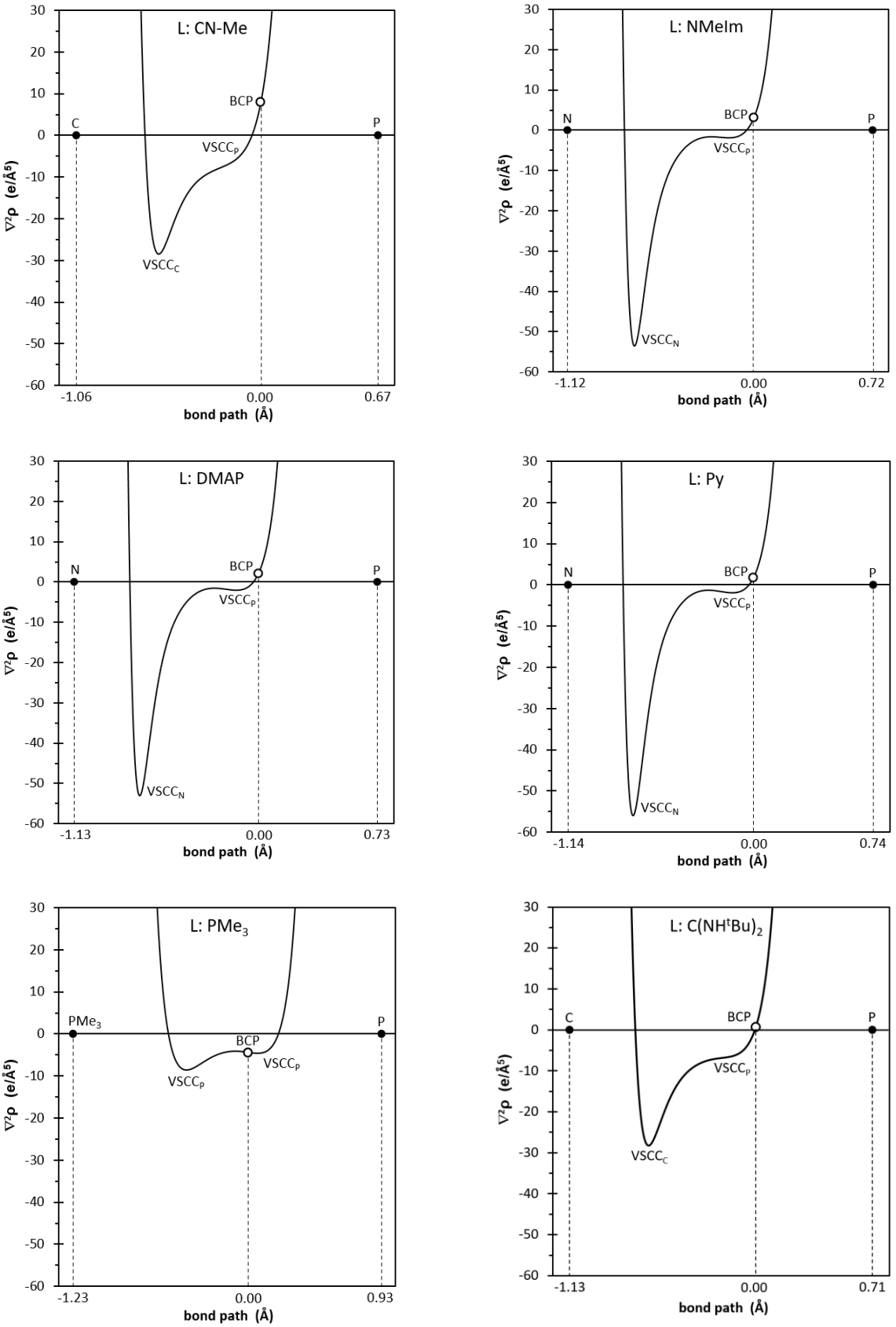

Figure 73: Computed [B3LYP-D3/def2-TZVPP(ecp)//B3LYP-D3/def2-TZVP(ecp)] variation of the Laplacian of electron density $\nabla^2\rho$ for complexes **6c^{Me}**, **13b**, **14b**, **15b**, **19b** and **71** along the L-P bond path.[216]

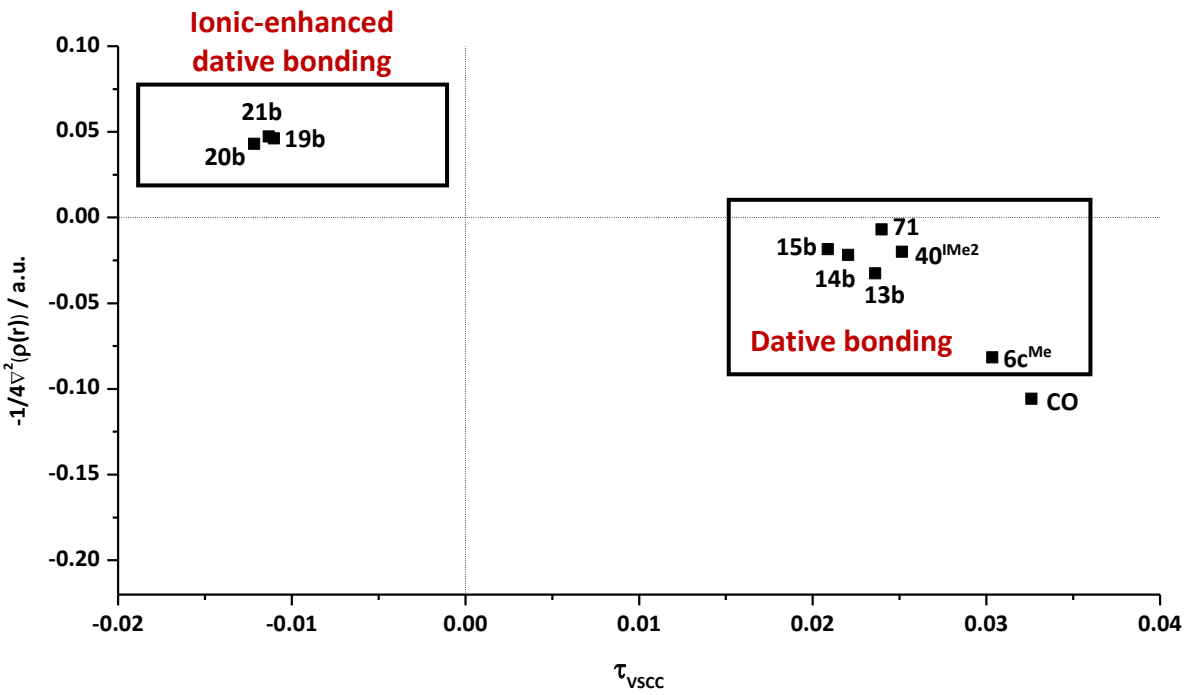

Figure 74: Plot of Laplacian of ρ(r) versus relative position of charge-concentration bands for the donor-to-phosphinidene complex adducts **6c**, **13b**, **14b**, **15b**, **19b**, **20b**, **21b**, **40^{IMe2}**, **71** and a CO adduct.[216]

Furthermore, adduct complexes **13–21**, **40^{IMe2}** and **71** also show a significant electron density transfer from the ligand to the phosphinidene complex unit of ca. 0.5 e and relatively high HOMO energy values above −6.12 eV (Table 21). Adducts resulting from phosphane and carbene donors (**19–21**, **40^{IMe2}** and **71**) exhibit a robust L-P bond with Wiberg bond indices (WBI)[278] close to unity and rather large complexation Gibbs free energies, whereas those arising from heteroaromatic N-donors (**13–15**) display moderately weak N-P bonds and rather low complexation energies. Complexes **13** and **14** represent interesting cases because they constitute the most labile isolable adducts and, thus, being the optimal case in point for ligand substitution reactions (*vide infra*).

The most different situation was observed for **6c^{Me}** featuring a remarkably high $\nabla^2\rho$ value (7.87 e/Å^5) that indicates mostly covalent character for the ligand-P linkage. This is in line with low electron density transfer to the phosphinidene complex unit (0.33 e) because of π-backdonation to the isocyanide ligand, which is supported by the partial double bond character, as pointed out by the high WBI (Table 21).

Table 21: Computed [CPCM$_{tol}$/PWPB95-D3/def2-QZVPP(ecp)//CPCM$_{tol}$/B3LYP-D3/def2-TZVP(ecp)] energetic, electronic and bond-strength related parameters for **6c^{Me}**, **13b**, **14b**, **15b**, **19b**, **20b**, **21b**, **40^{IMe2}** and **71**.[216]

Complex	Donor	ΔG_{comp} / kcal/mol	E_{def} / kcal/mol	ε_{HOMO} / eV	ε_{LUMO} / eV	q_P / e Mulliken/Löwdin	WBI_{L-P}
6c^{Me}	CNMe	−21.44	13.86	−6.34	−0.66	−0.33 / −0.24	1.244
13b	*N*-MeIm	−13.26	15.79	−6.07	−0.21	−0.51 / −0.50	0.628
14b	DMAP	−15.30	15.26	−5.92	−0.42	−0.51 / −0.48	0.622
15b	Py	−9.94	14.86	−6.12	−1.19	−0.45 / −0.42	0.628
19b	PMe_3	−29.08	19.24	−6.07	−0.29	−0.57 / −0.51	1.030
20b	PEt_3	−24.71	21.11	−6.00	−0.31	−0.46 / −0.49	1.043
21b	P^nBu_3	−30.96	20.74	−6.04	−0.24	−0.52 / −0.49	1.025
40^{IMe2}	IMe_2	−36.05	18.13	−5.88	−0.30	−0.53 / −0.38	0.999
71	$C(NH^tBu)_2$	−36.53	24.05	−5.90	−0.30	−0.55 / −0.62	1.046

The deformation energy E_{def} of the phosphinidene complex fragment upon formal association with donor molecules reflects the geometrical change induced upon electron donation and the resulting steric pressure. Therefore, E_{def} is increasing for a larger charge transfer q_P and a increasing steric demand of the donor. The largest deformation energy (E_{def} = 24.05 kcal/mol) was found for the bisaminocarbene-to-phosphinidene complex adduct **71** which is in accordance with the large charge transfer ($q_p^{Mulliken}$ = −0.55 e / $q_p^{Löwdin}$ = −0.62 e) and the steric demand of the *N*-^{t}Bu substituents while the deformation energies for the N-donor adducts **13b–15b** are significantly smaller due to their small charge transfer and sterically less demanding properties. The smallest deformation energy (E_{def} = 13.86 kcal/mol) was found for the methyl isocyanide-to-phosphinidene complex adduct **6c^{Me}** which coincides with the low charge transfer ($q_p^{Mulliken}$ = −0.33 e / $q_p^{Löwdin}$ = −0.24 e) and the linear donor molecule which is bearing only a methyl group as organic substituent.

3.4.2 Thermodynamic oxygen-transfer potential and fluoride ion affinity

Organyl-substituted phosphinidene-κ*P* pentacarbonyltungsten(0) complexes, R-P-W(CO)$_5$, possess highly electrophilic phosphorus centers as recently pointed out[73] by their thermodynamic oxygen-transfer potentials (TOP),[279] that revealed augmented ease to be oxidized (to the respective phosphinidene oxide) of *P*-methyl substituted phosphinidene complexes (TOP = −414 kJ/mol) compared to ethyl isocyanide (TOP = −395 kJ/mol). Espinosa

Ferao has repeated the calculations at a much higher level of theory (PW5B95-D3/def2-QZVPP(ecp)//RIJCOSX-B3LYP-D3/def2-TZVP(ecp)) and expanded it by the *P*-triphenylmethyl and *P-tert*-butyl substituted complexes.[216] The computed TOP increases in the order CPh_3 < Me < ^{t}Bu (−438 kJ/mol, −473 kJ/mol and −480 kJ/mol, respectively) (Figure 75).

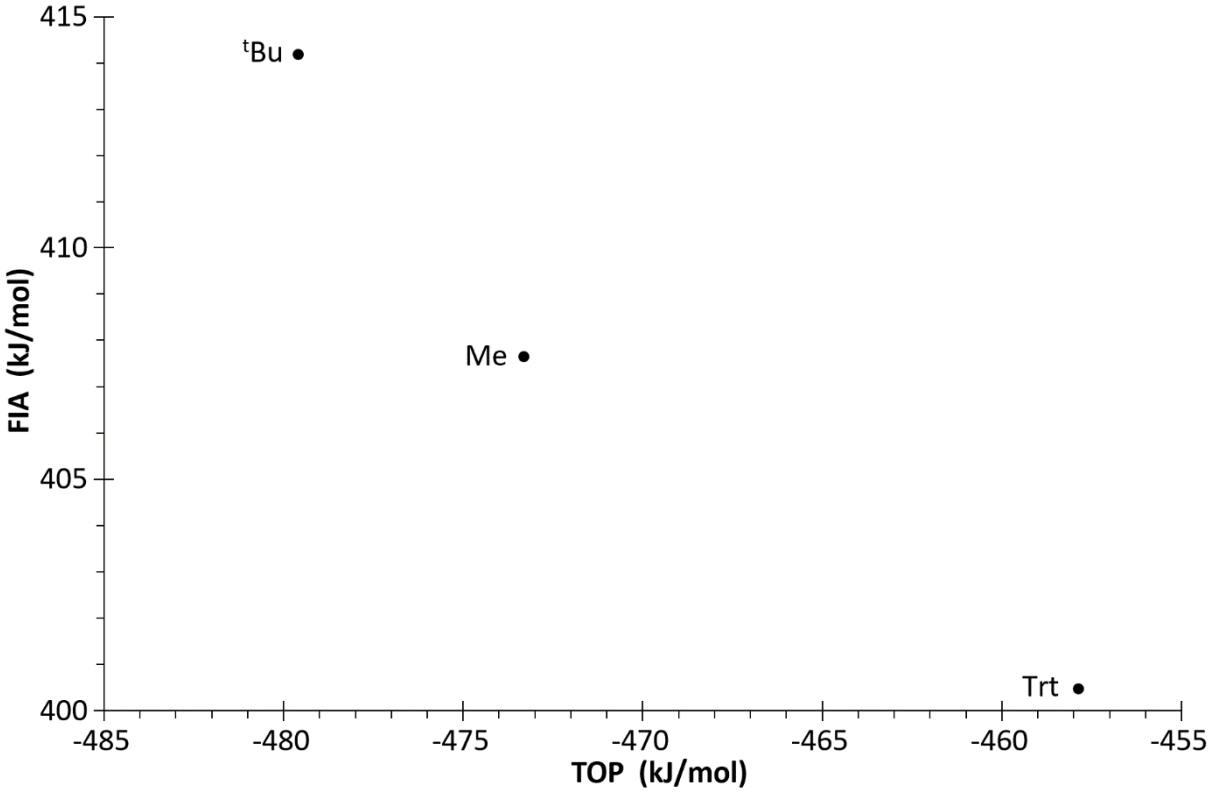

Figure 75: Computed [CPCM$_{tol}$/PWPB95-D3/def2-QZVPP(ecp)//CPCM$_{tol}$/B3LYP-D3/def2-TZVP(ecp)] fluoride ion affinity and thermodynamic oxygen transfer potentials for differently *P*-substituted phosphinidene tungsten(0) complexes.[216]

The fluoride ion affinity (FIA),[280,281] defined as the negative enthalpy change of the gas-phase reaction of a (neutral) acid A to form the adduct $[A\text{-}F]^-$, has been used as benchmark for the quantification of Lewis acidity for many different species including phosphorus centers, such as phosphenium cations;[282] but it is questionable if cationic Lewis acids can be easily included and compared. According to the FIA, the (hard) acidity for phosphinidene complexes R-P-$W(CO)_5$ increases in the order CPh_3 < Me < ^{t}Bu (400.5 kJ/mol, 407.6 kJ/mol, 414.2 kJ/mol, respectively) (Figure 75). For comparison, also the FIAs of the common reference compounds BF_3, AlF_3, SiF_4, PF_5 and SbF_5 were calculated on the same level of theory (CCSD(T)/CBS//PBEh-3c) by Espinosa Ferao (355.0 kJ/mol, 491.5 kJ/mol, 318.5 kJ/mol, 390.8 kJ/mol and 498.0 kJ/mol, respectively).[216] The important contribution of the coordination number and the oxidation state on the FIA was not studied thouroughly but usually the FIA increased for increasing coordination number/oxidation state.[280]

3.4.3 GIAO ^{31}P NMR calculations

The ^{31}P NMR chemical shifts of the donor-to-phosphinidene tungsten(0) complexes **6c**, **13b**, **14b**, **15b**, **19b**, **20b**, **21b**, **40^{IMe2}** and **71** as well as the phosphinidene complex **24b** were investigated using gauge-independent atomic orbital (GIAO) DFT calculations by Espinosa Ferao at [CPCM$_{tol}$/PBE0/def2-TZVP(ecp)//COSMO$_{THF}$/B3LYPD3/def2-TZVP] level of theory (Table 22).[216]

Table 22: Calculated [GIAO/CPCM$_{tol}$/PBE0/def2-TZVP(ecp)//COSMO$_{THF}$/B3LYP-D3/def2-TZVP] ^{31}P NMR chemical shifts and experimental data for complexes **6c**, **13b**, **14b**, **15b**, **19b**, **20b**, **24b**, **40^{IMe2}** and **71**.[216]

Compound	Donor	δ_{calc}(^{31}P) / ppm[a]	δ_{exp}(^{31}P) / ppm	solvent$_{exp}$
24b	—	1195.7	—	—
6c	tBuNC[b]	−37.3	−50.5	$CDCl_3$
13b	*N*-MeIm	254.4	199.4	C_6D_6
14b	DMAP	253.4	234.8	THF-d_8
15b	Py	278.4	284.6	THF
19b	PMe_3	−15.4	12.5	CD_2Cl_2
20b	PEt_3	−3.6	−28.6	C_6D_6
40^{IMe2}	IMe_2	−12.8	—	—
71	$C(NH^tBu)_2$	8.7	−33.8	THF

[a] ^{31}P NMR chemical shifts of the phosphinidene nucleus. [b] Calculated for Do = MeNC.

The calculated ^{31}P NMR chemical shifts show a good linear correlation (R^2 = 0.956) with the experimental obntained values (Figure 76) despite the changes in the solvent. The mean average deviation of 26.9 ppm for the small set of compounds is reasonable. However, some calculations gave significantly different values, *e.g.* for complex **13b** where the calculated ^{31}P NMR chemical shift is found 55 ppm downfield shifted compared to the experimentally obtained data. Therefore, the calculated ^{31}P NMR chemical shifts of the donor-to-phosphinidene complex adducts cannot be used for an exact prediction for unknown adduct systems but a clear trend can be construed showing an increased electronic shielding of the P nucleus for strong donors with partial double bond character like carbenes, isocyanides or phosphanes, and for weak donors like the aforementioned N-donors that show a significantly deshielding of the phosphorus resulting in a strong downfield-shift.

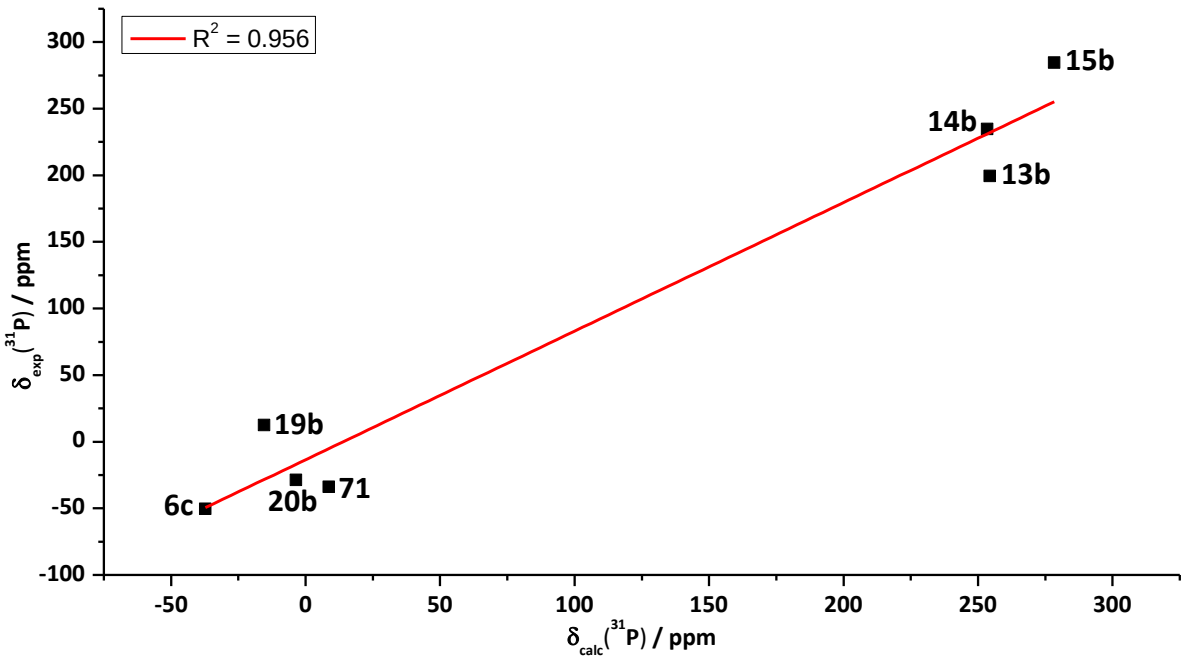

Figure 76: Correlation of the calculated [GIAO/CPCM$_{tol}$/PBE0/def2-TZVP(ecp)//COSMO$_{THF}$/B3LYP-D3/def2-TZVP] with the experimental ^{31}P NMR chemical shifts.

Therefore, the calculated ^{31}P NMR data strongly support the proposed formation of the pyridine-to-phosphinidene complex adduct **15b** and the diaminocarbene-to-phosphinidene complex adduct **71**. The computational data lie within the uncertainty of the calculated value which differed by 42.5 ppm from the experiment.

4 SUMMARY

Low-oxidation state, low-coordinate phosphorus compounds exhibit an extraordinary reactivity and, hence, are of fundamental interest for academic research. Among them are neutral electrophilic, terminal phosphinidene complexes, still fleeting species and highly reactive. The donor stabilization of such complexes may make them easier to handle but it should be pointed out that this can lead to a switch of reactivity, *i.e.*, becoming ambigous.

This PhD thesis focused on the synthesis and reactions of neutral, donor-stabilized electrophilic, terminal phosphinidene complexes bearing only π-accepting coligands starting from very strained P-heterocycle complexes or acyclic donor-to-phosphinidene complex adducts.

In chapter 3.1.1.1, synthesis of highly strained 3-imino-azaphosphiridine chromium(0) and molybdenum(0) complexes **4a,b** are described and the exchange reaction with *tert*-butyl isocyanide (**5**) was performed (Scheme 76). While the isocyanide-to-phosphinidene chromium(0) complex **6a** was isolated, the respective molybdenum complex **6b** decomposed rapidly which is in stark contrast to the (known) tungsten(0) complex **6c**.

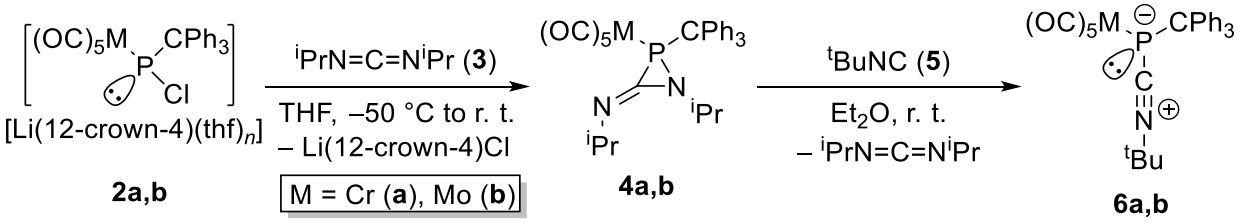

Scheme 76: Synthesis of *tert*-butylisocyanide-to-phosphinidene complexes **6a–b**.

However, complexes **4a,b** turned out to be problematic since they show a thermal instability and an extreme sensitivity towards moisture.

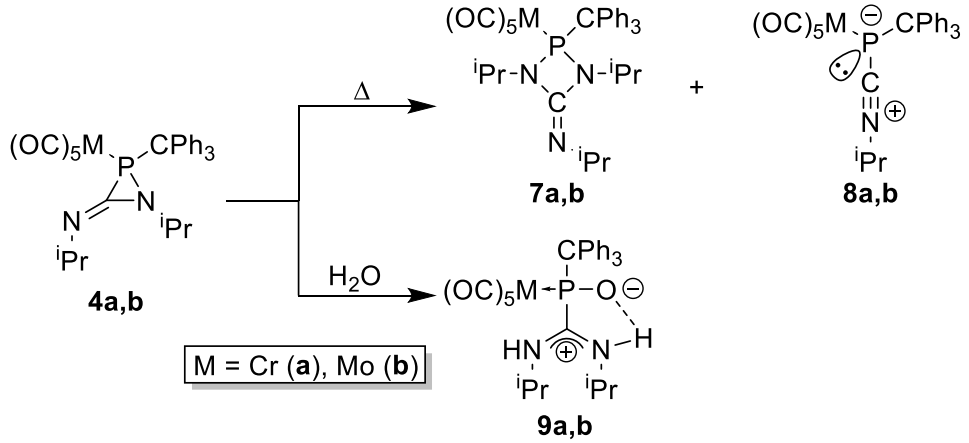

Scheme 77: Thermal decomposition and hydrolysis reactions of complexes **4a,b**.

Therefore, complexes **4a–c** deemed not to be suitable for experimental studies, and it was decided to examine the "direct" synthesis using Li/Cl phosphinidenoid complexes **2a,c** in reactions with promising donors. In doing so the scope of P-adducts could be expanded to a broader family of C-, N- and P-donors such as ^{t}BuNC, *N*-methylimidazole, DMAP and trialkylphosphanes (Scheme 78).

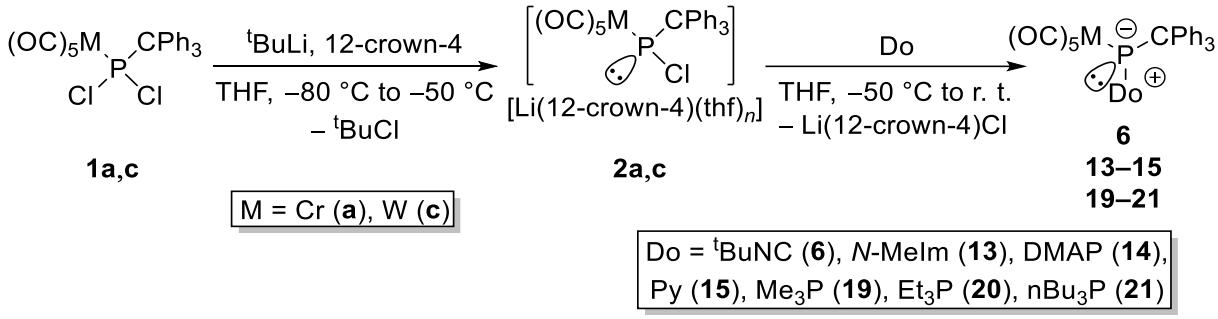

Scheme 78: Synthesis of donor-to-phosphinidene complex adducts **6**, **13–15** and **19–21** via the Li/Cl phosphinidenoid complexes **2a,c**.

For example, the yields could be increased significantly from 21 % to 94 % for **6a** and from 52 % to 82 % for **6c**. The molecular structure of most adducts was confirmed by single crystal X-ray diffraction analysis. Especially, for the N-donor adducts **13** and **14** an elongated P-N distance was observed, being significantly larger than typical P-N single bonds (Figure 77). The adduct formation did not alter much of the bond lengths and angles of the donor fragments, thus, confirming also the theoretically proposed dative character of the donor-P bond including the calculations on the bond order, the charge transfer, the bond dissociation energies as well as the relative charge concentration bands position parameter τ_{VSCC} together with the position of the valence shell charge concentration of phosphorus compared to the bond critical point. Additionally, the experimentally obtained ^{31}P NMR data provided insight into the electronic properties at the P center and, hence, also into the donor-P bond. Weak donor-

to-P bonds, *i.e.* the N-donor adducts, are associated with a deshielded phosphorus nucleus due to the reduced charge transfer from the donor to the phosphinidene complex. The $^{1}J_{W,P}$ coupling constant also showed in general a small value for all donor-to-phosphinidene complex adducts which was also significantly dependent on the “steric pressure” at the phosphorus center.

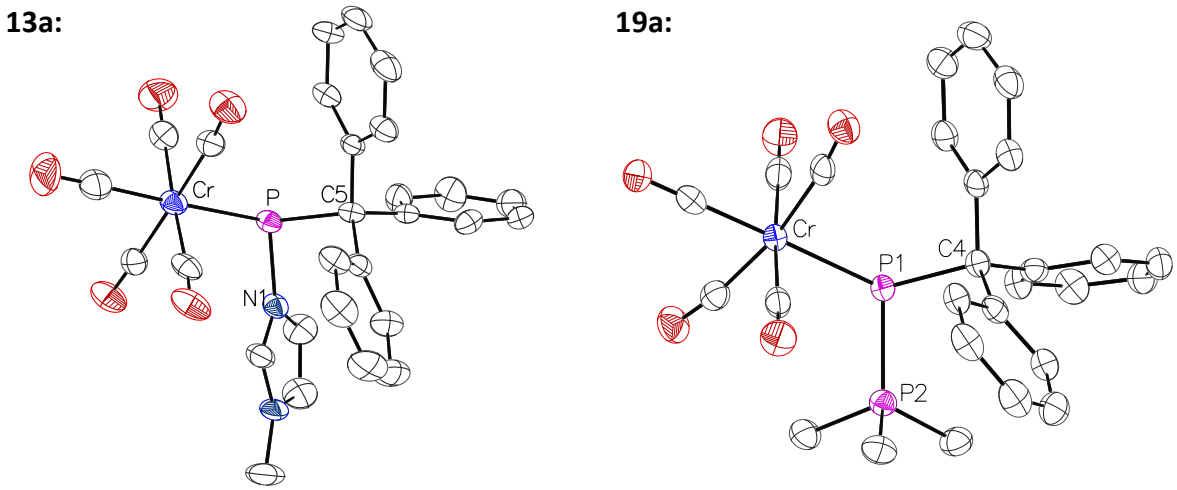

Figure 77: Molecular structures of **13a** and **19a** in the single crystal lattice. Hydrogen atoms and solvent molecules were omitted for clarity.

The redox properties of the obtained donor-to-phosphinidene complex adducts were investigated by cyclic voltammetry (Figure 78). All complexes, except of **6**, show a similar behavior in the cyclic voltammograms displaying three redox processes. While for the second oxidation and the reduction process no return wave was found, for the first oxidation process a return wave was observed that was getting suppressed by the second oxidation. The oxidation waves corresponded to one-electron step processes while in the reduction process at least two electrons were involved. All observed electrochemical processes were freely diffusion-controlled without participation of an electrode-absorption process which was tested by measurement of the cyclic voltammograms at different scan rates and checking for a linear correlation of the peak current i_p with the square root of the scan rate according to the Randles-Ševčik equation.

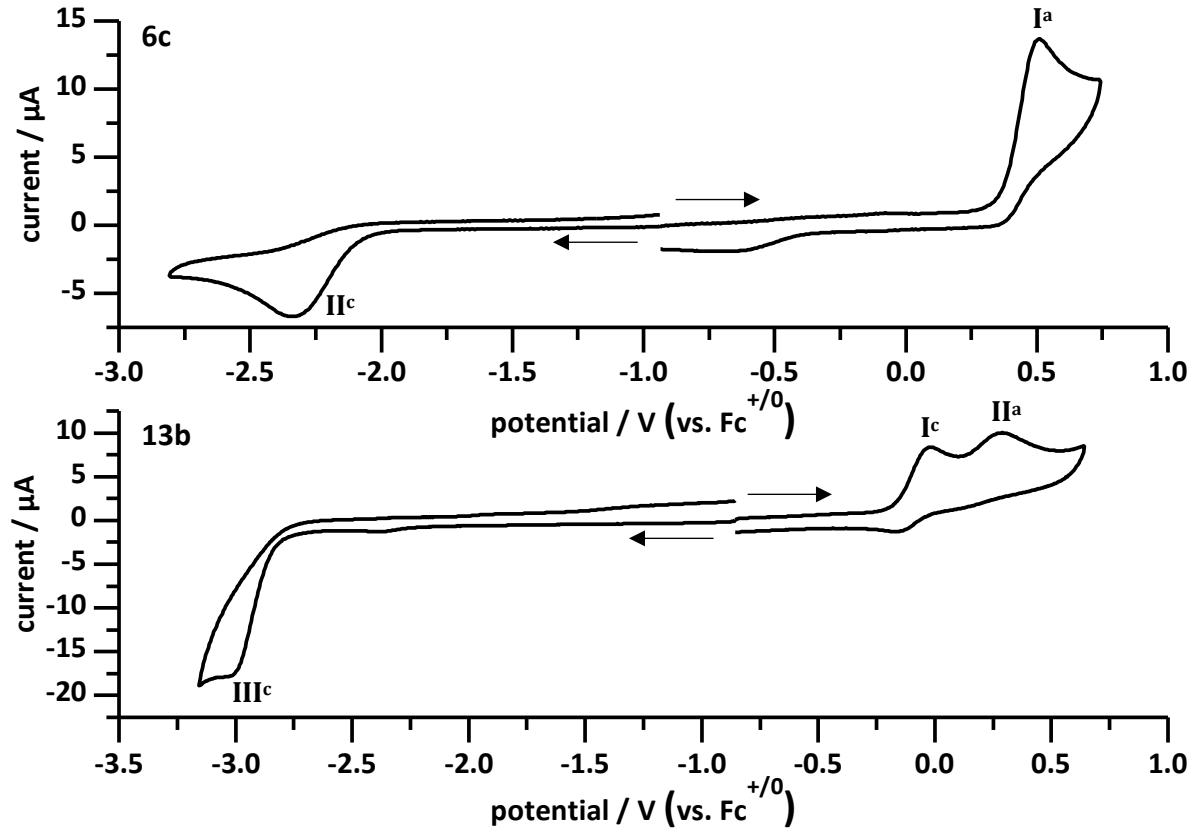

Figure 78: Overlay of cyclic voltammograms of **6c** and **13b** (1 mM) at a Pt electrode in a 0.2 M $^{n}Bu_4PF_6$/THF solution; oxidation parts with anodic initial scan direction and reduction parts with cathodic initial scan direction as denoted with arrows; scan rate: 200 mV/s; potentials are referenced against $Fc^{+/0}$.

Additionally, a correlation of the obtained peak potentials, that represent the HOMO and LUMO energies, with the ^{31}P NMR chemical shifts was tested (Figure 79).

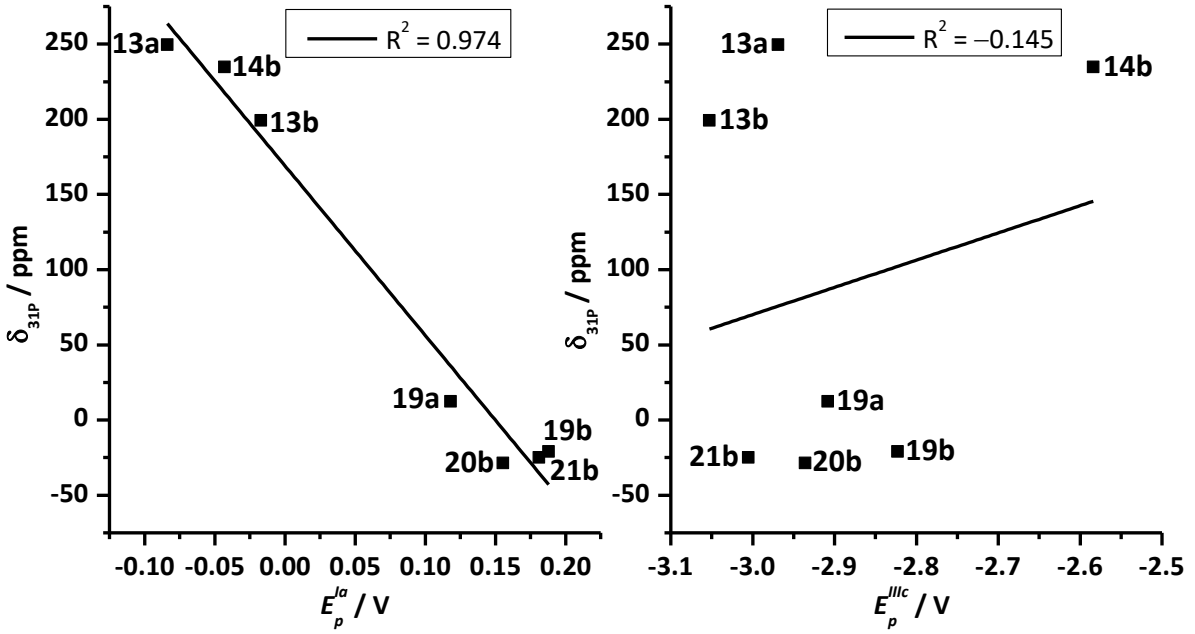

Figure 79: Correlation of the ^{31}P NMR chemical shifts of complexes **13a,b**, **14b**, **19a,b**, **20b** and **21b** with the anodic peak potentials E_p^{Ia} (left) and cathodic peak potentials E_p^{IIIc} (right) ; potentials are referenced against $Fc^{+/0}$.

Interestingly, only a correlation for the anodic peak potential of the first oxidation process was found but neither for the cathodic peak potential of the reduction event nor by the difference of the potentials. This is in agreement with the the HOMO and LUMO which are predominantly located on the phosphorus atom and the metal fragment, respectively (Figure 80).

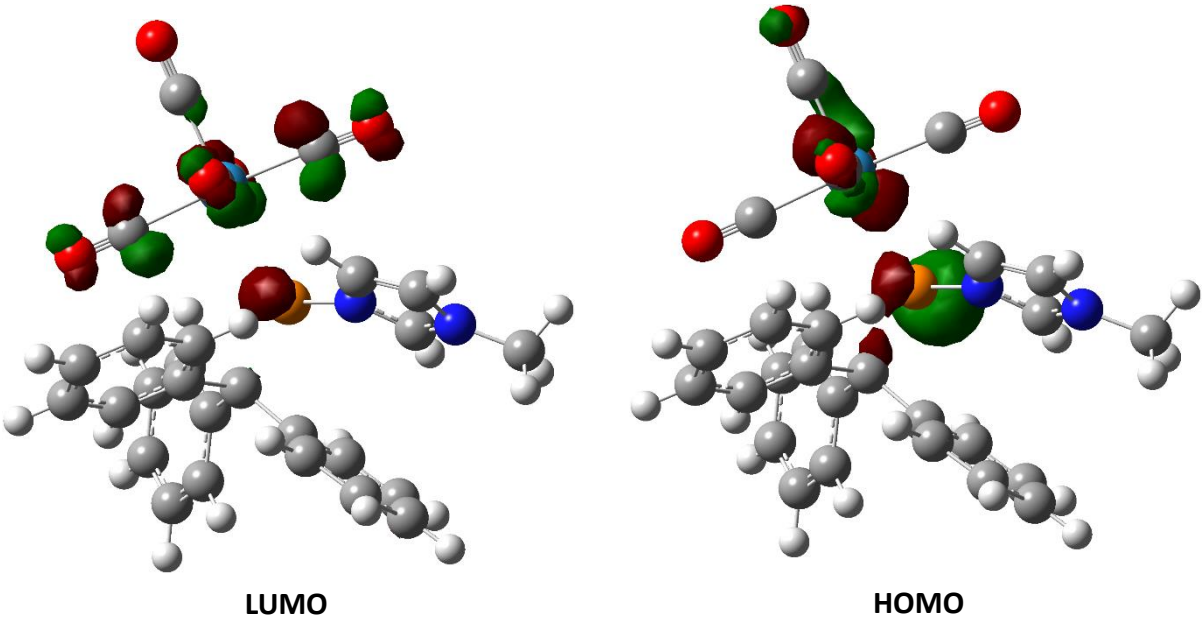

Figure 80: [CPCM$_{tol}$/B3LYP-D3/def2-TZVP(ecp)] lots of the LUMO (left) and HOMO (right) of the *N*-methyl-imidazole-to-phosphinidene complex adduct **13b**.[216]

The donor-to-phosphinidene complex adducts were also studied towards a thermal dissociation of the P-donor bond to form the highly reactive electrophilic, terminal phosphinidene complexes **24a,b**. However, for the N-donor-to-phosphinidene complex adducts the formation of white phosphorus (**22**) was observed (Scheme 79).

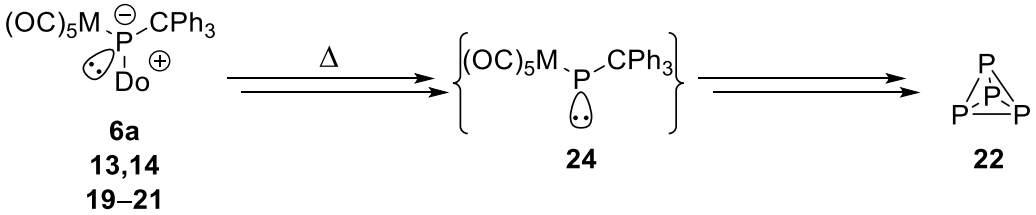

Scheme 79: Thermal decomposition of donor-to-phosphinidene complex adducts into white phosphorus (**22**).

Further studies on the decomposition revealed that probably the first step is the formation of the phosphinidene complex **24**, followed by the formation of the diphosphene **26**. The latter may dimerize and decompose via a consecutive, formal loss of the triphenylmethyl groups and the intermediate butterfly compound **29**, which eventually gives **22** (Scheme 80).

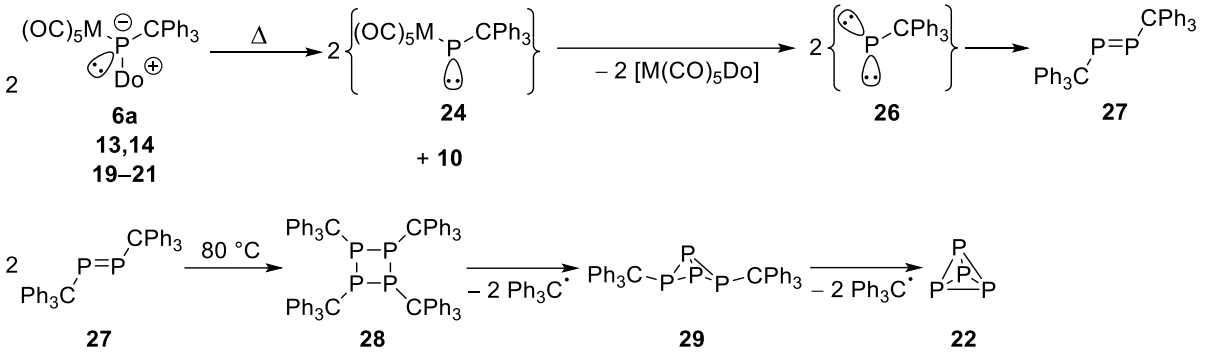

Scheme 80: Proposed potential pathway of the thermal decomposition of the donor-to-phosphinidene complex adducts to furnish white phosphorus as the final product.

Notably, the isocyanide-to-phosphinidene complex adduct **6c** decomposed via a different pathway, *i.e.*, the cyanophosphane complex **23b** was obtained via 1,2-elimination of *iso*-butene (Scheme 81).

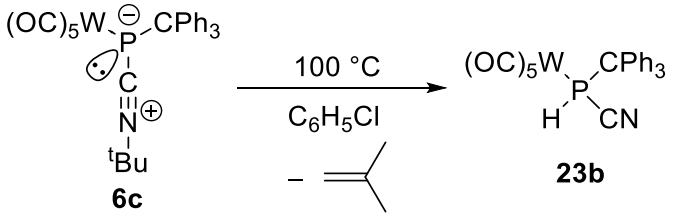

Scheme 81: Thermal decomposition of **6c** into cyanophosphane complex **23b** at 100 °C in chlorobenzene.

When a solution of the most labile N-donor adduct **13b** was heated, the transient formation of the phosphinidene complex **24** was confirmed by clear-cut trapping experiments with alkenes and 2,3-dimethyl-1,3-butadiene to give **36–38** and **39**, respectively (Scheme 82); An X-ray diffraction analysis confirmed **39**.

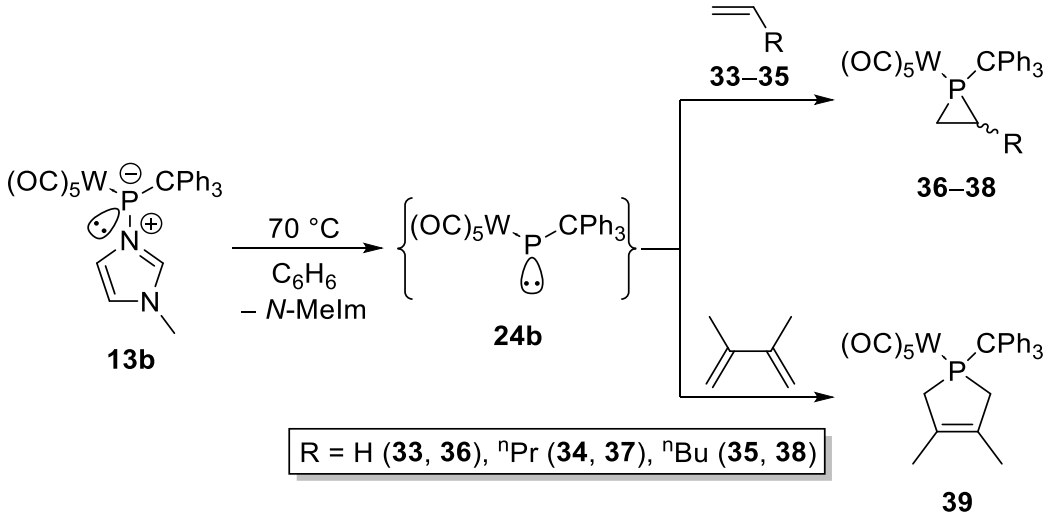

Scheme 82: Trapping reactions of the transient electrophilic, terminal phosphinidene complex **24b** using ethylene (**33**), 1-pentene (**34**), 1-hexene (**35**) and 2,3-dimethyl-1,3-butadiene.

Due to the lability of the *N*-methylimidazole adduct **13b**, it was particularly suited for the study of donor substitution reactions. Complex **13b** reacted with donors such as DMAP

(**11**), tertiary phosphanes (**16–18**) and *tert*-butylisocyanide (**5**) to form the respective complex adducts **6**, **14**, **15** and **19–21** (Scheme 83). Remarkably, all donor substitutions proceeded at ambient temperature, however, reactions with the carbenes IMe_4, IMes and Me_2cAAC (1-(2,6-diisopropylphenyl)-3,3,5,5-tetramethylpyrrolidin-2-ylidene) resulted in the rather unselective formation of product mixtures, *e.g.*, the reaction of **13b** with IMe_4 afforded a maximum content of 15 % of the proposed IMe_4-to-phosphinidene complex adduct **40** in the reaction mixture.

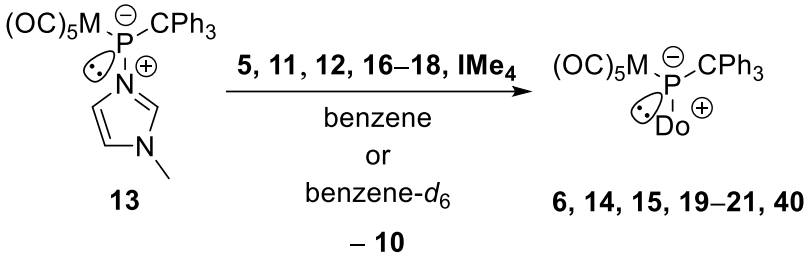

Scheme 83: *P*-donor substitution reactions at the *N*-methylimidazole-to-phosphinidene complexes **13**.

The nucleophilic character of P-adduct complexes was examined using complex **13b** as a case in point and various Lewis acids such as labile $[W(CO)_5L]$ **41** and **42**. The latter gave the dinuclear complex **43** but only with a maximum content of 22 % in the reaction mixture. **43** was identified by the resonance signal at 811.2 ppm in the ^{31}P NMR spectrum, showing a remarkably deshielded phosphorus nucleus (Scheme 84). The extremely high reactivity of **43** led to decomposition and formation of several new compounds via C-H activation, reactions with π-bonds or hydrolysis.

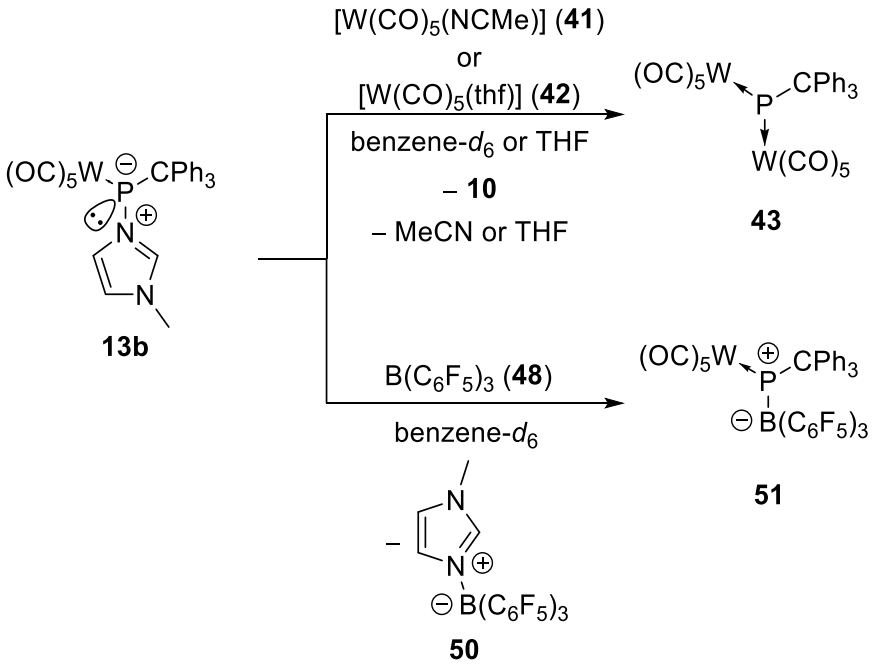

Scheme 84: μ_2-Phosphinidene complexes bridging two transition metals and/or one metal and one metalloid.

When the strong Lewis acid tris(pentafluorophenyl)borane was added to **13b** the analogous hetero-dinuclear phosphinidene complex **51** did form (maximum content of 24 % in the reaction mixture) showing a resonance signal at 1040.3 ppm ($^{1}J_{W,P}$ = 180.1 Hz) in the ^{31}P NMR spectrum, and it represents the first example ever of a μ_2-phosphinidene ligand bridging a transition metal and a metalloid center (Scheme 84). Complex **51** showed a similar high reactivity and low thermal stability as **43** and, hence, could not be isolated. Assuming that steric overcrowding was the origin of the instability of **43** and **51**, the proposed formation of the borane adduct **49** as intermediate (and of **51** as final product) was further studied by using the sterically much less demanding borane BH_3 using the borane dimethylsulfane adduct (**53**) (Scheme 85).

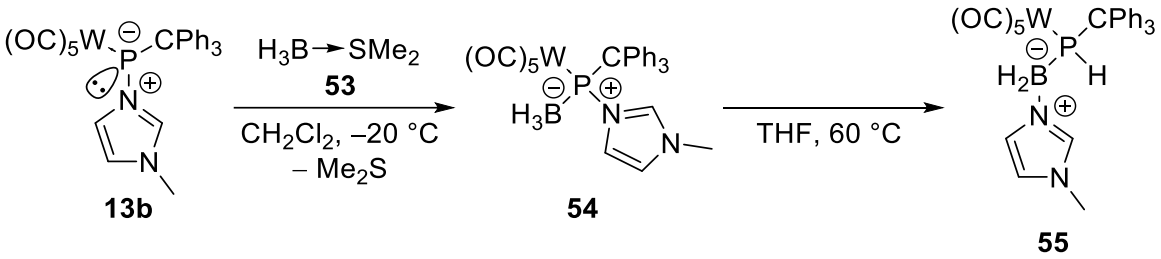

Scheme 85: Synthesis of the *N*-methylimidazole-to-*P*-stabilized phosphinidene complex borane adduct **54** and its thermal rearrangement.

Surprisingly, isolated complex **54** showed a remarkable low thermal stability; the decomposition product was identified as B-H insertion product combined with a migration of the *N*-methylimidazole to the boron atom. Complexes **54** and **55** could be isolated and fully characterized including X-ray diffraction analyses (Figure 81).

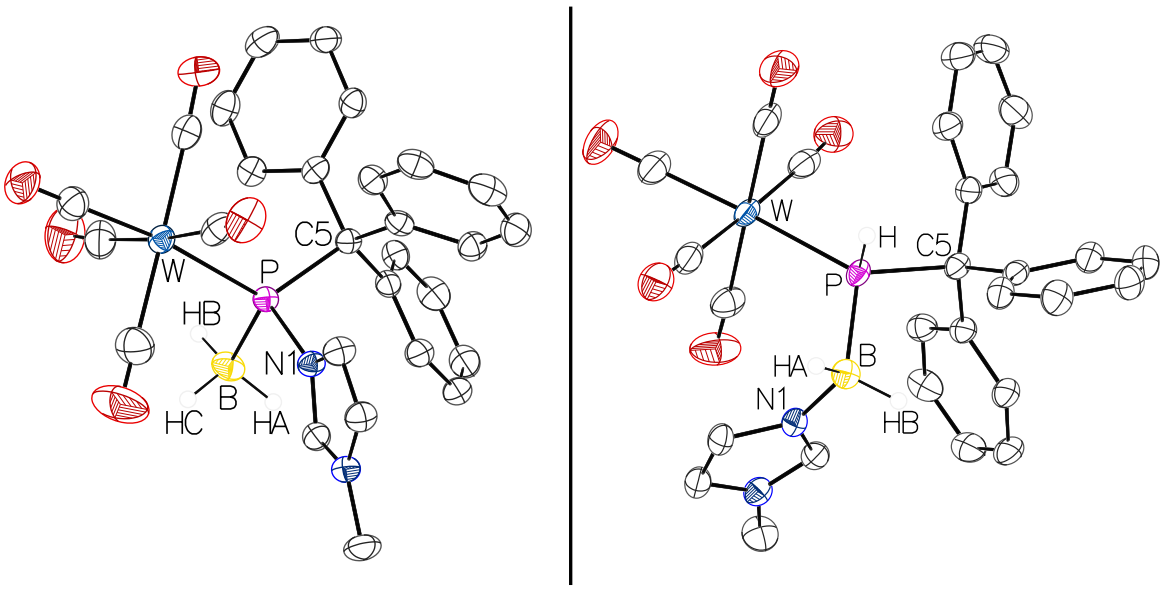

Figure 81: Molecular structures of **54** (left) and **55** (right) in the single crystal lattice at 100(2) K.

As the reactions with Lewis acids gave products with a remarkable low thermal stability and high sensitivity, the reactivity with Brønsted-Lowry acids was tested next. **13b** showed a high and selective reaction with water, alcohols and primary amines (as very weak acids) under formation of the formal O-H and N-H insertion products (Scheme 86).

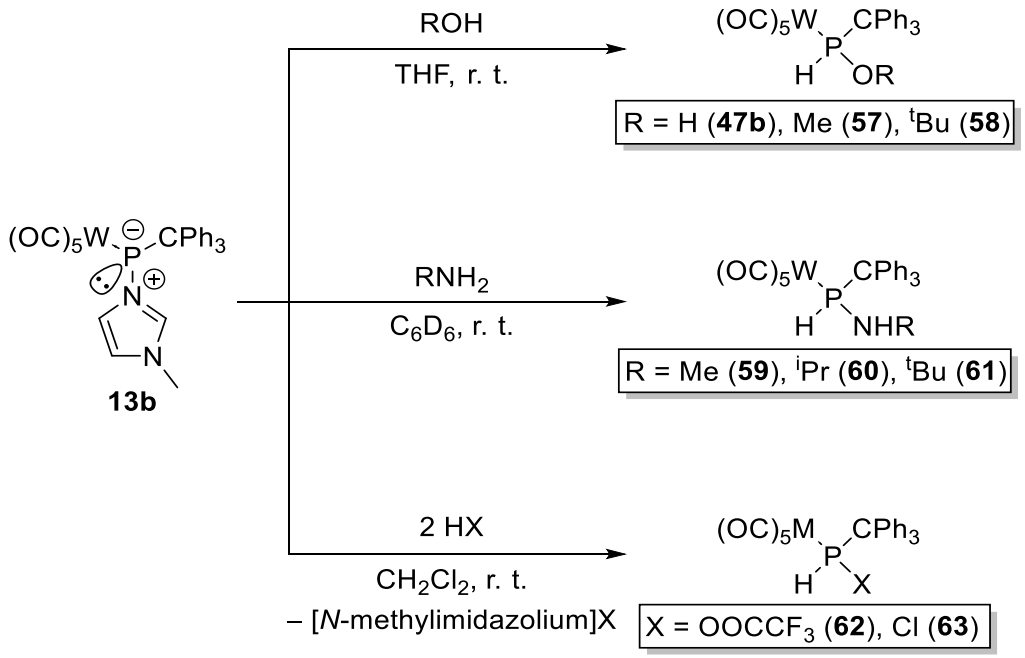

Scheme 86: Reactivity of complex **13b** with water, alcohols and primary amines.

The obtained complexes of the reactions with methanol, *tert*-butanol, methylamine, isopropylamine and *tert*-butylamine were already described by the Streubel group using different routes. The hydroxyphosphane complex **47b** was isolated and fully characterized, including an X-ray structure confirmation. The hydroxyphosphane complex adducts **56a,b**, obtained as hydrogen-bound *N*-methylimidazole adduct, could only be separated/purified by column chromatography. Reactions of complex adducts **13** with strong(er) acids such as trifluoroacetic acid and hydrogen chloride selectively formed the respective formal insertion products **62** and **63**. Since for strong acids also a reaction with the *N*-methylimidazole happened under formation of the respective *N*-methylimidazolium salts, the addition of two equivalents of the acid was essential.

To get evidence for the primary reaction step, *i.e.* the protonation of phosphorus, the reactions with strong acids of weakly coordinating anions (WCA) were examined. While for the reaction with trifluoromethanesulfonic acid still a weak interaction of the trifluoromethanesulfonate anion with the C^2H proton of the formed phosphanylimidazolium complexes was observed, the use of tetrakis(3,5-bis{trifluoromethyl}phenyl)borate and

tetrakis(nonafluoro-*tert*-butoxy)aluminate led to a better separation of the cation and anion (Scheme 87).

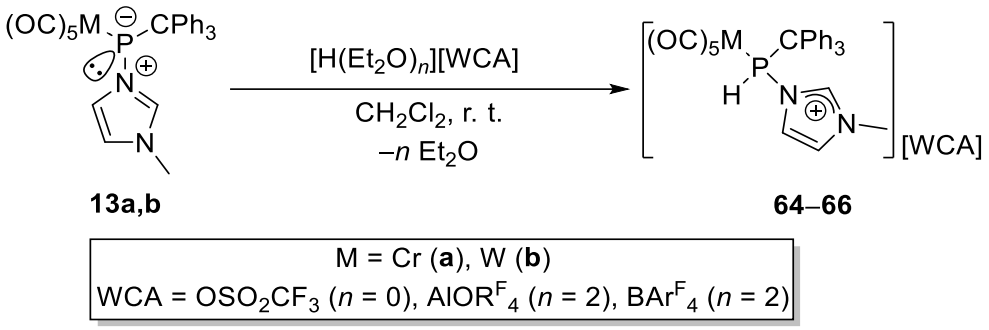

Scheme 87: Synthesis of phosphanylimidazolium complexes **64–66**.

All complexes were fully characterized and single crystal X-ray diffraction analyses confirmed the formation of the phosphanylimidazolium complexes (**66b**: Figure 60). Surprisingly, the fully separated phosphanylimidazolium complexes **65** and **66** were remarkably unstable in THF due to the astonishingly distinct acidity of the P-H proton in such cations.

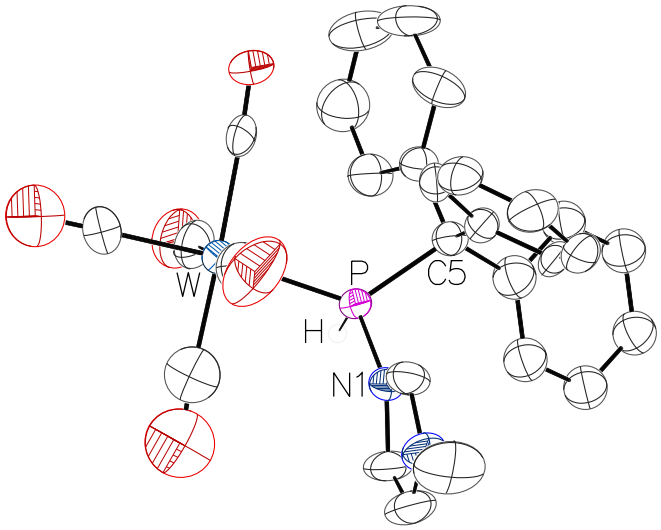

Figure 82: Molecular structure of **66b** in the single crystal lattice at 100(2) K; only the predominant split layer site (50.6 %) is displayed. Thermal ellipsoids are set at 50 % probability level. Hydrogen atoms were omitted for clarity except for those bound to phosphorus atoms.

Finally, the transformation of a donor molecule into a modified donor while keeping the Do-P connectivity, *i.e.*, 1,2-addition to the C-N bond, was investigated in analogy to transition metal coordination chemistry. Due to the well-established reactivity of isocyanide transition metal complexes with primary amines under formation heterocarbene complexes, the study was performed using complex **6** (Scheme 88).

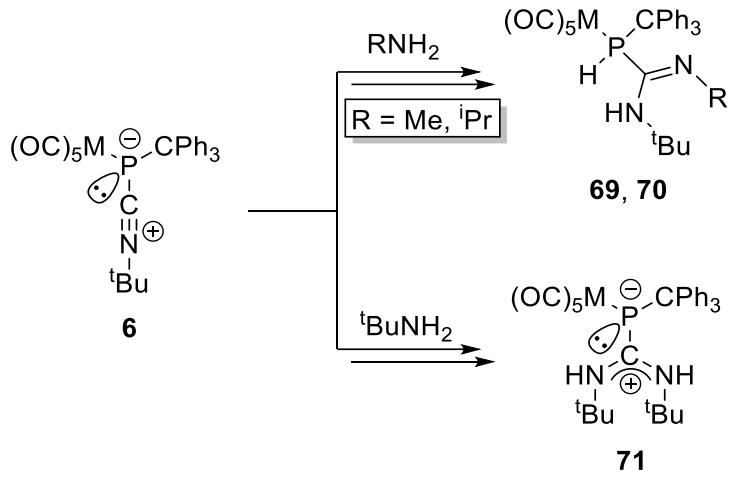

Scheme 88: Reactivity of the isocyanide-to-phosphinidene complex adducts **6** towards primary amines.

The reaction of **6** with methylamine and isopropylamine gave the phosphaguanidine complexes **69** and **70** by a formal 1,2-addition at the P-C bond combined with a protropic shift; both could be isolated and fully characterized. When the steric demand of the organic substituent at the amine was increased, and *tert*-butylamine was used, the reactivity changed and a formal 1,2 addition at the C-N bond was observed. The formation of the final product, the diaminocarbene-to-phosphinidene complex adduct **71**, is very reminiscent to organo-metallic chemistry and represents an unprecedented example in p-block chemistry. The mechanism of the product formation was further investigated by theoretical calculations.

5 EXPERIMENTAL SECTION

5.1 GENERAL WORKING TECHNIQUES

All reactions were performed under dried and deoxygenated argon atmosphere using Schlenk or glovebox techniques. The used argon (>99.998 %) was purified by a system of three columns (deoxygenation by a BTS copper catalyst (BASF PuriStar® R3-15S) at ca. 100 °C, removing moisture with silica gel, phosphorus pentoxide desiccant with indicator (Sicapent®) and calcium chloride). Glassware, spatulae, cannulae as well as filter papers were dried in a compartment dryer at 110 °C for at least one hour. Additionally, the glassware was heated with a heat gun (up to 550 °C) under active vacuum (<0.02 mbar) and filled with argon three times. Sterile syringes were purged with argon three times before use. The solvents were dried by standard procedures[283] by refluxing over proper desiccants under an argon atmosphere (*n*-pentane, petroleum ether 40/65 and toluene over sodium wire (Ø = 2 mm); diethyl ether stabilized with 3,5-di-*tert*-butyl-4-hydroxytoluene (BHT) and tetrahydrofuran over benzophenone and sodium wire) for several days and distilled before use. Alternatively, diethyl ether and toluene were dried using a Mbraun SPS-800 solvent purification system. For filtration Schlenk frits or stainless steel cannulae (Ø = 1 mm and 2 mm) with Whatman® glass microfiber filters (grade GF/B) were used. After use, devices made of stainless steel were cleaned with acetone, water and diluted hydrochloric acid and glassware by storage in a concentrated solution of potassium hydroxide in isopropanol for at least two days and in diluted hydrochloric acid for one day. Afterwards, the glassware was washed with water and soap, acetone and petroleum ether 40/65. All joints were greased with OKS 1112 grease or with PTFE paste (Carl Roth).

5.2 METHODS AND DEVICES

5.2.1 Nuclear magnetic resonance (NMR) spectroscopy

NMR spectra were recorded on a Bruker Avance I 300 MHz, Bruker Avance I 400 MHz, Bruker Avance I 500 MHz or Bruker Avance III HD Ascend 500 MHz spectrometer at the NMR department of the University of Bonn and subsequently analyzed by the program *Mestrenova 14.2*. The calibration of the ^{1}H and ^{13}C NMR spectra was done via the solvent residual signals

relative to tetramethylsilane (<1 % in $CDCl_3$) ($CDCl_3$: $\delta(^1H)$ = 7.26 ppm and $\delta(^{13}C)$ = 77.16 ppm, CD_2Cl_2: $\delta(^1H)$ = 5.32 ppm and $\delta(^{13}C)$ = 53.84 ppm, C_6D_6: $\delta(^1H)$ = 7.16 ppm and $\delta(^{13}C)$ = 128.06 ppm, toluene-d_8: $\delta(^1H)$ = 2.08 ppm, 6.97 ppm, 7.01 ppm or 7.09 ppm and $\delta(^{13}C)$ = 20.43 ppm, 125.13 ppm, 127.96 ppm, 128.87 ppm or 137.48 ppm, CD_3CN: $\delta(^1H)$ = 1.94 ppm or 3.58 ppm and $\delta(^{13}C)$ = 1.32 ppm or 118.26 ppm, THF-d_8: $\delta(^1H)$ = 1.72 ppm or 3.58 ppm and $\delta(^{13}C)$ = 25.31 ppm or 67.21 ppm).[284] ^{31}P NMR spectra were measured relative to 85 % H_3PO_4 in water as external reference by using the ^2H frequency of the deuterated solvent (lock frequency) and the frequency ratio ratio value $\Xi(^{31}P)$ = 40.480742 % as recommended by IUPAC, ^7Li NMR spectra relative to 9.7 M LiCl in D_2O using the ^2H frequency of the deuterated solvent (lock frequency) and the frequency ratio value $\Xi(^7Li)$ = 14.716086 %, ^{11}B NMR spectra relative to $BF_3{\cdot}OEt_2$ in $CDCl_3$ using the ^2H frequency of the deuterated solvent (lock frequency) and the frequency ratio value $\Xi(^{11}B)$ = 32.083974 %, ^{19}F NMR spectra relative to $CFCl_3$ using the ^2H frequency of the deuterated solvent (lock frequency) and the frequency ratio value $\Xi(^{19}F)$ = 94.094011 %, ^{27}Al NMR spectra relative to 1.1 M $Al(NO_3)_3$ in D_2O using the ^2H frequency of the deuterated solvent (lock frequency) and the frequency ratio value $\Xi(^{27}Al)$ = 26.056859 %, ^{29}Si NMR spectra relative to tetramethylsilane (<1 % in $CDCl_3$) by using the ^2H frequency of the deuterated solvent (lock frequency) and the frequency ratio value $\Xi(^{29}Si)$ = 19.867187 %, and ^{15}N NMR spectra via ge-2D NMR $^1H,^{15}N$ HMBC experiments relative to liquid ammonia by using the ^2H frequency of the deuterated solvent (lock frequency) and the frequency ratio value $\Xi(^{15}N)$ = 10.132912 %.[285] To obtain the ^{15}N NMR chemical shifts relative to CH_3NO_2, 380.5 ppm were subtracted.[286] All lock frequencies were calibrated internally against the ^1H signals of solutions of tetramethylsilane with a volume fraction of $\Phi \leq 1$ % in the corresponding deuterated solvent. The used deuterated solvents were purified via distillation over proper desiccants ($CDCl_3$ and CD_2Cl_2 over CaH_2, and C_6D_6 and THF-d_8 over a potassium mirror, CD_3CN over molecular sieves (3 Å)), trap-to-trap recondensation and degassing by three freeze-pump-thaw cycles. The purified solvents were stored over 3 Å or 4 Å molecular sieves. The chemical shift (δ) is given in parts per million (ppm) and the coupling constant ($^nJ_{X,Y}$) in Hertz (Hz) as absolute values neglecting the sign where *n* is the number of bonds between the coupling nuclei X and Y. For assigning the multiplicity following abbreviations were used: s = singlet, d = doublet, dd = doublet of doublets, ddd = doubet of doublets of doublets, t = triplet, q = quartet, q* = quartet (intensities 1:1:1:1), qd = quartet of doublets, dq = doublet of quartets, qq* = quartet of quartets (1:1:1:1), sept = septet, sept d =

septet of doublets, m = multiplet and br = broad. For ^{1}H NMR spectra additionally the number of nuclei is given according which is determined via integration. The ^{1}H and ^{13}C NMR signals of compounds were assigned by a combination of COSY, NOESY, HMQC and HMBC experiments to unequivocally assign protons and carbon resonances of diastereotopic substituents. All measurements were performed at ambient temperature (298 K) if not stated otherwise.

5.2.2 Mass spectrometry (MS)

Mass spectra using liquid injection field desorption ionization (LIFDI) were recorded on a Thermo Finnigan MAT 90 sector field instrument equipped with a LIFDI ion source (Linden CMS). The samples were dissolved in toluene or tetrahydrofuran. Electron impact ionization (EI) measurements were performed on a Thermo Finnigan MAT 95 XL sector field instrument using an ionization energy of 70 eV. The calibration and referencing was done using perfluorokerosene (PFK). Electrospray ionization (ESI) and atmospheric pressure chemical ionization (APCI) measurements were performed on a Thermo Fisher Scientific Orbitrap XL spectrometer with an HPLC autosampler using acetonitrile or dichloromethane as solvents. Solutions of highly air sensitive compounds for LIFDI and ESI measurements were prepared in a glovebox using dried, recondensed and degassed solvents. Only selected data are given for detected ions. The peaks are given in mass-to-charge ratio (m/z) while only the isotopomer with the highest relative abundance is represented. Additionally, the relative intensities of the peaks are given in parentheses and the proposed molecule fragments in square brackets. High resolution mass spectra (HRMS) that were obtained using ESI or APCI were recorded in a single measurement and, hence, no standard deviations for ESI/APCI HRMS were obtained.

5.2.3 Infrared spectroscopy (IR)

ATR-IR spectra of solids were recorded in the spectral range of 4000–400 cm^{-1} on a Bruker Alpha FTIR spectrometer with a single-reflection ATR measurement attachment (Platinum-ATR Diamond) or a Shimadzu IRSpirit FTIR spectrometer with a single-reflection ATR measurement attachment (QATR-S) in a glovebox at ambient temperature. The FT-IR spectra of solutions were recorded in the spectral range of 4000–400 cm^{-1} on a Shimdazu IRSpirit FTIR spectrometer using a stainless-steel cell with KBr windows (Omni-Cell SPECAC) separated by a 6 μm PTFE spacer (OMNI). For apodization the Happ-Genzel function was used. All analyses were performed using the programs *EZ OMNIC 7.3* of *Fisher Scientific*, *OPUS* of *Bruker* and

LabSolutions IR 2.26 of *Shimadzu*. The intensities of the bands are marked as very strong (vs), strong (s), medium (m) or weak (w). Only selected wavenumbers of the absorption bands are given using reciprocal centimeters (cm^{-1}).

5.2.4 Elemental analysis (EA)

Elemental analyses were performed on a Elementar Vario Micro analysis device in quadruplicate or triplicate for each sample. All samples were prepared and weighed up in tin or silver sample containers using a micro-analytical balance in a glovebox. The mean C, H, N and S values are given for each compound.

5.2.5 Melting point determination

Melting points were measured using an SRS DigiMelt device or a Büchi melting point determination device according to Dr. Tottoli. The samples were flame-sealed in a glass capillary (Ø = 0.1 mm) *in vacuo* (<0.02 mbar) and heated quickly (ca. 5 K/min) for a rough determination of the melting point or decomposition temperature. Afterwards, a heating rate of approximately 2 K/min was used until the sample melted or decomposed. The thermally treated samples were cooled to ambient temperature and studied by ^{1}H and/or ^{31}P NMR spectroscopy to confirm whether decomposition had occurred. No internal or external temperature corrections were performed.

5.2.6 Single crystal X-ray diffraction analysis

Single crystal X-ray diffraction analyses were performed on a Bruker X8-KappaApex II diffractometer, a Bruker D8 Venture diffractometer, a STOE IPDS-2T diffractometer or a STOE STADIVARI diffractometer, equipped with a low-temperature device (Bruker Kryoflex, Oxford Cryostream 700 series or Oxford Cryostream 800 series) at 100(2) K, 123(2) K or 180(2) K by using graphite monochromated Mo-Kα radiation (λ = 0.71073 Å) or Cu-Kα radiation (λ = 1.54186 Å). Intensities were measured by fine-slicing ϕ and ω scans and corrected background, polarization and Lorentz effects. A semi-empirical absorption correction was applied for the data sets following Blessing's method.[287] The structure was solved by direct methods and refined anisotropically by the least-squares procedure implemented in ShelX program system.[288] All non-hydrogen atoms were refined anisotropically. The hydrogen atoms were included isotropically refined using a riding model at the bound carbon atoms. The quality of the crystals was evaluated by the X-ray diffraction service within the chemical

institutes of the University of Bonn with an in-house grading: A = solving and refinement without any (identifiable) errors (excellent structure), B = only marginal problems during refinement (very good structure), C = small problems during refinement (good structure), D = significant problems during refinement (moderate structure), E = not for precise discussions, only structural motive confirmed, F = structural motive vague, 1 = found structure was identical with the beforehand proposed structure, 2 = found structure was close to the beforehand proposed structure, 3 = found structure contained motives of the beforehand proposed structure, 4 = found structure was not related to the beforehand proposed structure. The program *Olex2 1.5*[289] of *OlexSys* was used for analyses and the ellipsoid representations of the molecular structures with the probability level set to 50 %. Detailed crystallographic data including bond lengths and bond angles as well as the refinement parameters of the respective compounds can be found in the appendix.

5.2.7 Cyclic voltammetry (CV)

Figure 83: Potentiostat and galvanostat system WaveNowXV® of Pine Research (left), low volume glass cell with a PTFE insert and a ceramic screen-printed electrode (middle), and a close-up of the electrode (right). Copyright 2023 Pine Research Instrumentation. Reprinted with permission.

The measurement of cyclic voltammograms were performed using the potentiostat and galvanostat system WaveNowXV® of Pine Research with scan rates of 20–10000 mV/s. For all CV measurements Pine Research ceramic screen-printed platinum electrodes containing an Ag/AgCl reference electrode were used. These electrodes combine working, counter and reference electrodes on one ceramic plate. As cell a low volume glass cell with a special PTFE insert at the bottom that features a narrow slit for the ceramic screen-printed electrodes was used. The internal volume of the slit is approximately 1 mL. If tetrahydrofuran was used as solvent a 0.2 M electrolyte solution of $[^{n}Bu_4N]PF_6$ was prepared. For dichloromethane or acetonitrile, a 0.4 M or 0.1 M electrolyte solution was prepared. The electrolyte was dried *in vacuo* (<0.02 mbar) at 80 °C for 24 h. All used solvents were freshly

purified by drying over proper desiccants, trap-to-trap recondensation and degassing by three freeze-pump-thaw cycles. The used analyte solution was prepared with a concentration of 1 mM. All measurements were performed in a glovebox under argon atmosphere at ambient temperature. After background scans on the electrolyte solution were measured to identify the anodic and cathodic limits with respect to the nominal voltage of the solid silver reference, the analyte was added. Next, open circuit potential measurements were performed to establish the starting potential of the cyclic voltammetry experiments. Careful cyclic voltammetry scans were then measured in the anodic and cathodic directions to encounter the most accessible processes, and only after these were investigated thoroughly, further scans to higher positive and negative potentials were measured. After all measurements were completed, cobaltocenium hexafluorophosphate ($(\eta^5\text{-}C_5H_5)_2Co$)) was added to the same concentration as the analyte and served as internal reference using the cobaltocenium/cobaltocene ($Cc^{+/0}$) redox couple, set to −1.35 V,[290] and thus, the cyclic voltammograms were indirectly referenced to the ferrocene/ferrocenium ($Fc^{+/0}$) redox couple, set to 0 V, according to IUPAC recommendations.[291] For measurement and data processing the program *Aftermath* of *Pine Research* was used. All plots of the cyclic voltammograms were obtained using the program *OriginPro 8G* of *OriginLab*.

5.2.8 UV/vis spectroscopy

UV/vis spectra were measured using the spectrometer UV-1650PC of Shimadzu with a double-beam optics photometric system and a maximum wavelength range of 190.0 to 1100 nm, a spectra band width of 2 nm and a wavelength accuracy of ±0.5 nm with an automatic wavelength correction. To avoid the measurement of the lamp interchange of the 50W halogen lamp (340.8 nm) all speactra were measured between 350 to 700 nm. Before the measurement of the analyte solution, an automatic baseline correction was performed (baseline stability: ±0.001 abs./hour). A silicon photodiode was used as detector with a photometric range of −0.5 to 3.999 abs. with an accuracy of ±0.004 abs. at 1.0 abs. (±0.002 abs. at 0.5 abs.).The used cuvettes (Hellma precision cells 110-QS) (46 mm × 12.5 mm × 12.5 mm) were made of quartz glass (Suprasil® quartz, Heraeus) with two polished windows. The used cuvettes had a spectral range of 200 to 2500 nm, a light pathlength of 10 mm and a chamber volume of 3.5 μL. For *in situ* UV/vis spectra an aliquot of the reaction mixture was taken in the glovebox and diluted by the same solvent which was used in the experiment until

only a light color was visible. The diluted analyte solution was then added to the cuvettes and closed with a PTFE stopper and quickly transported to the spectrometer outside of the glovebox and the measurement was started immediately. The determination of the extinction coefficient was not possible for all *in situ* measurements due to the involvement of air sensitive compounds and the variable amount of analyte in the reaction mixture.

5.3 USED CHEMICALS

The used chemicals were purified according to standard procedures.[283]

Table 23: Sources of the commercially obtained chemicals.

Chemical	**producer**	**lot**
12-crown-4	Acros, 99.4 % Acros, 98.6 % Thermo Scientific, 98.5 %	A0424427 A0417212 A0447620
1-hexene	Aldrich, 99.9 % Acros, 99.5 %	BCBX4244 A0432701
1-pentene	Aldrich, 99.5 %	BCBZ3107
2-methylpropanal	Acros, 99.3 %	A0252150
2,3-dimethyl-1,3-butadiene	Aldrich, 98.6 % Alfa Aesar, 99.7 %	S11268 10225534
2,6-diisopropylphenylamine	Acros, 94.3 %	A0308962
3-chloro-2-methyl-1-propene	TCI, 98 %	IU63E
4-dimethylaminopyridine	Aldrich, 99 %	04424725
acetic acid, glacial	VWR VWR	19F054008 20G164012
Acetone	Julius Hoesch, 99.9 %	—
acetonitrile	VWR, 99.9 % VWR, 99.9 %	18l274029 19J011793
acetonitrile-d_3	125midazol, 99.8 %	B24467
aluminum oxide 90 active neutral (70–230 mesh ASTM)	Merck	TA1599977 TA5070677046
Benzene	AppliChem, 99.5 %	2E007623
benzene-d_6	Aldrich, 99.9 % 125midazol, 99.5 %	MKCL4685 B 23356
borane dimethylsulfide	Aldrich, 9.9 M	STBJ5836

calcium hydride	abcr, 92 % Alfa Aesar, 92 %	1425147 A0172430
carbon dioxide	AirLiquide, 99.995 %	P0760S10R0A001
carbon monoxide	AirLiquide, 99.997 %	P0755S10R2A001
Chlorobenzene	Aldrich, 99 %	S17660-433
chlorobenzene-d_5	abcr, 99 %	1379471
Chloroform	VWR, 99 %	13F110505
chloroform-d_1	deutero	—
chromium hexacarbonyl	abcr, 99 % Merck, 98.5 %	1306058 S5434096
cobaltocenium hexafluorophosphate	Aldrich, 98 %	—
Dichloromethane	Fisher, 99.8 %	—
dichloromethane-d_2	Aldrich, 99.95 % Aldrich, 99.95 %	MKCP3644 MKCP8630
diethyl ether	VWR VWR VWR VWR VWR VWR VWR VWR Riedel-de-Haën	18A084116 19l104101 20G234167 20J054143 21B044102 21H194104 22C224121 22H224133 10450
diethylene glycol dimethyl ether	Aldrich, 99 %	S60248-029
Ethanol	Julius Hoesch, 99 %	—
Ethylene	Aldrich, Messer®, 99.95 %	STBK5314
hydrochloric acid, 35–37 %	Th. Geyer VWR	26.1891012 21B044011
hydrogen chloride, 2 M in Et_2O	Acros	A0433759
hydrogen chloride, 4 M in dioxane	abcr	AB117077
Iodomethane	Merck, 99 %	S7531764801
Isopropylamine	Acros, 99.9 %	A0362038
Magnesium	Carl Roth, 99.9 %	503201380
magnesium sulfate	VWR, 99 %	20K164113
Methanol	Alfa Aesar	G26Z331
methyl trifluoromethanesulfonate	fluorochem, 99 %	FCB077709

methylamine, 2 M in THF	Aldrich	STBH9722
methyl lithium lithium bromide complex, 1.5 M in Et_2O	Aldrich	81797APV
molecular sieves, 3 Å, 1.7–2.4 mm	Carl Roth	8487
molecular sieves, 4 Å, 1–2 mm	Alfa Aesar	10162013
molybdenum hexacarbonyl	abcr, 98 %	1162056
N,*N*'-diisopropylcarbodiimide	abcr, 99 % Merck, 99 % Acros, 99.5 %	1307931 S35440203 A015582101
n-butyllithium, 1.6 M in *n*-hexane	Acros	A0413255
N-methylimidazole	Alfa Aesar, 99 %	10228851
n-pentane	Fisher, 99 %	—
para-toluenesulfonic acid hydrate	Riedel-de-Haën	03550
petroleum ether 40/65	Julius Hoesch	—
phosphorus, white	Thermphos	—
phosphorus trichloride	Acros, 100 % Acros, 99.6 %	A0400601 A0414901
phosphorus pentoxide	J. T. Baker, 99 % (granular) J. T. Baker, 99 % (powder)	9714710002 13495
Potassium	Riedel-de-Haën, 98 %	52080
potassium hydroxide	Aldrich, 94 % (powder)	STBK3639
Pyridine	Fisher, 99.5 %	2033812
silica gel 60 (63–200 mesh)	Merck Geduran Si60	TA1637532
Sodium	Aldrich	S782384217
sodium carbonate	Riedel-de-Haën, 99.8 %	2311A
sodium hydroxide	VWR, 99 % Th. Geyer	13l020011 170-07-19
sodium hypophosphite monohydrate	Alfa Aesar	G01Z032
sulfuric acid, 95–97 %	Merck Th. Geyer	K42080431 1099/02/17
tert-butanol	Riedel-de-Haën	50300
tert-butyl isocyanide	Aldrich, 99.2 % Alfa Aesar, 99.5 % TCI, 99.8 %	BCBM8296V 10221027 CQ4DF
tert-butylamine	Acros, 99.1 %	A0265971

tert-butyllithium, 1.6 M in *n*-pentane	Aldrich	STBJ1565 STBJ6836
tert-butyllithium, 1.7 M in *n*-pentane	Aldrich	STBH4975 STBH8561
Tetrahydrofuran	Fisher, 99.8 %	—
tetrahydrofuran-d_8	Carl Roth, 99.5 % 128midazol, 99.5 %	1001501 B23442
tetra-*n*-butylammonium hexafluorophosphate	Alfa Aesar	—
Tolane	Alfa Aesar, 99.1 %	10202355
Toluene	VWR, 99.9 %	—
toluene-d_8	euriso-top, 99.5 %	D005F K2581
Triethylphosphane	Cytec, Cytop® 320, 98 %	WE00-001
trifluoroacetic acid	abcr, 99.9 %	1408625
trifluoromethanesulfonic acid	fluorochem, 99 %	FCB085046
Trimesitylphosphane	Alfa Aesar, 98.5 %	J3162A
trimethylamine *N*-oxide dihydrate	Glentham, 99.1 %	852WNE
tri-*n*-butylphosphane	Alfa Aesar, 94.5 %	10228257
Triphenylmethanol	TCI, 99.9 %	W6QMG
tris(pentafluorophenyl)borane	Alfa Aesar, 97 %	LY001151
tungsten hexacarbonyl	Acros, 99 % Acros, 99 %	A0405586 A0424435

Table 24: Syntheses of starting materials according to literature-described procedures.

Compound	Experimentalist	Reaction code	Reference
$[Cr(CO)_5(thf)]$	D. Biskup	DB-79 DB-137 DB-268 DB-371	[292]
$[Cr(CO)_5\{P(CPh_3)Cl_2\}]$	D. Biskup	DB-2 DB-21 DB-79 DB-137 DB-268 DB-371	[80]
$[H(OEt_2)_2][Al\{OC(CF_3)_3\}_4]$	AK Streubel	—	[275]
$[H(OEt_2)_2][BAr^F{}_4]$	D. Biskup	DB-596	[293]

$[Mo(CO)_5\{P(CPh_3)Cl_2\}]$	D.Biskup F. Gleim	DB-34 FLG-284	[80]
[pentacarbonyl{1-isopropyl-3-isopropylimino-2-(triphenylmethyl)-1,2-azaphosphiridine-κ*P*}tungsten(0)]	D. Biskup	DB-6 DB-12 DB-18 DB-36 DB-39 DB-50 DB-60 DB-239 DB-243 DB-247 DB-534 DB-539 DB-545 DB-621	[94]
$[W(CO)_5(NCMe)]$	D. Biskup T. Bergmann	DB-188 TB-021	[294]
$[W(CO)_5(thf)]$	D. Biskup	DB-73 DB-186 DB-187 DB-200 DB-201 DB-244 DB-310 DB-332 DB-392 DB-433 DB-485 DB-554	[295]
$[W(CO)_5\{P(CPh_3)(CN^tBu)\}]$	D. Biskup	DB-15 DB-20 DB-42 DB-51 DB-52 DB-53 DB-54 DB-55 DB-57	[103]
$[W(CO)_5\{P(CPh_3)Cl_2\}]$	D.Biskup	DB-3 DB-41 DB-73 DB-186 DB-191 DB-201 DB-244	[78]

		DB-310 DB-332 DB-392 DB-433 DB-485 DB-554	
	P. Brehm	PB-254	
	P. Junker	PJ-143	
IMe_4	T. Kalisch	TK-181	[296]
$IMes_2$	R. Kunzmann	—	[296]
	AK Filippou	—	
lithium diisopropylamide	S. Kermanshahian	SHK-69	[297]
lithium *N*-(2,6-diisopropylphenyl)-2-methylpropan-1-iminide	D. Biskup	DB-346	[298]
Me_2cAAC	D. Biskup	DB-356	[25]
	P. Brehm	PB-388	
N-(2,6-diisopropylphenyl)-2,2,4-trimethylpent-4-en-1-imine	D. Biskup	DB-347	[298]
N-(2,6-diisopropylphenyl)-2-methylpropan-1-imine	D. Biskup	DB-345	[298]
$Na[BAr^F{}_4]$	F. Gleim	FLG-391	[299]
Ph_3CPCl_2	D. Biskup	DB-33	[300]
		DB-199	
		DB-370	
	F. Gleim	FLG-367	
		FLG-418	
	N. Volk	NV-458	
PMe_3	T. Kalisch	TK-310	[301]
trimethylphenylphosphinic acid	D. Biskup	DB-198	[300]

5.4 WASTE DISPOSAL

The disposal of laboratory chemical waste was performed according to the Hazardous Substances Ordinance (Gefahrstoffverordnung) (GefStoffV). Solvents, solids, column waste, heavy metal waste and syringes were separated from each other and collected in designed containers before disposing. Remaining reactive compounds or their residues were neutralized and/or quenched before disposal. The waste was submitted to the department 4.2 *Arbeits- und Umweltschutz* of the University of Bonn.

5.5 SYNTHESIS AND CHARACTERIZATION

5.5.1 Preparation of Li/Cl phosphinidenoid metal(0) complexes (2)

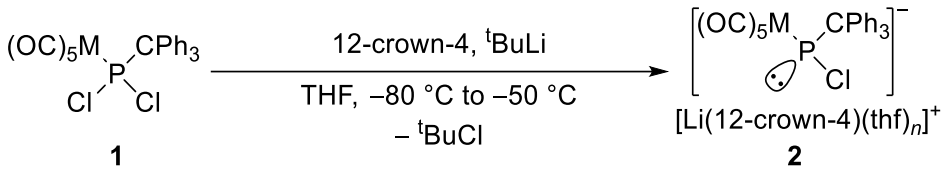

1 **2**

One equivalent of $[M(CO)_5\{P(CPh_3)Cl_2\}]$ (M = Cr (**1a**), Mo (**1b**), W (**1c**)) and one equivalent of 12-crown-4 were dissolved in THF. Subsequently, 1.3 equivalents of a *tert*-butyllithium solution were added dropwise at −80 °C. The reaction mixtures of **2a–c** were warmed up slowly (ca. 1 h) to −50 °C while stirring. The reaction mixture of **2d** is further stirred at −80 °C for 15 minutes.

5.5.2 Synthesis of [pentacarbonyl{1-isopropyl-3-isopropylimino-2-(triphenylmethyl)azaphosphiridine-κ*P*}chromium(0)] (4a)

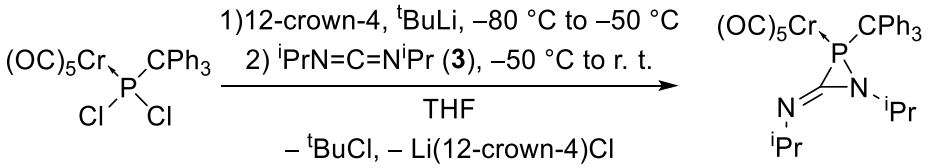

1a **4a**

Synthesis

A solution of a Li/Cl phosphinidenoid chromium(0) complex **2a** was prepared using 0.213 g (0.40 mmol, 1.0 eq.) of $[Cr(CO)_5\{P(CPh)_3Cl_2\}]$ (**1a**), 0.06 mL (0.37 mmol, 0.9 eq.) of 12-crown-4 and 0.26 mL (c = 1.6 M in *n*-pentane, 0.42 mmol, 1.0 eq.) of a *tert*-butyllithium solution in 6.0 mL of THF at −80 °C. Afterwards, 0.10 mL (0.65 mmol, 1.6 eq.) of *N*,*N*'-

diisopropylcarbodiimide (**3**) was added dropwise at −50 °C. The reaction mixture was stirred for 21 h while it was allowed to slowly warm up to ambient temperature. All volatiles were removed *in vacuo* (<0.02 mbar) at ambient temperature within 4 minutes and the obtained brown solid was further dried for 25 minutes. The product was extracted four times with 10 mL of *n*-pentane. The solvent was removed *in vacuo* (<0.02 mbar) at ambient temperature and the obtained yellow solid was dried under the same conditions for 1 h. The solid was washed three times with 2 mL of a 50:1 *n*-pentane/diethyl ether mixture at −90 °C. The product was obtained as yellow solid after drying for 1 h *in vacuo* (0.02 mbar) at ambient temperature. Due to the low thermal stability no elemental analyses were performed.

Reaction codes: DB-23, 27, 47, 304 (18m3b016.18, 18p5a042.18)

Molecular formula: $C_{31}H_{29}N_2O_5PCr$

Molecular weight: 592.552 g/mol

Yield: 0.118 g (0.20 mmol, 50.3 %)

Melting point: 105 °C (dec.)

MS (LIFDI, selected data): m/z (%) = 592.2 (100) $[M]^{\bullet+}$, 243.1 (21) $[CPh_3]^+$.

IR (ATR Diamond, selected data): $\tilde{\nu}$ / cm^{-1} = 1920 (vs) (C≡O), 1984 (w) (C≡O), 2063 (s) (C≡O).

^{1}H NMR (300.13 MHz, $CDCl_3$, 298 K): δ / ppm = 7.40–7.35 (m, 9H; CPh_3), 7.28–7.20 (m, 6H; CPh_3), 3.60 (sept d, $^3J_{H,H}$ = 6.53 Hz, $^3J_{P,H}$ = 2.50 Hz, 1H; P-N-C*H*$(CH_3)_2$), 3.24 (sept, $^3J_{H,H}$ = 6.34 Hz, 1H; C=N-C*H*$(CH_3)_2$), 1.20 (d, $^3J_{H,H}$ = 6.53 Hz, 3H; P-N-CH-C*H*$_3$), 1.15 (d, $^3J_{H,H}$ = 6.34 Hz, 3H; C=N-CH-C*H*$_3$), 1.01 (d, $^3J_{H,H}$ = 6.53 Hz, 3H; P-N-CH-C*H*$_3$), 0.67 (d, $^3J_{H,H}$ = 6.34 Hz, 3H; C=N-CH-C*H*$_3$).

^{13}C{^{1}H} NMR (75.48 MHz, $CDCl_3$, 298 K): δ / ppm = 219.8 (d, $^2J_{P,C}$ = 1.2 Hz; *trans*-*C*O), 214.9 (d, $^2J_{P,C}$ = 12.0 Hz; *cis*-*C*O), 141.4 (d, $^2J_{P,C}$ = 3.5 Hz; *ipso*-*C*), 138.3 (d, $^1J_{P,C}$ = 9.4 Hz; P-*C*=N), 131.1 (d, $J_{P,C}$ = 6.6 Hz; Ph), 128.5 (s; Ph), 127.9 (d, $J_{P,C}$ = 2.0 Hz; Ph), 69.6 (d, $^1J_{P,C}$ = 23.2 Hz; P-*C*Ph_3), 58.2 (d, $^2J_{P,C}$ = 13.1 Hz; C=N-*C*H$(CH_3)_2$), 50.7 (s; P-N-*C*H$(CH_3)_2$), 25.3 (s; C=N-CH-*C*H_3), 24.2 (s; C=N-CH-*C*H_3), 21.7 (d, $^3J_{P,C}$ = 1.0 Hz; P-N-CH-*C*H_3), 21.3 (d, $^3J_{P,C}$ = 1.8 Hz; P-N-CH-*C*H_3).

^{15}N{^{1}H} NMR (50.68 MHz, $CDCl_3$, 298 K): δ / ppm = −169.5 (s; C=*N*-^{i}Pr), −285.2 (s; P-*N*-^{i}Pr).

^{31}P{^{1}H} NMR (121.51 MHz, $CDCl_3$, 298 K): δ / ppm = 53.1 (s).

^{31}P NMR (121.51 MHz, $CDCl_3$, 298 K): δ / ppm = 53.1 (s).

5.5.3 Synthesis of [pentacarbonyl{1-isopropyl-3-isopropylimino-2-(triphenylmethyl)azaphosphiridine-κ*P*}molybdenum(0)] (4b)

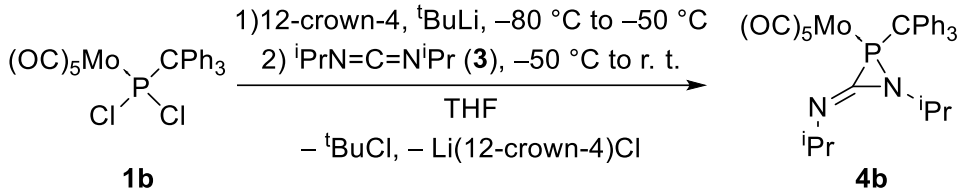

1b **4b**

Synthesis

A solution of a Li/Cl phosphinidenoid molybdenum(0) complex (**2b**) was prepared using 0.206 g (0.36 mmol, 1.0 eq.) of [$Mo(CO)_5${$P(CPh_3)Cl_2$}] (**1b**), 0.057 mL (0.35 mmol, 1.0 eq.) of 12-crown-4 and 0.23 mL (c = 1.6 M in *n*-pentane, 0.37 mmol, 1.0 eq.) of a *tert*-butyllithium solution in 6.0 mL of THF at −80 °C. Afterwards, 0.08 mL (0.52 mmol, 1.5 eq.) of *N*,*N*'-diisopropylcarbodiimide (**3**) was added dropwise at −50 °C. The reaction mixture was stirred for 19.5 h while it was allowed to slowly warm up to ambient temperature. All volatiles were removed *in vacuo* (<0.02 mbar) at ambient temperature within 15 minutes and the obtained brown solid was further dried for 15 minutes. The product was extracted four times with 10 mL of *n*-pentane. The solvent was removed *in vacuo* (<0.02 mbar) at ambient temperature and the obtained yellow solid was dried under the same conditions for 25 minutes. The solid was washed three times with 2 mL of a 50:1 *n*-pentane/diethyl ether mixture at −90 °C. The product was obtained as yellow solid after drying for 1 h *in vacuo* (<0.02 mbar) at ambient temperature.

Reaction codes: DB-40, 305 (27p5a032.18)

Molecular formula: $C_{31}H_{29}N_2O_5PMo$

Molecular weight: 636.507 g/mol

Yield: 0.189 g (0.30 mmol, 83.6 %)

Melting point: 91 °C (dec.)

MS (LIFDI, selected data): m/z (%) = 638 (100) $[M]^{\bullet+}$, 243 (78) $[CPh_3]^+$.

IR (ATR Diamond, selected data): $\tilde{\nu}$ / cm^{-1} = 1928 (vs) (C≡O), 1996 (w) (C≡O), 2075 (s) (C≡O).

^{1}H NMR (500.14 MHz, $CDCl_3$, 298 K): δ / ppm = 7.39–7.10 (m, 15H; CPh_3), 3.53 (sept d, $^{3}J_{H,H}$ = 6.52 Hz, $^{3}J_{P,H}$ = 1.85 Hz, 1H; P-N-C*H*$(CH_3)_2$), 3.22 (sept, $^{3}J_{H,H}$ = 6.34 Hz, 1H; C=N-C*H*$(CH_3)_2$), 1.21 (d, $^{3}J_{H,H}$ = 6.52 Hz, 3H; P-N-CH-C*H*$_3$), 1.14 (d, $^{3}J_{H,H}$ = 6.34 Hz, 3H; C=N-CH-C*H*$_3$), 0.99 (d, $^{3}J_{H,H}$ = 6.52 Hz, 3H; P-N-CH-C*H*$_3$), 0.65 (d, $^{3}J_{H,H}$ = 6.34 Hz, 3H; C=N-CH-C*H*$_3$).

^{13}C{^{1}H} NMR (125.78 MHz, $CDCl_3$, 298 K): δ / ppm = 208.9 (d, $^{2}J_{P,C}$ = 36.3 Hz; *trans*-*C*O), 204.1 (d, $^{2}J_{P,C}$ = 8.4 Hz; *cis*-*C*O), 141.5 (s; *ipso*-*C*), 139.1 (d, $^{1}J_{P,C}$ = 10.8 Hz; P-*C*=N), 131.1 (d, $J_{P,C}$ = 6.8 Hz; Ph), 128.4 (s; Ph), 127.9 (s; Ph), 67.1 (d, $^{1}J_{P,C}$ = 21.9 Hz; P-*C*Ph_3), 58.0 (d, $^{2}J_{P,C}$ = 12.9 Hz; C=N-*C*H$(CH_3)_2$), 51.3 (s; P-N-*C*H$(CH_3)_2$), 25.3 (s; C=N-CH-*C*H_3), 24.1 (s; C=N-CH-*C*H_3), 21.7 (d, $^{3}J_{P,C}$ = 1.0 Hz; P-N-CH-*C*H_3), 21.3 (s; P-N-CH-*C*H_3).

^{15}N{^{1}H} NMR (50.69 MHz, $CDCl_3$, 298 K): δ / ppm = −168.3 (s; C=*N*-^{i}Pr), −287.4 (s; P-*N*-^{i}Pr).

^{31}P{^{1}H} NMR (202.48 MHz, $CDCl_3$, 298 K): δ / ppm = 23.6 (s).

^{31}P NMR (202.48 MHz, $CDCl_3$, 298 K): δ / ppm = 23.6 (s).

5.5.4 Synthesis of [pentacarbonyl{(*tert*-butylazaniumylidyne)methyl(triphenylmethyl)phosphanido-κ*P*}chromium(0)] (6a)

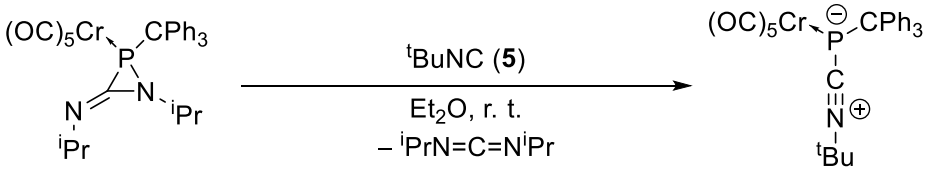

4a **6a**

Synthesis via the azaphosphiridine complex 4a

0.31 mL (2.74 mmol, 1.5 eq.) of *tert*-butyl isocyanide (**5**) was added dropwise to a solution of 1.07 g (1.81 mmol, 1.0 eq.) of **4a** in 70 mL of diethyl ether at ambient temperature. The reaction mixture was stirred for 24 h. All volatiles were removed *in vacuo* (<0.02 mbar) at ambient temperature and the obtained yellow oil was dried under the same conditions for 1 h. The oil was washed three times with 4 mL of a 3:1 *n*-pentane/diethyl ether mixture at −40 °C and the obtained yellow solid was dried *in vacuo* (<0.02 mbar) at ambient temperature for 7 h.

Reaction code: DB-49

Molecular formula: $C_{29}H_{24}NO_5PCr$

Molecular weight: 549.483 g/mol

Yield: 0.414 g (0.75 mmol, 41.8 %)

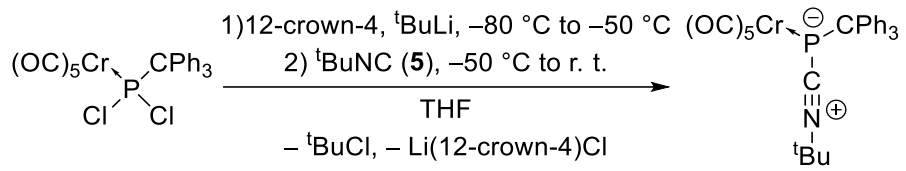

1a **6a**

Synthesis via the phosphinidenoid complex 2a

A solution of a Li/Cl phosphinidenoid chromium(0) complex (**2a**) was prepared using 0.54 g (1.00 mmol, 1.0 eq.) of [$Cr(CO)_5${$P(CPh_3)Cl_2$}] (**1a**), 0.15 mL (0.93 mmol, 0.9 eq.) of 12-crown-4 and 0.65 mL (c = 1.7 M in *n*-pentane, 1.10 mmol, 1.1 eq.) of a *tert*-butyllithium solution in 30 mL of THF at −80 °C. Afterwards, 0.17 mL (1.50 mmol, 1.5 eq.) of *tert*-butyl isocyanide (**5**) was added dropwise at −50 °C. The reaction mixture was stirred for 19 h while it was allowed to slowly warm up to ambient temperature. All volatiles were removed *in vacuo* (<0.02 mbar) at ambient temperature. The product was extracted six times with 20 mL of *n*-pentane. The solvent was removed *in vacuo* (<0.02 mbar) at ambient temperature and the product was obtained as yellow solid after drying under the same conditions for 10 minutes.

Reaction codes: DB-49, 83, 285 (31m3a017.18, 31p5a015.18)

Molecular formula: $C_{29}H_{24}NO_5PCr$

Molecular weight: 549.483 g/mol

Yield: 0.52 g (0.94 mmol, 94 %)

Melting point: 93 °C (dec.)

Elemental analysis:	calculated (%)	C 63.39	H 4.40	N 2.55
	found (%)	C 63.76	H 4.64	N 2.45

X-ray diffraction analysis: excellent structure (A1, GSTR649, GXray5842f)

MS (LIFDI, selected data): m/z (%) = 549.1 (100) $[M]^{\bullet+}$, 243.1 (24) $[CPh_3]^+$.

IR (ATR Diamond, selected data): $\tilde{\nu}$ / cm^{-1} = 1894 (vs) (C≡O), 1925 (vs) (C≡O), 2049 (m) (C≡O), 2132 (w) (C≡N).

^{1}H NMR (300.13 MHz, C_6D_6, 299 K): δ / ppm = 7.44–6.96 (m, 15H; CPh_3), 0.72 (s, 9H; $C(CH_3)_3$).

^{13}C{^{1}H} NMR (75.48 MHz, C_6D_6, 300 K): δ / ppm = 224.1 (d, $^{2}J_{P,C}$ = 3.6 Hz; *trans*-*C*O), 217.4 (s; *cis*-*C*O), 147.3 (d, $^{2}J_{P,C}$ = 6.8 Hz; *ipso*-*C*), 143.6 (s; N*C*), 130.6 (d, $J_{P,C}$ = 8.1 Hz; Ph), 128.3 (s; Ph), 127.0 (d, $J_{P,C}$ = 1.6 Hz; Ph), 61.3 (s; $C(CH_3)_3$), 60.0 (d, $^{1}J_{P,C}$ = 28.4 Hz; P-CPh_3), 29.0 (d, $^{4}J_{P,C}$ = 1.6 Hz; $C(CH_3)_3$).

^{15}N{^{1}H} NMR (50.69 MHz, C_6D_6, 298 K): δ / ppm = −170.0 (s).

^{31}P{^{1}H} NMR (121.51 MHz, $CDCl_3$, 300 K): δ / ppm = −11.4 (s).

^{31}P NMR (121.51 MHz, $CDCl_3$, 300 K): δ / ppm = −11.4 (s).

5.5.5 Attempted synthesis of [pentacarbonyl{(*tert*-butylazaniumylidyne)methyl(triphenylmethyl)phosphanido-κ*P*}molybdenum(0)] (6b)

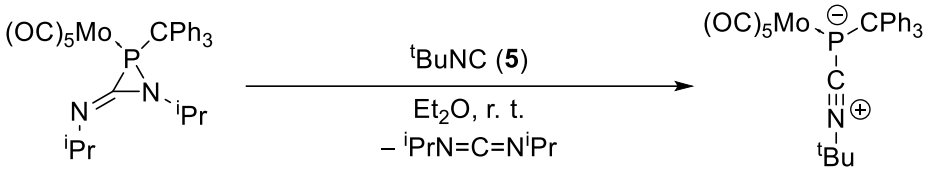

4b **6b**

Synthesis via the azaphosphiridine complex 4b

0.10 mL (0.90 mmol, 1.5 eq.) of *tert*-butyl isocyanide (**5**) was added dropwise to a solution of 0.38 g (0.60 mmol, 1.0 eq.) of **4b** in 40 mL of diethyl ether at ambient temperature. The reaction mixture was stirred for 24 h to obtain a brown suspension.

Reaction code: DB-48 (29t4a096.18)

Molecular formula: $C_{29}H_{24}NO_5PMo$

Molecular weight: 593.437 g/mol

Content in solution: 13 % (^{31}P NMR integration of reaction mixture)

^{31}P{^{1}H} NMR (162.00 MHz, Et_2O, 295 K): δ / ppm = −27.8 (s).

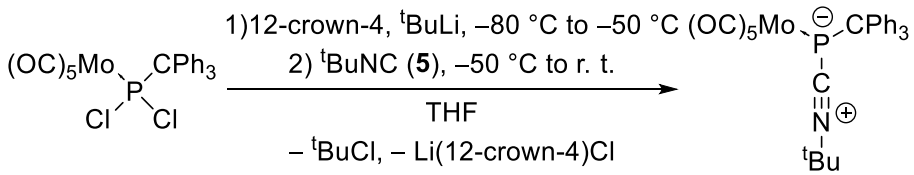

1b **6b**

Synthesis via the phosphinidenoid complex 2b

A solution of a Li/Cl phosphinidenoid molybdenum(0) complex **2b** was prepared using 53 mg (0.09 mmol, 1.0 eq.) of [Mo(CO)$_5${P(CPh$_3$)Cl$_2$}] (**1b**), 13 µL (0.08 mmol, 0.9 eq.) of 12-crown-4 and 0.06 mL (c = 1.7 M in *n*-pentane, 0.10 mmol, 1.1 eq.) of a *tert*-butyllithium solution in 2 mL of THF at −80 °C. Afterwards, 0.02 mL (0.18 mmol, 1.9 eq.) of *tert*-butyl isocyanide (**5**) was added dropwise at −50 °C. The reaction mixture was stirred for 21 h while it was allowed to slowly warm up to ambient temperature to obtain a brown suspension.

Reaction code: DB-84 (48m3a053.18)

Content in solution: 76 % (^{31}P NMR integration of reaction mixture)

^{31}P{^{1}H} NMR (121.51 MHz, THF, 298 K): δ / ppm = −29.0 (s).

5.5.6 Synthesis of [pentacarbonyl{(*tert*-butylazaniumylidyne)methyl(triphenylmethyl)phosphanido-κ*P*}tungsten(0)] (6c)

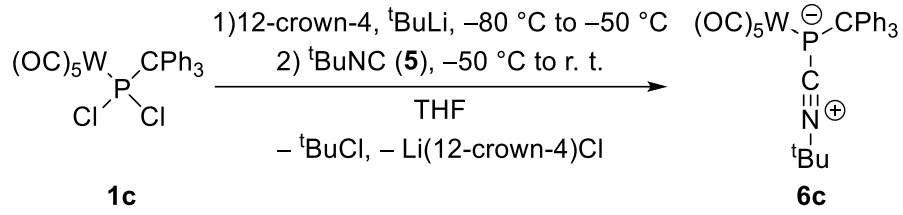

Synthesis

A solution of a Li/Cl phosphinidenoid tungsten(0) complex **2c** was prepared using 0.67 g (1.00 mmol, 1.0 eq.) of [W(CO)$_5${P(CPh$_3$)Cl$_2$}] (**1c**), 0.14 mL (0.87 mmol, 0.9 eq.) of 12-crown-4 and 0.77 mL (c = 1.7 M in *n*-pentane, 1.31 mmol, 1.3 eq.) of a *tert*-butyllithium solution in 30 mL of THF at −80 °C. Afterwards, 0.17 mL (1.50 mmol, 1.5 eq.) of *tert*-butyl isocyanide (**5**) was added dropwise at −50 °C. The reaction mixture was stirred for 16 h while it was allowed to slowly warm up to ambient temperature. All volatiles were removed *in vacuo* (<0.02 mbar) at ambient temperature. The product was extracted three times with 20 mL of diethyl ether. The solvent was removed *in vacuo* (<0.02 mbar) at ambient temperature and the product was obtained as yellow solid after drying under the same conditions for 2 h.

Reaction code: DB-20, 74 (17m3b004.18, 46p5a017.18)

Molecular formula: $C_{29}H_{24}NO_5PW$

Molecular weight: 681.327 g/mol

Yield: 0.56 g (0.82 mmol, 82 %)

MS (EI, 70 eV, selected data): m/z (%) = 681 (0.1) $[M]^{\bullet+}$, 244 (100) $[CPh_3+H]^+$.

^{1}H NMR (300.13 MHz, $CDCl_3$, 298 K): δ / ppm = 7.33–7.24 (m, 15H; CPh_3), 1.28 (s, 9H; $C(CH_3)_3$).

^{1}H NMR (500.14 MHz, C_6D_6, 298 K): δ / ppm = 7.45–6.98 (m, 15H; CPh_3), 0.68 (s, 9H; $C(CH_3)_3$).

^{13}C{^{1}H} NMR (125.76 MHz, $CDCl_3$, 298 K): δ / ppm = 201.3 (d, $^2J_{P,C}$ = 16.9 Hz; *trans*-*C*O), 197.7 (d_{sat}, $^2J_{P,C}$ = 3.5 Hz, $^1J_{W,C}$ = 126.7 Hz; *cis*-*C*O), 146.8 (d, $^2J_{P,C}$ = 6.6 Hz; *ipso*-*C*), 143.0 (d, $^1J_{P,C}$ = 104.0 Hz; N*C*), 130.4 (d, $J_{P,C}$ = 8.2 Hz; Ph), 128.1 (s; Ph), 126.8 (d, $J_{P,C}$ = 1.1 Hz; Ph), 61.5 (s; $C(CH_3)_3$), 58.4 (d, $^1J_{P,C}$ = 24.8 Hz; P-*C*Ph_3), 29.7 (s; $C(CH_3)_3$).

^{15}N{^{1}H} NMR (50.69 MHz, C_6D_6, 298 K): δ / ppm = −170.7 (s).

^{31}P{^{1}H} NMR (121.51 MHz, $CDCl_3$, 298 K): δ / ppm = −50.5 (s_{sat}, $^1J_{W,P}$ = 117.5 Hz).

^{31}P NMR (121.51 MHz, $CDCl_3$, 298 K): δ / ppm = −50.5 (s_{sat}, $^1J_{W,P}$ = 117.5 Hz).

5.5.7 Synthesis of [pentacarbonyl{(isopropylamino)(isopropylimino)methyl(triphenylmethyl)phosphinito-κ*P*}molybdenum(0)] (9b)

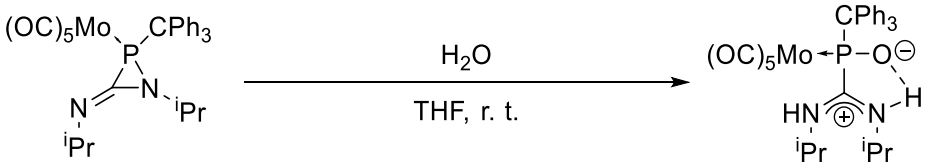

4b **9b**

Synthesis

0.102 g (0.16 mmol, 1.0 eq.) of the azaphosphiridine complex **4b** was reacted with 8 µL (0.44 mmol, 2.8 eq.) of water in 10 mL of tetrahydrofuran. The yellow solution was stirred for 2 h at ambient temperature. All volatiles were removed *in vacuo* (<0.02 mbar) at ambient temperature. The crude material was washed three times with 1.0 mL of an *n*-pentane/diethyl ether (1:50) mixture at −40 °C. After removing the volatiles *in vacuo* (<0.02 mbar) and drying under the same conditions for 3.5 h the product was obtained as yellow solid.

Reaction codes: DB-38, 59 (26p5a006.18)

Molecular formula: $C_{31}H_{31}N_2O_6PMo$

Molecular weight: 654.521 g/mol

Yield: 0.059 g (0.09 mmol, 56 %)

Elemental analysis:	calculated (%)	C 56.89	H 4.77	N 4.28
	found (%)	C 59.20	H 5.44	N 3.92

MS (ESI pos., selected data): m/z (%) = 657.105 (68) $[M+H]^+$, 629.109 (2) $[M-CO+H]^+$, 573.120 (2) $[M-3CO+H]^+$, 243.116 (31) $[CPh_3]^+$.

HRMS (ESI pos.): *m/z* calcd for $[C_{31}H_{32}N_2O_6PMo]^+$: 657.1050 $[M+H]^+$; found: 657.1050.

IR (ATR Diamond, selected data): $\tilde{\nu}$ / cm^{-1} = 1904 (vs) (C≡O), 1994 (w) (C≡O), 2069 (s) (C≡O), 3346 (w) (N-H).

^{1}H NMR (500.14 MHz, $CDCl_3$, 298 K): δ / ppm = 8.85 (br s, 2H; N*H*), 7.69–6.76 (m, 15H; CPh_3), 3.89 (br s, 2H; C*H*$(CH_3)_2$), 1.35–1.20 (m, 2H; CH(C*H*$_3)_2$).

^{13}C{^{1}H} NMR (125.78 MHz, $CDCl_3$, 298 K): δ / ppm = 212.1 (d, $^2J_{P,C}$ = 29.3 Hz; *trans*-*C*O), 206.1 (d, $^2J_{P,C}$ = 10.1 Hz; *cis*-*C*O), 173.4 (d, $^1J_{P,C}$ = 41.5 Hz; N-*C*-N), 145.5 (d, $^2J_{P,C}$ = 12.0 Hz; *ipso*-*C*), 142.1 (d, $^2J_{P,C}$ = 2.7 Hz; *ipso*-*C*), 141.1 (d, $^2J_{P,C}$ = 5.1 Hz; *ipso*-*C*), 131.6 (d, $J_{P,C}$ = 7.4 Hz; Ph), 131.0 (d, $J_{P,C}$ = 1.4 Hz; Ph), 130.2 (d, $J_{P,C}$ = 6.8 Hz; Ph), 128.8 (s; Ph), 128.5 (s; Ph), 127.9 (s; Ph), 127.6 (s; Ph), 127.4 (s; Ph), 126.4 (s; Ph), 69.7 (d, $^1J_{P,C}$ = 10.2 Hz; *C*Ph_3), 47.5 (br s; *C*H$(CH_3)_2$), 29.8 (s; CH(*C*$H_3)_2$).

^{31}P{^{1}H} NMR (202.48 MHz, $CDCl_3$, 298 K): δ / ppm = 110.6 (s).

^{31}P NMR (202.48 MHz, $CDCl_3$, 298 K): δ / ppm = 110.6 (s).

5.5.8 Synthesis of [pentacarbonyl{1-methylimidazol-3-iumyl(triphenylmethyl)phosphanido-κ*P*}chromium(0)] (13a)

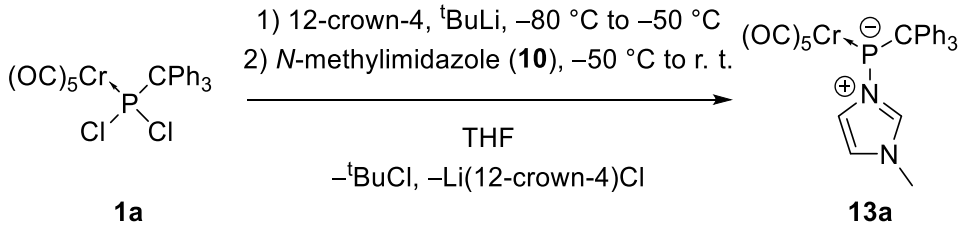

1a **13a**

Synthesis

A solution of a Li/Cl phosphinidenoid chromium(0) complex **2a** was prepared using 4.721 g (8.79 mmol, 1.0 eq.) of $[Cr(CO)_5\{P(CPh_3)Cl_2\}]$ (**1a**), 1.42 mL (8.78 mmol, 1.0 eq.) of 12-crown-4 and 5.50 mL (c = 1.6 M in *n*-pentane, 8.80 mmol, 1.0 eq.) of a *tert*-butyllithium solution in 50 mL of THF at −80 °C. Afterwards, 1.06 mL (13.30 mmol, 1.5 eq.) of *N*-methylimidazole (**10**) were added dropwise at −50 °C. The reaction mixture was stirred for 17 h while it was allowed to slowly warm up to ambient temperature. All volatiles were removed *in vacuo* (<0.02 mbar) at ambient temperature. The product was extracted five times with 60 mL of diethyl ether using a filter cannula (Ø = 2 mm) with a glass microfiber filter paper (Whatman® GF/B) and a P3 Schlenk frit (filled with dry SiO_2, Ø = 3 cm, h = 3 cm). Residual product was extracted from the SiO_2 using five times 60 mL of diethyl ether. Afterwards, 420 mL of *n*-pentane were added to the solution. The obtained yellow suspension was stirred for 30 minutes at ambient temperature and stored stationary at −40 °C for 40 h. The supernatant was filtered off using a filter cannula (Ø = 2 mm) with a Whatman® 595 filter paper at ambient temperature and the yellow solid residue was washed three times using 44 mL of a 10:1 *n*-pentane/diethyl ether mixture at ambient temperature. The product was obtained as yellow solid after drying for 3 h *in vacuo* (<0.02 mbar) at ambient temperature.

Reaction codes: DB-373, 543 (20m3b052.22, 33p5a001.21, 32m3b032.21)

Molecular formula: $C_{28}H_{21}N_2O_5PCr$

Molecular weight: 548.455 g/mol

Yield: 2.62 g (4.78 mmol, 54.4 %)

Melting point: 141 °C (dec.)

Elemental analysis:	calculated (%)	C 61.32	H 3.86	N 5.11
	found (%)	C 61.34	H 4.12	N 5.10

X-ray diffraction analysis: good structure, + 1.5 benzene (C1, GSTR730, GXray6654)

MS (LIFDI, selected data): m/z (%) = 548.1 (100) $[M]^{\bullet+}$, 274.0 (25) $[Cr(CO)_5(N\text{-MeIm})]^+$, 243.1 (98) $[CPh_3]^+$.

IR (solution in THF, c = 1.5 mM, selected data): $\tilde{\nu}$ / cm^{-1} = 1920 (s) (C≡O), 1963 (w) (C≡O), 2043 (m) (C≡O).

^{1}H NMR (300.13 MHz, C_6D_6, 300 K): δ / ppm = 7.78–7.69 (m, 6H; CPh_3), 7.15–7.11 (m, 6H; CPh_3), 6.99–6.96 (m, 3H; CPh_3), 6.45–6.44 (m, 1H; Im), 6.33 (m, 1H; Im), 5.11–5.10 (m, 1H; Im), 1.81 (s, 3H; C*H*$_3$).

^{13}C{^{1}H} NMR (125.75 MHz, C_6D_6, 298 K): δ / ppm = 225.3 (s; *trans*-*C*O), 219.8 (d, $^{2}J_{P,C}$ = 4.5 Hz; *cis*-*C*O), 147.5 (d, $^{2}J_{P,C}$ = 9.9 Hz; *ipso*-*C*), 141.4 (d, $J_{P,C}$ = 3.1 Hz; Im), 130.5 (br s; Ph), 130.3 (d, $J_{P,C}$ = 8.0 Hz; Im), 128.2 (s; Ph), 125.9 (s; Ph), 119.5 (s; Im), 63.5 (d, $^{1}J_{P,C}$ = 56.6 Hz; P-*C*Ph_3), 33.8 (s; *C*H_3).

^{15}N{^{1}H} NMR (50.68 MHz, C_6D_6, 298 K): δ / ppm = −177.7 (s; P-*N*), −215.2 (s; *N*-CH_3).

^{31}P{^{1}H} NMR (202.44 MHz, C_6D_6, 298 K): δ / ppm = 249.5 (br s).

^{31}P NMR (121.51 MHz, C_6D_6, 299 K): δ / ppm = 248.0 (br s).

5.5.9 Synthesis of [pentacarbonyl{1-methylimidazol-3-iumyl(triphenylmethyl)phosphanido-κ*P*}tungsten(0)] (13b)

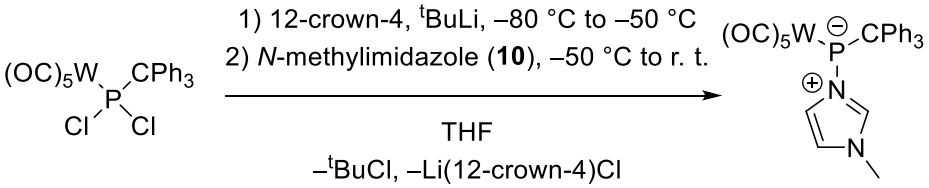

1c **13b**

Synthesis

A solution of a Li/Cl phosphinidenoid tungsten(0) complex **2c** was prepared using 1.425 g (2.13 mmol, 1.0 eq.) of [W(CO)$_5${P(CPh$_3$)Cl$_2$}] (**1c**), 0.34 mL (2.10 mmol, 1.0 eq.) of 12-crown-4 and 1.34 mL (c = 1.6 M in *n*-pentane, 2.14 mmol, 1.0 eq.) of a *tert*-butyllithium solution in 22 mL of THF at −80 °C. Afterwards, 0.26 mL (3.26 mmol, 1.5 eq.) of *N*-methylimidazole (**10**) were added dropwise at −50 °C. The reaction mixture was stirred for 15.5 h while it was allowed to slowly warm up to ambient temperature. All volatiles were removed *in vacuo* (<0.02 mbar) at ambient temperature. The product was extracted six times with 30 mL of diethyl ether using a filter cannula (Ø = 2 mm) with a glass microfiber filter paper (Whatman® GF/B) and a P3 Schlenk frit (filled with dry SiO_2, Ø = 3 cm, h = 3 cm). Residual product was extracted from the SiO_2 using three times 40 mL of diethyl ether. Afterwards, 420 mL of *n*-pentane were added to the solution. The obtained yellow suspension was stirred for 1 h at ambient temperature. The supernatant was filtered off using a filter cannula (Ø = 2 mm) with

a Whatman® 595 filter paper at ambient temperature and the yellow solid residue was washed three times using 20 mL of *n*-pentane at ambient temperature. The product was obtained as yellow solid after drying for 9 h *in vacuo* (<0.02 mbar) at ambient temperature.

Reaction codes: DB-362, 367, 521, 561 (18m3a018.22, 28p5a002.21, 28m3a001.21)

Molecular formula: $C_{28}H_{21}N_2O_5PW$

Molecular weight: 680.299 g/mol

Yield: 0.805 g (1.18 mmol, 54.9 %)

Melting point: 146 °C (dec.)

Elemental analysis:	calculated (%)	C 49.44	H 3.11	N 4.12
	found (%)	C 49.22	H 3.20	N 4.11

X-ray diffraction analysis: good structure, + 1.5 benzene (C1, GSTR723, GXray6613)

MS (LIFDI, selected data): m/z (%) = 680.8 (38) $[M]^{\bullet+}$, 243.1 (100) $[CPh_3]^+$.

IR (ATR Diamond, selected data): $\tilde{\nu}$ / cm^{-1} = 1921 (s) (C≡O), 1966 (w) (C≡O), 2053 (m) (C≡O).

^{1}H NMR (300.13 MHz, C_6D_6, 298 K): δ / ppm = 7.75–7.73 (m, 6H; CPh_3), 7.14–7.09 (m, 6H; CPh_3), 7.00–6.94 (m, 3H; CPh_3), 6.41–6.40 (m, 1H; Im), 6.33–6.32 (m, 1H; Im), 5.11–5.10 (m, 1H; Im), 1.83 (s, 3H; C*H*$_3$).

^{13}C{^{1}H} NMR (125.75 MHz, C_6D_6, 298 K): δ / ppm = 203.2 (d, $^2J_{P,C}$ = 14.0 Hz; *trans*-*C*O), 200.4 (d_{sat}, $^2J_{P,C}$ = 7.4 Hz, $^1J_{W,C}$ = 126.2 Hz; *cis*-*C*O), 147.4 (d, $^2J_{P,C}$ = 8.4 Hz; *ipso*-*C*), 142.1 (s; Im), 130.5 (br s; Ph), 130.3 (d, $J_{P,C}$ = 7.9 Hz; Im), 128.4 (s; Ph), 125.9 (s; Ph), 119.8 (s; Im), 62.9 (d, $^1J_{P,C}$ = 49.9 Hz; P-*C*Ph_3), 33.9 (s; *C*H_3).

^{15}N{^{1}H} NMR (50.68 MHz, C_6D_6, 298 K): δ / ppm = −183.9 (s; P-*N*), −215.2 (s; *N*-CH_3).

^{31}P{^{1}H} NMR (202.44 MHz, C_6D_6, 298 K): δ / ppm = 199.4 (br s_{sat}, $^1J_{W,P}$ = 107.2 Hz).

^{31}P NMR (121.51 MHz, C_6D_6, 298 K): δ / ppm = 199.2 (br s_{sat}, $^1J_{W,P}$ = 107.2 Hz).

5.5.10 Synthesis of [pentacarbonyl{4-(dimethylamino)pyridin-1-iumyl(triphenylmethyl)phosphanido-κ*P*}chromium(0)] (14a)

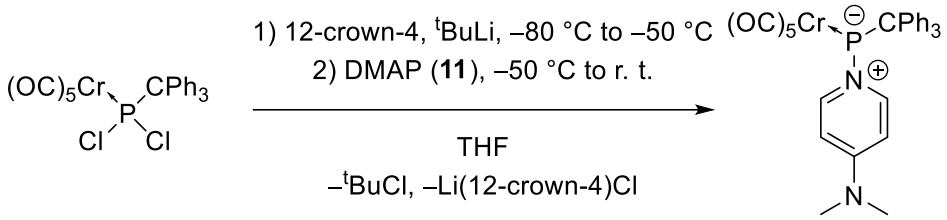

1a **14a**

Synthesis

A solution of a Li/Cl phosphinidenoid chromium(0) complex **2a** was prepared using 0.564 g (1.05 mmol, 1.0 eq.) of [$Cr(CO)_5${$P(CPh_3)Cl_2$}] (**1a**), 0.16 mL (0.99 mmol, 0.9 eq.) of 12-crown-4 and 0.66 mL (c = 1.6 M in *n*-pentane, 1.06 mmol, 1.0 eq.) of a *tert*-butyllithium solution in 20 mL of THF at −80 °C. Afterwards, 0.237 g (1.94 mmol, 1.8 eq.) of 4-dimethylaminopyridine (DMAP) (**11**) was added at −50 °C. The reaction mixture was stirred for 17 h while it was allowed to slowly warm up to ambient temperature. All volatiles were removed *in vacuo* (<0.02 mbar) at ambient temperature. The product was extracted five times with 20 mL of diethyl ether using a filter cannula (Ø = 2 mm) with a glass microfiber filter paper (Whatman® GF/B) and a Schlenk frit (filled with dry SiO_2, Ø = 3 cm, h = 3 cm). Residual product was extracted from the SiO_2 using three times 10 mL of diethyl ether at ambient temperature. Afterwards, 120 mL of *n*-pentane were added to the solution. The obtained yellow suspension was stirred for 1 h at ambient temperature. The supernatant was filtered off using a filter cannula (Ø = 2 mm) with a Whatman® 595 filter paper at ambient temperature and the yellow solid residue was washed once with 15 mL and twice with 5 mL of *n*-pentane at ambient temperature. The product was obtained as yellow solid after drying for 2 h *in vacuo* (<0.02 mbar) at ambient temperature.

Reaction codes: DB-426, 585 (48p5a029.21, 48m3a038.21)

Molecular formula: $C_{31}H_{25}N_2O_5PCr$

Molecular weight: 588.520 g/mol

Yield: 0.199 g (0.34 mmol, 32.1 %)

Melting point: 145 °C (dec.)

Elemental analysis: calculated (%) C 63.27 H 4.28 N 4.76

found (%) C 62.90 H 4.62 N 4.64

X-ray diffraction analysis: good structure, + 0.5 diethyl ether (C1, GSTR740, GXray6736)

MS (LIFDI, selected data): m/z (%) = 588.1 (100) $[M]^{\bullet+}$, 314.0 (9) $[Cr(CO)_5(dmap)]^+$, 243.1 (22) $[CPh_3]^+$.

IR (ATR Diamond, selected data): $\tilde{\nu}$ / cm^{-1} = 1920 (s) (C≡O), 1970 (m) (C≡O), 2042 (m) (C≡O).

^{1}H NMR (500.04 MHz, THF-d_8, 298 K): δ / ppm = 7.67 (d, $^3J_{H,H}$ = 6.1 Hz, 2H; DMAP-C*H*), 7.55–7.53 (m, 6H; CPh_3), 7.19–7.15 (m, 6H; CPh_3), 7.09–7.06 (m, 3H; CPh_3), 6.48–6.46 (m, 2H; DMAP-C*H*), 3.06 (s_{sat}, $^1J_{C,H}$ = 67.29 Hz, 6H; $N(CH_3)_2$).

^{13}C{^{1}H} NMR (125.75 MHz, THF-d_8, 298 K): δ / ppm = 225.7 (d, $^2J_{P,C}$ = 2.8 Hz; *trans*-*C*O), 219.8 (d, $^2J_{P,C}$ = 4.2 Hz; *cis*-*C*O), 156.8 (s; *p*-C^{DMAP}), 151.0 (d, $^2J_{P,C}$ = 11.7 Hz; *o*-CH^{DMAP}), 147.6 (s; *ipso*-*C*), 130.8 (d, $J_{P,C}$ = 8.5 Hz; Ph), 128.3 (s; Ph), 126.0 (s; Ph), 106.4 (s; *m*-CH^{DMAP}), 64.5 (d, $^1J_{P,C}$ = 60.8 Hz; P-*C*Ph_3), 39.4 (s; $N(CH_3)_2$).

^{15}N{^{1}H} NMR (50.68 MHz, THF-d_8, 298 K): δ / ppm = −192.1 (s; P-*N*), −297.6 (s; *N*$(CH_3)_2$).

^{31}P{^{1}H} NMR (202.44 MHz, THF-d_8, 298 K): δ / ppm = 281.2 (br s).

^{31}P NMR (121.51 MHz, THF-d_8, 298 K): δ / ppm = 281.1 (br s).

5.5.11 Synthesis of [pentacarbonyl{(4-(dimethylamino)pyridin-1-iumyl(triphenylmethyl)phosphanido-κ*P*}tungsten(0)] (14b)

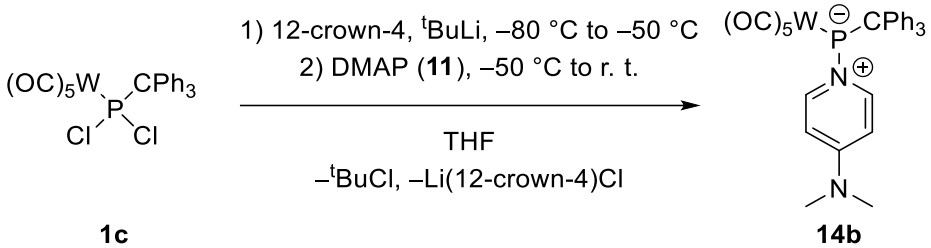

1c **14b**

Synthesis

A solution of a Li/Cl phosphinidenoid tungsten(0) complex **2c** was prepared using 0.078 g (0.12 mmol, 1.0 eq.) of $[W(CO)_5\{P(CPh_3)Cl_2\}]$ (**1c**), 18 µL (0.11 mmol, 1.0 eq.) of 12-crown-4 and 0.08 mL (c = 1.6 M in *n*-pentane, 0.13 mmol, 1.1 eq.) of a *tert*-butyllithium solution in 2 mL of THF at −80 °C. Afterwards, 0.030 g (0.24 mmol, 2.1 eq.) of 4-dimethylaminopyridine

(DMAP) (**11**) was added at −50 °C. The reaction mixture was stirred for 18 h while it was allowed to slowly warm up to ambient temperature. All volatiles were removed *in vacuo* (<0.02 mbar) at ambient temperature. The product was extracted five times with 5 mL of diethyl ether using a filter cannula (Ø = 2 mm) with a glass microfiber filter paper (Whatman® GF/B) and a Schlenk frit (filled with dry SiO_2, Ø = 1 cm, h = 2 cm). Afterwards, 40 mL of *n*-pentane were added to the solution. The obtained yellow suspension was stirred for 1 h at ambient temperature. The supernatant was filtered off using a filter cannula (Ø = 2 mm) with a Whatman® 595 filter paper at ambient temperature and the yellow solid residue was washed three times using 5 mL of *n*-pentane at ambient temperature. The product was obtained as yellow solid after drying for 1 h *in vacuo* (<0.02 mbar) at ambient temperature.

Reaction codes: DB-417, 425, 584 (48p5a028.21)

Molecular formula: $C_{31}H_{25}N_2O_5PW$

Molecular weight: 720.364 g/mol

Yield: 0.045 g (0.06 mmol, 53.7 %)

Melting point: 141 °C (dec.)

Elemental analysis:	calculated (%)	C 51.69	H 3.50	N 3.89
	found (%)	C 51.51	H 3.76	N 3.74

X-ray diffraction analysis: good structure, + 0.5 diethyl ether (C1, GSTR741, GXray6737)

MS (LIFDI, selected data): m/z (%) = 721.2 (38) $[M+H]^{\bullet+}$, 446.0 (10) $[W(CO)_5(dmap)]^+$, 243.2 (22) $[CPh_3]^+$.

MS (EI, 70 eV, selected data): m/z (%) = 598.0 (<1) $[W(CO)_5PCPh_3)]^+$, 569.9 (<1) $[W(CO)_4(PCPh_3)]^+$, 541.9 (<1) $[W(CO)_3(PCPh_3)]^+$, 514.0 (<1) $[W(CO)_2(PCPh_3)]^+$, 274.0 (<1) $[PCPh_3]$, 243.0 (100) $[CPh_3]^+$, 121.0 (48) $[DMAP-H]^+$.

IR (ATR Diamond, selected data): $\tilde{\nu}$ / cm^{-1} = 1917 (s) (C≡O), 1971 (m) (C≡O), 2054 (m) (C≡O).

^{1}H NMR (500.04 MHz, THF-d_8, 298 K): δ / ppm = 7.65 (d, $^3J_{H,H}$ = 6.7 Hz, 2H; DMAP-C*H*), 7.57–7.55 (m, 6H; CPh_3), 7.18–7.14 (m, 6H; CPh_3), 7.09–7.05 (m, 3H; CPh_3), 6.47–6.46 (m, 2H; DMAP-C*H*), 3.06 (s_{sat}, $^1J_{C,H}$ = 75.25 Hz, 6H; $N(CH_3)_2$).

$^{13}C\{^1H\}$ NMR (125.75 MHz, THF-d_8, 298 K): δ / ppm = 203.5 (d, $^2J_{P,C}$ = 13.6 Hz; *trans*-*C*O), 200.4 (d_{sat}, $^2J_{P,C}$ = 7.6 Hz, $^1J_{W,C}$ = 126.1 Hz; *cis*-*C*O), 156.8 (s; *p*-C^{DMAP}), 151.5 (d, $^2J_{P,C}$ = 10.7 Hz; *o*-CH^{DMAP}), 147.4 (s; *ipso*-*C*), 130.9 (d, $J_{P,C}$ = 11.5 Hz; Ph), 128.3 (s; Ph), 125.9 (s; Ph), 106.5 (s; *m*-CH^{DMAP}), 63.9 (d, $^1J_{P,C}$ = 53.4 Hz; P-*C*Ph_3), 39.4 (s; N(*C*H_3)$_2$).

$^{15}N\{^1H\}$ NMR (50.68 MHz, THF-d_8, 298 K): δ / ppm = −193.9 (s; P-*N*), −298.3 (s; *N*$(CH_3)_2$).

$^{31}P\{^1H\}$ NMR (202.44 MHz, THF-d_8, 298 K): δ / ppm = 234.8 (br s_{sat}, $^1J_{W,P}$ = 102.5 Hz).

^{31}P NMR (202.44 MHz, THF-d_8, 298 K): δ / ppm = 234.8 (br s_{sat}, $^1J_{W,P}$ = 102.5 Hz).

5.5.12 Attempted synthesis of [pentacarbonyl{pyridin-1-iumyl(triphenylmethyl)phosphanido-κ*P*}chromium(0)] (15a)

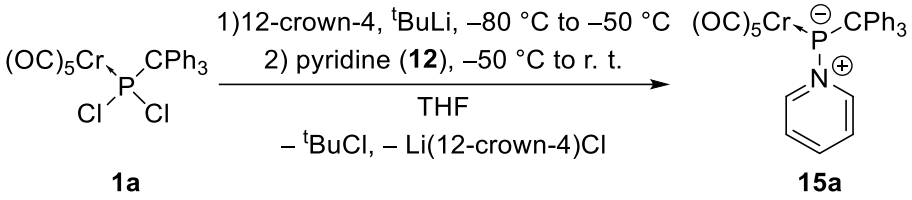

1a **15a**

Synthesis via the phosphinidenoid complex 2a

A solution of a Li/Cl phosphinidenoid chromium(0) complex **2a** was prepared using 0.606 g (1.13 mmol, 1.0 eq.) of [$Cr(CO)_5${$P(CPh_3)Cl_2$}] (**1a**), 0.18 mL (1.11 mmol, 1.0 eq.) of 12-crown-4 and 0.71 mL (c = 1.6 M in *n*-pentane, 1.14 mmol, 1.0 eq.) of a *tert*-butyllithium solution in 15 mL of THF at −80 °C. Afterwards, 1.82 mL (22.6 mmol, 20 eq.) of pyridine (**12**) were added dropwise at −50 °C. The reaction mixture was stirred for 7 h while it was allowed to slowly warm up to ambient temperature to obtain a dark brownish-violet suspension. All volatiles were removed *in vacuo* (<0.02 mbar) at ambient temperature. The product fully decomposed when extracted with diethyl ether using a filter cannula (Ø = 2 mm) with a glass microfiber filter (Whatman® GF/B) at ambient temperature.

Reaction code: DB-388 (36m3a002.21, 36m3a031.21)

Molecular formula: $C_{29}H_{20}NO_5PCr$

Molecular weight: 545.451 g/mol

Content in solution: 74 % (^{31}P NMR integration of reaction mixture)

$^{31}P\{^1H\}$ NMR (121.51 MHz, THF, 300 K): δ / ppm = 335.3 (br s).

$^{31}P\{^{1}H\}$ NMR of decomposed reaction mixture (121.51 MHz, Et_2O, 303 K): δ / ppm = 143.5 (br s; 67 %), 131.4 (s; 16 %), 123.5 (s; 3 %), 63.4 (s; 3 %), 43.3 (s; 6 %), 11.6 (s; 5 %).

^{31}P NMR of decomposed reaction mixture (121.51 MHz, Et_2O, 303 K): δ / ppm = 143.5 (br d, $J_{P,H}$ cannot be determined due to the broadness of the signal; 68 %), 131.4 (d, $^{1}J_{P,H}$ = 330.4 Hz; 18 %), 11.5 (t, $^{1}J_{P,H}$ = 627.8 Hz; 14 %).

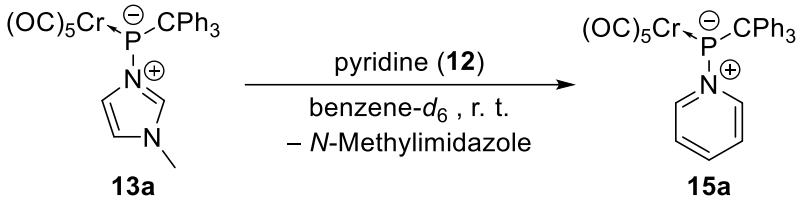

Synthesis via the *N*-methylimidazole adduct 13a

0.10 mL (1.24 mmol, 25.4 eq.) of pyridine (**12**) was added dropwise to a solution of 0.027 g (0.05 mmol, 1.0 eq.) of **13a** in 0.5 mL of benzene-d_6 at ambient temperature. The yellow reaction solution was kept for 2 minutes at ambient temperature.

Reaction code: DB-390 (36m3a042.21)

Molecular formula: $C_{29}H_{20}NO_5PCr$

Molecular weight: 545.451 g/mol

Content in solution: 3 % (^{31}P NMR integration of reaction mixture)

$^{31}P\{^{1}H\}$ NMR (121.51 MHz, C_6D_6, 303 K): δ / ppm = 339.1 (br s).

5.5.13 Attempted synthesis of [pentacarbonyl{pyridin-1-iumyl(triphenylmethyl)phosphanido-κ*P*}tungsten(0)] (15b)

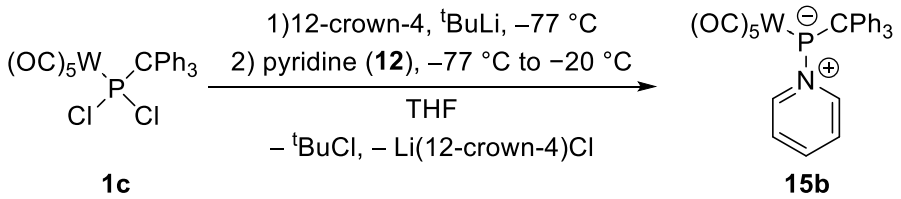

Synthesis via the phosphinidenoid complex 2c

A solution of a Li/Cl phosphinidenoid tungsten(0) complex **2c** was prepared using 0.114 g (0.17 mmol, 1.0 eq.) of $[W(CO)_5\{P(CPh_3)Cl_2\}]$ (**1c**), 27 µL (0.17 mmol, 1.0 eq.) of 12-crown-4 and 0.11 mL (c = 1.6 M in *n*-pentane, 0.18 mmol, 1.0 eq.) of a *tert*-butyllithium solution in 2 mL

of THF using a 10 mL Schlenk tube with cooling mantle attached to a cryostat (Thermo Haake PhoenixII CT80L with ethanol as refrigerant) at −77 °C. The obtained red solution was stirred for 40 minutes at −77 °C. Afterwards, 0.28 mL (3.47 mmol, 20 eq.) of pyridine (**12**) was added dropwise at −77 °C. The reaction mixture was stirred for 5 h while it was allowed to constantly warm up to −20 °C using the ramp function of the cryostat to obtain a dark reddish-brown suspension. All volatiles were removed *in vacuo* (<0.02 mbar) at −20 °C within 2 h. The product fully decomposed when extracted with diethyl ether using a P3 Schlenk frit (filled with dried Al_2O_3, Ø = 1 cm, h = 1 cm) at −40 °C.

Reaction code: DB-442 (04m3a015.22)

Molecular formula: $C_{29}H_{20}NO_5PW$

Molecular weight: 677.295 g/mol

Content in solution: 68 % (^{31}P NMR integration of reaction mixture)

^{31}P{^{1}H} NMR (121.51 MHz, THF, 298 K): δ / ppm = 284.6 (br s_{sat}, $^{1}J_{W,P}$ < 100 Hz). (The $^{1}J_{W,P}$ coupling constant cannot be determined exactly due to the broadness of the signal.)

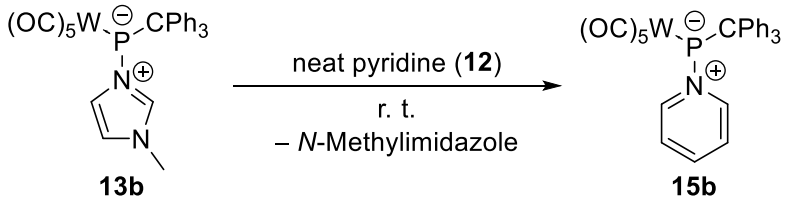

13b **15b**

Synthesis via the *N*-methylimidazole adduct 13b

0.016 g (0.02 mmol, 1.0 eq.) of **13b** was dissolved in 0.5 mL (6.19 mmol, 260 eq.) of pyridine (**12**) and shaken thoroughly for 1 minute at ambient temperature. The yellow reaction solution was kept for 21 h at ambient temperature.

Reaction code: DB-487 (12m3a048.22)

Molecular formula: $C_{29}H_{20}NO_5PW$

Molecular weight: 677.295 g/mol

Content in solution: 7 % (^{31}P NMR integration of reaction mixture)

^{31}P{^{1}H} NMR (121.51 MHz, pyridine, 298 K): δ / ppm = 281.7 (br s).

5.5.14 Synthesis of [pentacarbonyl{trimethylphosphoniumyl(triphenylmethyl)phosphanido-κ*P*}chromium(0)] (19a)

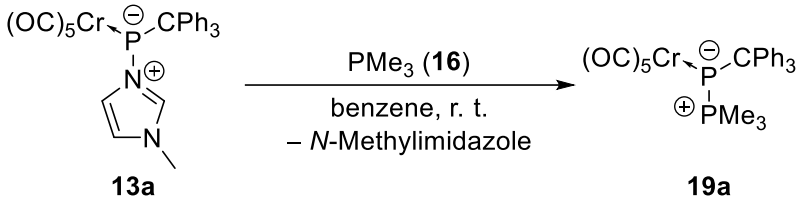

13a **19a**

Synthesis

0.24 mL (2.33 mmol, 5.2 eq.) of trimethylphosphane (**16**) was added to a solution of 0.246 g (0.45 mmol, 1.0 eq.) of [Cr(CO)$_5${P(CPh$_3$)(*N*-methylimidazole)}] (**13a**) in 10 mL of benzene at ambient temperature. The solution was stirred for 22 h at ambient temperature. The supernatant of the obtained yellow suspension was filtered off using a filter cannula (Ø = 1 mm) with a Whatman® 595 filter paper at ambient temperature. The solid was redissolved in 15 mL of dichloromethane. After addition of 15 mL of *n*-pentane the product was precipitated as yellow solid. The product was washed three times with 4 mL of *n*-pentane and dried for 1.5 h *in vacuo* (<0.02 mbar) at ambient temperature to obtain a yellow solid.

Reaction code: DB-565 (23t4a069.22, 23p5a024.22)

Molecular formula: $C_{27}H_{24}O_5P_2Cr$

Molecular weight: 542.428 g/mol

Yield: 0.191 g (0.35 mmol, 78.5 %)

Melting point: 150 °C (dec.)

Elemental analysis: calculated (%) C 59.79 H 4.46

found (%) C 59.53 H 4.75

X-ray diffraction analysis: excellent structure (AA1, GSTR771, GXray6923)

MS (LIFDI, selected data): m/z (%) = 542.0 (100) $[M]^{\bullet+}$, 243.1 (85) $[CPh_3]^+$.

IR (ATR Diamond, selected data): $\tilde{\nu}$ / cm^{-1} = 1875 (s) (C≡O), 1918 (s) (C≡O), 1974 (w) (C≡O), 2048 (m) (C≡O).

^{1}H NMR (400.13 MHz, CD_2Cl_2, 298 K): δ / ppm = 7.66–7.64 (m, 6H; CPh_3), 7.30–7.25 (m, 6H; CPh_3), 7.19–7.14 (m, 3H; CPh_3), 1.25 (dd, $^{2}J_{P,H}$ = 10.36 Hz, $^{3}J_{P,H}$ = 10.36 Hz, 9H; CH_3).

^{13}C{^{1}H} NMR (125.75 MHz, CD_2Cl_2, 298 K): δ / ppm = 224.0 (s; *trans*-*C*O), 218.5 (d, $^{2}J_{P,C}$ = 5.2 Hz; *cis*-*C*O), 147.8 (br s; *ipso*-*C*), 130.8 (d, $J_{P,C}$ = 9.2 Hz; Ph), 128.3 (s; Ph), 126.3 (s; Ph), 59.3 (d, $^{1}J_{P,C}$ = 41.7 Hz; P-*C*Ph_3), 16.0 (dd, $^{1}J_{P,C}$ = 39.4 Hz, $^{2}J_{P,C}$ = 11.2 Hz; P(*C*H_3)$_3$).

^{31}P{^{1}H} NMR (162.00 MHz, CD_2Cl_2, 298 K): δ / ppm = 17.3 (d, $^{1}J_{P,P}$ = 484.1 Hz; *P*Me_3), 12.5 (d, $^{1}J_{P,P}$ = 484.1 Hz; Cr-*P*CPh_3).

^{31}P NMR (162.00 MHz, CD_2Cl_2, 298 K): δ / ppm = 17.3 (dm, $^{1}J_{P,P}$ = 484.1 Hz; *P*Me_3), 12.5 (d, $^{1}J_{P,P}$ = 484.1 Hz; Cr-*P*CPh_3).

5.5.15 Synthesis of [pentacarbonyl{trimethylphosphoniumyl(triphenylmethyl)phosphanido-κ*P*}tungsten(0)] (19b)

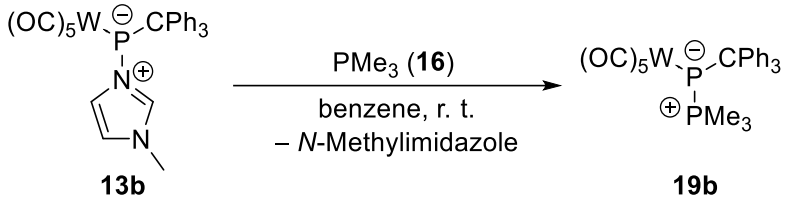

13b **19b**

Synthesis

0.08 mL (0.78 mmol, 5.4 eq.) of trimethylphosphane (**16**) was added to a solution of 0.098 g (0.14 mmol, 1.0 eq.) of [W(CO)$_5${P(CPh$_3$)(*N*-methylimidazole)}] (**13b**) in 5.0 mL of benzene at ambient temperature. The solution was stirred for 17 h at ambient temperature. The supernatant of the obtained yellow suspension was filtered off using a filter cannula (Ø = 1 mm) with a Whatman® 595 filter paper at ambient temperature. The product was obtained as yellow solid after drying for 80 minutes *in vacuo* (<0.02 mbar) at ambient temperature.

Reaction code: DB-491 (13p5a042.22)

Molecular formula: $C_{27}H_{24}O_5P_2W$

Molecular weight: 674.272 g/mol

Yield: 0.079 g (0.12 mmol, 80.8 %)

Melting point: 168 °C (dec.)

Elemental analysis: calculated (%) C 48.10 H 3.59

found (%) C 48.16 H 3.80

X-ray diffraction analysis: very good structure (AB1, GSTR758, GXray6857)

MS (LIFDI, selected data): m/z (%) = 674.0 (100) $[M]^{\bullet+}$, 243.1 (91) $[CPh_3]^+$.

IR (ATR Diamond, selected data): $\tilde{\nu}$ / cm^{-1} = 1911 (s) (C≡O), 1975 (m) (C≡O), 2059 (m) (C≡O).

^{1}H NMR (500.04 MHz, THF-d_8, 298 K): δ / ppm = 7.69–7.67 (m, 6H; CPh_3), 7.24–7.21 (m, 6H; CPh_3), 7.14–7.11 (m, 3H; CPh_3), 1.28 (dd, $^2J_{P,H}$ = 12.14 Hz, $^3J_{P,H}$ = 2.48 Hz, 9H; C*H*$_3$).

^{13}C{^{1}H} NMR (125.75 MHz, THF-d_8, 298 K): δ / ppm = 200.8 (d, $^2J_{P,C}$ = 15.5 Hz; *trans*-*C*O), 200.0 (dd_{sat}, $^2J_{P,C}$ = 4.3 Hz, $^3J_{P,C}$ = 4.3 Hz, $^1J_{W,C}$ = 125.4 Hz; *cis*-*C*O), 148.5 (br s; *ipso*-*C*), 131.6 (d, $J_{P,C}$ = 10.4 Hz; Ph), 128.8 (s; Ph), 126.8 (d, $J_{P,C}$ = 0.9 Hz; Ph), 59.3 (dd, $^1J_{P,C}$ = 33.5 Hz, $^2J_{P,C}$ = 3.2 Hz; P-*C*Ph_3), 15.4 (dd, $^1J_{P,C}$ = 42.6 Hz, $^2J_{P,C}$ = 8.7 Hz; P(*C*H_3)$_3$).

^{31}P{^{1}H} NMR (202.44 MHz, THF-d_8, 298 K): δ / ppm = 16.9 (d_{sat}, $^1J_{P,P}$ = 456.3 Hz, $^1J_{P,C}$ = 42.6 Hz; *P*Me_3), −20.9 (d_{sat}, $^1J_{P,P}$ = 456.3 Hz, $^1J_{W,P}$ = 120.6 Hz; W-*P*CPh_3).

^{31}P NMR (202.44 MHz, THF-d_8, 298 K): δ / ppm = 16.9 (dm_{sat}, $^1J_{P,P}$ = 456.3 Hz, $^1J_{P,C}$ = 42.6 Hz; *P*Me_3), −20.9 (d_{sat}, $^1J_{P,P}$ = 456.3 Hz, $^1J_{W,P}$ = 120.6 Hz; W-*P*CPh_3).

5.5.16 Synthesis of [pentacarbonyl{triethylphosphoniumyl(triphenylmethyl)phosphanido-κ*P*}-tungsten(0)] (20b)

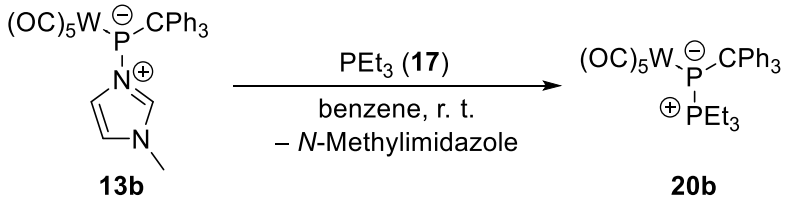

13b **20b**

Synthesis

0.13 mL (0.88 mmol, 5.0 eq.) of triethylphosphane (**17**) was added to a solution of 0.119 g (0.18 mmol, 1.0 eq.) of [W(CO)$_5${P(CPh_3)(*N*-methylimidazole)}] (**13b**) in 5.0 mL of benzene at ambient temperature. The solution was stirred for 16 h at ambient temperature. All volatiles were removed *in vacuo* (<0.02 mbar) at ambient temperature and the obtained yellow-orange solid was dried under the same conditions for 3.5 h.

Reaction code: DB-495 (13m3b018.22)

Molecular formula: $C_{30}H_{30}O_5P_2W$

Molecular weight: 716.353 g/mol

Yield: 0.112 g (0.16 mmol, 89.2 %)

Melting point: 122 °C (dec.)

Elemental analysis: calculated (%) C 50.30 H 4.22

found (%) C 50.39 H 4.34

X-ray diffraction analysis: very good structure (BC1, GSTR759, GXraymo_6858f)

MS (LIFDI, selected data): m/z (%) = 716.3 (56) $[M]^{\bullet+}$, 474.1 (17) $[M-CPh_3+H]^+$, 243.2 (100) $[CPh_3]^+$.

IR (ATR Diamond, selected data): $\tilde{\nu}$ / cm^{-1} = 1905 (s) (C≡O), 1978 (m) (C≡O), 2056 (m) (C≡O).

^{1}H NMR (300.13 MHz, C_6D_6, 298 K): δ / ppm = 7.84–7.80 (m, 6H; CPh_3), 7.10–7.04 (m, 6H; CPh_3), 6.95–6.90 (m, 3H; CPh_3), 1.26–1.15 (m, 6H; C*H*$_2$), 0.56–0.46 (m, 9H; C*H*$_3$).

^{13}C{^{1}H} NMR (75.48 MHz, C_6D_6, 298 K): δ / ppm = 200.0 (s; *trans*-*C*O), 199.5 (dd, $^2J_{P,C}$ = 3.9 Hz, $^3J_{P,C}$ = 3.9 Hz; *cis*-*C*O), 148.2 (dd, $J_{P,C}$ = 7.9 Hz, $J_{P,C}$ = 5.1 Hz ; *ipso*-*C*), 130.8 (dd, $J_{P,C}$ = 14.3 Hz, $J_{P,C}$ = 10.8 Hz; Ph), 128.7 (s; Ph), 126.1 (s; Ph), 58.5 (dd, $^1J_{P,C}$ = 35.4 Hz, $^2J_{P,C}$ = 3.5 Hz; P-*C*Ph_3), 16.6 (dd, $^1J_{P,C}$ = 36.4 Hz, $^2J_{P,C}$ = 6.6 Hz; P(*C*$H_2CH_3)_3$), 7.6 (br s; P(CH_2*C*$H_3)_3$).

^{31}P{^{1}H} NMR (121.51 MHz, C_6D_6, 298 K): δ / ppm = 33.3 (d, $^1J_{P,P}$ = 476.9 Hz; *P*Et_3), −28.6 (d_{sat}, $^1J_{P,P}$ = 476.9 Hz, $^1J_{W,P}$ = 123.9 Hz; W-*P*CPh_3).

^{31}P NMR (121.51 MHz, C_6D_6, 298 K): δ / ppm = 33.3 (dm, $^1J_{P,P}$ = 476.9 Hz; *P*Et_3), −28.6 (d_{sat}, $^1J_{P,P}$ = 476.9 Hz, $^1J_{W,P}$ = 123.9 Hz; W-*P*CPh_3).

5.5.17 Synthesis of [pentacarbonyl{tri-*n*-butylphosphoniumyl(triphenylmethyl)phosphanido-κ*P*}tungsten(0)] (21b)

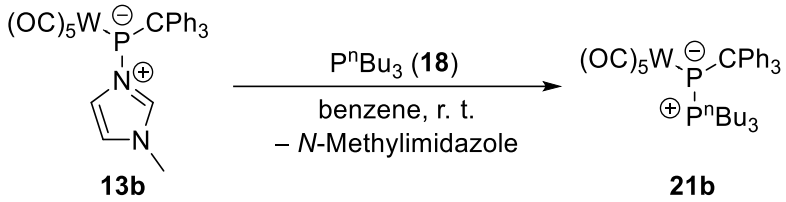

Synthesis

0.20 mL (0.81 mmol, 5.0 eq.) of tri-*n*-butylphosphane (**18**) was added to a solution of 0.109 g (0.16 mmol, 1.0 eq.) of [W(CO)$_5${P(CPh$_3$)(*N*-methylimidazole)}] (**13b**) in 5.0 mL of benzene at ambient temperature. The solution was stirred for 20 h at ambient temperature. All volatiles were removed *in vacuo* (<0.02 mbar) at ambient temperature and the obtained yellow solid was dried under the same conditions for 2 h. The product was recrystallized in 10 mL of a 7:1 *n*-pentane/diethyl ether mixture at −40 °C. The supernatant was filtered off using a filter cannula (Ø = 1 mm) with a Whatman® 595 filter paper at −40 °C and the yellow needle-shaped crystals were washed three times with 1 mL of *n*-pentane at −40 °C. The product was obtained as yellow solid after drying for 1.5 h *in vacuo* (<0.02 mbar) at ambient temperature.

Reaction code: DB-496 (14p5a010.22)

Molecular formula: $C_{36}H_{42}O_5P_2W$

Molecular weight: 800.515 g/mol

Yield: 0.076 g (0.09 mmol, 58.8 %)

Melting point: 120 °C (dec.)

Elemental analysis: calculated (%) C 54.01 H 5.29

found (%) C 53.97 H 5.47

MS (LIFDI, selected data): m/z (%) = 800 (18) $[M]^{\bullet+}$, 243 (100) $[CPh_3]^+$.

IR (ATR Diamond, selected data): $\tilde{\nu}$ / cm^{-1} = 1905 (s) (C≡O), 1968 (m) (C≡O), 2056 (m) (C≡O).

^{1}H NMR (500.04 MHz, THF-d_8, 298 K): δ / ppm = 7.75–7.73 (m, 6H; CPh$_3$), 7.24–7.20 (m, 6H; CPh$_3$), 7.13–7.10 (m, 3H; CPh$_3$), 1.62–1.56 (m, 6H; PC*H*$_2$), 1.48–1.41 (m, 6H; PCH$_2$C*H*$_2$), 1.29–1.22 (m, 6H; C*H*$_2$CH$_3$), 0.86 (t, $^3J_{H,H}$ = 7.36 Hz, 9H; C*H*$_3$).

$^{13}C\{^1H\}$ NMR (125.75 MHz, THF-d_8, 298 K): δ / ppm = 200.7 (d, $^1J_{P,C}$ = 15.4 Hz; *trans*-*C*O), 200.2 (dd_{sat}, $^2J_{P,C}$ = 3.9 Hz, $^3J_{P,C}$ = 3.9 Hz, $^1J_{W,C}$ = 125.6 Hz; *cis*-*C*O), 148.9 (dd, $J_{P,C}$ = 7.9 Hz, $J_{P,C}$ = 5.1 Hz; *ipso*-*C*), 131.5 (d, $J_{P,C}$ = 10.6 Hz; Ph), 128.8 (s; Ph), 126.7 (s; Ph), 59.4 (dd, $^1J_{P,C}$ = 36.1 Hz, $^2J_{P,C}$ = 3.7 Hz; P-*C*Ph_3), 26.5 (dd, $J_{P,C}$ = 6.5 Hz, $J_{P,C}$ = 3.5 Hz; PCH_2CH_2), 25.0 (d, $J_{P,C}$ = 13.7 Hz; CH_2CH_3), 24.7 (dd, $^1J_{P,C}$ = 35.2, $^2J_{P,C}$ = 5.8 Hz; PCH_2CH_2), 13.8 (s; CH_3).

$^{31}P\{^1H\}$ NMR (202.44 MHz, THF-d_8, 298 K): δ / ppm = 28.8 (d_{sat}, $^1J_{P,P}$ = 471.6 Hz, $^1J_{P,C}$ = 35.3 Hz; P^nBu_3), −25.0 (d_{sat}, $^1J_{P,P}$ = 471.6 Hz, $^1J_{W,P}$ = 122.1 Hz; W-*P*CPh_3).

^{31}P NMR (202.44 MHz, THF-d_8, 298 K): δ / ppm = 28.8 (dm, $^1J_{P,P}$ = 471.6 Hz; P^nBu_3), −25.0 (d_{sat}, $^1J_{P,P}$ = 471.6 Hz, $^1J_{W,P}$ = 122.1 Hz; W-*P*CPh_3).

5.5.18 Synthesis of [pentacarbonyl{(cyano(triphenylmethyl)phosphane-κ*P*}chromium(0)] (23a)

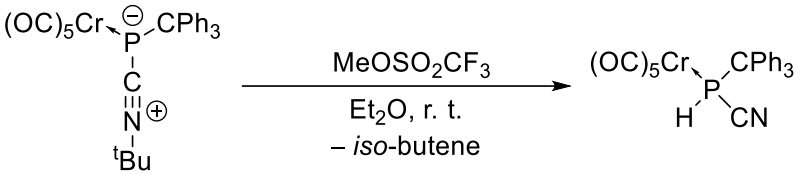

6a **23a**

Synthesis

0.05 mL (0.46 mmol, 1.2 eq.) of methyl trifluoromethanesulfonate was added to a solution of 0.209 g (0.38 mmol, 1.0 eq.) of $[Cr(CO)_5\{P(CPh_3)CN^tBu\}]$ (**6a**) in 30 mL of diethyl ether at ambient temperature. The solution was stirred for 24 h at ambient temperature. Afterwards, all volatiles were removed *in vacuo* (<0.02 mbar) at ambient temperature within 4 minutes and the obtained yellow-orange solid was further dried for 24 h. The product was washed twice with 2.0 mL and once with 1.0 mL of *n*-pentane at −70 °C. The yellow solid was dried for 100 minutes *in vacuo* (<0.02 mbar) at ambient temperature.

Reaction code: DB-292 (04m3a052.21)

Molecular formula: $C_{25}H_{16}NO_5PCr$

Molecular weight: 493.375 g/mol

Yield: 0.175 g (0.35 mmol, 93.2 %)

Melting point: 107 °C (dec.)

Elemental analysis: calculated (%) C 60.86 H 3.27 N 2.84

found (%) C 59.31 H 3.64 N 2.69

X-ray diffraction analysis: excellent structure (AA1, GSTR713, GXray6520)

MS (LIFDI, selected data): m/z (%) = 493.0 (100) $[M]^{\bullet+}$, 243.1 (50) $[CPh_3]^+$.

MS (EI, 70 eV, selected data): m/z (%) = 492.9 (<0.1) $[M]^{\bullet+}$, 352.9 (1) $[M-5CO]^+$, 244.0 (100) $[CPh_3+H]^+$.

IR (ATR Diamond, selected data): $\tilde{\nu}$ / cm^{-1} = 1934 (s) (C≡O), 1955 (s) (C≡O), 2002 (w) (C≡O), 2073 (m) (C≡O), 2178 (w) (C≡N).

^{1}H NMR (300.13 MHz, C_6D_6, 298 K): δ / ppm = 7.13–6.99 (m, 15H; CPh_3), 5.69 (d, $^1J_{P,H}$ = 354.62 Hz, 1H; P*H*).

^{13}C{^{1}H} NMR (75.48 MHz, C_6D_6, 298 K): δ / ppm = 219.5 (d, $^2J_{P,C}$ = 2.9 Hz; *trans*-*C*O), 214.4 (d, $^2J_{P,C}$ = 10.8 Hz; *cis*-*C*O), 141.8 (br s; *ipso*-*C*), 130.0 (d, $J_{P,C}$ = 7.0 Hz; Ph); 129.1 (s; Ph), 128.5 (s; Ph), 116.7 (d, $^1J_{P,C}$ = 7.4 Hz; *C*N), 61.6 (d, $^1J_{P,C}$ = 15.7 Hz; P-*C*Ph_3).

^{31}P{^{1}H} NMR (121.51 MHz, C_6D_6, 298 K): δ / ppm = 27.0 (s).

^{31}P NMR (121.51 MHz, C_6D_6, 298 K): δ / ppm = 27.0 (d, $^1J_{P,H}$ = 354.4 Hz).

5.5.19 Synthesis of [pentacarbonyl{(cyano(triphenylmethyl)phosphane-κ*P*}tungsten(0)] (23b)

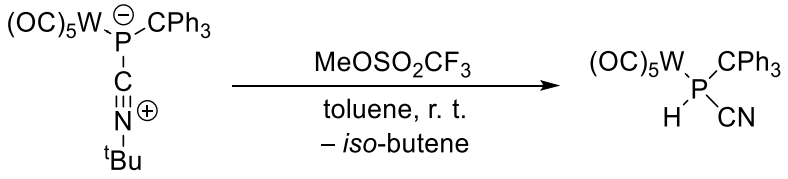

6c **23b**

Synthesis

0.05 mL (0.46 mmol, 1.5 eq.) of methyl trifluoromethanesulfonate was added to a solution of 0.153 g (0.23 mmol, 1.0 eq.) of $[W(CO)_5\{P(CPh_3)CN^tBu\}]$ (**6c**) in 13.5 mL of toluene at ambient temperature. The solution was stirred for 3 h at ambient temperature. Afterwards, all volatiles were removed *in vacuo* (<0.02 mbar) at ambient temperature within 15 minutes and the obtained orange oil was further dried for 8 minutes. The product was washed twice with 2.0 mL and once with 1.0 mL of *n*-pentane at −70 °C. After addition of 20 mL of *n*-pentane and

scratching at ambient temperature followed by removal of solvents *in vacuo* (<0.02 mbar) at ambient temperature a yellow solid was obtained.

Reaction codes: DB-231, 615 (29m3b027.20, 38p5a030.22)

Molecular formula: $C_{25}H_{16}NO_5PW$

Molecular weight: 625.219 g/mol

Yield: 0.116 g (0.19 mmol, 82.5 %)

Melting point: 119–120 °C (dec.)

Elemental analysis: calculated (%) C 50.58 H 4.10 N 3.93

found (%) C 52.26 H 4.60 N 3.60

MS (ESI neg., selected data): m/z (%) = 640.016 (33) $[M+O-H]^-$, 624.020 (10) $[M]^{\bullet-}$, 612.021 (21) $[M+O-H-CO]^-$, 584.026 (18) $[M+O-H-2CO]^-$.

MS (ESI pos., selected data): m/z (%) = 243.117 (54) $[CPh_3]^+$.

HRMS (ESI neg.): *m/z* calcd for $[C_{25}H_{15}NO_5PW]^-$: 624.0203 $[W(CO)_5\{P(CPh_3)CN\}]^-$; found: 624.0203.

IR (ATR Diamond, selected data): $\tilde{\nu}$ / cm^{-1} = 1935 (vs) (C≡O), 1955 (s) (C≡O), 1999 (m) (C≡O), 2081 (m) (C≡N), 2921 (w) (C-H), 2949 (w) (C-H).

^{1}H NMR (300.13 MHz, C_6D_6, 299 K): δ / ppm = 7.14–6.99 (m, 15H; CPh_3), 5.90 (d, $^1J_{P,H}$ = 366.97 Hz, 1H; P*H*).

^{13}C{^{1}H} NMR (75.48 MHz, C_6D_6, 299 K): δ / ppm = 197.2 (s; *trans*-*C*O), 195.0 (d, $^2J_{P,C}$ = 6.0 Hz; *cis*-*C*O), 141.9 (br s; *ipso*-*C*), 130.1 (d, $J_{P,C}$ = 7.5 Hz; Ph); 129.1 (d, $J_{P,C}$ = 1.3 Hz; Ph), 128.5 (s; Ph), 116.6 (s; *C*N), 60.4 (d, $^1J_{P,C}$ = 20.1 Hz; P-*C*Ph_3).

^{15}N{^{1}H} NMR (50.68 MHz, C_6D_6, 298 K): δ / ppm = −74.8 (s).

^{31}P{^{1}H} NMR (121.51 MHz, C_6D_6, 299 K): δ / ppm = −22.4 (s_{sat}, $^1J_{W,P}$ = 244.6 Hz).

^{31}P NMR (121.51 MHz, C_6D_6, 299 K): δ / ppm = −22.4 (d_{sat}, $^1J_{P,H}$ = 367.3 Hz, $^1J_{W,P}$ = 244.6 Hz).

5.5.20 Generation of [pentacarbonyl{1-triphenylmethylphosphirane-κ*P*}tungsten(0)] (36)

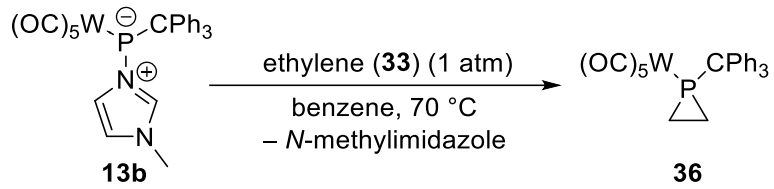

Synthesis

A solution of 0.021 g (0.03 mmol, 1.0 eq.) of [W(CO)$_5${P(CPh$_3$)(*N*-methylimidazole)}] (**13b**) in 0.7 mL of benzene was prepared in a PTFE valved NMR tube at ambient temperature. Afterwards all gases were removed *in vacuo* (<0.02 mbar) at −196 °C and 1 atm of ethylene (**33**) was applied to the tube. The reaction mixture was heated at 70 °C for 34.5 h.

Reaction code: DB-478 (11p5a012.22)

Molecular formula: $C_{26}H_{19}O_5PW$

Molecular weight: 626.247 g/mol

Content in solution: 0.017 g (0.03 mmol, 85 %) (^{31}P NMR integration of reaction mixture)

^{1}H NMR (500.04 MHz, C_6D_6, 298 K): δ / ppm = 7.33–7.31 (m, 6H; CPh$_3$), 7.10–6.98 (m, 9H; CPh$_3$), 0.93–0.90 (m, 4H; ring-C*H*$_2$).

^{13}C{^{1}H} NMR (125.75 MHz, C_6D_6, 298 K): δ / ppm = 199.2 (s$_{sat}$, $^1J_{W,C}$ = 130.0 Hz; *trans*-*C*O), 196.7 (d$_{sat}$, $^2J_{P,C}$ = 7.1 Hz, $^1J_{W,C}$ = 126.9 Hz; *cis*-*C*O), 141.8 (s; *ipso*-*C*), 131.2 (d, $J_{P,C}$ = 8.0 Hz; Ph), 128.4–127.8 (m; Ph), 60.6 (d, $^1J_{P,C}$ = 2.0 Hz; P-*C*Ph$_3$), 10.9 (d, $^1J_{P,C}$ = 17.0 Hz; ring-*C*H$_2$).

^{31}P{^{1}H} NMR (202.44 MHz, C_6D_6, 298 K): δ / ppm = −167.4 (s$_{sat}$, $^1J_{W,P}$ = 257.2 Hz).

^{31}P NMR (202.44 MHz, C_6D_6, 298 K): δ / ppm = −167.4 (s$_{sat}$, $^1J_{W,P}$ = 257.2 Hz).

5.5.21 Synthesis of [pentacarbonyl{2-*n*-propyl-1-triphenylmethylphosphirane-κ*P*}tungsten(0)] (37)

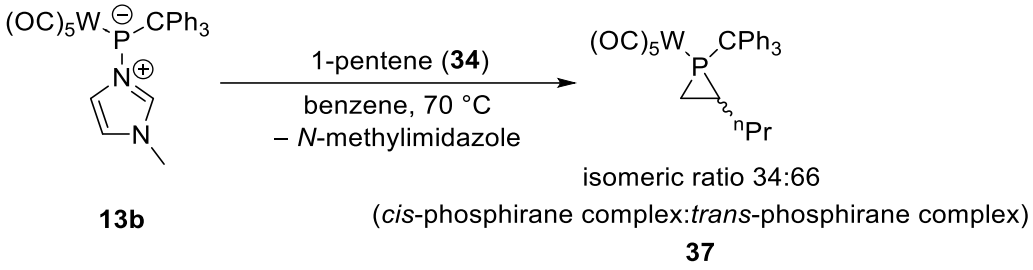

13b

isomeric ratio 34:66
(*cis*-phosphirane complex:*trans*-phosphirane complex)

37

Synthesis

A solution of 0.233 g (0.34 mmol, 1.0 eq.) of [W(CO)$_5${P(CPh$_3$)(*N*-methylimidazole)}] (**13b**) and 0.38 mL (3.47 mmol, 10.1 eq.) of 1-pentene (**34**) in 10 mL of benzene was stirred for 14 h at 70 °C. Afterwards, all volatiles were removed *in vacuo* (<0.02 mbar) at 70 °C. The obtained brown oil was further dried for 3 h at ambient temperature. The crude product was purified via column chromatography (SiO_2, Ø = 1 cm, h = 7 cm) using 200 mL of *n*-pentane. All volatiles were removed *in vacuo* (<0.02 mbar) at ambient temperature and the yellow oil was further dried for 1.5 h.

Reaction code: DB-569 (24m3a015.22)

Molecular formula: $C_{29}H_{25}O_5PW$

Molecular weight: 668.328 g/mol

Yield: 0.115 g (0.17 mmol, 50.3 %)

MS (LIFDI, selected data): m/z (%) = 668.1 (100) $[M]^{\bullet+}$, 243.1 (10) $[CPh_3]^+$.

IR (ATR Diamond, selected data): $\tilde{\nu}$ / cm^{-1} = 1913 (vs) (C≡O), 1983 (w) (C≡O), 2071 (m) (C≡O), 2959 (w) (C-H).

Isomeric ratio: 34:66 (*cis*-phosphirane complex : *trans*-phosphirane complex)

Major isomer: *trans*-phosphirane complex:

^{1}H NMR (500.04 MHz, C_6D_6, 298 K): δ / ppm = 7.45–7.42 (m, 6H; CPh_3), 7.10–6.98 (m, 9H; CPh_3), 1.71–1.63 (m, 1H; C*H*$_2$-C_2H_5), 1.45–1.17 (m, 5H; C*H*$_2$-C_2H_5 & CH_2-C*H*$_2$-CH_3 & ring-C*H*^{n}Pr & ring-C*H*$_2$), 0.81 (t, $^3J_{H,H}$ = 7.14 Hz, 3H, C*H*$_3$), 0.78–0.75 (m, 1H; ring-C*H*$_2$).

$^{13}C\{^1H\}$ NMR (125.75 MHz, C_6D_6, 298 K): δ / ppm = 197.4 (d, $^2J_{P,C}$ = 33.4 Hz; *trans*-*C*O), 196.8 (d_{sat}, $^2J_{P,C}$ = 7.2 Hz, $^1J_{W,C}$ = 126.6 Hz; *cis*-*C*O), 142.1 (s; *ipso*-*C*), 131.5 (d, $J_{P,C}$ = 7.8 Hz; Ph), 128.3 (s; Ph), 127.7 (s; Ph), 62.1 (d, $^1J_{P,C}$ = 1.6 Hz; *C*Ph_3), 34.1 (d, $^2J_{P,C}$ = 1.9 Hz; *C*H_2-C_2H_5), 23.0 (d, $^3J_{P,C}$ = 6.6 Hz; CH_2-*C*H_2-CH_3), 22.9 (d, $^1J_{P,C}$ = 18.8 Hz; ring-*C*H^{n}Pr), 17.3 (d, $^1J_{P,C}$ = 18.3 Hz; ring-*C*H_2), 13.8 (s; *C*H_3).

$^{31}P\{^1H\}$ NMR (202.44 MHz, C_6D_6, 298 K): δ / ppm = −145.4 (s_{sat}, $^1J_{W,P}$ = 259.7 Hz).

^{31}P NMR (202.44 MHz, C_6D_6, 298 K): δ / ppm = −145.4 (d_{sat}, $^2J_{P,H}$ = 19.6 Hz, $^1J_{W,P}$ = 259.7 Hz).

Minor isomer: *cis*-phosphirane complex:

^1H NMR (500.04 MHz, C_6D_6, 298 K): δ / ppm = 7.45–7.42 (m, 6H; CPh_3), 7.10–6.98 (m, 9H; CPh_3), 1.71–1.63 (m, 1H; ring-C*H*$_2$), 1.60–1.54 (m, 2H; ring-C*H*$_2$ & ring-C*H*^{n}Pr), 1.06–0.88 (m, 3H; C*H*$_2$-C_2H_5 & CH_2-C*H*$_2$-CH_3), 0.58 (t, $^3J_{H,H}$ = 7.06 Hz, 3H; C*H*$_3$), −0.18–−0.25 (m, 1H; C*H*$_2$-C_2H_5).

$^{13}C\{^1H\}$ NMR (125.75 MHz, C_6D_6, 298 K): δ / ppm = 198.3 (d, $^2J_{P,C}$ = 32.9 Hz; *trans*-*C*O), 197.2 (d_{sat}, $^2J_{P,C}$ = 7.1 Hz, $^1J_{W,C}$ = 126.7 Hz; *cis*-*C*O), 142.6 (s; *ipso*-*C*), 131.7 (d, $J_{P,C}$ = 7.7 Hz; Ph), 128.5 (s; Ph), 127.7 (s; Ph), 61.7 (d, $^1J_{P,C}$ = 3.2 Hz; *C*Ph_3), 33.5 (d, $^1J_{P,C}$ = 18.8 Hz; ring-*C*H^{n}Pr), 29.8 (d, $^2J_{P,C}$ = 3.7 Hz; *C*H_2-C_2H_5), 24.1 (d, $^3J_{P,C}$ = 6.7 Hz; CH_2-*C*H_2-CH_3), 16.9 (d, $^1J_{P,C}$ = 18.3 Hz; ring-*C*H_2), 13.8 (s; *C*H_3).

$^{31}P\{^1H\}$ NMR (202.44 MHz, C_6D_6, 298 K): δ / ppm = −137.7 (s_{sat}, $^1J_{W,P}$ = 258.8 Hz).

^{31}P NMR (202.44 MHz, C_6D_6, 298 K): δ / ppm = −137.7 (s_{sat}, $^1J_{W,P}$ = 258.8 Hz).

5.5.22 Synthesis of [pentacarbonyl{2-*n*-butyl-1-triphenylmethylphosphirane-κ*P*}tungsten(0)] (38)

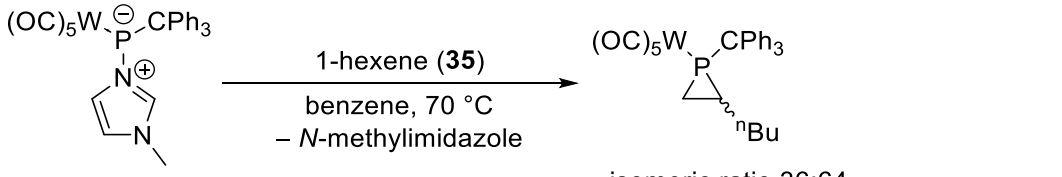

13b

isomeric ratio 36:64
(*cis*-phosphirane complex:*trans*-phosphirane complex)

38

Synthesis

A solution of 0.217 g (0.32 mmol, 1.0 eq.) of [W(CO)$_5${P(CPh_3)(*N*-methylimidazole)}] (**13b**) and 0.40 mL (3.20 mmol, 10.0 eq.) of 1-hexene (**35**) in 12 mL of benzene was stirred for 16.5 h at

70 °C. Afterwards, all volatiles were removed *in vacuo* (<0.02 mbar) at ambient temperature. The crude product was purified via column chromatography (SiO_2, Ø = 1 cm, h = 10 cm) at ambient temperature using *n*-pentane.

Reaction codes: DB-461, 475 (08p5a033.22, 08m3b006.22)

Molecular formula: $C_{30}H_{27}O_5PW$

Molecular weight: 682.355 g/mol

Yield: 0.120 g (0.18 mmol, 55.1 %)

MS (LIFDI, selected data): m/z (%) = 682.3 (100) $[M]^{\bullet+}$, 243.2 (5) $[CPh_3]^+$.

IR (ATR Diamond, selected data): $\tilde{\nu}$ / cm^{-1} = 1904 (vs) (C≡O), 1982 (w) (C≡O), 2070 (m) (C≡O), 2957 (w) (C-H).

Isomeric ratio: 36:64 (*cis*-phosphirane complex : *trans*-phosphirane complex)

Major isomer: *trans*-phosphirane complex:

^{1}H NMR (500.04 MHz, C_6D_6, 298 K): δ / ppm = 7.45–7.43 (m, 6H; CPh_3), 7.10–7.05 (m, 6H; CPh_3), 7.03–6.97 (m, 3H; CPh_3), 1.74–1.65 (m, 1H; C*H*$_2$-C_3H_7), 1.44–1.32 (m, 2H; CH_2-C*H*$_2$-C_2H_5), 1.28–1.18 (m, 3H; C*H*$_2$-C_3H_7 & ring-C*H*^{n}Bu & ring-C*H*$_2$), 1.03–0.92 (m, 2H; C_2H_4-C*H*$_2$-CH_3), 0.85–0.83 (m, 3H; C*H*$_3$), 0.80–0.76 (m, 1H; ring-C*H*$_2$).

^{13}C{^{1}H} NMR (125.75 MHz, C_6D_6, 298 K): δ / ppm = 197.4 (d, $^2J_{P,C}$ = 33.3 Hz; *trans*-*C*O), 196.8 (d_{sat}, $^2J_{P,C}$ = 7.1 Hz, $^1J_{W,C}$ = 118.9 Hz; *cis*-*C*O), 142.2 (s; *ipso*-*C*), 131.5 (d, $J_{P,C}$ = 7.9 Hz; Ph), 128.3 (s; Ph), 127.7 (s; Ph), 62.1 (d, $^1J_{P,C}$ = 1.5 Hz; P-*C*Ph_3), 32.0 (d, $^3J_{P,C}$ = 6.5 Hz, CH_2-*C*H_2-C_2H_5), 31.8 (d, $^2J_{P,C}$ = 1.9 Hz; *C*H_2-C_3H_7), 23.1 (d, $^1J_{P,C}$ = 18.8 Hz; ring-*C*H-^{n}Bu), 22.8 (s; C_2H_4-*C*H_2-CH_3), 17.4 (d, $^1J_{P,C}$ = 18.3 Hz; ring-*C*H_2), 14.1 (s; *C*H_3).

^{31}P{^{1}H} NMR (202.40 MHz, C_6D_6, 298 K): δ / ppm = −145.5 (s_{sat}, $^1J_{W,P}$ = 260.2 Hz).

^{31}P NMR (121.51 MHz, C_6D_6, 298 K): δ / ppm = −145.5 (br d_{sat}, $^2J_{P,H}$ = 15.2 Hz, $^1J_{W,P}$ = 260.2 Hz).

Minor isomer: *cis*-phosphirane complex:

^{1}H NMR (500.04 MHz, C_6D_6, 298 K): δ / ppm = 7.45–7.43 (m, 6H; CPh_3), 7.10–7.05 (m, 6H; CPh_3), 7.03–6.97 (m, 3H; CPh_3), 1.74–1.65 (m, 1H; ring-C*H*$_2$), 1.62–1.53 (m, 2H; ring-C*H*$_2$ & ring-

C*H*-^{n}Bu), 1.28–1.18 (m, 2H; C_2H_4-C*H*$_2$-CH_3), 1.16–1.09 (m, 1H; C*H*$_2$-C_3H_7), 1.03–0.92 (m, 2H; CH_2-C*H*$_2$-C_2H_5), 0.70–0.67 (m, 3H; C*H*$_3$), −0.09–−0.18 (m, 1H; C*H*$_2$-C_3H_7).

^{13}C{^{1}H} NMR (125.75 MHz, C_6D_6, 298 K): δ / ppm = 198.3 (d, $^{2}J_{P,C}$ = 32.9 Hz; *trans*-*C*O), 197.2 (d$_{sat}$, $^{2}J_{P,C}$ = 7.1 Hz, $^{1}J_{W,C}$ = 127.0 Hz; *cis*-*C*O), 142.6 (s; *ipso*-*C*), 131.7 (d, $J_{P,C}$ = 7.7 Hz; Ph), 128.5 (s; Ph), 127.7 (s; Ph), 61.7 (d, $^{1}J_{P,C}$ = 3.2 Hz; P-*C*Ph$_3$), 33.5 (d, $^{1}J_{P,C}$ = 18.8 Hz; ring-*C*H-^{n}Bu), 33.1 (d, $^{3}J_{P,C}$ = 6.6 Hz; CH_2-*C*H_2-C_2H_5), 27.7 (d, $^{2}J_{P,C}$ = 3.8 Hz; *C*H_2-C_3H_7), 22.7 (s; C_2H_4-*C*H_2-CH_3), 17.1 (d, $^{1}J_{P,C}$ = 18.5 Hz; ring-*C*H_2), 14.0 (s; *C*H_3).

^{31}P{^{1}H} NMR (202.40 MHz, C_6D_6, 298 K): δ / ppm = −137.4 (s$_{sat}$, $^{1}J_{W,P}$ = 258.9 Hz).

^{31}P NMR (121.51 MHz, C_6D_6, 298 K): δ / ppm = −137.4 (br s$_{sat}$, $^{1}J_{W,P}$ = 258.9 Hz).

5.5.23 Generation of [pentacarbonyl(3,4-dimethyl-1-triphenylmethyl-2,5-dihydro-1*H*-phosphole-κ*P*)tungsten(0) (39)

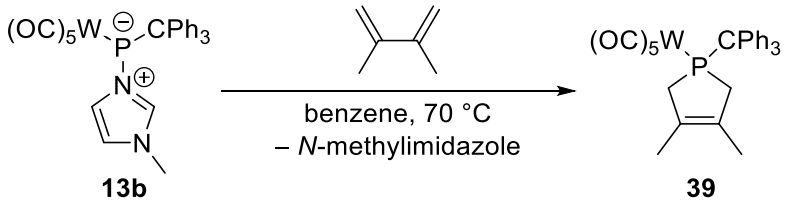

13b **39**

Synthesis

A solution of 0.207 g (0.30 mmol, 1.0 eq.) of [W(CO)$_5${P(CPh$_3$)(*N*-methylimidazole)}] (**13b**) and 0.68 mL (6.04 mmol, 20 eq.) of 2,3-dimethyl-1,3-butadiene in 20 mL of benzene was stirred for 23 h at 70 °C.

Reaction codes: DB-476, 574 (25m3a005.22)

Molecular formula: $C_{30}H_{25}O_5PW$

Molecular weight: 680.339 g/mol

Yield: 91 % (content in the reaction solution via ^{31}P{^{1}H} NMR integration)

X-ray diffraction analysis: very good structure, (A1, GSTR753, GXray6848)

^{31}P{^{1}H} NMR (121.51 MHz, C_6H_6, 300 K): δ / ppm = 30.1 (s$_{sat}$, $^{1}J_{W,P}$ = 241.8 Hz).

^{31}P NMR (121.51 MHz, C_6H_6, 300 K): δ / ppm = 30.1 (m$_{sat}$, $^{1}J_{W,P}$ = 241.8 Hz).

5.5.24 Synthesis of [pentacarbonyl-2κ*C*-μ{(1-methylimidazol-3-iumyl)triphenylmethyl-phosphanido-1κ*P*:2κ*P*}boranetungsten(0)] (54)

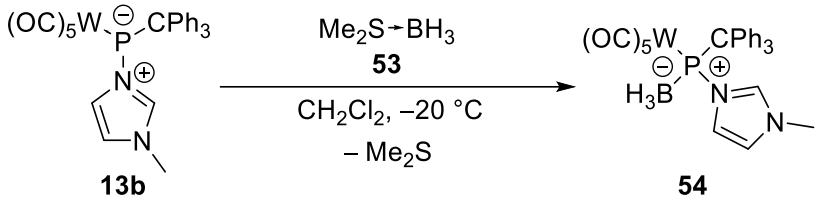

Synthesis

0.03 mL (0.32 mmol, 1.3 eq.) of borane dimethylsulfide was added dropwise to a solution of 0.165 g (0.24 mmol, 1.0 eq.) of [W(CO)$_5${P(CPh$_3$)(*N*-methylimidazole)}] (**13b**) in 3.0 mL of dichloromethane at −20 °C. The solution was stirred for 70 minutes at −20 °C and then warmed up to ambient temperature within 3 minutes. Afterwards, 8.0 mL of *n*-pentane were added to the formed colorless turbid solution under formation of colorless precipitate. The colorless solution was filtered off using a filter cannula (Ø = 1 mm) with a Whatman® 595 filter paper. The colorless solid residue was washed two times with 4 mL of *n*-pentane at ambient temperature and then dried *in vacuo* (<0.02 mbar) for 45 minutes.

Reaction codes: DB-630, 634 (48t4a025.22)

Molecular formula: $C_{28}H_{24}BN_2O_5PW$

Molecular weight: 694.133 g/mol

Yield: 0.149 g (0.21 mmol, 88.8 %)

Melting point: 173 °C (dec.)

X-ray diffraction analysis: excellent structure (AA1, GSTR793, GXraymo_7114_0m_4)

MS (pos. APCI, selected data): m/z (%) = 693.094 (100) $[M-H]^+$, 555.052 (48) [M−H−2CO−*N*-methylimidazole]$^+$, 371.184 (80) $[M-W(CO)_5+H]^+$, 243.117 (85) $[CPh_3]^+$.

MS (pos. ESI, selected data): m/z (%) = 691.076 (97) $[M-3H]^+$.

HRMS (pos. APCI): *m/z* calcd for $[C_{28}H_{23}BN_2O_5PW]^+$: 693.0950 $[M-H]^+$; found: 693.0944.

HRMS (pos. ESI): *m/z* calcd for $[C_{28}H_{21}BN_2O_5PW]^+$: 691.0795 $[M-3H]^+$; found: 691.0767.

IR (ATR Diamond, selected data): $\tilde{\nu}$ / cm^{-1} = 1910 (vs) (C≡O), 1974 (w) (C≡O), 2064 (m) (C≡O), 2402 (w) (B-H), 3155 (w) (C-H).

^{1}H NMR (400.13 MHz, CD_2Cl_2, 298 K): δ / ppm = 8.13 (s, 1H; Im), 7.81 (br s, 2H; *ortho*-C*H*), 7.62 (br s, 2H; *ortho*-C*H*), 7.44–7.12 (m, 9H; CPh_3), 6.93–6.92 (m, 1H; Im), 6.85 (s, 1H; Im), 6.45 (br s, 2H; *ortho*-C*H*), 3.73 (s, 3H; NCH_3), 1.78–1.00 (br m, 3H; BH_3).

^{11}B{^{1}H} NMR (128.38 MHz, CD_2Cl_2, 298 K): δ / ppm = −24.9 (s).

^{11}B NMR (128.38 MHz, CD_2Cl_2, 298 K): δ / ppm = −24.9 (br s).

^{13}C{^{1}H} NMR (100.63 MHz, CD_2Cl_2, 298 K): δ / ppm = 201.4 (d, $^{2}J_{P,C}$ = 23.3 Hz; *trans*-*C*O), 198.7 (d, $^{2}J_{P,C}$ = 4.7 Hz; *cis*-*C*O), 146.8 (s; *ipso*-*C*), 140.5 (s; Im), 132.1 (br s; *ortho*-*C*H), 131.5 (d, $J_{P,C}$ = 4.9 Hz; Ph), 128.5 (br s; *ortho*-*C*H), 128.2 (s; Ph), 127.9 (d, $J_{P,C}$ = 1.2 Hz; Ph), 127.6 (br s; *ortho*-*C*H), 126.4 (d, $J_{P,C}$ = 1.6 Hz; Im), 122.4 (s; Ph), 121.4 (s; Im), 64.7 (d, $^{1}J_{P,C}$ = 12.0 Hz; *C*Ph_3), 36.6 (s; *C*H_3).

^{31}P{^{1}H} NMR (162.00 MHz, CD_2Cl_2, 298 K): δ / ppm = 163.5 (s).

^{31}P NMR (162.00 MHz, CD_2Cl_2, 298 K): δ / ppm = 163.5 (s).

5.5.25 Synthesis of [pentacarbonyl{({1-methylimidazol-3-iumyl}boratyl)(triphenylmethyl)-phosphane-κ*P*}tungsten(0)] (55)

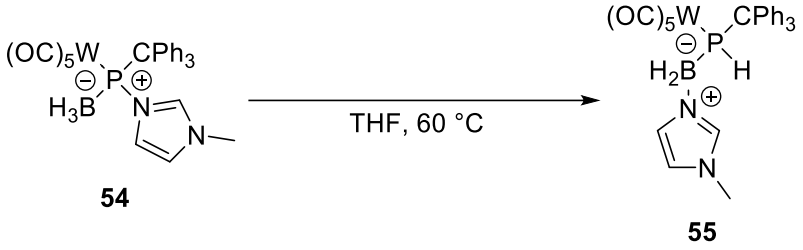

54 **55**

Synthesis

A solution of 0.121 g (0.17 mmol, 1.0 eq.) of the borane adduct **54** in tetrahydrofuran was stirred for 22 hours at 60 °C. All volatiles of the pale yellow solution were removed *in vacuo* (<0.02 mbar) at 60 °C and further dried under the same conditions for 45 minutes. The obtained pale yellow solid was redissolved in 15 mL of diethyl ether and 40 mL of *n*-pentane were added to the pale yellow solution at ambient temperature. The solution was stirred for 45 minutes at −80 °C to form a pale yellow fine suspension. The pale yellow solution was filtered off using a filter cannula (Ø = 1 mm) with a Whatman® 595 filter paper at −80 °C. The

pale yellow solid residue was washed two times with *n*-pentane at −80 °C and then dried *in vacuo* (<0.02 mbar) for 21.5 hours at ambient temperature.

Reaction codes: DB-632, 635, 636 (49p5a001.22, 47t4a038.22)

Molecular formula: $C_{28}H_{24}BN_2O_5PW$

Molecular weight: 694.133 g/mol

Yield: 0.090 g (0.13 mmol, 74.7 %)

Melting point: 166 °C

X-ray diffraction analysis: excellent structure (AA1, GSTR804, GXraymo_7283f)

MS (pos. APCI, selected data): m/z (%) = 693.095 (74) $[M-H]^+$, 555.052 (44) [M−H−2CO−*N*-methylimidazole], 371.184 (19) $[M-W(CO)_5+H]^+$, 243.117 (100) $[CPh_3]^+$.

MS (pos. ESI, selected data): m/z (%) = 371.182 (100) $[M-W(CO)_5+H]^+$, 243.116 (54) $[CPh_3]^+$.

HRMS (pos. APCI): *m/z* calcd for $[C_{28}H_{23}BN_2O_5PW]^+$: 693.0952 $[M-H]^+$; found: 693.0950.

IR (ATR Diamond, selected data): $\tilde{\nu}$ / cm^{-1} = 1895 (vs) (C≡O), 1979 (w) (C≡O), 1993 (w) (C≡O), 2062 (m) (C≡O), 2386 (w) (B-H), 3010 (w) (C-H), 3154 (w) (C-H).

^{1}H NMR (500.04 MHz, CD_3CN, 298 K): δ / ppm = 7.36–7.33 (m, 6H; CPh_3), 7.28–7.21 (m, 9H; CPh_3), 6.94–6.92 (m, 1H; Im), 6.65–6.63 (m, 1H; Im), 6.60 (s, 1H; Im), 5.38 (ddd, $^1J_{P,H}$ = 289.11, $^3J_{H,H}$ = 6.48 Hz, $^3J_{H,H}$ = 1.77 Hz, 1H; P*H*), 3.51 (s, 3H; NCH_3), 2.95 (br d, $^2J_{P,H}$ = 57.3 Hz, 2H; BH_2).

^{11}B{^{1}H} NMR (128.38 MHz, THF-d_8, 298 K): δ / ppm = −13.3 (s).

^{11}B NMR (128.38 MHz, THF-d_8, 298 K): δ / ppm = −13.4 (s).

^{13}C{^{1}H} NMR (125.75 MHz, CD_3CN, 298 K): δ / ppm = 201.7 (d, $^2J_{P,C}$ = 17.8 Hz; *trans-C*O), 199.1 (d_{sat}, $^1J_{W,C}$ = 125.9 Hz, $^2J_{P,C}$ = 5.5 Hz; *cis-C*O), 147.1 (s; *ipso-C*), 139.0 (s; Im), 131.6 (d, $J_{P,C}$ = 4.9 Hz; Ph), 128.6 (s; Ph), 127.5 (d, $J_{P,C}$ = 2.0 Hz; Ph), 127.1 (d, $J_{P,C}$ = 1.6 Hz; Im), 123.0 (s; Im), 57.9 (d, $^1J_{P,C}$ = 8.7 Hz; *C*Ph_3), 35.4 (s; *C*H_3).

^{15}N{^{1}H} NMR (50.68 MHz, CD_3CN, 298 K): δ / ppm = −182.8 (s; P-*N*), −212.5 (s; *N*-CH_3).

^{31}P{^{1}H} NMR (162.00 MHz, THF-d_8, 298 K): δ / ppm = −38.3 (br s).

^{31}P NMR (162.00 MHz, THF-d_8, 298 K): δ / ppm = −38.3 (br d, $^1J_{P,H}$ = 289.3 Hz).

5.5.26 Synthesis of [pentacarbonyl{hydroxy(triphenylmethyl)phosphane-κ*P*}tungsten(0)] (47b)

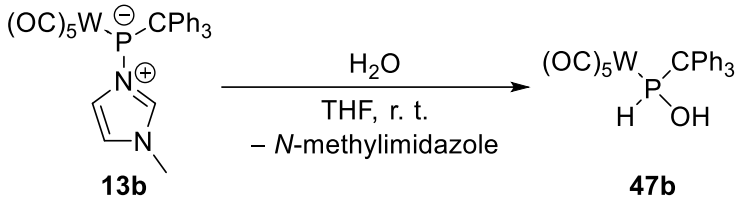

13b **47b**

Synthesis

0.07 mL (3.87 mmol, 20.8 eq.) of water was added to a solution of 0.127 g (0.19 mmol, 1.0 eq.) of [W(CO)$_5${P(CPh$_3$)(*N*-methylimidazole)}] (**13b**) in 2.0 mL of THF at ambient temperature. The solution was stirred for 3 h at ambient temperature. Afterwards, all volatiles were removed *in vacuo* (<0.02 mbar) at ambient temperature within 5 minutes and the obtained yellow sticky solid was further dried for 30 minutes. The crude product was purified via column chromatography (SiO_2, Ø = 1 cm, h = 10 cm) using a 1:9 *n*-pentane/diethyl ether mixture at ambient temperature.

Reaction codes: DB-403, 501 (21p5a015.22)

Molecular formula: $C_{24}H_{17}O_6PW$

Molecular weight: 616.208 g/mol

Yield: 0.095 g (0.15 mmol, 82.8 %)

Melting point: 181 °C (dec.)

Elemental analysis: calculated (%) C 46.78 H 2.78

found (%) C 47.30 H 3.05

X-ray diffraction analysis: good structure, + 0.5 THF (B1, GSTR738, GXraymo_6721_0m_4)

MS (EI, 70 eV, selected data): m/z (%) = 616.0 (21) $[M]^{\bullet+}$, 476.0 (45) $[M-5CO]^+$, 243.3 (100) $[CPh_3]^+$.

MS (ESI neg., selected data): m/z (%) = 615.021 (100) $[M-H]^-$, 1231.051 (42) $[2M-H]^-$.

MS (ESI pos., selected data): m/z (%) = 243.117 (100) $[CPh_3]^+$.

HRMS (ESI neg.): *m/z* calcd for $[C_{24}H_{16}O_6PW]^-$: 615.0202 $[M-H]^-$; found: 615.0209.

IR (ATR Diamond, selected data): $\tilde{\nu}$ / cm^{-1} = 1924 (s) (C≡O), 1944 (m) (C≡O), 1993 (m) (C≡O), 2076 (m) (C≡O).

^{1}H NMR (500.04 MHz, CD_2Cl_2, 298 K): δ / ppm = 7.93 (d_{sat}, $^{1}J_{P,H}$ = 340.31 Hz, $^{2}J_{W,H}$ = 6.83 Hz, 1H; P*H*), 7.43–7.38 (m, 9H; CPh_3), 7.29–7.27 (m, 6H; CPh_3), 3.79 (d, $^{2}J_{P,H}$ = 5.06 Hz, 1H; PO*H*).

^{13}C{^{1}H} NMR (125.75 MHz, CD_2Cl_2, 298 K): δ / ppm = 199.3 (d_{sat}, $^{2}J_{P,C}$ = 30.5 Hz, $^{1}J_{W,C}$ = 142.8 Hz; *trans*-*C*O), 196.3 (d_{sat}, $^{2}J_{P,C}$ = 7.4 Hz, $^{1}J_{W,C}$ = 126.4 Hz; *cis*-*C*O), 141.7 (s; *ipso*-*C*), 130.4 (d, $J_{P,C}$ = 5.5 Hz; Ph), 129.4 (s; Ph), 128.3 (d, $J_{P,C}$ = 2.1 Hz; Ph).

^{31}P{^{1}H} NMR (202.44 MHz, CD_2Cl_2, 298 K): δ / ppm = 100.7 (s_{sat}, $^{1}J_{W,P}$ = 278.7 Hz).

^{31}P NMR (202.44 MHz, CD_2Cl_2, 298 K): δ / ppm = 100.7 (d_{sat}, $^{1}J_{P,H}$ = 340.5 Hz, $^{1}J_{W,P}$ = 278.7 Hz).

5.5.27 Generation of [pentacarbonyl{methoxy(triphenylmethyl)phosphane-κ*P*}tungsten(0)] (57)

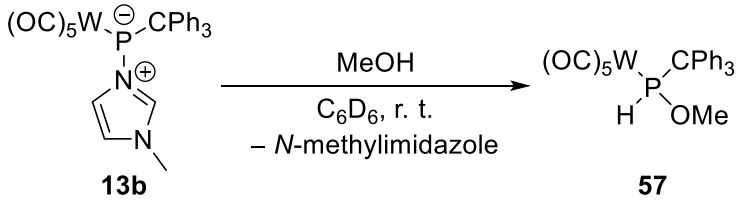

13b **57**

Synthesis

0.01 mL (0.25 mmol, 12.9 eq.) of methanol was added to a solution of 0.013 g (0.02 mmol, 1.0 eq.) of [$W(CO)_5${$P(CPh_3)$(*N*-methylimidazole)}] (**13b**) in 0.5 mL of benzene-d_6. The reaction mixture was shaken thoroughly for 30 seconds and then kept for 16 h at ambient temperature to obtain a yellow solution.

Reaction code: DB-599 (35m3c001.22)

Molecular formula: $C_{25}H_{19}O_6PW$

Molecular weight: 630.235 g/mol

Content in solution: 97 % (^{31}P NMR integration of reaction mixture)

^{1}H NMR (300.13 MHz, C_6D_6, 298 K): δ / ppm = 7.68 (d, $^{1}J_{P,H}$ = 342.79 Hz, 1H; P*H*), 7.28–7.24 (m, 6H; CPh_3), 7.12–7.04 (m, 9H; CPh_3), 2.75 (d, $^{3}J_{P,H}$ = 12.39 Hz, 3H; POCH_3).

^{31}P{^{1}H} NMR (121.51 MHz, C_6D_6, 298 K): δ / ppm = 127.2 (s_{sat}, $^{1}J_{W,P}$ = 274.1 Hz).

^{31}P NMR (121.51 MHz, C_6D_6, 298 K): δ / ppm = 127.2 (dq_{sat}, $^1J_{P,H}$ = 342.7 Hz, $^3J_{P,H}$ = 12.5 Hz, $^1J_{W,P}$ = 274.1 Hz).

Reference: Streubel, **2014**.[88]

5.5.28 Generation of [pentacarbonyl{*tert*-butoxy(triphenylmethyl)phosphane-κ*P*}tungsten(0)] (58)

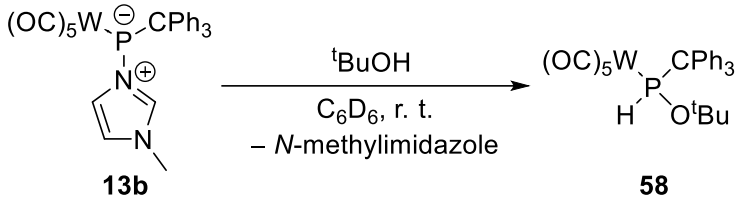

13b **58**

Synthesis

0.01 mL (0.11 mmol, 3.9 eq.) of *tert*-butanol was added to a solution of 0.0184 g (0.03 mmol, 1.0 eq.) of [$W(CO)_5${$P(CPh_3)$(*N*-methylimidazole)}] (**13b**) in 0.5 mL of benzene-d_6. The reaction mixture was shaken thoroughly for 30 seconds and then kept for 14 days at ambient temperature to obtain a yellow solution.

Reaction code: DB-600 (37t4b040.22)

Molecular formula: $C_{28}H_{25}O_6PW$

Molecular weight: 672.316 g/mol

Content in solution: 77 % (^{31}P NMR integration of reaction mixture)

^{1}H NMR (400.13 MHz, C_6D_6, 298 K): δ / ppm = 7.79 (d, $^1J_{P,H}$ = 322.30 Hz, 1H; P*H*), 7.39–7.36 (m, 6H; CPh_3), 7.12–6.94 (m, 9H; CPh_3), 0.83 (d, $^4J_{P,H}$ = 0.62 Hz, 9H; $POC(CH_3)_3$).

^{31}P{^{1}H} NMR (162.00 MHz, C_6D_6, 298 K): δ / ppm = 97.4 (s_{sat}, $^1J_{W,P}$ = 282.6 Hz).

^{31}P NMR (162.00 MHz, C_6D_6, 298 K): δ / ppm = 97.4 (d_{sat}, $^1J_{P,H}$ = 322.3 Hz, $^1J_{W,P}$ = 282.6 Hz).

5.5.29 Generation of [pentacarbonyl{methylamino(triphenylmethyl)phosphane-κ*P*}-tungsten(0)] (59)

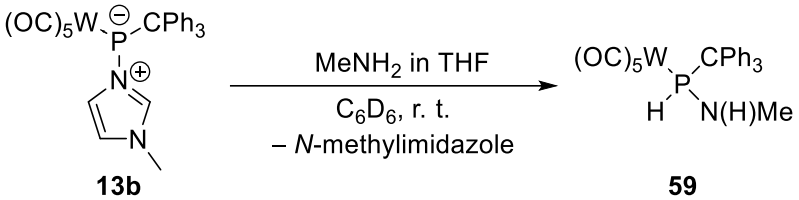

13b **59**

Synthesis

0.02 mL (c = 2 M in THF, 0.04 mmol, 1.3 eq.) of a methylamine solution was added to a solution of 0.0205 g (0.03 mmol, 1.0 eq.) of [W(CO)$_5${P(CPh$_3$)(*N*-methylimidazole)}] (**13b**) in 0.5 mL of benzene-d_6. The reaction mixture was kept for 63 h at ambient temperature.

Reaction code: DB-423 (48t4a012.21)

Molecular formula: $C_{25}H_{20}NO_5PW$

Molecular weight: 629.251 g/mol

Content in solution: 100 % (^{31}P NMR integration of reaction mixture)

^{1}H NMR (400.13 MHz, C_6D_6, 298 K): δ / ppm = 7.31–7.29 (m, 6H; CPh$_3$), 7.10–7.08 (m, 6H; CPh$_3$), 7.06 (dd, $^1J_{P,H}$ = 348.94 Hz, $^3J_{H,H}$ = 5.14 Hz, 1H; P*H*), 7.05–7.01 (m, 3H; CPh$_3$), 1.92–1.87 (m, 3H; NC*H*$_3$), 1.87–1.82 (m, 1H; N*H*).

^{31}P{^{1}H} NMR (162.00 MHz, C_6D_6, 298 K): δ / ppm = 55.3 (s$_{sat}$, $^1J_{W,P}$ = 257.8 Hz).

^{31}P NMR (162.00 MHz, C_6D_6, 298 K): δ / ppm = 55.3 (dm$_{sat}$, $^1J_{P,H}$ = 348.6 Hz, $^1J_{W,P}$ = 257.8 Hz).

Reference: Streubel, **2016**.[89]

5.5.30 Generation of [pentacarbonyl{isopropylamino(triphenylmethyl)phosphane-κ*P*}-tungsten(0)] (60)

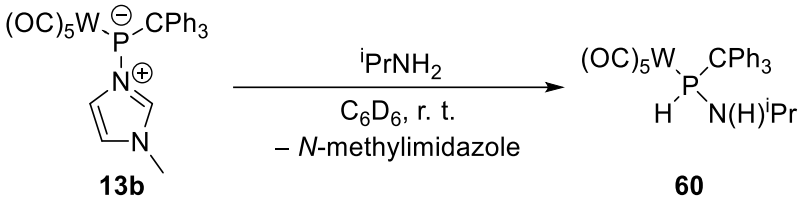

Synthesis

0.01 mL (0.12 mmol, 7.2 eq.) of isopropylamine was added to a solution of 0.011 g (0.02 mmol, 1.0 eq.) of [W(CO)$_5${P(CPh$_3$)(*N*-methylimidazole)}] (**60**) in 0.5 mL of benzene-d_6. The reaction mixture was shaken thoroughly for 30 seconds at ambient temperature to obtain a yellow solution.

Reaction code: DB-576 (25m3a038.22)

Molecular formula: $C_{27}H_{24}NO_5PW$

Molecular weight: 657.305 g/mol

Content in solution: 97 % (^{31}P NMR integration of reaction mixture)

^{31}P{^{1}H} NMR (121.51 MHz, C_6D_6, 301 K): δ / ppm = 49.2 (s_{sat}, $^1J_{W,P}$ = 260.5 Hz).

^{31}P NMR (121.51 MHz, C_6D_6, 301 K): δ / ppm = 49.2 (ddd_{sat}, $^1J_{P,H}$ = 336.5 Hz, $^2J_{P,H}$ = 7.8 Hz, $^3J_{P,H}$ = 7.8 Hz, $^1J_{W,P}$ = 260.5 Hz).

Reference: Streubel, **2016**.[89]

5.5.31 Generation of [pentacarbonyl{*tert*-butylamino(triphenylmethyl)phosphane-κ*P*}-tungsten(0)] (61)

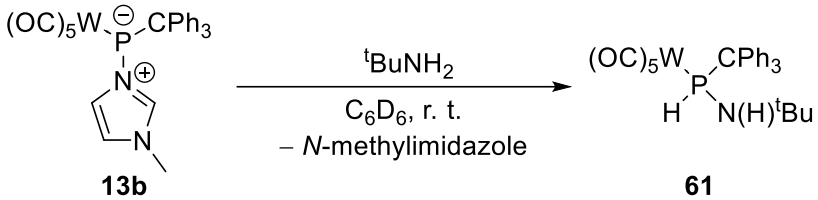

Synthesis

0.01 mL (0.10 mmol, 4.7 eq.) of *tert*-butylamine was added to a solution of 0.014 g (0.02 mmol, 1.0 eq.) of [W(CO)$_5${P(CPh$_3$)(*N*-methylimidazole)}] (**13b**) in 0.5 mL of benzene-d_6. The reaction mixture was shaken thoroughly for 30 seconds and then kept for 18 h at ambient temperature to obtain a yellow solution.

Reaction code: DB-577 (25m3a026.22)

Molecular formula: $C_{28}H_{26}NO_5PW$

Molecular weight: 671.332 g/mol

Content in solution: 99 % (^{31}P NMR integration of reaction mixture)

^{1}H NMR (300.13 MHz, C_6D_6, 301 K): δ / ppm = 7.48–7.44 (m, 6H; CPh_3), 7.44 (dd, $^1J_{H,H}$ = 342.60 Hz, $^3J_{H,H}$ = 10.04 Hz, 1H; P*H*), 7.13–7.07 (m, 6H; CPh_3), 7.04–6.98 (m, 3H; CPh_3), 1.14 (dd, $^3J_{H,H}$ = 10.04 Hz, $^4J_{H,H}$ = 5.01 Hz, 1H; N*H*), 0.99 (d, $^4J_{H,H}$ = 5.01 Hz, 9H; C(C*H*$_3$)$_3$).

^{31}P{^{1}H} NMR (121.51 MHz, C_6D_6, 301 K): δ / ppm = 36.8 (s_{sat}, $^1J_{W,P}$ = 263.8 Hz).

^{31}P NMR (121.51 MHz, C_6D_6, 301 K): δ / ppm = 36.8 (dd_{sat}, $^1J_{P,H}$ = 342.8 Hz, $^2J_{P,H}$ = 15.4 Hz, $^1J_{W,P}$ = 263.8 Hz).

Reference: Streubel, **2016**.[89]

5.5.32 Synthesis of [pentacarbonyl{trifluoroacetyl(triphenylmethyl)phosphane-κ*P*}-chromium(0)] (62a)

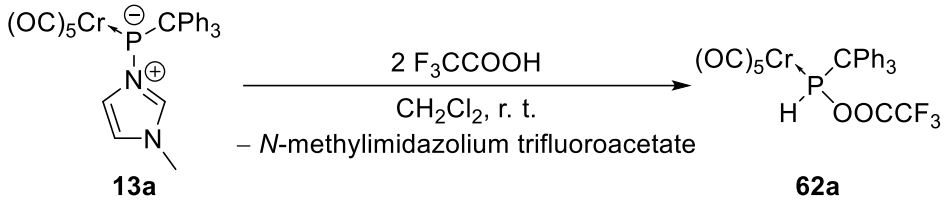

13a **62a**

Synthesis

0.11 mL (1.43 mmol, 5.9 eq.) of trifluoroacetic acid was added dropwise to a solution of 0.133 g (0.24 mmol, 1.0 eq.) of [$Cr(CO)_5${$P(CPh_3)$(*N*-methylimidazole)}] (**13a**) in 10 mL of dichloromethane at ambient temperature. The solution was stirred for 3.5 h at ambient temperature. Afterwards, all volatiles were removed *in vacuo* (<0.02 mbar) at ambient temperature within 7 minutes and the obtained pale yellow solid was further dried for 50 minutes. The product was extracted using six times 3 mL of *n*-pentane at ambient temperature via a filter cannula (Ø = 1 mm) with a glass microfiber filter paper (Whatman® GF/B). All volatiles were removed from the extract *in vacuo* (<0.02 mbar) at ambient temperature. The obtained colorless solid was further dried for 1 h at ambient temperature.

Reaction codes: DB-557 (22t4a032.22, 27p5a022.22)

Molecular formula: $C_{26}H_{16}O_7F_3PCr$

Molecular weight: 580.372 g/mol

Yield: 0.136 g (0.23 mmol, 96.2 %)

Melting point: 160 °C (dec.)

Elemental analysis: calculated (%) C 53.81 H 2.78

found (%) C 54.26 H 2.95

X-ray diffraction analysis: very good structure (A1, GSTR770, GXray6913)

MS (LIFDI, selected data): m/z (%) = 580.1 (100) $[M]^{\bullet+}$, 243.2 (5) $[CPh_3]^+$.

MS (ESI neg., selected data): m/z (%) = 578.993 (21) $[M-H]^-$.

HRMS (ESI neg.): *m/z* calcd for $[C_{26}H_{15}O_7F_3PCr]^-$: 578.9921 $[M-H]^-$; found: 578.9930.

IR (ATR Diamond, selected data): $\tilde{\nu}$ / cm^{-1} = 1944 (s) (C≡O), 1956 (s) (C≡O), 2003 (w) (C≡O), 2075 (m) (C≡O).

^{1}H NMR (400.13 MHz, C_6D_6, 298 K): δ / ppm = 8.19 (d, $^{1}J_{P,H}$ = 349.99 Hz, 1H; P*H*), 7.20–7.11 (m, 6H; CPh_3), 7.06–6.97 (m, 9H; CPh_3).

^{13}C{^{1}H} NMR (100.63 MHz, C_6D_6, 298 K): δ / ppm = 219.1 (d, $^{2}J_{P,C}$ = 1.9 Hz; *trans*-*C*O), 214.3 (d, $^{2}J_{P,C}$ = 12.6 Hz; *cis*-*C*O), 153.7 (qd, $^{2}J_{F,C}$ = 44.9 Hz, $^{2}J_{P,C}$ = 12.6 Hz; OO*C*CF_3), 140.3 (br s; *ipso*-*C*), 130.3 (br s; Ph), 129.1 (s; Ph), 128.5 (s; Ph), 114.6 (q, $^{1}J_{F,C}$ = 287.1 Hz; OOC*C*F_3), 66.9 (d, $^{1}J_{P,C}$ = 9.8 Hz; *C*Ph_3).

^{19}F NMR (470.51 MHz, C_6D_6, 298 K): δ / ppm = −75.5 (s).

^{31}P{^{1}H} NMR (162.00 MHz, C_6D_6, 298 K): δ / ppm = 164.8 (s).

^{31}P NMR (162.00 MHz, C_6D_6, 298 K): δ / ppm = 164.8 (d, $^{1}J_{P,H}$ = 350.1 Hz).

5.5.33 Synthesis of [pentacarbonyl{trifluoroacetyl(triphenylmethyl)phosphane-κ*P*}-tungsten(0)] (62b)

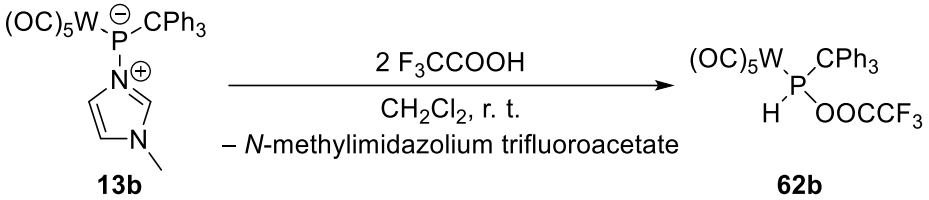

Synthesis

0.10 mL (1.30 mmol, 5.5 eq.) of trifluoroacetic acid was added dropwise to a solution of 0.16 g (0.2 mmol, 1.0 eq.) of [W(CO)$_5${P(CPh_3)(*N*-methylimidazole)}] (**13b**) in 30 mL of dichloromethane at ambient temperature. The solution was stirred for 20.5 h at ambient temperature. Afterwards, all volatiles were removed *in vacuo* (<0.02 mbar) at ambient temperature within 30 minutes and the obtained pale yellow solid was further dried for 15 minutes. The product was extracted using three times 10 mL of *n*-pentane at ambient temperature via a filter cannula (Ø = 1 mm) with a glass microfiber filter paper (Whatman® GF/B). All volatiles were removed from the extract *in vacuo* (<0.02 mbar) at ambient temperature. The obtained colorless solid was further dried for 2 h at ambient temperature.

Reaction codes: DB-550, 566 (23p5a013.22, 23c5a011.22)

Molecular formula: $C_{26}H_{16}O_7F_3PW$

Molecular weight: 712.216 g/mol

Yield: 0.131 g (0.18 mmol, 78 %)

Melting point: 158 °C (dec.)

Elemental analysis: calculated (%) C 43.85 H 2.26

found (%) C 44.83 H 2.65

X-ray diffraction analysis: medium good structure (C1, GSTR777, GXray6912)

MS (LIFDI, selected data): m/z (%) = 712.2 (100) $[M]^{\bullet+}$, 243.2 (50) $[CPh_3]^+$.

IR (ATR Diamond, selected data): $\tilde{\nu}$ / cm^{-1} = 1930 (s) (C≡O), 1960 (s) (C≡O), 1999 (w) (C≡O), 2079 (m) (C≡O).

^{1}H NMR (500.04 MHz, C_6D_6, 298 K): δ / ppm = 8.42 (d_{sat}, $^1J_{P,H}$ = 362.18 Hz, $^2J_{W,H}$ = 6.9 Hz, 1H; P*H*), 7.23–7.12 (m, 6H; CPh_3), 7.05–6.99 (m, 9H; CPh_3).

^{13}C{^{1}H} NMR (125.52 MHz, C_6D_6, 298 K): δ / ppm = 197.1 (d, $^2J_{P,C}$ = 34.4 Hz; *trans*-*C*O), 194.7 (d_{sat}, $^2J_{P,C}$ = 6.8 Hz, $^1J_{W,C}$ = 126.1 Hz; *cis*-*C*O), 153.7 (qd, $^2J_{F,C}$ = 44.7 Hz, $^2J_{P,C}$ = 11.9 Hz; OO*C*CF_3), 140.2 (br s; *ipso*-*C*), 130.4 (br s; Ph), 129.1 (s; Ph), 128.5 (s; Ph), 114.7 (q, $^1J_{F,C}$ = 286.7 Hz; OOC*C*F_3), 65.2 (d, $^1J_{P,C}$ = 15.6 Hz; *C*Ph_3).

^{19}F NMR (470.51 MHz, C_6D_6, 298 K): δ / ppm = −75.4 (s).

^{31}P{^{1}H} NMR (202.44 MHz, C_6D_6, 298 K): δ / ppm = 112.1 (s_{sat}, $^1J_{W,P}$ = 285.3 Hz).

^{31}P NMR (162.00 MHz, C_6D_6, 298 K): δ / ppm = 112.1 (d_{sat}, $^1J_{P,H}$ = 362.4 Hz, $^1J_{W,P}$ = 285.3 Hz).

5.5.34 Synthesis of [pentacarbonyl{chloro(triphenylmethyl)phosphane-κ*P*}tungsten(0)] (63)

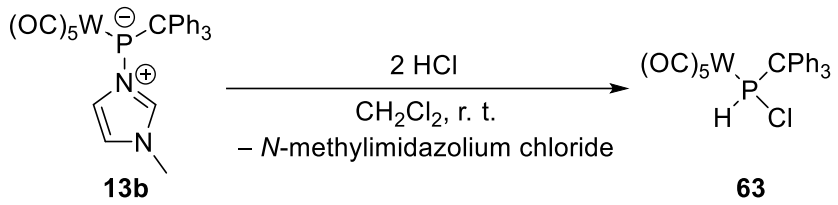

13b **63**

Synthesis

0.16 mL (0.32 mmol, 2.5 eq.) of a hydrogen chloride solution (c = 2 M in diethyl ether) was added to a solution of 0.086 g (0.13 mmol, 1.0 eq.) of [$W(CO)_5${$P(CPh_3)$(*N*-methylimidazole)}] (**13b**) in 8.0 mL of dichloromethane at ambient temperature. The formed pale yellow suspension was stirred for 1 hour at ambient temperature. Afterwards, all volatiles were removed *in vacuo* (<0.02 mbar) at ambient temperature within 10 minutes and the obtained pale yellow solid was further dried for 10 minutes. The product was extracted using three times 5.0 mL of diethyl ether at ambient temperature via a filter cannula (Ø = 1 mm) with a glass microfiber filter paper (Whatman® GF/B). All volatiles were removed from the extract *in vacuo* (<0.02 mbar) at ambient temperature. The obtained colorless solid was further dried for 30 minutes at ambient temperature.

Reaction codes: DB-541 (19m3b020.22)

Molecular formula: $C_{24}H_{16}O_5PClW$

Molecular weight: 634.651 g/mol

Yield: 0.081 g (0.13 mmol, 100 %)

$^{31}P\{^1H\}$ NMR (121.51 MHz, CH_2Cl_2, 298 K): δ / ppm = 71.2 (s_{sat}, $^1J_{W,P}$ = 270.9 Hz).

^{31}P NMR (121.51 MHz, CH_2Cl_2, 298 K): δ / ppm = 71.2 (d_{sat}, $^1J_{P,H}$ = 345.4 Hz, $^1J_{W,P}$ = 270.9 Hz).

Reference: Streubel, **2017**.[224]

5.5.35 Synthesis of [pentacarbonyl{1-methylimidazol-3-iumyl(triphenylmethyl)phosphane-κ*P*}chromium(0)] trifluoromethanesulfonate (64a)

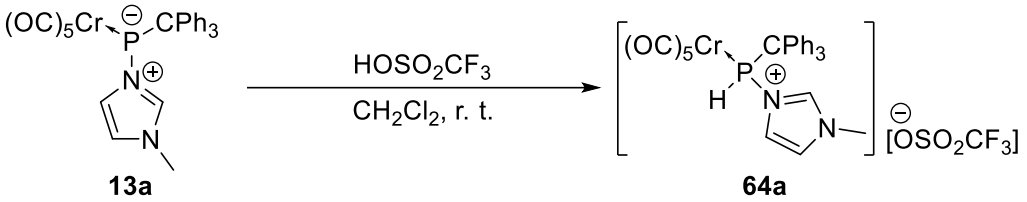

Synthesis

0.03 mL (0.34 mmol, 1.2 eq.) of trifluoromethanesulfonic acid was added dropwise to a solution of 0.161 g (0.29 mmol, 1.0 eq.) of [$Cr(CO)_5${$P(CPh_3)$(*N*-methylimidazole)}] (**13a**) in 10 mL of dichloromethane at ambient temperature. The solution was stirred for 2 h at ambient temperature. Afterwards, 26 mL of *n*-pentane were added to the reaction solution forming a colorless suspension. After additional stirring for 1 minute the solid transformed to a yellow oil. All volatiles were removed *in vacuo* (<0.02 mbar) at ambient temperature within 8 minutes and the obtained colorless and blue-green solids were further dried for 1.5 h. After addition of 10 mL of diethyl ether the solids formed a yellow oil. The mixture was stirred for 20 minutes obtaining a pale yellow suspension. The supernatant was filtered off using a filter cannula (Ø = 1 mm) with a Whatman® 595 filter paper. The pale yellow solid residue was washed two times using 10 mL of diethyl ether and four times using 10 mL of *n*-pentane at ambient temperature. The obtained pale yellow solid was dried for 16.5 h *in vacuo* (<0.02 mbar) at ambient temperature.

Reaction codes: DB-572 (24p5a036.22)

Molecular formula: $C_{29}H_{22}N_2O_8F_3PSCr$

Molecular weight: 698.526 g/mol

Yield: 0.181 g (0.26 mmol, 88.1 %)

Melting point: 144 °C (dec.)

Elemental analysis:	calculated (%)	C 49.86	H 3.17	N 4.01	S 4.59
	found (%)	C 49.53	H 3.21	N 4.07	S 4.60

MS (ESI pos., selected data): m/z (%) = 549.071 (100) $[Cr(CO)_5\{P(CPh_3)(H)(N\text{-MeIm})\}]^+$, 357.155 (3) $[P(CPh_3)(H)(N\text{-MeIm})]^+$, 243.119 (51) $[CPh_3]^+$.

MS (ESI neg., selected data): m/z (%) = 149.1 (100) $[OSO_2CF_3]^-$.

HRMS (ESI pos.): *m/z* calcd for $[C_{28}H_{22}N_2O_5PCr]^-$: 549.0666 $[Cr(CO)_5\{P(CPh_3)(H)(N\text{-MeIm})\}]^+$; found: 549.0676.

IR (ATR Diamond, selected data): $\tilde{\nu}$ / cm^{-1} = 1941 (s) (C≡O), 1972 (m) (C≡O), 2001 (w) (C≡O), 2076 (m) (C≡O).

^{1}H NMR (500.04 MHz, CD_2Cl_2, 298 K): δ / ppm = 9.11 (s, 1H; Im-*H*), 8.94 (d, $^1J_{P,H}$ = 361.86 Hz, 1H; P*H*), 7.47–7.40 (m, 9H; CPh_3), 7.34–7.32 (m, 7H; CPh_3 & Im-*H*), 6.49 (s, 1H; Im-*H*), 3.87 (s, 3H; CH_3).

^{13}C{^{1}H} NMR (125.75 MHz, CD_2Cl_2, 298 K): δ / ppm = 218.8 (d, $^2J_{P,C}$ = 0.8 Hz; *trans*-*C*O), 214.0 (d, $^2J_{P,C}$ = 11.6 Hz; *cis*-*C*O), 141.2 (d, $^2J_{P,C}$ = 3.7 Hz; Im), 139.9 (br s; *ipso*-*C*), 130.3 (br s; Ph), 129.7 (s; Ph), 129.1 (s; Ph), 125.5 (d, $^3J_{P,C}$ = 2.4 Hz; Im), 124.9 (d, $^2J_{P,C}$ = 4.6 Hz; Im), 121.3 (q, $^1J_{F,C}$ = 321.3 Hz; *C*F_3), 66.0 (d, $^1J_{P,C}$ = 3.0 Hz; *C*Ph_3), 37.1 (s; *C*H_3).

^{15}N{^{1}H} NMR (50.68 MHz, CD_2Cl_2, 298 K): δ / ppm = −200.3 (s; *N*-P), −205.8 (s; *N*-CH_3).

^{19}F NMR (470.51 MHz, CD_2Cl_2, 298 K): δ / ppm = −78.9 (s).

^{31}P{^{1}H} NMR (202.44 MHz, CD_2Cl_2, 298 K): δ / ppm = 116.4 (s).

^{31}P NMR (202.44 MHz, CD_2Cl_2, 298 K): δ / ppm = 116.4 (d, $^1J_{P,H}$ = 362.2 Hz).

5.5.36 Synthesis of [pentacarbonyl{1-methylimidazol-3-iumyl(triphenylmethyl)phosphane-κ*P*}tungsten(0)] trifluoromethanesulfonate (64b)

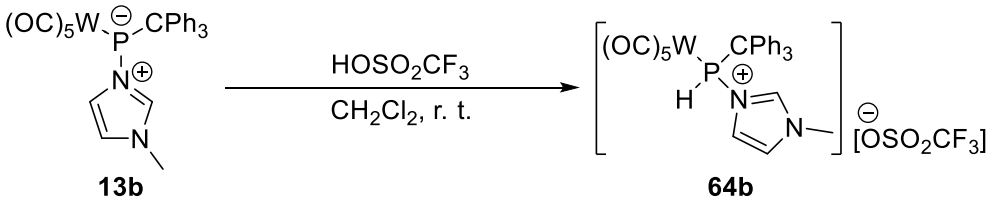

13b **64b**

Synthesis

0.02 mL (0.23 mmol, 1.1 eq.) of trifluoromethanesulfonic acid was added dropwise to a solution of 0.145 g (0.21 mmol, 1.0 eq.) of $[W(CO)_5\{P(CPh_3)(N\text{-methylimidazole})\}]$ (**13b**) in

10 mL of dichloromethane at ambient temperature. The solution was stirred for 1.5 h at ambient temperature. Afterwards, 30 mL of *n*-pentane were added to the reaction solution forming a colorless suspension. After additional stirring for 1 minute the solid transformed to a yellow oil. All volatiles were removed *in vacuo* (<0.02 mbar) at ambient temperature within 15 minutes and the obtained pale yellow solid was further dried for 2 h. After addition of 10 mL of diethyl ether the solid formed a yellow oil. The mixture was stirred for 10 minutes obtaining a pale yellow suspension. The supernatant was filtered off using a filter cannula (Ø = 1 mm) with a Whatman® 595 filter paper. The pale yellow solid residue was washed two times using 10 mL of diethyl ether and three times using 10 mL of *n*-pentane at ambient temperature. The obtained colorless solid was dried for 19 h *in vacuo* (<0.02 mbar) at ambient temperature.

Reaction codes: DB-571 (24p5a037.22)

Molecular formula: $C_{29}H_{22}N_2O_8F_3PSW$

Molecular weight: 830.370 g/mol

Yield: 0.153 g (0.18 mmol, 86.0 %)

Melting point: 142 °C (dec.)

Elemental analysis:	calculated (%)	C 41.95	H 2.67	N 3.37	S 3.86
	found (%)	C 42.13	H 2.83	N 3.42	S 3.92

X-ray diffraction analysis: very good structure (B1, GSTR794, GXraymo_7115f)

MS (ESI pos., selected data): m/z (%) = 681.076 (100) $[W(CO)_5\{P(CPh_3)(H)(N\text{-MeIm})\}]^+$, 243.117 (11) $[CPh_3]^+$.

MS (ESI neg., selected data): m/z (%) = 149.0 (100) $[OSO_2CF_3]^-$.

HRMS (ESI pos.): *m/z* calcd for $[C_{28}H_{22}N_2O_5PW]^-$: 681.0775 $[W(CO)_5\{P(CPh_3)(H)(N\text{-MeIm})\}]^+$; found: 681.0774.

IR (ATR Diamond, selected data): $\tilde{\nu}$ / cm^{-1} = 1932 (s) (C≡O), 1940 (m) (C≡O), 2001 (w) (C≡O), 2081 (m) (C≡O).

^{1}H NMR (500.04 MHz, CD_2Cl_2, 298 K): δ / ppm = 9.41 (d, $^{1}J_{P,H}$ = 373.01 Hz, 1H; P*H*), 9.12 (s, 1H; Im-*H*), 7.46–7.36 (m, 15H; CPh_3), 7.30 (br s, 1H; Im-*H*), 6.48–6.46 (m, 1H; Im-*H*), 3.87 (s, 3H; C*H*$_3$).

^{13}C{^{1}H} NMR (125.75 MHz, CD_2Cl_2, 298 K): δ / ppm = 196.5 (d_{sat}, $^{2}J_{P,C}$ = 34.9 Hz, $^{1}J_{W,C}$ = 143.1 Hz; *trans*-*C*O), 194.5 (d_{sat}, $^{2}J_{P,C}$ = 6.0 Hz, $^{1}J_{W,C}$ = 126.7 Hz; *cis*-*C*O), 141.2 (s; Im), 139.8 (br s; *ipso*-*C*), 130.4 (br s; Ph), 129.7 (s; Ph), 129.0 (s; Ph), 125.3 (s; Im), 125.2 (s; Im), 121.1 (q, $^{1}J_{F,C}$ = 320.3 Hz; *C*F_3), 64.7 (d, $^{1}J_{P,C}$ = 8.0 Hz; *C*Ph_3), 37.1 (s; *C*H_3).

^{15}N{^{1}H} NMR (50.68 MHz, CD_2Cl_2, 298 K): δ / ppm = −200.3 (s; *N*-P), −205.0 (s; *N*-CH_3).

^{19}F NMR (470.51 MHz, CD_2Cl_2, 298 K): δ / ppm = −79.0 (s).

^{31}P{^{1}H} NMR (202.44 MHz, CD_2Cl_2, 298 K): δ / ppm = 65.5 (s_{sat}, $^{1}J_{W,P}$ = 277.8 Hz).

^{31}P NMR (202.44 MHz, CD_2Cl_2, 298 K): δ / ppm = 65.5 (d_{sat}, $^{1}J_{P,H}$ = 373.3 Hz, $^{1}J_{W,P}$ = 277.8 Hz).

5.5.37 Synthesis of [pentacarbonyl{1-methylimidazol-3-iumyl(triphenylmethyl)phosphane-κ*P*}tungsten(0)] tetrakis{3,5-bis(trifluoromethyl)phenyl}borate (65b)

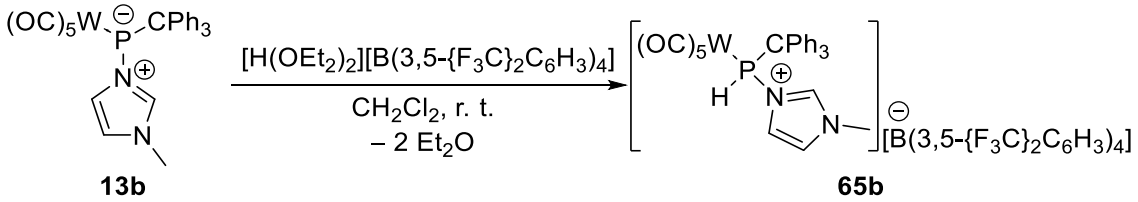

13b **65b**

Synthesis

A solution of 0.1225 g (0.18 mmol, 1.0 eq.) of $[W(CO)_5\{P(CPh_3)$(*N*-methylimidazole)$\}]$ (**13b**) and 0.1847 g (0.18 mmol, 1.0 eq.) of $[H(OEt_2)_2][B(3,5\text{-}\{F_3C\}_2C_6H_3)_4]$ in 10 mL of dichloromethane was stirred for 1.5 h at ambient temperature. Afterwards, 60 mL of *n*-pentane were added to the reaction solution forming a colorless suspension with brown oil. The supernatant was filtered off using a filter cannula (Ø = 1 mm) with a Whatman® 595 filter paper. The pale brown residue was washed once with 5.0 mL of *n*-pentane at −40 °C. The obtained pale yellow solid was dried for 3.5 h *in vacuo* (<0.02 mbar) at ambient temperature.

Reaction codes: DB-604 (37p5a038.22)

Molecular formula: $C_{60}H_{34}BN_2O_5F_{24}PW$

Molecular weight: 1544.526 g/mol

Yield: 0.251 g (0.16 mmol, 90.1 %)

Melting point: 84 °C (dec.)

Elemental analysis: calculated (%) C 46.66 H 2.22 N 1.81

found (%) C 46.86 H 2.56 N 1.93

X-ray diffraction analysis: very good structure (A1, GSTR796, GXraymo_7138v)

MS (ESI pos., selected data): m/z (%) = 681.084 (8) $[W(CO)_5\{P(CPh_3)(H)(\textit{N}\text{-MeIm})\}]^+$, 599.030 (29) $[W(CO)_5\{P(CPh_3)H]^+$, 571.035 (11) $[W(CO)_4\{P(CPh_3)H\}]^+$, 543.040 (35) $[W(CO)_3\{P(CPh_3)H\}]^+$, 515.044 (100) $[W(CO)_2\{P(CPh_3)H\}]^+$, 487.050 (12) $[W(CO)\{P(CPh_3)H\}]^+$, 459.054 (23) $[W\{P(CPh_3)H\}]^+$, 357.156 (24) $[P(CPh_3)(H)(\textit{N}\text{-MeIm})\}]^+$.

MS (ESI neg., selected data): m/z (%) = 863.064 (100) $[B(3,5\text{-}\{F_3C\}_2C_6H_3)_4]^-$.

HRMS (ESI pos.): *m/z* calcd for $[C_{28}H_{22}N_2O_5PW]^-$: 681.0775 $[W(CO)_5\{P(CPh_3)(H)(\textit{N}\text{-MeIm})\}]^+$; found: 681.0775.

IR (ATR Diamond, selected data): $\tilde{\nu}$ / cm^{-1} = 1949 (s) (C≡O), 1963 (m) (C≡O), 2001 (w) (C≡O), 2086 (m) (C≡O).

^{1}H NMR (500.04 MHz, CD_2Cl_2, 298 K): δ / ppm = 8.84 (d, $^1J_{P,H}$ = 353.01 Hz, 1H; P*H*), 7.75–7.73 (m, 8H; *ortho*-C*H*^{BarF}), 7.57 (s, 4H; *para*-C*H*^{BarF}), 7.48–7.44 (m, 9H; CPh_3), 7.28–7.23 (m, 7H; CPh_3 & Im-*H*), 7.19–7.17 (m, 1H; Im-*H*), 7.08 (br s, 1H; Im-*H*), 3.76 (s, 3H; CH_3).

^{11}B{^{1}H} NMR (160.43 MHz, CD_2Cl_2, 298 K): δ / ppm = −6.6 (s).

^{13}C{^{1}H} NMR (125.75 MHz, CD_2Cl_2, 298 K): δ / ppm = 195.1 (d_{sat}, $^2J_{P,C}$ = 36.4 Hz, $^1J_{W,C}$ = 141.2 Hz; *trans*-*C*O), 194.3 (d_{sat}, $^2J_{P,C}$ = 5.9 Hz, $^1J_{W,C}$ = 126.6 Hz; *cis*-*C*O), 162.2 (q*, $^1J_{C,B}$ = 49.8 Hz; *ipso*-*C*^{BArF}), 139.4 (br s; *ipso*-*C*^{Ph}), 138.3 (s; Im), 135.2 (s; *ortho*-*C*^{BArF}), 130.3 (br s; Ph), 130.1 (s; Ph), 129.8 (d, $J_{P,C}$ = 1.5 Hz; Ph), 129.3 (qq*, $^2J_{F,C}$ = 31.5 Hz, $^3J_{C,B}$ = 3.0 Hz; *meta*-*C*^{BArF}), 126.4 (s; Im), 125.2 (d, $J_{P,C}$ = 1.7 Hz; Im), 125.0 (q, $^1J_{F,C}$ = 272.4 Hz; *C*F_3), 117.9 (sept, $^3J_{F,C}$ = 4.4 Hz; *para*-*C*^{BArF}), 65.5 (d, $^1J_{P,C}$ = 7.3 Hz; *C*Ph_3), 37.7 (s; *C*H_3).

^{15}N{^{1}H} NMR (50.68 MHz, CD_2Cl_2, 298 K): δ / ppm = −194.6 (s; *N*-P), −203.1 (s; *N*-CH_3).

^{19}F NMR (470.51 MHz, CD_2Cl_2, 298 K): δ / ppm = −62.8 (s).

^{31}P{^{1}H} NMR (202.44 MHz, CD_2Cl_2, 298 K): δ / ppm = 77.7 (s_{sat}, $^1J_{W,P}$ = 283.9 Hz).

^{31}P NMR (202.44 MHz, CD_2Cl_2, 298 K): δ / ppm = 77.7 (d_{sat}, $^1J_{P,H}$ = 353.3 Hz, $^1J_{W,P}$ = 283.9 Hz).

5.5.38 Synthesis of [pentacarbonyl{(1-methylimidazol-3-iumyl)(triphenylmethyl)phosphane-κ*P*}chromium(0)] tetrakis(nonafluoro-*tert*-butoxy)aluminate (66a)

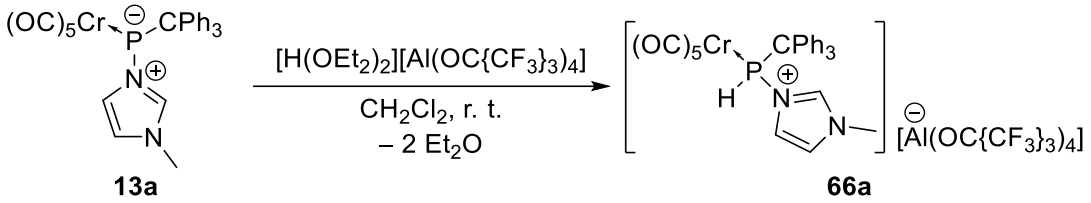

Synthesis

A solution of 0.167 g (0.30 mmol, 1.0 eq.) of $[Cr(CO)_5\{P(CPh_3)(N\text{-methylimidazole})\}]$ (**13a**) and 0.339 g (0.30 mmol, 1.0 eq.) of $[H(OEt_2)_2][Al(OC\{CF_3\}_3)_4]$ in 16 mL of dichloromethane was stirred for 3 h at ambient temperature. Afterwards, 100 mL of *n*-pentane were added to the reaction solution forming a yellow suspension. The supernatant was filtered off using a filter cannula (Ø = 2 mm) with a Whatman® 595 filter paper. The pale yellow residue was washed three times using 11 mL of a 10:1 *n*-pentane/dichloromethane mixture and three times using 10 mL of *n*-pentane at ambient temperature. The obtained pale yellow solid was dried for 19 h *in vacuo* (<0.02 mbar) at ambient temperature.

Reaction codes: DB-573 (24p5a038.22)

Molecular formula: $C_{44}H_{22}N_2O_9F_{36}AlPCr$

Molecular weight: 1516.559 g/mol

Yield: 0.44 g (0.29 mmol, 95.6 %)

Melting point: 151 °C (dec.)

Elemental analysis:	calculated (%)	C 34.85	H 1.46	N 1.85
	found (%)	C 33.50	H 1.52	N 1.84

MS (ESI pos., selected data): m/z (%) = 549.067 (36) $[Cr(CO)_5\{P(CPh_3)(H)(N\text{-MeIm})\}]^+$.

MS (ESI neg., selected data): m/z (%) = 966.9 (100) $[Al(OC\{CF_3\}_3)_4]^-$.

HRMS (ESI pos.): *m/z* calcd for $[C_{28}H_{22}N_2O_5PCr]^-$: 549.0666 $[Cr(CO)_5\{P(CPh_3)(H)(N\text{-MeIm})\}]^+$; found: 549.0669.

IR (ATR Diamond, selected data): $\tilde{\nu}$ / cm^{-1} = 1953 (s) (C≡O), 1969 (s) (C≡O), 2014 (w) (C≡O), 2079 (m) (C≡O).

^{1}H NMR (500.04 MHz, CD_2Cl_2, 298 K): δ / ppm = 8.34 (d, $^{1}J_{P,H}$ = 341.49 Hz, 1H; P*H*), 7.50–7.49 (m, 9H; CPh_3), 7.28 (m, 1H; Im-*H*), 7.26–7.18 (m, 6H; CPh_3), 7.20–7.19 (m, 1H; Im-*H*), 7.03 (br s, 1H; Im-*H*), 3.80 (s, 3H; CH_3).

^{13}C{^{1}H} NMR (125.75 MHz, CD_2Cl_2, 298 K): δ / ppm = 217.4 (s; *trans*-*C*O), 213.8 (d, $^{2}J_{P,C}$ = 11.4 Hz; *cis*-*C*O), 139.5 (br s; *ipso*-*C*), 138.2 (d, $^{2}J_{P,C}$ = 4.8 Hz; Im), 130.2–129.9 (m; Ph), 126.3 (d, $J_{P,C}$ = 4.8 Hz; Im), 125.3 (s; Im), 121.7 (q, $^{1}J_{F,C}$ = 293.0 Hz; *C*F_3), 67.0 (d, $^{1}J_{P,C}$ = 2.2 Hz; *C*Ph_3), 37.7 (d, $^{4/5}J_{P,C}$ = 0.9 Hz ; *C*H_3).

^{15}N{^{1}H} NMR (50.68 MHz, CD_2Cl_2, 298 K): δ / ppm = −195.7 (s; *N*-P), −204.2 (s; *N*-CH_3).

^{19}F NMR (470.51 MHz, CD_2Cl_2, 298 K): δ / ppm = −75.7 (s).

^{27}Al{^{1}H} NMR (130.29 MHz, CD_2Cl_2, 298 K): δ / ppm = 34.6 (s).

^{31}P{^{1}H} NMR (202.44 MHz, CD_2Cl_2, 298 K): δ / ppm = 132.0 (s).

^{31}P NMR (202.44 MHz, CD_2Cl_2, 298 K): δ / ppm = 132.0 (d, $^{1}J_{P,H}$ = 341.9 Hz).

5.5.39 Synthesis of [pentacarbonyl{(1-methylimidazol-3-iumyl(triphenylmethyl)phosphane-κ*P*}tungsten(0)] tetrakis(nonafluoro-*tert*-butoxy)aluminate (66b)

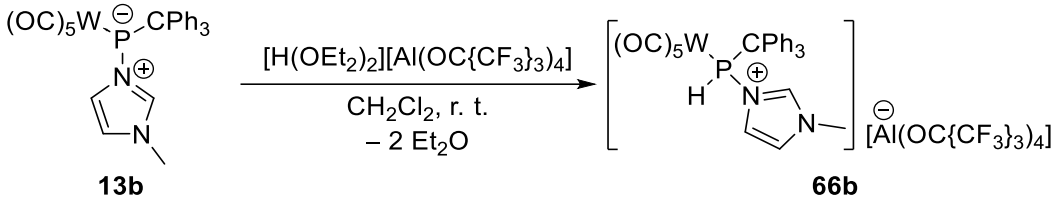

13b **66b**

Synthesis

A solution of 0.109 g (0.16 mmol, 1.0 eq.) of [W(CO)$_5${P(CPh_3)(*N*-methylimidazole)}] (**13b**) and 0.178 g (0.16 mmol, 1.0 eq.) of [H(OEt_2)$_2$][Al(OC{CF_3}$_3$)$_4$] in 16 mL of dichloromethane was stirred for 3 h at ambient temperature. Afterwards, 80 mL of *n*-pentane were added to the reaction solution forming a pale yellow suspension. The supernatant was filtered off using a filter cannula (Ø = 2 mm) with a glass microfiber filter paper (Whatman® GF/B). The pale yellow residue was washed three times using 11 mL of a 10:1 *n*-pentane/dichloromethane

mixture and two times using 5 mL of *n*-pentane at ambient temperature. The obtained colorless solid was dried for 14 h *in vacuo* (<0.02 mbar) at ambient temperature.

Reaction codes: DB-510, 568 (16t4a080.22, 17p5a007.22, 16m3a049.22)

Molecular formula: $C_{44}H_{22}N_2O_9F_{36}AlPW$

Molecular weight: 1648.403 g/mol

Yield: 0.234 g (0.14 mmol, 89.0 %)

Melting point: 160 °C (dec.)

Elemental analysis:	calculated (%)	C 32.06	H 1.35	N 1.70
	found (%)	C 31.32	H 1.56	N 1.73

X-ray diffraction analysis: medium good structure (CD1, GSTR789, GXraymo_7046f)

MS (ESI pos., selected data): m/z (%) = 681.077 (<1) $[W(CO)_5\{P(CPh_3)(H)(N\text{-MeIm})\}]^+$, 243.116 (100) $[CPh_3]^+$.

MS (ESI neg., selected data): m/z (%) = 966.907 (100) $[Al(OC\{CF_3\}_3)_4]^-$.

HRMS (ESI pos.): *m/z* calcd for $[C_{28}H_{22}N_2O_5PW]^-$: 681.0775 $[W(CO)_5\{P(CPh_3)(H)(N\text{-MeIm})\}]^+$; found: 681.0782.

IR (ATR Diamond, selected data): $\tilde{\nu}$ / cm^{-1} = 1949 (s) (C≡O), 1963 (m) (C≡O), 2009 (w) (C≡O), 2085 (m) (C≡O).

^{1}H NMR (400.13 MHz, CD_2Cl_2, 298 K): δ / ppm = 8.84 (d, $^1J_{P,H}$ = 352.91 Hz, 1H; P*H*), 7.49–7.48 (m, 9H; CPh_3), 7.29–7.25 (m, 7H; CPh_3 & Im-*H*), 7.20–7.19 (m, 1H; Im-*H*), 7.08 (br s, 1H; Im-*H*), 3.81 (s, 3H; CH_3).

^{13}C{^{1}H} NMR (100.63 MHz, CD_2Cl_2, 298 K): δ / ppm = 195.1 (d, $^2J_{P,C}$ = 36.2 Hz; *trans*-*C*O), 194.3 (d, $^2J_{P,C}$ = 6.0 Hz; *cis*-*C*O), 139.3 (br s; *ipso*-*C*), 138.3 (s; Im), 130.3 (br d, $J_{P,C}$ = 8.7 Hz; Ph), 130.1 (s; Ph), 129.8 (d, $J_{P,C}$ = 2.1 Hz; Ph), 126.4 (s; Im), 126.0 (s; $C(CF_3)_3$), 125.2 (d, $J_{P,C}$ = 1.6 Hz; Im), 121.7 (q, $^1J_{F,C}$ = 293.1 Hz; CF_3), 65.5 (d, $^1J_{P,C}$ = 7.3 Hz; CPh_3), 37.8 (s; CH_3).

^{15}N{^{1}H} NMR (50.68 MHz, CD_2Cl_2, 298 K): δ / ppm = −195.7 (s; *N*-P), −204.2 (s; *N*-CH_3).

^{19}F NMR (470.51 MHz, CD_2Cl_2, 298 K): δ / ppm = −75.7 (s).

^{27}Al{^{1}H} NMR (78.20 MHz, CD_2Cl_2, 298 K): δ / ppm = 34.7 (s).

^{31}P{^{1}H} NMR (162.00 MHz, CD_2Cl_2, 298 K): δ / ppm = 77.8 (s_{sat}, $^{1}J_{W,P}$ = 283.8 Hz).

^{31}P NMR (162.00 MHz, CD_2Cl_2, 298 K): δ / ppm = 77.8 (d_{sat}, $^{1}J_{P,H}$ = 353.6 Hz, $^{1}J_{W,P}$ = 283.8 Hz).

5.5.40 Synthesis of [pentacarbonyl{methyl(1-methylimidazol-3-iumyl)(triphenylmethyl)phosphane-κ*P*}chromium(0)] trifluoromethanesulfonate (68a)

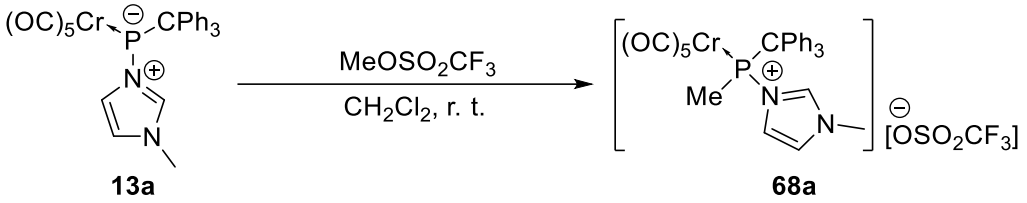

Synthesis

0.04 mL (0.37 mmol, 1.2 eq.) of methyl trifluoromethanesulfonate was added to a solution of 0.171 g (0.31 mmol, 1.0 eq.) of [Cr(CO)$_5${P(CPh$_3$)(*N*-methylimidazole)}] (**13a**) in 16 mL of dichloromethane at ambient temperature. The solution was stirred for 80 minutes in a glovebox at ambient temperature. Afterwards, all volatiles were removed *in vacuo* (<0.02 mbar) at ambient temperature. The obtained yellow solid was redissolved in 15 mL of dichloromethane at ambient temperature. After addition of 50 mL of *n*-pentane the formed yellow suspension was stirred for 3 minutes at ambient temperature. The supernatant was filtered off using a filter cannula (Ø = 2 mm) with a Whatman® 595 filter paper and the pale yellow solid residue was washed three times with 5.0 mL of *n*-pentane at ambient temperature. The product was dried for 2.5 h *in vacuo* (<0.02 mbar) at ambient temperature.

Reaction codes: DB-558 (22p5a046.22, 22p5a055.22)

Molecular formula: $C_{30}H_{24}N_2O_8F_3PSCr$

Molecular weight: 712.553 g/mol

Yield: 0.194 g (0.27 mmol, 86.9 %)

Melting point: 142 °C (dec.)

Elemental analysis:	calculated (%)	C 50.57	H 3.40	N 3.93	S 4.50
	found (%)	C 47.04	H 3.46	N 3.60	S 4.31

X-ray diffraction analysis: good structure, + dichloromethane (B1, GSTR773, GXray6925)

MS (ESI pos., selected data): m/z (%) = 563.082 (12) $[Cr(CO)_5\{P(CPh_3)(Me)(N\text{-MeIm})\}]^+$, 481.029 (7) $[Cr(CO)_5\{P(CPh_3)Me\}]^+$, 425.039 (1) $[Cr(CO)_3\{P(CPh_3)Me\}]^+$, 397.044 (8) $[Cr(CO)_2\{P(CPh_3)Me\}]^+$, 382.081 (4) $[Cr(CO)_2(PCPh_3)]^+$, 371.167 (100) $[P(CPh_3)(Me)(N\text{-MeIm})]^+$, 289.114 (64) $[P(CPh_3)Me]^+$, 243.117 (26) $[CPh_3]^+$, 237.983 (1) $[Cr(CO)_5(PMe)]^+$.

MS (ESI neg., selected data): m/z (%) = 149.0 (100) $[OSO_2CF_3]^-$.

HRMS (ESI pos.): *m/z* calcd for $[C_{29}H_{24}N_2O_5PCr]^+$: 563.0825 $[Cr(CO)_5\{P(CPh_3)(Me)(N\text{-MeIm})\}]^+$; found: 563.0820.

HRMS (ESI pos.): *m/z* calcd for $[C_{24}H_{24}N_2P]^+$: 371.1672 $[P(CPh_3)(Me)(N\text{-MeIm})]^+$; found: 371.1670.

IR (ATR Diamond, selected data): $\tilde{\nu}$ / cm^{-1} = 1934 (s) (C≡O), 1981 (m) (C≡O), 2001 (w) (C≡O), 2073 (m) (C≡O).

^{1}H NMR (500.04 MHz, CD_2Cl_2, 298 K): δ / ppm = 8.66 (s, 1H; Im-*H*), 7.67–7.63 (m, 2H; CPh_3), 7.56–7.45 (m, 6H; CPh_3), 7.45–7.33 (m, 3H; CPh_3), 7.28 (s, 1H; Im-*H*), 7.26–7.17 (m, 2H; CPh_3), 6.58 (s, 1H; Im-*H*), 6.56–6.45 (m, 2H; CPh_3), 3.97 (s, 3H; N-CH_3), 2.28 (s, 3H; P-CH_3).

^{13}C{^{1}H} NMR (125.75 MHz, CD_2Cl_2, 298 K): δ / ppm = 219.3 (d, $^2J_{P,C}$ = 2.0 Hz; *trans*-*C*O), 214.8 (d, $^2J_{P,C}$ = 10.9 Hz; *cis*-*C*O), 141.1 (br s; *ipso*-*C*), 139.8 (d, $J_{P,C}$ = 2.2 Hz; Im), 139.5 (br s; *ipso*-*C*), 137.8 (br s; *ipso*-*C*), 131.7–131.3 (m; Ph), 130.0–129.5 (m; Ph), 125.4 (d, $J_{P,C}$ = 2.0 Hz; Im), 124.9 (d, $J_{P,C}$ = 3.9 Hz; Im), 121.4 (br q, $^1J_{F,C}$ = 323.7 Hz; *C*F_3), 69.7 (d, $^1J_{P,C}$ = 2.4 Hz; *C*Ph_3), 37.5 (s; N-*C*H_3), 24.8 (d, $^1J_{P,C}$ = 15.6 Hz; P-*C*H_3).

^{15}N{^{1}H} NMR (50.68 MHz, CD_2Cl_2, 298 K): δ / ppm = −191.4 (s; *N*-P), −203.1 (s; *N*-CH_3).

^{19}F NMR (470.51 MHz, CD_2Cl_2, 298 K): δ / ppm = −78.8 (s).

^{31}P{^{1}H} NMR (202.44 MHz, CD_2Cl_2, 298 K): δ / ppm = 165.1 (s).

^{31}P NMR (202.44 MHz, CD_2Cl_2, 298 K): δ / ppm = 165.1 (s).

5.5.41 Synthesis of [pentacarbonyl{methyl(1-methylimidazol-3-iumyl)(triphenylmethyl)phosphane-κ*P*}tungsten(0)] trifluoromethanesulfonate (68b)

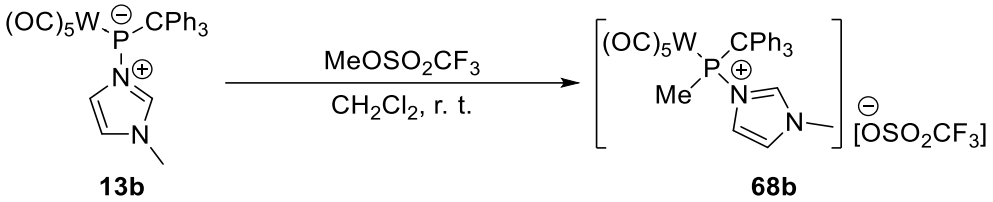

13b **68b**

Synthesis

0.02 mL (0.18 mmol, 1.1 eq.) of methyl trifluoromethanesulfonate was added to a solution of 0.111 g (0.16 mmol, 1.0 eq.) of [$W(CO)_5${$P(CPh_3)$(*N*-methylimidazole)}] (**13b**) in 10 mL of dichloromethane at ambient temperature. The solution was stirred for 3 h at ambient temperature. After addition of 40 mL of *n*-pentane the formed colorless suspension was stirred for 2 h at ambient temperature. The supernatant was filtered off using a filter cannula (Ø = 2 mm) with a Whatman® 595 filter paper and the colorless solid residue was washed three times with 4.0 mL of *n*-pentane at ambient temperature. The solid was dried for 14 h *in vacuo* (<0.02 mbar) at ambient temperature. The product was isolated by recrystallization in 20 mL of a 1:1 diethylether/THF mixture at −40 °C. After the supernatant was filtered off using a filter cannula (Ø = 2 mm) with a Whatman® 595 filter paper and washing the colorless solid three times with 3 mL of *n*-pentane at −40 °C the product was dried for 75 minutes at ambient temperature.

Reaction codes: DB-519, 594 (21p5a028.22, 21m3a033.22, 32p5b033.22)

Molecular formula: $C_{30}H_{24}N_2O_8F_3PSW$

Molecular weight: 844.397 g/mol

Yield: 0.078 g (0.09 mmol, 56.3 %)

Melting point: 155 °C (dec.)

Elemental analysis:	calculated (%)	C 42.67	H 2.87	N 3.32	S 3.80
	found (%)	C 41.74	H 2.92	N 3.35	S 4.32

X-ray diffraction analysis: very good structure, + dichloromethane (B1, GSTR763, GXray6876)

MS (ESI pos., selected data): m/z (%) = 695.092 (4) $[W(CO)_5\{P(CPh_3)(Me)(N\text{-MeIm})\}]^+$, 613.039 (3) $[W(CO)_5\{P(CPh_3)Me\}]^+$, 585.044 (1) $[W(CO)_4\{P(CPh_3)Me\}]^+$, 529.054 (1) $[W(CO)_2\{P(CPh_3)Me\}]^+$, 501.059 (1) $[W(CO)\{P(CPh_3)Me\}]^+$, 371.166 (12) $[P(CPh_3)(Me)(N\text{-MeIm})]^+$, 289.113 (44) $[P(CPh_3)Me]^+$, 243.116 (100) $[CPh_3]^+$.

MS (ESI neg., selected data): m/z (%) = 148.9 (100) $[OSO_2CF_3]^-$.

HRMS (ESI pos.): *m/z* calcd for $[C_{29}H_{24}N_2O_5PW]^+$: 695.0928 $[W(CO)_5\{P(CPh_3)(Me)(N\text{-MeIm})\}]^+$; found: 695.0921.

IR (ATR Diamond, selected data): $\tilde{\nu}$ / cm^{-1} = 1927 (s) (C≡O), 1995 (w) (C≡O), 2079 (m) (C≡O).

^{1}H NMR (500.04 MHz, CD_2Cl_2, 298 K): δ / ppm = 8.71 (s, 1H; Im-*H*), 7.70–7.57 (m, 2H; CPh_3), 7.54–7.35 (m, 9H; CPh_3), 7.35–7.27 (m, 2H; CPh_3), 7.25 (s, 1H; Im-*H*), 6.69–6.98 (m, 1H; Im-*H*), 6.65–6.55 (m, 2H; CPh_3), 3.96 (s, 3H; N-CH_3), 2.53 (d, $^2J_{P,H}$ = 1.13 Hz, 3H; P-CH_3).

^{13}C{^{1}H} NMR (125.75 MHz, CD_2Cl_2, 298 K): δ / ppm = 197.1 (d, $^2J_{P,C}$ = 33.6 Hz; *trans*-*C*O), 196.0 (d_{sat}, $^2J_{P,C}$ = 6.0 Hz, $^1J_{W,C}$ = 127.2 Hz; *cis*-*C*O), 141.2 (br s; *ipso*-*C*), 139.9 (d, $J_{P,C}$ = 1.4 Hz; Im), 139.6 (br s; *ipso*-*C*), 137.3 (br s; *ipso*-*C*), 131.8–131.4 (m; Ph), 130.1–129.6 (m; Ph), 125.3 (d, $J_{P,C}$ = 5.1 Hz; Im), 125.1 (d, $J_{P,C}$ = 2.7 Hz; Im), 121.2 (q, $^1J_{F,C}$ = 320.4 Hz; *C*F_3), 68.1 (d, $^1J_{P,C}$ = 2.3 Hz; *C*Ph_3), 37.5 (s; N-*C*H_3), 26.1 (d, $^1J_{P,C}$ = 20.2 Hz; P-*C*H_3).

^{15}N{^{1}H} NMR (50.68 MHz, CD_2Cl_2, 298 K): δ / ppm = −191.4 (s; *N*-P), −202.4 (s; *N*-CH_3).

^{19}F NMR (470.51 MHz, CD_2Cl_2, 298 K): δ / ppm = −79.0 (s).

^{31}P{^{1}H} NMR (202.44 MHz, CD_2Cl_2, 298 K): δ / ppm = 116.4 (s_{sat}, $^1J_{W,P}$ = 273.9 Hz).

^{31}P NMR (121.51 MHz, CD_2Cl_2, 299 K): δ / ppm = 116.4 (s_{sat}, $^1J_{W,P}$ = 273.7 Hz).

5.5.42 Synthesis of [pentacarbonyl{2-*tert*-butyl-3-methyl-1-(triphenylmethyl)phosphaguanidine-κ*P*}chromium(0)] (69a)

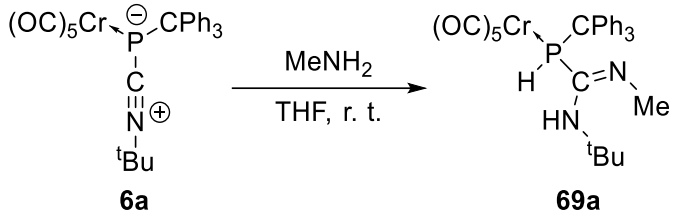

6a **69a**

Synthesis

2.2 mL (c = 2 M in THF, 4.40 mmol, 10.2 eq.) of a methylamine solution were added to a solution of 0.238 g (0.43 mmol, 1.0 eq.) of [$Cr(CO)_5${$P(CPh_3)CN^tBu$}] (**6a**) in 10 mL of THF. The solution was stirred for 18 h at ambient temperature. Afterwards, all volatiles were removed *in vacuo* (<0.02 mbar) at ambient temperature and the obtained yellow solid was further dried under the same conditions for 35 minutes.

Reaction codes: DB-56, 58, 245, 398 (31m3b030.18, 32p5a053.18, 31p5b001.18)

Molecular formula: $C_{30}H_{29}N_2O_5PCr$

Molecular weight: 580.541 g/mol

Yield: 0.188 g (0.32 mmol, 74.9 %)

Melting point: 129–130 °C (dec.)

Elemental analysis:	calculated (%)	C 62.07	H 5.04	N 4.83
	found (%)	C 62.04	H 5.32	N 4.71

X-ray diffraction analysis: good structure, two independent structures (B1, GSTR734, GXray6704)

MS (LIFDI, selected data): m/z (%) = 580.0 (100) $[M]^{\bullet+}$, 243.1 (12) $[CPh_3]^+$.

IR (ATR Diamond, selected data): $\tilde{\nu}$ / cm^{-1} = 1919 (vs) (C≡O), 2000 (w) (C≡O), 2064 (s) (C≡O), 2371 (w) (P-H), 3413 (m) (N-H).

^{1}H NMR (300.13 MHz, C_6D_6, 299 K): δ / ppm = 7.42–7.02 (m, 15H; CPh_3), 6.33 (d, $^1J_{P,H}$ = 338.87 Hz, 1H; P*H*), 3.30 (s, 1H; N*H*), 2.98 (s, 3H; NCH_3), 1.18 (s, 9H; N(H)C(CH)$_3$).

$^{13}C\{^1H\}$ NMR (125.78 MHz, C_6D_6, 297 K): δ / ppm = 220.7 (d, $^2J_{P,C}$ = 4.1 Hz; *trans*-*C*O), 215.7 (d, $^2J_{P,C}$ = 10.6 Hz; *cis*-*C*O), 151.9 (d, $^1J_{P,C}$ = 3.0 Hz; N=*C*-N), 143.1 (s; *ipso*-*C*), 129.4 (s; Ph), 127.5 (s; Ph), 127.2 (s; Ph), 60.4 (d, $^1J_{P,C}$ = 6.8 Hz; P-*C*Ph$_3$), 52.3 (d, $^3J_{P,C}$ = 5.7 Hz; N(H)*C*(CH$_3$)$_3$), 37.8 (d, $^3J_{P,C}$ = 13.4 Hz; N*C*H$_3$), 28.2 (s; N(H)C(*C*H$_3$)$_3$).

$^{15}N\{^1H\}$ NMR (50.69 MHz, C_6D_6, 298 K): δ / ppm = −144.8 (s; C=*N*-Me), −258.7 (s; C-*N*H-^{t}Bu).

$^{31}P\{^1H\}$ NMR (121.51 MHz, C_6D_6, 299 K): δ / ppm = 14.4 (s).

^{31}P NMR (121.51 MHz, C_6D_6, 299 K): δ / ppm = 14.4 (d, $^1J_{P,H}$ = 339.5 Hz).

5.5.43 Synthesis of [pentacarbonyl{2-*tert*-butyl-3-methyl-1-(triphenylmethyl)phosphaguanidine-κ*P*}tungsten(0)] (69b)

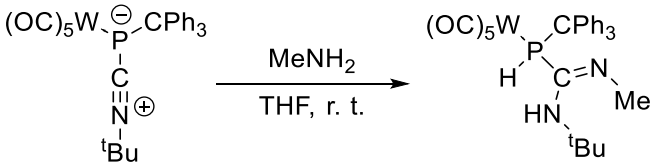

6c **69b**

Synthesis

0.63 mL (c = 2 M in THF, 1.26 mmol, 5.0 eq.) of a methylamine solution was added to a solution of 0.17 g (0.25 mmol, 1.0 eq.) of [W(CO)$_5${P(CPh$_3$)CN^{t}Bu}] (**6c**) in 20 mL of THF. The solution was stirred for 21 h at ambient temperature. Afterwards, all volatiles were removed *in vacuo* (<0.02 mbar) at ambient temperature. The product was isolated as pale yellow solid by column chromatography (Al_2O_3, Ø = 5 cm, h = 4 cm) using diethyl ether at ambient temperature.

Reaction codes: DB-108, 116, 246, 393 (11m3a038.19, 28p5a008.22)

Molecular formula: $C_{30}H_{29}N_2O_5PW$

Molecular weight: 712.385 g/mol

Yield: 0.03 g (0.05 mmol, 20 %)

Melting point: 131–132 °C (dec.)

Elemental analysis:	calculated (%)	C 50.58	H 4.10	N 3.93
	found (%)	C 52.26	H 4.60	N 3.60

X-ray diffraction analysis: very good structure, two independent structures (B2, GSTR672, GXray6002f)

MS (EI, 70 eV, selected data): m/z (%) = 712.0 (0.1) $[M]^{\bullet+}$, 684.0 (2) $[M-CO]^+$, 628.0 (0.1) [M−3CO], 599.9 (0.1) $[M-4CO]^+$, 572.1 (0.1) $[M-5CO]^+$, 542.9 (0.1) $[M-4CO-{}^tBu]^+$, 514.9 (0.1) $[M-5CO-{}^tBu]^+$, 440.9 (5) $[M-CPh_3-CO]^+$, 384.9 (2) $[M-CPh_3-3CO]^+$, 356.8 (1) $[M-CPh_3-4CO]^+$, 244.0 (100) $[CPh_3+H]^+$, 166.0 (32) $[CPh_2]^+$, 113.0 (48) $[C(NMe)N(H){}^tBu]^+$, 77.0 (2) $[Ph]^+$, 57.0 (65) $[{}^tBu]^+$.

IR (ATR Diamond, selected data): $\tilde{\nu}$ / cm^{-1} = 1914 (vs) (C≡O), 1988 (w) (C≡O), 2072 (m) (C≡O), 2372 (w) (P-H), 3411 (m) (N-H).

^{1}H NMR (300.13 MHz, $CDCl_3$, 298 K): δ / ppm = 7.36–7.11 (m, 15H; CPh_3), 6.78 (d, $^1J_{P,H}$ = 349.16 Hz, 1H; P*H*), 3.22 (s, 1H; N*H*), 2.96 (s, 3H; NCH_3), 1.04 (s, 9H; N(H)C(C*H*)$_3$).

^{13}C{^{1}H} NMR (75.48 MHz, $CDCl_3$, 298 K): δ / ppm = 198.1 (d, $^2J_{P,C}$ = 26.0 Hz; *trans*-*C*O), 196.3 (d, $^2J_{P,C}$ = 5.7 Hz; *cis*-*C*O), 151.7 (s; N=*C*-N), 143.9 (s; *ipso*-*C*), 129.6 (s; Ph), 128.4 (s; Ph), 127.5 (s; Ph), 66.0 (s; N(H)*C*$(CH_3)_3$), 58.9 (d, $^1J_{P,C}$ = 11.2 Hz; P-*C*Ph_3), 29.9 (s; N*C*H_3), 28.3 (s; N(H)C(*C*$H_3)_3$).

^{15}N{^{1}H} NMR (50.68 MHz, C_6D_6, 298 K): δ / ppm = −144.6 (s; C=*N*-Me), −259.3 (s; C-*N*H-^{t}Bu).

^{31}P{^{1}H} NMR (121.51 MHz, $CDCl_3$, 298 K): δ / ppm = −27.2 (s_{sat}, $^1J_{W,P}$ = 220.5 Hz).

^{31}P NMR (121.51 MHz, $CDCl_3$, 298 K): δ / ppm = −27.2 (d_{sat}, $^1J_{P,H}$ = 349.2 Hz, $^1J_{W,P}$ = 220.5 Hz).

5.5.44 Synthesis of [pentacarbonyl{2-*tert*-butyl-1-(triphenylmethyl)-3-isopropylphospha-guanidine-κ*P*}chromium(0)] (70a)

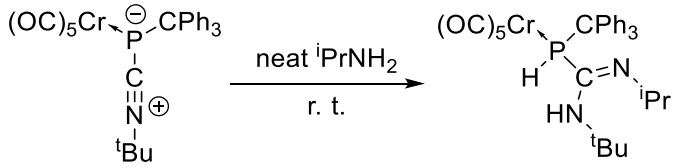

6a **70a**

Synthesis

0.215 g (0.39 mmol, 1.0 eq.) of $[Cr(CO)_5\{P(CPh_3)CN{}^tBu\}]$ (**6a**) was dissolved in 10 mL (117 mmol, 299 eq.) of isopropylamine at ambient temperature. The reaction mixture was stirred for 11 h at ambient temperature. All volatiles were removed *in vacuo* (<0.02 mbar) at ambient temperature.

Reaction codes: DB-257, 301, 399 (10m3a024.21, 10p5a027.21)

Molecular formula: $C_{32}H_{33}N_2O_5PCr$

Molecular weight: 608.595 g/mol

Yield: 0.226 g (0.37 mmol, 95.0 %)

Melting point: 130–131 °C (dec.)

Elemental analysis: calculated (%) C 63.15 H 5.47 N 4.60

found (%) C 62.79 H 5.67 N 4.50

X-ray diffraction analysis: very good structure (B1, GSTR714, GXray6529)

MS (LIFDI, selected data): m/z (%) = 608.2 (100) $[M]^{\bullet+}$, 580.4 (73) $[M-CO]^+$, 417.5 (9) $[M-Cr(CO)_5+H]^+$, 243.3 (20) $[CPh_3]^+$.

MS (EI, 70 eV, selected data): m/z (%) = 608.0 (<0.1) $[M]^{\bullet+}$, 468.0 (3) $[M-5CO]^+$, 243.0 (100) $[CPh_3]^+$, 165.0 (83) $[HCPh_2]^+$, 141.1 (17) $[C(N^iPr)N(H)^tBu]^+$, 77.0 (3) $[Ph]^+$, 57.0 (12) $[^tBu]^+$.

IR (ATR Diamond, selected data): $\tilde{\nu}$ / cm^{-1} = 1918 (vs) (C≡O), 1989 (w) (C≡O), 2062 (m) (C≡O), 2377 (w) (P-H), 3410 (m) (N-H).

^{1}H NMR (300.13 MHz, C_6D_6, 298 K): δ / ppm = 7.59–7.00 (m, 15H; CPh_3), 6.20 (dd, $^1J_{P,H}$ = 336.73 Hz, $^4J_{H,H}$ = 1.22 Hz, 1H; P*H*), 3.36 (s, 1H; N*H*), 3.27 (sept, $^3J_{H,H}$ = 6.10 Hz, 1H; NC(*H*)$(CH_3)_2$), 1.21 (d, $^3J_{H,H}$ = 6.10 Hz, 3H; NC(H)C*H*$_3$), 1.21 (s, 9H; N(H)C(C*H*)$_3$), 0.91 (d, $^3J_{H,H}$ = 6.10 Hz, 3H; NC(H)C*H*$_3$).

^{13}C{^{1}H} NMR (75.48 MHz, C_6D_6, 298 K): δ / ppm = 221.0 (d, $^2J_{P,C}$ = 4.0 Hz; *trans*-*C*O), 216.2 (d, $^2J_{P,C}$ = 10.5 Hz; *cis*-*C*O), 147.5 (d, $^2J_{P,C}$ = 4.4 Hz; *ipso*-*C*), 144.4 (s; N=*C*-N), 129.9 (s; Ph), 128.6 (s; Ph), 127.9 (s; Ph), 60.9 (d, $^1J_{P,C}$ = 5.8 Hz; P-*C*Ph_3), 52.6 (d, $^3J_{P,C}$ = 6.1 Hz; N(H)*C*$(CH_3)_3$), 51.4 (d, $^3J_{P,C}$ = 10.5 Hz; N*C*(H)$(CH_3)_2$), 28.4 (s; N(H)C(*C*H)$_3$), 25.0 (s; NC(H)*C*H$_3$), 24.8 (s; NC(H)*C*H$_3$).

^{15}N{^{1}H} NMR (50.69 MHz, C_6D_6, 298 K): δ / ppm = −112.6 (s; C=*N*-^{i}Pr), −259.3 (s; C-*N*H-^{t}Bu).

^{31}P{^{1}H} NMR (121.51 MHz, C_6D_6, 298 K): δ / ppm = 17.6 (s).

^{31}P NMR (121.51 MHz, C_6D_6, 298 K): δ / ppm = 17.6 (d, $^1J_{P,H}$ = 339.9 Hz).

5.5.45 Synthesis of [pentacarbonyl{2-*tert*-butyl-1-(triphenylmethyl)-3-isopropylphosphaguanidine-κ*P*}tungsten(0)] (70b)

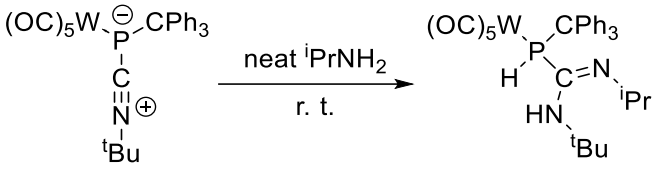

6c **70b**

Synthesis

0.251 g (0.37 mmol, 1.0 eq.) of $[W(CO)_5\{P(CPh_3)CN^tBu\}]$ (**6c**) was dissolved in 13 mL (159 mmol, 431 eq.) of isopropylamine at ambient temperature. The reaction mixture was stirred for 25 h at ambient temperature. All volatiles were removed *in vacuo* (<0.02 mbar) at ambient temperature.

Reaction codes: DB-256, 400 (43m3a025.21, 37p5a036.20)

Molecular formula: $C_{32}H_{33}N_2O_5PW$

Molecular weight: 740.439 g/mol

Yield: 0.191 g (0.26 mmol, 75.9 %)

Melting point: 147–148 °C (dec.)

Elemental analysis:	calculated (%)	C 51.91	H 4.49	N 3.78
	found (%)	C 52.22	H 4.53	N 3.59

X-ray diffraction analysis: good structure (C1, GSTR735, GXray6705)

MS (LIFDI, selected data): m/z (%) = 740.3 (100) $[M]^{\bullet+}$, 599.1 (3) $[M-5CO-H]^+$, 417 (16) $[M-W(CO)_5+H]^+$, 243.2 (82) $[CPh_3]^+$.

IR (ATR Diamond, selected data): $\tilde{\nu}$ / cm^{-1} = 1915 (vs) (C≡O), 1987 (w) (C≡O), 2070 (m) (C≡O), 2379 (w) (P-H), 3408 (m) (N-H).

^{1}H NMR (300.13 MHz, C_6D_6, 298 K): δ / ppm = 7.59–6.99 (m, 15H; CPh_3), 6.64 (d, $^1J_{P,H}$ = 346.43 Hz, 1H; P*H*), 3.33 (s, 1H; N*H*), 3.27 (sept, $^3J_{H,H}$ = 6.09 Hz, 1H; NC(*H*)$(CH_3)_2$), 1.19 (s, 9H; N(H)C(C*H*)$_3$), 1.19 (d, $^3J_{H,H}$ = 6.09 Hz, 3H; NC(H)C*H*$_3$), 0.97 (d, $^3J_{H,H}$ = 6.09 Hz, 3H; NC(H)C*H*$_3$).

$^{13}C\{^1H\}$ NMR (125.78 MHz, C_6D_6, 298 K): δ / ppm = 198.1 (d_{sat}, $^2J_{P,C}$ = 26.0 Hz, $^1J_{W,P}$ = 146.3 Hz; *trans*-*C*O), 196.6 (d_{sat}, $^2J_{P,C}$ = 5.7 Hz, $^1J_{W,P}$ = 126.3 Hz; *cis*-*C*O), 146.6 (s; *ipso*-*C*), 144.0 (s; N=*C*-N), 131.3–126.4 (m; Ph), 59.1 (d, $^1J_{P,C}$ = 10.2 Hz; P-*C*Ph_3), 52.4 (d, $^3J_{P,C}$ = 6.3 Hz; N(H)*C*$(CH_3)_3$), 50.8 (d, $^3J_{P,C}$ = 11.4 Hz; N*C*(H)$(CH_3)_2$), 28.3 (s; N(H)C(*C*H)$_3$), 24.8 (s; NC(H)*C*H_3), 24.7 (s; NC(H)*C*H_3).

$^{15}N\{^1H\}$ NMR (50.69 MHz, C_6D_6, 298 K): δ / ppm = −112.4 (s; C=*N*-^{i}Pr), −260.0 (s; C-*N*H-^{t}Bu).

$^{31}P\{^1H\}$ NMR (121.51 MHz, C_6D_6, 298 K): δ / ppm = −25.8 (s_{sat}, $^1J_{W,P}$ = 230.9 Hz).

^{31}P NMR (121.51 MHz, C_6D_6, 298 K): δ / ppm = −25.8 (d_{sat}, $^1J_{P,H}$ = 346.9 Hz, $^1J_{W,P}$ = 230.9 Hz).

5.5.46 Attempted synthesis of [pentacarbonyl{bis(*tert*-butylamino)methylium(triphenylmethyl)phosphanido-κ*P*}chromium(0)] (71a)

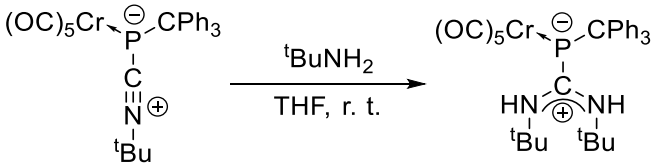

6a **71a**

Synthesis

0.06 mL (0.57 mmol, 1.9 eq.) of *tert*-butylamine was added to a solution of 0.16 g (0.30 mmol, 1.0 eq.) of [Cr(CO)$_5${P(CPh$_3$)CN^{t}Bu}] (**6a**) in 20 mL of THF. The reaction mixture was stirred for 8 days at ambient temperature.

Reaction code: DB-97 (04p5a031.19)

Molecular formula: $C_{33}H_{35}N_2O_5PCr$

Molecular weight: 622.622 g/mol

Content in solution: 54 % (^{31}P NMR integration of reaction mixture)

^{31}P NMR (202.48 MHz, THF, 298 K): δ / ppm = −29.1 (s).

5.5.47 Attempted synthesis of [pentacarbonyl{bis(*tert*-butylamino)methylium(triphenylmethyl)phosphanido-κ*P*}tungsten(0)] (71b)

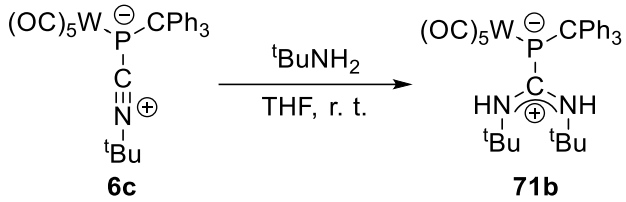

6c **71b**

Synthesis

0.05 mL (0.48 mmol, 4.4 eq.) of *tert*-butylamine was added to a solution of 0.073 g (0.11 mmol, 1.0 eq.) of [W(CO)$_5${P(CPh$_3$)CN^{t}Bu}] (**6c**) in 3 mL of THF. The reaction mixture was stirred for 12 days at 40 °C.

Reaction code: DB-130 (23p5a014.19)

Molecular formula: $C_{33}H_{35}N_2O_5PW$

Molecular weight: 754.466 g/mol

Content in solution: 74 % (^{31}P NMR integration of reaction mixture)

^{31}P NMR (202.48 MHz, THF, 298 K): δ / ppm = −33.8 (s_{sat}, $^1J_{W,P}$ = 103.8 Hz).

6 REFERENCES

[1] Norman E. Holden, *Standard Atomic Weight Values for the Mononuclidic Elements - 2001*, Brisbane, Australia, **2001**.

[2] John R. van Wazer, *Phosphorus and its Compounds, Volume I: Chemistry*, Interscience Publishers, New York, **1958**.

[3] A. F. Holleman, E. Wiberg, N. Wiberg, *Anorganische Chemie, Band 1, Grundlagen und Hauptgruppenelemente,* Vol. 103, De Gruyter, Berlin, **2017**.

[4] F. Krafft, *Angew. Chem.* **1969**, *81*, 634–645; *Angew. Chem. Int. Ed. Engl.* **1969**, *8*, 660–671.

[5] E. Riedel, C. Janiak, *Anorganische Chemie,* Vol. 10, De Gruyter, Berlin, **2022**.

[6] a) J. Li, X. Wang, T. Zhang, C. Wang, Z. Huang, X. Luo, Y. Deng, *Asian J. Pharm. Sci.* **2015**, *10*, 81–98; b) A. Travers, G. Muskhelishvili, *FEBS J.* **2015**, *282*, 2279–2295; c) Food and Nutrition Board, Institute of Medicine, *Dietary Reference Intakes: A Risk Assessment Model for Establishing Upper Intake Levels for Nutrients*, National Academies Press (US), Washington (DC), **1998**.

[7] J. M. Berg, J. L. Tymoczko, L. Stryer, *Biochemie,* Vol. 6, Spektrum Akademischer Verlag, Heidelberg, **2011**.

[8] H. Lüllmann, K. Mohr, L. Hein, *Pharmakologie und Toxikologie,* Vol. 16, Thieme, Stuttgart, **2006**.

[9] G. Schrader, *Die Entwicklung neuer insektizider Phosphorsäure-Erster,* Vol. 3, Verlag Chemie, Weinheim, **1963**.

[10] S. Havelange, N. van Lierde, A. Germeau, E. Martins, T. Theys, M. Sonveaux, C. Toussaint, K. Schrödter, G. Bettermann, T. Staffel et al., *Ullmann's Encycl. Ind. Chem.* **2008**, *26*, 679–724.

[11] I. van der Veen, J. de Boer, *Chemosphere* **2012**, *88*, 1119–1153.

[12] C. Elschenbroich, *Organometallchemie,* Vol. 6, Vieweg+Teubner Verlag / GWV Fachverlage GmbH Wiesbaden, Wiesbaden, **2008**.

[13] B. D. Vineyard, W. S. Knowles, M. J. Sabacky, G. L. Bachman, D. J. Weinkauff, *J. Am. Chem. Soc.* **1977**, *99*, 5946–5952.

[14] A. L. Clevenger, R. M. Stolley, J. Aderibigbe, J. Louie, *Chem. Rev.* **2020**, *120*, 6124–6196.

[15] G. Wittig, U. Schöllkopf, *Chem. Ber.* **1954**, *87*, 1318–1330.

[16] A. A. Nazarov, P. J. Dyson in *Catalysis by Metal Complexes*, Vol. 37 (Eds.: M. Peruzzini, L. Gonsalvi), Springer, Dordrecht, **2011**, pp. 445–461.

[17] L. D. Quin, *A guide to organophosphorus chemistry*, Wiley-Interscience, New York, Chichester, Weinheim, **2000**.

[18] a) H. A. Favre, W. H. Powell, *Nomenclature of Organic Chemistry*, Royal Society of Chemistry, Cambridge, **2013**; b) W. H. Powell, *Pure Appl. Chem.* **1984**, *56*, 769–778.

[19] N. G. Connelly, T. Damhus, R. M. Hartshorn, A. T. Hutton, *Nomenclature of Inorganic Chemistry*. *IUPAC Recommendations 2005*, RSC Publishing, Cambridge, **2005**.

[20] a) W. M. Butler, J. H. Enemark, J. Parks, A. L. Balch, *Inorg. Chem.* **1973**, *12*, 451–457; b) L. Tschugajeff, M. Skanawy-Grigorjewa, A. Posnjak, *Z. Anorg. Allg. Chem.* **1925**, *148*, 37–42; c) L. Chugaev, M. Skanavy-Grigorieva, *J. Russ. Chem. Soc.* **1915**, *47*, 776–782.

[21] E. O. Fischer, A. Maasböl, *Angew. Chem.* **1964**, *76*, 645; *Angew. Chem. Int. Ed. Engl.* **1964**, *3*, 580–581.

[22] R. R. Schrock, *J. Am. Chem. Soc.* **1974**, *96*, 6796–6797.

[23] A. Igau, H. Grutzmacher, A. Baceiredo, G. Bertrand, *J. Am. Chem. Soc.* **1988**, *110*, 6463–6466.

[24] A. J. Arduengo, R. L. Harlow, M. Kline, *J. Am. Chem. Soc.* **1991**, *113*, 361–363.

[25] V. Lavallo, Y. Canac, C. Präsang, B. Donnadieu, G. Bertrand, *Angew. Chem.* **2005**, *117*, 5851–5855; *Angew. Chem. Int. Ed.* **2005**, *44*, 5705–5709.

[26] K. B. Dillon, F. Mathey, J. F. Nixon, *Phosphorus: The Carbon Copy*. *From Organophosphorus to Phospha-Organic Chemistry*, Wiley, Chichester, **1998**.

[27] J. Warkentin in *Advances in carbene chemistry*, Vol. 2 (Ed.: U. H. Brinker), JAI Press, Greenwich, CT, **1998**, pp. 245–295.

[28] M. Weidenbruch, *Coord. Chem. Rev.* **1994**, *130*, 275–300.

[29] a) D. E. Falvey, A. D. Gudmundsdottir, *Nitrenes and nitrenium ions*. *Wiley series on reactive intermediates in chemistry and biology,* Vol. 1, Wiley, Hoboken, **2013**; b) A. Schulz, A. Villinger, *Angew. Chem.* **2013**, *125*, 3146–3148; *Angew. Chem. Int. Ed.* **2013**, *52*, 3068–3070; c) H. F. Sleiman, S. Mercer, L. McElwee-White, *J. Am. Chem. Soc.* **1989**, *111*, 8007–8009; d) C. Wentrup, *Adv. Heterocycl. Chem.* **1981**, *28*, 231–361.

[30] M. T. Nguyen, A. van Keer, L. G. Vanquickenborne, *J. Org. Chem.* **1996**, *61*, 7077–7084.

[31] Z. Benko, R. Streubel, L. Nyulászi, *Dalton Trans.* **2006**, 4321–4327.

[32] S. Grigoleit, A. Alijah, A. B. Rozhenko, R. Streubel, W. W. Schoeller, *J. Organomet. Chem.* **2002**, *643-644*, 223–230.

[33] a) G. Bucher, M. L. G. Borst, A. W. Ehlers, K. Lammertsma, S. Ceola, M. Huber, D. Grote, W. Sander, *Angew. Chem.* **2005**, *117*, 3353–3357; *Angew. Chem. Int. Ed.* **2005**, *44*, 3289–3293; b) X. Li, S. I. Weissman, T.-S. Lin, P. P. Gaspar, A. H. Cowley, A. I. Smirnov, *J. Am. Chem. Soc.* **1994**, *116*, 7899–7900; c) H.-F. Grützmacher, W. Silhan, U. Schmidt, *Chem. Ber.* **1969**, *102*, 3230–3232.

[34] a) W. J. Transue, A. Velian, M. Nava, C. García-Iriepa, M. Temprado, C. C. Cummins, *J. Am. Chem. Soc.* **2017**, *139*, 10822–10831; b) E. Niecke, J. Böske, D. Gudat, W. Güth, M. Lysek, E. Symalla, *Nova Acta Leopold.* **1985**, *59*, 83–91; c) W. Mahler, A. B. Burg, *J. Am. Chem. Soc.* **1958**, *80*, 6161–6167; d) U. Schmidt, *Angew. Chem.* **1975**, *87*, 535–540; *Angew. Chem. Int. Ed. Engl.* **1975**, *14*, 523–528.

[35] L. Liu, D. A. Ruiz, D. Munz, G. Bertrand, *Chem* **2016**, *1*, 147–153.

[36] M. M. Hansmann, R. Jazzar, G. Bertrand, *J. Am. Chem. Soc.* **2016**, *138*, 8356–8359.

[37] a) R. H. V. Nishimura, V. E. Murie, R. A. Soldi, J. L. C. Lopes, G. C. Clososki, *J. Braz. Chem. Soc.* **2015**; b) G. Köbrich, A. Akhtar, F. Ansari, W. E. Breckoff, H. Büttner, W. Drischel, R. H. Fischer, K. Flory, H. Fröhlich, W. Goyert et al., *Angew. Chem.* **1967**, *79*, 15–27; *Angew. Chem. Int. Ed. Engl.* **1967**, *6*, 41–52; c) H. E. Simmons, R. D. Smith, *J. Am. Chem. Soc.* **1959**, *81*, 4256–4264.

[38] M. Yoshifuji, T. Sato, N. Inamoto, *Chem. Lett.* **1988**, *17*, 1735–1738.

[39] M. Yoshifuji, I. Shima, N. Inamoto, K. Hirotsu, T. Higuchi, *J. Am. Chem. Soc.* **1981**, *103*, 4587–4589.

[40] J. D. Protasiewicz, *Eur. J. Inorg. Chem.* **2012**, *2012*, 4539–4549.

[41] S. Shah, J. D. Protasiewicz, *Chem. Commun.* **1998**, 1585–1586.

[42] a) R. Streubel, E. Niecke, P. Paetzold, *Chem. Ber.* **1991**, *124*, 765–767; b) E. Niecke, R. Streubel, M. Nieger, D. Stalke, *Angew. Chem.* **1989**, *101*, 1708–1710; *Angew. Chem. Int. Ed. Engl.* **1989**, *28*, 1673–1674.

[43] E. Niecke, R. Rüger, M. Lysek, W. W. Schoeller, *Phosphorus Sulfur Relat. Elem.* **1983**, *18*, 35–38.

[44] R. Streubel, *PhD thesis*, Bonn, University of Bonn, **1990**.

[45] a) T. Krachko, J. C. Slootweg, *Eur. J. Inorg. Chem.* **2018**, *2018*, 2734–2754; b) S. Kundu, S. Sinhababu, A. V. Luebben, T. Mondal, D. Koley, B. Dittrich, H. W. Roesky, *J. Am.*

Chem. Soc. **2018**, *140*, 151–154; c) S. Roy, K. C. Mondal, S. Kundu, B. Li, C. J. Schürmann, S. Dutta, D. Koley, R. Herbst-Irmer, D. Stalke, H. W. Roesky, *Chem. Eur. J.* **2017**, *23*, 12153–12157; d) M. Bispinghoff, H. Grützmacher, *Chimia* **2016**, *70*, 279–283; e) K. Pal, O. B. Hemming, B. M. Day, T. Pugh, D. J. Evans, R. A. Layfield, *Angew. Chem.* **2016**, *128*, 1722–1725; *Angew. Chem. Int. Ed.* **2016**, *55*, 1690–1693; f) M. Cicač-Hudi, J. Bender, S. H. Schlindwein, M. Bispinghoff, M. Nieger, H. Grützmacher, D. Gudat, *Eur. J. Inorg. Chem.* **2016**, *2016*, 649–658; g) M. Scheer, G. Balázs, A. Seitz, *Chem. Rev.* **2010**, *110*, 4236–4256; h) A. J. Arduengo, J. C. Calabrese, A. H. Cowley, H. V. R. Dias, J. R. Goerlich, W. J. Marshall, B. Riegel, *Inorg. Chem.* **1997**, *36*, 2151–2158; i) I. A. J. Arduengo, H. V. R. Dias, J. C. Calabrese, *Chem. Lett.* **1997**, *26*, 143–144; j) A. J. Arduengo III, C. J. Carmalt, J. A. C. Clyburne, A. H. Cowley, R. Pyati, *Chem. Commun.* **1997**, 981–982; k) A. N. Chernega, A. V. Ruban, V. D. Romanenko, L. N. Markovski, A. A. Korkin, M. Y. Antipin, Y. T. Struchkov, *Heteroat. Chem.* **1991**, *2*, 229–241; l) A. N. Chernega, M. Y. Antipin, Y. T. Struchkov, T. V. Sarina, v. d. Romanenko, *J. Struct. Chem.* **1987**, *27*, 741–745.

[46] M. M. Hansmann, G. Bertrand, *J. Am. Chem. Soc.* **2016**, *138*, 15885–15888.

[47] a) M. Yoshifuji, T. Niitsu, K. Toyota, N. Inamoto, K. Hirotsu, Y. Odagaki, T. Higuchi, S. Nagase, *Polyhedron* **1988**, *7*, 2213–2216; b) O. I. Kolodiazhnyi, *Phosphorus Sulfur Relat. Elem.* **1983**, *18*, 39–42.

[48] K. Lammertsma, *Top. Curr. Chem.* **2003**, *229*, 95–119.

[49] A. H. Cowley, M. C. Cushner, *Inorg. Chem.* **1980**, *19*, 515–518.

[50] a) K. Hansen, T. Szilvási, B. Blom, E. Irran, M. Driess, *Chem. Eur. J.* **2014**, *20*, 1947–1956; b) K. Hansen, T. Szilvási, B. Blom, S. Inoue, J. Epping, M. Driess, *J. Am. Chem. Soc.* **2013**, *135*, 11795–11798.

[51] A. N. Kornev, Y. S. Panova, V. V. Sushev, *Phosphorus, Sulfur Silicon Relat. Elem.* **2020**, *195*, 905–909.

[52] I. Kalinina, F. Mathey, *Organometallics* **2006**, *25*, 5031–5034.

[53] C. Janiak, D. Gudat, P. Kurz, *Moderne anorganische Chemie,* Vol. 5, De Gruyter, Berlin, Boston, **2018**.

[54] A. W. Ehlers, E. J. Baerends, K. Lammertsma, *J. Am. Chem. Soc.* **2002**, *124*, 2831–2838.

[55] P. B. Hitchcock, M. F. Lappert, W.-P. Leung, *J. Chem. Soc., Chem. Commun.* **1987**, 1282–1283.

[56] E. Niecke, J. Hein, M. Nieger, *Organometallics* **1989**, *8*, 2290–2291.

[57] F. Mathey, N. H. T. Huy, A. Marinetti, *Helv. Chim. Acta* **2001**, *84*, 2938–2957.

[58] A. Marinetti, F. Mathey, J. Fischer, A. Mitschler, *J. Am. Chem. Soc.* **1982**, *104*, 4484–4485.

[59] F. Mercier, B. Deschamps, F. Mathey, *J. Am. Chem. Soc.* **1989**, *111*, 9098–9100.

[60] R. Streubel, A. Kusenberg, J. Jeske, P. G. Jones, *Angew. Chem.* **1994**, *106*, 2564–2566; *Angew. Chem. Int. Ed. Engl.* **1995**, *33*, 2427–2428.

[61] a) R. Streubel, J. Jeske, P. G. Jones, R. Herbst-Irmer, *Angew. Chem.* **1994**, *106*, 115–117; *Angew. Chem. Int. Ed. Engl.* **1994**, *33*, 80–82; b) R. Streubel, *Top. Curr. Chem.* **2002**, *223*, 91–109.

[62] R. Streubel, *Coord. Chem. Rev.* **2002**, *227*, 175–192.

[63] M. L. G. Borst, R. E. Bulo, C. W. Winkel, D. J. Gibney, A. W. Ehlers, M. Schakel, M. Lutz, A. L. Spek, K. Lammertsma, *J. Am. Chem. Soc.* **2005**, *127*, 5800–5801.

[64] A. Marinetti, F. Mathey, *Organometallics* **1984**, *3*, 456–461.

[65] F. Mathey, *Angew. Chem.* **1987**, *99*, 285–296; *Angew. Chem. Int. Ed. Engl.* **1987**, *26*, 275–286.

[66] J. B. M. Wit, G. T. van Eijkel, F. J. J. de Kanter, M. Schakel, A. W. Ehlers, M. Lutz, A. L. Spek, K. Lammertsma, *Angew. Chem.* **1999**, *111*, 2716–2719; *Angew. Chem. Int. Ed.* **1999**, *38*, 2596–2599.

[67] K. Lammertsma, A. W. Ehlers, M. L. McKee, *J. Am. Chem. Soc.* **2003**, *125*, 14750–14759.

[68] C. Compain, F. Mathey, *Z. Anorg. Allg. Chem.* **2006**, *632*, 421–424.

[69] G. Huttner, H.-D. Müller, A. Frank, H. Lorenz, *Angew. Chem.* **1975**, *87*, 597–598; *Angew. Chem. Int. Ed. Engl.* **1975**, *14*, 572–573.

[70] a) H. Lang, G. Huttner, I. Jibril, *Z. Naturforsch. B* **1986**, *41*, 473–485; b) G. Huttner, K. Evertz, *Acc. Chem. Res.* **1986**, *19*, 406–413.

[71] A. Özbolat, G. von Frantzius, E. Ionescu, S. Schneider, M. Nieger, P. G. Jones, R. Streubel, *Organometallics* **2007**, *26*, 4021–4024.

[72] A. Özbolat, G. von Frantzius, J. M. Pérez, M. Nieger, R. Streubel, *Angew. Chem.* **2007**, *119*, 9488–9491; *Angew. Chem. Int. Ed.* **2007**, *46*, 9327–9330.

[73] C. Schulten, G. von Frantzius, G. Schnakenburg, A. Espinosa, R. Streubel, *Chem. Sci.* **2012**, *3*, 3526–3533.

[74] V. Nesterov, T. Heurich, R. Streubel, *Pure Appl. Chem.* **2012**, *85*, 829–834.

[75] A. Özbolat, G. von Frantzius, W. Hoffbauer, R. Streubel, *Dalton Trans.* **2008**, 2674–2676.

[76] R. Streubel, A. Özbolat-Schön, G. von Frantzius, H. Lee, G. Schnakenburg, D. Gudat, *Inorg. Chem.* **2013**, *52*, 3313–3325.

[77] M. Bode, J. Daniels, R. Streubel, *Organometallics* **2009**, *28*, 4636–4638.

[78] V. Nesterov, G. Schnakenburg, A. Espinosa, R. Streubel, *Inorg. Chem.* **2012**, *51*, 12343–12349.

[79] C. Albrecht, M. Bode, J. M. Pérez, J. Daniels, G. Schnakenburg, R. Streubel, *Dalton Trans.* **2011**, *40*, 2654–2665.

[80] C. M. García, A. E. Ferao, G. Schnakenburg, R. Streubel, *Dalton Trans.* **2016**, *45*, 2378–2385.

[81] A. Schmer, N. Volk, A. Espinosa Ferao, R. Streubel, *Dalton Trans.* **2019**, *48*, 339–345.

[82] J. Fassbender, G. Schnakenburg, A. Espinosa Ferao, R. Streubel, *Dalton Trans.* **2018**, *47*, 9347–9354.

[83] A. Schmer, P. Junker, A. Espinosa Ferao, R. Streubel, *Acc. Chem. Res.* **2021**, *54*, 1754–1765.

[84] V. Nesterov, L. Duan, G. Schnakenburg, R. Streubel, *Eur. J. Inorg. Chem.* **2011**, *2011*, 567–572.

[85] M. Klein, G. Schnakenburg, A. Espinosa Ferao, N. Tokitoh, R. Streubel, *Eur. J. Inorg. Chem.* **2016**, *2016*, 685–690.

[86] A. Espinosa Ferao, R. Streubel, *Chem. Eur. J.* **2017**, *23*, 8632–8643.

[87] A. Espinosa Ferao, A. García Alcaraz, S. Zaragoza Noguera, R. Streubel, *Inorg. Chem.* **2020**, *59*, 12829–12841.

[88] R. Streubel, A. W. Kyri, L. Duan, G. Schnakenburg, *Dalton Trans.* **2014**, *43*, 2088–2097.

[89] P. K. Majhi, A. W. Kyri, A. Schmer, G. Schnakenburg, R. Streubel, *Chem. Eur. J.* **2016**, *22*, 15413–15419.

[90] a) A. W. Kyri, V. Nesterov, G. Schnakenburg, R. Streubel, *Angew. Chem.* **2014**, *126*, 10985–10988; *Angew. Chem. Int. Ed.* **2014**, *53*, 10809–10812; b) A. W. Kyri, F. Gleim, A. García Alcaraz, G. Schnakenburg, A. Espinosa Ferao, R. Streubel, *Chem. Commun.* **2018**, *54*, 7123–7126; c) A. W. Kyri, F. Gleim, D. Biskup, G. Schnakenburg, A. Espinosa Ferao, R. Streubel, *Chem. Commun.* **2019**, *55*, 1615–1618.

[91] S. Fankel, H. Helten, G. von Frantzius, G. Schnakenburg, J. Daniels, V. Chu, C. Müller, R. Streubel, *Dalton Trans.* **2010**, *39*, 3472–3481.

[92] N. Volk, P. Malik, A. G. Alcaraz, A. Espinosa Ferao, R. Streubel, *Coord. Chem. Rev.* **2021**, *437*, 213818.

[93] J. M. Villalba Franco, G. Schnakenburg, A. Espinosa Ferao, R. Streubel, *Chem. Eur. J.* **2015**, *21*, 3727–3735.

[94] J. M. Villalba Franco, T. Sasamori, G. Schnakenburg, A. Espinosa Ferao, R. Streubel, *Chem. Commun.* **2015**, *51*, 3878–3881.

[95] R. Streubel, N. Volk, G. Schnakenburg, A. García Alcaraz, A. Espinosa Ferao, *Eur. J. Inorg. Chem.* **2021**, *2021*, 252–257.

[96] a) A. Özbolat-Schön, M. Bode, G. Schnakenburg, A. Anoop, M. van Gastel, F. Neese, R. Streubel, *Angew. Chem.* **2010**, *122*, 7047–7051; *Angew. Chem. Int. Ed.* **2010**, *49*, 6894–6898; b) P. Junker, J. M. Villalba Franco, G. Schnakenburg, V. Nesterov, R. T. Boere, Z.-W. Qu, R. Streubel, *Dalton Trans.* **2020**, *49*, 13544–13548; c) C. M. García, A. Bauzá, G. Schnakenburg, A. Frontera, R. Streubel, *Chem. Commun.* **2017**, *53*, 933–936.

[97] P. Junker, Z.-W. Qu, T. Kalisch, G. Schnakenburg, A. Espinosa Ferao, R. Streubel, *Dalton Trans.* **2021**, *50*, 739–745.

[98] J. M. Villalba Franco, G. Schnakenburg, T. Sasamori, A. Espinosa Ferao, R. Streubel, *Chem. Eur. J.* **2015**, *21*, 9650–9655.

[99] a) R. Streubel, M. Bode, J. Marinas Pérez, G. Schnakenburg, J. Daniels, M. Nieger, P. G. Jones, *Z. Anorg. Allg. Chem.* **2009**, *635*, 1163–1171; b) S. Bauer, A. Marinetti, L. Ricard, F. Mathey, *Angew. Chem.* **1990**, *102*, 1188–1189; *Angew. Chem. Int. Ed. Engl.* **1990**, *29*, 1166–1167; c) C. M. García, G. Schnakenburg, R. Streubel, *Aust. J. Chem.* **2017**, *70*, 442–446; d) A. Espinosa Ferao, R. Streubel, *Eur. J. Inorg. Chem.* **2017**, *2017*, 2707–2712; e) J. Faßbender, N. Künemund, A. Espinosa Ferao, G. Schnakenburg, R. Streubel, *Organometallics* **2018**, *37*, 1331–1336.

[100] R. Streubel, J. M. Villalba Franco, G. Schnakenburg, A. Espinosa Ferao, *Chem. Commun.* **2012**, *48*, 5986–5988.

[101] J. M. Villalba Franco, A. Espinosa Ferao, G. Schnakenburg, R. Streubel, *Chem. Commun.* **2013**, *49*, 9648–9650.

[102] J. M. Villalba Franco, *PhD thesis*, University of Bonn, Bonn, **2015**.

[103] J. M. Villalba Franco, G. Schnakenburg, A. Espinosa Ferao, R. Streubel, *Dalton Trans.* **2016**, *45*, 13951–13956.

[104] E. Ionescu, G. von Frantzius, P. G. Jones, R. Streubel, *Organometallics* **2005**, *24*, 2237–2240.

[105] M. Seidl, M. Schiffer, M. Bodensteiner, A. Y. Timoshkin, M. Scheer, *Chem. Eur. J.* **2013**, *19*, 13783–13791.

[106] L. Weber, M. Meyer, H.-G. Stammler, B. Neumann, *Chem. Eur. J.* **2001**, *7*, 5401–5408.

[107] A. Doddi, D. Bockfeld, A. Nasr, T. Bannenberg, P. G. Jones, M. Tamm, *Chem. Eur. J.* **2015**, *21*, 16178–16189.

[108] M. Klein, *PhD thesis*, University of Bonn, Bonn, **2015**.

[109] D. Bockfeld, A. Doddi, P. G. Jones, M. Tamm, *Eur. J. Inorg. Chem.* **2016**, 3704–3713.

[110] T. W. Graham, K. A. Udachin, A. J. Carty, *Chem. Commun.* **2006**, 2699–2701.

[111] R. Streubel, H. Wilkens, A. Ostrowski, C. Neumann, F. Ruthe, P. G. Jones, *Angew. Chem.* **1997**, *109*, 1549–1550; *Angew. Chem. Int. Ed. Engl.* **1997**, *36*, 1492–1494.

[112] H. Wilkens, F. Ruthe, P. G. Jones, R. Streubel, *Chem. Commun.* **1998**, 1529–1530.

[113] R. Streubel, U. Schiemann, P. G. Jones, N. H. Tran Huy, F. Mathey, *Angew. Chem.* **2000**, *112*, 3845–3847; *Angew. Chem. Int. Ed.* **2000**, *39*, 3686–3688.

[114] a) A. A. Khan, C. Wismach, P. G. Jones, R. Streubel, *Dalton Trans.* **2003**, 2483–2487; b) V. Nesterov, A. Espinosa, G. Schnakenburg, R. Streubel, *Chem. Eur. J.* **2014**, *20*, 7010–7016.

[115] a) O. I. Kolodiazhnyi, *Phosphorus ylides*. *Chemistry and application in organic synthesis,* Vol. 1, Wiley-VCH, Weinheim, New York, **1999**; b) P. Molina, M. J. Vilaplana, *Synthesis* **1994**, *1994*, 1197–1218; c) P. Potin, R. de Jaeger, *Eur. Polym. J.* **1991**, *27*, 341–348.

[116] A. B. Burg, W. Mahler, *J. Am. Chem. Soc.* **1961**, *83*, 2388–2389.

[117] A. B. Burg, *J. Inorg. Nucl. Chem.* **1971**, *33*, 1575–1581.

[118] D. Weber, E. Fluck, *Z. Anorg. Allg. Chem.* **1976**, *424*, 103–107.

[119] a) G. Fritz, T. Vaahs, H. Fleischer, E. Matern, *Angew. Chem.* **1989**, *101*, 324–325; *Angew. Chem. Int. Ed. Engl.* **1989**, *28*, 315–316; b) G. Fritz, T. Vaahs, H. Fleischer, E. Matern, *Z. Anorg. Allg. Chem.* **1989**, *570*, 54–66.

[120] F. Zurmühlen, M. Regitz, *Angew. Chem.* **1987**, *99*, 65–67; *Angew. Chem. Int. Ed. Engl.* **1987**, *26*, 83–84.

[121] R. Armbrust, M. Sanchez, R. Reau, U. Bergstraesser, M. Regitz, G. Bertrand, *J. Am. Chem. Soc.* **1995**, *117*, 10785–10786.

[122] M. Sanchez, R. Réau, C. J. Marsden, M. Regitz, G. Bertrand, *Chem. Eur. J.* **1999**, *5*, 274–279.

[123] M. Sanchez, R. Réau, F. Dahan, M. Regitz, G. Bertrand, *Angew. Chem.* **1996**, *108*, 2386–2388; *Angew. Chem. Int. Ed. Engl.* **1996**, *35*, 2228–2230.

[124] M. Sanchez, R. Réau, H. Gornitzka, F. Dahan, M. Regitz, G. Bertrand, *J. Am. Chem. Soc.* **1997**, *119*, 9720–9728.

[125] B. A. Surgenor, M. Bühl, A. M. Z. Slawin, J. D. Woollins, P. Kilian, *Angew. Chem.* **2012**, *124*, 10297–10300; *Angew. Chem. Int. Ed.* **2012**, *51*, 10150–10153.

[126] P. Le Floch, F. Mathey, *Synlett* **1990**, *1990*, 171–172.

[127] R. C. Smith, S. Shah, J. D. Protasiewicz, *J. Organomet. Chem.* **2002**, *646*, 255–261.

[128] C. C. Cummins, R. R. Schrock, W. M. Davis, *Angew. Chem.* **1993**, *105*, 758–761; *Angew. Chem. Int. Ed. Engl.* **1993**, *32*, 756–759.

[129] P. P. Power, *Angew. Chem.* **1993**, *105*, 893–894; *Angew. Chem. Int. Ed. Engl.* **1993**, *32*, 850–851.

[130] S. Shah, M. C. Simpson, R. C. Smith, J. D. Protasiewicz, *J. Am. Chem. Soc.* **2001**, *123*, 6925–6926.

[131] a) A. I. Arkhypchuk, Y. V. Svyaschenko, A. Orthaber, S. Ott, *Angew. Chem.* **2013**, *125*, 6612–6615; *Angew. Chem. Int. Ed.* **2013**, *52*, 6484–6487; b) A. I. Arkhypchuk, M.-P. Santoni, S. Ott, *Organometallics* **2012**, *31*, 1118–1126.

[132] a) S. Shah, G. P. Yap, J. D. Protasiewicz, *J. Organomet. Chem.* **2000**, *608*, 12–20; b) A. B. Burg, K. K. Joshi, J. F. Nixon, *J. Am. Chem. Soc.* **1966**, *88*, 31–37.

[133] P. Le Floch, A. Marinetti, L. Ricard, F. Mathey, *J. Am. Chem. Soc.* **1990**, *112*, 2407–2410.

[134] A. Marinetti, S. Bauer, L. Ricard, F. Mathey, *Organometallics* **1990**, *9*, 793–798.

[135] B. A. Surgenor, B. A. Chalmers, K. S. Athukorala Arachchige, A. M. Z. Slawin, J. D. Woollins, M. Bühl, P. Kilian, *Inorg. Chem.* **2014**, *53*, 6856–6866.

[136] D. V. Partyka, M. P. Washington, J. B. Updegraff, R. A. Woloszynek, J. D. Protasiewicz, *Angew. Chem.* **2008**, *120*, 7599–7602; *Angew. Chem. Int. Ed.* **2008**, *47*, 7489–7492.

[137] M. Stubenhofer, C. Kuntz, M. Bodensteiner, A. Y. Timoshkin, M. Scheer, *Organometallics* **2013**, *32*, 3521–3528.

[138] M. Scheer, C. Kuntz, M. Stubenhofer, M. Zabel, A. Y. Timoshkin, *Angew. Chem.* **2010**, *122*, 192–196; *Angew. Chem. Int. Ed.* **2010**, *49*, 188–192.

[139] a) B. T. Sterenberg, K. A. Udachin, A. J. Carty, *Organometallics* **2001**, *20*, 4463–4465; b) B. T. Sterenberg, O. S. Senturk, K. A. Udachin, A. J. Carty, *Organometallics* **2007**, *26*, 925–937; c) T. W. Graham, R. P.-Y. Cariou, J. Sánchez-Nieves, A. E. Allen, K. A. Udachin, R. Regragui, A. J. Carty, *Organometallics* **2005**, *24*, 2023–2026.

[140] K. Dimroth, P. Hoffmann, *Angew. Chem.* **1964**, *76*, 433; *Angew. Chem. Int. Ed.* **1964**, *3*, 384.

[141] K. Dimroth, P. Hoffmann, *Chem. Ber.* **1966**, *99*, 1325–1331.

[142] a) R. Allmann, *Angew. Chem.* **1965**, *77*, 134; *Angew. Chem. Int. Ed.* **1965**, *4*, 150–151; b) R. Allmann, *Chem. Ber.* **1966**, *99*, 1332–1340.

[143] M. G. Thomas, C. W. Schultz, R. W. Parry, *Inorg. Chem.* **1977**, *16*, 994–1001.

[144] S. Fleming, M. K. Lupton, K. Jekot, *Inorg. Chem.* **1972**, *11*, 2534–2540.

[145] B. E. Maryanoff, R. O. Hutchins, *J. Org. Chem.* **1972**, *37*, 3475–3480.

[146] A. H. Cowley, M. C. Cushner, J. S. Szobota, *J. Am. Chem. Soc.* **1978**, *100*, 7784–7786.

[147] J. Luber, A. Schmidpeter, *Angew. Chem.* **1976**, *88*, 91–92; *Angew. Chem. Int. Ed. Engl.* **1976**, *15*, 111–112.

[148] P. Friedrich, G. Huttner, J. Luber, A. Schmidpeter, *Chem. Ber.* **1978**, *111*, 1558–1563.

[149] E. Niecke, R. Kröher, *Angew. Chem.* **1976**, *88*, 758–759; *Angew. Chem. Int. Ed. Engl.* **1976**, *15*, 692–693.

[150] S. Pohl, *Chem. Ber.* **1979**, *112*, 3159–3165.

[151] I. A. Litvinov, V. A. Naumov, T. V. Griaznova, A. N. Pudovik, A. M. Kibardin, *Dokl. Akad. Nauk SSSR* **1990**, *312*, 623–625.

[152] M. K. Denk, S. Gupta, A. J. Lough, *Eur. J. Inorg. Chem.* **1999**, *1999*, 41–49.

[153] D. Gudat, A. Haghverdi, H. Hupfer, M. Nieger, *Chem. Eur. J.* **2000**, *6*, 3414–3425.

[154] M. Olaru, S. Mebs, J. Beckmann, *Angew. Chem.* **2021**, *133*, 19282–19287; *Angew. Chem. Int. Ed.* **2021**, *60*, 19133–19138.

[155] a) A. H. Cowley, R. A. Kemp, *Chem. Rev.* **1985**, *85*, 367–382; b) M. Yoshifuji, *Sci. Synth.* **2009**, *42*, 63-70.

[156] S. Loss, C. Widauer, H. Grützmacher, *Angew. Chem.* **1999**, *111*, 3546–3548; *Angew. Chem. Int. Ed.* **1999**, *38*, 3329–3331.

[157] N. Burford, P. Losier, S. V. Sereda, T. S. Cameron, G. Wu, *J. Am. Chem. Soc.* **1994**, *116*, 6474–6475.

[158] N. Burford, J. A. C. Clyburne, P. Losier, T. M. Parks, T. S. Cameron, J. F. Richardson, *Phosphorus, Sulfur Silicon Relat. Elem.* **1994**, *93*, 301–304.

[159] N. Burford, J. A. C. Clyburne, P. K. Bakshi, T. S. Cameron, *Organometallics* **1995**, *14*, 1578–1585.

[160] N. Burford, T. S. Cameron, J. A. C. Clyburne, K. Eichele, K. N. Robertson, S. Sereda, R. E. Wasylishen, W. A. Whitla, *Inorg. Chem.* **1996**, *35*, 5460–5467.

[161] N. Burford, P. Losier, P. K. Bakshi, T. S. Cameron, *Chem. Commun.* **1996**, 307–308.

[162] N. Burford, T. S. Cameron, D. J. LeBlanc, P. Losier, S. Sereda, G. Wu, *Organometallics* **1997**, *16*, 4712–4717.

[163] N. Burford, T. Stanley Cameron, K. N. Robertson, A. D. Phillips, H. A. Jenkins, *Chem. Commun.* **2000**, 2087–2088.

[164] N. Burford, T. S. Cameron, P. J. Ragogna, E. Ocando-Mavarez, M. Gee, R. McDonald, R. E. Wasylishen, *J. Am. Chem. Soc.* **2001**, *123*, 7947–7948.

[165] N. Burford, P. J. Ragogna, K. N. Robertson, T. S. Cameron, N. J. Hardman, P. P. Power, *J. Am. Chem. Soc.* **2002**, *124*, 382–383.

[166] N. Burford, P. J. Ragogna, R. McDonald, M. J. Ferguson, *J. Am. Chem. Soc.* **2003**, *125*, 14404–14410.

[167] N. Burford, P. Losier, A. D. Phillips, P. J. Ragogna, T. S. Cameron, *Inorg. Chem.* **2003**, *42*, 1087–1091.

[168] S. S. Chitnis, N. Burford, *Dalton Trans.* **2015**, *44*, 17–29.

[169] L. Rosenberg, *Coord. Chem. Rev.* **2012**, *256*, 606–626.

[170] D. Gudat, A. Haghverdi, M. Nieger, *J. Organomet. Chem.* **2001**, *617-618*, 383–394.

[171] R. W. Parry, J. M. Higashi, *J. Fluorine Chem.* **1995**, *71*, 221–222.

[172] H. Nakazawa, Y. Yamaguchi, T. Mizuta, S. Ichimura, K. Miyoshi, *Organometallics* **1995**, *14*, 4635–4643.

[173] Y. Yamaguchi, H. Nakazawa, M. Kishishita, K. Miyoshi, *Organometallics* **1996**, *15*, 4383–4388.

[174] J. Andrieu, M. Azouri, P. Richard, *Inorganic Chemistry Communications* **2008**, *11*, 1401–1404.

[175] S. Saleh, E. Fayad, M. Azouri, J.-C. Hierso, J. Andrieu, M. Picquet, *Adv. Synth. Catal.* **2009**, *351*, 1621–1628.

[176] A. Kozma, T. Deden, J. Carreras, C. Wille, J. Petuškova, J. Rust, M. Alcarazo, *Chem. Eur. J.* **2014**, *20*, 2208–2214.

[177] P. Ai, C. Gourlaouen, A. A. Danopoulos, P. Braunstein, *Inorg. Chem.* **2016**, *55*, 1219–1229.

[178] A. E. R. Watson, M. J. Grant, P. D. Boyle, P. J. Ragogna, J. B. Gilroy, *Inorg. Chem.* **2022**, *61*, 18719–18728.

[179] N. Tokitoh, H. Suzuki, N. Takeda, T. Kajiwara, T. Sasamori, R. Okazaki, *Silicon Chem.* **2002**, *1*, 313–319.

[180] N. Takeda, H. Suzuki, N. Tokitoh, R. Okazaki, S. Nagase, *J. Am. Chem. Soc.* **1997**, *119*, 1456–1457.

[181] N. Takeda, T. Kajiwara, N. Tokitoh, *Chem. Lett.* **2001**, *30*, 1076–1077.

[182] a) M. Weidenbruch, B. Brand-Roth, S. Pohl, W. Saak, *Angew. Chem.* **1990**, *102*, 93–95; *Angew. Chem. Int. Ed. Engl.* **1990**, *29*, 90–92; b) M. Weidenbruch, B. Brand-Roth, S. Pohl, W. Saak, *Polyhedron* **1991**, *10*, 1147–1152.

[183] N. Takeda, T. Kajiwara, H. Suzuki, R. Okazaki, N. Tokitoh, *Chem. Eur. J.* **2003**, *9*, 3530–3543.

[184] T. Abe, T. Iwamoto, C. Kabuto, M. Kira, *J. Am. Chem. Soc.* **2006**, *128*, 4228–4229.

[185] S. Karwasara, L. R. Maurer, B. Peerless, G. Schnakenburg, U. Das, A. C. Filippou, *J. Am. Chem. Soc.* **2021**, *143*, 14780–14794.

[186] A. Jana, V. Huch, H. S. Rzepa, D. Scheschkewitz, *Angew. Chem.* **2015**, *127*, 291–295; *Angew. Chem. Int. Ed.* **2015**, *54*, 289–292.

[187] a) C. A. Arrington, J. T. Petty, S. E. Payne, W. C. Haskins, *J. Am. Chem. Soc.* **1988**, *110*, 6240–6241; b) M. A. Pearsall, R. West, *J. Am. Chem. Soc.* **1988**, *110*, 7228–7229; c) G. Maier, H. P. Reisenauer, H. Egenolf, *Organometallics* **1999**, *18*, 2155–2161; d) H. Bornemann, W. Sander, *J. Organomet. Chem.* **2002**, *641*, 156–164.

[188] N. Tokitoh, Y. Mizuhata, T. Sato, *Heterocycles* **2012**, *84*, 413–418.

[189] R. Holzner, D. Reiter, P. Frisch, S. Inoue, *RSC Adv.* **2020**, *10*, 3402–3406.

[190] A. Werner, *Z. Anorg. Allg. Chem.* **1893**, *3*, 267–330.

[191] R. H. Crabtree, *The organometallic chemistry of the transition metals*, Wiley, Hoboken, NJ, **2019**.

[192] a) L. Vaska, J. W. DiLuzio, *J. Am. Chem. Soc.* **1961**, *83*, 2784–2785; b) J. P. Collman, W. R. Roper, *J. Am. Chem. Soc.* **1965**, *87*, 4008–4009; c) J. P. Collman, *Acc. Chem. Res.* **1968**, *1*, 136–143; d) J. F. Hartwig, F. Paul, *J. Am. Chem. Soc.* **1995**, *117*, 5373–5374; e) J. A. Labinger, *Organometallics* **2015**, *34*, 4784–4795.

[193] P. M. Treichel, *Adv. Organomet. Chem.* **1973**, *11*, 21–86.

[194] E. Singleton, H. E. Oosthuizen, *Adv. Organomet. Chem.* **1983**, *22*, 209–310.

[195] F. P. Pruchnik, S. A. Duraj in *Organometallic Chemistry of the Transition Elements* (Eds.: F. P. Pruchnik, S. A. Duraj), Springer, Boston, **1990**, pp. 617–645.

[196] J. P. Collman, L. S. Hegedus, J. R. Norton, R. G. Finke, *Principles and Applications of Organotransition Metal Chemistry,* Vol. 2, University Science Books, Mill Valley, Calif., **1987**.

[197] a) W. A. LaRue, A. T. Liu, J. San Filippo, *Inorg. Chem.* **1980**, *19*, 315–320; b) W. S. Mialki, R. E. Wild, R. A. Walton, *Inorg. Chem.* **1981**, *20*, 1380–1384; c) P. Brant, F. A. Cotton, J. C. Sekutowski, T. E. Wood, R. A. Walton, *J. Am. Chem. Soc.* **1979**, *101*, 6588–6593; d) G. S. Girolami, R. A. Andersen, *J. Organomet. Chem.* **1979**, *182*, C43-C45; e) D. D. Klendworth, W. W. Welters, R. A. Walton, *Organometallics* **1982**, *1*, 336–343.

[198] W. S. Mialki, D. E. Wigley, T. E. Wood, R. A. Walton, *Inorg. Chem.* **1982**, *21*, 480–485.

[199] A. J. L. Pombeiro, R. L. Richards, *Rev. Port. Quim.* **1979**, *21*, 132–138.

[200] G. A. Minghetti, A. L. Bandini, G. Banditelli, F. Bonati, *J. Organomet. Chem.* **1979**, *179*, C13-C15.

[201] a) V. W. Day, R. O. Day, J. S. Kristoff, F. J. Hirsekorn, E. L. Muetterties, *J. Am. Chem. Soc.* **1975**, *97*, 2571–2573; b) L. S. Benner, M. M. Olmstead, A. L. Balch, *J. Organomet. Chem.* **1978**, *159*, 289–298; c) R. D. Adams, D. A. Katahira, L. W. Yang, *Organometallics* **1982**, *1*, 231–235.

[202] a) H. B. Gray, K. R. Mann, N. S. Lewis, J. A. Thich, R. M. Richman, *Adv. Chem.* **1978**, *168*, 44–56; b) K. R. Mann, H. B. Gray, G. S. Hammond, *J. Am. Chem. Soc.* **1977**, *99*, 306–307.

[203] a) P. M. Treichel, G. E. Dirreen, *J. Organomet. Chem.* **1972**, *39*, C20-C22; b) P. M. Treichel, G. E. Dirreen, H. J. Mueh, *J. Organomet. Chem.* **1972**, *44*, 339–352; c) K. R. Mann, J. A. Thich, R. A. Bell, C. L. Coyle, H. B. Gray, *Inorg. Chem.* **1980**, *19*, 2462–2468.

[204] J. A. S. Howell, A. J. Rowan, *J. Chem. Soc., Dalton Trans.* **1981**, 297–301.

[205] E. de Boer, J. H. Teuben, *J. Organomet. Chem.* **1979**, *166*, 193–198.

[206] a) E. M. Badley, J. Chatt, R. L. Richards, G. A. Sim, *J. Chem. Soc. D* **1969**, 1322–1323; b) W. M. Butler, J. H. Enemark, *Inorg. Chem.* **1973**, *12*, 540–544; c) D. J. Doonan, A. L. Balch, *J. Am. Chem. Soc.* **1973**, *95*, 4769–4771.

[207] L. Calligaro, P. Uguagliati, B. Crociani, U. Belluco, *J. Organomet. Chem.* **1975**, *92*, 399–408.

[208] M. L. Kuznetsov, V. Y. Kukushkin, *Molecules* **2017**, *22*, 1141.

[209] F. E. Hahn, M. Tamm, *J. Chem. Soc., Chem. Commun.* **1993**, 842–844.

[210] a) P. Brant, J. H. Enemark, A. L. Balch, *J. Organomet. Chem.* **1976**, *114*, 99–106; b) G. M. Bancroft, P. L. Sears, *Inorg. Chem.* **1975**, *14*, 2716–2720.

[211] a) S. O. Grim, D. A. Wheatland, W. McFarlane, *J. Am. Chem. Soc.* **1967**, *89*, 5573–5577; b) U. Kunze, S. Budhi Sastrawan, *Chem. Ber.* **1979**, *112*, 3149–3158; c) D. H. Harris, M. F. Lappert, J. S. Poland, W. McFarlane, *J. Chem. Soc., Dalton Trans.* **1975**, 311–316.

[212] H. Quast, S. Aldenkortt, B. Freudenreich, P. Schäfer, M. Hagedorn, J. Lehmann, K. Banert, *J. Org. Chem.* **2007**, *72*, 1659–1666.

[213] D. Becker, *Master thesis*, University of Bonn, Bonn, **2018**.

[214] F. H. Allen, O. Kennard, D. G. Watson, L. Brammer, A. G. Orpen, R. Taylor, *J. Chem. Soc., Perkin Trans. 2* **1987**, S1–S19.

[215] a) E. D. Glendening, F. Weinhold, *J. Comput. Chem.* **1998**, *19*, 610–627; b) E. D. Glendening, J. K. Badenhoop, F. Weinhold, *J. Comput. Chem.* **1998**, *19*, 628–646.

[216] D. Biskup, G. Schnakenburg, R. Boeré, A. Espinosa Ferao, R. K. Streubel, *manuscript in preparation*.

[217] A. Espinosa Ferao, A. García Alcaraz, *New J. Chem.* **2020**, *44*, 8763–8770.

[218] G. S. Reddy, R. T. Hobgood, J. H. Goldstein, *J. Am. Chem. Soc.* **1962**, *84*, 336–340.

[219] I. I. Schuster, J. D. Roberts, *J. Org. Chem.* **1979**, *44*, 3864–3867.

[220] R. Kleinmaier, S. Arenz, A. Karim, A.-C. C. Carlsson, M. Erdélyi, *Magn. Reson. Chem.* **2013**, *51*, 46–53.

[221] a) L. Pazderski, *Magn. Reson. Chem.* **2008**, *46*, S3–S15; b) N. Juranic, R. L. Lichter, *J. Am. Chem. Soc.* **1983**, *105*, 406–410.

[222] B. M. Craven, R. K. McMullan, J. D. Bell, H. C. Freeman, *Acta Crystallogr., Sect. B: Struct. Crystallogr. Cryst. Chem.* **1977**, *33*, 2585–2589.

[223] U. Ohms, H. Guth, *Z. Kristallogr. - Cryst. Mater.* **1984**, *166*, 213–218.

[224] R. Streubel, A. Schmer, A. W. Kyri, G. Schnakenburg, *Organometallics* **2017**, *36*, 1488–1495.

[225] A. Marinetti, F. Mathey, *Angew. Chem.* **1988**, *100*, 1435–1437; *Angew. Chem. Int. Ed. Engl.* **1988**, *27*, 1382–1384.

[226] A. Sarbajna, V. S. V. S. N. Swamy, V. H. Gessner, *Chem. Sci.* **2020**, *12*, 2016–2024.

[227] W. Nernst, *Zeitschrift für Physikalische Chemie* **1889**, *4U*, 129–181.

[228] P. Zanello, F. F. de Biani, C. Nervi, *Inorganic electrochemistry*. *Theory, practice and application,* Vol. 2, RSC The Royal Soc. of Chemistry, Cambridge, **2012**.

[229] a) J.-M. Savéant, *Elements of molecular and biomolecular electrochemistry*. *An electrochemical approach to electron transfer chemistry*, Wiley-Interscience, Hoboken, NJ, **2006**; b) W. Schmickler, *Grundlagen der Elektrochemie*, Vieweg, Braunschweig, Wiesbaden, **1996**.

[230] N. Elgrishi, K. J. Rountree, B. D. McCarthy, E. S. Rountree, T. T. Eisenhart, J. L. Dempsey, *J. Chem. Educ.* **2018**, *95*, 197–206.

[231] A. J. Bard, L. R. Faulkner, *Electrochemical methods*. *Fundamentals and applications,* Vol. 2, Wiley, New York, Weinheim, **2001**.

[232] a) A. Ševčík, *Collect. Czech. Chem. Commun.* **1948**, *13*, 349–377; b) J. E. B. Randles, *Trans. Faraday Soc.* **1948**, *44*, 327–338.

[233] G. Huttner, K. Knoll, *Angew. Chem.* **1987**, *99*, 765–783; *Angew. Chem. Int. Ed. Engl.* **1987**, *26*, 743–760.

[234] a) G. David, V. von der Gönna, E. Niecke, T. Busch, W. W. Schoeller, P. Rademacher, *J. Chem. Soc., Faraday Trans.* **1994**, *90*, 2611–2616; b) E. Niecke, D. Gudat, *Angew. Chem.* **1991**, *103*, 251–270; *Angew. Chem. Int. Ed. Engl.* **1991**, *30*, 217–237.

[235] D. B. Chesnut, L. D. Quin, K. D. Moore, *J. Am. Chem. Soc.* **1993**, *115*, 11984–11990.

[236] L. Weber, *Coord. Chem. Rev.* **2005**, *249*, 741–763.

[237] A. Orthaber, R. Pietschnig, *Phosphorus, Sulfur Silicon Relat. Elem.* **2013**, *188*, 128–131.

[238] a) A. H. Cowley, J. E. Kilduff, J. G. Lasch, S. K. Mehrotra, N. C. Norman, M. Pakulski, B. R. Whittlesey, J. L. Atwood, W. E. Hunter, *Inorg. Chem.* **1984**, *23*, 2582–2593; b) A. H. Cowley, N. C. Norman, *Prog. Inorg. Chem.* **1986**, *34*, 1–63.

[239] L. Weber, *Chem. Rev.* **1992**, *92*, 1839–1906.

[240] K. A. Schugart, R. F. Fenske, *J. Am. Chem. Soc.* **1985**, *107*, 3384–3385.

[241] a) J. T. Jaeger, J. S. Field, D. Collison, G. P. Speck, B. M. Peake, J. Haehnle, H. Vahrenkamp, *Organometallics* **1988**, *7*, 1753–1760; b) K. Eichele, R. E. Wasylishen, J. F. Corrigan, N. J. Taylor, A. J. Carty, *J. Am. Chem. Soc.* **1995**, *117*, 6961–6969.

[242] O. Kühl, *Phosphorus-31 NMR Spectroscopy*, Springer, Berlin, Heidelberg, **2009**.

[243] V. Plack, J. R. Goerlich, A. Fischer, R. Schmutzler, *Z. Anorg. Allg. Chem.* **1999**, *625*, 1979–1984.

[244] P. Jutzi, U. Meyer, *J. Organomet. Chem.* **1987**, *333*, C18–C20.

[245] A. H. Cowley, P. C. Knueppel, C. M. Nunn, *Organometallics* **1989**, *8*, 2490–2492.

[246] A. N. Kornev, V. E. Galperin, V. V. Sushev, N. V. Zolotareva, E. V. Baranov, G. K. Fukin, G. A. Abakumov, *Eur. J. Inorg. Chem.* **2016**, *2016*, 3629–3633.

[247] A. R. Fox, R. J. Wright, E. Rivard, P. P. Power, *Angew. Chem.* **2005**, *117*, 7907–7911; *Angew. Chem. Int. Ed.* **2005**, *44*, 7729–7733.

[248] a) R. Riedel, H.-D. Hausen, E. Fluck, *Angew. Chem.* **1985**, *97*, 1050; *Angew. Chem. Int. Ed. Engl.* **1985**, *24*, 1056–1057; b) E. Fluck, R. Riedel, H.-D. Hausen, G. Heckmann, *Z. Anorg. Allg. Chem.* **1987**, *551*, 85–94.

[249] J. E. Borger, A. W. Ehlers, M. Lutz, J. C. Slootweg, K. Lammertsma, *Angew. Chem.* **2016**, *128*, 623–627; *Angew. Chem. Int. Ed.* **2016**, *55*, 613–617.

[250] S. Heinl, S. Reisinger, C. Schwarzmaier, M. Bodensteiner, M. Scheer, *Angew. Chem.* **2014**, *126*, 7769–7773; *Angew. Chem. Int. Ed.* **2014**, *53*, 7639–7642.

[251] a) A. Schisler, P. Lönnecke, T. Gelbrich, E. Hey-Hawkins, *Dalton Trans.* **2004**, 2895–2898; b) M. Baudler, M. Bock, *Z. Anorg. Allg. Chem.* **1973**, *395*, 37–49; c) C. Frenzel, E. Hey-Hawkins, *Phosphorus, Sulfur Silicon Relat. Elem.* **1998**, *143*, 1–17; d) J.-E. Siewert, A. Schumann, C. Hering-Junghans, *Dalton Trans.* **2021**, *50*, 15111–15117; e) C. N. Smit, T. van der Knaap, F. Bickelhaupt, *Tetrahedron Lett.* **1983**, *24*, 2031–2034.

[252] R. Streubel, S. Sauerbrey, M. Nieger, *J. Organomet. Chem.* **2011**, *696*, 2035–2039.

[253] M. Baudler, Y. Aktalay, *Z. Anorg. Allg. Chem.* **1983**, *496*, 29–39.

[254] J. T. Hung, S. W. Yang, G. M. Gray, K. Lammertsma, *J. Org. Chem.* **1993**, *58*, 6786–6790.

[255] J. T. Hung, P. Chand, F. R. Fronczek, S. F. Watkins, K. Lammertsma, *Organometallics* **1993**, *12*, 1401–1405.

[256] K. Lammertsma, J. T. Hung, P. Chand, G. M. Gray, *J. Org. Chem.* **1992**, *57*, 6557–6560.

[257] J. T. Hung, K. Lammertsma, *J. Org. Chem.* **1993**, *58*, 1800–1803.

[258] E. P. A. Couzijn, A. W. Ehlers, J. C. Slootweg, M. Schakel, S. Krill, M. Lutz, A. L. Spek, K. Lammertsma, *Chem. Eur. J.* **2008**, *14*, 1499–1507.

[259] N. H. Tran Huy, S. Hao, L. Ricard, F. Mathey, *Organometallics* **2006**, *25*, 3152–3155.

[260] E. Deschamps, F. Mathey, *J. Organomet. Chem.* **1987**, *332*, 141–152.

[261] Y. Hao, C. Zhang, Y. Mei, R. Tian, Z. Duan, F. Mathey, *Dalton Trans.* **2016**, *45*, 8284–8290.

[262] B. Deschamps, F. Mathey, *J. Chem. Soc., Chem. Commun.* **1985**, 1010–1012.

[263] M. P. Duffy, F. Mathey, *J. Am. Chem. Soc.* **2009**, *131*, 7534–7535.

[264] R. G. Pearson in *Advances in Chemistry* (Eds.: J. M. Harris, S. P. McManus), American Chemical Society, Washington, DC, **1987**, pp. 233–244.

[265] R. E. Dessy, R. L. Pohl, R. B. King, *J. Am. Chem. Soc.* **1966**, *88*, 5121–5124.

[266] M. Besora, A. Lledós, F. Maseras, *Chem. Soc. Rev.* **2009**, *38*, 957–966.

[267] H. Lang, O. Orama, G. Huttner, *J. Organomet. Chem.* **1985**, *291*, 293–309.

[268] P. Jutzi, R. Kroos, *J. Organomet. Chem.* **1990**, *390*, 317–322.

[269] G. Huttner, J. Borm, L. Zsolnai, *J. Organomet. Chem.* **1984**, *263*, C33–C36.

[270] M. E. García, D. García-Vivó, A. Ramos, M. A. Ruiz, *Coord. Chem. Rev.* **2017**, *330*, 1–36.

[271] a) H. Lang, L. Zsolnai, G. Huttner, *Z. Naturforsch. B* **1985**, *40*, 500–506; b) H. Lang, G. Mohr, O. Scheidsteger, G. Huttner, *Chem. Ber.* **1985**, *118*, 574–596.

[272] R. J. Kwaan, C. J. Harlan, J. R. Norton, *Organometallics* **2001**, *20*, 3818–3820.

[273] I. M. Riddlestone, A. Kraft, J. Schaefer, I. Krossing, *Angew. Chem.* **2018**, *130*, 14178–14221; *Angew. Chem. Int. Ed.* **2018**, *57*, 13982–14024.

[274] L. Liu, D. A. Ruiz, F. Dahcheh, G. Bertrand, *Chem. Commun.* **2015**, *51*, 12732–12735.

[275] I. Krossing, A. Reisinger, *Eur. J. Inorg. Chem.* **2005**, *2005*, 1979–1989.

[276] H. Ambrosius, A. van der Linden, J. J. Steggerda, *J. Organomet. Chem.* **1981**, *204*, 211–220.

[277] a) V. Nesterov, R. Baierl, F. Hanusch, A. E. Ferao, S. Inoue, *J. Am. Chem. Soc.* **2019**, *141*, 14576–14580; b) M. W. Stanford, J. I. Schweizer, M. Menche, G. S. Nichol, M. C. Holthausen, M. J. Cowley, *Angew. Chem.* **2019**, *131*, 1343–1347; *Angew. Chem. Int. Ed.* **2019**, *58*, 1329–1333.

[278] K. B. Wiberg, *Tetrahedron* **1968**, *24*, 1083–1096.

[279] D. V. Deubel, *J. Am. Chem. Soc.* **2004**, *126*, 996–997.

[280] P. Erdmann, J. Leitner, J. Schwarz, L. Greb, *ChemPhysChem* **2020**, *21*, 987–994.

[281] a) J. F. Kögel, D. A. Sorokin, A. Khvorost, M. Scott, K. Harms, D. Himmel, I. Krossing, J. Sundermeyer, *Chem. Sci.* **2018**, *9*, 245–253; b) J. C. Haartz, D. H. McDaniel, *J. Am. Chem. Soc.* **1973**, *95*, 8562–8565.

[282] J. M. Slattery, S. Hussein, *Dalton Trans.* **2012**, *41*, 1808–1815.

[283] W. Armarego, *Purification of Laboratory Chemicals,* Vol. 8, Butterworth-Heinemann, Elsevier, Oxford, **2003**.

[284] G. R. Fulmer, A. J. M. Miller, N. H. Sherden, H. E. Gottlieb, A. Nudelman, B. M. Stoltz, J. E. Bercaw, K. I. Goldberg, *Organometallics* **2010**, *29*, 2176–2179.

[285] R. K. Harris, E. D. Becker, S. M. Cabral de Menezes, P. Granger, R. E. Hoffman, K. W. Zilm, *Pure Appl. Chem.* **2008**, *80*, 59–84.

[286] R. K. Harris, E. D. Becker, S. M. Cabral de Menezes, R. Goodfellow, P. Granger, *Pure Appl. Chem.* **2001**, *73*, 1795–1818.

[287] R. H. Blessing, *Acta Crystallogr., Sect. A: Found. Crystallogr.* **1995**, *51*, 33–38.

[288] G. M. Sheldrick, *ShelXS97 and ShelXL97*, University of Göttingen, Germany, **1997**.

[289] O. V. Dolomanov, L. J. Bourhis, R. J. Gildea, J. A. K. Howard, H. Puschmann, *J. Appl. Crystallogr.* **2009**, *42*, 339–341.

[290] R. S. Stojanovic, A. M. Bond, *Anal. Chem.* **1993**, *65*, 56–64.

[291] G. Gritzner, J. Kuta, *Pure Appl. Chem.* **1984**, *56*, 461–466.

[292] W. Strohmeier, G. Matthias, D. von Hobe, *Z. Naturforsch. B* **1960**, *15*, 813–814.

[293] M. Brookhart, B. Grant, A. F. Volpe, *Organometallics* **1992**, *11*, 3920–3922.

[294] U. Koelle, *J. Organomet. Chem.* **1977**, *133*, 53–58.

[295] I. W. Stolz, H. Haas, R. K. Sheline, *J. Am. Chem. Soc.* **1965**, *87*, 716–718.

[296] A. J. Arduengo, H. V. R. Dias, R. L. Harlow, M. Kline, *J. Am. Chem. Soc.* **1992**, *114*, 5530–5534.

[297] B. Edelbach, B. Pharoah, S. Bellows, P. Thayer, C. Fennie, R. Cowley, P. Holland, *Synthesis* **2012**, *44*, 3595–3597.

[298] R. Jazzar, R. D. Dewhurst, J.-B. Bourg, B. Donnadieu, Y. Canac, G. Bertrand, *Angew. Chem.* **2007**, *119*, 2957–2960; *Angew. Chem. Int. Ed.* **2007**, *46*, 2899–2902.

[299] K. Fujiki, M. Kashiwagi, H. Miyamoto, A. Sonoda, J. Ichikawa, H. Kobayashi, T. Sonoda, *J. Fluorine Chem.* **1992**, *57*, 307–321.

[300] V. Plack, J. R. Goerlich, A. Fischer, H. Thnnessen, P. G. Jones, R. Schmutzler, *Z. Anorg. Allg. Chem.* **1995**, *621*, 1080–1092.

[301] M. L. Luetkens, A. P. Sattelberger, H. H. Murray, J. D. Basil, J. P. Fackler, R. A. Jones, D. E. Heaton, *Inorg. Synth.* **1989**, *26*, 7–12.

7 APPENDIX

7.1 ABBREVIATIONS

7.1.1 Chemical Abbreviations

$[BAr^F{}_4]^-$	tetrakis[3,5-bis(trifluoromethyl)phenyl]borate
12-crown-4	1,4,7,10-tetraoxacyclododecane
Ad	adamantly
Ar	aryl
Ar^{Dipp}	2,6-bis(2,6-diisopropylphenyl)phenyl
ATP	adenosine triphosphate
BHT	3,5-di-*tert*-butyl-4-hydroxytoluene
BINAP	bis(diphenylphosphanyl)-1,1'-binaphtyl
Bisyl	bis(trimethylsilyl)methyl
cAAC	cyclic alkyl(amino)carbene
Cp	cyclopentadienyl
Cp*	pentamethylcyclopentadienyl
Cp'''	tri-*tert*-butylcyclopentadienyl
Cp^{4iPr}	tetraisopropylcyclopentadienyl
Cp^{BIG}	penta(4-*n*-butylphenyl)cyclopentadienyl
CPS	*O,O*-diethyl-*O*-(3,5,6-trichloropyridin-2-yl)phosphorothioate
Cy	cyclohexyl
DFP	diisopropylfluorophosphate
DIPAMP	bis[(2-methoxyphenyl)phenylphosphanyl]ethane
Dipp	2,6-diisopropylphenyl
DIPPE	1,2-bis(diisopropylphosphino)ethane
DMAD	dimethylacetylenedicarboxylate
DMAP	4-dimethylaminopyridine
Dmp	2,6-bis(2,4,6-trimethylphenyl)phenyl
DNA	deoxyribonucleic acid
DPPE	(ethane-1,2-diyl)bis(diphenylphosphane)
Et	ethyl

Fc	ferrocenyl
$Fc^{+/0}$	ferrocenium/ferrocene redox couple
GTP	guanosine triphosphate
HMPT	hexamethylphosphoric triamide
IDipp	1,3-bis(2,6-diisopropylphenyl)-imidazol-2-ylidene
Im	imidazole
IMe_4	1,3,4,5-tetramethylimidazol-2-ylidene
IMes	1,3-bis(2,4,6-trimethylphenyl)-imidazol-2-ylidene
^{i}Pr	isopropyl
LDA	lithium diisopropylamide
Me	methyl
Me_2cAAC	1-(2,6-diisopropylphenyl)-3,3,5,5-tetramethylpyrrolidin-2-ylidene
Mes	2,4,6-trimethylphenyl
Mes*	2,4,6-tri-*tert*-butylphenyl
^{n}Bu	*n*-butyl
NHC	*N*-heterocyclic carbene
N-MeIm	*N*-methylimidazole
^{n}Pr	*n*-propyl
OTf	trifluoromethanesulfonate
PFK	perfluorokerosene
Ph	phenyl
Phen	1,10-phenantroline
PTFE	polytetrafluoroethylene
p-Tol	*para*-tolyl
Py	pyridine
Tbt	2,4,6-tris[bis(trimethylsilyl)methyl]phenyl
^{t}Bu	*tert*-butyl
THF	tetrahydrofuran
Tip	2,4,6-triisopropylphenyl
Tol	toluene
Xantphos	(9,9-dimethyl-9*H*-xanthene-4,5-diyl)bis(diphenylphosphane)
Xyl	xylyl

7.1.2 Other Abbreviations

$\nabla^2\rho(r)$	variation of the Laplacian of electron density
Ø	diameter
2D	two-dimensional
Å	Ångström (10^{-10} m)
a, *b*, *c*, α, β, γ	unit cell parameters
A	electrode surface area
a.u.	atomic units
APCI	atmospheric pressure chemical ionization
atm	atmospheric pressure
ATR	attenuated total reflection
BCP	bond critical point
br	broad
c	concentration
C^0	bulk concentration
ca.	circa
calc	calculated
CCSD(T)	coupled cluster single-double and perturbative triple
COSMO	conductor-like screening model
COSY	correlated spectroscopy
CPCM	conductor-like polarized continuum model
CV	cyclic voltammetry
d	doublet (1:1) or bond distance
D_{ox}	diffusion coefficient of the oxidized species
dd	doublet of doublets
ddd	doublet of doublets of doublets
dec.	decomposition
def2-QZVP	valence quadruple-zeta polarization
def2-QZVPP	valence quadruple-zeta with two sets of polarization functions
def2-TZVP	valence triple-zeta polarization
DFT	density-functional theory
dm	doublet of multiplets

Do	donor
dq	doublet of quartets
E_p^a	anodic peak potential
E_p^c	cathodic peak potential
e.g.	*exempli gratia*, “for example”
EA	elemental analysis
ecp	effective core potential
EI	electron impact ionization
eq.	equivalent
ESI	electrospray ionization
et al.	*et alii* / *et aliae*, “and others”
exp	experimental
F(000)	structure factor evaluated in the zeroth order case $h = k = l = 0$
FIA	fluoride ion affinity
FLP	frustrated Lewis pair
FTIR	Fourier-transform infrared
ge-NMR	gradient enhanced nuclear magnetic resonance
h	hour or height
HMQC	heteronuclear multiple quantum correlation
HOMO	highest occupied molecular orbital
HPLC	high-performance liquid chromatography
HRMS	high resolution mass spectrometry
HSQC	heteronuclear single quantum coherence
i_p^a	anodic peak current
i_p^c	cathodic peak current
i.e.	*id est*, “it is”
IUPAC	International Union of Pure and Applied Chemistry
IR	infrared
irrev	irreversible
L	ligand
LIFDI	liquid injection field desorption
lit.	literature

LUMO	lowest unoccupied molecular orbital
m	*meta*
$[M]^{+\cdot}$	molecular ion
m	multiplet or medium
M	metal or molar
max.	maximum
MBO	Mayer bond order
min.	minimum
MS	mass spectrometry
neg.	negative
$^{n}J_{X,Y}$	coupling constant
NMR	nuclear magnetic resonance
NOESY	nuclear Overhauser effect spectroscopy
NRT	natural resonance theory
o	*ortho*
p	*para*
pos.	positive
ppm	parts per million
q	quartet (1:3:3:1)
q*	quartet (1:1:1:1)
qd	quartet of doublets
qq*	quartet (1:3:3:1) of quartets (1:1:1:1)
QTAIM	quantum theory of atoms in molecules
R	organic substituent
R^2	coefficient of determination
r.t.	room temperature
rev	reversible
s	singlet or strong
sat	satellites
sept	septet
sept d	septet of doublets
SET	single electron transfer

SPS	solvent purification system
t	triplet (1:2:1)
T	temperature
TOP	thermodynamic oxygen-transfer potential
UV	ultraviolet
V	volume
vis	visible
vs	very strong
vs.	versus
VSCC	valence shell charge concentration
VT	variable temperature
w	weak
WBI	Wiberg bond index
Z	number of formula units in unit cell
δ	chemical shift
Δ	thermal energy or difference
ΔE_p	peak-to-peak potential
Δq^{nat}	electron transfer
ε	redox orbital energy
η^n	hapticity
Θ	Bragg angle
λ^m	number *m* of all bonds
μ	attenuation coefficient
ν	scan rate
$\tilde{\nu}$	wavenumber
Ξ	frequency ratio
ρ	density
σ^n	number *n* of σ-bonds
τ_{VSCC}	relative charge concentration bands position parameter
Φ	volume fraction
Φ_0	equilibrium potential
Φ_{00}	standard equilibrium potential

7.2 CRYSTAL DATA AND STRUCTURE REFINEMENTS

7.2.1 [Pentacarbonyl{(*tert*-butylazaniumylidyne)methyl(triphenylmethyl)phosphanido-κ*P*}chromium(0)] (6a)

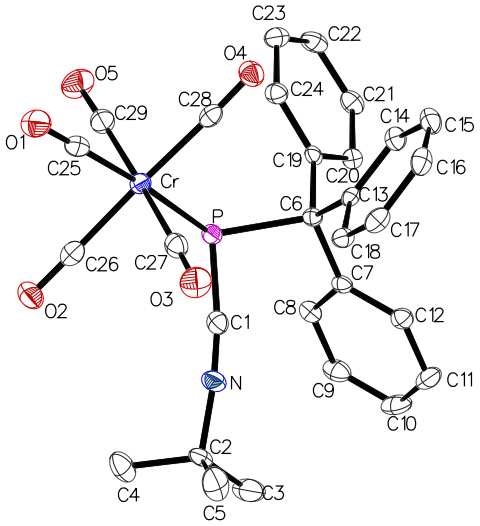

Figure 84: Molecular structures of **6a** in the single crystal lattice at 100(2) K. Thermal ellipsoids are set at 50 % probability level. Hydrogen atoms were omitted for clarity.

Table 25: Crystal data and structure refinements for **6a**.

Identification code	GSTR649, DB-83 // GXray5842f
Crystal habitus	yellow plate
Device type	Bruker X8-KappaApexII
Empirical formula	$C_{29}H_{24}NO_5PCr$
Moiety formula	$C_{29}H_{24}CrNO_5P$
Formula weight / g/mol	549.46
T / K	100
Crystal system	Monoclinic
Space group	$P2_1/n$
a / Å	13.1380(11)
b / Å	13.1116(11)
c / Å	15.6049(13)
α / °	90
β / °	90.806(3)
γ / °	90
V / Å^3	2687.8(4)
Z	4
ρ_{calc} / g/cm^3	1.358
μ / mm^{-1}	0.524
F(000)	1136.0

Crystal size / mm^3	0.26 × 0.24 × 0.04
Absorption correction	Empirical
Min. and max. transmission	0.6541 and 0.7462
Radiation	Mo-K_α (λ = 0.71073 Å)
2Θ range for data collection / °	5.084 to 55.99
Completeness to Θ	0.998
Index ranges	$-17 \leq h \leq 17$, $-17 \leq k \leq 17$, $-20 \leq l \leq 20$
Reflections collected	44084
Independent reflections	6480 (R_{int} = 0.0956, R_σ = 0.0631)
Data / restraints / parameters	6480 / 0 / 337
Goodness-of-fit on F^2	1.016
Final R indexes ($I \geq 2\sigma(I)$)	R_1 = 0.0399, ωR_2 = 0.0809
Final R indexes (all data)	R_1 = 0.0760, ωR_2 = 0.0947
Largest diff. peak and hole / e/Å^3	0.35 and −0.51

Table 26: Bond lengths for **6a**.

Atom	Atom	Length / Å	Atom	Atom	Length / Å
Cr	P	2.4656(7)	C6	C19	1.547(3)
Cr	C25	1.851(2)	C7	C8	1.402(3)
Cr	C26	1.903(2)	C7	C12	1.393(3)
Cr	C27	1.906(2)	C8	C9	1.376(3)
Cr	C28	1.908(2)	C9	C10	1.394(3)
Cr	C29	1.909(2)	C10	C11	1.380(3)
P	C1	1.750(2)	C11	C12	1.392(3)
P	C6	1.954(2)	C13	C14	1.395(3)
O1	C25	1.157(3)	C13	C18	1.398(3)
O2	C26	1.147(3)	C14	C15	1.396(3)
O3	C27	1.145(3)	C15	C16	1.384(3)
O4	C28	1.146(3)	C16	C17	1.389(3)
O5	C29	1.142(3)	C17	C18	1.388(3)
N	C1	1.156(3)	C19	C20	1.394(3)
N	C2	1.464(3)	C19	C24	1.394(3)
C2	C3	1.518(3)	C20	C21	1.396(3)
C2	C4	1.525(3)	C21	C22	1.378(3)
C2	C5	1.522(3)	C22	C23	1.388(3)
C6	C7	1.531(3)	C23	C24	1.382(3)
C6	C13	1.536(3)			

Table 27: Bond angles for **6a**.

Atom	Atom	Atom	Angle / °	Atom	Atom	Atom	Angle /°
C25	Cr	P	172.61(8)	C19	C6	P	103.69(13)
C25	Cr	C26	89.05(10)	C8	C7	C6	119.51(18)
C25	Cr	C27	90.22(10)	C12	C7	C6	122.67(19)
C25	Cr	C28	92.19(10)	C12	C7	C8	117.76(19)
C25	Cr	C29	88.66(10)	C9	C8	C7	121.5(2)
C26	Cr	P	85.55(7)	C8	C9	C10	120.2(2)
C26	Cr	C27	88.76(10)	C11	C10	C9	119.1(2)
C26	Cr	C28	178.10(9)	C10	C11	C12	120.7(2)
C26	Cr	C29	90.52(10)	C11	C12	C7	120.7(2)
C27	Cr	P	94.70(7)	C14	C13	C6	121.50(18)
C27	Cr	C28	89.81(10)	C14	C13	C18	117.64(19)
C27	Cr	C29	178.67(10)	C18	C13	C6	120.84(18)
C28	Cr	P	93.33(7)	C13	C14	C15	121.2(2)
C28	Cr	C29	90.94(10)	C16	C15	C14	120.2(2)
C29	Cr	P	86.35(7)	C15	C16	C17	119.4(2)
C1	P	Cr	101.57(8)	C18	C17	C16	120.3(2)
C1	P	C6	98.18(10)	C17	C18	C13	121.3(2)
C6	P	Cr	125.45(7)	C20	C19	C6	121.84(18)
C1	N	C2	163.7(2)	C20	C19	C24	117.80(19)
N	C1	P	173.0(2)	C24	C19	C6	120.35(18)
N	C2	C3	106.83(18)	C19	C20	C21	120.8(2)
N	C2	C4	106.02(18)	C22	C21	C20	120.5(2)
N	C2	C5	108.23(19)	C21	C22	C23	119.1(2)
C3	C2	C4	112.7(2)	C24	C23	C22	120.5(2)
C3	C2	C5	112.8(2)	C23	C24	C19	121.3(2)
C5	C2	C4	109.90(19)	O1	C25	Cr	178.2(2)
C7	C6	P	106.32(13)	O2	C26	Cr	178.2(2)
C7	C6	C13	112.70(17)	O3	C27	Cr	177.6(2)
C7	C6	C19	110.66(17)	O4	C28	Cr	177.49(19)
C13	C6	P	111.96(14)	O5	C29	Cr	177.6(2)
C13	C6	C19	111.07(16)				

7.2.2 [Pentacarbonyl{1-methylimidazol-3-iumyl(triphenylmethyl)phosphanido-κ*P*}-chromium(0)] (13a)

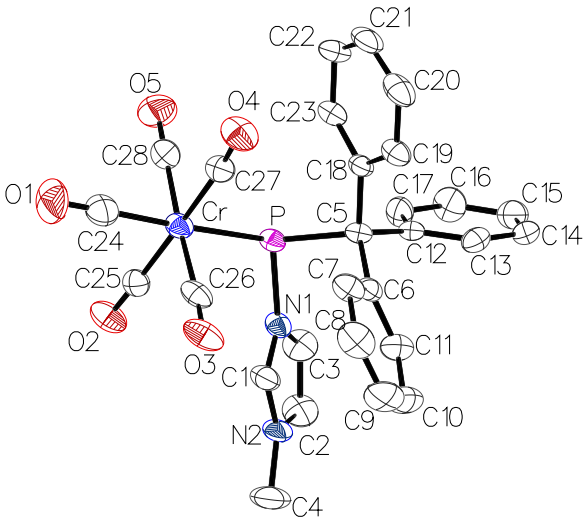

Figure 85: Molecular structures of **13a** in the single crystal lattice at 180(2) K. Thermal ellipsoids are set at 50 % probability level. Hydrogen atoms and solvent molecules were omitted for clarity.

Table 28: Crystal data and structure refinements for **13a**.

Identification code	GSTR730, DB-373 // GXray6654
Crystal habitus	clear yellow block
Device type	STOE IPDS-2T
Empirical formula	$C_{37}H_{30}CrN_2O_5P$
Moiety formula	$C_{28}H_{21}CrN_2O_5P$, 1.5 (C_6H_6)
Formula weight / g/mol	665.60
T / K	180
Crystal system	triclinic
Space group	$P\bar{1}$
a / Å	10.0539(7)
b / Å	11.6733(9)
c / Å	14.6554(10)
α / °	90.504(6)
β / °	100.483(5)
γ / °	94.922(6)
V / Å^3	1684.5
Z	2
ρ_{calc} / g/cm^3	1.312
μ / mm^{-1}	0.432
F(000)	690.0
Crystal size / mm^3	0.35 × 0.15 × 0.15
Absorption correction	integration
Min. and max. transmission	0.7056 and 0.9405

Radiation	Mo-K_α (λ = 0.71073 Å)
2Θ range for data collection / °	5.422 to 56
Completeness to Θ	0.982
Index ranges	$-13 \le h \le 13$, $-15 \le k \le 15$, $-18 \le l \le 19$
Reflections collected	14869
Independent reflections	7987 (R_{int} = 0.0638, R_σ = 0.2033)
Data / restraints / parameters	7987 / 0 / 404
Goodness-of-fit on F^2	0.635
Final R indexes ($I \ge 2\sigma(I)$)	R_1 = 0.0398, ωR_2 = 0.0599
Final R indexes (all data)	R_1 = 0.1225, ωR_2 = 0.0691
Largest diff. peak and hole / e/Å^3	0.34 and −0.26

Table 29: Bond lengths for **13a**.

Atom	Atom	Length / Å	Atom	Atom	Length / Å
Cr	P	2.4580(8)	C8	C9	1.376(4)
Cr	C24	1.832(3)	C9	C10	1.376(4)
Cr	C25	1.882(3)	C10	C11	1.386(4)
Cr	C26	1.891(3)	C12	C13	1.386(3)
Cr	C27	1.904(3)	C12	C17	1.385(3)
Cr	C28	1.894(3)	C13	C14	1.383(3)
P	N1	1.817(2)	C14	C15	1.380(4)
P	C5	1.946(2)	C15	C16	1.370(3)
O1	C24	1.172(3)	C16	C17	1.385(3)
O2	C25	1.140(3)	C18	C19	1.389(3)
O3	C26	1.147(3)	C18	C23	1.397(4)
O4	C27	1.146(3)	C19	C20	1.395(4)
O5	C28	1.138(3)	C20	C21	1.379(4)
N1	C1	1.330(3)	C21	C22	1.378(4)
N1	C3	1.370(3)	C22	C23	1.389(3)
N2	C1	1.338(3)	C29	C34	1.3900
N2	C2	1.357(3)	C29	C30	1.3900
N2	C4	1.466(3)	C34	C33	1.3900
C2	C3	1.350(4)	C33	C32	1.3900
C5	C6	1.537(3)	C32	C31	1.3900
C5	C12	1.544(3)	C31	C30	1.3900
C5	C18	1.531(3)	C35	C36	1.363(6)
C6	C7	1.395(3)	C35	C37[a]	1.348(6)
C6	C11	1.398(3)	C36	C37	1.356(6)
C7	C8	1.373(4)			

[a] 2–X,2–Y,2–Z

Table 30: Bond angles for **13a**.

Atom	Atom	Atom	Angle / °	Atom	Atom	Atom	Angle / °
C24	Cr	P	169.18(10)	C8	C7	C6	121.5(3)
C24	Cr	C25	88.76(11)	C7	C8	C9	120.8(3)
C24	Cr	C26	90.53(13)	C10	C9	C8	119.2(3)
C24	Cr	C27	89.11(12)	C9	C10	C11	120.3(3)
C24	Cr	C28	90.33(13)	C10	C11	C6	121.3(3)
C25	Cr	P	85.15(8)	C13	C12	C5	119.1(2)
C25	Cr	C26	90.77(11)	C17	C12	C5	123.4(2)
C25	Cr	C27	177.54(12)	C17	C12	C13	116.9(2)
C25	Cr	C28	92.45(12)	C14	C13	C12	122.0(3)
C26	Cr	P	98.47(8)	C15	C14	C13	119.8(3)
C26	Cr	C27	88.04(11)	C16	C15	C14	119.1(3)
C26	Cr	C28	176.69(12)	C15	C16	C17	120.7(3)
C27	Cr	P	97.15(8)	C12	C17	C16	121.4(2)
C28	Cr	P	81.03(9)	C19	C18	C5	122.9(2)
C28	Cr	C27	88.78(12)	C19	C18	C23	117.3(2)
N1	P	Cr	109.27(7)	C23	C18	C5	119.5(2)
N1	P	C5	96.87(9)	C18	C19	C20	121.2(3)
C5	P	Cr	117.84(8)	C21	C20	C19	120.1(3)
C1	N1	P	129.51(18)	C22	C21	C20	119.9(3)
C1	N1	C3	107.0(2)	C21	C22	C23	119.6(3)
C3	N1	P	123.46(19)	C22	C23	C18	121.7(3)
C1	N2	C2	107.9(2)	O1	C24	Cr	179.0(3)
C1	N2	C4	125.7(3)	O2	C25	Cr	178.0(2)
C2	N2	C4	126.3(2)	O3	C26	Cr	175.6(3)
N1	C1	N2	109.6(2)	O4	C27	Cr	173.9(2)
C3	C2	N2	107.3(2)	O5	C28	Cr	179.7(3)
C2	C3	N1	108.1(3)	C34	C29	C30	120.0
C6	C5	P	108.83(14)	C29	C34	C33	120.0
C6	C5	C12	111.5(2)	C32	C33	C34	120.0
C12	C5	P	111.82(16)	C33	C32	C31	120.0
C18	C5	P	105.45(16)	C32	C31	C30	120.0
C18	C5	C6	114.8(2)	C31	C30	C29	120.0
C18	C5	C12	104.32(18)	C37[a]	C35	C36	121.2(4)
C7	C6	C5	122.5(2)	C37	C36	C35	118.6(5)
C7	C6	C11	116.9(2)	C35[a]	C37	C36	120.3(5)
C11	C6	C5	120.4(2)				

[a] 2–X,2–Y,2–Z

7.2.3 [Pentacarbonyl{1-methylimidazol-3-iumyl(triphenylmethyl)phosphanido-κ*P*}-tungsten(0)] (13b)

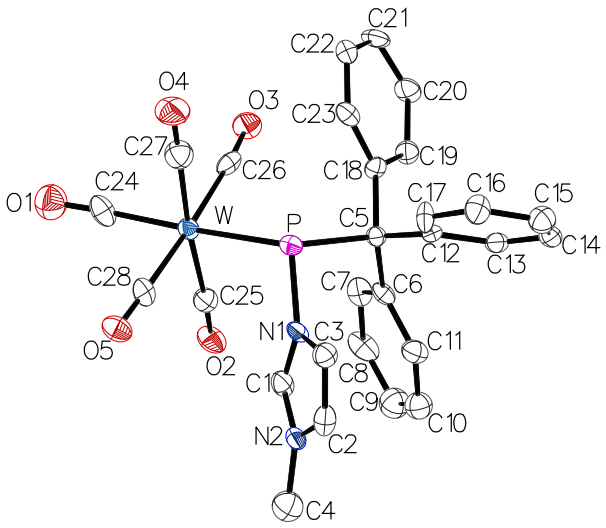

Figure 86: Molecular structures of **13b** in the single crystal lattice at 123(2) K. Thermal ellipsoids are set at 50 % probability level. Hydrogen atoms and solvent molecules were omitted for clarity.

Table 31: Crystal data and structure refinements for **13b**.

Identification code	GSTR723, DB-362 // 6613
Crystal habitus	clear yellow block
Device type	STOE IPDS-2T
Empirical formula	$C_{37}H_{30}N_2O_5PW$
Moiety formula	$C_{28}H_{21}N_2O_5PW$, 1.5 (C_6H_6)
Formula weight / g/mol	797.45
T / K	123(2)
Crystal system	triclinic
Space group	$P\bar{1}$
a / Å	10.0209(7)
b / Å	11.6994(9)
c / Å	14.8295(11)
α / °	92.666(6)
β / °	101.738(6)
γ / °	94.449(6)
V / Å^3	1693.6(2)
Z	2
ρ_{calc} / g/cm^3	1.564
μ / mm^{-1}	3.502
F(000)	790.0
Crystal size / mm^3	0.15 × 0.12 × 0.08
Absorption correction	integration
Min. and max. transmission	0.1644 and 0.6078

Radiation	Mo-K_α (λ = 0.71073 Å)
2Θ range for data collection / °	5.492 to 55.996
Completeness to Θ	0.989
Index ranges	$-13 \leq h \leq 13$, $-15 \leq k \leq 15$, $-19 \leq l \leq 17$
Reflections collected	17922
Independent reflections	8113 (R_{int} = 0.1668, R_σ = 0.3153)
Data / restraints / parameters	8113 / 86 / 416
Goodness-of-fit on F^2	0.706
Final R indexes ($I \geq 2\sigma(I)$)	R_1 = 0.0633, ωR_2 = 0.1134
Final R indexes (all data)	R_1 = 0.1357, ωR_2 = 0.1327
Largest diff. peak and hole / e/Å^3	2.50 and −2.72

Table 32: Bond lengths for **13b**.

Atom	Atom	Length / Å	Atom	Atom	Length / Å
W	P	2.588(3)	C8	C9	1.390(16)
W	C24	1.969(11)	C9	C10	1.357(17)
W	C25	2.069(12)	C10	C11	1.365(14)
W	C26	2.049(14)	C12	C13	1.402(14)
W	C27	2.006(13)	C12	C17	1.350(16)
W	C28	2.021(13)	C13	C14	1.351(13)
P	N1	1.813(8)	C14	C15	1.409(16)
P	C5	1.946(10)	C15	C16	1.415(16)
O1	C24	1.176(13)	C16	C17	1.386(13)
O2	C25	1.134(12)	C18	C19	1.411(15)
O3	C26	1.151(14)	C18	C23	1.413(14)
O4	C27	1.151(13)	C19	C20	1.363(14)
O5	C28	1.152(14)	C20	C21	1.421(16)
N1	C1	1.304(12)	C21	C22	1.415(17)
N1	C3	1.417(13)	C22	C23	1.354(14)
N2	C1	1.318(13)	C29	C30	1.342(18)
N2	C2	1.379(14)	C29	C34	1.38(2)
N2	C4	1.479(13)	C30	C31	1.309(19)
C2	C3	1.333(14)	C31	C32	1.40(2)
C5	C6	1.529(13)	C32	C33	1.36(2)
C5	C12	1.556(13)	C33	C34	1.34(2)
C5	C18	1.523(13)	C35	C36	1.329(16)
C6	C7	1.406(14)	C35	C37[a]	1.3901(10)
C6	C11	1.397(14)	C36	C37	1.3901(10)
C7	C8	1.380(14)			

[a]−X,−Y,1−Z

Table 33: Bond angles for **13b**.

Atom	Atom	Atom	Angle / °	Atom	Atom	Atom	Angle / °
C24	W	P	169.4(4)	C8	C7	C6	120.8(10)
C24	W	C25	89.2(5)	C7	C8	C9	120.4(11)
C24	W	C26	87.8(5)	C10	C9	C8	119.6(11)
C24	W	C27	92.7(5)	C9	C10	C11	119.9(11)
C24	W	C28	89.1(5)	C10	C11	C6	123.1(10)
C25	W	P	100.1(3)	C13	C12	C5	117.9(10)
C26	W	P	97.7(3)	C17	C12	C5	125.9(9)
C26	W	C25	86.6(4)	C17	C12	C13	115.9(9)
C27	W	P	78.5(3)	C14	C13	C12	124.1(11)
C27	W	C25	174.4(6)	C13	C14	C15	119.0(10)
C27	W	C26	88.3(5)	C14	C15	C16	118.4(10)
C27	W	C28	91.7(5)	C17	C16	C15	118.7(11)
C28	W	P	85.3(3)	C12	C17	C16	123.9(10)
C28	W	C25	93.6(5)	C19	C18	C5	123.0(9)
C28	W	C26	176.9(5)	C19	C18	C23	115.9(9)
N1	P	W	108.2(2)	C23	C18	C5	120.8(10)
N1	P	C5	97.0(4)	C20	C19	C18	122.3(10)
C5	P	W	116.7(3)	C19	C20	C21	119.9(12)
C1	N1	P	130.8(7)	C22	C21	C20	118.9(10)
C1	N1	C3	106.5(8)	C23	C22	C21	119.0(11)
C3	N1	P	122.7(6)	C22	C23	C18	123.7(11)
C1	N2	C2	106.7(8)	O1	C24	W	177.7(10)
C1	N2	C4	126.6(10)	O2	C25	W	176.7(9)
C2	N2	C4	126.4(10)	O3	C26	W	175.3(9)
N1	C1	N2	111.8(10)	O4	C27	W	177.9(11)
C3	C2	N2	108.4(10)	O5	C28	W	177.3(9)
C2	C3	N1	106.4(9)	C30	C29	C34	118.6(13)
C6	C5	P	107.6(6)	C31	C30	C29	123.4(15)
C6	C5	C12	112.9(8)	C30	C31	C32	120.4(13)
C12	C5	P	110.8(7)	C33	C32	C31	115.1(13)
C18	C5	P	104.8(6)	C34	C33	C32	124.9(17)
C18	C5	C6	116.2(9)	C33	C34	C29	117.5(15)
C18	C5	C12	104.2(7)	C36	C35	C37[a]	120.3(12)
C7	C6	C5	123.1(9)	C35	C36	C37	122.1(13)
C11	C6	C5	121.0(9)	C36	C37	C35[a]	117.5(13)
C11	C6	C7	115.9(9)				

[a] −X,−Y,1−Z

7.2.4 [Pentacarbonyl{4-(dimethylamino)pyridin-1-iumyl(triphenylmethyl)phosphanido-κ*P*}-chromium(0)] (14a)

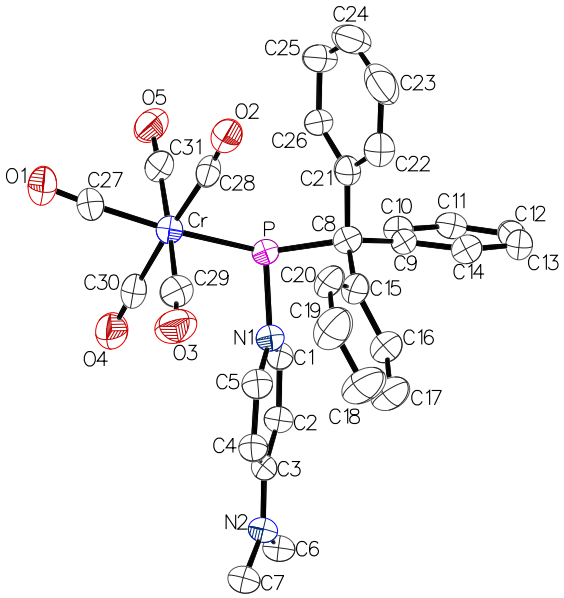

Figure 87: Molecular structures of **14a** in the single crystal lattice at 123(2) K. Thermal ellipsoids are set at 50 % probability level. Hydrogen atoms and solvent molecules were omitted for clarity.

Table 34: Crystal data and structure refinements for **14a**.

Identification code	GSTR740, DB-426 // GXray6736
Crystal habitus	clear yellow plate
Device type	STOE IPDS-2T
Empirical formula	$C_{66}H_{60}Cr_2N_4O_{11}P_2$
Moiety formula	2 ($C_{31}H_{25}CrN_2O_5P$), $C_4H_{10}O$
Formula weight / g/mol	1251.12
T / K	123
Crystal system	monoclinic
Space group	$P2_1/c$
a / Å	15.7633(15)
b / Å	9.6245(7)
c / Å	20.6670(19)
α / °	90
β / °	93.619(8)
γ / °	90
V / Å^3	3129.2(5)
Z	2
ρ_{calc} / g/cm^3	1.328
μ / mm^{-1}	0.461
F(000)	1300.0
Crystal size / mm^3	0.12 × 0.06 × 0.06

Absorption correction	integration
Min. and max. transmission	0.7408 and 0.9613
Radiation	Mo-K_α (λ = 0.71073 Å)
2Θ range for data collection / °	5.178 to 56
Completeness to Θ	0.997
Index ranges	$-20 \le h \le 20$, $-12 \le k \le 12$, $-27 \le l \le 27$
Reflections collected	29406
Independent reflections	7540 (R_{int} = 0.1380, R_σ = 0.1215)
Data / restraints / parameters	7540 / 32 / 410
Goodness-of-fit on F^2	0.990
Final R indexes ($I \ge 2\sigma(I)$)	R_1 = 0.0870, ωR_2 = 0.2111
Final R indexes (all data)	R_1 = 0.1675, ωR_2 = 0.2512
Largest diff. peak and hole / e/Å^3	1.08 and −0.80

Table 35: Bond lengths for **14a**.

Atom	**Atom**	**Length / Å**	**Atom**	**Atom**	**Length / Å**
Cr	P	2.4741(16)	C8	C21	1.532(7)
Cr	C27	1.859(6)	C9	C10	1.369(8)
Cr	C28	1.893(7)	C9	C14	1.427(7)
Cr	C29	1.895(7)	C10	C11	1.388(7)
Cr	C30	1.873(7)	C11	C12	1.387(8)
Cr	C31	1.865(6)	C12	C13	1.356(9)
P	N1	1.834(4)	C13	C14	1.385(8)
P	C8	1.938(5)	C15	C16	1.412(7)
O1	C27	1.146(7)	C15	C20	1.357(8)
O2	C28	1.161(7)	C16	C17	1.388(9)
O3	C29	1.153(7)	C17	C18	1.364(9)
O4	C30	1.160(7)	C18	C19	1.389(9)
O5	C31	1.167(7)	C19	C20	1.398(8)
N1	C1	1.335(7)	C21	C22	1.370(8)
N1	C5	1.368(7)	C21	C26	1.423(8)
N2	C3	1.361(6)	C22	C23	1.412(9)
N2	C6	1.439(7)	C23	C24	1.382(10)
N2	C7	1.459(7)	C24	C25	1.362(10)
C1	C2	1.388(7)	C25	C26	1.386(8)
C2	C3	1.407(7)	O6	C33	1.51(2)
C3	C4	1.394(8)	O6	C34	1.365(9)
C4	C5	1.384(7)	C32	C33	1.42(2)
C8	C9	1.555(7)	C34	C35	1.493(10)
C8	C15	1.518(8)			

Table 36: Bond angles of **14a**.

Atom	Atom	Atom	Angle / °	Atom	Atom	Atom	Angle / °
C27	Cr	P	166.3(2)	C21	C8	P	104.9(3)
C27	Cr	C28	88.9(2)	C21	C8	C9	103.0(4)
C27	Cr	C29	90.7(3)	C10	C9	C8	124.5(5)
C27	Cr	C30	92.8(2)	C10	C9	C14	117.2(5)
C27	Cr	C31	86.1(2)	C14	C9	C8	117.9(5)
C28	Cr	P	96.72(16)	C9	C10	C11	121.7(5)
C28	Cr	C29	87.0(3)	C12	C11	C10	120.2(6)
C29	Cr	P	101.99(18)	C13	C12	C11	119.4(5)
C30	Cr	P	82.23(17)	C12	C13	C14	121.1(6)
C30	Cr	C28	176.7(2)	C13	C14	C9	120.3(6)
C30	Cr	C29	90.2(3)	C16	C15	C8	119.8(5)
C31	Cr	P	81.32(17)	C20	C15	C8	123.2(5)
C31	Cr	C28	91.3(2)	C20	C15	C16	116.8(5)
C31	Cr	C29	176.4(2)	C17	C16	C15	120.4(6)
C31	Cr	C30	91.6(3)	C18	C17	C16	121.8(6)
N1	P	Cr	108.87(14)	C17	C18	C19	118.6(6)
N1	P	C8	99.1(2)	C18	C19	C20	119.4(6)
C8	P	Cr	117.19(18)	C15	C20	C19	123.1(6)
C1	N1	P	116.9(3)	C22	C21	C8	123.5(5)
C1	N1	C5	118.1(4)	C22	C21	C26	116.1(5)
C5	N1	P	124.6(4)	C26	C21	C8	120.0(5)
C3	N2	C6	120.5(4)	C21	C22	C23	121.3(6)
C3	N2	C7	121.2(5)	C24	C23	C22	120.6(7)
C6	N2	C7	118.2(4)	C25	C24	C23	119.6(6)
N1	C1	C2	122.7(5)	C24	C25	C26	119.7(7)
C1	C2	C3	120.0(5)	C25	C26	C21	122.5(6)
N2	C3	C2	120.9(5)	O1	C27	Cr	176.7(5)
N2	C3	C4	122.4(5)	O2	C28	Cr	173.4(4)
C4	C3	C2	116.7(5)	O3	C29	Cr	173.8(5)
C5	C4	C3	120.6(5)	O4	C30	Cr	177.4(6)
N1	C5	C4	121.9(5)	O5	C31	Cr	177.5(5)
C9	C8	P	112.7(4)	C34	O6	C33	112.1(12)
C15	C8	P	109.1(3)	C32	C33	O6	113.0(15)
C15	C8	C9	112.2(4)	O6	C34	C35	119.4(16)
C15	C8	C21	114.7(5)				

7.2.5 [Pentacarbonyl{(4-(dimethylamino)pyridin-1-iumyl(triphenylmethyl)phosphanido-κ*P*}-tungsten(0)] (14b)

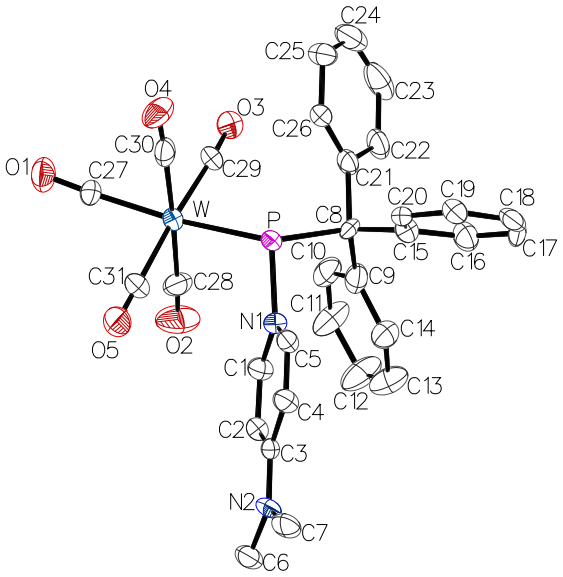

Figure 88: Molecular structures of **14b** in the single crystal lattice at 123(2) K. Thermal ellipsoids are set at 50 % probability level. Hydrogen atoms and solvent molecules were omitted for clarity.

Table 37: Crystal data and structure refinements for **14b**.

Identification code	GSTR741, DB-425 // GXray6737
Crystal habitus	clear yellow plank
Device type	STOE IPDS-2T
Empirical formula	$C_{66}H_{60}N_4O_{11}P_2W_2$
Moiety formula	2 ($C_{31}H_{25}N_2O_5PW$), $C_4H_{10}O$
Formula weight / g/mol	1514.82
T / K	123
Crystal system	monoclinic
Space group	$P2_1/c$
a / Å	15.8124(12)
b / Å	9.6562(6)
c / Å	20.8092(16)
α / °	90
β / °	93.151(6)
γ / °	90
V / Å^3	3172.5(4)
Z	2
ρ_{calc} / g/cm^3	1.586
μ / mm^{-1}	3.735
F(000)	1500.0
Crystal size / mm^3	0.35 × 0.12 × 0.04

Absorption correction	integration
Min. and max. transmission	0.4355 and 0.7479
Radiation	Mo-K_α (λ = 0.71073 Å)
2Θ range for data collection / °	5.372 to 55.992
Completeness to Θ	0.994
Index ranges	$-20 \leq h \leq 20$, $-12 \leq k \leq 12$, $-24 \leq l \leq 27$
Reflections collected	23804
Independent reflections	7604 (R_{int} = 0.1071, R_σ = 0.1868)
Data / restraints / parameters	7604 / 35 / 410
Goodness-of-fit on F^2	0.784
Final R indexes ($I \geq 2\sigma(I)$)	R_1 = 0.0540, ωR_2 = 0.1099
Final R indexes (all data)	R_1 = 0.1299, ωR_2 = 0.1311
Largest diff. peak and hole / e/Å^3	2.25 and −4.25

Table 38: Bond lengths for **14b**.

Atom	**Atom**	**Length / Å**	**Atom**	**Atom**	**Length / Å**
W	P	2.586(2)	C8	C21	1.530(12)
W	C27	1.990(9)	C9	C10	1.408(14)
W	C28	2.047(11)	C9	C14	1.393(14)
W	C29	2.052(9)	C10	C11	1.380(15)
W	C30	2.020(12)	C11	C12	1.384(16)
W	C31	2.036(10)	C12	C13	1.398(16)
P	N1	1.826(8)	C13	C14	1.366(15)
P	C8	1.936(8)	C15	C16	1.389(13)
O1	C27	1.153(10)	C15	C20	1.386(13)
O2	C28	1.160(12)	C16	C17	1.368(14)
O3	C29	1.145(10)	C17	C18	1.380(15)
O4	C30	1.153(12)	C18	C19	1.370(14)
O5	C31	1.131(11)	C19	C20	1.401(12)
N1	C1	1.372(11)	C21	C22	1.401(13)
N1	C5	1.370(11)	C21	C26	1.395(13)
N2	C3	1.333(10)	C22	C23	1.409(16)
N2	C6	1.459(11)	C23	C24	1.357(17)
N2	C7	1.467(12)	C24	C25	1.370(16)
C1	C2	1.354(12)	C25	C26	1.376(13)
C2	C3	1.421(12)	O6	C33	1.53(3)
C3	C4	1.414(12)	O6	C34	1.37(3)
C4	C5	1.359(12)	C32	C33	1.499(10)
C8	C9	1.526(13)	C34	C35	1.507(10)
C8	C15	1.561(12)			

Table 39: Bond angles for **14b**.

Atom	Atom	Atom	Angle / °	Atom	Atom	Atom	Angle / °
C27	W	P	165.8(3)	C21	C8	P	104.7(6)
C27	W	C28	90.1(4)	C21	C8	C15	103.4(7)
C27	W	C29	88.1(4)	C10	C9	C8	120.9(9)
C27	W	C30	86.5(4)	C14	C9	C8	121.2(9)
C27	W	C31	93.3(4)	C14	C9	C10	117.4(10)
C28	W	P	103.2(3)	C11	C10	C9	120.2(11)
C28	W	C29	87.5(4)	C10	C11	C12	121.6(11)
C29	W	P	97.2(3)	C11	C12	C13	118.1(11)
C30	W	P	80.3(3)	C14	C13	C12	120.5(11)
C30	W	C28	176.3(4)	C13	C14	C9	122.0(10)
C30	W	C29	90.9(4)	C16	C15	C8	120.0(8)
C30	W	C31	93.8(4)	C20	C15	C8	121.9(8)
C31	W	P	82.5(3)	C20	C15	C16	117.4(9)
C31	W	C28	88.0(4)	C17	C16	C15	121.7(10)
C31	W	C29	175.2(4)	C16	C17	C18	120.7(9)
N1	P	W	108.3(2)	C19	C18	C17	118.9(9)
N1	P	C8	100.2(3)	C18	C19	C20	120.5(10)
C8	P	W	116.4(3)	C15	C20	C19	120.6(9)
C1	N1	P	125.0(6)	C22	C21	C8	121.6(9)
C5	N1	P	117.7(6)	C26	C21	C8	121.1(8)
C5	N1	C1	116.9(8)	C26	C21	C22	117.0(9)
C3	N2	C6	122.5(8)	C21	C22	C23	119.6(11)
C3	N2	C7	120.4(8)	C24	C23	C22	121.3(10)
C6	N2	C7	117.2(7)	C23	C24	C25	119.6(10)
C2	C1	N1	122.2(9)	C24	C25	C26	120.2(11)
C1	C2	C3	121.9(9)	C25	C26	C21	122.2(10)
N2	C3	C2	123.0(8)	O1	C27	W	177.0(8)
N2	C3	C4	122.1(8)	O2	C28	W	176.4(9)
C4	C3	C2	114.9(8)	O3	C29	W	175.3(8)
C5	C4	C3	121.0(9)	O4	C30	W	176.7(8)
C4	C5	N1	123.1(9)	O5	C31	W	178.7(10)
C9	C8	P	108.7(6)	C34	O6	C33	117.8(18)
C9	C8	C15	110.0(7)	C32	C33	O6	118(2)
C9	C8	C21	116.1(8)	O6	C34	C35	115(2)
C15	C8	P	113.9(6)				

7.2.6 [Pentacarbonyl{trimethylphosphoniumyl(triphenylmethyl)phosphanido-κ*P*}-chromium(0)] (19a)

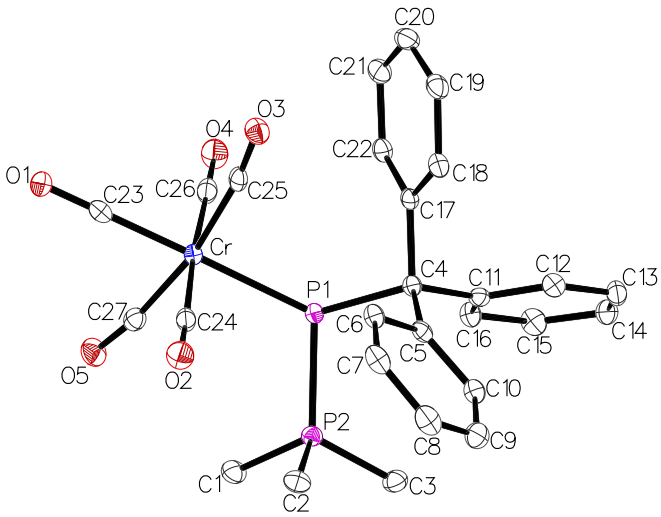

Figure 89: Molecular structures of **19a** in the single crystal lattice at 100(2) K. Thermal ellipsoids are set at 50 % probability level. Hydrogen atoms were omitted for clarity.

Table 40: Crystal data and structure refinements for **19a**.

Identification code	GSTR771, DB-565 // GXray6923
Crystal habitus	clear light yellow prisms
Device type	STOE STADIVARI
Empirical formula	$C_{27}H_{24}O_5P_2Cr$
Moiety formula	$C_{27}H_{24}CrO_5P_2$
Formula weight / g/mol	542.42
T / K	100
Crystal system	triclinic
Space group	$P\bar{1}$
a / Å	9.06234(20)
b / Å	9.31754(23)
c / Å	15.9532(3)
α / °	88.1908(19)
β / °	76.3409(17)
γ / °	70.2330(18)
V / Å^3	1230.12(5)
Z	2
ρ_{calc} / g/cm^3	1.464
μ / mm^{-1}	5.38
F(000)	560.0
Crystal size / mm^3	0.3 × 0.177 × 0.08
Absorption correction	multi-scan
Min. and max. transmission	0.1558 and 0.2633

Radiation	Cu-K_α (λ = 1.54186 Å)
2Θ range for data collection / °	10.102 to 141.05
Completeness to Θ	0.988
Index ranges	$-11 \leq h \leq 9$, $-11 \leq k \leq 5$, $-19 \leq l \leq 18$
Reflections collected	24426
Independent reflections	24037 (R_{int} = 0.0176, R_σ = 0.0122)
Data / restraints / parameters	24037 / 0 / 319
Goodness-of-fit on F^2	1.038
Final R indexes ($I \geq 2\sigma(I)$)	R_1 = 0.0290, ωR_2 = 0.0784
Final R indexes (all data)	R_1 = 0.0297, ωR_2 = 0.0789
Largest diff. peak and hole / e/Å^3	0.56 and −0.47

Table 41: Bond lengths for **19a**.

Atom	**Atom**	**Length / Å**	**Atom**	**Atom**	**Length / Å**
Cr	P1	2.5025(5)	C5	C6	1.405(2)
Cr	C23	1.8332(18)	C5	C10	1.398(2)
Cr	C24	1.9105(18)	C6	C7	1.388(2)
Cr	C25	1.9047(17)	C7	C8	1.384(3)
Cr	C26	1.9080(18)	C8	C9	1.386(3)
Cr	C27	1.8895(18)	C9	C10	1.390(3)
P1	P2	2.1621(6)	C11	C12	1.401(2)
P1	C4	1.9586(16)	C11	C16	1.390(2)
P2	C1	1.8095(17)	C12	C13	1.387(2)
P2	C2	1.8116(17)	C13	C14	1.381(3)
P2	C3	1.8058(18)	C14	C15	1.383(3)
O1	C23	1.165(2)	C15	C16	1.395(2)
O2	C24	1.143(2)	C17	C18	1.398(2)
O3	C25	1.148(2)	C17	C22	1.401(2)
O4	C26	1.139(2)	C18	C19	1.389(3)
O5	C27	1.146(2)	C19	C20	1.390(3)
C4	C5	1.535(2)	C20	C21	1.389(3)
C4	C11	1.549(2)	C21	C22	1.395(3)
C4	C17	1.542(2)			

Table 42: Bond angles for **19a**.

Atom	Atom	Atom	Angle / °	Atom	Atom	Atom	Angle / °
C23	Cr	P1	172.36(5)	C6	C5	C4	119.30(15)
C23	Cr	C24	91.10(7)	C10	C5	C4	123.34(15)
C23	Cr	C25	87.52(7)	C10	C5	C6	117.27(16)
C23	Cr	C26	92.30(7)	C7	C6	C5	121.29(17)
C23	Cr	C27	83.68(7)	C8	C7	C6	120.46(17)
C24	Cr	P1	94.64(5)	C7	C8	C9	119.09(16)
C25	Cr	P1	97.67(5)	C8	C9	C10	120.65(17)
C25	Cr	C24	88.32(7)	C9	C10	C5	121.17(16)
C25	Cr	C26	90.76(7)	C12	C11	C4	118.05(14)
C26	Cr	P1	82.06(5)	C16	C11	C4	124.28(14)
C26	Cr	C24	176.43(7)	C16	C11	C12	117.56(15)
C27	Cr	P1	90.85(5)	C13	C12	C11	121.30(15)
C27	Cr	C24	94.36(7)	C14	C13	C12	120.31(16)
C27	Cr	C25	170.84(7)	C13	C14	C15	119.35(16)
C27	Cr	C26	87.08(7)	C14	C15	C16	120.37(16)
P2	P1	Cr	110.72(2)	C11	C16	C15	121.06(16)
C4	P1	Cr	119.91(5)	C18	C17	C4	122.53(15)
C4	P1	P2	102.45(5)	C18	C17	C22	117.65(16)
C1	P2	P1	107.38(6)	C22	C17	C4	119.67(14)
C1	P2	C2	103.32(8)	C19	C18	C17	121.11(17)
C2	P2	P1	122.58(6)	C18	C19	C20	120.62(17)
C3	P2	P1	111.93(6)	C21	C20	C19	119.14(17)
C3	P2	C1	103.80(8)	C20	C21	C22	120.15(17)
C3	P2	C2	106.01(9)	C21	C22	C17	121.21(16)
C5	C4	P1	109.07(10)	O1	C23	Cr	178.96(16)
C5	C4	C11	112.63(13)	O2	C24	Cr	176.18(15)
C5	C4	C17	112.52(13)	O3	C25	Cr	172.33(14)
C11	C4	P1	111.30(10)	O4	C26	Cr	178.60(16)
C17	C4	P1	106.53(11)	O5	C27	Cr	172.35(15)
C17	C4	C11	104.58(13)				

Table 43: Torsion angles for **19a**.

A	**B**	**C**	**D**	**Angle / °**	**A**	**B**	**C**	**D**	**Angle / °**
P1	C4	C5	C6	−67.98(16)	C10	C5	C6	C7	−0.9(2)
P1	C4	C5	C10	108.38(15)	C11	C4	C5	C6	167.92(14)
P1	C4	C11	C12	−175.56(12)	C11	C4	C5	C10	−15.7(2)
P1	C4	C11	C16	8.3(2)	C11	C4	C17	C18	−102.42(17)
P1	C4	C17	C18	139.63(14)	C11	C4	C17	C22	72.96(17)
P1	C4	C17	C22	−44.99(17)	C11	C12	C13	C14	1.2(3)
C4	C5	C6	C7	175.63(15)	C12	C11	C16	C15	2.1(3)
C4	C5	C10	C9	−174.34(15)	C12	C13	C14	C15	0.9(3)
C4	C11	C12	C13	−179.03(16)	C13	C14	C15	C16	−1.4(3)
C4	C11	C16	C15	178.22(16)	C14	C15	C16	C11	−0.1(3)
C4	C17	C18	C19	178.23(15)	C16	C11	C12	C13	−2.6(3)
C4	C17	C22	C21	−179.78(15)	C17	C4	C5	C6	50.01(19)
C5	C4	C11	C12	−52.7(2)	C17	C4	C5	C10	−133.63(16)
C5	C4	C11	C16	131.17(17)	C17	C4	C11	C12	69.79(18)
C5	C4	C17	C18	20.1(2)	C17	C4	C11	C16	−106.33(18)
C5	C4	C17	C22	−164.47(14)	C17	C18	C19	C20	0.1(3)
C5	C6	C7	C8	−1.3(3)	C18	C17	C22	C21	−4.2(2)
C6	C5	C10	C9	2.1(2)	C18	C19	C20	C21	−1.6(3)
C6	C7	C8	C9	2.5(3)	C19	C20	C21	C22	0.2(3)
C7	C8	C9	C10	−1.3(3)	C20	C21	C22	C17	2.8(3)
C8	C9	C10	C5	−1.0(3)	C22	C17	C18	C19	2.8(2)

7.2.7 [Pentacarbonyl{trimethylphosphoniumyl(triphenylmethyl)phosphanido-κ*P*}-tungsten(0)] (19b)

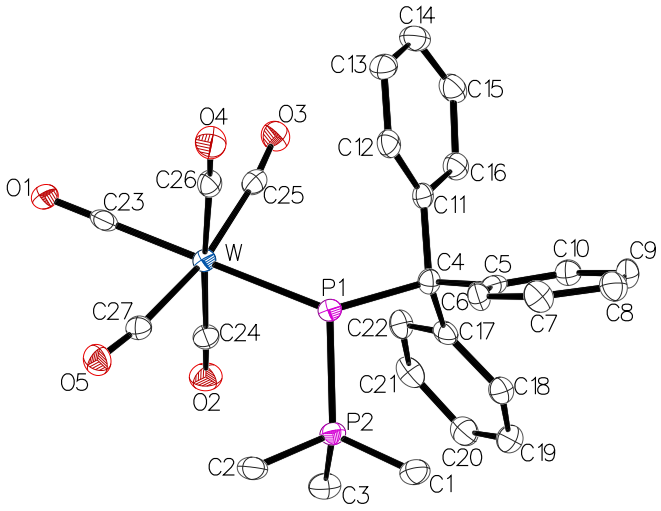

Figure 90: Molecular structures of **19b** in the single crystal lattice at 123(2) K. Thermal ellipsoids are set at 50 % probability level. Hydrogen atoms were omitted for clarity.

Table 44: Crystal data and structure refinements for **19b**.

Identification code	GSTR758, DB-491 // GXray6857
Crystal habitus	clear yellow plate
Device type	STOE IPDS-2T
Empirical formula	$C_{27}H_{24}O_5P_2W$
Moiety formula	$C_{27}H_{24}O_5P_2W$
Formula weight / g/mol	674.25
T / K	123(2)
Crystal system	triclinic
Space group	$P\bar{1}$
a / Å	9.1192(4)
b / Å	9.4046(5)
c / Å	16.0948(8)
α / °	88.489(4)
β / °	76.363(4)
γ / °	70.182(4)
V / Å^3	1259.80(11)
Z	2
ρ_{calc} / g/cm^3	1.777
μ / mm^{-1}	4.748
F(000)	660.0
Crystal size / mm^3	0.21 × 0.15 × 0.1
Absorption correction	integration
Min. and max. transmission	0.2582 and 0.5544

Radiation	Mo-K_α (λ = 0.71073 Å)
2Θ range for data collection / °	4.892 to 56
Completeness to Θ	0.993
Index ranges	$-12 \leq h \leq 12$, $-12 \leq k \leq 10$, $-21 \leq l \leq 21$
Reflections collected	11644
Independent reflections	6004 (R_{int} = 0.0455, R_σ = 0.0648)
Data / restraints / parameters	6004 / 0 / 319
Goodness-of-fit on F^2	0.955
Final R indexes ($I \geq 2\sigma(I)$)	R_1 = 0.0316, ωR_2 = 0.0689
Final R indexes (all data)	R_1 = 0.0432, ωR_2 = 0.0709
Largest diff. peak and hole / e/Å^3	1.62 and −1.83

Table 45: Bond lengths for **19b**.

Atom	**Atom**	**Length / Å**	**Atom**	**Atom**	**Length / Å**
W	P1	2.6151(11)	C5	C6	1.384(6)
W	C23	1.978(5)	C5	C10	1.384(6)
W	C24	2.052(5)	C6	C7	1.394(6)
W	C25	2.047(4)	C7	C8	1.383(7)
W	C26	2.054(5)	C8	C9	1.390(7)
W	C27	2.031(4)	C9	C10	1.379(6)
P1	P2	2.1584(14)	C11	C12	1.402(6)
P1	C4	1.958(4)	C11	C16	1.395(6)
P2	C1	1.804(5)	C12	C13	1.384(6)
P2	C2	1.807(5)	C13	C14	1.377(7)
P2	C3	1.811(5)	C14	C15	1.394(7)
O1	C23	1.161(5)	C15	C16	1.393(6)
O2	C24	1.139(5)	C17	C18	1.399(6)
O3	C25	1.147(5)	C17	C22	1.404(6)
O4	C26	1.132(5)	C18	C19	1.382(6)
O5	C27	1.138(5)	C19	C20	1.376(7)
C4	C5	1.560(6)	C20	C21	1.399(6)
C4	C11	1.545(6)	C21	C22	1.381(6)
C4	C17	1.536(6)			

Table 46: Bond angles for **19b**.

Atom	Atom	Atom	Angle / °	Atom	Atom	Atom	Angle / °
C23	W	P1	171.70(14)	C6	C5	C4	123.3(4)
C23	W	C24	90.88(17)	C6	C5	C10	118.5(4)
C23	W	C25	87.66(17)	C10	C5	C4	118.1(4)
C23	W	C26	91.99(17)	C5	C6	C7	120.8(4)
C23	W	C27	83.17(17)	C8	C7	C6	120.3(4)
C24	W	P1	95.87(12)	C7	C8	C9	118.8(4)
C24	W	C26	176.59(18)	C10	C9	C8	120.5(4)
C25	W	P1	97.38(12)	C9	C10	C5	121.1(4)
C25	W	C24	88.07(17)	C12	C11	C4	120.2(4)
C25	W	C26	90.21(17)	C16	C11	C4	122.0(4)
C26	W	P1	81.43(12)	C16	C11	C12	117.6(4)
C27	W	P1	91.45(12)	C13	C12	C11	121.2(4)
C27	W	C24	94.52(17)	C14	C13	C12	120.5(4)
C27	W	C25	170.51(16)	C13	C14	C15	119.3(4)
C27	W	C26	87.65(17)	C16	C15	C14	120.1(4)
P2	P1	W	109.87(5)	C15	C16	C11	121.1(4)
C4	P1	W	119.36(13)	C18	C17	C4	123.4(4)
C4	P1	P2	102.93(13)	C18	C17	C22	117.2(4)
C1	P2	P1	112.21(15)	C22	C17	C4	119.4(4)
C1	P2	C2	103.8(2)	C19	C18	C17	121.2(4)
C1	P2	C3	106.5(2)	C20	C19	C18	120.8(4)
C2	P2	P1	107.49(15)	C19	C20	C21	119.3(4)
C2	P2	C3	103.2(2)	C22	C21	C20	119.8(4)
C3	P2	P1	121.89(16)	C21	C22	C17	121.6(4)
C5	C4	P1	111.1(3)	O1	C23	W	179.1(4)
C11	C4	P1	106.3(3)	O2	C24	W	177.1(4)
C11	C4	C5	105.1(3)	O3	C25	W	173.4(4)
C17	C4	P1	108.7(3)	O4	C26	W	177.8(4)
C17	C4	C5	112.8(3)	O5	C27	W	173.5(4)
C17	C4	C11	112.7(3)				

Table 47: Torsion angles for **19b**.

A	B	C	D	Angle / °	A	B	C	D	Angle / °
P1	C4	C5	C6	−9.1(5)	C10	C5	C6	C7	−1.5(6)
P1	C4	C5	C10	174.9(3)	C11	C4	C5	C6	105.4(4)
P1	C4	C11	C12	44.2(4)	C11	C4	C5	C10	−70.6(4)
P1	C4	C11	C16	−140.9(4)	C11	C4	C17	C18	133.7(4)
P1	C4	C17	C18	−108.8(4)	C11	C4	C17	C22	−48.9(5)
P1	C4	C17	C22	68.6(4)	C11	C12	C13	C14	−2.9(7)
C4	C5	C6	C7	−177.5(4)	C12	C11	C16	C15	−1.7(6)
C4	C5	C10	C9	178.4(4)	C12	C13	C14	C15	−0.5(7)
C4	C11	C12	C13	179.1(4)	C13	C14	C15	C16	2.8(7)
C4	C11	C16	C15	−176.8(4)	C14	C15	C16	C11	−1.7(7)
C4	C17	C18	C19	174.9(4)	C16	C11	C12	C13	4.0(6)
C4	C17	C22	C21	−175.8(4)	C17	C4	C5	C6	−131.4(4)
C5	C4	C11	C12	−73.7(5)	C17	C4	C5	C10	52.6(5)
C5	C4	C11	C16	101.3(4)	C17	C4	C11	C12	163.1(4)
C5	C4	C17	C18	14.9(5)	C17	C4	C11	C16	−21.9(6)
C5	C4	C17	C22	−167.7(4)	C17	C18	C19	C20	0.9(7)
C5	C6	C7	C8	−0.7(6)	C18	C17	C22	C21	1.8(6)
C6	C5	C10	C9	2.2(6)	C18	C19	C20	C21	1.6(7)
C6	C7	C8	C9	2.3(7)	C19	C20	C21	C22	−2.3(7)
C7	C8	C9	C10	−1.7(6)	C20	C21	C22	C17	0.6(7)
C8	C9	C10	C5	−0.6(6)	C22	C17	C18	C19	−2.6(6)

7.2.8 [Pentacarbonyl{triethylphosphoniumyl(triphenylmethyl)phosphanido-κ*P*}tungsten(0)] (20b)

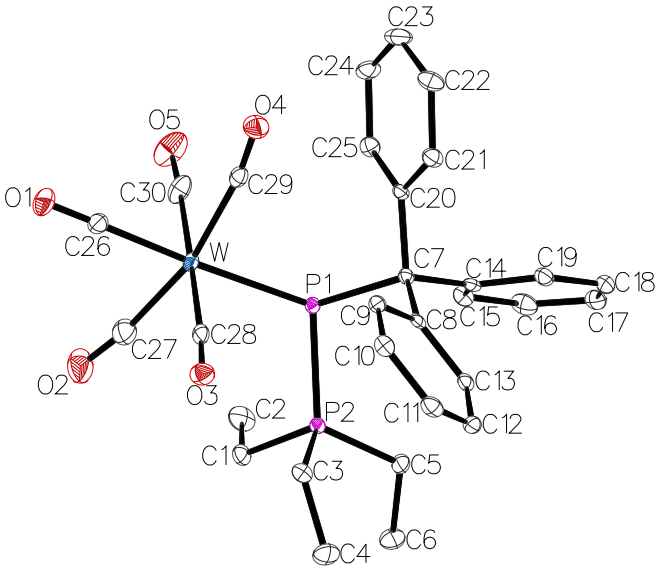

Figure 91: Molecular structures of **20b** in the single crystal lattice at 100(2) K. Thermal ellipsoids are set at 50 % probability level. Hydrogen atoms were omitted for clarity.

Table 48: Crystal data and structure refinements for **20b**.

Identification code	GSTR759, DB-495 // GXraymo_6858f
Crystal habitus	clear yellow block
Device type	Bruker D8 Venture
Empirical formula	$C_{30}H_{30}O_5P_2W$
Moiety formula	$C_{30}H_{30}O_5P_2W$
Formula weight / g/mol	716.33
T / K	100.0
Crystal system	monoclinic
Space group	$P2_1/c$
a / Å	9.5507(4)
b / Å	14.6045(5)
c / Å	20.9543(7)
α / °	90
β / °	101.0820(10)
γ / °	90
V / Å^3	2868.27(18)
Z	4
ρ_{calc} / g/cm^3	1.659
μ / mm^{-1}	4.176
F(000)	1416.0
Crystal size / mm^3	0.28 × 0.25 × 0.24
Absorption correction	empirical

Min. and max. transmission	0.5165 and 0.7461
Radiation	Mo-K_α (λ = 0.71073 Å)
2Θ range for data collection / °	4.346 to 51.998
Completeness to Θ	0.939
Index ranges	$-11 \leq h \leq 11$, $-18 \leq k \leq 18$, $-25 \leq l \leq 25$
Reflections collected	30521
Independent reflections	5325 (R_{int} = 0.0421, R_σ = 0.0242)
Data / restraints / parameters	5325 / 18 / 346
Goodness-of-fit on F^2	1.209
Final R indexes ($I \geq 2\sigma(I)$)	R_1 = 0.0204, ωR_2 = 0.0476
Final R indexes (all data)	R_1 = 0.0206, ωR_2 = 0.0477
Largest diff. peak and hole / e/Å^3	0.61 and −0.82

Table 49: Bond lengths for **20b**.

Atom	**Atom**	**Length / Å**	**Atom**	**Atom**	**Length / Å**
W	P1	2.6373(6)	C7	C14	1.545(3)
W	C26	1.984(2)	C7	C20	1.545(3)
W	C27	2.022(3)	C8	C9	1.403(3)
W	C28	2.037(3)	C8	C13	1.403(3)
W	C29	2.062(3)	C9	C10	1.386(3)
W	C30	2.051(3)	C10	C11	1.394(4)
P1	P2	2.1747(8)	C11	C12	1.387(4)
P1	C7	1.945(2)	C12	C13	1.391(3)
P2	C1	1.815(2)	C14	C15	1.390(4)
P2	C3	1.824(2)	C14	C19	1.405(3)
P2	C5	1.833(2)	C15	C16	1.389(4)
O1	C26	1.150(3)	C16	C17	1.388(4)
O2	C27	1.146(4)	C17	C18	1.386(4)
O3	C28	1.147(3)	C18	C19	1.391(4)
O4	C29	1.138(3)	C20	C21	1.398(3)
O5	C30	1.135(4)	C20	C25	1.396(3)
C1	C2	1.527(4)	C21	C22	1.390(4)
C3	C4	1.531(3)	C22	C23	1.387(4)
C5	C6	1.534(3)	C23	C24	1.388(4)
C7	C8	1.533(3)	C24	C25	1.391(4)

Table 50: Bond angles for **20b**.

Atom	Atom	Atom	Angle / °	Atom	Atom	Atom	Angle / °
C26	W	P1	175.02(7)	C14	C7	C20	104.01(18)
C26	W	C27	85.30(11)	C20	C7	P1	105.75(15)
C26	W	C28	89.55(10)	C9	C8	C7	120.4(2)
C26	W	C29	83.38(10)	C13	C8	C7	122.2(2)
C26	W	C30	89.90(10)	C13	C8	C9	117.3(2)
C27	W	P1	94.17(8)	C10	C9	C8	121.3(2)
C27	W	C28	92.19(11)	C9	C10	C11	120.6(2)
C27	W	C29	167.67(10)	C12	C11	C10	119.0(2)
C27	W	C30	87.30(12)	C11	C12	C13	120.4(2)
C28	W	P1	95.42(7)	C12	C13	C8	121.4(2)
C28	W	C29	92.61(10)	C15	C14	C7	123.8(2)
C28	W	C30	179.28(10)	C15	C14	C19	117.4(2)
C29	W	P1	96.68(7)	C19	C14	C7	118.6(2)
C30	W	P1	85.12(7)	C16	C15	C14	121.4(2)
C30	W	C29	87.80(11)	C17	C16	C15	120.4(3)
P2	P1	W	109.25(3)	C18	C17	C16	119.2(2)
C7	P1	W	116.69(7)	C17	C18	C19	120.2(2)
C7	P1	P2	103.45(8)	C18	C19	C14	121.2(2)
C1	P2	P1	105.15(8)	C21	C20	C7	122.1(2)
C1	P2	C3	105.08(12)	C25	C20	C7	119.8(2)
C1	P2	C5	104.72(12)	C25	C20	C21	117.8(2)
C3	P2	P1	117.60(8)	C22	C21	C20	121.0(2)
C3	P2	C5	108.88(12)	C23	C22	C21	120.5(2)
C5	P2	P1	114.11(8)	C22	C23	C24	119.2(2)
C2	C1	P2	113.97(18)	C23	C24	C25	120.2(2)
C4	C3	P2	116.32(18)	C24	C25	C20	121.2(2)
C6	C5	P2	116.62(18)	O1	C26	W	179.2(2)
C8	C7	P1	109.17(15)	O2	C27	W	172.1(3)
C8	C7	C14	112.09(19)	O3	C28	W	176.2(2)
C8	C7	C20	113.69(19)	O4	C29	W	171.3(2)
C14	C7	P1	111.93(16)	O5	C30	W	177.3(2)

7.2.9 [Pentacarbonyl{(cyano(triphenylmethyl)phosphane-κ*P*}chromium(0)] (23a)

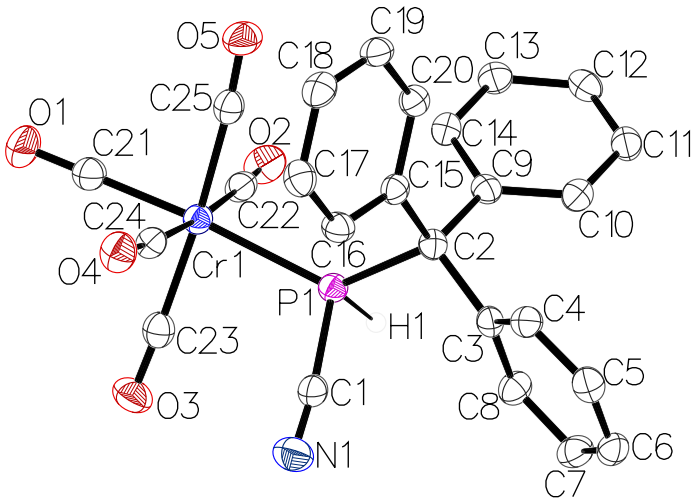

Figure 92: Molecular structures of **23a** in the single crystal lattice at 123(2) K. Thermal ellipsoids are set at 50 % probability level. Hydrogen atoms were omitted for clarity except for those bound to phosphorus atoms.

Table 51: Crystal data and structure refinements for **23a**.

Identification code	GSTR713, DB-292 // GXray6520
Crystal habitus	clear colorless plate
Device type	STOE IPDS 2T
Empirical formula	$C_{25}H_{16}NO_5PCr$
Moiety formula	$C_{25}H_{16}CrNO_5P$
Formula weight / g/mol	493.36
T / K	123(2)
Crystal system	monoclinic
Space group	$P2_1/c$
a / Å	10.8079(3)
b / Å	10.7875(3)
c / Å	19.4365(4)
α / °	90
β / °	99.574(2)
γ / °	90
V / Å^3	2234.54(10)
Z	4
ρ_{calc} / g/cm^3	1.467
μ / mm^{-1}	0.621
F(000)	1008.0
Crystal size / mm^3	0.4 × 0.24 × 0.04
Absorption correction	integration
Min. and max. transmission	0.82841 and 1.00000
Radiation	Mo-K_α (λ = 0.71073 Å)

2Θ range for data collection / °	3.822 to 54
Completeness to Θ	1.000
Index ranges	$-13 \leq h \leq 13$, $-12 \leq k \leq 13$, $-24 \leq l \leq 23$
Reflections collected	17203
Independent reflections	4889 (R_{int} = 0.0609, R_σ = 0.0601)
Data / restraints / parameters	4889 / 1 / 302
Goodness-of-fit on F^2	1.018
Final R indexes ($I \geq 2\sigma(I)$)	R_1 = 0.0379, ωR_2 = 0.0808
Final R indexes (all data)	R_1 = 0.0650, ωR_2 = 0.0881
Largest diff. peak and hole / e/Å^3	0.31 and −0.36

Table 52: Bond lengths for **23a**.

Atom	**Atom**	**Length / Å**	**Atom**	**Atom**	**Length / Å**
Cr1	P1	2.3587(7)	C3	C8	1.401(3)
Cr1	C21	1.872(2)	C4	C5	1.394(3)
Cr1	C22	1.902(2)	C5	C6	1.381(3)
Cr1	C23	1.909(2)	C6	C7	1.384(3)
Cr1	C24	1.908(2)	C7	C8	1.387(3)
Cr1	C25	1.913(2)	C9	C10	1.396(3)
P1	C1	1.809(2)	C9	C14	1.393(3)
P1	C2	1.921(2)	C10	C11	1.390(3)
O1	C21	1.140(3)	C11	C12	1.385(3)
O2	C22	1.142(3)	C12	C13	1.382(3)
O3	C23	1.140(3)	C13	C14	1.392(3)
O4	C24	1.143(3)	C15	C16	1.397(3)
O5	C25	1.140(3)	C15	C20	1.391(3)
N1	C1	1.147(3)	C16	C17	1.393(3)
C2	C3	1.543(3)	C17	C18	1.390(3)
C2	C9	1.551(3)	C18	C19	1.377(3)
C2	C15	1.540(3)	C19	C20	1.395(3)
C3	C4	1.394(3)			

Table 53: Bond angles for **23a**.

Atom	Atom	Atom	Angle / °	Atom	Atom	Atom	Angle / °
C21	Cr1	P1	173.50(8)	C8	C3	C2	120.70(19)
C21	Cr1	C22	87.81(10)	C3	C4	C5	120.8(2)
C21	Cr1	C23	87.48(10)	C6	C5	C4	120.5(2)
C21	Cr1	C24	89.31(10)	C5	C6	C7	119.5(2)
C21	Cr1	C25	89.27(10)	C6	C7	C8	120.2(2)
C22	Cr1	P1	89.19(7)	C7	C8	C3	121.2(2)
C22	Cr1	C23	91.93(10)	C10	C9	C2	120.46(19)
C22	Cr1	C24	175.66(10)	C14	C9	C2	121.89(19)
C22	Cr1	C25	90.50(10)	C14	C9	C10	117.59(19)
C23	Cr1	P1	86.86(7)	C11	C10	C9	121.1(2)
C23	Cr1	C25	175.86(10)	C12	C11	C10	120.4(2)
C24	Cr1	P1	93.99(7)	C13	C12	C11	119.2(2)
C24	Cr1	C23	91.19(10)	C12	C13	C14	120.2(2)
C24	Cr1	C25	86.22(10)	C13	C14	C9	121.3(2)
C25	Cr1	P1	96.53(7)	C16	C15	C2	120.02(19)
C1	P1	Cr1	109.09(7)	C20	C15	C2	122.11(19)
C1	P1	C2	101.75(10)	C20	C15	C16	117.9(2)
C2	P1	Cr1	129.59(7)	C17	C16	C15	121.5(2)
N1	C1	P1	174.6(2)	C18	C17	C16	119.7(2)
C3	C2	P1	110.00(14)	C19	C18	C17	119.5(2)
C3	C2	C9	108.90(17)	C18	C19	C20	120.8(2)
C9	C2	P1	106.21(14)	C15	C20	C19	120.7(2)
C15	C2	P1	105.34(14)	O1	C21	Cr1	179.4(2)
C15	C2	C3	113.37(17)	O2	C22	Cr1	177.4(2)
C15	C2	C9	112.72(17)	O3	C23	Cr1	177.8(2)
C4	C3	C2	121.11(19)	O4	C24	Cr1	174.7(2)
C4	C3	C8	117.8(2)	O5	C25	Cr1	176.0(2)

Table 54: Torsion angles for **23a**.

A	B	C	D	Angle / °	A	B	C	D	Angle / °
P1	C2	C3	C4	−138.08(17)	C8	C3	C4	C5	2.4(3)
P1	C2	C3	C8	49.5(2)	C9	C2	C3	C4	105.9(2)
P1	C2	C9	C10	−137.84(18)	C9	C2	C3	C8	−66.5(2)
P1	C2	C9	C14	45.2(2)	C9	C2	C15	C16	173.57(19)
P1	C2	C15	C16	58.2(2)	C9	C2	C15	C20	−5.2(3)
P1	C2	C15	C20	−120.54(19)	C9	C10	C11	C12	−0.6(3)
C2	C3	C4	C5	−170.23(18)	C10	C9	C14	C13	1.1(3)
C2	C3	C8	C7	171.6(2)	C10	C11	C12	C13	1.3(3)
C2	C9	C10	C11	−177.68(19)	C11	C12	C13	C14	−0.8(3)
C2	C9	C14	C13	178.1(2)	C12	C13	C14	C9	−0.4(4)
C2	C15	C16	C17	−177.3(2)	C14	C9	C10	C11	−0.6(3)
C2	C15	C20	C19	178.0(2)	C15	C2	C3	C4	−20.4(3)
C3	C2	C9	C10	−19.4(3)	C15	C2	C3	C8	167.18(19)
C3	C2	C9	C14	163.64(19)	C15	C2	C9	C10	107.3(2)
C3	C2	C15	C16	−62.1(3)	C15	C2	C9	C14	−69.6(3)
C3	C2	C15	C20	119.1(2)	C15	C16	C17	C18	−1.0(4)
C3	C4	C5	C6	−1.9(3)	C16	C15	C20	C19	−0.7(3)
C4	C3	C8	C7	−1.0(3)	C16	C17	C18	C19	−0.4(4)
C4	C5	C6	C7	0.0(3)	C17	C18	C19	C20	1.1(3)
C5	C6	C7	C8	1.4(3)	C18	C19	C20	C15	−0.5(3)
C6	C7	C8	C3	−0.9(3)	C20	C15	C16	C17	1.5(3)

7.2.10 [Pentacarbonyl(3,4-dimethyl-1-triphenylmethyl-2,5-dihydro-1*H*-phosphole-κ*P*)tungsten(0) (39)

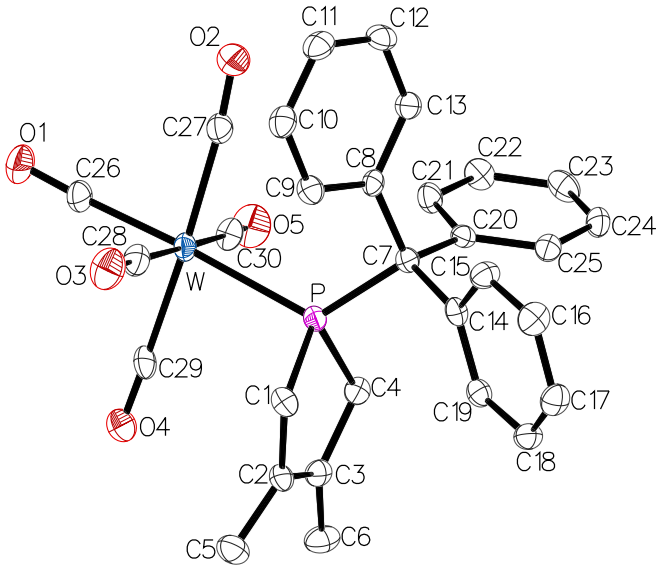

Figure 93: Molecular structures of **39** in the single crystal lattice at 123(2) K. Thermal ellipsoids are set at 50 % probability level. Hydrogen atoms were omitted for clarity.

Table 55: Crystal data and structure refinements for **39**.

Identification code	GSTR753, DB-476 // GXray6848
Crystal habitus	clear colorless block
Device type	STOE IPDS2T
Empirical formula	$C_{30}H_{25}O_5PW$
Moiety formula	$C_{30}H_{25}O_5PW$
Formula weight / g/mol	680.32
T / K	123
Crystal system	monoclinic
Space group	$P2_1/c$
a / Å	10.117(2)
b / Å	14.733(8)
c / Å	17.855(4)
α / °	90
β / °	92.33(2)
γ / °	90
V / Å^3	2659.1(17)
Z	4
ρ_{calc} / g/cm^3	1.699
μ / mm^{-1}	4.443
F(000)	1336.0
Crystal size / mm^3	0.14 × 0.12 × 0.1

Absorption correction	integration
Min. and max. transmission	0.3942 and 0.6523
Radiation	Mo-K_α (λ = 0.71073 Å)
2Θ range for data collection / °	5.324 to 55.998
Completeness to Θ	0.998
Index ranges	$-11 \leq h \leq 13$, $-18 \leq k \leq 19$, $-23 \leq l \leq 23$
Reflections collected	18638
Independent reflections	6414 (R_{int} = 0.0449, R_σ = 0.0486)
Data / restraints / parameters	6414 / 5 / 336
Goodness-of-fit on F^2	0.882
Final R indexes ($I \geq 2\sigma(I)$)	R_1 = 0.0236, ωR_2 = 0.0386
Final R indexes (all data)	R_1 = 0.0402, ωR_2 = 0.0406
Largest diff. peak and hole / e/Å^3	0.68 and −0.72

Table 56: Bond lengths for **39**.

Atom	**Atom**	**Length / Å**	**Atom**	**Atom**	**Length / Å**
W	P	2.5576(10)	C7	C14	1.544(3)
W	C26	2.000(3)	C7	C20	1.547(4)
W	C27	2.045(3)	C8	C9	1.392(4)
W	C28	2.041(3)	C8	C13	1.395(4)
W	C29	2.051(3)	C9	C10	1.390(4)
W	C30	2.046(3)	C10	C11	1.386(4)
P	C1	1.856(3)	C11	C12	1.377(4)
P	C4	1.852(3)	C12	C13	1.395(4)
P	C7	1.929(3)	C14	C15	1.402(4)
O1	C26	1.149(4)	C14	C19	1.393(4)
O2	C27	1.145(4)	C15	C16	1.387(4)
O3	C28	1.146(4)	C16	C17	1.382(4)
O4	C29	1.137(4)	C17	C18	1.381(4)
O5	C30	1.143(4)	C18	C19	1.391(4)
C1	C2	1.513(4)	C20	C21	1.396(4)
C2	C3	1.335(4)	C20	C25	1.391(4)
C2	C5	1.505(4)	C21	C22	1.386(4)
C3	C4	1.520(4)	C22	C23	1.385(4)
C3	C6	1.498(4)	C23	C24	1.379(4)
C7	C8	1.536(4)	C24	C25	1.397(4)

Table 57: Bond angles for **39**.

Atom	Atom	Atom	Angle / °	Atom	Atom	Atom	Angle / °
C26	W	P	176.59(9)	C14	C7	P	113.10(17)
C26	W	C27	84.70(12)	C14	C7	C20	110.2(2)
C26	W	C28	89.68(13)	C20	C7	P	106.36(18)
C26	W	C29	91.50(12)	C9	C8	C7	120.5(2)
C26	W	C30	88.36(12)	C9	C8	C13	118.0(3)
C27	W	P	97.82(9)	C13	C8	C7	121.3(2)
C27	W	C29	175.46(12)	C10	C9	C8	121.4(3)
C27	W	C30	89.19(13)	C11	C10	C9	119.7(3)
C28	W	P	87.96(9)	C12	C11	C10	119.9(3)
C28	W	C27	91.74(13)	C11	C12	C13	120.3(3)
C28	W	C29	90.73(13)	C8	C13	C12	120.7(3)
C28	W	C30	177.74(13)	C15	C14	C7	120.2(2)
C29	W	P	86.08(9)	C19	C14	C7	122.4(2)
C30	W	P	93.96(8)	C19	C14	C15	117.2(3)
C30	W	C29	88.21(12)	C16	C15	C14	121.0(3)
C1	P	W	109.01(10)	C17	C16	C15	120.8(3)
C1	P	C7	108.72(12)	C18	C17	C16	119.0(3)
C4	P	W	111.48(9)	C17	C18	C19	120.4(3)
C4	P	C1	93.68(13)	C18	C19	C14	121.5(3)
C4	P	C7	106.56(13)	C21	C20	C7	120.4(2)
C7	P	W	123.33(8)	C25	C20	C7	121.5(2)
C2	C1	P	103.62(19)	C25	C20	C21	118.0(3)
C3	C2	C1	117.2(3)	C22	C21	C20	121.2(3)
C3	C2	C5	126.3(3)	C23	C22	C21	120.4(3)
C5	C2	C1	116.4(2)	C24	C23	C22	119.1(3)
C2	C3	C4	116.5(2)	C23	C24	C25	120.8(3)
C2	C3	C6	126.8(3)	C20	C25	C24	120.5(3)
C6	C3	C4	116.6(2)	O1	C26	W	177.4(3)
C3	C4	P	104.03(19)	O2	C27	W	173.7(3)
C8	C7	P	107.02(17)	O3	C28	W	178.6(3)
C8	C7	C14	109.1(2)	O4	C29	W	177.8(3)
C8	C7	C20	111.0(2)	O5	C30	W	177.3(3)

7.2.11 [Pentacarbonyl-2κ*C*-μ{(1-methylimidazol-3-iumyl)triphenylmethylphosphanido-1κ*P*:2κ*P*}boranetungsten(0)] (54)

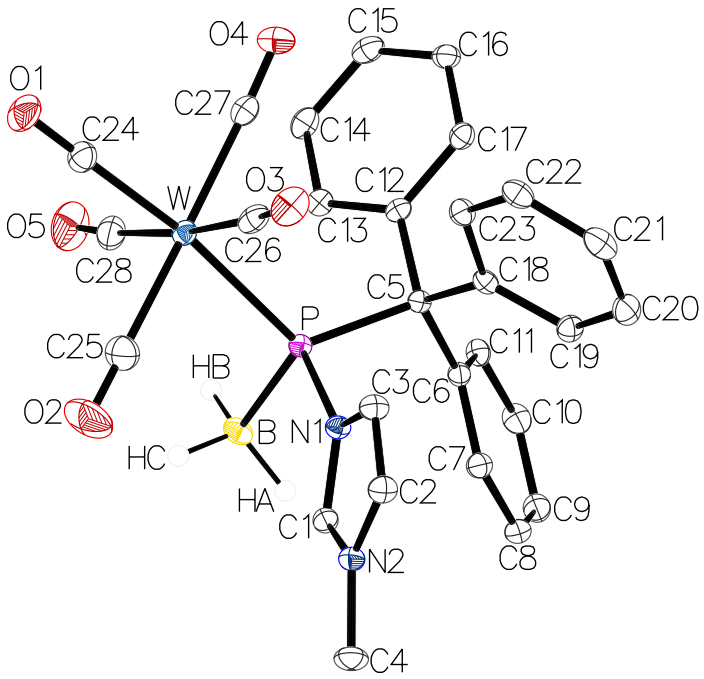

Figure 94: Molecular structures of **54** in the single crystal lattice at 100(2) K. Thermal ellipsoids are set at 50 % probability level. Solvent molecules and hydrogen atoms were omitted for clarity except for those bound to boron atoms.

Table 58: Crystal data and structure refinements for **54**.

Identification code	GSTR793, DB-630 // GXraymo_7114_om_4
Crystal habitus	clear colorless block
Device type	Bruker D8 Venture
Empirical formula	$C_{30}H_{28}BCl_4N_2O_5PW$
Moiety formula	$C_{28}H_{24}BN_2O_5PW$, 2 (CH_2Cl_2)
Formula weight / g/mol	863.97
T / K	100.0
Crystal system	triclinic
Space group	$P\bar{1}$
a / Å	11.0075(6)
b / Å	12.3330(7)
c / Å	12.9754(7)
α / °	85.521(2)
β / °	73.945(2)
γ / °	81.084(2)
V / Å^3	1671.17(16)
Z	2
ρ_{calc} / g/cm^3	1.717
μ / mm^{-1}	3.865

F(000)	848.0
Crystal size / mm^3	0.6 × 0.48 × 0.44
Absorption correction	empirical
Min. and max. transmission	0.338087 and 0.746427
Radiation	Mo-K_α (λ = 0.71073 Å)
2Θ range for data collection / °	5.884 to 58.498
Completeness to Θ	0.995
Index ranges	$-14 \le h \le 15$, $-16 \le k \le 16$, $0 \le l \le 17$
Reflections collected	9067
Independent reflections	9067 (R_{int} = 0.0618, R_σ = 0.0252)
Data / restraints / parameters	9067 / 3 / 411
Goodness-of-fit on F^2	1.111
Final *R* indexes ($I \ge 2\sigma(I)$)	R_1 = 0.0199, ωR_2 = 0.0471
Final *R* indexes (all data)	R_1 = 0.0219, ωR_2 = 0.0483
Largest diff. peak and hole / e/Å^3	1.10 and −0.77

Table 59: Bond lengths for **54**.

Atom	Atom	Length / Å	Atom	Atom	Length / Å
W	P	2.5688(5)	C6	C7	1.405(3)
W	C24	1.994(2)	C6	C11	1.398(3)
W	C25	2.059(2)	C7	C8	1.391(3)
W	C26	2.033(2)	C8	C9	1.391(3)
W	C27	2.046(2)	C9	C10	1.386(3)
W	C28	2.063(2)	C10	C11	1.396(3)
P	N1	1.8138(16)	C12	C13	1.400(3)
P	C5	1.9540(19)	C12	C17	1.400(3)
P	B	1.959(2)	C13	C14	1.391(3)
O1	C24	1.148(3)	C14	C15	1.391(3)
O2	C25	1.133(3)	C15	C16	1.383(3)
O3	C26	1.141(3)	C16	C17	1.395(3)
O4	C27	1.137(3)	C18	C19	1.395(3)
O5	C28	1.138(3)	C18	C23	1.406(3)
N1	C1	1.346(2)	C19	C20	1.399(3)
N1	C3	1.389(2)	C20	C21	1.383(3)
N2	C1	1.324(3)	C21	C22	1.391(3)
N2	C2	1.384(3)	C22	C23	1.386(3)
N2	C4	1.466(2)	Cl1	C29	1.757(3)
C2	C3	1.357(3)	Cl2	C29	1.754(3)
C5	C6	1.540(3)	Cl3	C30	1.764(2)
C5	C12	1.540(2)	Cl4	C30	1.754(2)
C5	C18	1.540(3)			

Table 60: Bond angles for **54**.

Atom	Atom	Atom	Angle / ˚	Atom	Atom	Atom	Angle / ˚
C24	W	P	172.79(6)	C18	C5	C6	112.55(15)
C24	W	C25	90.24(9)	C18	C5	C12	110.02(14)
C24	W	C26	87.53(9)	C7	C6	C5	120.86(16)
C24	W	C27	88.09(8)	C11	C6	C5	121.89(16)
C24	W	C28	88.45(9)	C11	C6	C7	117.24(17)
C25	W	P	84.05(7)	C8	C7	C6	121.67(18)
C25	W	C28	93.76(10)	C7	C8	C9	120.14(18)
C26	W	P	96.87(6)	C10	C9	C8	119.12(18)
C26	W	C25	90.24(9)	C9	C10	C11	120.68(19)
C26	W	C27	88.41(8)	C10	C11	C6	121.14(18)
C26	W	C28	174.34(8)	C13	C12	C5	120.91(16)
C27	W	P	97.72(6)	C17	C12	C5	120.82(17)
C27	W	C25	177.90(8)	C17	C12	C13	117.98(17)
C27	W	C28	87.47(8)	C14	C13	C12	121.12(18)
C28	W	P	87.54(6)	C15	C14	C13	120.20(19)
N1	P	W	107.17(5)	C16	C15	C14	119.34(18)
N1	P	C5	101.73(8)	C15	C16	C17	120.70(18)
N1	P	B	100.26(9)	C16	C17	C12	120.66(18)
C5	P	W	121.14(6)	C19	C18	C5	123.47(17)
C5	P	B	111.77(9)	C19	C18	C23	117.15(17)
B	P	W	111.89(7)	C23	C18	C5	119.37(17)
C1	N1	P	124.34(13)	C18	C19	C20	121.19(19)
C1	N1	C3	107.21(16)	C21	C20	C19	120.6(2)
C3	N1	P	128.07(13)	C20	C21	C22	119.02(19)
C1	N2	C2	108.74(16)	C23	C22	C21	120.33(19)
C1	N2	C4	126.56(17)	C22	C23	C18	121.58(19)
C2	N2	C4	124.68(17)	O1	C24	W	178.9(2)
N2	C1	N1	109.48(17)	O2	C25	W	178.1(2)
C3	C2	N2	106.78(17)	O3	C26	W	176.02(18)
C2	C3	N1	107.79(17)	O4	C27	W	175.58(17)
C6	C5	P	109.45(12)	O5	C28	W	175.0(2)
C6	C5	C12	109.55(14)	Cl2	C29	Cl1	112.35(14)
C12	C5	P	106.38(12)	Cl4	C30	Cl3	111.90(13)
C18	C5	P	108.70(12)				

Table 61: Torsion angles for **54**.

A	**B**	**C**	**D**	**Angle / ˚**	**A**	**B**	**C**	**D**	**Angle / ˚**
W	P	N1	C1	119.77(15)	C6	C7	C8	C9	−0.5(3)
W	P	N1	C3	−52.26(17)	C7	C6	C11	C10	−0.5(3)
P	N1	C1	N2	−173.41(13)	C7	C8	C9	C10	−0.1(3)
P	N1	C3	C2	173.17(14)	C8	C9	C10	C11	0.3(3)
P	C5	C6	C7	−60.2(2)	C9	C10	C11	C6	0.0(3)
P	C5	C6	C11	121.10(17)	C11	C6	C7	C8	0.8(3)
P	C5	C12	C13	−42.3(2)	C12	C5	C6	C7	−176.53(17)
P	C5	C12	C17	143.96(15)	C12	C5	C6	C11	4.8(2)
P	C5	C18	C19	118.38(17)	C12	C5	C18	C19	−125.50(19)
P	C5	C18	C23	−62.97(19)	C12	C5	C18	C23	53.1(2)
N2	C2	C3	N1	−0.1(2)	C12	C13	C14	C15	0.3(3)
C1	N1	C3	C2	0.0(2)	C13	C12	C17	C16	0.8(3)
C1	N2	C2	C3	0.1(2)	C13	C14	C15	C16	0.1(3)
C2	N2	C1	N1	−0.1(2)	C14	C15	C16	C17	−0.1(3)
C3	N1	C1	N2	0.0(2)	C15	C16	C17	C12	−0.4(3)
C4	N2	C1	N1	−178.51(18)	C17	C12	C13	C14	−0.8(3)
C4	N2	C2	C3	178.57(19)	C18	C5	C6	C7	60.7(2)
C5	P	N1	C1	−112.13(16)	C18	C5	C6	C11	−117.92(19)
C5	P	N1	C3	75.84(18)	C18	C5	C12	C13	−159.88(17)
C5	C6	C7	C8	−177.94(18)	C18	C5	C12	C17	26.4(2)
C5	C6	C11	C10	178.18(17)	C18	C19	C20	C21	−0.2(3)
C5	C12	C13	C14	−174.65(17)	C19	C18	C23	C22	−3.6(3)
C5	C12	C17	C16	174.71(17)	C19	C20	C21	C22	−1.9(3)
C5	C18	C19	C20	−178.43(17)	C20	C21	C22	C23	1.2(3)
C5	C18	C23	C22	177.68(17)	C21	C22	C23	C18	1.6(3)
C6	C5	C12	C13	75.9(2)	C23	C18	C19	C20	2.9(3)
C6	C5	C12	C17	−97.83(19)	B	P	N1	C1	2.87(18)
C6	C5	C18	C19	−3.0(2)	B	P	N1	C3	−169.17(17)
C6	C5	C18	C23	175.62(16)					

7.2.12 [Pentacarbonyl{({1-methylimidazol-3-iumyl}boratyl)(triphenylmethyl)phosphane-κ*P*}tungsten(0)] (55)

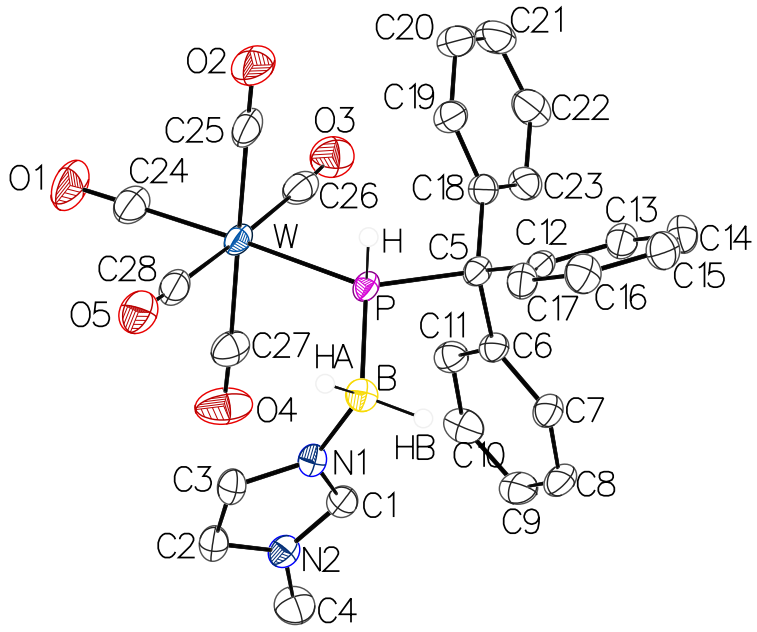

Figure 95: Molecular structures of **55** in the single crystal lattice at 100(2) K. Thermal ellipsoids are set at 50 % probability level. Solvent molecules and hydrogen atoms were omitted for clarity except for those bound to phosphorus and boron atoms.

Table 62: Crystal data and structure refinements for **55**.

Identification code	GSTR804, DB-636 // GXraymo_7283f
Crystal habitus	clear yellow block
Device type	Bruker D8 Venture
Empirical formula	$C_{32}H_{32}BN_2O_6PW$
Moiety formula	$C_{28}H_{24}BN_2O_5PW$, C_4H_8O
Formula weight / g/mol	766.22
T / K	100.0
Crystal system	triclinic
Space group	$P\bar{1}$
a / Å	9.5360(6)
b / Å	12.7052(8)
c / Å	13.0180(7)
α / °	86.357(2)
β / °	80.306(2)
γ / °	85.980(2)
V / Å^3	1548.73(16)
Z	2
ρ_{calc} / g/cm^3	1.643
μ / mm^{-1}	3.828

F(000)	760.0
Crystal size / mm^3	0.4 × 0.28 × 0.24
Absorption correction	multi-scan
Min. and max. transmission	0.4882 and 0.7461
Radiation	Mo-K_α (λ = 0.71073 Å)
2Θ range for data collection / °	4.342 to 55.998
Completeness to Θ	0.985
Index ranges	$-12 \le h \le 12$, $-16 \le k \le 16$, $-17 \le l \le 17$
Reflections collected	50193
Independent reflections	7393 (R_{int} = 0.0381, R_σ = 0.0296)
Data / restraints / parameters	7393 / 0 / 398
Goodness-of-fit on F^2	1.050
Final *R* indexes ($I \ge 2\sigma(I)$)	R_1 = 0.0154, ωR_2 = 0.0359
Final *R* indexes (all data)	R_1 = 0.0159, ωR_2 = 0.0361
Largest diff. peak and hole / e/Å^3	0.63 and −1.05

Table 63: Bond lengths for **55**.

Atom	Atom	Length / Å	Atom	Atom	Length / Å
W	P	2.5650(4)	C6	C7	1.397(2)
W	C24	1.9943(16)	C6	C11	1.4048(19)
W	C25	2.0465(16)	C7	C8	1.397(2)
W	C26	2.0377(17)	C8	C9	1.388(2)
W	C27	2.0510(16)	C9	C10	1.394(2)
W	C28	2.0509(17)	C10	C11	1.390(2)
P	C5	1.9179(14)	C12	C13	1.402(2)
P	B	1.9904(16)	C12	C17	1.395(2)
O1	C24	1.149(2)	C13	C14	1.388(2)
O2	C25	1.132(2)	C14	C15	1.390(2)
O3	C26	1.147(2)	C15	C16	1.383(2)
O4	C27	1.137(2)	C16	C17	1.3970(19)
O5	C28	1.142(2)	C18	C19	1.400(2)
N1	C1	1.3261(19)	C18	C23	1.398(2)
N1	C3	1.3853(18)	C19	C20	1.394(2)
N1	B	1.5586(19)	C20	C21	1.390(3)
N2	C1	1.3328(18)	C21	C22	1.384(3)
N2	C2	1.3757(19)	C22	C23	1.397(2)
N2	C4	1.4565(19)	O6	C29	1.428(2)
C2	C3	1.357(2)	O6	C32	1.425(2)
C5	C6	1.5379(19)	C29	C30	1.532(2)
C5	C12	1.5487(18)	C30	C31	1.542(2)
C5	C18	1.5387(19)	C31	C32	1.524(2)

Table 64: Bond lengths for **55**.

Atom	Atom	Atom	Angle / ˚	Atom	Atom	Atom	Angle / ˚
C24	W	P	173.51(5)	C7	C6	C11	117.67(13)
C24	W	C25	90.56(6)	C11	C6	C5	119.86(12)
C24	W	C26	89.31(6)	C8	C7	C6	120.99(14)
C24	W	C27	88.44(6)	C9	C8	C7	120.69(14)
C24	W	C28	89.92(6)	C8	C9	C10	119.01(14)
C25	W	P	87.84(4)	C11	C10	C9	120.33(14)
C25	W	C27	177.15(6)	C10	C11	C6	121.30(14)
C25	W	C28	90.27(6)	C13	C12	C5	117.91(12)
C26	W	P	96.91(4)	C17	C12	C5	124.65(13)
C26	W	C25	87.80(6)	C17	C12	C13	117.44(13)
C26	W	C27	89.53(6)	C14	C13	C12	121.51(14)
C26	W	C28	177.91(6)	C13	C14	C15	120.19(14)
C27	W	P	93.45(4)	C16	C15	C14	119.24(14)
C28	W	P	83.80(4)	C15	C16	C17	120.52(14)
C28	W	C27	92.40(6)	C12	C17	C16	121.11(14)
C5	P	W	123.10(4)	C19	C18	C5	119.55(13)
C5	P	B	107.48(6)	C23	C18	C5	122.31(13)
B	P	W	118.20(5)	C23	C18	C19	118.00(14)
C1	N1	C3	107.09(12)	C20	C19	C18	121.05(15)
C1	N1	B	124.91(12)	C21	C20	C19	120.06(15)
C3	N1	B	128.00(12)	C22	C21	C20	119.60(15)
C1	N2	C2	108.47(12)	C21	C22	C23	120.33(15)
C1	N2	C4	125.11(13)	C22	C23	C18	120.85(15)
C2	N2	C4	126.42(13)	O1	C24	W	179.56(15)
N1	C1	N2	109.88(13)	O2	C25	W	178.79(15)
C3	C2	N2	106.40(12)	O3	C26	W	176.80(13)
C2	C3	N1	108.15(13)	O4	C27	W	175.47(13)
C6	C5	P	104.42(9)	O5	C28	W	178.36(14)
C6	C5	C12	111.54(11)	N1	B	P	111.31(9)
C6	C5	C18	112.47(11)	C32	O6	C29	104.68(13)
C12	C5	P	112.25(9)	O6	C29	C30	105.52(13)
C18	C5	P	109.58(9)	C29	C30	C31	103.61(13)
C18	C5	C12	106.68(11)	C32	C31	C30	103.54(13)
C7	C6	C5	122.41(12)	O6	C32	C31	105.69(14)

Table 65: Torsion lengths for **55**.

A	**B**	**C**	**D**	**Angle / ˚**	**A**	**B**	**C**	**D**	**Angle / ˚**
P	C5	C6	C7	105.9(12)	C9	C10	C11	C6	0(2)
P	C5	C6	C11	−70.2(14)	C11	C6	C7	C8	0(2)
P	C5	C12	C13	−52.3(14)	C12	C5	C6	C7	−135.6(13)
P	C5	C12	C17	134.6(12)	C12	C5	C6	C11	48.4(17)
P	C5	C18	C19	172.1(10)	C12	C5	C18	C19	52.8(15)
P	C5	C18	C23	−5.3(18)	C12	C5	C18	C23	−124.6(14)
N2	C2	C3	N1	1.1(16)	C12	C13	C14	C15	1(2)
C1	N1	C3	C2	−1.5(17)	C13	C12	C17	C16	1(2)
C1	N1	B	P	100.1(16)	C13	C14	C15	C16	0(2)
C1	N2	C2	C3	−0.3(16)	C14	C15	C16	C17	−1(2)
C2	N2	C1	N1	−0.7(17)	C15	C16	C17	C12	0(2)
C3	N1	C1	N2	1.3(18)	C17	C12	C13	C14	−2(2)
C3	N1	B	P	−81.5(16)	C18	C5	C6	C7	−15.6(18)
C4	N2	C1	N1	−176.2(13)	C18	C5	C6	C11	168.4(12)
C4	N2	C2	C3	175.1(13)	C18	C5	C12	C13	68.8(14)
C5	C6	C7	C8	−176.5(13)	C18	C5	C12	C17	−104.3(14)
C5	C6	C11	C10	176.4(13)	C18	C19	C20	C21	−3(2)
C5	C12	C13	C14	−175.9(12)	C19	C18	C23	C22	0(2)
C5	C12	C17	C16	174.5(13)	C19	C20	C21	C22	5(2)
C5	C18	C19	C20	−177.1(13)	C20	C21	C22	C23	−4(2)
C5	C18	C23	C22	177.4(14)	C21	C22	C23	C18	2(2)
C6	C5	C12	C13	−167.5(12)	C23	C18	C19	C20	1(2)
C6	C5	C12	C17	19.4(18)	B	N1	C1	N2	−180.0(13)
C6	C5	C18	C19	−71.4(16)	B	N1	C3	C2	179.8(13)
C6	C5	C18	C23	111.2(15)	O6	C29	C30	C31	23.3(14)
C6	C7	C8	C9	0(2)	C29	O6	C32	C31	−25.7(16)
C7	C6	C11	C10	0(2)	C29	C30	C31	C32	−37.3(15)
C7	C8	C9	C10	0(2)	C30	C31	C32	O6	39.1(15)
C8	C9	C10	C11	0(2)	C32	O6	C29	C30	0.9(15)

7.2.13 [Pentacarbonyl{hydroxy(triphenylmethyl)phosphane-κ*P*}chromium(0)] (47a)

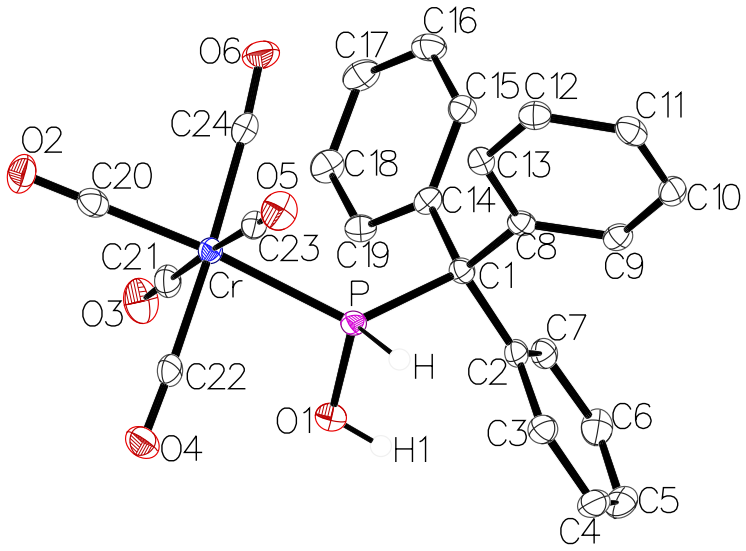

Figure 96: Molecular structures of **47a** in the single crystal lattice at 100(2) K. Thermal ellipsoids are set at 50 % probability level. Hydrogen atoms were omitted for clarity except for those bound to phosphorus and oxygen atoms.

Table 66: Crystal data and structure refinements for **47a**.

Identification code	GSTR772, DB-547 // GXray6924
Crystal habitus	clear colorless plate
Device type	STOE STADIVARI
Empirical formula	$C_{24}H_{17}CrO_6P$
Moiety formula	$C_{24}H_{17}CrO_6P$
Formula weight / g/mol	484.34
T / K	100
Crystal system	triclinic
Space group	$P\bar{1}$
a / Å	9.2146(3)
b / Å	10.4151(3)
c / Å	11.5363(3)
α / °	89.614(2)
β / °	83.365(2)
γ / °	84.417(2)
V / Å^3	1094.51(6)
Z	2
ρ_{calc} / g/cm^3	1.470
μ / mm^{-1}	5.331
F(000)	496.0
Crystal size / mm^3	0.24 × 0.167 × 0.04
Absorption correction	multi-scan
Min. and max. transmission	0.5412 and 0.7082

Radiation	Cu-K_α (λ = 1.54186 Å)
2Θ range for data collection / °	7.716 to 140.566
Completeness to Θ	0.984
Index ranges	$-11 \leq h \leq 5$, $-12 \leq k \leq 12$, $-14 \leq l \leq 12$
Reflections collected	14695
Independent reflections	4045 (R_{int} = 0.0248, R_σ = 0.0193)
Data / restraints / parameters	4045 / 0 / 294
Goodness-of-fit on F^2	1.059
Final R indexes ($I \geq 2\sigma(I)$)	R_1 = 0.0314, ωR_2 = 0.0858
Final R indexes (all data)	R_1 = 0.0350, ωR_2 = 0.0878
Largest diff. peak and hole / e/Å^3	0.34 and −0.39

Table 67: Bond lengths for **47a**.

Atom	**Atom**	**Length / Å**	**Atom**	**Atom**	**Length / Å**
Cr	P	2.3360(5)	C2	C7	1.394(3)
Cr	C20	1.874(2)	C3	C4	1.389(3)
Cr	C21	1.910(2)	C4	C5	1.388(3)
Cr	C22	1.889(2)	C5	C6	1.380(3)
Cr	C23	1.900(2)	C6	C7	1.395(3)
Cr	C24	1.915(2)	C8	C9	1.391(3)
P	O1	1.6319(14)	C8	C13	1.398(3)
P	C1	1.9145(18)	C9	C10	1.393(3)
O2	C20	1.147(3)	C10	C11	1.385(3)
O3	C21	1.137(3)	C11	C12	1.394(3)
O4	C22	1.147(2)	C12	C13	1.390(3)
O5	C23	1.140(2)	C14	C15	1.396(3)
O6	C24	1.139(2)	C14	C19	1.398(3)
C1	C2	1.543(2)	C15	C16	1.390(3)
C1	C8	1.541(2)	C16	C17	1.385(3)
C1	C14	1.534(2)	C17	C18	1.390(3)
C2	C3	1.402(3)	C18	C19	1.385(3)

Table 68: Bond angles for **47a**.

Atom	Atom	Atom	Angle / °	Atom	Atom	Atom	Angle / °
C20	Cr	P	174.15(6)	C4	C3	C2	121.08(19)
C20	Cr	C21	92.00(8)	C5	C4	C3	120.07(19)
C20	Cr	C22	88.96(8)	C6	C5	C4	119.67(19)
C20	Cr	C23	89.27(8)	C5	C6	C7	120.35(19)
C20	Cr	C24	89.05(8)	C2	C7	C6	120.85(18)
C21	Cr	P	89.97(6)	C9	C8	C1	121.02(16)
C21	Cr	C24	89.14(8)	C9	C8	C13	118.06(17)
C22	Cr	P	85.60(6)	C13	C8	C1	120.84(16)
C22	Cr	C21	88.16(8)	C8	C9	C10	120.94(18)
C22	Cr	C23	90.08(8)	C11	C10	C9	120.49(18)
C22	Cr	C24	176.59(8)	C10	C11	C12	119.26(18)
C23	Cr	P	88.60(6)	C13	C12	C11	120.00(18)
C23	Cr	C21	177.82(8)	C12	C13	C8	121.22(17)
C23	Cr	C24	92.66(8)	C15	C14	C1	122.34(17)
C24	Cr	P	96.48(6)	C15	C14	C19	117.95(17)
O1	P	Cr	107.02(5)	C19	C14	C1	119.71(16)
O1	P	C1	104.28(8)	C16	C15	C14	120.78(18)
C1	P	Cr	128.33(6)	C17	C16	C15	120.57(19)
C2	C1	P	106.73(12)	C16	C17	C18	119.28(18)
C8	C1	P	107.92(12)	C19	C18	C17	120.15(19)
C8	C1	C2	110.13(14)	C18	C19	C14	121.27(18)
C14	C1	P	107.64(12)	O2	C20	Cr	178.28(18)
C14	C1	C2	112.13(15)	O3	C21	Cr	178.36(18)
C14	C1	C8	112.03(15)	O4	C22	Cr	177.52(16)
C3	C2	C1	119.75(16)	O5	C23	Cr	178.68(17)
C7	C2	C1	122.24(16)	O6	C24	Cr	176.59(16)
C7	C2	C3	117.96(17)				

Table 69: Torsion angles for **47a**.

A	**B**	**C**	**D**	**Angle / °**	**A**	**B**	**C**	**D**	**Angle / °**
P	C1	C2	C3	-54.74(19)	C7	C2	C3	C4	-1.0(3)
P	C1	C2	C7	127.92(16)	C8	C1	C2	C3	62.2(2)
P	C1	C8	C9	133.86(15)	C8	C1	C2	C7	-115.18(19)
P	C1	C8	C13	-49.5(2)	C8	C1	C14	C15	10.8(2)
P	C1	C14	C15	129.31(16)	C8	C1	C14	C19	-169.39(16)
P	C1	C14	C19	-50.91(19)	C8	C9	C10	C11	0.7(3)
C1	C2	C3	C4	-178.44(17)	C9	C8	C13	C12	-1.2(3)
C1	C2	C7	C6	177.17(17)	C9	C10	C11	C12	-1.5(3)
C1	C8	C9	C10	177.38(16)	C10	C11	C12	C13	1.0(3)
C1	C8	C13	C12	-177.93(17)	C11	C12	C13	C8	0.4(3)
C1	C14	C15	C16	-179.07(17)	C13	C8	C9	C10	0.6(3)
C1	C14	C19	C18	178.90(17)	C14	C1	C2	C3	-172.37(17)
C2	C1	C8	C9	17.7(2)	C14	C1	C2	C7	10.3(2)
C2	C1	C8	C13	-165.63(16)	C14	C1	C8	C9	-107.82(19)
C2	C1	C14	C15	-113.60(19)	C14	C1	C8	C13	68.8(2)
C2	C1	C14	C19	66.2(2)	C14	C15	C16	C17	-0.3(3)
C2	C3	C4	C5	1.4(3)	C15	C14	C19	C18	-1.3(3)
C3	C2	C7	C6	-0.2(3)	C15	C16	C17	C18	-0.4(3)
C3	C4	C5	C6	-0.7(3)	C16	C17	C18	C19	0.3(3)
C4	C5	C6	C7	-0.5(3)	C17	C18	C19	C14	0.6(3)
C5	C6	C7	C2	1.0(3)	C19	C14	C15	C16	1.1(3)

7.2.14 [Pentacarbonyl{hydroxy(triphenylmethyl)phosphane-κ*P*}tungsten(0)] (47b)

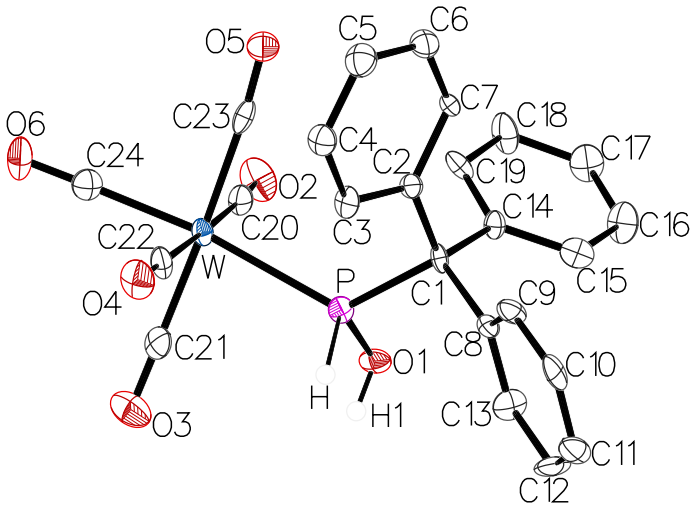

Figure 97: Molecular structures of **47b** in the single crystal lattice at 100(2) K. Thermal ellipsoids are set at 50 % probability level. Hydrogen atoms and solvent molecules were omitted for clarity except for those bound to phosphorus and oxygen atoms.

Table 70: Crystal data and structure refinements for **47b**.

Identification code	GSTR738, DB-403 // GXraymo_6721_0m_4
Crystal habitus	clear colorless block
Device type	Bruker D8 Venture
Empirical formula	$C_{52}H_{42}O_{13}P_2W_2$
Moiety formula	2 ($C_{24}H_{17}O_6PW$), C_4H_8O
Formula weight / g/mol	1304.49
T / K	100.0
Crystal system	triclinic
Space group	$P\bar{1}$
a / Å	9.3995(9)
b / Å	11.6790(10)
c / Å	12.0501(11)
α / °	97.985(3)
β / °	91.166(4)
γ / °	109.171(3)
V / Å^3	1234.3(2)
Z	1
ρ_{calc} / g/cm^3	1.755
μ / mm^{-1}	4.786
F(000)	636.0
Crystal size / mm^3	0.4 × 0.24 × 0.2
Absorption correction	empirical
Min. and max. transmission	0.588614 and 0.745472
Radiation	Mo-K_α (λ = 0.71073 Å)

2Θ range for data collection / °	3.736 to 52
Completeness to Θ	0.969
Index ranges	$-11 \leq h \leq 11$, $-14 \leq k \leq 14$, $0 \leq l \leq 14$
Reflections collected	4891
Independent reflections	4891 (R_{int} = ?, R_σ = 0.0860)
Data / restraints / parameters	4891 / 117 / 342
Goodness-of-fit on F^2	1.110
Final R indexes ($I \geq 2\sigma(I)$)	R_1 = 0.0565, ωR_2 = 0.1230
Final R indexes (all data)	R_1 = 0.0745, ωR_2 = 0.1317
Largest diff. peak and hole / e/Å^3	2.06 and −2.81

Table 71: Bond lengths for **47b**.

Atom	**Atom**	**Length / Å**	**Atom**	**Atom**	**Length / Å**
W	P	2.527(3)	C5	C6	1.390(16)
W	C20	2.053(12)	C6	C7	1.385(15)
W	C21	1.986(12)	C8	C9	1.401(14)
W	C22	2.032(11)	C8	C13	1.383(15)
W	C23	2.017(12)	C9	C10	1.393(15)
W	C24	1.991(11)	C10	C11	1.371(17)
P	O1	1.575(8)	C11	C12	1.404(16)
P	C1	1.919(10)	C12	C13	1.395(15)
O2	C20	1.135(13)	C14	C15	1.386(15)
O3	C21	1.184(14)	C14	C19	1.394(15)
O4	C22	1.154(13)	C15	C16	1.390(16)
O5	C23	1.172(13)	C16	C17	1.387(17)
O6	C24	1.150(13)	C17	C18	1.378(17)
C1	C2	1.521(14)	C18	C19	1.398(15)
C1	C8	1.538(14)	O7	C25	1.361(13)
C1	C14	1.565(14)	O7	C28	1.396(14)
C2	C3	1.405(13)	C25	C26	1.465(13)
C2	C7	1.410(14)	C26	C27	1.474(13)
C3	C4	1.366(15)	C27	C28	1.458(13)
C4	C5	1.391(16)			

Table 72: Bond angles for **47b**.

Atom	Atom	Atom	Angle / °	Atom	Atom	Atom	Angle / °
C20	W	P	91.5(3)	C6	C5	C4	117.8(11)
C21	W	P	86.3(3)	C7	C6	C5	121.6(11)
C21	W	C20	90.7(4)	C6	C7	C2	119.8(10)
C21	W	C22	89.2(4)	C9	C8	C1	120.9(9)
C21	W	C23	177.3(5)	C13	C8	C1	122.5(9)
C21	W	C24	87.0(5)	C13	C8	C9	116.6(10)
C22	W	P	90.1(3)	C10	C9	C8	122.2(11)
C22	W	C20	178.4(4)	C11	C10	C9	120.5(10)
C23	W	P	96.0(3)	C10	C11	C12	118.5(10)
C23	W	C20	88.0(4)	C13	C12	C11	120.4(11)
C23	W	C22	92.1(4)	C8	C13	C12	121.8(10)
C24	W	P	173.1(3)	C15	C14	C1	122.6(9)
C24	W	C20	90.1(4)	C15	C14	C19	118.1(10)
C24	W	C22	88.4(4)	C19	C14	C1	119.3(9)
C24	W	C23	90.7(4)	C14	C15	C16	120.6(11)
O1	P	W	113.8(3)	C17	C16	C15	120.2(11)
O1	P	C1	105.8(4)	C18	C17	C16	120.6(11)
C1	P	W	124.1(3)	C17	C18	C19	118.4(11)
C2	C1	P	109.2(6)	C14	C19	C18	122.1(11)
C2	C1	C8	110.2(8)	O2	C20	W	176.6(10)
C2	C1	C14	111.9(9)	O3	C21	W	178.6(9)
C8	C1	P	109.0(7)	O4	C22	W	179.3(9)
C8	C1	C14	111.0(8)	O5	C23	W	174.4(8)
C14	C1	P	105.3(6)	O6	C24	W	178.9(11)
C3	C2	C1	118.8(9)	C25	O7	C28	109.0(13)
C3	C2	C7	118.3(10)	O7	C25	C26	112.0(11)
C7	C2	C1	122.8(9)	C25	C26	C27	103.0(10)
C4	C3	C2	120.5(10)	C28	C27	C26	107.6(10)
C3	C4	C5	122.0(10)	O7	C28	C27	108.3(12)

Table 73: Torsion angles for **47b**.

A	B	C	D	Angle / °	A	B	C	D	Angle / °
P	C1	C2	C3	50.3(11)	C8	C1	C14	C15	−1.7(14)
P	C1	C2	C7	−133.5(9)	C8	C1	C14	C19	177.2(9)
P	C1	C8	C9	−129.0(9)	C8	C9	C10	C11	−1.5(17)
P	C1	C8	C13	49.9(12)	C9	C8	C13	C12	0.2(17)
P	C1	C14	C15	−119.6(10)	C9	C10	C11	C12	1.8(17)
P	C1	C14	C19	59.3(11)	C10	C11	C12	C13	−1.1(18)
C1	C2	C3	C4	177.2(9)	C11	C12	C13	C8	0.1(18)
C1	C2	C7	C6	−176.0(9)	C13	C8	C9	C10	0.5(16)
C1	C8	C9	C10	179.4(9)	C14	C1	C2	C3	166.5(9)
C1	C8	C13	C12	−178.7(10)	C14	C1	C2	C7	−17.3(13)
C1	C14	C15	C16	178.8(10)	C14	C1	C8	C9	115.4(11)
C1	C14	C19	C18	−179.7(10)	C14	C1	C8	C13	−65.8(13)
C2	C1	C8	C9	−9.1(13)	C14	C15	C16	C17	0.7(18)
C2	C1	C8	C13	169.7(10)	C15	C14	C19	C18	−0.7(17)
C2	C1	C14	C15	121.9(11)	C15	C16	C17	C18	0(2)
C2	C1	C14	C19	−59.2(12)	C16	C17	C18	C19	−0.4(19)
C2	C3	C4	C5	−2.2(17)	C17	C18	C19	C14	1.0(18)
C3	C2	C7	C6	0.2(15)	C19	C14	C15	C16	−0.1(17)
C3	C4	C5	C6	2.4(17)	O7	C25	C26	C27	1(2)
C4	C5	C6	C7	−1.3(17)	C25	O7	C28	C27	1(2)
C5	C6	C7	C2	0.0(16)	C25	C26	C27	C28	−1(2)
C7	C2	C3	C4	0.8(15)	C26	C27	C28	O7	0(2)
C8	C1	C2	C3	−69.5(11)	C28	O7	C25	C26	−1(2)
C8	C1	C2	C7	106.8(11)					

7.2.15 [Pentacarbonyl{trifluoroacetyl(triphenylmethyl)phosphane-κ*P*}chromium(0)] (62a)

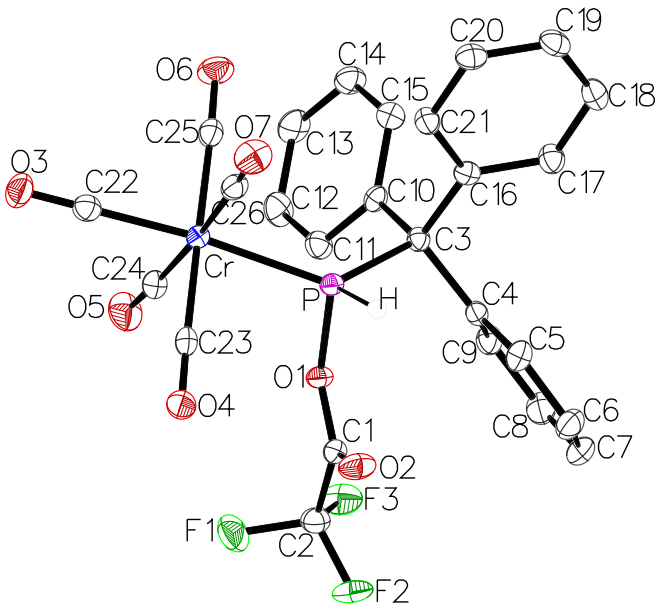

Figure 98: Molecular structures of **62a** in the single crystal lattice at 123(2) K. Thermal ellipsoids are set at 50 % probability level. Hydrogen atoms were omitted for clarity except for those bound to phosphorus atoms.

Table 74: Crystal data and structure refinements for **62a**.

Identification code	GSTR770, DB-557 // GXray6913
Crystal habitus	clear colorless plate
Device type	STOE IPDS-2T
Empirical formula	$C_{26}H_{16}CrF_3O_7P$
Moiety formula	$C_{26}H_{16}CrF_3O_7P$
Formula weight / g/mol	580.36
T / K	123(2)
Crystal system	monoclinic
Space group	$P2_1/c$
a / Å	11.7074(11)
b / Å	10.9879(9)
c / Å	19.4438(23)
α / °	90.00
β / °	95.019(8)
γ / °	90.00
V / Å^3	2491.7(4)
Z	4
ρ_{calc} / g/cm^3	1.547
μ / mm^{-1}	0.17
F(000)	1176.0
Crystal size / mm^3	0.3 × 0.25 × 0.14

Absorption correction	integration
Min. and max. transmission	0.8377 and 0.9602
Radiation	Mo-K_α (λ = 0.71073 Å)
2Θ range for data collection / °	4.206 to 55.992
Completeness to Θ	0.990
Index ranges	$-15 \leq h \leq 12$, $-14 \leq k \leq 13$, $-24 \leq l \leq 25$
Reflections collected	12331
Independent reflections	13501 (R_{int} = 0.0396, R_σ = 0.0468)
Data / restraints / parameters	13501 / 0 / 346
Goodness-of-fit on F^2	1.013
Final R indexes ($I \geq 2\sigma(I)$)	R_1 = 0.0296, ωR_2 = 0.0776
Final R indexes (all data)	R_1 = 0.0433, ωR_2 = 0.0814
Largest diff. peak and hole / e/Å^3	0.39 and −0.50

Table 75: Bond lengths for **62a**.

Atom	**Atom**	**Length / Å**	**Atom**	**Atom**	**Length / Å**
Cr	P	2.3224(5)	C3	C10	1.543(2)
Cr	C22	1.8880(17)	C3	C16	1.5394(19)
Cr	C23	1.9096(17)	C4	C5	1.401(2)
Cr	C24	1.9071(17)	C4	C9	1.393(2)
Cr	C25	1.9158(17)	C5	C6	1.388(2)
Cr	C26	1.9115(16)	C6	C7	1.391(2)
P	O1	1.7017(10)	C7	C8	1.378(3)
P	C3	1.9148(16)	C8	C9	1.395(2)
F1	C2	1.3311(19)	C10	C11	1.400(2)
F2	C2	1.3259(19)	C10	C15	1.392(2)
F3	C2	1.3385(19)	C11	C12	1.385(2)
O1	C1	1.3280(18)	C12	C13	1.392(3)
O2	C1	1.1958(19)	C13	C14	1.381(2)
O3	C22	1.143(2)	C14	C15	1.390(2)
O4	C23	1.143(2)	C16	C17	1.397(2)
O5	C24	1.1388(19)	C16	C21	1.397(2)
O6	C25	1.140(2)	C17	C18	1.389(2)
O7	C26	1.1378(19)	C18	C19	1.393(2)
C1	C2	1.536(2)	C19	C20	1.383(2)
C3	C4	1.548(2)	C20	C21	1.393(2)

Table 76: Bond angles for **62a**.

Atom	Atom	Atom	Angle / °	Atom	Atom	Atom	Angle / °
C22	Cr	P	174.95(5)	C16	C3	C4	110.18(12)
C22	Cr	C23	90.45(7)	C16	C3	C10	110.43(12)
C22	Cr	C24	87.59(7)	C5	C4	C3	119.15(13)
C22	Cr	C25	90.37(7)	C9	C4	C3	122.72(14)
C22	Cr	C26	88.88(7)	C9	C4	C5	118.13(14)
C23	Cr	P	84.68(5)	C6	C5	C4	121.21(15)
C23	Cr	C25	178.85(7)	C5	C6	C7	119.95(16)
C23	Cr	C26	89.25(7)	C8	C7	C6	119.37(15)
C24	Cr	P	91.10(5)	C7	C8	C9	120.91(15)
C24	Cr	C23	90.88(7)	C4	C9	C8	120.40(15)
C24	Cr	C25	88.36(7)	C11	C10	C3	120.07(13)
C24	Cr	C26	176.46(7)	C15	C10	C3	121.96(13)
C25	Cr	P	94.47(5)	C15	C10	C11	117.96(14)
C26	Cr	P	92.43(5)	C12	C11	C10	121.05(15)
C26	Cr	C25	91.56(7)	C11	C12	C13	120.36(16)
O1	P	Cr	106.46(4)	C14	C13	C12	119.03(15)
O1	P	C3	97.56(6)	C13	C14	C15	120.73(16)
C3	P	Cr	131.96(5)	C14	C15	C10	120.87(15)
C1	O1	P	124.16(9)	C17	C16	C3	119.58(13)
O1	C1	C2	109.26(12)	C17	C16	C21	118.30(13)
O2	C1	O1	127.93(14)	C21	C16	C3	121.86(14)
O2	C1	C2	122.74(14)	C18	C17	C16	120.82(14)
F1	C2	F3	107.63(14)	C17	C18	C19	120.32(16)
F1	C2	C1	109.83(13)	C20	C19	C18	119.44(14)
F2	C2	F1	108.75(13)	C19	C20	C21	120.32(14)
F2	C2	F3	108.41(13)	C20	C21	C16	120.80(15)
F2	C2	C1	110.39(13)	O3	C22	Cr	178.80(14)
F3	C2	C1	111.75(13)	O4	C23	Cr	178.32(15)
C4	C3	P	106.61(10)	O5	C24	Cr	176.75(15)
C10	C3	P	107.29(10)	O6	C25	Cr	177.71(14)
C10	C3	C4	113.57(12)	O7	C26	Cr	177.31(15)
C16	C3	P	108.54(10)				

7.2.16 [Pentacarbonyl{trifluoroacetyl(triphenylmethyl)phosphane-κ*P*}tungsten(0)] (62b)

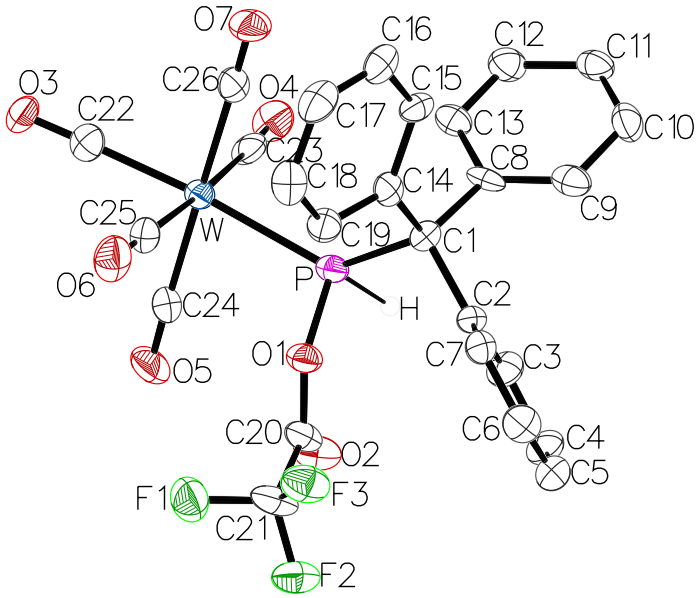

Figure 99: Molecular structures of **62b** in the single crystal lattice at 123(2) K. Thermal ellipsoids are set at 50 % probability level. Hydrogen atoms were omitted for clarity except for those bound to phosphorus atoms.

Table 77: Crystal data and structure refinements for **62b**.

Identification code	GSTR777, DB-550 // GXray6912
Crystal habitus	clear colorless block
Device type	STOE IPDS2T
Empirical formula	$C_{26}H_{16}F_3O_7PW$
Moiety formula	$C_{26}H_{16}F_3O_7PW$
Formula weight / g/mol	712.21
T / K	123(2)
Crystal system	monoclinic
Space group	$P2_1/c$
a / Å	11.7247(3)
b / Å	11.0478(4)
c / Å	19.5690(5)
α / °	90
β / °	95.179(2)
γ / °	90
V / Å^3	2524.47(13)
Z	4
ρ_{calc} / g/cm^3	1.874
μ / mm^{-1}	4.706
F(000)	1376.0
Crystal size / mm^3	0.12 × 0.11 × 0.08
Absorption correction	multi-scan
Min. and max. transmission	0.0215 and 0.9140

Radiation	Mo-K_α (λ = 0.71073 Å)
2Θ range for data collection / °	5.076 to 50.5
Completeness to Θ	0.956
Index ranges	$-13 \leq h \leq 14$, $-13 \leq k \leq 13$, $-23 \leq l \leq 23$
Reflections collected	18095
Independent reflections	4366 (R_{int} = 0.1136, R_σ = 0.0689)
Data / restraints / parameters	4366 / 1 / 347
Goodness-of-fit on F^2	1.064
Final R indexes ($I \geq 2\sigma(I)$)	R_1 = 0.0731, ωR_2 = 0.1711
Final R indexes (all data)	R_1 = 0.0923, ωR_2 = 0.2016
Largest diff. peak and hole / e/Å^3	2.73 and −1.74

Table 78: Bond lengths for **62b**.

Atom	Atom	Length / Å	Atom	Atom	Length / Å
W	P	2.452(3)	C1	C14	1.503(18)
W	C22	2.001(14)	C2	C3	1.393(19)
W	C23	2.054(14)	C2	C7	1.403(18)
W	C24	2.070(14)	C3	C4	1.42(2)
W	C25	2.043(16)	C4	C5	1.38(2)
W	C26	2.064(13)	C5	C6	1.38(2)
P	O1	1.695(9)	C6	C7	1.40(2)
P	C1	1.915(12)	C8	C9	1.37(2)
F1	C21	1.34(2)	C8	C13	1.402(19)
F2	C21	1.296(18)	C9	C10	1.427(18)
F3	C21	1.339(17)	C10	C11	1.39(2)
O1	C20	1.349(16)	C11	C12	1.41(2)
O2	C20	1.170(17)	C12	C13	1.377(18)
O3	C22	1.143(17)	C14	C15	1.408(17)
O4	C23	1.132(17)	C14	C19	1.403(18)
O5	C24	1.118(17)	C15	C16	1.390(19)
O6	C25	1.125(18)	C16	C17	1.36(2)
O7	C26	1.110(16)	C17	C18	1.38(2)
C1	C2	1.551(17)	C18	C19	1.38(2)
C1	C8	1.553(15)	C20	C21	1.515(18)

Table 79: Bond angles for **62b**.

Atom	Atom	Atom	Angle / °	Atom	Atom	Atom	Angle / °
C22	W	P	175.5(4)	C6	C7	C2	121.0(13)
C22	W	C23	89.5(5)	C9	C8	C1	119.0(11)
C22	W	C24	90.4(6)	C9	C8	C13	120.1(11)
C22	W	C25	87.4(5)	C13	C8	C1	120.5(12)
C22	W	C26	90.0(5)	C8	C9	C10	120.1(13)
C23	W	P	92.0(4)	C11	C10	C9	119.8(13)
C23	W	C24	88.4(5)	C10	C11	C12	119.0(12)
C23	W	C26	91.6(5)	C13	C12	C11	120.8(13)
C24	W	P	85.3(4)	C12	C13	C8	120.2(13)
C25	W	P	91.2(4)	C15	C14	C1	121.9(11)
C25	W	C23	176.8(5)	C19	C14	C1	121.6(11)
C25	W	C24	92.3(5)	C19	C14	C15	116.5(13)
C25	W	C26	87.7(5)	C16	C15	C14	121.6(13)
C26	W	P	94.2(4)	C17	C16	C15	119.3(13)
C26	W	C24	179.5(5)	C16	C17	C18	122.0(14)
O1	P	W	106.6(3)	C17	C18	C19	118.5(14)
O1	P	C1	97.5(5)	C18	C19	C14	122.1(13)
C1	P	W	130.6(4)	O1	C20	C21	109.8(12)
C20	O1	P	124.0(9)	O2	C20	O1	126.1(12)
C2	C1	P	105.8(8)	O2	C20	C21	124.0(12)
C2	C1	C8	109.3(10)	F1	C21	C20	110.4(12)
C8	C1	P	108.2(8)	F2	C21	F1	107.3(11)
C14	C1	P	107.0(8)	F2	C21	F3	109.0(12)
C14	C1	C2	113.9(10)	F2	C21	C20	111.3(14)
C14	C1	C8	112.2(9)	F3	C21	F1	106.5(13)
C3	C2	C1	118.3(12)	F3	C21	C20	112.1(11)
C3	C2	C7	118.9(12)	O3	C22	W	178.8(12)
C7	C2	C1	122.8(11)	O4	C23	W	176.6(12)
C2	C3	C4	119.3(13)	O5	C24	W	178.8(13)
C5	C4	C3	120.6(13)	O6	C25	W	177.6(13)
C6	C5	C4	120.6(14)	O7	C26	W	178.7(13)
C5	C6	C7	119.5(14)				

Table 80: Torsion angles for **62b**.

A	B	C	D	Angle / °	A	B	C	D	Angle / °
W	P	O1	C20	102.8(10)	C2	C3	C4	C5	−2(2)
P	O1	C20	O2	−4(2)	C3	C2	C7	C6	−0.7(18)
P	O1	C20	C21	−179.2(9)	C3	C4	C5	C6	0(2)
P	C1	C2	C3	60.1(13)	C4	C5	C6	C7	1(2)
P	C1	C2	C7	−119.6(11)	C5	C6	C7	C2	−1(2)
P	C1	C8	C9	−148.7(10)	C7	C2	C3	C4	1.8(19)
P	C1	C8	C13	38.1(13)	C8	C1	C2	C3	−56.2(14)
P	C1	C14	C15	−126.6(11)	C8	C1	C2	C7	124.1(12)
P	C1	C14	C19	53.7(14)	C8	C1	C14	C15	−8.0(16)
O1	C20	C21	F1	79.9(14)	C8	C1	C14	C19	172.3(12)
O1	C20	C21	F2	−161.1(12)	C8	C9	C10	C11	−1(2)
O1	C20	C21	F3	−38.7(18)	C9	C8	C13	C12	0.9(19)
O2	C20	C21	F1	−95.6(19)	C9	C10	C11	C12	2(2)
O2	C20	C21	F2	23(2)	C10	C11	C12	C13	−1(2)
O2	C20	C21	F3	145.8(15)	C11	C12	C13	C8	−1(2)
C1	P	O1	C20	−120.7(11)	C13	C8	C9	C10	0.1(19)
C1	C2	C3	C4	−177.9(12)	C14	C1	C2	C3	177.4(11)
C1	C2	C7	C6	179.0(12)	C14	C1	C2	C7	−2.3(16)
C1	C8	C9	C10	−173.2(12)	C14	C1	C8	C9	93.4(14)
C1	C8	C13	C12	174.1(12)	C14	C1	C8	C13	−79.8(14)
C1	C14	C15	C16	178.8(12)	C14	C15	C16	C17	1(2)
C1	C14	C19	C18	−179.6(12)	C15	C14	C19	C18	1(2)
C2	C1	C8	C9	−33.9(15)	C15	C16	C17	C18	1(2)
C2	C1	C8	C13	152.8(11)	C16	C17	C18	C19	−2(2)
C2	C1	C14	C15	116.8(12)	C17	C18	C19	C14	1(2)
C2	C1	C14	C19	−62.9(15)	C19	C14	C15	C16	−1.5(18)

7.2.17 [Pentacarbonyl{1-methylimidazol-3-iumyl(triphenylmethyl)phosphane-κ*P*}tungsten(0)] trifluoromethanesulfonate (64b)

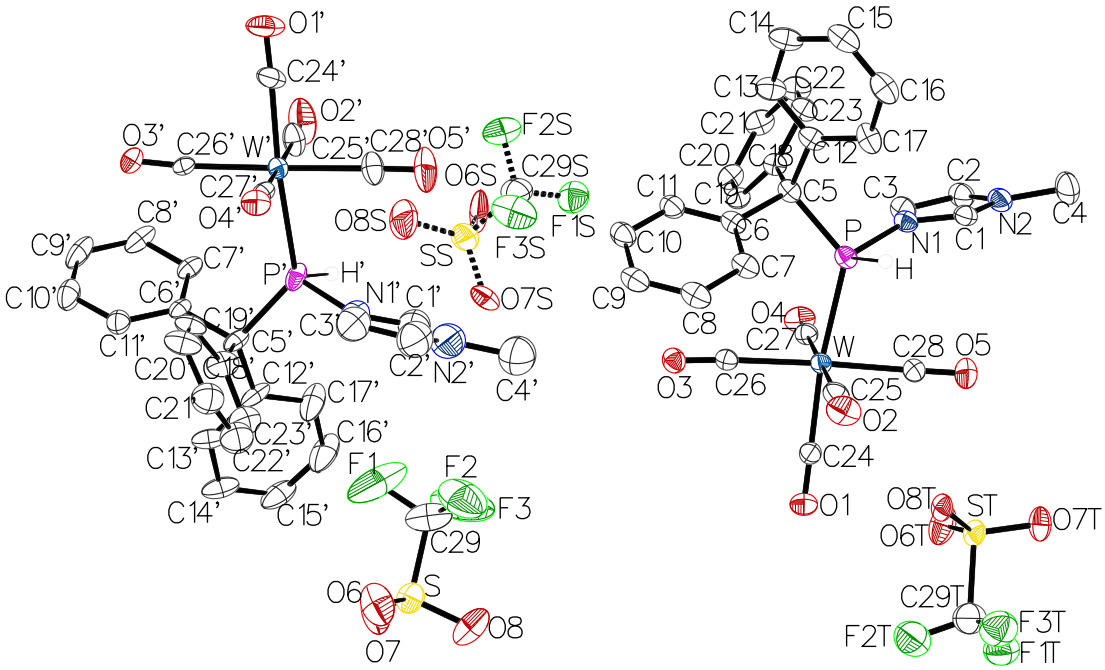

Figure 100: Molecular structures of **64b** in the single crystal lattice at 100(2) K. Thermal ellipsoids are set at 50 % probability level. Solvent molecules and hydrogen atoms were omitted for clarity except for those bound to phosphorus atoms.

Table 81: Crystal data and structure refinements for **64b**.

Identification code	GSTR794, DB-571-2 // GXraymo_7115f
Crystal habitus	clear colorless block
Device type	Bruker D8 Venture
Empirical formula	$C_{30.25}H_{25}F_3N_2O_8PSW$
Moiety formula	$C_{28}H_{22}N_2O_5PW$, CF_3O_3S, 0.25 (C_5H_{12})
Formula weight / g/mol	848.40
T / K	100.0
Crystal system	monoclinic
Space group	*C*2/*c*
a / Å	54.221(3)
b / Å	8.9542(5)
c / Å	32.5364(19)
α / °	90
β / °	125.097(2)
γ / °	90
V / Å^3	12924.5(13)
Z	16
ρ_{calc} / g/cm^3	1.744
μ / mm^{-1}	3.758

F(000)	6664.0
Crystal size / mm^3	0.24 × 0.08 × 0.06
Absorption correction	multi-scan
Min. and max. transmission	0.5844 and 0.7464
Radiation	Mo-K_α (λ = 0.71073 Å)
2Θ range for data collection / °	3.672 to 58.5
Completeness to Θ	0.999
Index ranges	$-74 \le h \le 74$, $-12 \le k \le 12$, $-44 \le l \le 43$
Reflections collected	145150
Independent reflections	17600 (R_{int} = 0.0551, R_σ = 0.0319)
Data / restraints / parameters	17600 / 942 / 940
Goodness-of-fit on F^2	1.035
Final *R* indexes ($I \ge 2\sigma(I)$)	R_1 = 0.0452, ωR_2 = 0.1066
Final *R* indexes (all data)	R_1 = 0.0510, ωR_2 = 0.1104
Largest diff. peak and hole / e/Å^3	2.91 and −1.68

Table 82: Bond lengths for **64b**.

Atom	Atom	Length / Å	Atom	Atom	Length / Å
W	P	2.4815(12)	N1'	C1'	1.372(9)
W	C24	2.018(5)	N1'	C3'	1.423(9)
W	C25	2.051(5)	N2'	C1'	1.363(10)
W	C26	2.055(5)	N2'	C2'	1.291(11)
W	C27	2.046(5)	N2'	C4'	1.529(11)
W	C28	2.039(5)	C2'	C3'	1.382(11)
P	N1	1.776(4)	C5'	C6'	1.530(6)
P	C5	1.894(5)	C5'	C12'	1.547(6)
O1	C24	1.147(6)	C5'	C18'	1.538(7)
O2	C25	1.136(6)	C6'	C7'	1.394(6)
O3	C26	1.140(6)	C6'	C11'	1.394(7)
O4	C27	1.140(6)	C7'	C8'	1.387(6)
O5	C28	1.143(6)	C8'	C9'	1.373(9)
N1	C1	1.334(6)	C9'	C10'	1.391(9)
N1	C3	1.398(6)	C10'	C11'	1.386(7)
N2	C1	1.322(6)	C12'	C13'	1.395(8)
N2	C2	1.386(7)	C12'	C17'	1.366(8)
N2	C4	1.460(7)	C13'	C14'	1.386(7)
C2	C3	1.346(7)	C14'	C15'	1.372(9)
C5	C6	1.540(6)	C15'	C16'	1.359(10)
C5	C12	1.545(6)	C16'	C17'	1.420(8)
C5	C18	1.537(6)	C18'	C19'	1.394(7)
C6	C7	1.399(7)	C18'	C23'	1.388(8)

C6	C11	1.378(7)	C19'	C20'	1.389(7)
C7	C8	1.399(7)	C20'	C21'	1.376(9)
C8	C9	1.371(8)	C21'	C22'	1.340(10)
C9	C10	1.391(8)	C22'	C23'	1.409(9)
C10	C11	1.400(7)	S	O6	1.446(5)
C12	C13	1.393(7)	S	O7	1.426(5)
C12	C17	1.390(7)	S	O8	1.433(5)
C13	C14	1.395(7)	S	C29	1.775(8)
C14	C15	1.395(8)	F1	C29	1.330(11)
C15	C16	1.382(9)	F2	C29	1.349(11)
C16	C17	1.405(7)	F3	C29	1.322(11)
C18	C19	1.397(6)	SS	O6S	1.435(8)
C18	C23	1.402(6)	SS	O7S	1.394(9)
C19	C20	1.394(6)	SS	O8S	1.455(8)
C20	C21	1.390(7)	SS	C29S	1.806(11)
C21	C22	1.392(7)	F1S	C29S	1.275(12)
C22	C23	1.393(6)	F2S	C29S	1.326(11)
W'	P'	2.4947(13)	F3S	C29S	1.337(12)
W'	C24'	2.002(5)	ST	O6T	1.442(9)
W'	C25'	2.041(5)	ST	O7T	1.417(8)
W'	C26'	2.044(4)	ST	O8T	1.441(7)
W'	C27'	2.065(5)	ST	C29T	1.859(12)
W'	C28'	2.052(5)	F1T	C29T	1.334(12)
P'	N1'	1.776(5)	F2T	C29T	1.297(13)
P'	C5'	1.889(5)	F3T	C29T	1.350(13)
O1'	C24'	1.144(6)	C30	C31	1.5191(10)
O2'	C25'	1.135(7)	C31	C32	1.5200(10)
O3'	C26'	1.138(5)	C32	C33	1.5204(10)
O4'	C27'	1.129(6)	C33	C34	1.5201(10)
O5'	C28'	1.135(7)			

Table 83: Bond angles for **64b**.

Atom	Atom	Atom	Angle / ˚	Atom	Atom	Atom	Angle / ˚
C24	W	P	172.72(14)	C3'	N1'	P'	125.3(5)
C24	W	C25	88.8(2)	C1'	N2'	C4'	116.9(7)
C24	W	C26	88.69(18)	C2'	N2'	C1'	112.7(7)
C24	W	C27	90.23(18)	C2'	N2'	C4'	130.4(8)
C24	W	C28	88.73(19)	N2'	C1'	N1'	103.5(6)
C25	W	P	86.12(14)	N2'	C2'	C3'	110.5(8)
C25	W	C26	89.52(19)	C2'	C3'	N1'	102.4(7)
C26	W	P	96.43(13)	C6'	C5'	P'	105.7(3)
C27	W	P	94.85(13)	C6'	C5'	C12'	106.4(3)
C27	W	C25	178.9(2)	C6'	C5'	C18'	113.6(4)
C27	W	C26	90.87(18)	C12'	C5'	P'	116.3(4)
C28	W	P	86.22(15)	C18'	C5'	P'	103.4(3)
C28	W	C25	91.2(2)	C18'	C5'	C12'	111.6(4)
C28	W	C26	177.29(19)	C7'	C6'	C5'	119.3(4)
C28	W	C27	88.3(2)	C11'	C6'	C5'	122.2(4)
N1	P	W	110.94(14)	C11'	C6'	C7'	118.4(4)
N1	P	C5	103.78(19)	C8'	C7'	C6'	121.0(5)
C5	P	W	127.57(15)	C9'	C8'	C7'	120.3(5)
C1	N1	P	124.9(3)	C8'	C9'	C10'	119.3(5)
C1	N1	C3	107.9(4)	C11'	C10'	C9'	120.8(5)
C3	N1	P	125.4(3)	C10'	C11'	C6'	120.2(5)
C1	N2	C2	109.0(4)	C13'	C12'	C5'	116.5(5)
C1	N2	C4	125.7(5)	C17'	C12'	C5'	125.6(5)
C2	N2	C4	125.3(5)	C17'	C12'	C13'	117.8(5)
N2	C1	N1	109.0(5)	C14'	C13'	C12'	121.5(6)
C3	C2	N2	107.0(5)	C15'	C14'	C13'	120.0(6)
C2	C3	N1	107.1(5)	C16'	C15'	C14'	119.8(5)
C6	C5	P	104.6(3)	C15'	C16'	C17'	120.3(7)
C6	C5	C12	106.3(4)	C12'	C17'	C16'	120.6(7)
C12	C5	P	117.2(3)	C19'	C18'	C5'	119.5(5)
C18	C5	P	103.6(3)	C23'	C18'	C5'	123.1(5)
C18	C5	C6	114.5(4)	C23'	C18'	C19'	117.3(5)
C18	C5	C12	110.8(4)	C20'	C19'	C18'	120.7(5)
C7	C6	C5	118.4(4)	C21'	C20'	C19'	120.3(6)
C11	C6	C5	122.4(4)	C22'	C21'	C20'	120.5(7)
C11	C6	C7	119.1(4)	C21'	C22'	C23'	119.9(7)
C6	C7	C8	120.3(5)	C18'	C23'	C22'	121.2(6)
C9	C8	C7	120.4(5)	O1'	C24'	W'	177.6(5)
C8	C9	C10	119.4(5)	O2'	C25'	W'	177.1(6)
C9	C10	C11	120.5(5)	O3'	C26'	W'	175.4(4)

C6	C11	C10	120.2(5)	O4'	C27'	W'	177.0(4)
C13	C12	C5	116.4(4)	O5'	C28'	W'	178.6(6)
C17	C12	C5	125.0(5)	O6	S	C29	104.6(4)
C17	C12	C13	118.6(5)	O7	S	O6	117.4(3)
C12	C13	C14	121.5(5)	O7	S	O8	113.8(3)
C15	C14	C13	119.6(6)	O7	S	C29	103.0(4)
C16	C15	C14	119.1(5)	O8	S	O6	113.1(3)
C15	C16	C17	121.1(5)	O8	S	C29	102.5(4)
C12	C17	C16	120.0(5)	F1	C29	S	110.9(8)
C19	C18	C5	120.8(4)	F1	C29	F2	106.6(8)
C19	C18	C23	118.5(4)	F2	C29	S	110.8(6)
C23	C18	C5	120.3(4)	F3	C29	S	111.8(6)
C20	C19	C18	120.4(4)	F3	C29	F1	109.4(8)
C21	C20	C19	121.0(5)	F3	C29	F2	107.1(9)
C20	C21	C22	118.8(5)	O6S	SS	O8S	114.0(5)
C21	C22	C23	120.6(5)	O6S	SS	C29S	100.5(5)
C22	C23	C18	120.7(5)	O7S	SS	O6S	117.9(5)
O1	C24	W	179.3(4)	O7S	SS	O8S	116.6(5)
O2	C25	W	178.8(7)	O7S	SS	C29S	101.8(8)
O3	C26	W	176.6(4)	O8S	SS	C29S	102.0(6)
O4	C27	W	177.5(4)	F1S	C29S	SS	110.4(7)
O5	C28	W	177.6(5)	F1S	C29S	F2S	108.3(9)
C24'	W'	P'	173.81(17)	F1S	C29S	F3S	107.3(10)
C24'	W'	C25'	88.5(2)	F2S	C29S	SS	111.4(8)
C24'	W'	C26'	87.3(2)	F2S	C29S	F3S	109.6(9)
C24'	W'	C27'	88.8(2)	F3S	C29S	SS	109.7(8)
C24'	W'	C28'	91.9(2)	O6T	ST	C29T	104.4(6)
C25'	W'	P'	86.61(18)	O7T	ST	O6T	115.4(5)
C25'	W'	C26'	89.44(19)	O7T	ST	O8T	116.3(6)
C25'	W'	C27'	177.2(2)	O7T	ST	C29T	101.2(5)
C25'	W'	C28'	89.7(2)	O8T	ST	O6T	114.8(5)
C26'	W'	P'	96.50(12)	O8T	ST	C29T	101.7(5)
C26'	W'	C27'	91.40(17)	F1T	C29T	ST	109.6(8)
C26'	W'	C28'	178.8(2)	F1T	C29T	F3T	107.4(8)
C27'	W'	P'	95.98(13)	F2T	C29T	ST	112.7(9)
C28'	W'	P'	84.25(17)	F2T	C29T	F1T	110.5(9)
C28'	W'	C27'	89.4(2)	F2T	C29T	F3T	109.5(9)
N1'	P'	W'	110.87(17)	F3T	C29T	ST	107.0(8)
N1'	P'	C5'	103.1(2)	C30	C31	C32	113.45(11)
C5'	P'	W'	127.84(15)	C31	C32	C33	113.30(11)
C1'	N1'	P'	122.2(5)	C32	C33	C34	113.32(11)
C1'	N1'	C3'	110.9(6)				

Table 84: Torsion angles for **64b**.

A	B	C	D	Angle / ˚	A	B	C	D	Angle / ˚
W	P	N1	C1	−104.3(4)	N1'	P'	C5'	C18'	53.1(4)
W	P	N1	C3	58.9(4)	N2'	C2'	C3'	N1'	−1.9(9)
W	P	C5	C6	43.1(3)	C1'	N1'	C3'	C2'	1.1(8)
W	P	C5	C12	160.4(2)	C1'	N2'	C2'	C3'	2.1(10)
W	P	C5	C18	−77.2(3)	C2'	N2'	C1'	N1'	−1.3(8)
P	N1	C1	N2	165.9(3)	C3'	N1'	C1'	N2'	0.0(8)
P	N1	C3	C2	−166.5(4)	C4'	N2'	C1'	N1'	−179.7(6)
P	C5	C6	C7	45.6(5)	C4'	N2'	C2'	C3'	−179.8(8)
P	C5	C6	C11	−138.5(4)	C5'	P'	N1'	C1'	113.9(5)
P	C5	C12	C13	177.6(3)	C5'	P'	N1'	C3'	−81.8(6)
P	C5	C12	C17	−4.0(6)	C5'	C6'	C7'	C8'	178.2(4)
P	C5	C18	C19	71.1(5)	C5'	C6'	C11'	C10'	−176.1(4)
P	C5	C18	C23	−101.4(4)	C5'	C12'	C13'	C14'	177.0(5)
N1	P	C5	C6	173.8(3)	C5'	C12'	C17'	C16'	−177.6(6)
N1	P	C5	C12	−68.8(3)	C5'	C18'	C19'	C20'	−174.1(5)
N1	P	C5	C18	53.5(3)	C5'	C18'	C23'	C22'	174.0(6)
N2	C2	C3	N1	1.3(6)	C6'	C5'	C12'	C13'	−56.3(6)
C1	N1	C3	C2	−1.0(6)	C6'	C5'	C12'	C17'	120.9(6)
C1	N2	C2	C3	−1.1(6)	C6'	C5'	C18'	C19'	−44.3(6)
C2	N2	C1	N1	0.4(6)	C6'	C5'	C18'	C23'	139.9(5)
C3	N1	C1	N2	0.3(5)	C6'	C7'	C8'	C9'	−2.4(7)
C4	N2	C1	N1	178.8(5)	C7'	C6'	C11'	C10'	−0.4(7)
C4	N2	C2	C3	−179.5(5)	C7'	C8'	C9'	C10'	0.4(8)
C5	P	N1	C1	115.7(4)	C8'	C9'	C10'	C11'	1.5(8)
C5	P	N1	C3	−81.2(4)	C9'	C10'	C11'	C6'	−1.5(8)
C5	C6	C7	C8	179.5(4)	C11'	C6'	C7'	C8'	2.4(6)
C5	C6	C11	C10	−176.8(4)	C12'	C5'	C6'	C7'	−77.9(5)
C5	C12	C13	C14	179.7(4)	C12'	C5'	C6'	C11'	97.7(5)
C5	C12	C17	C16	−179.5(4)	C12'	C5'	C18'	C19'	−164.6(5)
C5	C18	C19	C20	−173.4(4)	C12'	C5'	C18'	C23'	19.7(7)
C5	C18	C23	C22	173.4(5)	C12'	C13'	C14'	C15'	1.4(8)
C6	C5	C12	C13	−66.0(5)	C13'	C12'	C17'	C16'	−0.3(10)
C6	C5	C12	C17	112.5(5)	C13'	C14'	C15'	C16'	−1.4(9)
C6	C5	C18	C19	−42.1(6)	C14'	C15'	C16'	C17'	0.6(12)
C6	C5	C18	C23	145.3(4)	C15'	C16'	C17'	C12'	0.3(13)
C6	C7	C8	C9	−3.3(7)	C17'	C12'	C13'	C14'	−0.4(8)
C7	C6	C11	C10	−0.9(7)	C18'	C5'	C6'	C7'	158.9(4)
C7	C8	C9	C10	0.5(7)	C18'	C5'	C6'	C11'	−25.5(6)
C8	C9	C10	C11	2.1(8)	C18'	C5'	C12'	C13'	68.1(6)
C9	C10	C11	C6	−1.9(8)	C18'	C5'	C12'	C17'	−114.6(7)

C11	C6	C7	C8	3.5(7)	C18'	C19'	C20'	C21'	0.6(9)
C12	C5	C6	C7	−79.0(5)	C19'	C18'	C23'	C22'	−1.9(9)
C12	C5	C6	C11	96.9(5)	C19'	C20'	C21'	C22'	−3.3(10)
C12	C5	C18	C19	−162.4(4)	C20'	C21'	C22'	C23'	3.4(11)
C12	C5	C18	C23	25.0(6)	C21'	C22'	C23'	C18'	−0.7(10)
C12	C13	C14	C15	−0.2(8)	C23'	C18'	C19'	C20'	1.9(8)
C13	C12	C17	C16	−1.1(7)	O6	S	C29	F1	−61.1(8)
C13	C14	C15	C16	−0.9(8)	O6	S	C29	F2	57.2(8)
C14	C15	C16	C17	1.0(8)	O6	S	C29	F3	176.6(7)
C15	C16	C17	C12	0.0(8)	O7	S	C29	F1	62.2(8)
C17	C12	C13	C14	1.2(7)	O7	S	C29	F2	−179.5(6)
C18	C5	C6	C7	158.2(4)	O7	S	C29	F3	−60.2(8)
C18	C5	C6	C11	−25.9(6)	O8	S	C29	F1	−179.3(7)
C18	C5	C12	C13	59.1(5)	O8	S	C29	F2	−61.1(7)
C18	C5	C12	C17	−122.5(5)	O8	S	C29	F3	58.3(8)
C18	C19	C20	C21	0.8(7)	O6S	SS	C29S	F1S	−57.1(9)
C19	C18	C23	C22	0.7(7)	O6S	SS	C29S	F2S	63.3(9)
C19	C20	C21	C22	−0.9(8)	O6S	SS	C29S	F3S	−175.1(8)
C20	C21	C22	C23	1.0(8)	O7S	SS	C29S	F1S	64.6(9)
C21	C22	C23	C18	−0.8(8)	O7S	SS	C29S	F2S	−175.0(8)
C23	C18	C19	C20	−0.7(7)	O7S	SS	C29S	F3S	−53.4(9)
W'	P'	N1'	C1'	−106.4(5)	O8S	SS	C29S	F1S	−174.6(8)
W'	P'	N1'	C3'	57.9(6)	O8S	SS	C29S	F2S	−54.2(9)
W'	P'	C5'	C6'	42.6(4)	O8S	SS	C29S	F3S	67.3(9)
W'	P'	C5'	C12'	160.3(3)	O6T	ST	C29T	F1T	64.3(9)
W'	P'	C5'	C18'	−77.0(3)	O6T	ST	C29T	F2T	−59.2(9)
P'	N1'	C1'	N2'	166.3(4)	O6T	ST	C29T	F3T	−179.6(7)
P'	N1'	C3'	C2'	−164.7(5)	O7T	ST	C29T	F1T	−55.9(9)
P'	C5'	C6'	C7'	46.3(5)	O7T	ST	C29T	F2T	−179.4(8)
P'	C5'	C6'	C11'	−138.1(4)	O7T	ST	C29T	F3T	60.2(8)
P'	C5'	C12'	C13'	−173.6(4)	O8T	ST	C29T	F1T	−176.1(7)
P'	C5'	C12'	C17'	3.6(7)	O8T	ST	C29T	F2T	60.4(9)
P'	C5'	C18'	C19'	69.7(5)	O8T	ST	C29T	F3T	−60.0(8)
P'	C5'	C18'	C23'	−106.1(5)	C30	C31	C32	C33	−161.6(12)
N1'	P'	C5'	C6'	172.7(3)	C31	C32	C33	C34	−142.1(11)
N1'	P'	C5'	C12'	−69.6(4)					

7.2.18 [Pentacarbonyl{1-methylimidazol-3-iumyl(triphenylmethyl)phosphane-κ*P*}tungsten(0)] tetrakis{3,5-bis(trifluoromethyl)phenyl}borate (65b)

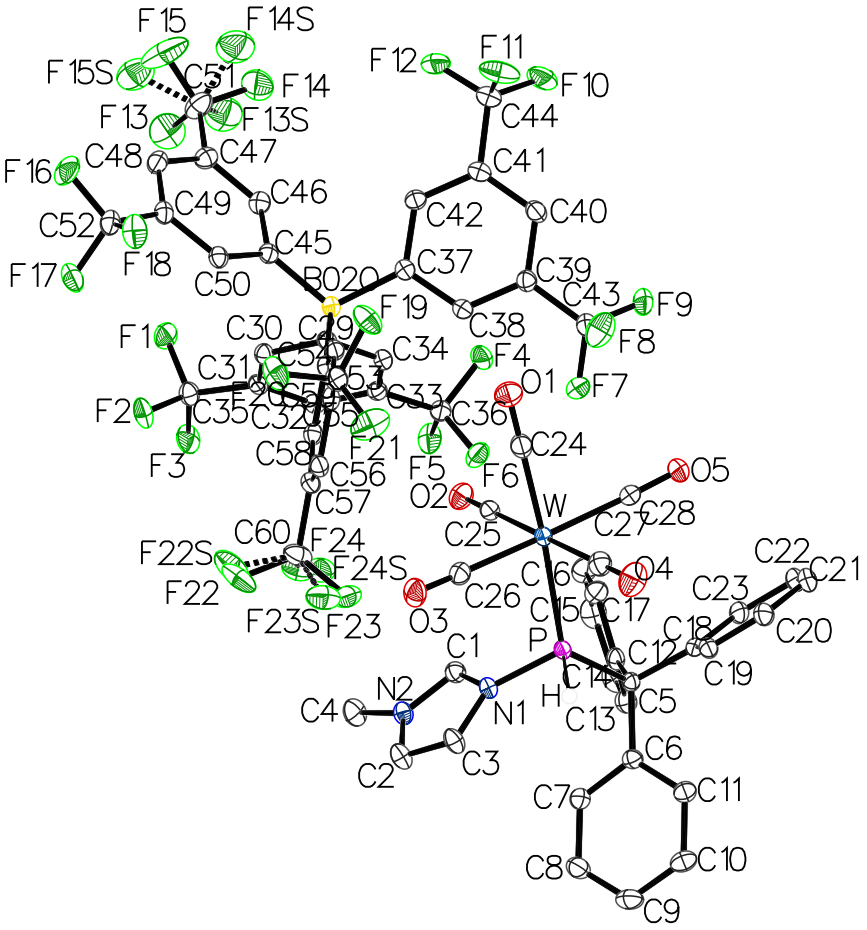

Figure 101: Molecular structures of **65b** in the single crystal lattice at 100(2) K. Thermal ellipsoids are set at 50 % probability level. Solvent molecules and hydrogen atoms were omitted for clarity except for those bound to phosphorus atoms.

Table 85: Crystal data and structure refinements for **65b**.

Identification code	GSTR796, DB-604 // GXraymo_7138v
Crystal habitus	clear colorless plate
Device type	Bruker D8 Venture
Empirical formula	$C_{61}H_{36}BCl_2F_{24}N_2O_5PW$
Moiety formula	$C_{28}H_{22}N_2O_5PW$, CH_2Cl_2, $C_{32}H_{12}BF_{24}$
Formula weight / g/mol	1629.45
T / K	100.0
Crystal system	triclinic
Space group	$P\bar{1}$
a / Å	11.3237(5)
b / Å	14.0365(6)
c / Å	20.5226(7)
α / °	98.0490(10)

β / °	104.5540(10)
γ / °	94.751(2)
V / Å^3	3102.4(2)
Z	2
ρ_{calc} / g/cm^3	1.744
μ / mm^{-1}	2.097
F(000)	1600.0
Crystal size / mm^3	0.22 × 0.18 × 0.1
Absorption correction	multi-scan
Min. and max. transmission	0.6329 and 0.7461
Radiation	Mo-K$_\alpha$ (λ = 0.71073 Å)
2Θ range for data collection / °	3.884 to 55.998
Completeness to Θ	0.995
Index ranges	$-14 \le h \le 14$, $-18 \le k \le 18$, $-27 \le l \le 27$
Reflections collected	89491
Independent reflections	14911 (R_{int} = 0.0233, R_σ = 0.0189)
Data / restraints / parameters	14911 / 126 / 944
Goodness-of-fit on F^2	1.059
Final R indexes ($I \ge 2\sigma(I)$)	R_1 = 0.0188, ωR_2 = 0.0470
Final R indexes (all data)	R_1 = 0.0192, ωR_2 = 0.0473
Largest diff. peak and hole / e/Å^3	1.17 and −0.71

Table 86: Bond lengths for **65b**.

Atom	Atom	Length / Å	Atom	Atom	Length / Å
W	P	2.4611(4)	F13	C51	1.350(3)
W	C24	2.0189(18)	F13S	C51	1.262(11)
W	C25	2.0411(18)	F14	C51	1.322(3)
W	C26	2.0532(17)	F14S	C51	1.407(12)
W	C27	2.0571(18)	F15	C51	1.305(3)
W	C28	2.0499(17)	F15S	C51	1.402(12)
P	N1	1.7773(14)	F16	C52	1.344(2)
P	C5	1.9239(16)	F17	C52	1.347(2)
O1	C24	1.141(2)	F18	C52	1.336(2)
O2	C25	1.142(2)	F19	C59	1.344(2)
O3	C26	1.135(2)	F20	C59	1.340(2)
O4	C27	1.136(2)	F21	C59	1.337(2)
O5	C28	1.135(2)	F22	C60	1.333(4)
N1	C1	1.341(2)	F22S	C60	1.336(7)
N1	C3	1.390(2)	F23	C60	1.386(3)
N2	C1	1.326(2)	F23S	C60	1.305(5)
N2	C2	1.380(2)	F24	C60	1.306(4)

N2	C4	1.469(2)	F24S	C60	1.402(7)
C2	C3	1.350(2)	C29	C30	1.406(2)
C5	C6	1.540(2)	C29	C34	1.397(2)
C5	C12	1.535(2)	C29	B02O	1.646(2)
C5	C18	1.539(2)	C30	C31	1.391(2)
C6	C7	1.404(2)	C31	C32	1.389(2)
C6	C11	1.396(2)	C31	C35	1.496(2)
C7	C8	1.388(2)	C32	C33	1.388(2)
C8	C9	1.391(3)	C33	C34	1.395(2)
C9	C10	1.386(3)	C33	C36	1.495(2)
C10	C11	1.394(2)	C37	C38	1.406(2)
C12	C13	1.395(2)	C37	C42	1.404(2)
C12	C17	1.400(2)	C37	B02O	1.649(2)
C13	C14	1.398(2)	C38	C39	1.391(2)
C14	C15	1.383(3)	C39	C40	1.391(2)
C15	C16	1.385(3)	C39	C43	1.502(2)
C16	C17	1.393(2)	C40	C41	1.390(2)
C18	C19	1.399(2)	C41	C42	1.391(2)
C18	C23	1.396(2)	C41	C44	1.501(2)
C19	C20	1.391(2)	C45	C46	1.409(2)
C20	C21	1.391(2)	C45	C50	1.399(2)
C21	C22	1.383(3)	C45	B02O	1.639(2)
C22	C23	1.394(2)	C46	C47	1.387(2)
Cl1	C61	1.756(2)	C47	C48	1.390(2)
Cl2	C61	1.811(3)	C47	C51	1.499(2)
Cl2S	C61	1.649(4)	C48	C49	1.383(2)
F1	C35	1.3557(19)	C49	C50	1.399(2)
F2	C35	1.3333(19)	C49	C52	1.498(2)
F3	C35	1.346(2)	C53	C54	1.408(2)
F4	C36	1.3515(18)	C53	C58	1.398(2)
F5	C36	1.3365(19)	C53	B02O	1.641(2)
F6	C36	1.3429(19)	C54	C55	1.391(2)
F7	C43	1.336(2)	C55	C56	1.391(2)
F8	C43	1.342(2)	C55	C59	1.493(2)
F9	C43	1.337(2)	C56	C57	1.386(2)
F10	C44	1.336(2)	C57	C58	1.395(2)
F11	C44	1.346(2)	C57	C60	1.495(2)
F12	C44	1.331(2)			

Table 87: Bond angles for **65b**.

Atom	Atom	Atom	Angle / ˚	Atom	Atom	Atom	Angle / ˚
C24	W	P	175.92(5)	C42	C37	C38	115.62(14)
C24	W	C25	89.46(7)	C42	C37	B02O	124.54(14)
C24	W	C26	87.50(7)	C39	C38	C37	122.34(14)
C24	W	C27	91.99(7)	C38	C39	C43	120.23(14)
C24	W	C28	88.56(7)	C40	C39	C38	121.06(15)
C25	W	P	90.50(5)	C40	C39	C43	118.67(14)
C25	W	C26	93.23(6)	C41	C40	C39	117.50(15)
C25	W	C27	177.82(7)	C40	C41	C42	121.49(15)
C25	W	C28	92.00(7)	C40	C41	C44	117.80(15)
C26	W	P	88.43(5)	C42	C41	C44	120.68(15)
C26	W	C27	88.46(7)	C41	C42	C37	121.97(15)
C27	W	P	88.17(5)	F7	C43	F8	106.27(15)
C28	W	P	95.52(5)	F7	C43	F9	106.78(15)
C28	W	C26	173.42(7)	F7	C43	C39	112.62(14)
C28	W	C27	86.41(7)	F8	C43	C39	111.84(15)
N1	P	W	113.30(5)	F9	C43	F8	106.11(14)
N1	P	C5	102.46(7)	F9	C43	C39	112.75(14)
C5	P	W	130.29(5)	F10	C44	F11	106.07(15)
C1	N1	P	127.59(11)	F10	C44	C41	112.31(15)
C1	N1	C3	107.73(13)	F11	C44	C41	111.48(15)
C3	N1	P	124.68(11)	F12	C44	F10	107.16(15)
C1	N2	C2	108.85(14)	F12	C44	F11	106.05(16)
C1	N2	C4	125.66(15)	F12	C44	C41	113.30(15)
C2	N2	C4	125.49(14)	C46	C45	B02O	119.96(14)
N2	C1	N1	108.94(14)	C50	C45	C46	115.77(14)
C3	C2	N2	107.12(14)	C50	C45	B02O	124.13(14)
C2	C3	N1	107.35(15)	C47	C46	C45	122.20(15)
C6	C5	P	106.51(10)	C46	C47	C48	120.92(15)
C12	C5	P	110.44(10)	C46	C47	C51	119.93(15)
C12	C5	C6	112.87(13)	C48	C47	C51	119.12(15)
C12	C5	C18	111.16(12)	C49	C48	C47	118.11(15)
C18	C5	P	102.01(10)	C48	C49	C50	120.99(15)
C18	C5	C6	113.18(12)	C48	C49	C52	120.11(15)
C7	C6	C5	120.60(14)	C50	C49	C52	118.82(15)
C11	C6	C5	121.70(14)	C45	C50	C49	121.98(15)
C11	C6	C7	117.68(14)	F13	C51	C47	110.90(17)
C8	C7	C6	121.27(16)	F13S	C51	F14S	96.0(7)
C7	C8	C9	120.18(16)	F13S	C51	F15S	113.7(7)
C10	C9	C8	119.30(16)	F13S	C51	C47	121.4(5)
C9	C10	C11	120.46(16)	F14	C51	F13	103.25(17)

C10	C11	C6	121.00(16)	F14	C51	C47	112.85(16)
C13	C12	C5	121.53(14)	F14S	C51	C47	111.9(5)
C13	C12	C17	118.24(15)	F15	C51	F13	107.7(2)
C17	C12	C5	120.05(15)	F15	C51	F14	108.6(2)
C12	C13	C14	120.48(16)	F15	C51	C47	113.04(17)
C15	C14	C13	120.57(17)	F15S	C51	F14S	95.5(7)
C14	C15	C16	119.58(17)	F15S	C51	C47	113.4(5)
C15	C16	C17	120.13(17)	F16	C52	F17	106.06(13)
C16	C17	C12	120.95(17)	F16	C52	C49	112.54(14)
C19	C18	C5	120.23(13)	F17	C52	C49	112.04(14)
C23	C18	C5	121.60(14)	F18	C52	F16	107.09(14)
C23	C18	C19	118.15(15)	F18	C52	F17	105.65(14)
C20	C19	C18	121.32(15)	F18	C52	C49	112.94(13)
C21	C20	C19	119.74(16)	C54	C53	B02O	119.65(13)
C22	C21	C20	119.59(16)	C58	C53	C54	115.96(14)
C21	C22	C23	120.71(16)	C58	C53	B02O	124.39(14)
C22	C23	C18	120.47(16)	C55	C54	C53	122.22(14)
O1	C24	W	178.51(17)	C54	C55	C59	120.97(15)
O2	C25	W	178.37(15)	C56	C55	C54	120.74(15)
O3	C26	W	176.56(16)	C56	C55	C59	118.21(14)
O4	C27	W	178.25(16)	C57	C56	C55	117.97(15)
O5	C28	W	175.77(16)	C56	C57	C58	121.28(15)
Cl1	C61	Cl2	108.03(16)	C56	C57	C60	118.06(15)
Cl2S	C61	Cl1	119.7(2)	C58	C57	C60	120.66(15)
C30	C29	B02O	120.51(13)	C57	C58	C53	121.82(15)
C34	C29	C30	115.53(14)	F19	C59	C55	113.10(14)
C34	C29	B02O	123.91(13)	F20	C59	F19	105.89(14)
C31	C30	C29	122.30(14)	F20	C59	C55	111.88(14)
C30	C31	C35	118.70(14)	F21	C59	F19	106.44(14)
C32	C31	C30	121.20(14)	F21	C59	F20	105.95(14)
C32	C31	C35	120.04(14)	F21	C59	C55	113.02(14)
C33	C32	C31	117.47(14)	F22	C60	F23	106.4(2)
C32	C33	C34	121.23(14)	F22	C60	C57	113.8(2)
C32	C33	C36	120.78(14)	F22S	C60	F24S	107.1(4)
C34	C33	C36	117.99(14)	F22S	C60	C57	109.5(3)
C33	C34	C29	122.27(14)	F23	C60	C57	111.27(17)
F1	C35	C31	111.67(13)	F23S	C60	F22S	104.7(3)
F2	C35	F1	105.88(13)	F23S	C60	F24S	110.5(4)
F2	C35	F3	107.22(13)	F23S	C60	C57	113.8(2)
F2	C35	C31	113.47(13)	F24	C60	F22	104.9(2)
F3	C35	F1	105.18(13)	F24	C60	F23	104.4(2)
F3	C35	C31	112.83(14)	F24	C60	C57	115.3(2)

F4	C36	C33	111.94(13)	F24S	C60	C57	110.8(3)
F5	C36	F4	106.30(13)	C29	B02O	C37	109.71(12)
F5	C36	F6	106.78(13)	C45	B02O	C29	107.09(12)
F5	C36	C33	113.31(13)	C45	B02O	C37	112.21(13)
F6	C36	F4	105.35(13)	C45	B02O	C53	110.96(12)
F6	C36	C33	112.59(13)	C53	B02O	C29	109.59(12)
C38	C37	B02O	119.82(13)	C53	B02O	C37	107.28(12)

7.2.19 [Pentacarbonyl{(1-methylimidazol-3-iumyl(triphenylmethyl)phosphenium-κ*P*}-tungsten(0)] tetrakis(nonafluoro-*tert*-butoxy)aluminate (66b)

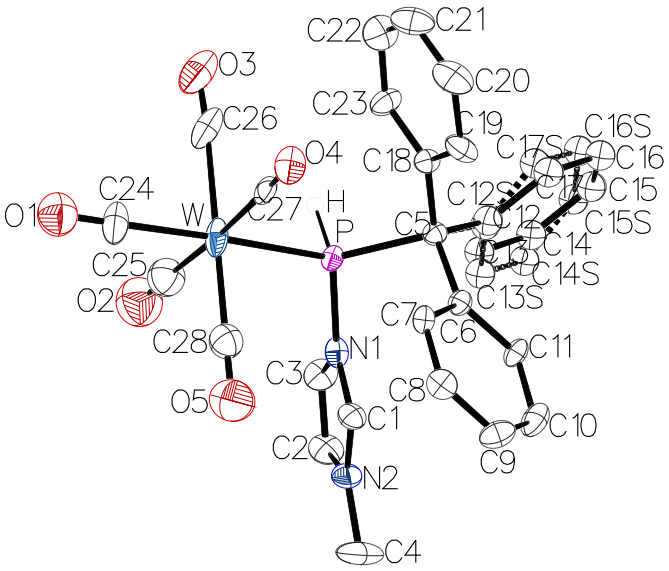

Figure 102: Molecular structures of **66b** in the single crystal lattice at 100(2) K. Thermal ellipsoids are set at 50 % probability level. Hydrogen atoms were omitted for clarity except for those bound to phosphorus atoms.

Table 88: Crystal data and structure refinements for **66b**.

Identification code	GSTR789, DB-568 // GXraymo_7046f
Crystal habitus	clear colorless block
Device type	Bruker D8 Venture
Empirical formula	$C_{28}H_{22}N_2O_5PW$
Moiety formula	$C_{28}H_{22}N_2O_5PW$
Formula weight / g/mol	681.29
T / K	100.0
Crystal system	monoclinic
Space group	$P2_1/n$
a / Å	9.9563(5)
b / Å	34.958(2)
c / Å	16.3809(13)
α / °	90
β / °	97.490(2)
γ / °	90
V / Å^3	5652.8(6)
Z	4
ρ_{calc} / g/cm^3	0.801
μ / mm^{-1}	2.091
F(000)	1322.0
Crystal size / mm^3	0.12 × 0.09 × 0.05
Absorption correction	multi-scan

Min. and max. transmission	0.6491 and 0.7461
Radiation	Mo-K_α (λ = 0.71073 Å)
2Θ range for data collection / °	4.288 to 55.998
Completeness to Θ	0.998
Index ranges	$-12 \leq h \leq 13$, $-46 \leq k \leq 46$, $-21 \leq l \leq 21$
Reflections collected	137230
Independent reflections	13629 (R_{int} = 0.0502, R_σ = 0.0241)
Data / restraints / parameters	13629 / 268 / 369
Goodness-of-fit on F^2	1.032
Final R indexes ($I \geq 2\sigma(I)$)	R_1 = 0.0824, ωR_2 = 0.2406
Final R indexes (all data)	R_1 = 0.0870, ωR_2 = 0.2447
Largest diff. peak and hole / e/Å^3	2.27 and −1.88

Table 89: Bond lengths for **66b**.

Atom	**Atom**	**Length / Å**	**Atom**	**Atom**	**Length / Å**
W	P	2.4643(17)	C6	C11	1.398(9)
W	C24	2.023(9)	C7	C8	1.382(10)
W	C25	2.012(11)	C8	C9	1.399(11)
W	C26	2.113(10)	C9	C10	1.388(12)
W	C27	2.051(8)	C10	C11	1.422(11)
W	C28	2.013(10)	C12	C17	1.3900
P	N1	1.784(6)	C12	C13	1.3900
P	C5	1.923(7)	C17	C16	1.3900
O1	C24	1.153(12)	C16	C15	1.3900
O2	C25	1.158(14)	C15	C14	1.3900
O3	C26	1.083(12)	C14	C13	1.3900
O4	C27	1.145(10)	C16S	C15S	1.3900
O5	C28	1.166(13)	C16S	C17S	1.3900
N1	C1	1.352(9)	C15S	C14S	1.3900
N1	C3	1.398(9)	C14S	C13S	1.3900
N2	C1	1.331(9)	C13S	C12S	1.3900
N2	C2	1.409(11)	C12S	C17S	1.3900
N2	C4	1.451(11)	C18	C19	1.373(10)
C2	C3	1.325(11)	C18	C23	1.413(9)
C5	C6	1.555(9)	C19	C20	1.409(12)
C5	C12	1.534(10)	C20	C21	1.355(14)
C5	C12S	1.586(10)	C21	C22	1.334(13)
C5	C18	1.501(9)	C22	C23	1.411(12)
C6	C7	1.409(9)			

Table 90: Bond angles for **66b**.

Atom	Atom	Atom	Angle / ˚	Atom	Atom	Atom	Angle / ˚
C24	W	P	174.0(3)	C11	C6	C5	121.6(6)
C24	W	C26	89.7(4)	C11	C6	C7	117.7(6)
C24	W	C27	87.4(3)	C8	C7	C6	120.9(6)
C25	W	P	82.5(3)	C7	C8	C9	120.7(7)
C25	W	C24	91.5(4)	C10	C9	C8	120.4(7)
C25	W	C26	87.5(4)	C9	C10	C11	118.2(7)
C25	W	C27	176.5(4)	C6	C11	C10	122.0(6)
C25	W	C28	93.0(4)	C17	C12	C5	114.6(7)
C26	W	P	89.3(2)	C17	C12	C13	120.0
C27	W	P	98.6(2)	C13	C12	C5	125.4(7)
C27	W	C26	89.2(3)	C12	C17	C16	120.0
C28	W	P	90.9(3)	C15	C16	C17	120.0
C28	W	C24	90.1(4)	C16	C15	C14	120.0
C28	W	C26	179.5(4)	C15	C14	C13	120.0
C28	W	C27	90.3(4)	C14	C13	C12	120.0
N1	P	W	111.5(2)	C15S	C16S	C17S	120.0
N1	P	C5	105.2(3)	C14S	C15S	C16S	120.0
C5	P	W	127.4(2)	C15S	C14S	C13S	120.0
C1	N1	P	127.0(5)	C12S	C13S	C14S	120.0
C1	N1	C3	106.8(6)	C13S	C12S	C5	122.9(7)
C3	N1	P	126.1(5)	C13S	C12S	C17S	120.0
C1	N2	C2	108.0(6)	C17S	C12S	C5	117.1(7)
C1	N2	C4	123.9(7)	C12S	C17S	C16S	120.0
C2	N2	C4	128.2(7)	C19	C18	C5	123.5(6)
N2	C1	N1	109.4(6)	C19	C18	C23	119.6(7)
C3	C2	N2	107.0(7)	C23	C18	C5	116.8(6)
C2	C3	N1	108.9(7)	C18	C19	C20	119.4(8)
C6	C5	P	103.5(4)	C21	C20	C19	121.4(8)
C6	C5	C12S	111.4(6)	C22	C21	C20	119.3(8)
C12	C5	P	114.3(6)	C21	C22	C23	122.8(9)
C12	C5	C6	111.5(7)	C22	C23	C18	117.5(7)
C12S	C5	P	110.0(6)	O1	C24	W	179.0(10)
C18	C5	P	103.9(4)	O2	C25	W	177.7(10)
C18	C5	C6	114.4(5)	O3	C26	W	176.3(9)
C18	C5	C12	109.0(6)	O4	C27	W	177.1(7)
C18	C5	C12S	112.9(6)	O5	C28	W	178.0(9)
C7	C6	C5	120.6(6)				

7.2.20 [Pentacarbonyl{methyl(1-methylimidazol-3-iumyl)(triphenylmethyl)phosphane-κ*P*}-chromium(0)] trifluoromethanesulfonate (68a)

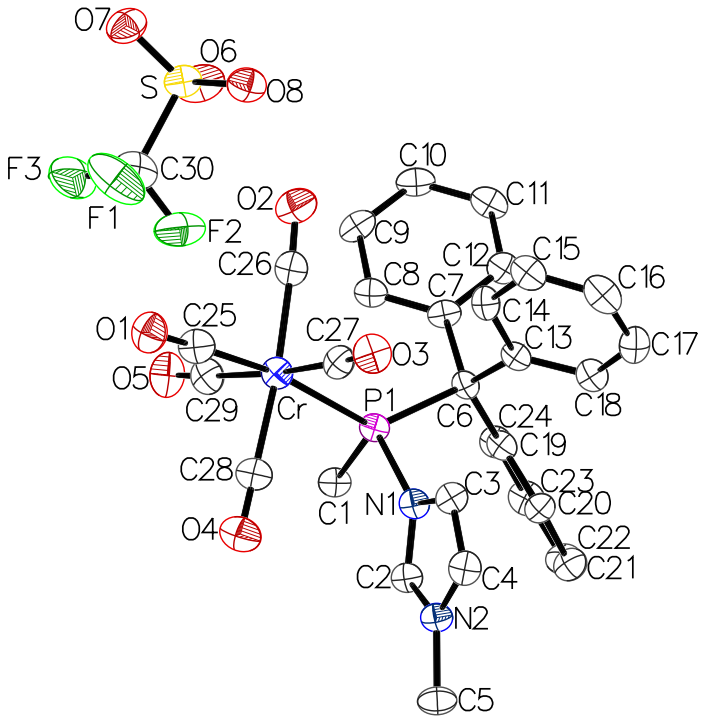

Figure 103: Molecular structures of **68a** in the single crystal lattice at 100(2) K. Thermal ellipsoids are set at 50 % probability level. Hydrogen atoms and solvent molecules were omitted for clarity.

Table 91: Crystal data and structure refinements for **68a**.

Identification code	GSTR773, DB-558 // GXray6925
Crystal habitus	clear colorless needle
Device type	Stadivari
Empirical formula	$C_{31}H_{26}Cl_2CrF_3N_2O_8PS$
Moiety formula	$C_{29}H_{24}CrN_2O_5P$, CH_2Cl_2, CF_3O_3S
Formula weight / g/mol	797.47
T / K	100
Crystal system	triclinic
Space group	$P\bar{1}$
a / Å	8.5285(6)
b / Å	12.2121(9)
c / Å	17.7662(12)
α / °	69.997(5)
β / °	78.901(5)
γ / °	79.928(6)
V / Å^3	1694.3(2)
Z	2
ρ_{calc} / g/cm^3	1.563

μ / mm^{-1}	5.868
F(000)	812.0
Crystal size / mm^3	0.2 × 0.077 × 0.01
Absorption correction	multi-scan
Min. and max. transmission	0.4156 and 0.9570
Radiation	Cu-K$_\alpha$ (λ = 1.54186 Å)
2Θ range for data collection / °	7.758 to 135.496
Completeness to Θ	0.990
Index ranges	−10 ≤ h ≤ 5, −14 ≤ k ≤ 14, −20 ≤ l ≤ 21
Reflections collected	36949
Independent reflections	6088 (R_{int} = 0.0948, R_σ = 0.0538)
Data / restraints / parameters	6088 / 0 / 444
Goodness-of-fit on F^2	1.032
Final R indexes ($I \geq 2\sigma(I)$)	R_1 = 0.0714, ωR_2 = 0.1777
Final R indexes (all data)	R_1 = 0.1047, ωR_2 = 0.2061
Largest diff. peak and hole / e/Å^3	0.72 and −0.62

Table 92: Bond lengths for **68a**.

Atom	Atom	Length / Å	Atom	Atom	Length / Å
Cr	P1	2.4024(15)	C8	C9	1.402(7)
Cr	C25	1.875(6)	C9	C10	1.360(8)
Cr	C26	1.909(6)	C10	C11	1.381(8)
Cr	C27	1.915(6)	C11	C12	1.389(7)
Cr	C28	1.891(6)	C13	C14	1.388(7)
Cr	C29	1.935(6)	C13	C18	1.393(8)
P1	N1	1.778(4)	C14	C15	1.398(7)
P1	C1	1.828(5)	C15	C16	1.374(9)
P1	C6	1.935(5)	C16	C17	1.375(8)
O1	C25	1.138(7)	C17	C18	1.390(8)
O2	C26	1.134(7)	C19	C20	1.403(7)
O3	C27	1.140(7)	C19	C24	1.409(7)
O4	C28	1.133(7)	C20	C21	1.390(7)
O5	C29	1.098(7)	C21	C22	1.391(8)
N1	C2	1.338(7)	C22	C23	1.378(8)
N1	C3	1.392(6)	C23	C24	1.389(8)
N2	C2	1.328(7)	Cl1	C31	1.736(7)
N2	C4	1.375(7)	Cl2	C31	1.762(8)
N2	C5	1.472(7)	S	O6	1.439(4)
C3	C4	1.339(8)	S	O7	1.442(4)
C6	C7	1.551(7)	S	O8	1.430(4)
C6	C13	1.552(7)	S	C30	1.814(7)

C6	C19	1.531(7)	F1	C30	1.335(8)
C7	C8	1.385(8)	F2	C30	1.335(8)
C7	C12	1.392(7)	F3	C30	1.324(8)

Table 93: Bond angles for **68a**.

Atom	**Atom**	**Atom**	**Angle / °**	**Atom**	**Atom**	**Atom**	**Angle / °**
C25	Cr	P1	170.99(19)	C7	C8	C9	120.2(5)
C25	Cr	C26	89.1(2)	C10	C9	C8	121.1(5)
C25	Cr	C27	85.4(2)	C9	C10	C11	119.6(5)
C25	Cr	C28	85.7(2)	C10	C11	C12	119.8(5)
C25	Cr	C29	89.3(2)	C11	C12	C7	121.4(5)
C26	Cr	P1	99.85(17)	C14	C13	C6	117.9(4)
C26	Cr	C27	90.1(2)	C14	C13	C18	117.9(5)
C26	Cr	C29	86.9(2)	C18	C13	C6	124.0(4)
C27	Cr	P1	95.43(17)	C13	C14	C15	121.4(5)
C27	Cr	C29	173.9(2)	C16	C15	C14	119.5(5)
C28	Cr	P1	85.30(17)	C15	C16	C17	119.9(5)
C28	Cr	C26	174.7(2)	C16	C17	C18	120.7(5)
C28	Cr	C27	90.8(2)	C17	C18	C13	120.5(5)
C28	Cr	C29	91.6(2)	C20	C19	C6	121.8(4)
C29	Cr	P1	90.31(17)	C20	C19	C24	117.4(5)
N1	P1	Cr	106.91(14)	C24	C19	C6	120.7(5)
N1	P1	C1	98.3(2)	C21	C20	C19	121.7(5)
N1	P1	C6	99.9(2)	C20	C21	C22	119.6(5)
C1	P1	Cr	111.61(18)	C23	C22	C21	119.8(5)
C1	P1	C6	103.2(2)	C22	C23	C24	120.9(5)
C6	P1	Cr	131.59(16)	C23	C24	C19	120.6(5)
C2	N1	P1	126.7(4)	O1	C25	Cr	176.4(5)
C2	N1	C3	106.9(4)	O2	C26	Cr	176.8(5)
C3	N1	P1	126.1(4)	O3	C27	Cr	175.8(5)
C2	N2	C4	108.7(4)	O4	C28	Cr	177.9(5)
C2	N2	C5	124.5(5)	O5	C29	Cr	176.9(6)
C4	N2	C5	126.8(4)	Cl1	C31	Cl2	112.1(4)
N2	C2	N1	109.3(4)	O6	S	O7	113.6(3)
C4	C3	N1	108.1(5)	O6	S	C30	103.2(3)
C3	C4	N2	107.1(5)	O7	S	C30	103.3(3)
C7	C6	P1	109.0(3)	O8	S	O6	116.0(3)
C7	C6	C13	106.2(4)	O8	S	O7	115.1(3)
C13	C6	P1	108.1(3)	O8	S	C30	103.1(3)
C19	C6	P1	107.6(3)	F1	C30	S	111.5(4)
C19	C6	C7	110.9(4)	F2	C30	S	111.6(5)

C19	C6	C13	114.8(4)	F2	C30	F1	106.3(6)
C8	C7	C6	124.5(4)	F3	C30	S	112.7(5)
C8	C7	C12	117.9(5)	F3	C30	F1	107.1(6)
C12	C7	C6	117.5(5)	F3	C30	F2	107.3(5)

Table 94: Torsion angles for **68a**.

A	**B**	**C**	**D**	**Angle / °**	**A**	**B**	**C**	**D**	**Angle / °**
Cr	P1	N1	C2	109.8(4)	C8	C9	C10	C11	-0.3(8)
Cr	P1	N1	C3	-62.1(4)	C9	C10	C11	C12	-0.5(8)
P1	N1	C2	N2	-172.3(3)	C10	C11	C12	C7	0.3(8)
P1	N1	C3	C4	172.4(4)	C12	C7	C8	C9	-1.4(7)
P1	C6	C7	C8	-9.5(6)	C13	C6	C7	C8	-125.8(5)
P1	C6	C7	C12	169.9(4)	C13	C6	C7	C12	53.6(5)
P1	C6	C13	C14	-57.7(5)	C13	C6	C19	C20	46.5(6)
P1	C6	C13	C18	128.5(4)	C13	C6	C19	C24	-136.2(5)
P1	C6	C19	C20	-73.9(5)	C13	C14	C15	C16	2.0(8)
P1	C6	C19	C24	103.4(5)	C14	C13	C18	C17	3.6(7)
N1	C3	C4	N2	0.5(6)	C14	C15	C16	C17	0.6(8)
C1	P1	N1	C2	-5.9(5)	C15	C16	C17	C18	-1.0(8)
C1	P1	N1	C3	-177.8(4)	C16	C17	C18	C13	-1.1(8)
C2	N1	C3	C4	-0.8(6)	C18	C13	C14	C15	-4.0(7)
C2	N2	C4	C3	0.0(6)	C19	C6	C7	C8	108.8(5)
C3	N1	C2	N2	0.9(6)	C19	C6	C7	C12	-71.8(6)
C4	N2	C2	N1	-0.6(6)	C19	C6	C13	C14	-177.8(4)
C5	N2	C2	N1	178.5(5)	C19	C6	C13	C18	8.3(7)
C5	N2	C4	C3	-179.0(5)	C19	C20	C21	C22	0.6(8)
C6	P1	N1	C2	-111.0(4)	C20	C19	C24	C23	-0.4(8)
C6	P1	N1	C3	77.1(4)	C20	C21	C22	C23	-0.9(9)
C6	C7	C8	C9	178.0(4)	C21	C22	C23	C24	0.5(9)
C6	C7	C12	C11	-178.8(5)	C22	C23	C24	C19	0.2(9)
C6	C13	C14	C15	-178.2(4)	C24	C19	C20	C21	0.0(8)
C6	C13	C18	C17	177.4(5)	O6	S	C30	F1	179.1(5)
C6	C19	C20	C21	177.4(5)	O6	S	C30	F2	60.4(5)
C6	C19	C24	C23	-177.8(5)	O6	S	C30	F3	-60.4(6)
C7	C6	C13	C14	59.2(5)	O7	S	C30	F1	-62.3(6)
C7	C6	C13	C18	-114.6(5)	O7	S	C30	F2	179.0(4)
C7	C6	C19	C20	166.9(5)	O7	S	C30	F3	58.2(6)
C7	C6	C19	C24	-15.8(7)	O8	S	C30	F1	57.9(6)
C7	C8	C9	C10	1.2(8)	O8	S	C30	F2	-60.8(5)
C8	C7	C12	C11	0.6(7)	O8	S	C30	F3	178.4(5)

7.2.21 [Pentacarbonyl{methyl(1-methylimidazol-3-iumyl)(triphenylmethyl)phosphane-κ*P*}-tungsten(0)] trifluoromethanesulfonate (68b)

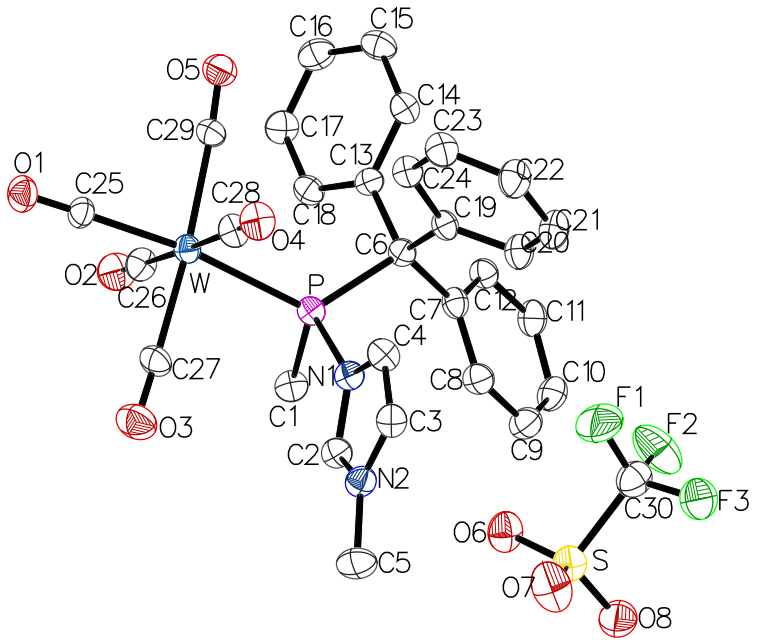

Figure 104: Molecular structures of **68b** in the single crystal lattice at 123(2) K. Thermal ellipsoids are set at 50 % probability level. Hydrogen atoms and solvent molecules were omitted for clarity.

Table 95: Crystal data and structure refinements for **68b**.

Identification code	GSTR763, DB-519 // GXray6876
Crystal habitus	clear colorless block
Device type	STOE IPDS-2T
Empirical formula	$C_{31}H_{26}Cl_2F_3N_2O_8PSW$
Moiety formula	$C_{29}H_{24}N_2O_5PW$, CF_3O_3S, CH_2Cl_2
Formula weight / g/mol	929.32
T / K	123(2)
Crystal system	triclinic
Space group	$P\bar{1}$
a / Å	9.1342(3)
b / Å	10.5960(4)
c / Å	18.7994(6)
α / °	87.804(3)
β / °	79.701(3)
γ / °	77.720(3)
V / Å^3	1749.24(11)
Z	2
ρ_{calc} / g/cm^3	1.764
μ / mm^{-1}	3.627
F(000)	912.0
Crystal size / mm^3	0.12 × 0.09 × 0.06

Absorption correction	multi-scan
Min. and max. transmission	0.0000 and 0.0000
Radiation	Mo-K_α (λ = 0.71073 Å)
2Θ range for data collection / °	3.934 to 56
Completeness to Θ	0.999
Index ranges	$-12 \leq h \leq 12$, $-13 \leq k \leq 13$, $-24 \leq l \leq 24$
Reflections collected	44205
Independent reflections	44205 (R_{int} = 0.0711, R_σ = 0.0591)
Data / restraints / parameters	44205 / 0 / 448
Goodness-of-fit on F^2	0.991
Final R indexes ($I \geq 2\sigma(I)$)	R_1 = 0.0586, ωR_2 = 0.1512
Final R indexes (all data)	R_1 = 0.0771, ωR_2 = 0.1631
Largest diff. peak and hole / e/Å^3	1.45 and −2.11

Table 96: Bond lengths for **68b**.

Atom	Atom	Length / Å	Atom	Atom	Length / Å
W	P	2.4996(19)	C8	C9	1.375(10)
W	C25	2.022(7)	C9	C10	1.388(11)
W	C26	2.050(7)	C10	C11	1.382(11)
W	C27	2.046(8)	C11	C12	1.388(10)
W	C28	2.068(7)	C13	C14	1.395(10)
W	C29	2.083(7)	C13	C18	1.391(10)
P	N1	1.801(6)	C14	C15	1.388(10)
P	C1	1.837(7)	C15	C16	1.387(11)
P	C6	1.947(7)	C16	C17	1.383(11)
O1	C25	1.117(9)	C17	C18	1.389(10)
O2	C26	1.128(9)	C19	C20	1.385(10)
O3	C27	1.119(10)	C19	C24	1.407(10)
O4	C28	1.120(9)	C20	C21	1.395(11)
O5	C29	1.108(9)	C21	C22	1.392(11)
N1	C2	1.335(9)	C22	C23	1.383(11)
N1	C4	1.389(9)	C23	C24	1.387(10)
N2	C2	1.321(9)	S	O6	1.437(6)
N2	C3	1.380(10)	S	O7	1.432(7)
N2	C5	1.457(10)	S	O8	1.447(7)
C3	C4	1.344(11)	S	C30	1.824(10)
C6	C7	1.538(9)	F1	C30	1.315(10)
C6	C13	1.544(9)	F2	C30	1.324(11)
C6	C19	1.542(9)	F3	C30	1.334(10)
C7	C8	1.406(10)	Cl1	C31	1.766(12)
C7	C12	1.394(10)	Cl2	C31	1.748(13)

Table 97: Bond angles for **68b**.

Atom	Atom	Atom	Angle / °	Atom	Atom	Atom	Angle / °
C25	W	P	172.7(2)	C9	C8	C7	120.6(7)
C25	W	C26	89.6(3)	C8	C9	C10	120.9(7)
C25	W	C27	88.3(3)	C11	C10	C9	119.3(7)
C25	W	C28	90.0(3)	C10	C11	C12	120.1(7)
C25	W	C29	88.0(3)	C11	C12	C7	121.1(7)
C26	W	P	88.2(2)	C14	C13	C6	120.3(6)
C26	W	C28	178.8(3)	C18	C13	C6	121.7(6)
C26	W	C29	88.3(3)	C18	C13	C14	117.7(6)
C27	W	P	84.8(2)	C15	C14	C13	120.8(7)
C27	W	C26	90.2(3)	C16	C15	C14	120.6(7)
C27	W	C28	91.0(3)	C17	C16	C15	119.2(7)
C27	W	C29	176.0(3)	C16	C17	C18	119.9(7)
C28	W	P	92.3(2)	C17	C18	C13	121.7(7)
C28	W	C29	90.5(3)	C20	C19	C6	122.8(6)
C29	W	P	98.9(2)	C20	C19	C24	118.3(7)
N1	P	W	109.4(2)	C24	C19	C6	118.9(6)
N1	P	C1	97.1(3)	C19	C20	C21	121.0(7)
N1	P	C6	104.6(3)	C22	C21	C20	119.9(7)
C1	P	W	111.5(3)	C23	C22	C21	119.9(7)
C1	P	C6	106.3(3)	C22	C23	C24	120.1(7)
C6	P	W	124.3(2)	C23	C24	C19	120.8(7)
C2	N1	P	124.6(5)	O1	C25	W	178.7(7)
C2	N1	C4	107.0(6)	O2	C26	W	178.6(7)
C4	N1	P	127.4(5)	O3	C27	W	177.9(8)
C2	N2	C3	108.2(6)	O4	C28	W	178.7(7)
C2	N2	C5	126.2(7)	O5	C29	W	176.2(7)
C3	N2	C5	125.7(7)	O6	S	O8	114.4(4)
N2	C2	N1	110.0(7)	O6	S	C30	103.4(4)
C4	C3	N2	107.2(7)	O7	S	O6	115.5(4)
C3	C4	N1	107.7(7)	O7	S	O8	114.4(5)
C7	C6	P	111.7(5)	O7	S	C30	103.3(4)
C7	C6	C13	110.6(6)	O8	S	C30	103.6(4)
C7	C6	C19	111.8(6)	F1	C30	S	111.7(7)
C13	C6	P	106.0(5)	F1	C30	F2	108.1(8)
C19	C6	P	105.3(5)	F1	C30	F3	107.0(7)
C19	C6	C13	111.1(6)	F2	C30	S	111.6(6)
C8	C7	C6	121.6(6)	F2	C30	F3	107.2(8)
C12	C7	C6	120.5(6)	F3	C30	S	111.1(6)
C12	C7	C8	117.9(7)	Cl2	C31	Cl1	112.0(6)

Table 98: Torsion angles for **68b**.

A	B	C	D	Angle / °	A	B	C	D	Angle / °
W	P	N1	C2	96.0(6)	C8	C9	C10	C11	1.4(12)
W	P	N1	C4	−71.1(7)	C9	C10	C11	C12	−2.1(12)
P	N1	C2	N2	−169.2(5)	C10	C11	C12	C7	0.5(11)
P	N1	C4	C3	169.8(5)	C12	C7	C8	C9	−2.4(11)
P	C6	C7	C8	−48.2(8)	C13	C6	C7	C8	−166.0(7)
P	C6	C7	C12	133.9(6)	C13	C6	C7	C12	16.1(9)
P	C6	C13	C14	140.5(6)	C13	C6	C19	C20	−131.3(7)
P	C6	C13	C18	−45.3(8)	C13	C6	C19	C24	49.1(9)
P	C6	C19	C20	114.3(7)	C13	C14	C15	C16	0.4(12)
P	C6	C19	C24	−65.2(7)	C14	C13	C18	C17	−2.7(11)
N2	C3	C4	N1	−1.4(9)	C14	C15	C16	C17	−1.4(12)
C1	P	N1	C2	−19.8(7)	C15	C16	C17	C18	0.4(12)
C1	P	N1	C4	173.1(7)	C16	C17	C18	C13	1.7(12)
C2	N1	C4	C3	0.8(9)	C18	C13	C14	C15	1.6(11)
C2	N2	C3	C4	1.5(9)	C19	C6	C7	C8	69.6(8)
C3	N2	C2	N1	−1.0(9)	C19	C6	C7	C12	−108.3(7)
C4	N1	C2	N2	0.1(8)	C19	C6	C13	C14	26.5(9)
C5	N2	C2	N1	180.0(7)	C19	C6	C13	C18	−159.3(6)
C5	N2	C3	C4	−179.5(7)	C19	C20	C21	C22	−1.1(13)
C6	P	N1	C2	−128.8(6)	C20	C19	C24	C23	−4.0(11)
C6	P	N1	C4	64.1(7)	C20	C21	C22	C23	−1.1(14)
C6	C7	C8	C9	179.7(7)	C21	C22	C23	C24	0.6(13)
C6	C7	C12	C11	179.6(6)	C22	C23	C24	C19	2.0(12)
C6	C13	C14	C15	176.0(7)	C24	C19	C20	C21	3.6(12)
C6	C13	C18	C17	−177.0(7)	O6	S	C30	F1	61.5(7)
C6	C19	C20	C21	−176.0(7)	O6	S	C30	F2	−59.5(7)
C6	C19	C24	C23	175.5(7)	O6	S	C30	F3	−179.1(6)
C7	C6	C13	C14	−98.2(8)	O7	S	C30	F1	−59.2(7)
C7	C6	C13	C18	75.9(8)	O7	S	C30	F2	179.8(7)
C7	C6	C19	C20	−7.2(10)	O7	S	C30	F3	60.2(7)
C7	C6	C19	C24	173.2(6)	O8	S	C30	F1	−178.8(7)
C7	C8	C9	C10	0.8(12)	O8	S	C30	F2	60.1(7)
C8	C7	C12	C11	1.7(11)	O8	S	C30	F3	−59.5(7)

7.2.22 [Pentacarbonyl{2-*tert*-butyl-3-methyl-1-(triphenylmethyl)phosphaguanidine-κ*P*}chromium(0)] (69a)

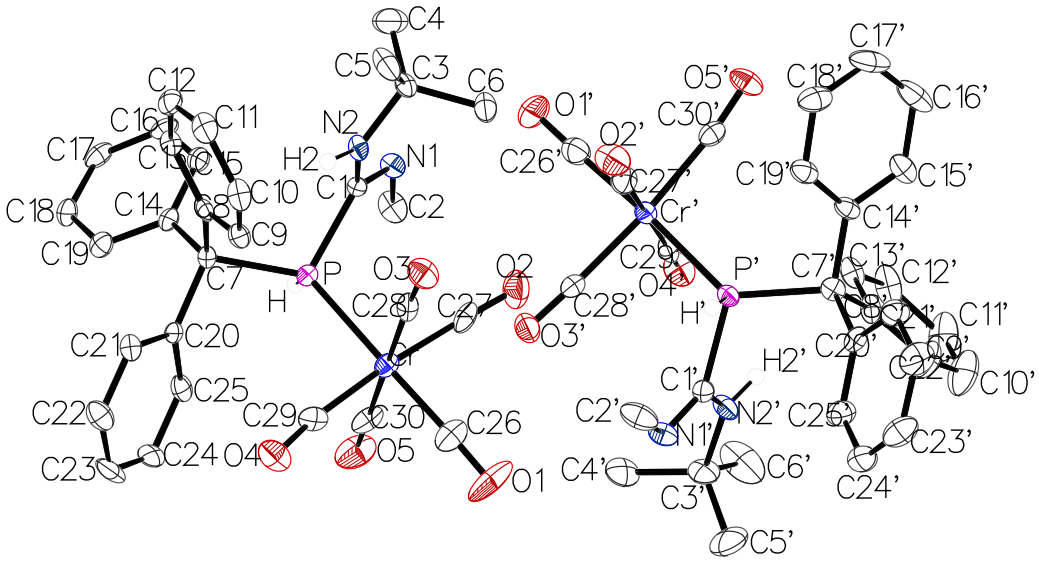

Figure 105: Molecular structures of **69a** in the single crystal lattice at 123(2) K. Thermal ellipsoids are set at 50 % probability level. Hydrogen atoms and solvent molecules were omitted for clarity except for those bound to phosphorus and nitrogen atoms.

Table 99: Crystal data and structure refinements for **69a**.

Identification code	GSTR734, DB-398 // GXray6704
Crystal habitus	clear light yellow needle
Device type	STOE IPDS-2T
Empirical formula	$C_{30}H_{29}CrN_2O_5P$
Moiety formula	$C_{30}H_{29}CrN_2O_5P$
Formula weight / g/mol	580.52
T / K	123(2)
Crystal system	triclinic
Space group	$P\bar{1}$
a / Å	9.1284(5)
b / Å	13.1778(6)
c / Å	24.2171(13)
α / °	89.744(4)
β / °	81.178(4)
γ / °	84.886(4)
V / Å^3	2867.1(3)
Z	4
ρ_{calc} / g/cm^3	1.345
μ / mm^{-1}	0.496
F(000)	1208.0

Crystal size / mm^3	0.18 × 0.04 × 0.03
Absorption correction	integration
Min. and max. transmission	0.9272 and 0.9909
Radiation	Mo-K_α (λ = 0.71073 Å)
2Θ range for data collection / °	5.32 to 56
Completeness to Θ	0.998
Index ranges	$-9 \le h \le 12$, $-16 \le k \le 17$, $-31 \le l \le 31$
Reflections collected	32389
Independent reflections	13808 (R_{int} = 0.1148, R_σ = 0.2248)
Data / restraints / parameters	13808 / 0 / 717
Goodness-of-fit on F^2	0.725
Final R indexes ($I \ge 2\sigma(I)$)	R_1 = 0.0529, ωR_2 = 0.0624
Final R indexes (all data)	R_1 = 0.1523, ωR_2 = 0.0784
Largest diff. peak and hole / e/$Å^3$	0.47 and −0.46

Table 100: Bond lengths for **69a**.

Atom	Atom	Length / Å	Atom	Atom	Length / Å
Cr	P	2.3804(13)	Cr'	P'	2.3946(13)
Cr	C26	1.849(4)	Cr'	C26'	1.855(5)
Cr	C27	1.882(4)	Cr'	C27'	1.913(4)
Cr	C28	1.930(4)	Cr'	C28'	1.907(3)
Cr	C29	1.912(4)	Cr'	C29'	1.925(4)
Cr	C30	1.894(4)	Cr'	C30'	1.898(4)
P	C1	1.873(3)	P'	C1'	1.873(3)
P	C7	1.938(3)	P'	C7'	1.938(3)
O1	C26	1.164(5)	O1'	C26'	1.163(5)
O2	C27	1.158(4)	O2'	C27'	1.127(5)
O3	C28	1.127(4)	O3'	C28'	1.137(4)
O4	C29	1.139(4)	O4'	C29'	1.128(4)
O5	C30	1.143(4)	O5'	C30'	1.146(4)
N1	C1	1.270(4)	N1'	C1'	1.269(4)
N1	C2	1.462(4)	N1'	C2'	1.459(5)
N2	C1	1.368(4)	N2'	C1'	1.370(4)
N2	C3	1.473(4)	N2'	C3'	1.481(4)
C3	C4	1.524(5)	C3'	C4'	1.511(5)
C3	C5	1.534(5)	C3'	C5'	1.523(6)
C3	C6	1.519(4)	C3'	C6'	1.523(5)
C7	C8	1.546(5)	C7'	C8'	1.537(5)
C7	C14	1.540(5)	C7'	C14'	1.544(5)
C7	C20	1.538(4)	C7'	C20'	1.530(5)
C8	C9	1.399(5)	C8'	C9'	1.387(5)

C8	C13	1.386(5)	C8'	C13'	1.391(5)
C9	C10	1.390(5)	C9'	C10'	1.388(6)
C10	C11	1.381(5)	C10'	C11'	1.370(7)
C11	C12	1.379(5)	C11'	C12'	1.379(6)
C12	C13	1.405(5)	C12'	C13'	1.382(5)
C14	C15	1.392(5)	C14'	C15'	1.389(4)
C14	C19	1.395(4)	C14'	C19'	1.397(5)
C15	C16	1.380(5)	C15'	C16'	1.383(5)
C16	C17	1.381(5)	C16'	C17'	1.381(6)
C17	C18	1.365(5)	C17'	C18'	1.363(5)
C18	C19	1.390(5)	C18'	C19'	1.375(5)
C20	C21	1.407(4)	C20'	C21'	1.402(5)
C20	C25	1.396(5)	C20'	C25'	1.386(5)
C21	C22	1.380(5)	C21'	C22'	1.393(5)
C22	C23	1.393(5)	C22'	C23'	1.373(6)
C23	C24	1.379(5)	C23'	C24'	1.385(5)
C24	C25	1.377(5)	C24'	C25'	1.383(6)

Table 101: Bond angles for **69a**.

Atom	**Atom**	**Atom**	**Angle / °**	**Atom**	**Atom**	**Atom**	**Angle / °**
C26	Cr	P	176.03(14)	C26'	Cr'	P'	175.32(13)
C26	Cr	C27	88.46(17)	C26'	Cr'	C27'	91.69(18)
C26	Cr	C28	90.21(17)	C26'	Cr'	C28'	88.70(16)
C26	Cr	C29	86.44(17)	C26'	Cr'	C29'	90.25(18)
C26	Cr	C30	90.76(17)	C26'	Cr'	C30'	86.80(16)
C27	Cr	P	88.87(12)	C27'	Cr'	P'	85.43(13)
C27	Cr	C28	86.99(15)	C27'	Cr'	C29'	177.64(18)
C27	Cr	C29	174.79(17)	C28'	Cr'	P'	87.60(11)
C27	Cr	C30	91.34(16)	C28'	Cr'	C27'	89.68(16)
C28	Cr	P	92.59(12)	C28'	Cr'	C29'	89.02(14)
C29	Cr	P	96.27(11)	C29'	Cr'	P'	92.55(12)
C29	Cr	C28	91.92(15)	C30'	Cr'	P'	96.80(12)
C30	Cr	P	86.36(12)	C30'	Cr'	C27'	88.59(16)
C30	Cr	C28	178.04(17)	C30'	Cr'	C28'	175.13(16)
C30	Cr	C29	89.84(16)	C30'	Cr'	C29'	92.86(15)
C1	P	Cr	109.60(11)	C1'	P'	Cr'	108.87(11)
C1	P	C7	109.46(15)	C1'	P'	C7'	109.16(15)
C7	P	Cr	127.27(11)	C7'	P'	Cr'	129.24(12)
C1	N1	C2	121.9(3)	C1'	N1'	C2'	121.3(3)
C1	N2	C3	126.5(3)	C1'	N2'	C3'	126.7(3)
N1	C1	P	125.5(3)	N1'	C1'	P'	126.1(3)
N1	C1	N2	121.2(3)	N1'	C1'	N2'	121.4(3)

N2	C1	P	113.0(2)	N2'	C1'	P'	112.1(2)
N2	C3	C4	111.3(3)	N2'	C3'	C4'	110.6(3)
N2	C3	C5	104.9(3)	N2'	C3'	C5'	110.2(3)
N2	C3	C6	110.6(3)	N2'	C3'	C6'	105.1(3)
C4	C3	C5	109.5(3)	C4'	C3'	C5'	111.0(3)
C6	C3	C4	111.2(3)	C4'	C3'	C6'	109.2(4)
C6	C3	C5	109.1(3)	C5'	C3'	C6'	110.5(4)
C8	C7	P	109.2(2)	C8'	C7'	P'	110.1(2)
C14	C7	P	108.2(2)	C8'	C7'	C14'	110.1(3)
C14	C7	C8	112.6(3)	C14'	C7'	P'	104.4(2)
C20	C7	P	105.1(2)	C20'	C7'	P'	107.9(2)
C20	C7	C8	111.2(3)	C20'	C7'	C8'	112.4(3)
C20	C7	C14	110.1(3)	C20'	C7'	C14'	111.5(3)
C9	C8	C7	119.5(3)	C9'	C8'	C7'	122.2(3)
C13	C8	C7	122.0(3)	C9'	C8'	C13'	117.7(3)
C13	C8	C9	118.5(3)	C13'	C8'	C7'	120.0(3)
C10	C9	C8	120.9(4)	C8'	C9'	C10'	121.0(4)
C11	C10	C9	120.2(4)	C11'	C10'	C9'	120.1(4)
C12	C11	C10	119.8(3)	C10'	C11'	C12'	120.2(4)
C11	C12	C13	120.3(4)	C11'	C12'	C13'	119.5(4)
C8	C13	C12	120.4(3)	C12'	C13'	C8'	121.6(4)
C15	C14	C7	122.4(3)	C15'	C14'	C7'	122.3(3)
C15	C14	C19	117.1(3)	C15'	C14'	C19'	116.8(3)
C19	C14	C7	120.4(3)	C19'	C14'	C7'	120.9(3)
C16	C15	C14	121.5(3)	C16'	C15'	C14'	121.3(4)
C15	C16	C17	120.3(3)	C17'	C16'	C15'	120.2(4)
C18	C17	C16	119.3(3)	C18'	C17'	C16'	119.4(4)
C17	C18	C19	120.8(3)	C17'	C18'	C19'	120.5(4)
C18	C19	C14	120.9(3)	C18'	C19'	C14'	121.7(3)
C21	C20	C7	121.8(3)	C21'	C20'	C7'	121.5(3)
C25	C20	C7	120.7(3)	C25'	C20'	C7'	121.9(3)
C25	C20	C21	117.4(3)	C25'	C20'	C21'	116.6(4)
C22	C21	C20	120.5(3)	C22'	C21'	C20'	121.4(4)
C21	C22	C23	120.9(3)	C23'	C22'	C21'	120.6(4)
C24	C23	C22	118.9(3)	C22'	C23'	C24'	119.0(4)
C25	C24	C23	120.6(4)	C25'	C24'	C23'	120.3(4)
C24	C25	C20	121.6(3)	C24'	C25'	C20'	122.3(4)
O1	C26	Cr	178.3(4)	O1'	C26'	Cr'	178.4(3)
O2	C27	Cr	176.5(3)	O2'	C27'	Cr'	178.0(3)
O3	C28	Cr	176.9(3)	O3'	C28'	Cr'	177.4(3)
O4	C29	Cr	173.3(3)	O4'	C29'	Cr'	177.2(3)
O5	C30	Cr	179.3(4)	O5'	C30'	Cr'	173.5(3)

7.2.23 [Pentacarbonyl{2-*tert*-butyl-3-methyl-1-(triphenylmethyl)phosphaguanidine-κ*P*}tungsten(0)] (69b)

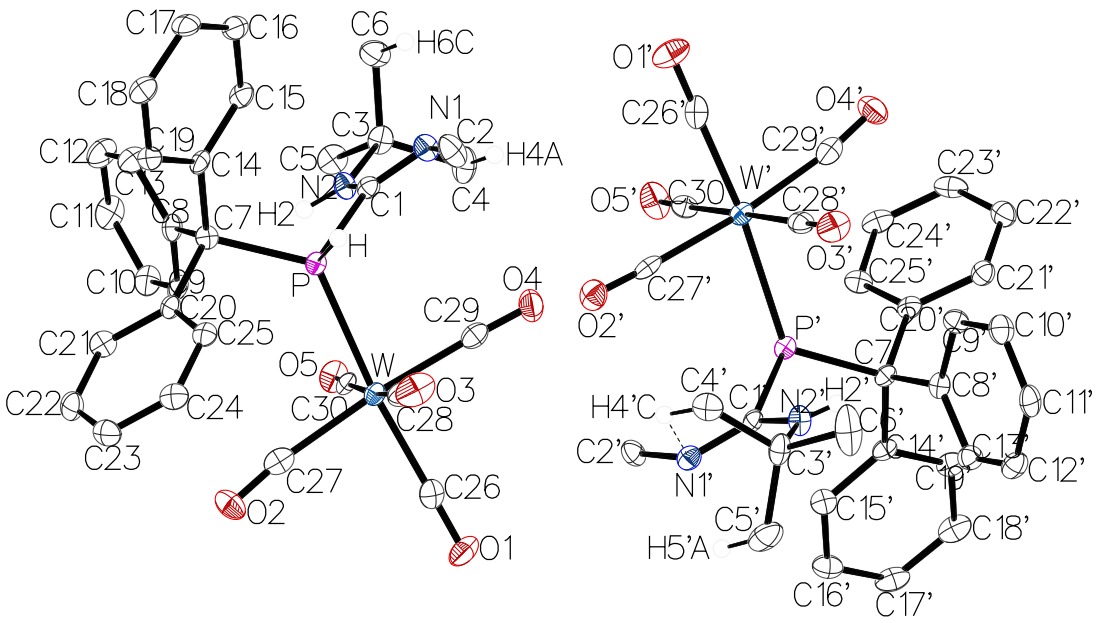

Figure 106: Molecular structures of **69b** in the single crystal lattice at 100(2) K. Thermal ellipsoids are set at 50 % probability level. Hydrogen atoms and solvent molecules were omitted for clarity except for those bound to phosphorus and nitrogen atoms or that are in close proximity to a nitrogen atom.

Table 102: Crystal data and structure refinements for **69b**.

Identification code	GSTR672, DB-116.1 // GXray6002f
Crystal habitus	clear light yellow plate
Device type	Bruker X8-KappaApexII
Empirical formula	$C_{30}H_{29}N_2O_5PW$
Moiety formula	$C_{30}H_{29}N_2O_5PW$
Formula weight / g/mol	712.37
T / K	100
Crystal system	triclinic
Space group	$P\bar{1}$
a / Å	9.2076(5)
b / Å	17.6788(10)
c / Å	17.9311(9)
α / °	87.109(3)
β / °	82.372(3)
γ / °	78.688(3)
V / Å^3	2835.9(3)
Z	4
ρ_{calc} / g/cm^3	1.669
μ / mm^{-1}	4.172
F(000)	1408.0
Crystal size / mm^3	0.18 × 0.1 × 0.04

Absorption correction	empirical
Min. and max. transmission	0.4487 and 0.7461
Radiation	Mo-K_α (λ = 0.71073 Å)
2Θ range for data collection / °	2.35 to 55.996
Completeness to Θ	0.998
Index ranges	$-12 \le h \le 12$, $-23 \le k \le 23$, $-23 \le l \le 23$
Reflections collected	133248
Independent reflections	13670 (R_{int} = 0.1023, R_σ = 0.0518)
Data / restraints / parameters	13670 / 0 / 723
Goodness-of-fit on F^2	1.113
Final R indexes ($I \ge 2\sigma(I)$)	R_1 = 0.0377, ωR_2 = 0.0689
Final R indexes (all data)	R_1 = 0.0595, ωR_2 = 0.0774
Largest diff. peak and hole / e/Å^3	1.86 and −1.82

Table 103: Bond lengths for **69b**.

Atom	Atom	Length / Å	Atom	Atom	Length / Å
W	P	2.5166(12)	W'	P'	2.5239(12)
W	C26	2.002(5)	W'	C26'	1.989(5)
W	C27	2.046(6)	W'	C27'	2.040(5)
W	C28	2.040(5)	W'	C28'	2.044(5)
W	C29	2.034(5)	W'	C29'	2.052(6)
W	C30	2.055(5)	W'	C30'	2.046(5)
P	C1	1.867(5)	P'	C1'	1.889(5)
P	C7	1.931(5)	P'	C7'	1.915(5)
O1	C26	1.146(6)	O1'	C26'	1.152(6)
O2	C27	1.145(6)	O2'	C27'	1.145(6)
O3	C28	1.135(6)	O3'	C28'	1.141(6)
O4	C29	1.133(6)	O4'	C29'	1.143(6)
O5	C30	1.140(6)	O5'	C30'	1.129(6)
N1	C1	1.272(6)	N1'	C1'	1.270(6)
N1	C2	1.455(6)	N1'	C2'	1.452(6)
N2	C1	1.371(6)	N2'	C1'	1.361(6)
N2	C3	1.474(6)	N2'	C3'	1.479(6)
C3	C4	1.518(7)	C3'	C4'	1.523(7)
C3	C5	1.529(7)	C3'	C5'	1.520(7)
C3	C6	1.515(7)	C3'	C6'	1.517(7)
C7	C8	1.529(6)	C7'	C8'	1.529(6)
C7	C14	1.537(6)	C7'	C14'	1.547(6)
C7	C20	1.541(7)	C7'	C20'	1.541(6)
C8	C9	1.396(6)	C8'	C9'	1.398(6)
C8	C13	1.400(7)	C8'	C13'	1.397(6)

C9	C10	1.386(7)	C9'	C10'	1.391(7)
C10	C11	1.390(7)	C10'	C11'	1.367(7)
C11	C12	1.377(7)	C11'	C12'	1.381(7)
C12	C13	1.387(7)	C12'	C13'	1.394(7)
C14	C15	1.395(7)	C14'	C15'	1.381(7)
C14	C19	1.397(7)	C14'	C19'	1.388(6)
C15	C16	1.382(7)	C15'	C16'	1.399(7)
C16	C17	1.383(7)	C16'	C17'	1.372(7)
C17	C18	1.376(7)	C17'	C18'	1.383(8)
C18	C19	1.386(7)	C18'	C19'	1.390(7)
C20	C21	1.389(7)	C20'	C21'	1.390(7)
C20	C25	1.406(6)	C20'	C25'	1.397(6)
C21	C22	1.380(7)	C21'	C22'	1.387(7)
C22	C23	1.386(7)	C22'	C23'	1.381(7)
C23	C24	1.389(7)	C23'	C24'	1.394(7)
C24	C25	1.377(7)	C24'	C25'	1.379(7)

Table 104: Bond angles for **69b**.

Atom	**Atom**	**Atom**	**Angle / °**	**Atom**	**Atom**	**Atom**	**Angle / °**
C26	W	P	174.05(14)	C26'	W'	P'	174.35(15)
C26	W	C27	86.7(2)	C26'	W'	C27'	88.4(2)
C26	W	C28	92.88(19)	C26'	W'	C28'	90.82(19)
C26	W	C29	88.5(2)	C26'	W'	C29'	87.1(2)
C26	W	C30	91.79(18)	C26'	W'	C30'	90.8(2)
C27	W	P	97.99(14)	C27'	W'	P'	86.34(13)
C27	W	C30	92.67(19)	C27'	W'	C28'	90.44(19)
C28	W	P	83.50(14)	C27'	W'	C29'	174.68(19)
C28	W	C27	89.6(2)	C27'	W'	C30'	90.47(19)
C28	W	C30	174.94(19)	C28'	W'	P'	91.39(13)
C29	W	P	86.81(14)	C28'	W'	C29'	92.55(19)
C29	W	C27	175.19(19)	C28'	W'	C30'	178.15(19)
C29	W	C28	91.2(2)	C29'	W'	P'	97.98(14)
C29	W	C30	86.95(19)	C30'	W'	P'	87.07(14)
C30	W	P	91.68(13)	C30'	W'	C29'	86.66(19)
C1	P	W	108.46(15)	C1'	P'	W'	108.95(14)
C1	P	C7	110.2(2)	C1'	P'	C7'	110.1(2)
C7	P	W	127.79(15)	C7'	P'	W'	126.60(15)
C1	N1	C2	121.9(4)	C1'	N1'	C2'	123.2(4)
C1	N2	C3	126.3(4)	C1'	N2'	C3'	126.7(4)
N1	C1	P	125.5(4)	N1'	C1'	P'	125.3(4)
N1	C1	N2	121.7(4)	N1'	C1'	N2'	121.4(4)

N2	C1	P	112.2(3)	N2'	C1'	P'	112.5(3)
N2	C3	C4	110.1(4)	N2'	C3'	C4'	109.9(4)
N2	C3	C5	104.9(4)	N2'	C3'	C5'	110.6(4)
N2	C3	C6	110.5(4)	N2'	C3'	C6'	106.3(4)
C4	C3	C5	109.4(4)	C5'	C3'	C4'	110.5(4)
C6	C3	C4	111.5(4)	C6'	C3'	C4'	109.3(5)
C6	C3	C5	110.2(4)	C6'	C3'	C5'	110.1(5)
C8	C7	P	109.5(3)	C8'	C7'	P'	107.0(3)
C8	C7	C14	112.1(4)	C8'	C7'	C14'	111.5(4)
C8	C7	C20	111.3(4)	C8'	C7'	C20'	112.7(4)
C14	C7	P	108.1(3)	C14'	C7'	P'	113.6(3)
C14	C7	C20	111.2(4)	C20'	C7'	P'	105.2(3)
C20	C7	P	104.3(3)	C20'	C7'	C14'	106.8(4)
C9	C8	C7	120.3(4)	C9'	C8'	C7'	119.6(4)
C9	C8	C13	117.5(4)	C13'	C8'	C7'	122.3(4)
C13	C8	C7	122.2(4)	C13'	C8'	C9'	118.0(4)
C10	C9	C8	121.6(5)	C10'	C9'	C8'	120.7(5)
C9	C10	C11	119.7(5)	C11'	C10'	C9'	120.5(5)
C12	C11	C10	119.7(5)	C10'	C11'	C12'	120.1(5)
C11	C12	C13	120.4(5)	C11'	C12'	C13'	120.1(5)
C12	C13	C8	121.0(5)	C12'	C13'	C8'	120.7(5)
C15	C14	C7	121.2(4)	C15'	C14'	C7'	124.7(4)
C15	C14	C19	117.7(4)	C15'	C14'	C19'	118.4(4)
C19	C14	C7	121.0(4)	C19'	C14'	C7'	116.9(4)
C16	C15	C14	121.1(5)	C14'	C15'	C16'	120.6(5)
C15	C16	C17	120.4(5)	C17'	C16'	C15'	120.5(5)
C18	C17	C16	119.2(5)	C16'	C17'	C18'	119.4(5)
C17	C18	C19	120.8(5)	C17'	C18'	C19'	120.1(5)
C18	C19	C14	120.7(5)	C14'	C19'	C18'	121.0(5)
C21	C20	C7	122.9(4)	C21'	C20'	C7'	122.9(4)
C21	C20	C25	117.4(4)	C21'	C20'	C25'	117.6(4)
C25	C20	C7	119.7(4)	C25'	C20'	C7'	119.3(4)
C22	C21	C20	121.2(5)	C22'	C21'	C20'	121.1(5)
C21	C22	C23	120.5(5)	C23'	C22'	C21'	120.5(5)
C22	C23	C24	119.4(5)	C22'	C23'	C24'	119.2(5)
C25	C24	C23	119.7(5)	C25'	C24'	C23'	119.9(5)
C24	C25	C20	121.7(5)	C24'	C25'	C20'	121.6(5)
O1	C26	W	178.7(4)	O1'	C26'	W'	179.4(5)
O2	C27	W	173.4(4)	O2'	C27'	W'	177.4(4)
O3	C28	W	176.2(4)	O3'	C28'	W'	178.9(4)
O4	C29	W	177.3(5)	O4'	C29'	W'	172.9(4)
O5	C30	W	176.8(4)	O5'	C30'	W'	177.6(4)

Table 105: Hydrogen bonds for **69b**.

D	H	A	d(D-H) / Å	d(H-A) / Å	d(D-A) / Å	D-H-A / °
C4	H4A	N1	0.98	2.50	3.101(6)	119.4
C6	H6C	N1	0.98	2.51	3.103(6)	118.9
C4'	H4'C	N1'	0.98	2.51	3.124(6)	120.6
C5'	H5'A	N1'	0.98	2.48	3.085(7)	119.8

7.2.24 [Pentacarbonyl{2-*tert*-butyl-1-(triphenylmethyl)-3-isopropylphosphaguanidine-κ*P*}chromium(0)] (70a)

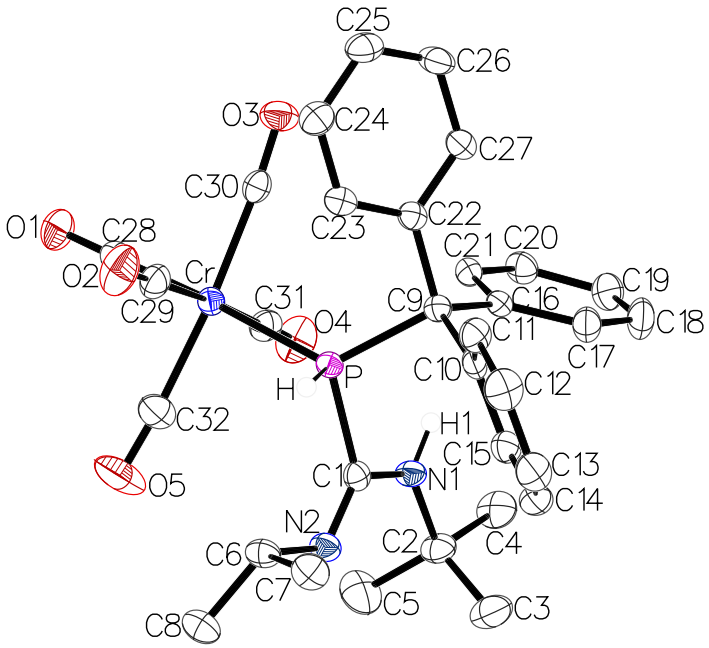

Figure 107: Molecular structures of **70a** in the single crystal lattice at 123(2) K. Thermal ellipsoids are set at 50 % probability level. Hydrogen atoms and solvent molecules were omitted for clarity except for those bound to phosphorus and nitrogen atoms.

Table 106: Crystal data and structure refinements for **70a**.

Identification code	GSTR714, DB-301 // GXray6529
Crystal habitus	clear light yellow block
Device type	STOE IPDS-2T
Empirical formula	$C_{32}H_{33}CrN_2O_5P$
Moiety formula	$C_{32}H_{33}CrN_2O_5P$
Formula weight / g/mol	608.57
T / K	123
Crystal system	monoclinic
Space group	$P2_1/n$
a / Å	17.2112(9)
b / Å	10.0937(4)
c / Å	19.2780(10)
α / °	90
β / °	113.077(4)
γ / °	90
V / Å^3	3081.1(3)
Z	4
ρ_{calc} / g/cm^3	1.312
μ / mm^{-1}	0.465

F(000)	1272.0
Crystal size / mm^3	0.14 × 0.09 × 0.07
Absorption correction	integration
Min. and max. transmission	0.8669 and 0.9766
Radiation	Mo-K_α (λ = 0.71073 Å)
2Θ range for data collection / °	5.146 to 55.998
Completeness to Θ	0.999
Index ranges	$-22 \le h \le 22$, $-13 \le k \le 13$, $-22 \le l \le 25$
Reflections collected	24207
Independent reflections	7447 (R_{int} = 0.0675, R_σ = 0.1004)
Data / restraints / parameters	7447 / 0 / 378
Goodness-of-fit on F^2	0.840
Final *R* indexes ($I \ge 2\sigma(I)$)	R_1 = 0.0420, ωR_2 = 0.0591
Final *R* indexes (all data)	R_1 = 0.0959, ωR_2 = 0.0691
Largest diff. peak and hole / e/Å^3	0.26 and −0.48

Table 107: Bond lengths for **70a**.

Atom	Atom	Length / Å	Atom	Atom	Length / Å
Cr	P	2.3952(6)	C9	C10	1.546(3)
Cr	C28	1.852(2)	C9	C16	1.532(3)
Cr	C29	1.899(3)	C9	C22	1.546(3)
Cr	C30	1.906(2)	C10	C11	1.386(3)
Cr	C31	1.894(2)	C10	C15	1.401(3)
Cr	C32	1.898(3)	C11	C12	1.394(3)
P	C1	1.880(2)	C12	C13	1.377(3)
P	C9	1.948(2)	C13	C14	1.379(3)
O1	C28	1.159(3)	C14	C15	1.388(3)
O2	C29	1.145(3)	C16	C17	1.390(3)
O3	C30	1.143(3)	C16	C21	1.407(3)
O4	C31	1.146(3)	C17	C18	1.391(3)
O5	C32	1.141(3)	C18	C19	1.387(3)
N1	C1	1.369(3)	C19	C20	1.379(3)
N1	C2	1.479(3)	C20	C21	1.378(3)
N2	C1	1.278(3)	C22	C23	1.393(3)
N2	C6	1.467(3)	C22	C27	1.396(3)
C2	C3	1.534(3)	C23	C24	1.382(3)
C2	C4	1.528(3)	C24	C25	1.386(3)
C2	C5	1.520(3)	C25	C26	1.376(3)
C6	C7	1.523(3)	C26	C27	1.399(3)
C6	C8	1.517(3)			

Table 108: Bond angles for **70a**.

Atom	Atom	Atom	Angle / °	Atom	Atom	Atom	Angle / °
C28	Cr	P	177.21(7)	C16	C9	P	110.58(14)
C28	Cr	C29	90.84(10)	C16	C9	C10	112.62(18)
C28	Cr	C30	87.14(10)	C16	C9	C22	110.04(17)
C28	Cr	C31	89.55(10)	C22	C9	P	105.60(14)
C28	Cr	C32	87.50(10)	C11	C10	C9	122.5(2)
C29	Cr	P	88.63(7)	C11	C10	C15	117.9(2)
C29	Cr	C30	91.28(10)	C15	C10	C9	119.62(19)
C30	Cr	P	95.61(7)	C10	C11	C12	120.6(2)
C31	Cr	P	90.88(7)	C13	C12	C11	120.9(2)
C31	Cr	C29	177.77(10)	C12	C13	C14	119.3(2)
C31	Cr	C30	90.93(10)	C13	C14	C15	120.2(2)
C31	Cr	C32	88.45(11)	C14	C15	C10	121.1(2)
C32	Cr	P	89.75(7)	C17	C16	C9	122.87(19)
C32	Cr	C29	89.37(11)	C17	C16	C21	117.5(2)
C32	Cr	C30	174.61(10)	C21	C16	C9	119.6(2)
C1	P	Cr	112.03(7)	C16	C17	C18	121.0(2)
C1	P	C9	107.60(9)	C19	C18	C17	120.4(2)
C9	P	Cr	126.93(6)	C20	C19	C18	119.3(2)
C1	N1	C2	126.85(18)	C21	C20	C19	120.4(2)
C1	N2	C6	123.80(18)	C20	C21	C16	121.3(2)
N1	C1	P	112.57(14)	C23	C22	C9	121.63(19)
N2	C1	P	125.97(16)	C23	C22	C27	117.7(2)
N2	C1	N1	121.23(19)	C27	C22	C9	120.7(2)
N1	C2	C3	109.88(19)	C24	C23	C22	121.6(2)
N1	C2	C4	105.29(18)	C23	C24	C25	120.2(2)
N1	C2	C5	110.7(2)	C26	C25	C24	119.3(2)
C4	C2	C3	109.2(2)	C25	C26	C27	120.6(2)
C5	C2	C3	111.5(2)	C22	C27	C26	120.5(2)
C5	C2	C4	110.1(2)	O1	C28	Cr	179.6(2)
N2	C6	C7	110.00(19)	O2	C29	Cr	178.4(2)
N2	C6	C8	107.16(18)	O3	C30	Cr	174.79(19)
C8	C6	C7	110.49(18)	O4	C31	Cr	177.7(2)
C10	C9	P	105.08(13)	O5	C32	Cr	175.4(2)
C10	C9	C22	112.59(17)				

7.2.25 [Pentacarbonyl{2-*tert*-butyl-1-(triphenylmethyl)-3-isopropylphosphaguanidine-κ*P*}tungsten(0)] (70b)

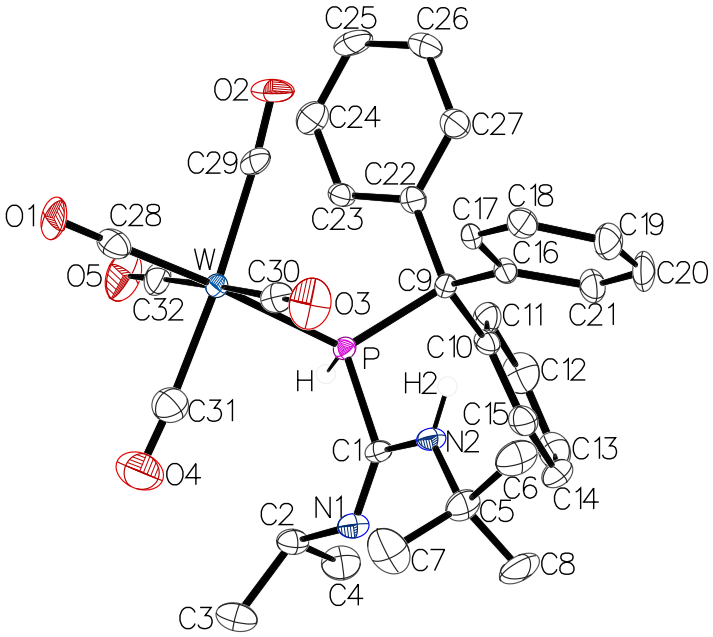

Figure 108: Molecular structures of **70b** in the single crystal lattice at 123(2) K. Thermal ellipsoids are set at 50 % probability level. Hydrogen atoms and solvent molecules were omitted for clarity except for those bound to phosphorus and nitrogen atoms.

Table 109: Crystal data and structure refinements for **70b**.

Identification code	GSTR735, DB-400 // GXray6705
Crystal habitus	clear colorless plate
Device type	STOE IPDS2T
Empirical formula	$C_{32}H_{33}N_2O_5PW$
Moiety formula	$C_{32}H_{33}N_2O_5PW$
Formula weight / g/mol	740.42
T / K	123
Crystal system	monoclinic
Space group	$P2_1/n$
a / Å	17.300(6)
b / Å	10.198(4)
c / Å	19.486(6)
α / °	90
β / °	113.21(2)
γ / °	90
V / Å^3	3159.6(19)
Z	4
ρ_{calc} / g/cm^3	1.557
μ / mm^{-1}	3.747
F(000)	1472.0

Crystal size / mm^3	0.15 × 0.11 × 0.04
Absorption correction	integration
Min. and max. transmission	0.5168 and 0.7481
Radiation	Mo-K_α (λ = 0.71073 Å)
2Θ range for data collection / °	5.346 to 56
Completeness to Θ	0.994
Index ranges	$-22 \le h \le 22$, $-13 \le k \le 13$, $-25 \le l \le 21$
Reflections collected	20556
Independent reflections	7598 (R_{int} = 0.0536, R_σ = 0.1256)
Data / restraints / parameters	7598 / 12 / 378
Goodness-of-fit on F^2	0.554
Final R indexes ($I \ge 2\sigma(I)$)	R_1 = 0.0246, ωR_2 = 0.0338
Final R indexes (all data)	R_1 = 0.0584, ωR_2 = 0.0368
Largest diff. peak and hole / e/$Å^3$	0.99 and −0.64

Table 110: Bond lengths for **70b**.

Atom	Atom	Length / Å	Atom	Atom	Length / Å
W	P	2.5256(11)	C9	C10	1.551(4)
W	C28	1.978(4)	C9	C16	1.542(4)
W	C29	2.048(3)	C9	C22	1.540(5)
W	C30	2.044(4)	C10	C11	1.392(4)
W	C31	2.027(4)	C10	C15	1.398(5)
W	C32	2.042(4)	C11	C12	1.399(4)
P	C1	1.879(3)	C12	C13	1.375(5)
P	C9	1.948(3)	C13	C14	1.376(5)
O1	C28	1.163(4)	C14	C15	1.380(5)
O2	C29	1.145(4)	C16	C17	1.404(4)
O3	C30	1.137(4)	C16	C21	1.384(5)
O4	C31	1.151(4)	C17	C18	1.379(4)
O5	C32	1.140(4)	C18	C19	1.381(5)
N1	C1	1.274(3)	C19	C20	1.379(5)
N1	C2	1.474(4)	C20	C21	1.395(5)
N2	C1	1.381(3)	C22	C23	1.389(5)
N2	C5	1.470(4)	C22	C27	1.396(4)
C2	C3	1.532(5)	C23	C24	1.379(5)
C2	C4	1.526(5)	C24	C25	1.386(4)
C5	C6	1.530(5)	C25	C26	1.380(5)
C5	C7	1.527(5)	C26	C27	1.394(5)
C5	C8	1.522(5)			

Table 111: Bond angles for **70b**.

Atom	Atom	Atom	Angle / °	Atom	Atom	Atom	Angle / °
C28	W	P	176.58(10)	C16	C9	C10	112.5(3)
C28	W	C29	87.96(14)	C22	C9	P	106.0(2)
C28	W	C30	89.59(15)	C22	C9	C10	112.8(3)
C28	W	C31	87.22(15)	C22	C9	C16	110.0(2)
C28	W	C32	91.84(15)	C11	C10	C9	121.8(3)
C29	W	P	95.46(10)	C11	C10	C15	118.1(3)
C30	W	P	90.32(11)	C15	C10	C9	120.1(3)
C30	W	C29	91.23(14)	C10	C11	C12	120.2(3)
C31	W	P	89.36(12)	C13	C12	C11	120.5(4)
C31	W	C29	175.13(16)	C12	C13	C14	119.6(3)
C31	W	C30	88.08(15)	C13	C14	C15	120.4(4)
C31	W	C32	90.31(15)	C14	C15	C10	121.1(3)
C32	W	P	88.15(11)	C17	C16	C9	118.9(3)
C32	W	C29	90.51(14)	C21	C16	C9	122.9(3)
C32	W	C30	177.79(16)	C21	C16	C17	118.1(3)
C1	P	W	111.35(10)	C18	C17	C16	121.0(3)
C1	P	C9	108.89(14)	C17	C18	C19	120.1(3)
C9	P	W	125.89(10)	C20	C19	C18	119.8(3)
C1	N1	C2	123.1(3)	C19	C20	C21	120.2(4)
C1	N2	C5	126.5(3)	C16	C21	C20	120.7(3)
N1	C1	P	126.3(2)	C23	C22	C9	121.7(3)
N1	C1	N2	121.0(3)	C23	C22	C27	117.4(3)
N2	C1	P	112.45(19)	C27	C22	C9	120.9(3)
N1	C2	C3	107.2(3)	C24	C23	C22	121.9(3)
N1	C2	C4	110.0(3)	C23	C24	C25	120.1(3)
C4	C2	C3	110.5(3)	C26	C25	C24	119.4(3)
N2	C5	C6	105.5(3)	C25	C26	C27	120.1(3)
N2	C5	C7	110.7(3)	C26	C27	C22	121.0(3)
N2	C5	C8	110.7(3)	O1	C28	W	179.3(3)
C7	C5	C6	109.8(3)	O2	C29	W	174.8(3)
C8	C5	C6	109.2(3)	O3	C30	W	179.1(3)
C8	C5	C7	110.8(4)	O4	C31	W	176.3(4)
C10	C9	P	104.9(2)	O5	C32	W	178.8(3)
C16	C9	P	110.4(2)				

7.3 CYCLIC VOLTAMMOGRAMS

Table 112: Cyclic voltammetric measurement details for donor-to-phosphinidene complex adducts.

Compound	*m* / mg	*M* / g/mol	*n* / μmol	*c* / mmol/L
6c	2.4	681.327	4	1.2
13a	1.6	548.455	3	1.0
13b	2.0	680.299	3	1.0
14b	<1	720.364	<1	<0.5
19a	1.6	542.428	3	1.0
19b	5.4	674.272	8	2.0
20b	2.1	716.353	3	1.0
21b	2.4	800.515	3	1.0

7.3.1 [Pentacarbonyl{(*tert*-butylazaniumylidyne)methyl(triphenylmethyl)phosphanido-κ*P*}tungsten(0)] (6c)

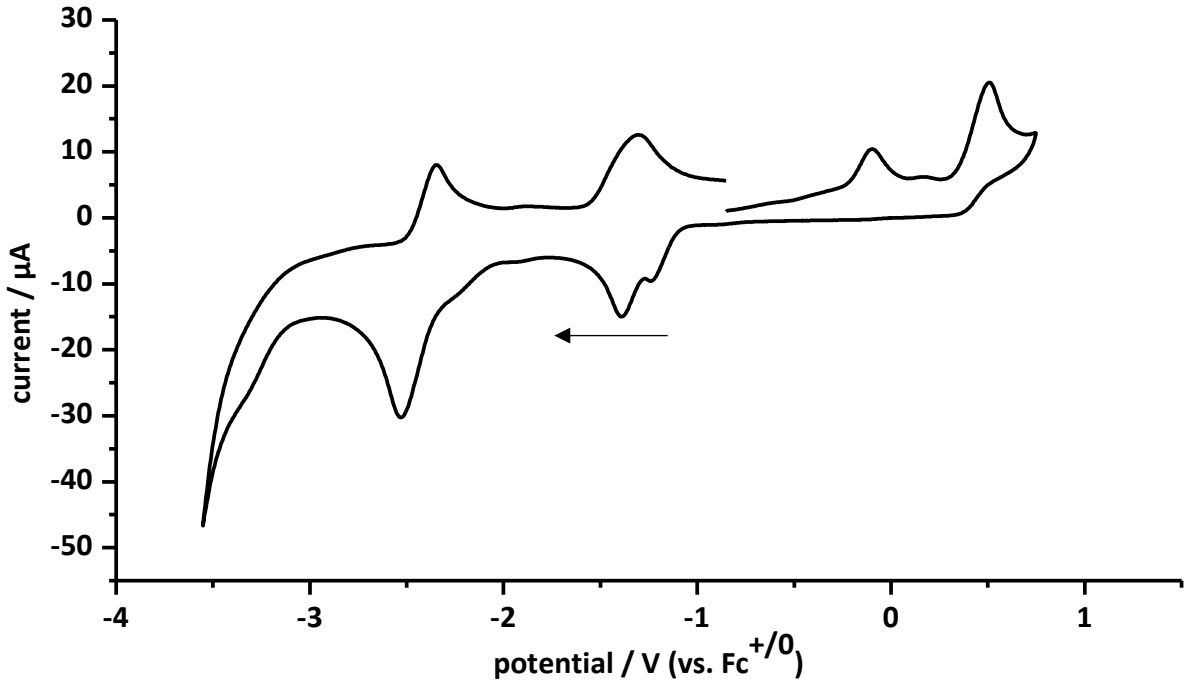

Figure 109: Cyclic voltammogram of complex **6c** (1 mM) at a Pt electrode in a 0.2 M $^{n}Bu_4PF_6$/THF solution with cobaltocenium hexafluorophosphate as internal reference; measurement with cathodic initial scan direction (denoted with an arrow); scan rate: 200 mV/s; potentials are referenced against $Fc^{+/0}$.

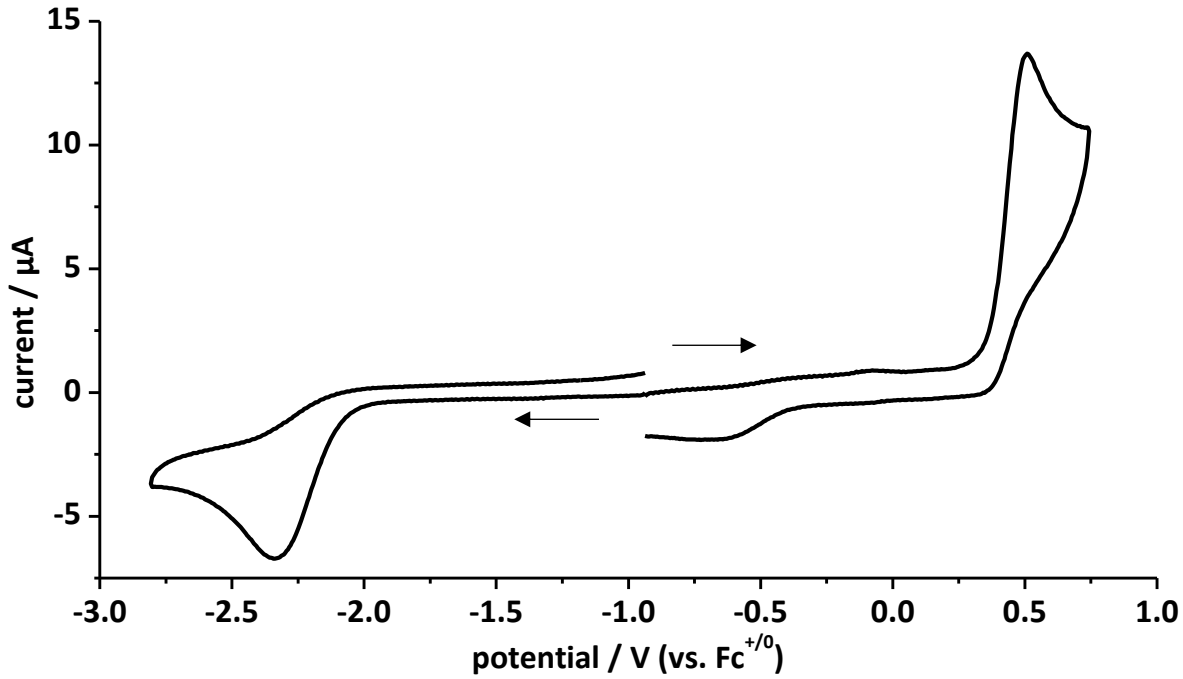

Figure 110: Overlay of cyclic voltammograms of **6c** (1 mM) at a Pt electrode in a 0.2 M $^{n}Bu_4PF_6$/THF solution; oxidation parts with anodic initial scan direction and reduction parts with cathodic initial scan direction as denoted with arrows; scan rate: 200 mV/s; potentials are referenced against $Fc^{+/0}$.

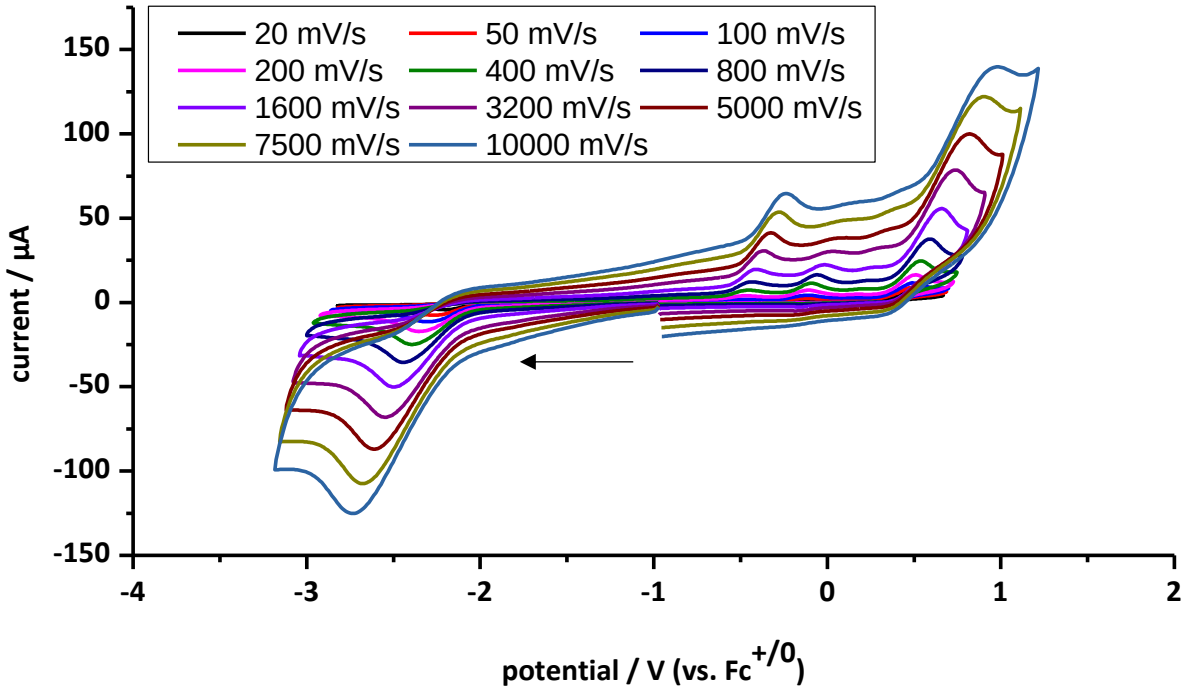

Figure 111: Cyclic voltammogram of complex **6c** (1 mM) at a Pt electrode in a 0.2 M $^{n}Bu_4PF_6$/THF solution at various scan rates; measurement with cathodic initial scan direction (denoted with an arrow); potentials are referenced against $Fc^{+/0}$.

Table 113: Selected results of the cyclic voltametric studies of **6c** in 0.2 M $^{n}Bu_4NPF_6$/THF solution at ambient temperature. Potentials are referenced against $Fc^{+/0}$.

ν / mV/s	E_p^{Ia} / V	i_p^{Ia} / µA	E_p^{IIc} / V	i_p^{IIc} / µA	E_p^{IIIa} / V	i_p^{IIIa} / µA	$\lvert i_p^{IIIa}/i_p^{IIc} \rvert$
20	0.47	7.28	−2.20	−4.28	−0.15	0.68	0.16
50	0.48	8.72	−2.26	−7.50	−0.13	2.51	0.33
100	0.49	11.6	−2.30	−11.4	−0.11	4.33	0.38
200	0.51	16.4	−2.35	−17.2	−0.11	7.31	0.42
400	0.54	24.6	−2.39	−24.9	−0.09	11.4	0.46
800	0.59	37.6	−2.44	−35.6	−0.05	16.4	0.46
1600	0.66	55.6	−2.50	−50.1	−0.01	22.4	0.45
3200	0.74	78.6	−2.55	−68.1	0.03	30.3	0.44
5000	0.82	100	−2.61	−87.0	0.11	38.4	0.44
7500	0.90	122	−2.68	−107	0.14	49.2	0.46
10000	0.98	140	−2.73	−125	0.21	59.9	0.48

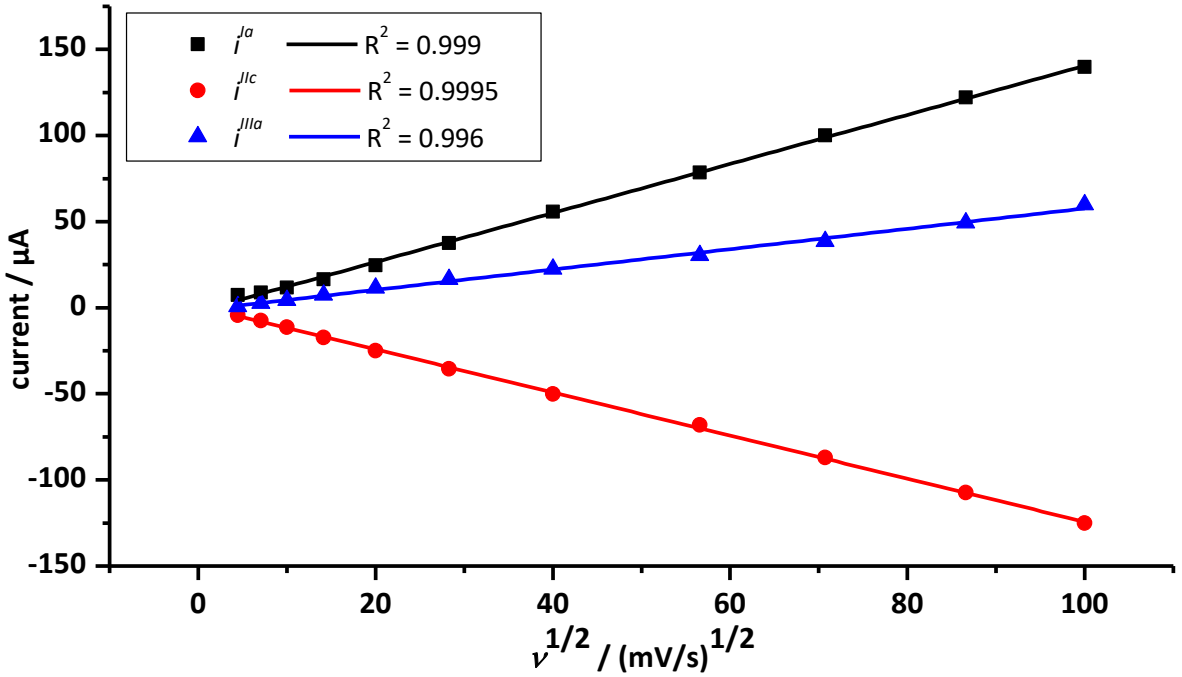

Figure 112: Plot of the peak currents against the square root of the scan rate $\nu^{1/2}$ of **6c**.

7.3.2 [Pentacarbonyl{1-methylimidazol-3-iumyl(triphenylmethyl)phosphanido-κ*P*}-chromium(0)] (13a)

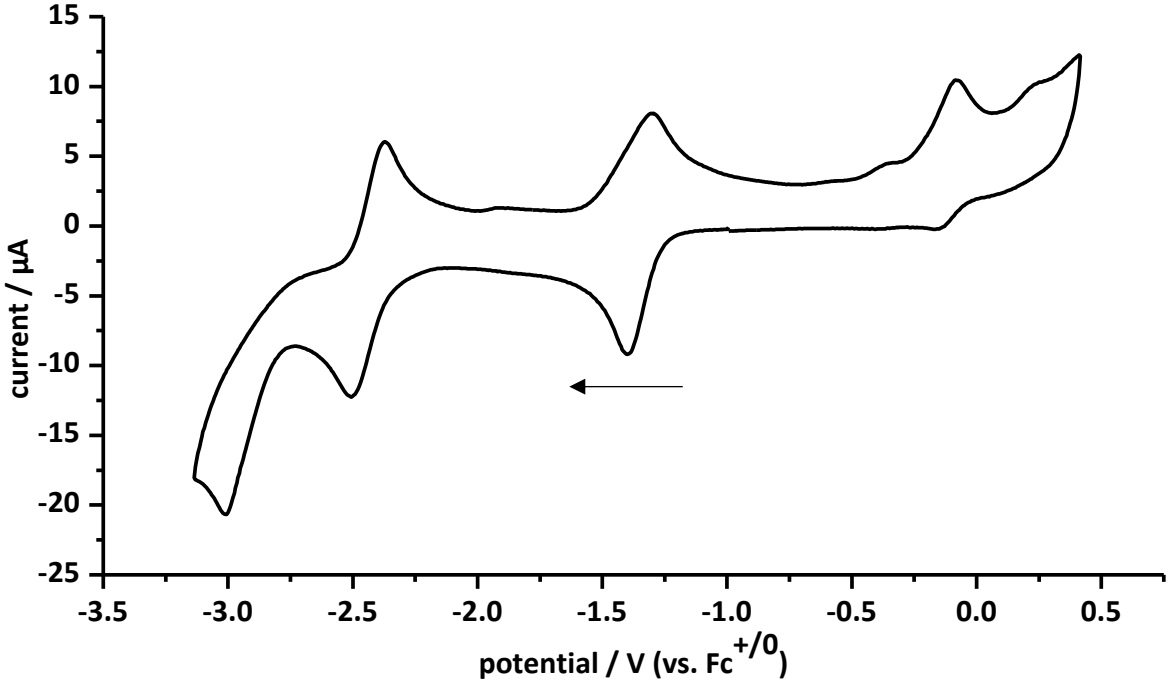

Figure 113: Cyclic voltammogram of complex **13a** (1 mM) at a Pt electrode in a 0.2 M $^{n}Bu_4PF_6$/THF solution with cobaltocenium hexafluorophosphate as internal reference; measurement with cathodic initial scan direction (denoted with an arrow); scan rate: 200 mV/s; potentials are referenced against $Fc^{+/0}$.

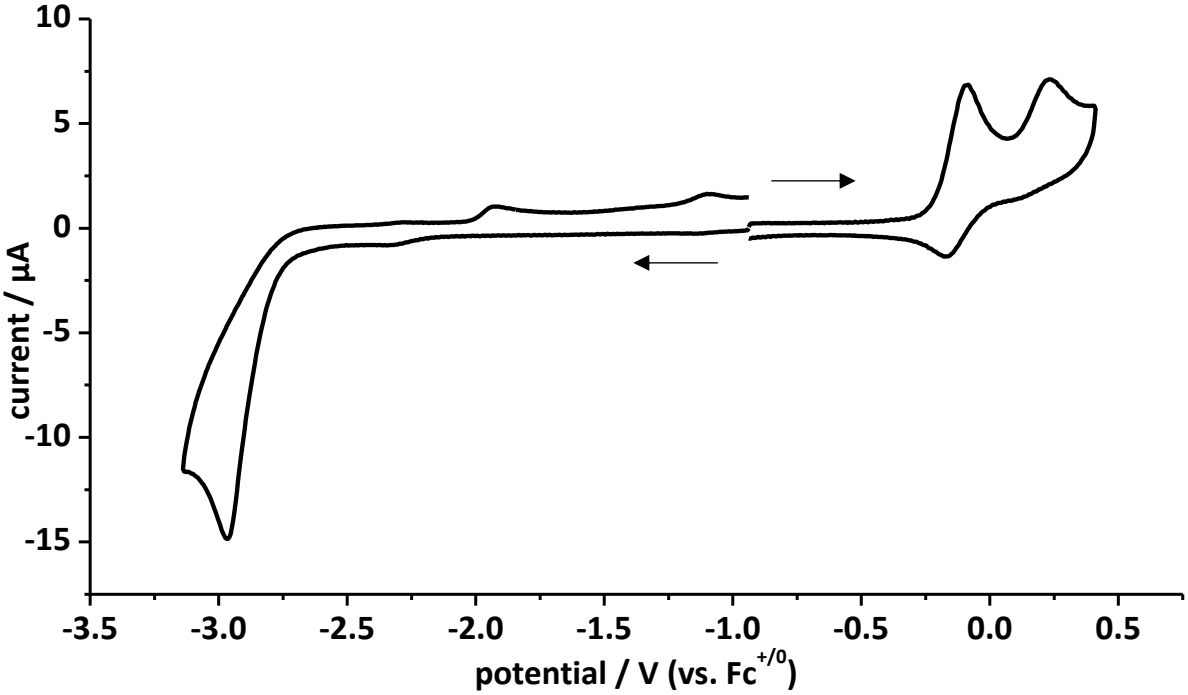

Figure 114: Overlay of cyclic voltammograms of **13a** (1 mM) at a Pt electrode in a 0.2 M $^{n}Bu_4PF_6$/THF solution; oxidation parts with anodic initial scan direction and reduction parts with cathodic initial scan direction as denoted with arrows; scan rate: 200 mV/s; potentials are referenced against $Fc^{+/0}$.

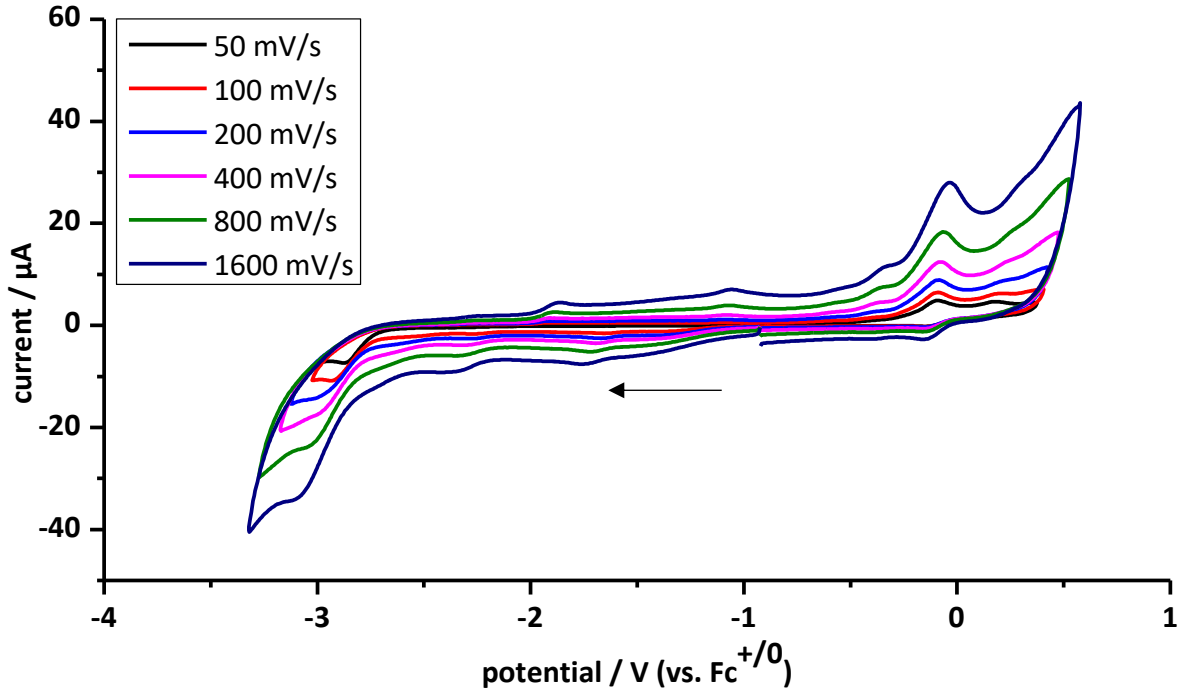

Figure 115: Cyclic voltammogram of complex **13a** (1 mM) at a Pt electrode in a 0.2 M $^{n}Bu_4PF_6$/THF solution at various scan rates; measurement with cathodic initial scan direction (denoted with an arrow); potentials are referenced against $Fc^{+/0}$.

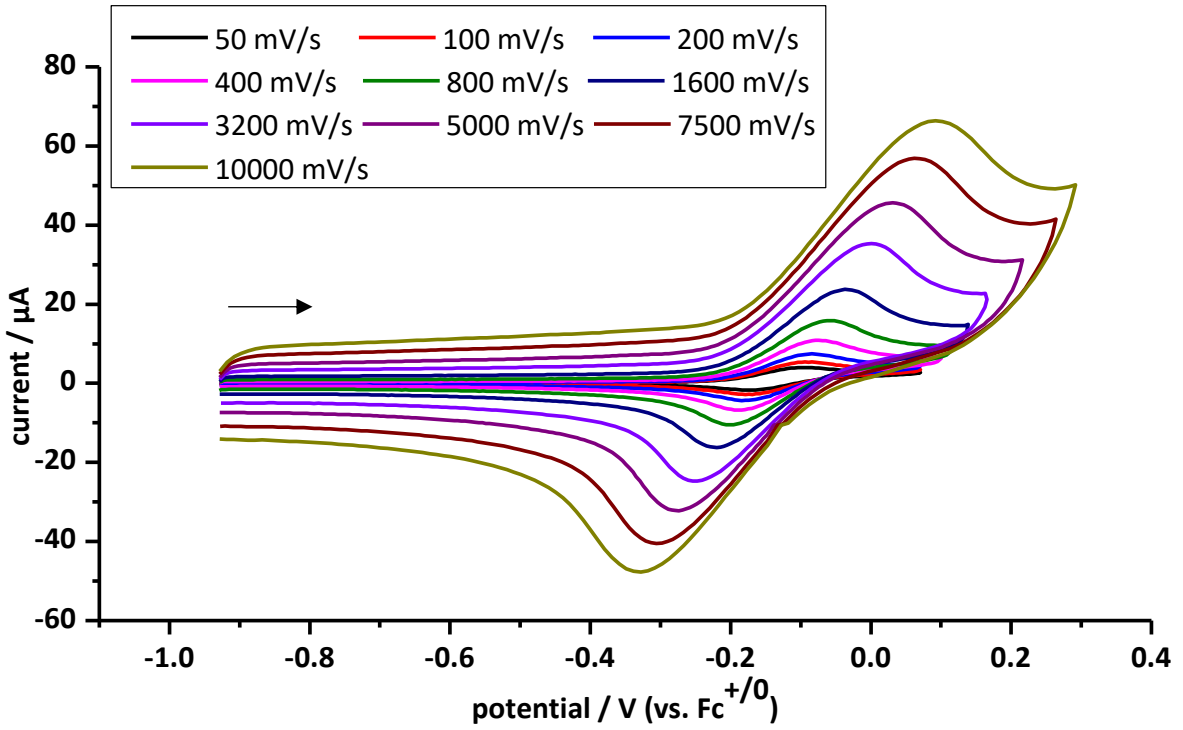

Figure 116: Cyclic voltammogram of complex **13a** (1 mM) at a Pt electrode in a 0.2 M $^{n}Bu_4PF_6$/THF solution at various scan rates; measurement with anodic initial scan direction (denoted with an arrow) of the first redox process; potentials are referenced against $Fc^{+/0}$.

Table 114: Selected results of the cyclic voltametric studies of **13a** in 0.2 M $^{n}Bu_4NPF_6$/THF solution at ambient temperature. Potentials are referenced against $Fc^{+/0}$.

ν / mV/s	E_p^{Ia} / V	i_p^{Ia} / µA	E_p^{Ic} / V	i_p^{Ic} / µA	$E_{1/2}^{I}$ / V	ΔE_p^{I} / mV	$\lvert i_p^c/i_p^a \rvert$
50	−0.10	2.69	−0.17	−2.62	0.14	75	0.97
100	−0.09	3.81	−0.18	−3.85	0.14	85	1.01
200	−0.08	5.38	−0.18	−5.63	0.13	100	1.05
400	−0.07	8.23	−0.18	−8.52	0.13	110	1.03
800	−0.06	12.4	−0.20	−12.8	0.13	139	1.03
1600	−0.04	18.8	−0.22	−19.6	0.13	183	1.04
3200	0.00	29.7	−0.25	−29.6	0.12	248	1.00
5000	0.03	36.9	−0.27	−39.5	0.12	305	1.07
7500	0.06	44.7	−0.31	−50.7	0.12	368	1.13
10000	0.09	49.90	−0.33	−61.0	0.12	420	1.22

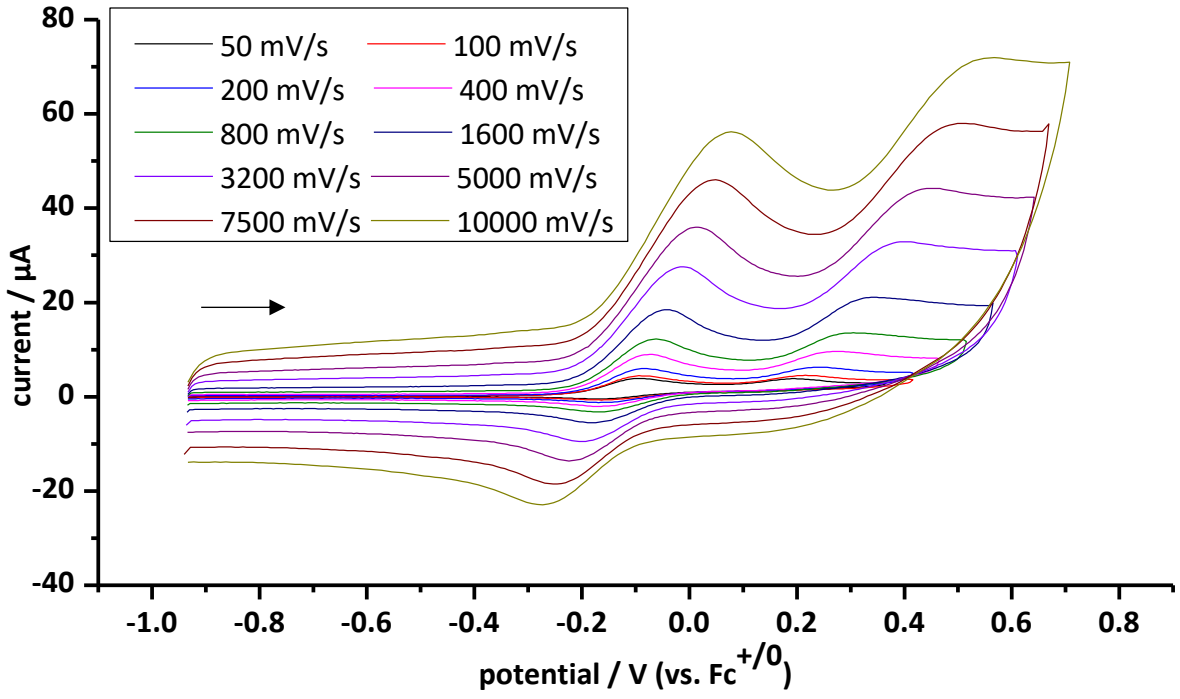

Figure 117: Cyclic voltammogram of complex **13a** (1 mM) at a Pt electrode in a 0.2 M $^{n}Bu_4PF_6$/THF solution at various scan rates; measurement with anodic initial scan direction (denoted with an arrow) of the first and second redox processes; potentials are referenced against $Fc^{+/0}$.

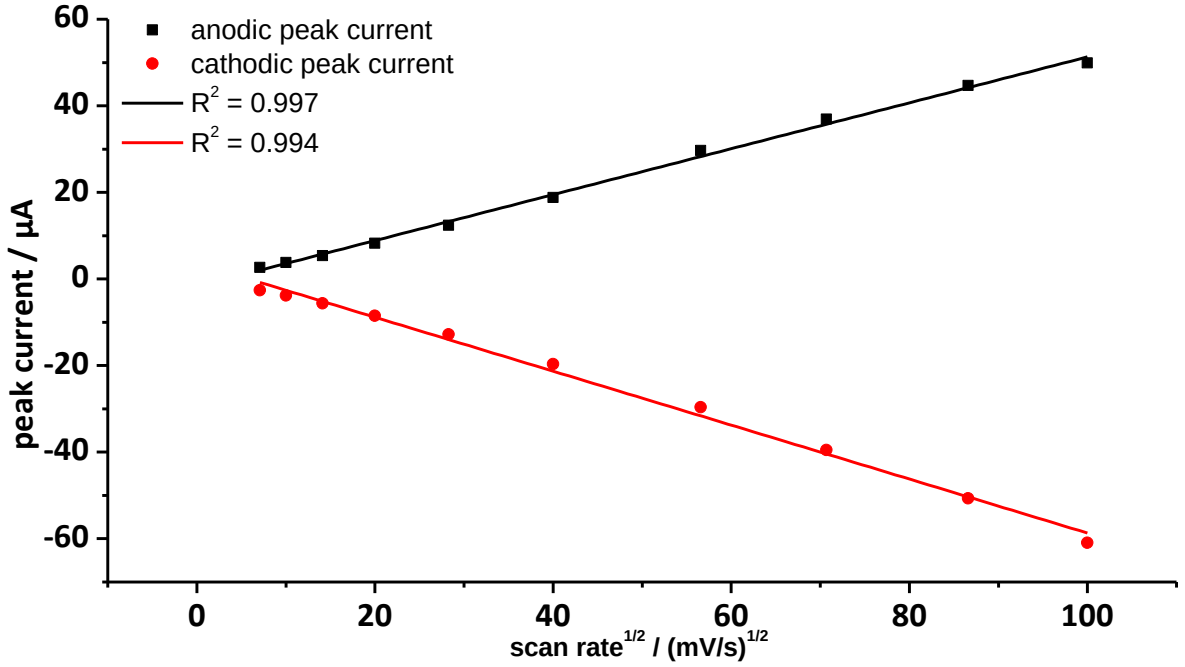

Figure 118: Plot of the peak currents against the square root of the scan rate $\nu^{1/2}$ for the first redox process of complex **13a**.

7.3.3 [Pentacarbonyl{1-methylimidazol-3-iumyl(triphenylmethyl)phosphanido-κ*P*}-tungsten(0)] (13b)

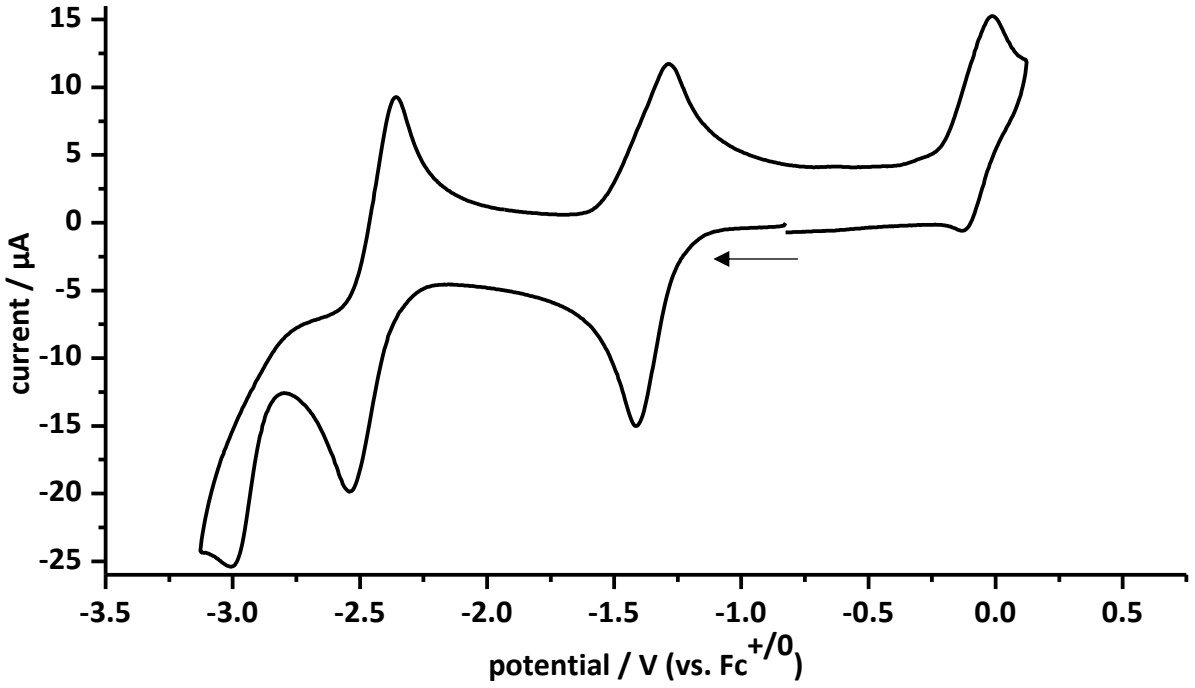

Figure 119: Cyclic voltammogram of complex **13b** (1 mM) at a Pt electrode in a 0.2 M $^{n}Bu_4PF_6$/THF solution with cobaltocenium hexafluorophosphate as internal reference; measurement with cathodic initial scan direction (denoted with an arrow); scan rate: 200 mV/s; potentials are referenced against $Fc^{+/0}$.

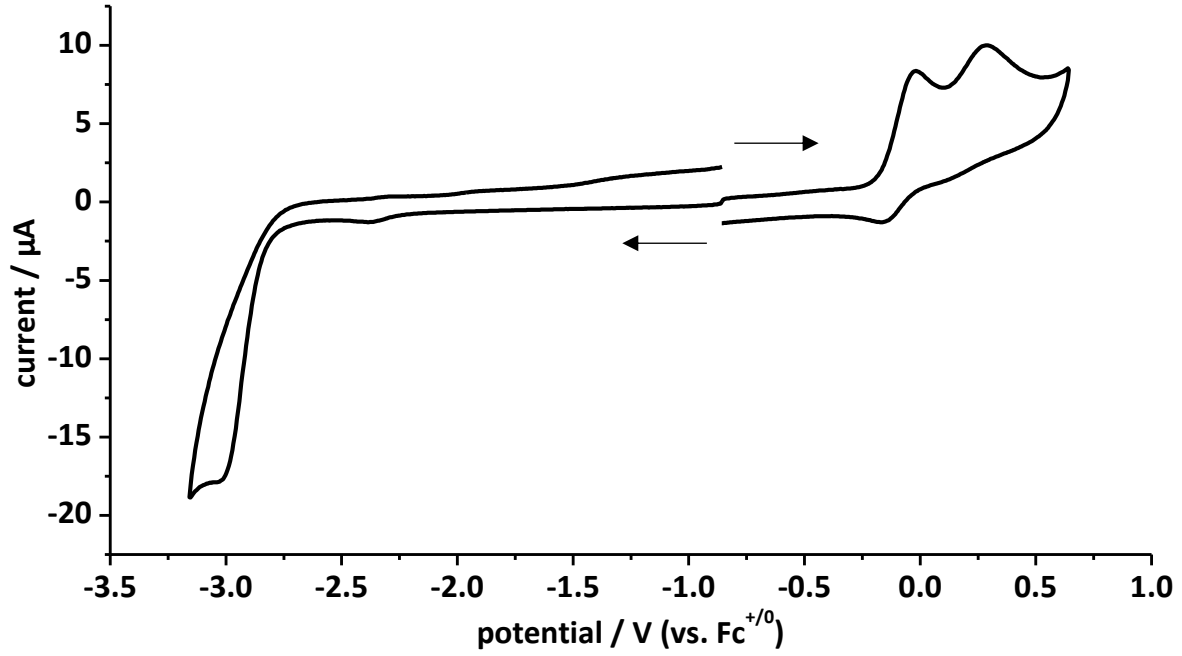

Figure 120: Overlay of cyclic voltammograms of **13b** (1 mM) at a Pt electrode in a 0.2 M $^{n}Bu_4PF_6$/THF solution; oxidation parts with anodic initial scan direction and reduction parts with cathodic initial scan direction as denoted with arrows; scan rate: 200 mV/s; potentials are referenced against $Fc^{+/0}$.

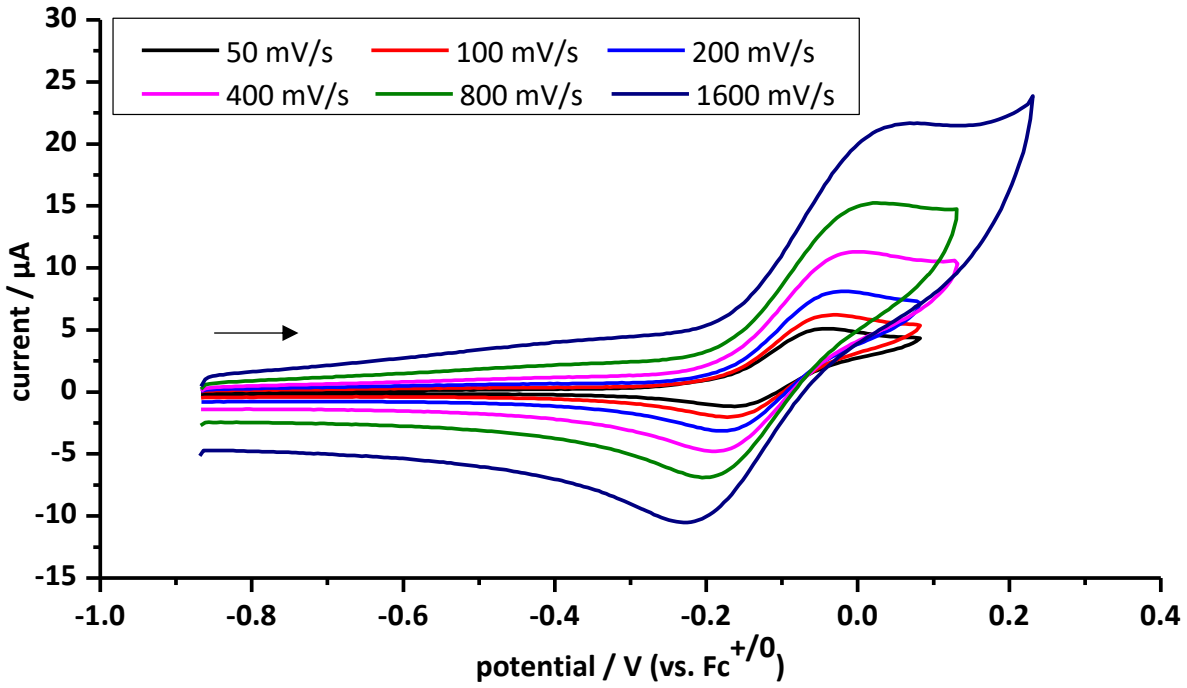

Figure 121: Cyclic voltammogram of complex **13b** (1 mM) at a Pt electrode in a 0.2 M $^{n}Bu_4PF_6$/THF solution at various scan rates; measurement with anodic initial scan direction (denoted with an arrow) of the first redox process; potentials are referenced against $Fc^{+/0}$.

Table 115: Selected results of the cyclic voltametric studies of **13b** in 0.2 M $^{n}Bu_4NPF_6$/THF solution at ambient temperature. Potentials are referenced against $Fc^{+/0}$.

ν / mV/s	E_p^{Ia} / V	i_p^{Ia} / µA	E_p^{Ic} / V	i_p^{Ic} / µA	$E_{1/2}^{I}$ / V	ΔE_p^{I} / mV	$\lvert i_p^c/i_p^a \rvert$
50	−0.04	2.69	−0.16	−2.46	−0.10	125	0.91
100	−0.03	3.39	−0.17	−3.33	−0.10	140	0.98
200	−0.02	4.71	−0.18	−4.69	−0.10	166	1.00
400	0.00	7.03	−0.19	−6.98	−0.10	191	0.99
800	0.03	9.80	−0.21	−10.0	−0.09	230	1.02
1600	0.07	15.4	−0.23	−15.4	−0.08	294	1.00

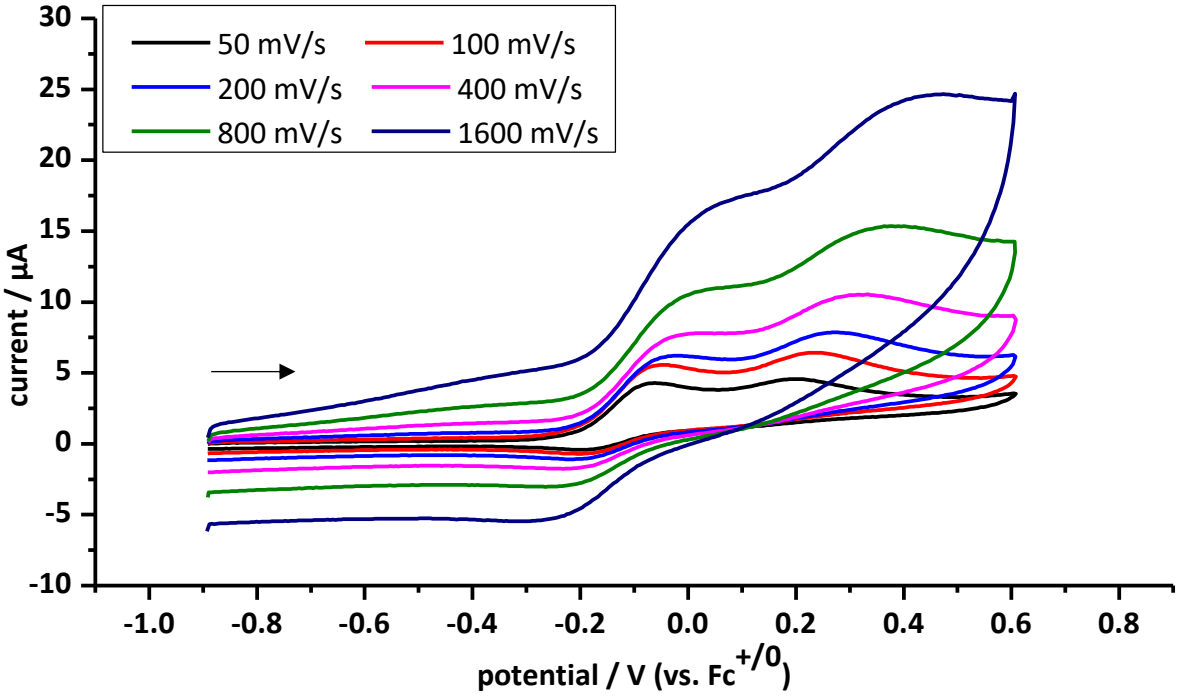

Figure 122: Cyclic voltammogram of complex **13b** (1 mM) at a Pt electrode in a 0.2 M $^{n}Bu_4PF_6$/THF solution at various scan rates; measurement with anodic initial scan direction (denoted with an arrow) of the first and second redox processes; potentials are referenced against $Fc^{+/0}$.

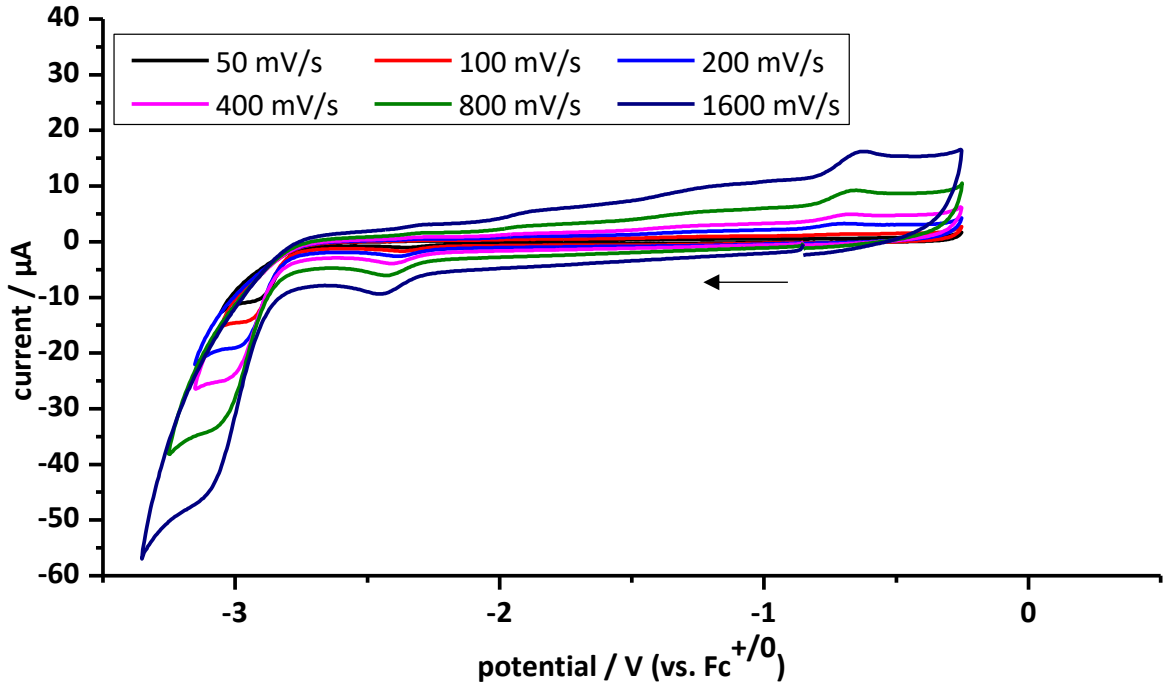

Figure 123: Cyclic voltammogram of complex **13b** (1 mM) at a Pt electrode in a 0.2 M $^{n}Bu_4PF_6$/THF solution at various scan rates; measurement with cathodic initial scan direction (denoted with an arrow) of the third redox process; potentials are referenced against $Fc^{+/0}$.

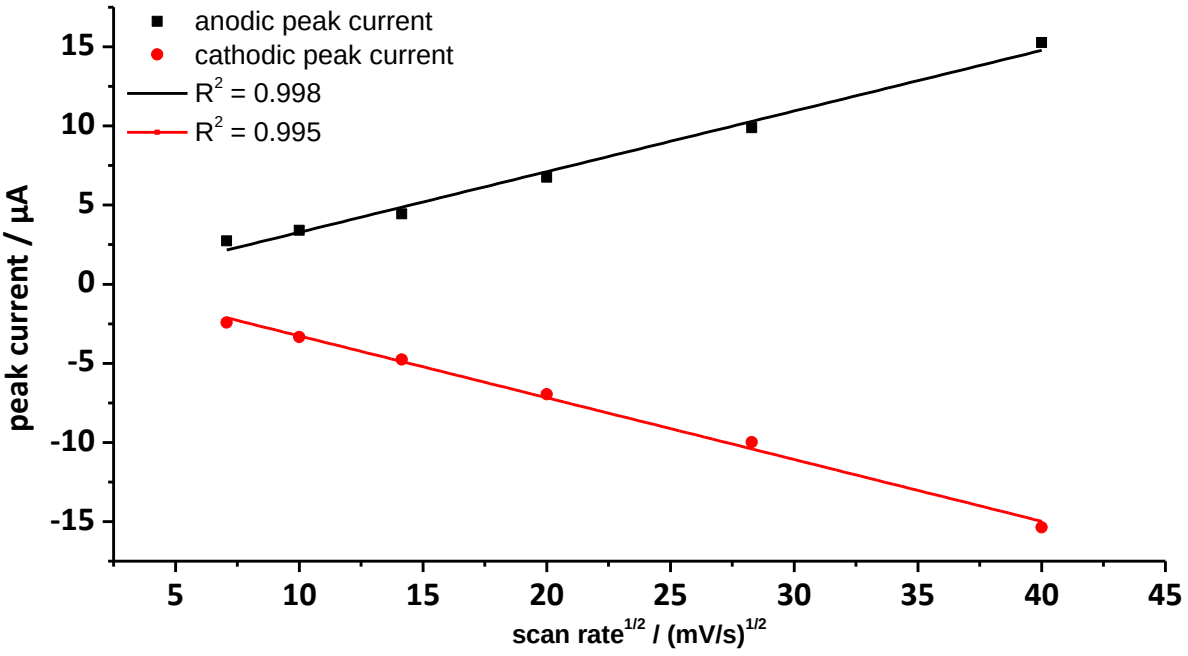

Figure 124: Plot of the peak currents against the square root of the scan rate $v^{1/2}$ for the first redox process of complex **13b**.

7.3.4 [Pentacarbonyl{(4-(dimethylamino)pyridin-1-iumyl(triphenylmethyl)phosphanido-κ*P*}-tungsten(0)] (14b)

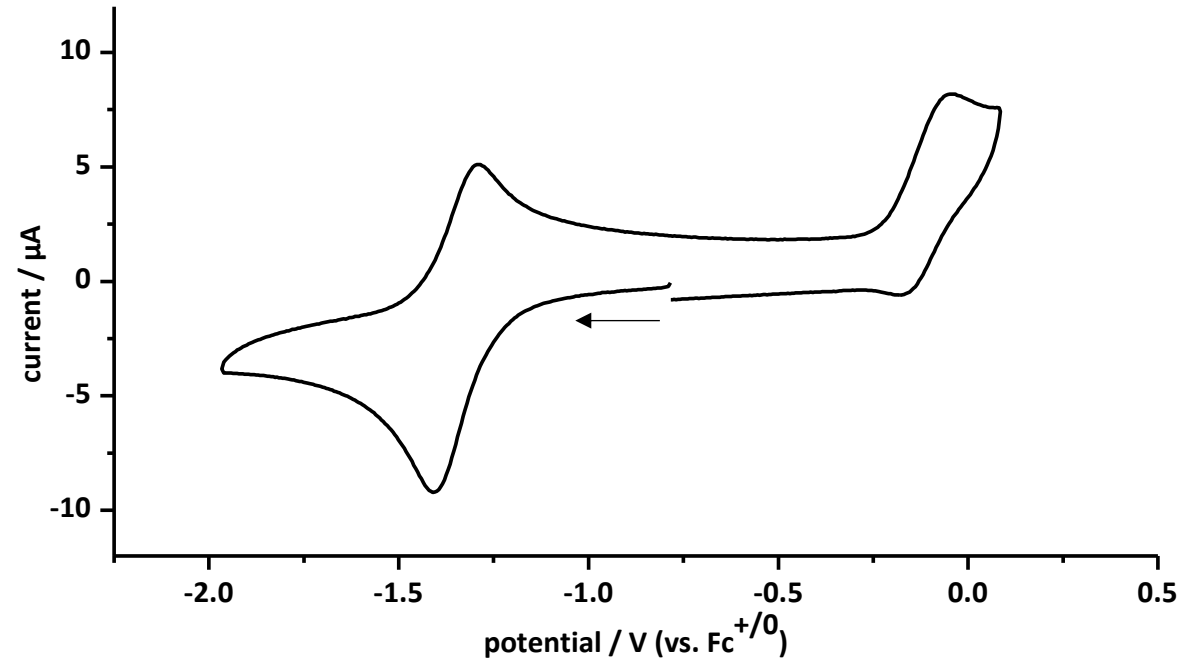

Figure 125: Cyclic voltammogram of complex **14b** (<0.5 mM) at a Pt electrode in a 0.2 M $^{n}Bu_4PF_6$/THF solution with cobaltocenium hexafluorophosphate as internal reference; measurement with cathodic initial scan direction (denoted with an arrow); scan rate: 200 mV/s; potentials are referenced against $Fc^{+/0}$.

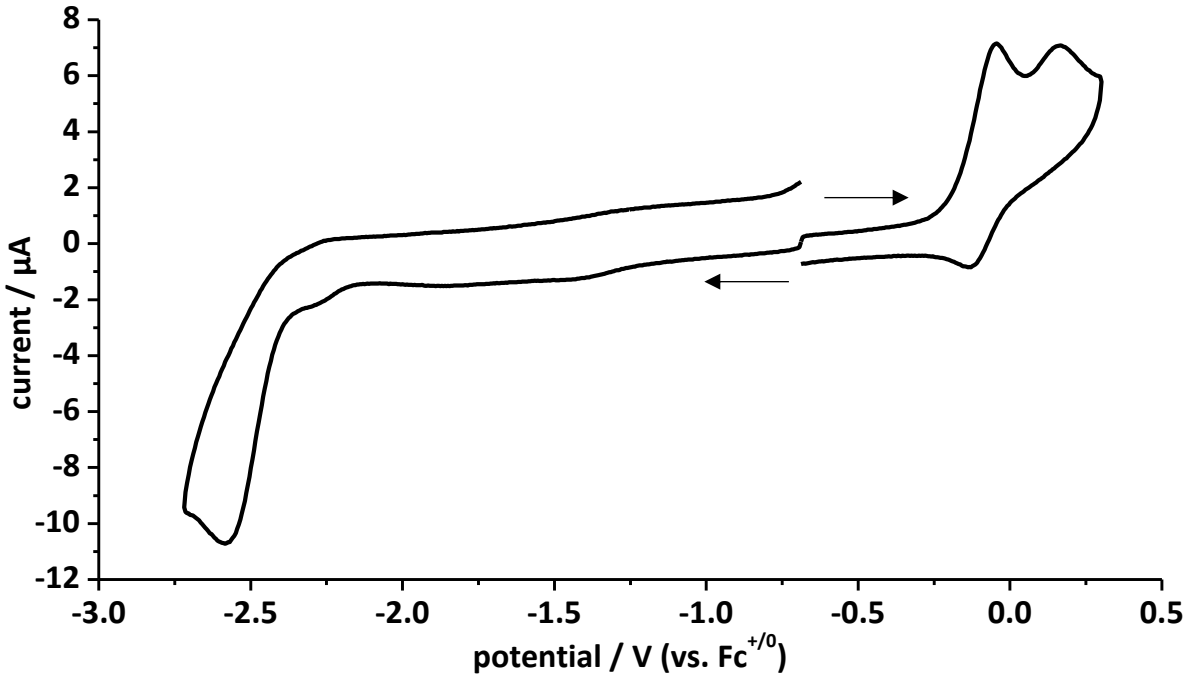

Figure 126: Overlay of cyclic voltammograms of **14b** (<0.5 mM) at a Pt electrode in a 0.2 M $^{n}Bu_4PF_6$/THF solution; oxidation parts with anodic initial scan direction and reduction parts with cathodic initial scan direction as denoted with arrows; scan rate: 200 mV/s; potentials are referenced against $Fc^{+/0}$.

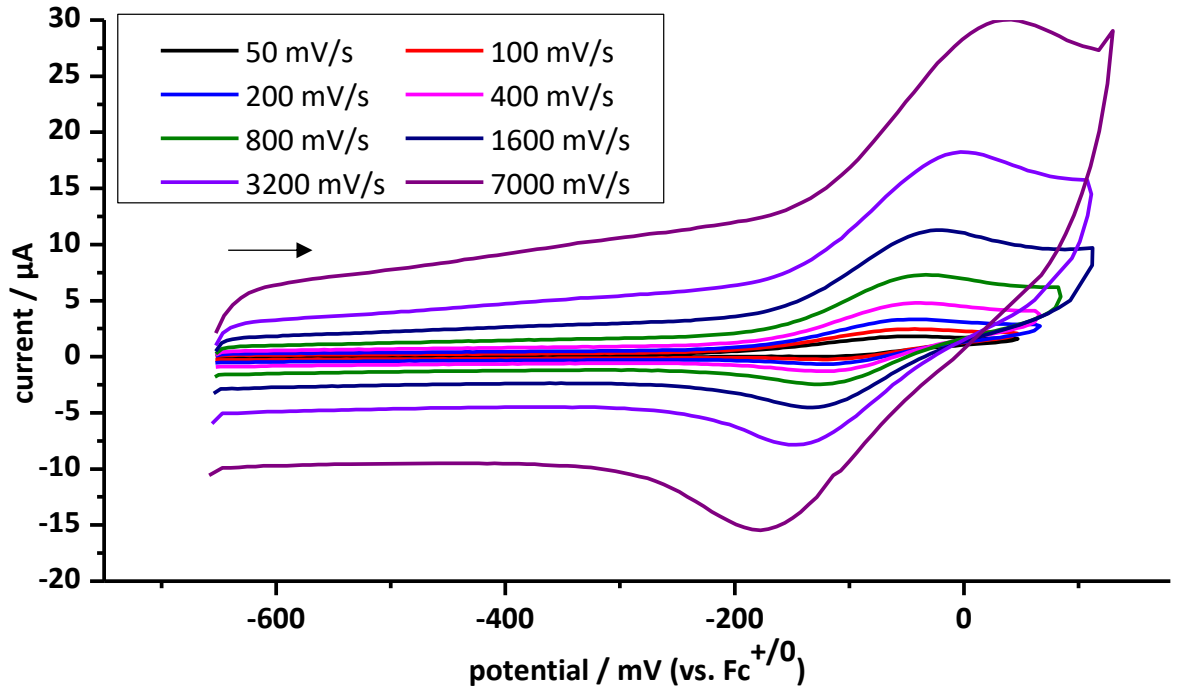

Figure 127: Cyclic voltammogram of complex **14b** (<0.5 mM) at a Pt electrode in a 0.2 M $^{n}Bu_4PF_6$/THF solution at various scan rates; measurement with anodic initial scan direction (denoted with an arrow) of the first redox process; potentials are referenced against $Fc^{+/0}$.

Table 116: Selected results of the cyclic voltametric studies of **14b** in 0.2 M $^{n}Bu_4NPF_6$/THF solution at ambient temperature. Potentials are referenced against $Fc^{+/0}$.

ν / mV/s	E_p^{Ia} / V	i_p^{Ia} / µA	E_p^{Ic} / V	i_p^{Ic} / µA	$E_{1/2}^{I}$ / V	ΔE_p^{I} / mV	$\lvert i_p^{c}/i_p^{a} \rvert$
50	−0.04	0.87	−0.13	−0.67	−0.09	85	0.77
100	−0.04	1.34	−0.12	−1.10	−0.08	76	0.82
200	−0.04	2.17	−0.12	−1.62	−0.08	75	0.75
400	−0.04	3.08	−0.12	−2.74	−0.08	81	0.89
800	−0.03	5.12	−0.13	−4.46	−0.08	92	0.87
1600	−0.02	7.28	−0.13	−8.12	−0.08	108	1.11
3200	0.00	10.9	−0.15	−14.2	−0.07	143	1.30
7000	0.04	15.8	−0.18	−27.1	−0.07	219	1.72

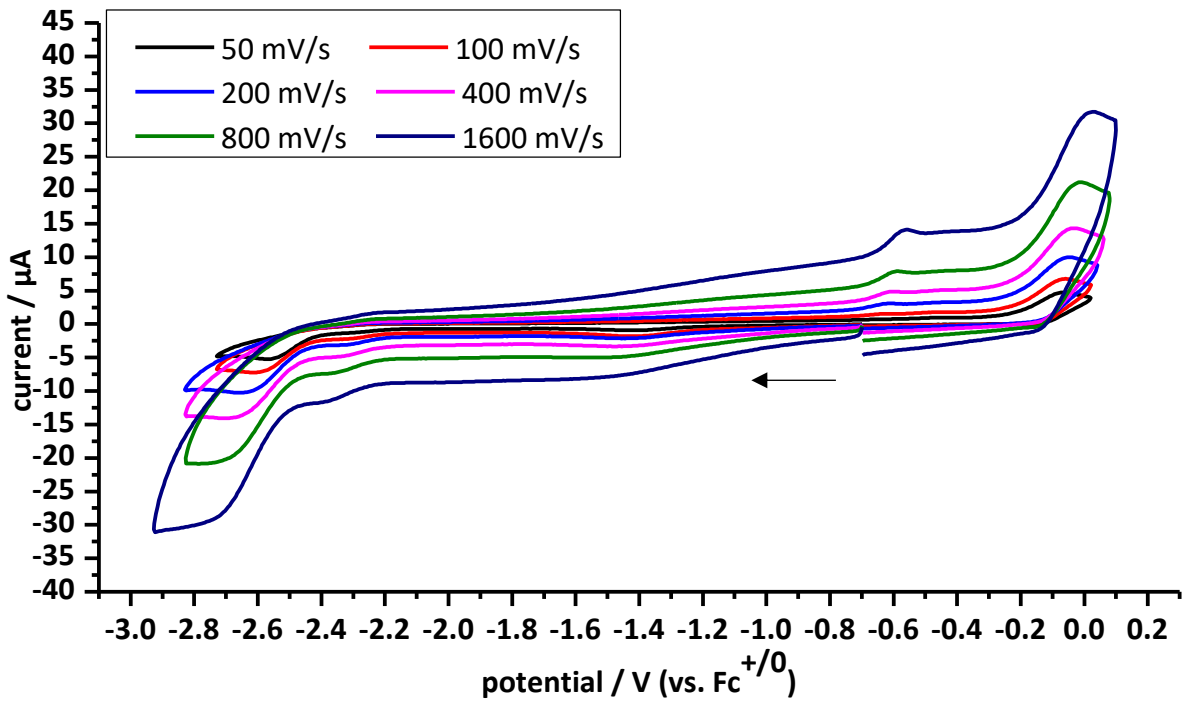

Figure 128: Cyclic voltammogram of complex **14b** (<0.5 mM) at a Pt electrode in a 0.2 M $^{n}Bu_4PF_6$/THF solution at various scan rates; measurement with cathodic initial scan direction (denoted with an arrow) of the first and third redox process; potentials are referenced against $Fc^{+/0}$.

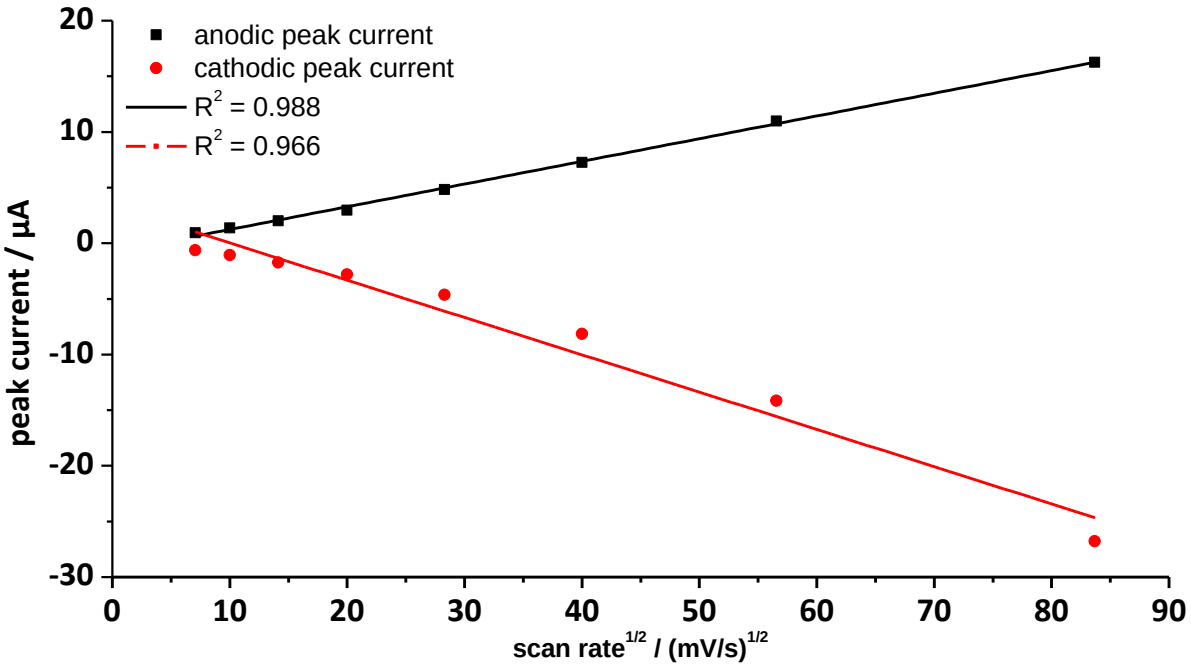

Figure 129: Plot of the peak currents against the square root of the scan rate $\nu^{1/2}$ for the first redox process of complex **14b**.

7.3.5 [Pentacarbonyl{trimethylphosphoniumyl(triphenylmethyl)phosphanido-κ*P*}-chromium(0)] (19a)

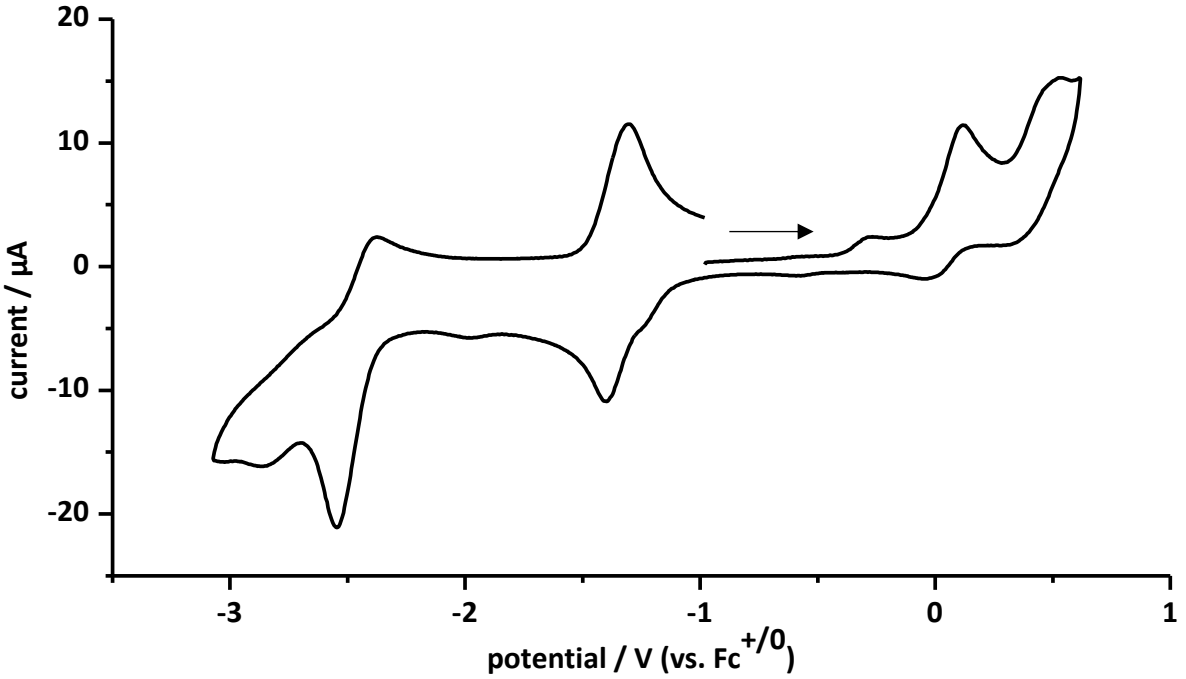

Figure 130: Cyclic voltammogram of complex **19a** (1 mM) at a Pt electrode in a 0.2 M $^{n}Bu_4PF_6$/THF solution with cobaltocenium hexafluorophosphate as internal reference; measurement with anodic initial scan direction (denoted with an arrow); scan rate: 200 mV/s; potentials are referenced against $Fc^{+/0}$.

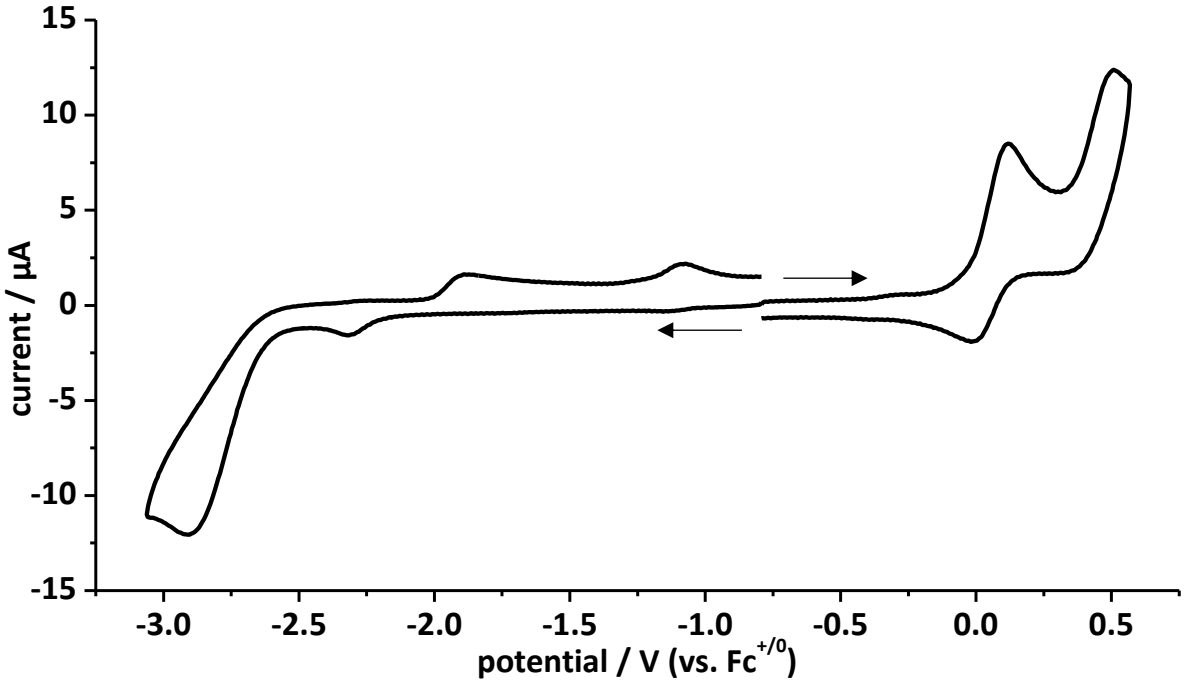

Figure 131: Overlay of cyclic voltammograms of **19a** (1 mM) at a Pt electrode in a 0.2 M $^{n}Bu_4PF_6$/THF solution; oxidation parts with anodic initial scan direction and reduction parts with cathodic initial scan direction as denoted with arrows; scan rate: 200 mV/s; potentials are referenced against $Fc^{+/0}$.

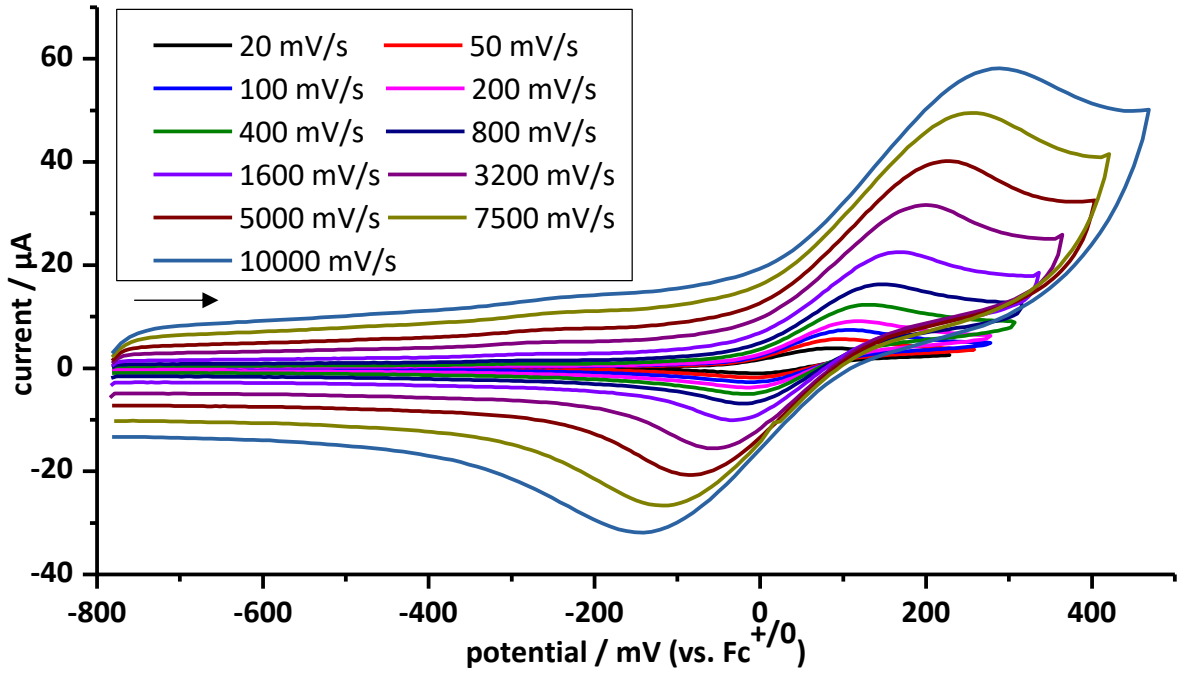

Figure 132: Cyclic voltammogram of complex **19a** (1 mM) at a Pt electrode in a 0.2 M $^{n}Bu_4PF_6$/THF solution at various scan rates; measurement with anodic initial scan direction (denoted with an arrow) of the first redox process; potentials are referenced against $Fc^{+/0}$.

Table 117: Selected results of the cyclic voltametric studies of **19a** in 0.2 M $^{n}Bu_4NPF_6$/THF solution at ambient temperature. Potentials are referenced against $Fc^{+/0}$.

ν / mV/s	E_p^{Ia} / V	i_p^{Ia} / µA	E_p^{Ic} / V	i_p^{Ic} / µA	$E_{1/2}^{I}$ / V	ΔE_p^{I} / mV	$\lvert i_p^c/i_p^a \rvert$
20	0.09	2.29	−0.01	−1.94	0.04	95	0.85
50	0.10	3.53	−0.01	−3.02	0.05	105	0.86
100	0.11	4.77	−0.01	−4.19	0.05	119	0.88
200	0.12	5.72	−0.01	−5.55	0.05	131	0.97
400	0.13	7.70	−0.02	−7.49	0.06	151	0.97
800	0.14	10.1	−0.02	−10.3	0.06	163	1.02
1600	0.17	14.5	−0.03	−14.8	0.07	202	1.02
3200	0.20	21.3	−0.06	−22.3	0.07	257	1.04
5000	0.22	30.0	−0.08	−29.1	0.07	306	0.97
7500	0.25	36.0	−0.12	−38.1	0.07	373	1.06
10000	0.29	39.6	−0.14	−45.8	0.07	430	1.16

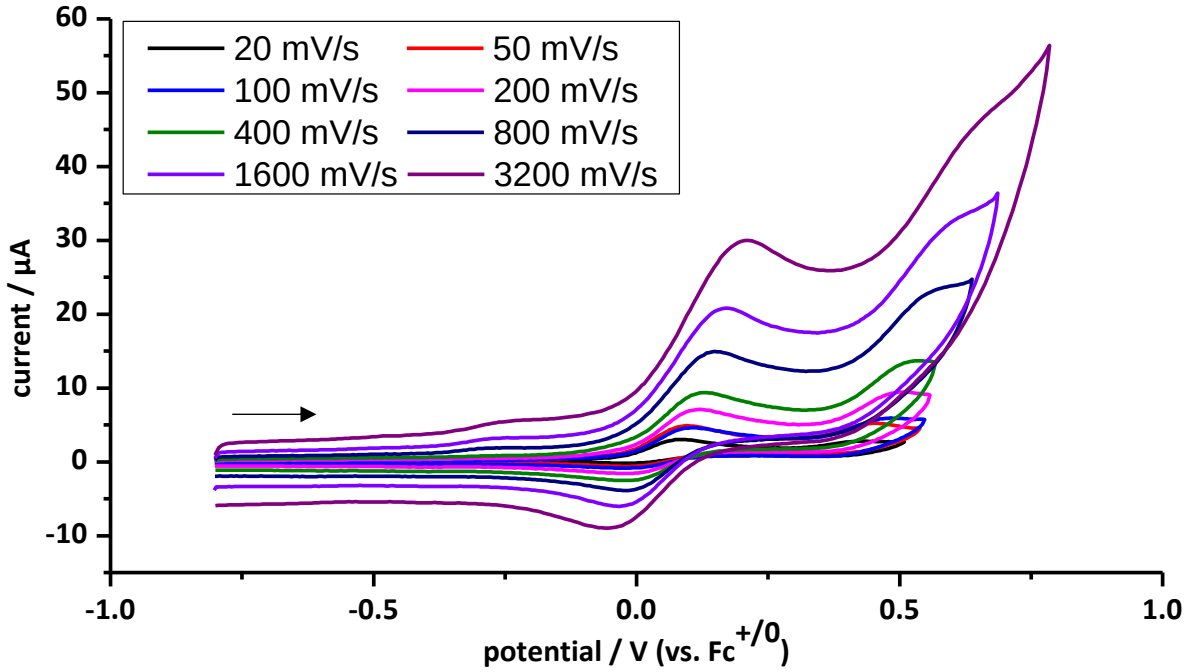

Figure 133: Cyclic voltammogram of complex **19a** (1 mM) at a Pt electrode in a 0.2 M $^{n}Bu_4PF_6$/THF solution at various scan rates; measurement with anodic initial scan direction (denoted with an arrow) of the first and second redox process; potentials are referenced against $Fc^{+/0}$.

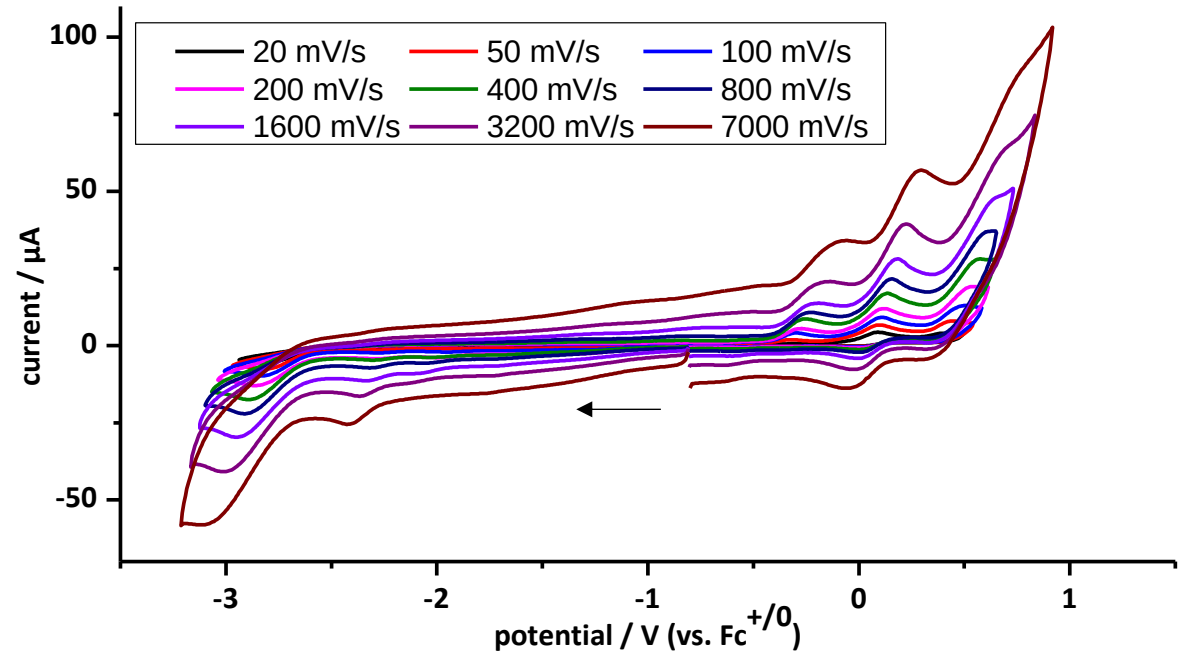

Figure 134: Cyclic voltammogram of complex **19a** (1 mM) at a Pt electrode in a 0.2 M $^{n}Bu_4PF_6$/THF solution at various scan rates; measurement with cathodic initial scan direction (denoted with an arrow) of the first, second and third redox process; potentials are referenced against $Fc^{+/0}$.

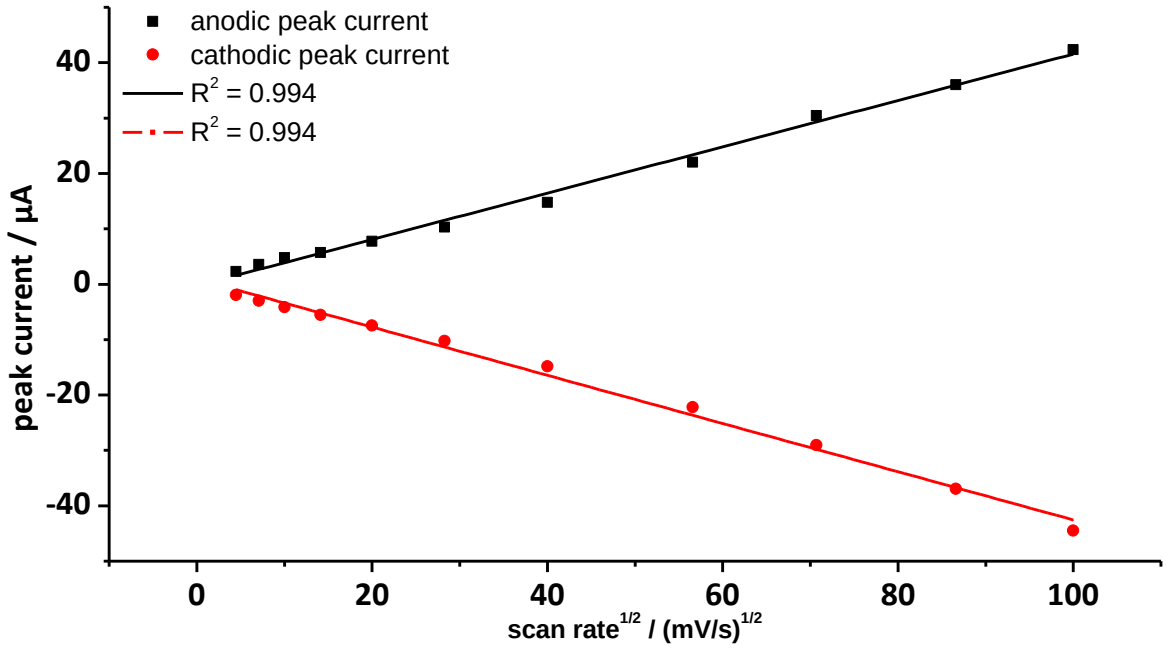

Figure 135: Plot of the peak currents against the square root of the scan rate $\nu^{1/2}$ for the first redox process of complex **19a**.

7.3.6 [Pentacarbonyl{trimethylphosphoniumyl(triphenylmethyl)phosphanido-κ*P*}-tungsten(0)] (19b)

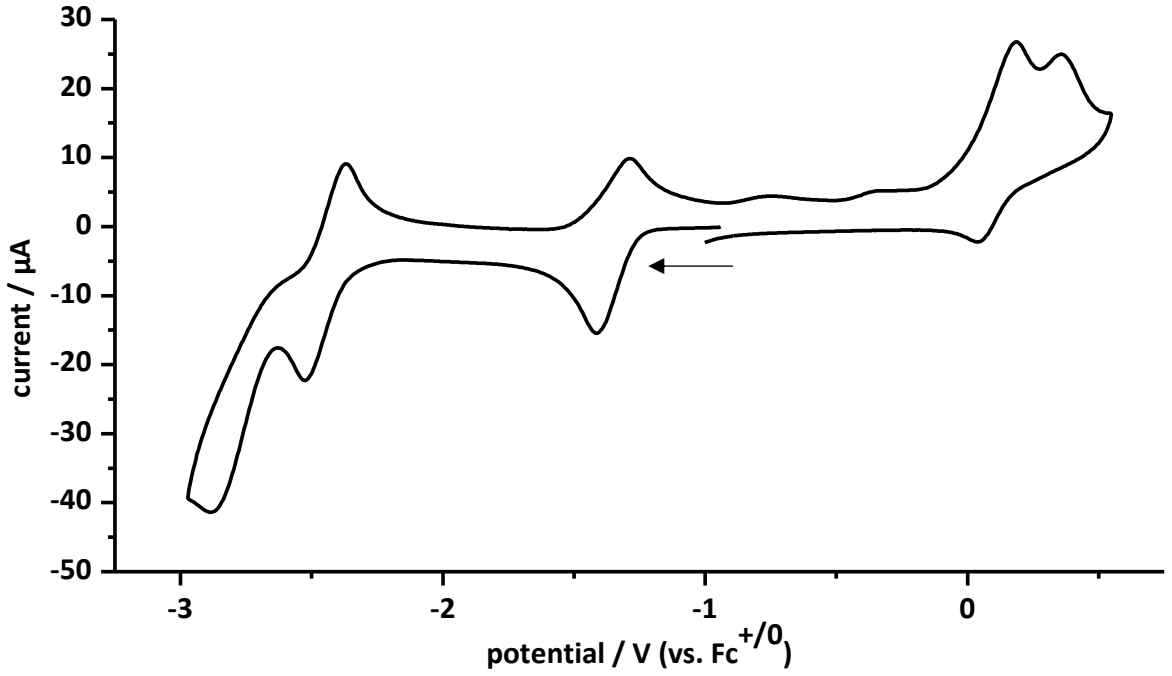

Figure 136: Cyclic voltammogram of complex **19b** (2 mM) at a Pt electrode in a 0.2 M $^{n}Bu_4PF_6$/THF solution with cobaltocenium hexafluorophosphate as internal reference; measurement with cathodic initial scan direction (denoted with an arrow); scan rate: 200 mV/s; potentials are referenced against $Fc^{+/0}$.

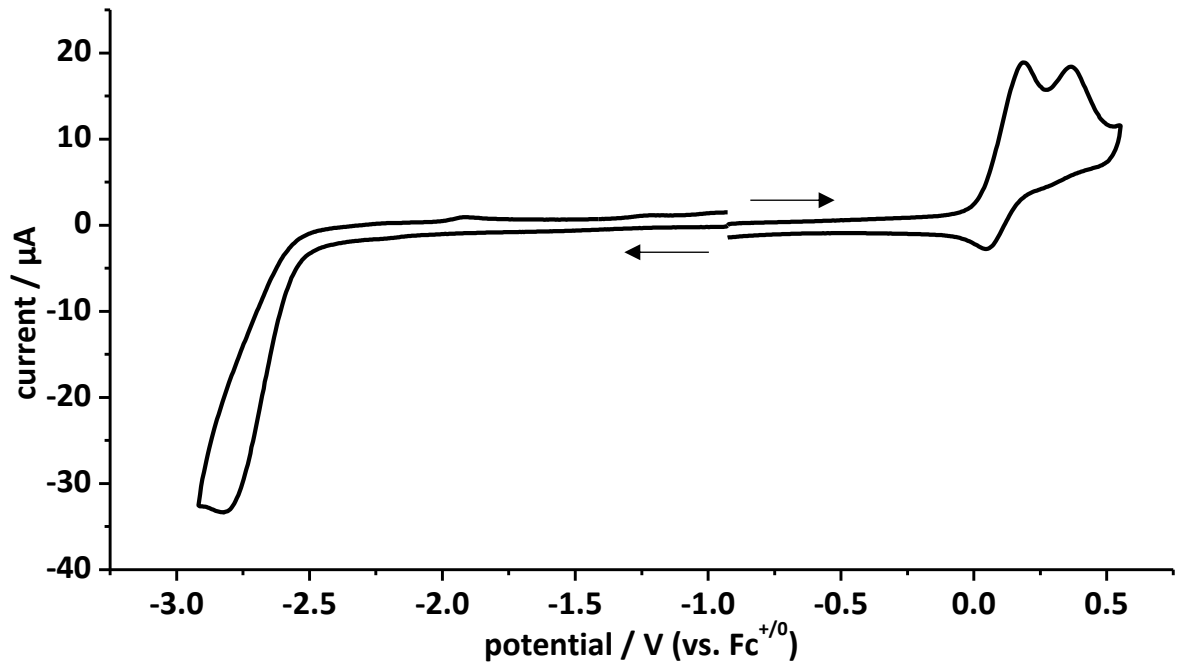

Figure 137: Overlay of cyclic voltammograms of **19b** (2 mM) at a Pt electrode in a 0.2 M $^{n}Bu_4PF_6$/THF solution; oxidation parts with anodic initial scan direction and reduction parts with cathodic initial scan direction as denoted with arrows; scan rate: 200 mV/s; potentials are referenced against $Fc^{+/0}$.

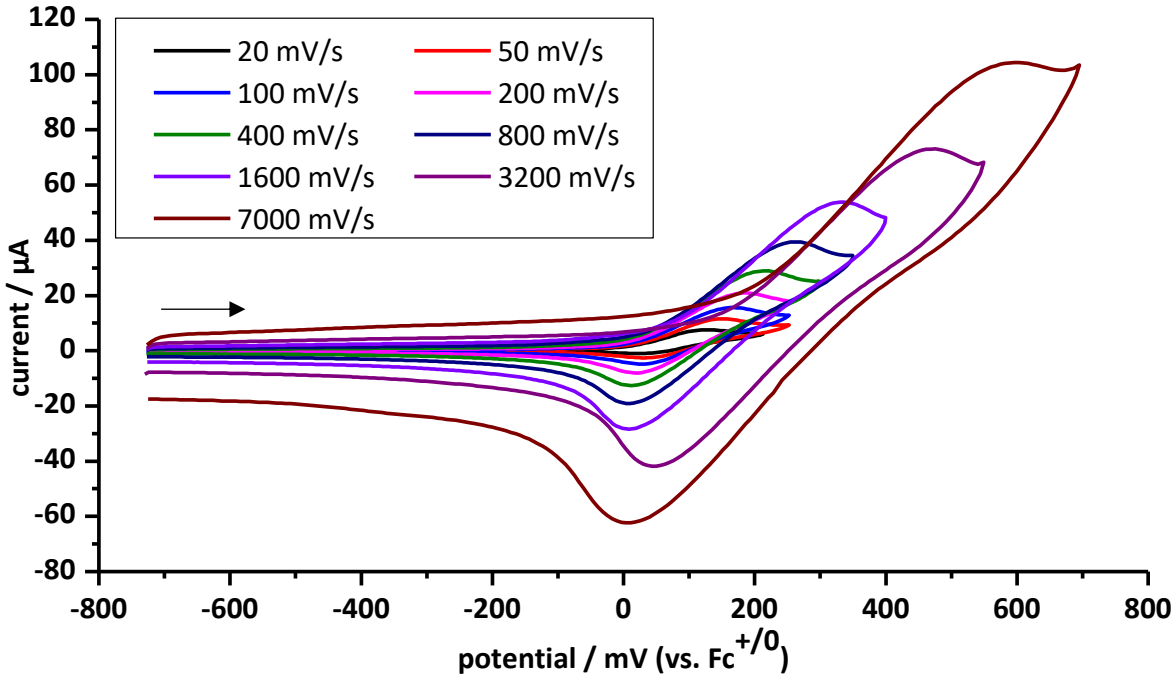

Figure 138: Cyclic voltammogram of complex **19b** (2 mM) at a Pt electrode in a 0.2 M $^{n}Bu_4PF_6$/THF solution at various scan rates; measurement with anodic initial scan direction (denoted with an arrow) of the first redox process; potentials are referenced against $Fc^{+/0}$.

Table 118: Selected results of the cyclic voltametric studies of **19b** in 0.2 M $^{n}Bu_4NPF_6$/THF solution at ambient temperature. Potentials are referenced against $Fc^{+/0}$.

ν / mV/s	E_p^{Ia} / V	i_p^{Ia} / µA	E_p^{Ic} / V	i_p^{Ic} / µA	$E_{1/2}^{I}$ / V	ΔE_p^{I} / mV	$\lvert i_p^{c}/i_p^{a} \rvert$
20	0.13	4.22	0.02	−1.01	0.08	105	0.24
50	0.15	6.69	0.03	−4.88	0.09	125	0.73
100	0.17	8.98	0.03	−7.83	0.10	140	0.87
200	0.19	11.0	0.02	−11.7	0.10	170	1.07
400	0.22	16.1	0.01	−17.2	0.11	206	1.07
800	0.26	22.1	0.01	−24.5	0.14	256	1.11
1600	0.34	30.6	0.01	−34.8	0.17	327	1.14
3200	0.48	44.8	0.04	−49.2	0.26	432	1.10
7000	0.60	66.8	0.00	−73.9	0.30	593	1.11

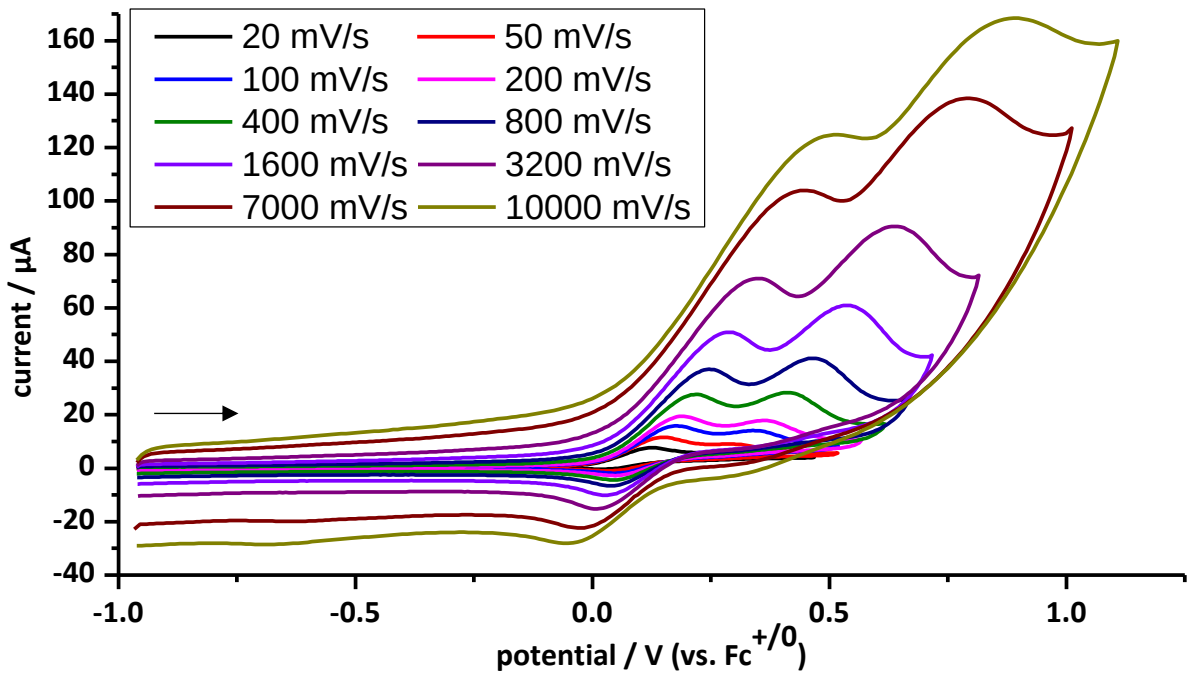

Figure 139: Cyclic voltammogram of complex **19b** (2 mM) at a Pt electrode in a 0.2 M $^{n}Bu_4PF_6$/THF solution at various scan rates; measurement with anodic initial scan direction (denoted with an arrow) of the first and second redox process; potentials are referenced against $Fc^{+/0}$.

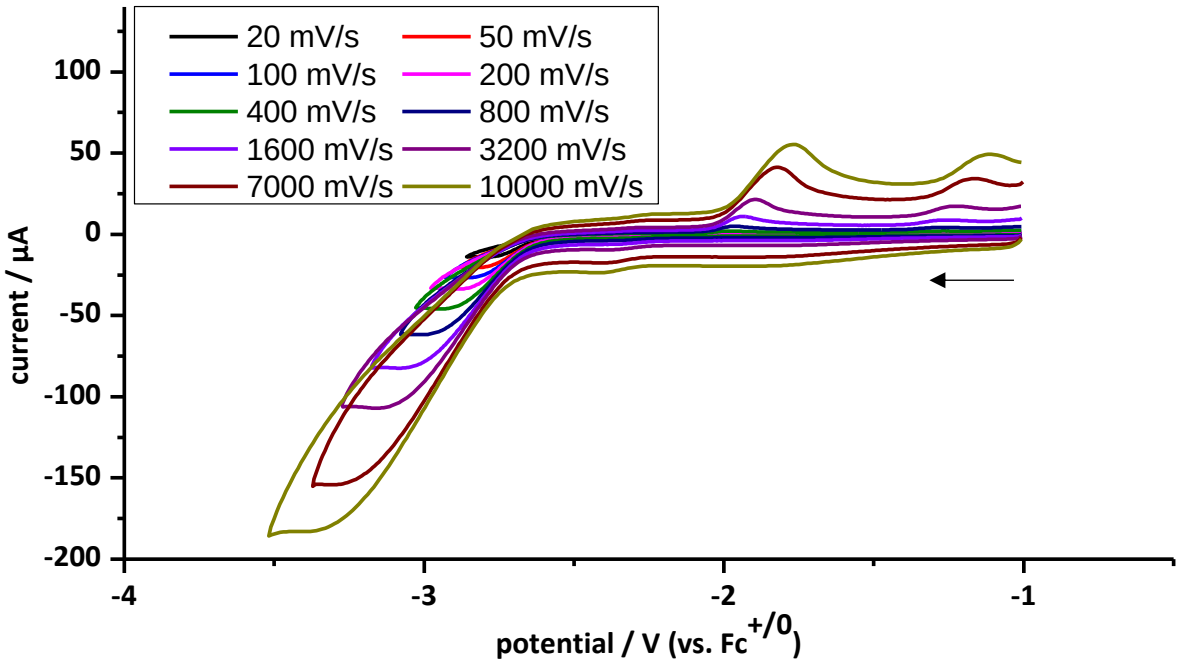

Figure 140: Cyclic voltammogram of complex **19b** (2 mM) at a Pt electrode in a 0.2 M $^{n}Bu_4PF_6$/THF solution at various scan rates; measurement with cathodic initial scan direction (denoted with an arrow) of the third redox process; potentials are referenced against $Fc^{+/0}$.

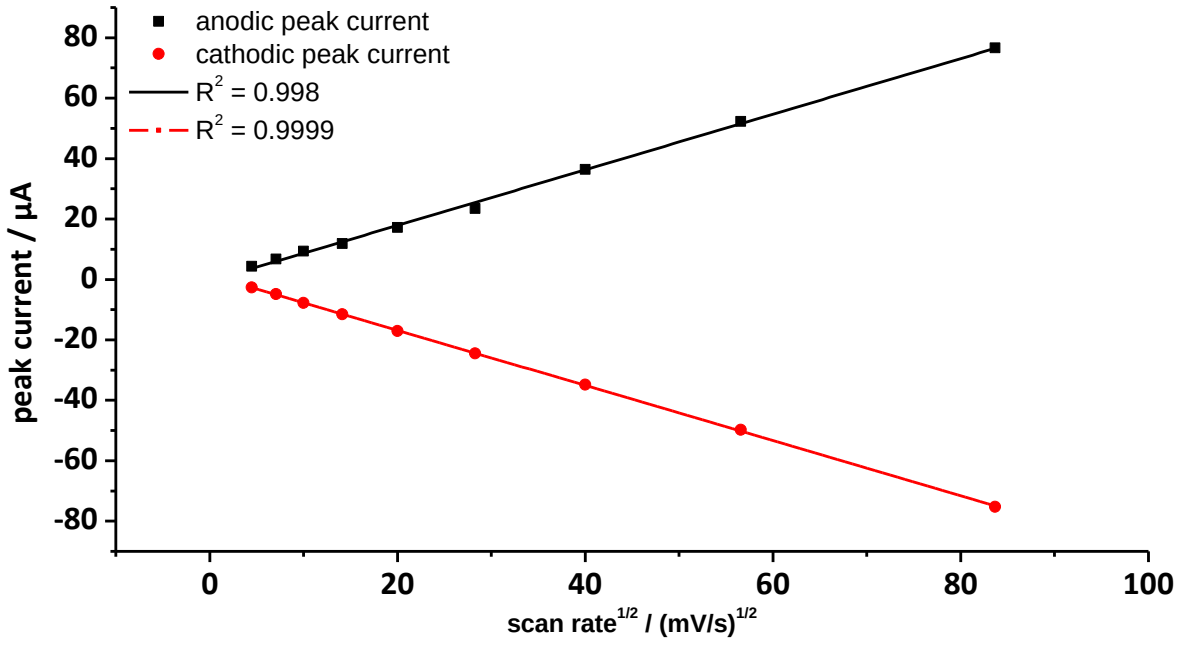

Figure 141: Plot of the peak currents against the square root of the scan rate $\nu^{1/2}$ for the first redox process of complex **19b**.

7.3.7 [Pentacarbonyl{triethylphosphoniumyl(triphenylmethyl)phosphanido-κ*P*}tungsten(0)] (20b)

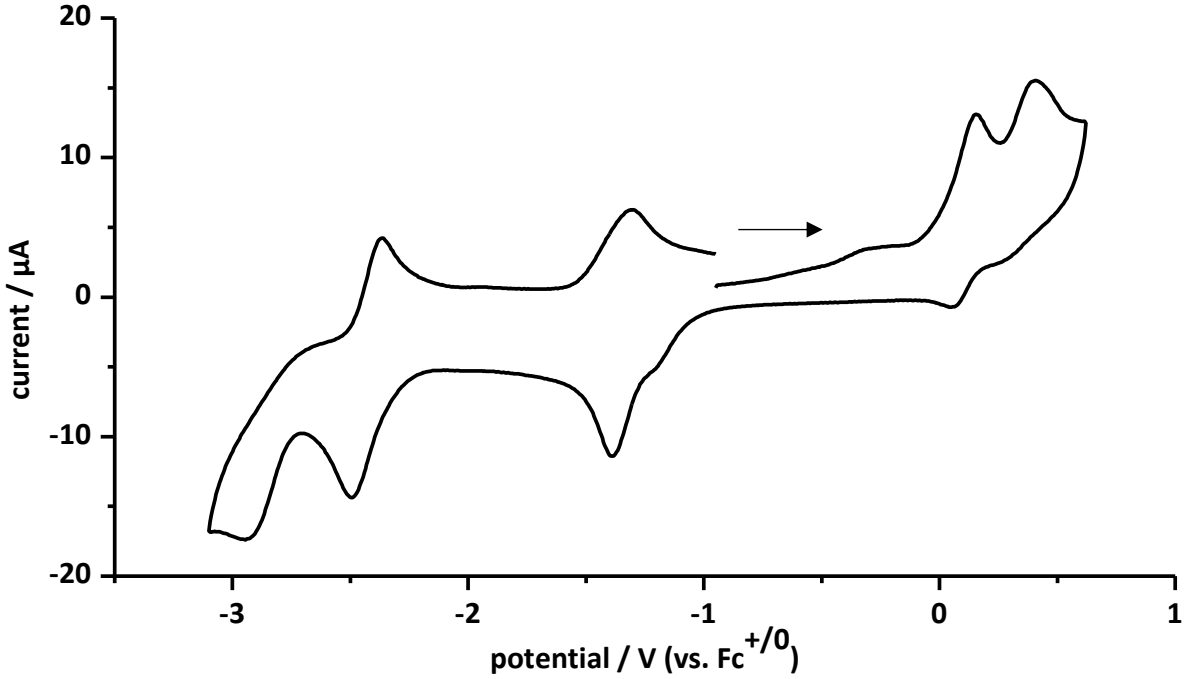

Figure 142: Cyclic voltammogram of complex **20b** (1 mM) at a Pt electrode in a 0.2 M $^{n}Bu_4PF_6$/THF solution with cobaltocenium hexafluorophosphate as internal reference; measurement with anodic initial scan direction (denoted with an arrow); scan rate: 200 mV/s; potentials are referenced against $Fc^{+/0}$.

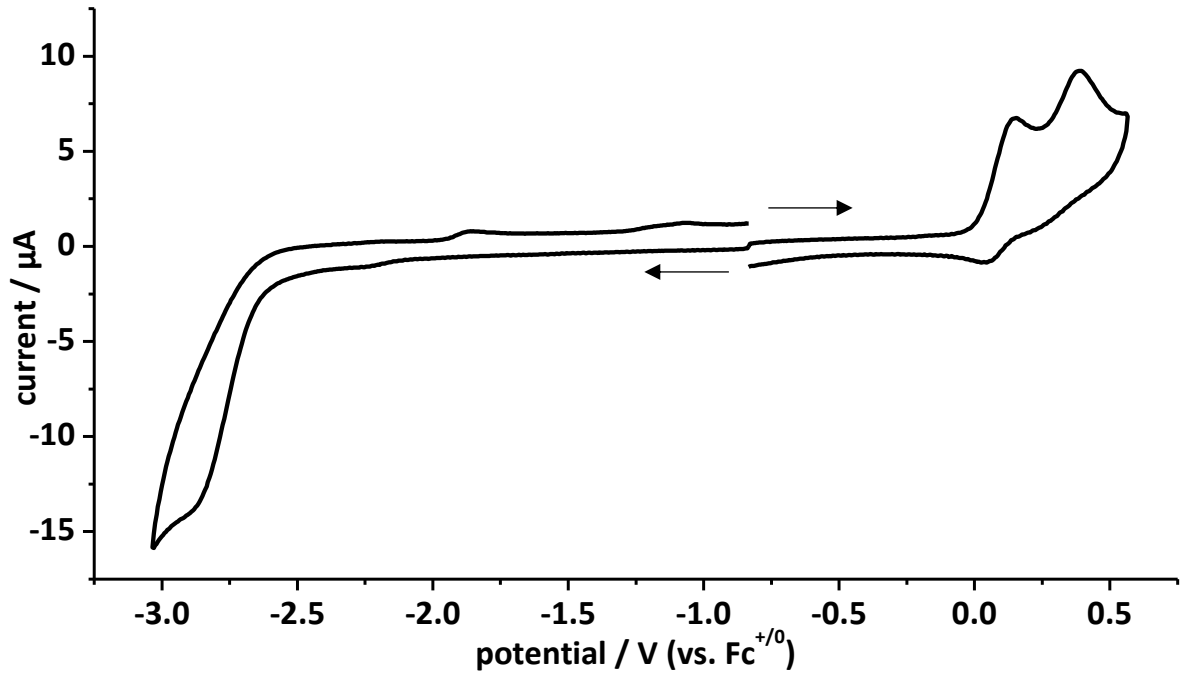

Figure 143: Overlay of cyclic voltammograms of **20b** (1 mM) at a Pt electrode in a 0.2 M $^{n}Bu_4PF_6$/THF solution; oxidation parts with anodic initial scan direction and reduction parts with cathodic initial scan direction as denoted with arrows; scan rate: 200 mV/s; potentials are referenced against $Fc^{+/0}$.

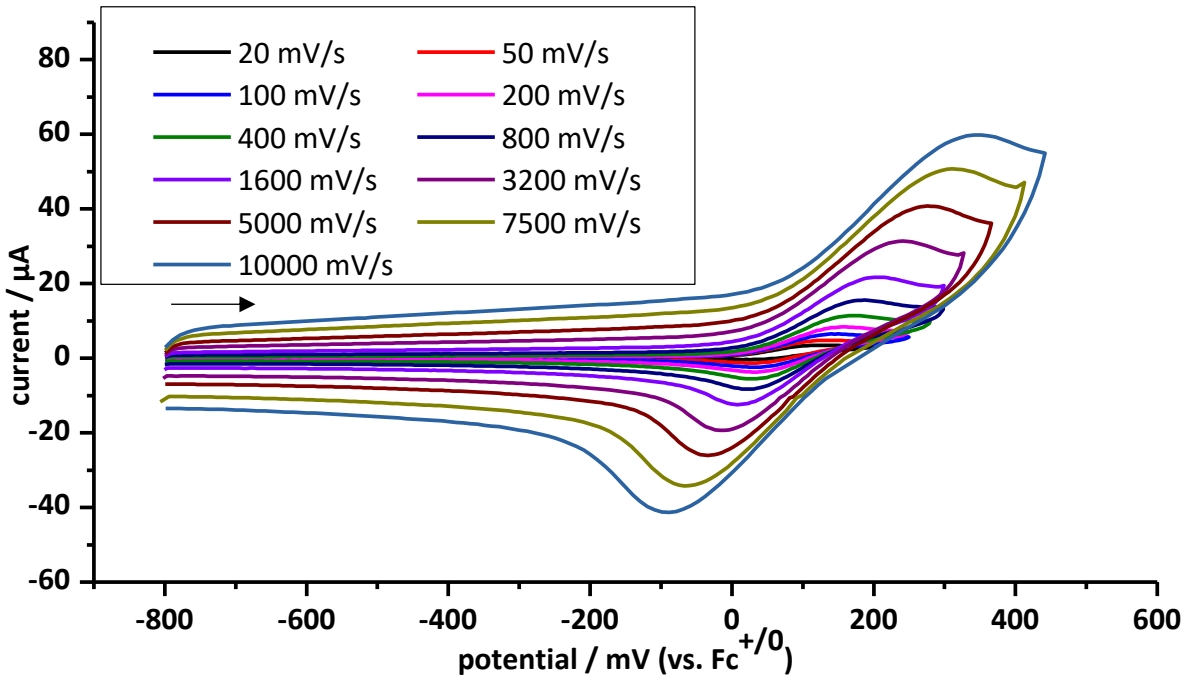

Figure 144: Cyclic voltammogram of complex **20b** (1 mM) at a Pt electrode in a 0.2 M $^{n}Bu_4PF_6$/THF solution at various scan rates; measurement with anodic initial scan direction (denoted with an arrow) of the first redox process; potentials are referenced against $Fc^{+/0}$.

Table 119: Selected results of the cyclic voltametric studies of **20b** in 0.2 M $^{n}Bu_4NPF_6$/THF solution at ambient temperature. Potentials are referenced against $Fc^{+/0}$.

ν / mV/s	E_p^{Ia} / V	i_p^{Ia} / µA	E_p^{Ic} / V	i_p^{Ic} / µA	$E_{1/2}^{I}$ / V	ΔE_p^{I} / mV	$\lvert i_p^c/i_p^a \rvert$
20	0.12	1.74	0.02	−1.18	0.07	105	0.68
50	0.14	2.41	0.03	−2.47	0.08	105	1.03
100	0.15	3.60	0.03	−3.84	0.09	115	1.07
200	0.16	4.76	0.03	−5.48	0.10	121	1.15
400	0.17	6.66	0.02	−7.77	0.10	146	1.17
800	0.19	9.60	0.02	−11.4	0.11	163	1.19
1600	0.20	14.2	0.01	−16.9	0.11	197	1.19
3200	0.24	21.5	−0.02	−25.8	0.11	258	1.20
5000	0.28	30.1	−0.03	−34.7	0.12	310	1.15
7500	0.31	36.1	−0.07	−46.0	0.12	378	1.27
10000	0.35	40.6	−0.09	−56.4	0.13	440	1.39

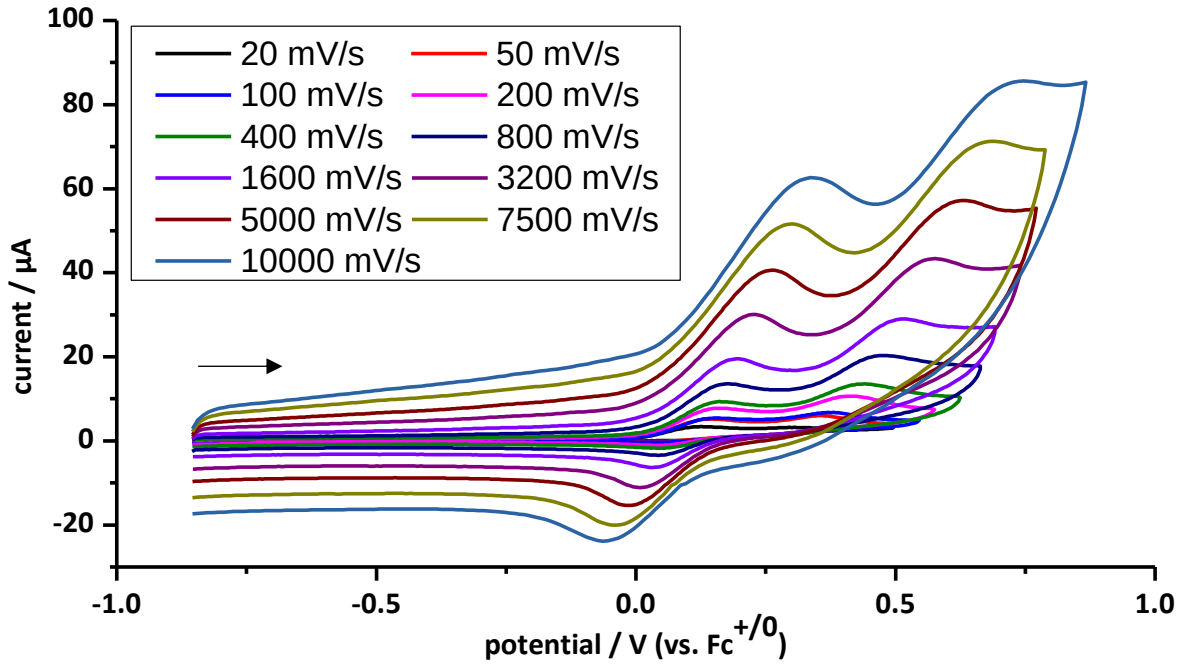

Figure 145: Cyclic voltammogram of complex **20b** (1 mM) at a Pt electrode in a 0.2 M $^{n}Bu_4PF_6$/THF solution at various scan rates; measurement with anodic initial scan direction (denoted with an arrow) of the first and second redox process; potentials are referenced against $Fc^{+/0}$.

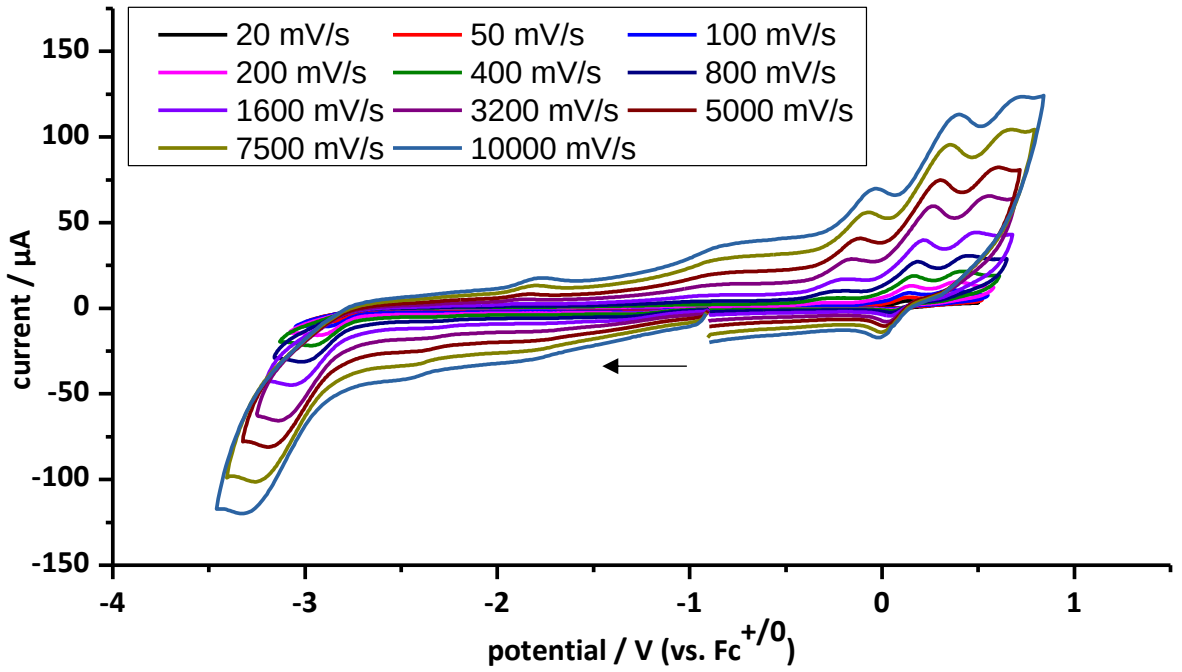

Figure 146: Cyclic voltammogram of complex **20b** (1 mM) at a Pt electrode in a 0.2 M $^{n}Bu_4PF_6$/THF solution at various scan rates; measurement with cathodic initial scan direction (denoted with an arrow) of the first, second and third redox process; potentials are referenced against $Fc^{+/0}$.

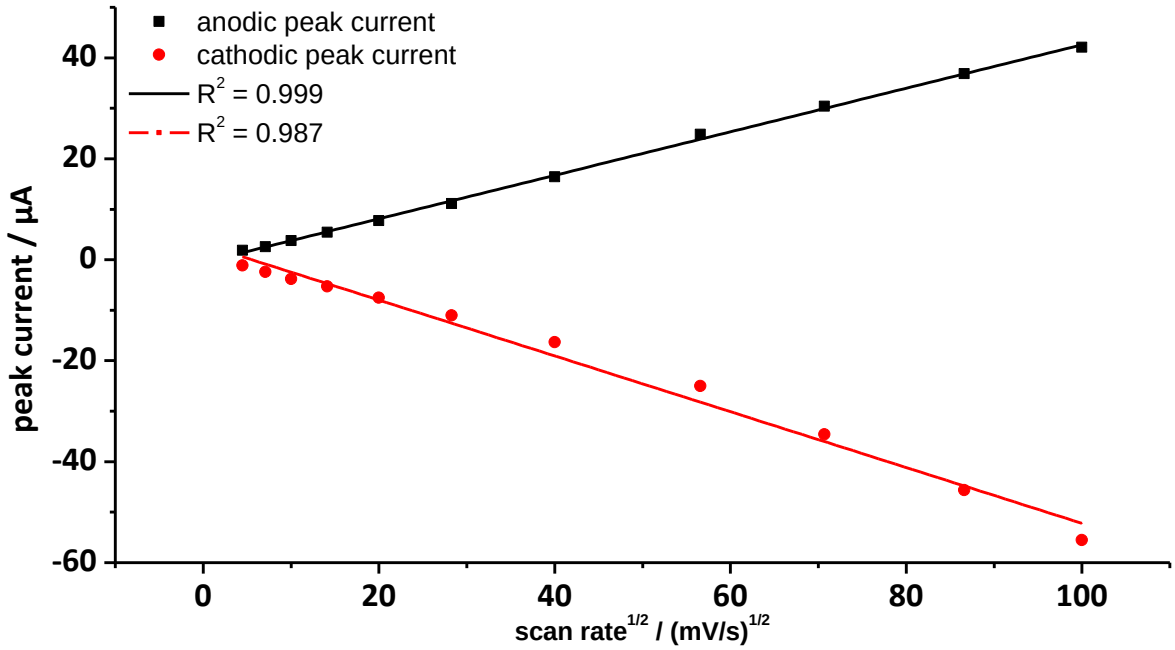

Figure 147: Plot of the peak currents against the square root of the scan rate $\nu^{1/2}$ for the first redox process of complex **20b**.

7.3.8 [Pentacarbonyl{tri-*n*-butylphosphoniumyl(triphenylmethyl)phosphanido-κ*P*}-tungsten(0)] (21b)

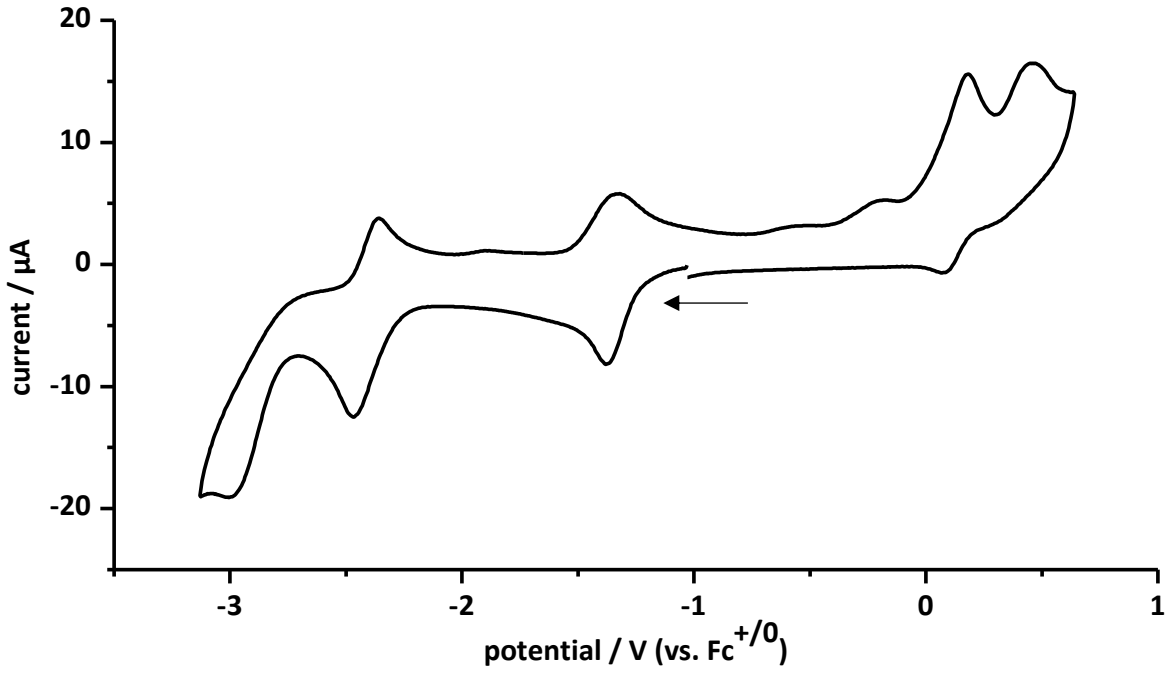

Figure 148: Cyclic voltammogram of complex **21b** (1 mM) at a Pt electrode in a 0.2 M $^{n}Bu_4PF_6$/THF solution with cobaltocenium hexafluorophosphate as internal reference; measurement with cathodic initial scan direction (denoted with an arrow); scan rate: 200 mV/s; potentials are referenced against $Fc^{+/0}$.

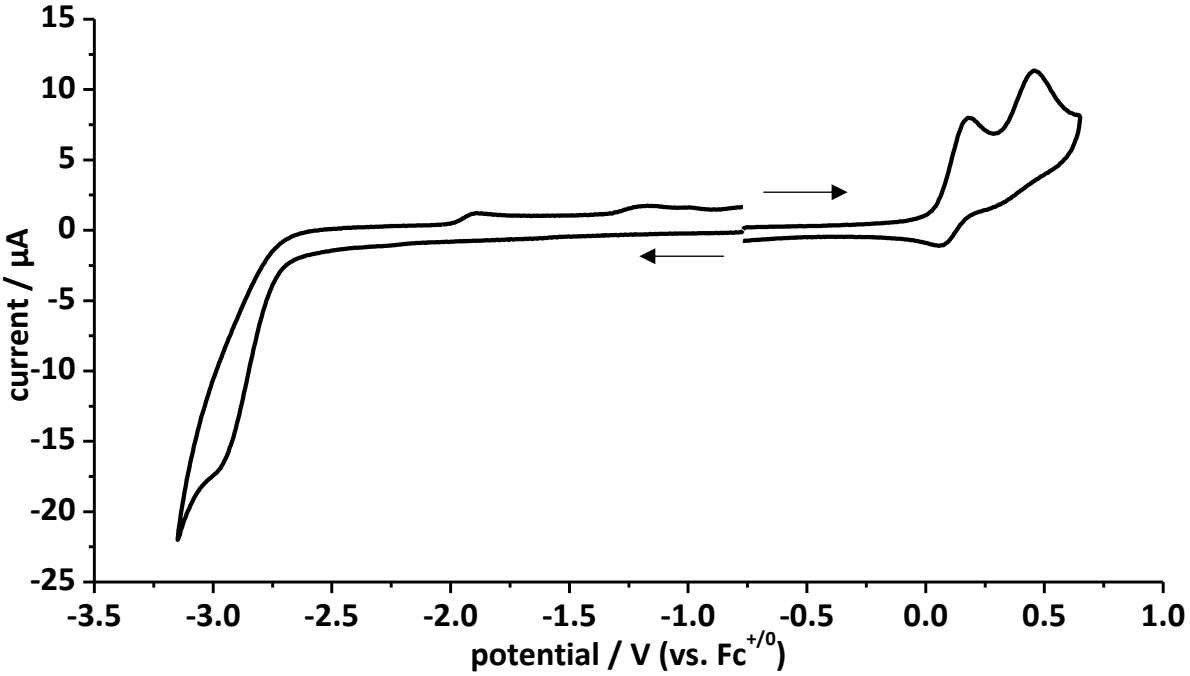

Figure 149: Overlay of cyclic voltammograms of **21b** (1 mM) at a Pt electrode in a 0.2 M $^{n}Bu_4PF_6$/THF solution; oxidation parts with anodic initial scan direction and reduction parts with cathodic initial scan direction as denoted with arrows; scan rate: 200 mV/s; potentials are referenced against $Fc^{+/0}$.

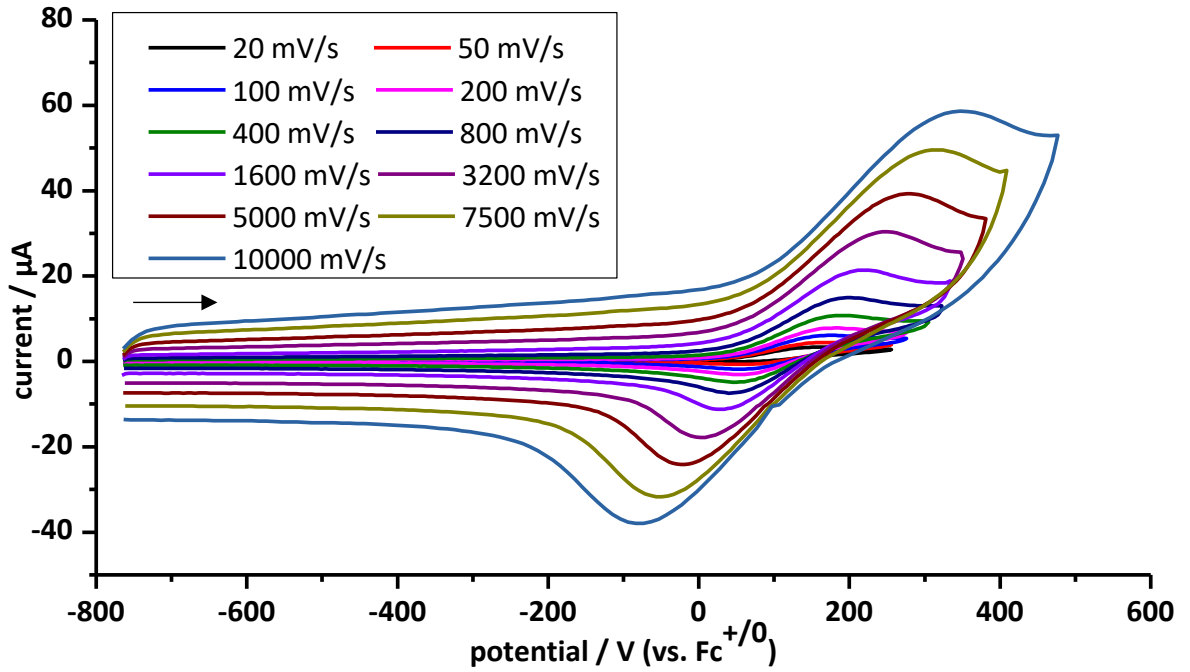

Figure 150: Cyclic voltammogram of complex **21b** (1 mM) at a Pt electrode in a 0.2 M $^{n}Bu_4PF_6$/THF solution at various scan rates; measurement with anodic initial scan direction (denoted with an arrow) of the first redox process; potentials are referenced against $Fc^{+/0}$.

Table 120: Selected results of the cyclic voltametric studies of **21b** in 0.2 M $^{n}Bu_4NPF_6$/THF solution at ambient temperature. Potentials are referenced against $Fc^{+/0}$.

ν / mV/s	E_p^{Ia} / V	i_p^{Ia} / µA	E_p^{Ic} / V	i_p^{Ic} / µA	$E_{1/2}^{I}$ / V	ΔE_p^{I} / mV	$\lvert i_p^c/i_p^a \rvert$
20	0.16	1.97	0.05	−0.71	0.10	115	0.36
50	0.17	2.36	0.05	−1.59	0.11	121	0.68
100	0.18	3.17	0.06	−3.16	0.12	120	1.00
200	0.18	4.19	0.06	−4.72	0.12	125	1.13
400	0.19	6.44	0.05	−7.11	0.12	136	1.11
800	0.20	9.25	0.04	−10.6	0.12	162	1.14
1600	0.22	14.4	0.03	−15.8	0.12	192	1.10
3200	0.25	23.0	0.00	−24.0	0.13	248	1.04
5000	0.28	28.7	−0.02	−32.7	0.13	305	1.14
7500	0.32	35.0	−0.06	−43.4	0.13	373	1.24
10000	0.35	40.4	−0.08	−52.2	0.13	430	1.29

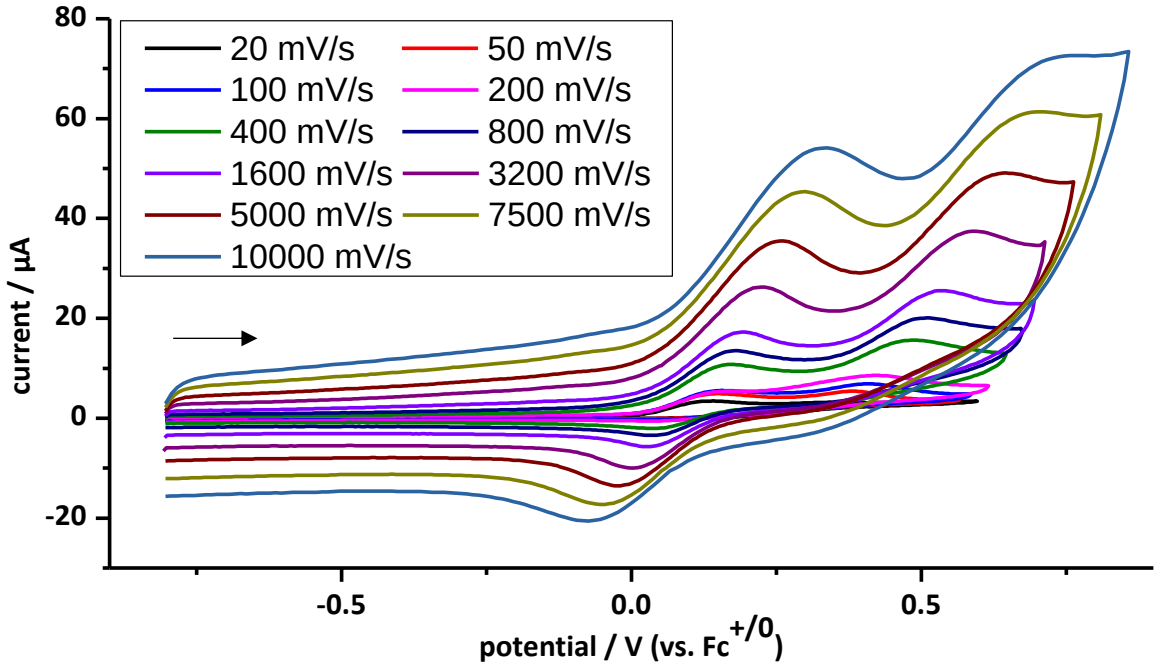

Figure 151: Cyclic voltammogram of complex **21b** (1 mM) at a Pt electrode in a 0.2 M $^{n}Bu_4PF_6$/THF solution at various scan rates; measurement with anodic initial scan direction (denoted with an arrow) of the first and second redox process; potentials are referenced against $Fc^{+/0}$.

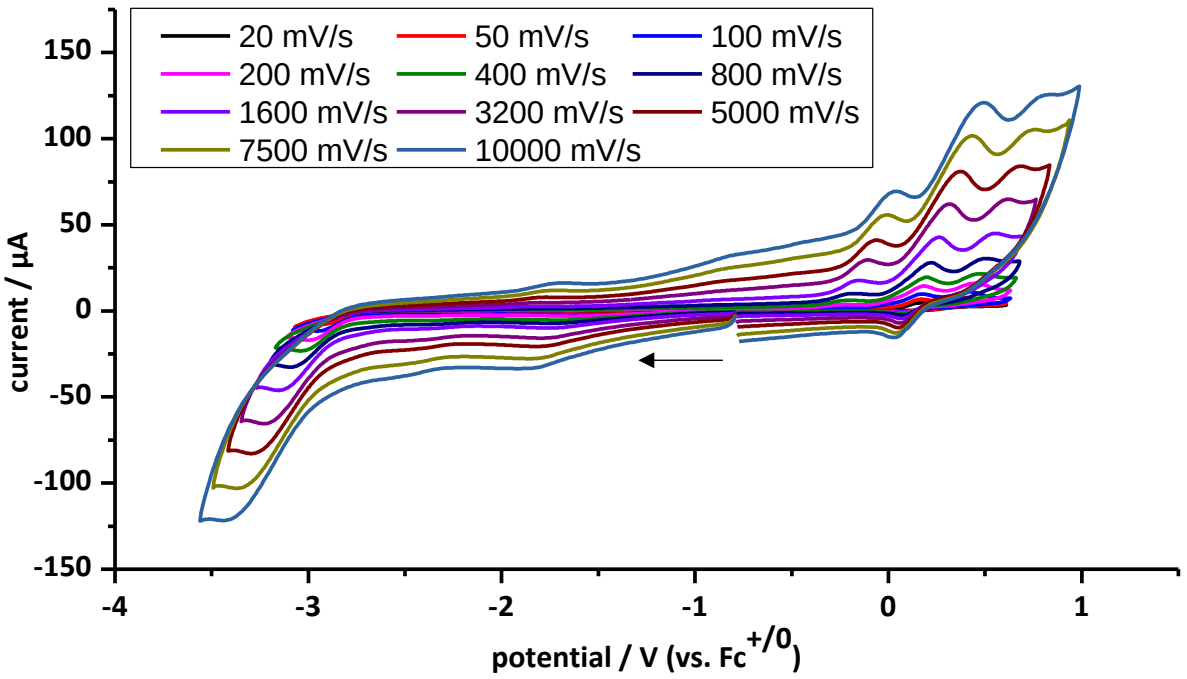

Figure 152: Cyclic voltammogram of complex **21b** (1 mM) at a Pt electrode in a 0.2 M $^{n}Bu_4PF_6$/THF solution at various scan rates; measurement with cathodic initial scan direction (denoted with an arrow) of the first, second and third redox process; potentials are referenced against $Fc^{+/0}$.

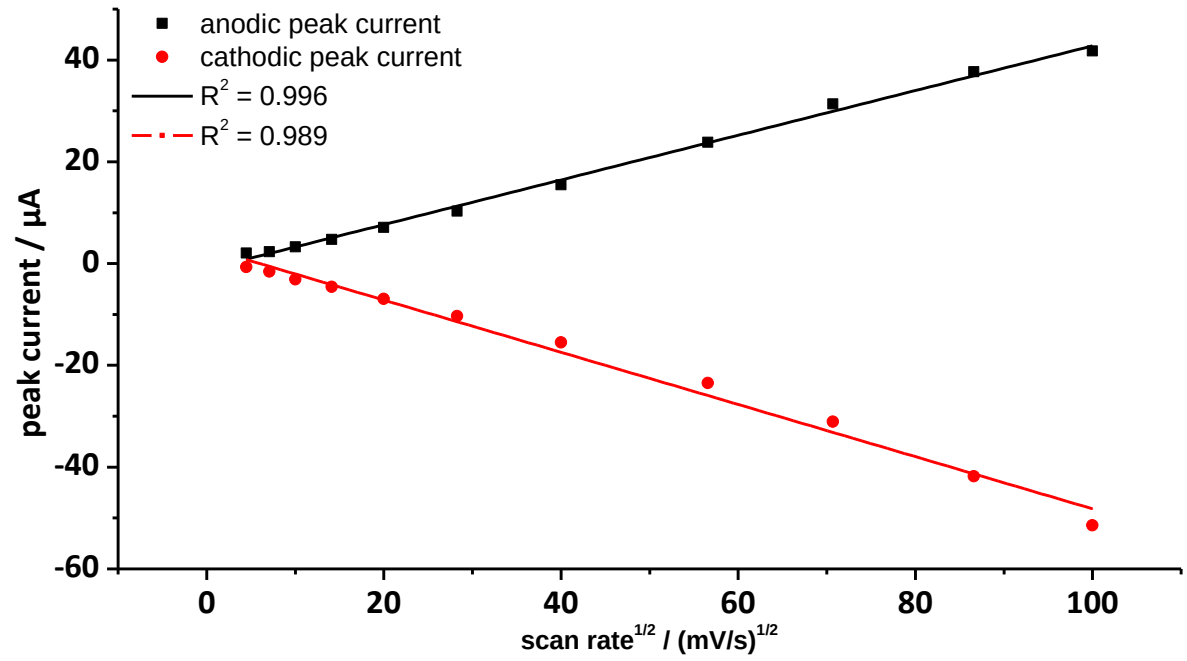

Figure 153: Plot of the peak currents against the square root of the scan rate $\nu^{1/2}$ for the first redox process of complex **21b**.

7.4 UV/VIS SPECTRA

7.4.1 Reaction mixture of complex 13b with $[W(CO)_5(NCMe)]$ (41) containing 43

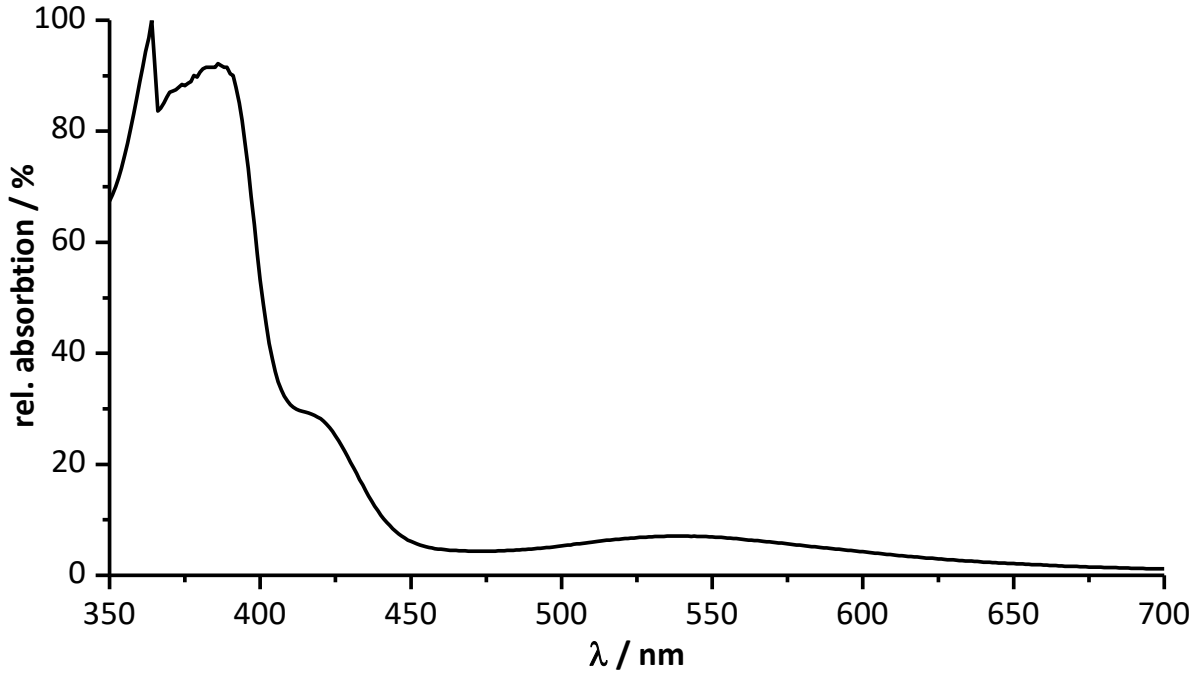

Figure 154: *in situ* UV/vis spectrum of the reaction mixture of complex **13b** with $[W(CO)_5(NCMe)]$ (**41**) in THF after stirring for 4 h at ambient temperature with a normalized absorption scale.

7.4.2 Reaction mixture of complex 13b with $B(C_6F_5)_3$ (48) containing 51

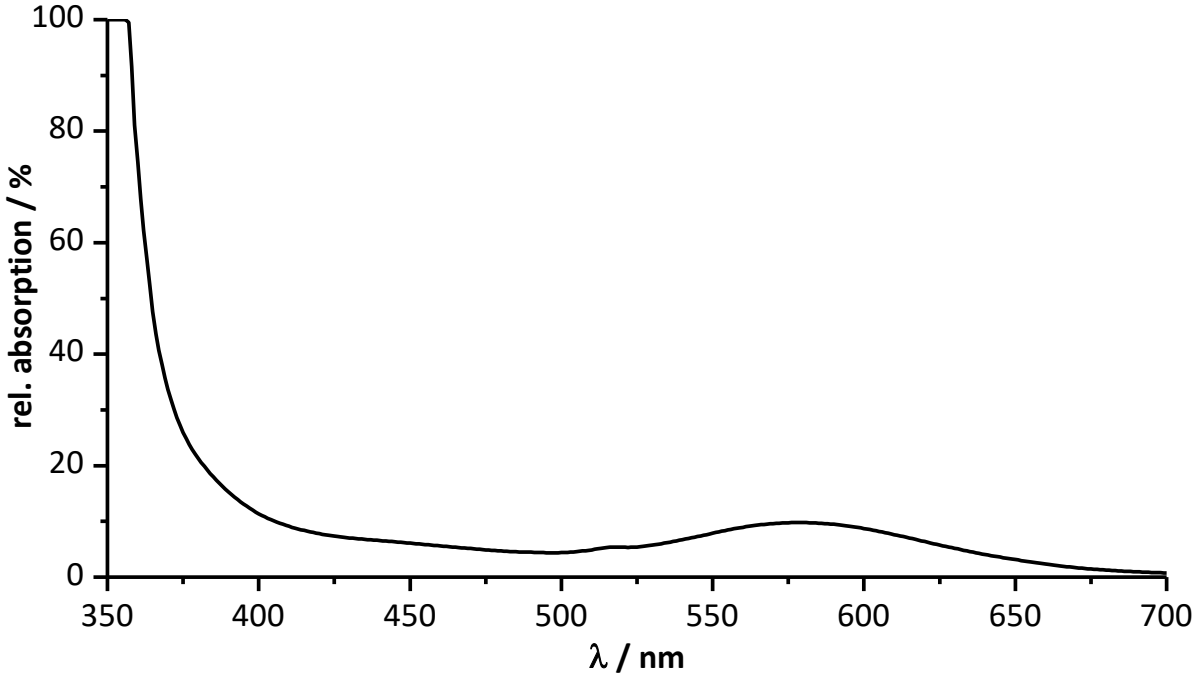

Figure 155: *in situ* UV/vis spectrum of the reaction mixture of complex **13b** with $B(C_6F_5)_3$ (**48**) in benzene after stirring for 30 minutes at ambient temperature with a normalized absorption scale.

7.5 Overview of isolated novel compounds

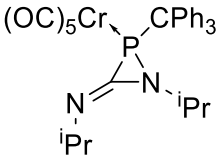

4a

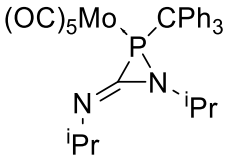

4b

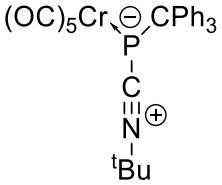

6a

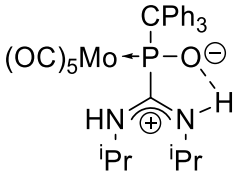

9b

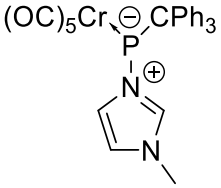

13a

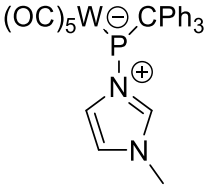

13b

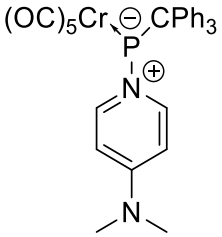

14a

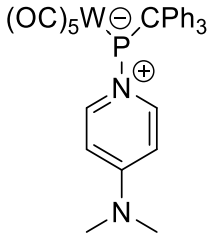

14b

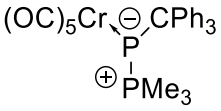

19a

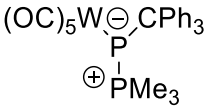

19b

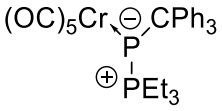

20b

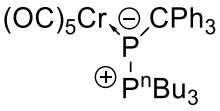

21b

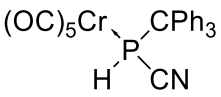

23a

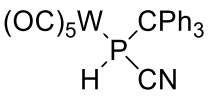

23b

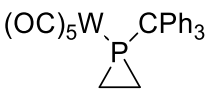

36

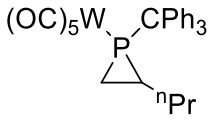

37

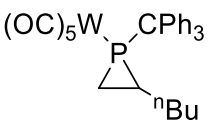

38

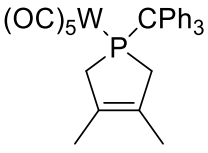

39

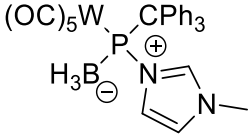

54

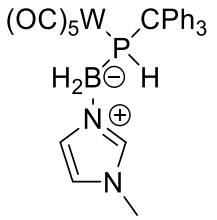

55

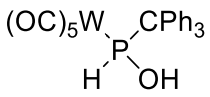

47b

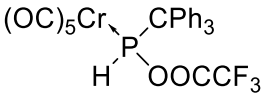

62a

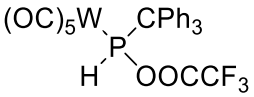

62b

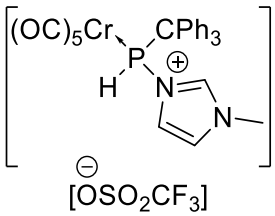

64a

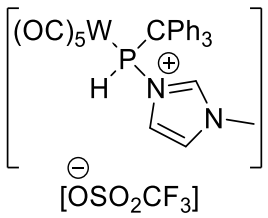

64b

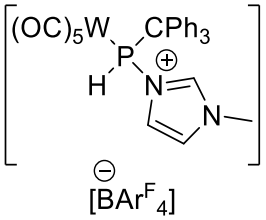

65b

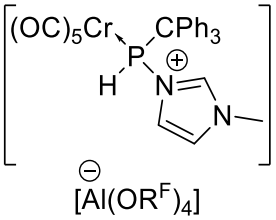

66a

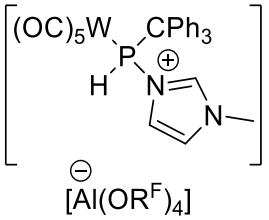

66b

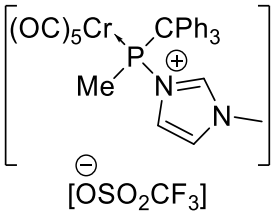

68a

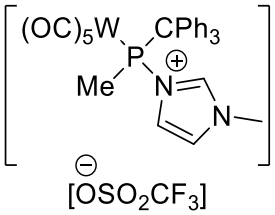

68b

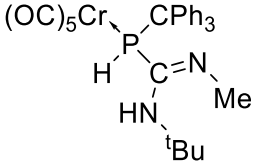

69a

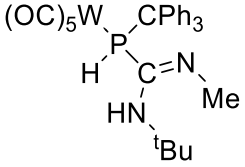

69b

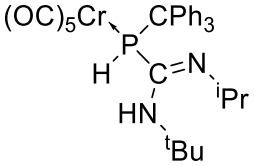

70a

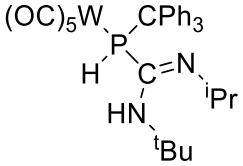

70b

7.6 LIST OF FIGURES

7.7 LIST OF SCHEMES

7.8 LIST OF TABLES